NBS SPECIAL PUBLICATION 461

U.S. DEPARTMENT OF COMMERCE / National Bureau of Standards

Radiation Physics

NATIONAL BUREAU OF STANDARDS

The National Bureau of Standards [1] was established by an act of Congress March 3, 1901. The Bureau's overall goal is to strengthen and advance the Nation's science and technology and facilitate their effective application for public benefit. To this end, the Bureau conducts research and provides: (1) a basis for the Nation's physical measurement system, (2) scientific and technological services for industry and government, (3) a technical basis for equity in trade, and (4) technical services to promote public safety. The Bureau consists of the Institute for Basic Standards, the Institute for Materials Research, the Institute for Applied Technology, the Institute for Computer Sciences and Technology, and the Office for Information Programs.

THE INSTITUTE FOR BASIC STANDARDS provides the central basis within the United States of a complete and consistent system of physical measurement; coordinates that system with measurement systems of other nations; and furnishes essential services leading to accurate and uniform physical measurements throughout the Nation's scientific community, industry, and commerce. The Institute consists of the Office of Measurement Services, the Office of Radiation Measurement and the following Center and divisions:

Applied Mathematics — Electricity — Mechanics — Heat — Optical Physics — Center for Radiation Research: Nuclear Sciences; Applied Radiation — Laboratory Astrophysics [2] — Cryogenics [2] — Electromagnetics [2] — Time and Frequency [2].

THE INSTITUTE FOR MATERIALS RESEARCH conducts materials research leading to improved methods of measurement, standards, and data on the properties of well-characterized materials needed by industry, commerce, educational institutions, and Government; provides advisory and research services to other Government agencies; and develops, produces, and distributes standard reference materials. The Institute consists of the Office of Standard Reference Materials, the Office of Air and Water Measurement, and the following divisions:

Analytical Chemistry — Polymers — Metallurgy — Inorganic Materials — Reactor Radiation — Physical Chemistry.

THE INSTITUTE FOR APPLIED TECHNOLOGY provides technical services to promote the use of available technology and to facilitate technological innovation in industry and Government; cooperates with public and private organizations leading to the development of technological standards (including mandatory safety standards), codes and methods of test; and provides technical advice and services to Government agencies upon request. The Institute consists of the following divisions and Centers:

Standards Application and Analysis — Electronic Technology — Center for Consumer Product Technology: Product Systems Analysis; Product Engineering — Center for Building Technology: Structures, Materials, and Life Safety; Building Environment; Technical Evaluation and Application — Center for Fire Research: Fire Science; Fire Safety Engineering.

THE INSTITUTE FOR COMPUTER SCIENCES AND TECHNOLOGY conducts research and provides technical services designed to aid Government agencies in improving cost effectiveness in the conduct of their programs through the selection, acquisition, and effective utilization of automatic data processing equipment; and serves as the principal focus within the executive branch for the development of Federal standards for automatic data processing equipment, techniques, and computer languages. The Institute consists of the following divisions:

Computer Services — Systems and Software — Computer Systems Engineering — Information Technology.

THE OFFICE FOR INFORMATION PROGRAMS promotes optimum dissemination and accessibility of scientific information generated within NBS and other agencies of the Federal Government; promotes the development of the National Standard Reference Data System and a system of information analysis centers dealing with the broader aspects of the National Measurement System; provides appropriate services to ensure that the NBS staff has optimum accessibility to the scientific information of the world. The Office consists of the following organizational units:

Office of Standard Reference Data — Office of Information Activities — Office of Technical Publications — Library — Office of International Relations — Office of International Standards.

---

[1] Headquarters and Laboratories at Gaithersburg, Maryland, unless otherwise noted; mailing address Washington, D.C. 20234.

[2] Located at Boulder, Colorado 80302.

Radiation Physics

Proceedings of the
International Symposium on Radiation Physics,
held at Bose Institute, Calcutta, India
November 30-December 4, 1974

Edited by:

A. M. Ghose
Nuclear Physics Laboratory
Bose Institute, Calcutta—700 009, India

D. V. Gopinath
Safety Research Laboratory
Reactor Research Center
Kalpakkam 603 102, India

J. H. Hubbell
Institute for Basic Standards
National Bureau of Standards
Washington, D.C. 20234

S. C. Roy
Nuclear Physics Laboratory
Bose Institute, Calcutta—700 009, India

Organized by:
Bose Institute, Calcutta, India

Co-sponsored by:
Department of Atomic Energy, India

Assistance from:
International Atomic Energy Agency

National Bureau of Standards

U.S. DEPARTMENT OF COMMERCE, Elliot L. Richardson, Secretary
Edward O. Vetter, Under Secretary
Dr. Betsy Ancker-Johnson, Assistant Secretary for Science and Technology
NATIONAL BUREAU OF STANDARDS, Ernest Ambler, Acting Director

Issued January 1977

Library of Congress Cataloging in Publication Data

International Symposium on Radiation Physics, Bose Institute, 1974.
Radiation physics.

(NBS special publication ; 461)
"CODEN: XNBSAV."
Supt. of Docs. No.; C 13.10:461

1. Ionizing radiation--Congresses. 2. Radiation--Congresses. 3. Radiation--Measurement--Congresses. 4. Cross sections (Nuclear physics)--Congresses. I. Ghose, A. M. II. Bose Research Institute, Calcutta. III. India (Republic). Dept. of Atomic Energy. IV. Title. V. Series: United States. National Bureau of Standards. Special publication ; 461.

QC100U57 no. 461 [QC474] 602'.1s [539.7'2] 76-608379

National Bureau of Standards Special Publication 461

Nat. Bur. Stand. (U.S.), Spec Publ. 461, 268 pages (Jan. 1977)

CODEN: XNBSAV

U.S. GOVERNMENT PRINTING OFFICE
WASHINGTON: 1977

For sale by the Superintendent of Documents, U.S. Government Printing Office, Washington, D.C. 20402
(Order by SD Catalog No. C13.10:461). Stock No. 003-003-01733-7 Price $3.25
(Add 25 percent additional for other than U.S. mailing)

PREFACE

Radiation Physics is an interdisciplinary science and in the past different aspects of the subject such as nuclear and atomic cross section measurements and analysis, shielding of accelerators, dosimetry, nuclear electronics, radiation biophysics, etc., have been discussed in specialized symposia and seminars. It has been increasingly felt that a symposium presenting the subject matter in an integrated manner would be useful to specialists working in isolated areas of radiation physics as well as to those interested in the global view of the entire subject. The International Symposium on Radiation Physics held in Bose Institute, Calcutta from November 30 to December 4, 1974, with these ends in view provided a forum for exchange of experiences and ideas among different workers in Radiation Physics from different countries.

The symposium was organized by Bose Institute, Calcutta. Moral and financial support was received from the Departments of Atomic Energy and Science and Technology, Govt. of India; National Bureau of Standards, U.S.A. and International Atomic Energy Agency, Vienna. We express our appreciation to those organizations.

Apart from a few minor changes, the papers published in these proceedings essentially represent what the authors submitted as the final versions of their presentations in the symposium. The editorial board apologizes for any mistake that might have crept in inadvertently.

All papers were retyped at Bose Institute, Calcutta, on composition (25% reduction) guide sheets supplied by the National Bureau of Standards for direct photo-reproduction. In some cases the inserted figures and tables, although the best available to the editors, suffer in legibility, particularly after the size-reduction. In these cases we suggest that interested readers write to the authors for more detailed versions of these papers which in most cases have been published elsewhere.

When commercial equipment, instruments and materials are mentioned or identified in these proceedings it is intended only to adequately specify experimental procedure. In no case does such identification imply recommendation or endorsement by the National Bureau of Standards, nor does it imply that the material or equipment identified is necessarily the best available for the purpose.

We regret the inordinate delay in publishing the proceedings, the reasons of which are beyond our control.

The editorial board gratefully acknowledges the assistance of the U.S. National Bureau of Standards Office of Technical Information and Publications received for printing and publishing these proceedings.

A. M. Ghose
D. V. Gopinath
J. H. Hubbell
S. C. Roy

ABSTRACT

These proceedings contain invited and contributed papers presented at the International Symposium on Radiation Physics organized by and held at the Bose Institute, Calcutta, India Nov. 30-Dec. 4, 1974. The purpose of this symposium, recognizing radiation physics as the thread held in common by a variety of medical, engineering and scientific disciplines, was to bring together specialists from these disciplines to report on, exchange, and make available through these proceedings, information and experiences of common interest to workers in these diverse disciplines. Topics thus brought together in this symposium include new measurements, theoretical developments, compilations and applications of basic cross section and transport data for photon, electron, neutron and heavy ion beams interacting with matter.

Key words: Cross sections; dosimetry; electrons; neutrons; photons; radiation physics; symposium.

TABLE OF CONTENTS

INAUGURAL ADDRESS

R. Ramanna
Director, Bhabha Atomic Research Centre
Trombay, Bombay-400085, India

Prof. Sircar, Prof. D.M. Bose, Prof. Ghose, Ladies and Gentlemen:

I feel deeply honoured in being asked to inaugurate this International Symposium on Radiation Physics. It is gratifying to note the magnitude of the participation in this symposium from various countries and India. I hope all of you will have a pleasant and useful time at Calcutta.

At this function, I would like to share some of my thoughts with you who represent a very wide cross section in nuclear physics on the future of nuclear research in countries like India. While we are classified as a developing country, we happen to have a very large number of nuclear physicists of ability and some facilities for the study of nuclear reactions and nuclear structure and at least one big facility for nuclear physics, the Variable Energy Cyclotron which we are fabricating entirely ourselves. I would therefore like to ask myself the question before all of you - what should be our future programme especially considering that providing facilities for Nuclear Physics takes both time and money ?

In the past, a greater part of the Nuclear Physics research in India has so far been closely connected with the expansion of the atomic energy programme. At the beginning of the programme, a 1 MeV cascade generator was installed at TIFR, in the early fifties. This together with radioactivity studies constituted the nuclear physics research facilities in the country till the reactors in Trombay, were commissioned. With the commissioning of the reactors, fission physics and reactor-based nuclear and solid state physics research started. In the early sixties the 5.5 MeV van de graaff accelerator at Trombay was installed. While the nuclear physics activity of BARC and TIFR centred around these facilities, several universities and DAE assisted institutes like the Saha Institute also started nuclear physics research using mainly radioactivity and low energy accelerators. Since these came into existence, there has been no further expansion of nuclear physics research facilities except for the forthcoming VEC project.

The performance of the nuclear physicists during this time can be rated very good considering the facilities available. Notable contributions were made in the fields of nuclear structure, fission and theoretical physics, apart from the contribution of the nuclear physicists to the atomic energy programme, development of electronics and in the field of technical physics.

It should be to the credit of the nuclear physicists in the country that the VEC facility is being built entirely with local effort. The commissioning of the VEC project is being eagerly awaited by the nuclear physics community of the country. In the first phase, experiments are planned with particles of energy up to 60 MeV. The enthusiasm of the physicists is evident from the experimental proposals submitted to the seminar on VEC utilisation to be held at the annual Nuclear Physics and Solid State Physics Symposium to be held in December this year in Trombay. Experiments are being made to study (a) the few particle nucleus interactions through elastic and inelastic scattering studies (b) nuclear structure studies through their electromagnetic and strong interactions and (c) fission phenomenon. Further proposals to enhance the utility of the Cyclotron is also under consideration for the second phase of the operation of the machine. For instance it is planned to have heavy ion facilities with Variable Energy Cyclotron. Looking even more further ahead we must ask ourselves whether we should have a versatile heavy ion facility at the VEC, by combining it with a straight accelerator like a tandem machine which I believe can also be made in the country. Is it worthwhile ? Can we afford it ?

This is as far as the immediate future is concerned. But what of the more distant future ? Should we expand our nuclear physics activity further or have we reached a stage where we cannot afford any further expansion ? In discussing this question, we should consider, forgetting for the time being our economic situation, the performance of the people so far, the experience they have gained during the past and the trend which nuclear physics

activity is taking in general in the rest of the world. It is true, unfortunately that days when small groups of people working on a simple problem and can achieve useful result have gone. To achieve tangible results, it is necessary to concentrate our efforts in major national facilities. Granting that the credibility of our nuclear physicists is established and that we should not let their past experience go to waste, we could think of the ways in which nuclear physics activity can grow in the country.

The two major areas in which nuclear physics may grow in the future are:

1. Phenomena involving the whole nucleus or a large number of particles in the nucleus : viz.

a) Production and study of exotic nuclei like super heavy nuclei and nuclei far off the stability line,

b) physics of nucleus at low nuclear densities like at the nuclear surface,

c) new phenomena involving various collective degrees of freedom like the giant resonances, high spin states leading to nuclear Meissner effect.

d) study of features like viscosity of the nuclear matter, through heavy ion studies.

These experiments require a heavy ion accelerator with upgrading of the VEC facility as envisaged above.

2. Phenomena involving a few nucleons and their correlations in nuclei are:

a) nuclear radius and surface studies using π, K and $\bar{p}$ absorption in nuclei,

b) importance of baryon resonances in nuclear systems, which should connect up the elementary particle physics and nuclear physics,

c) Mesic and hyperonic atoms giving rise to a wealth of information about the charge, mass and current distribution in nuclei,

d) investigation of unstable elementary particles themselves by secondary process, when they are produced in nuclei.

These studies require a machine with an energy of 4-6 GeV which is capable of giving K, π, μ, and $\bar{p}$ beams.

The listing of possible experiments under the circumstances can only be vague and very restricted. But I have made such a listing only for the purpose of discussion as to what should be done for the future. It is seen that the set of experiments involving the whole nucleus or a large number of particles can be undertaken in a upgraded VEC facility, we should therefore give it serious consideration and try to provide funds for it. However, in the case of phenomena of a few nucleons and their correlations in nuclei, the need for a large machine is beset by many question marks especially from the point of view of the cost, time of construction and the need for various maintenance facilities. But I do not see why the nuclear physicists in the country cannot start making feasibility studies just as we did when we planned the VEC project. Feasibility studies should not stop just because big machines are entirely out of our range financially though not technically as things stand.

I have great pleasure in inaugurating the conference and wish all of you a very successful meeting.

PRESENT STATUS OF PHOTON CROSS SECTION DATA 100 eV TO 100 GeV*

J. H. Hubbell
National Bureau of Standards
Washington, D.C. 20234

Recent developments in theoretical and experimental cross sections for the basic photon interactions with atoms (photoeffect, coherent and incoherent scattering, and electron-positron pair production) are reviewed. Emphasis is on the extensive total and subshell photoeffect calculations by J. Scofield, and on atomic form factor and incoherent scattering function data calculated by D. Cromer and by R. Brown. Some comparisons of these theoretical results with available explicit cross section and total attenuation coefficient measurements are presented.

(Atomic form factor, attenuation coefficients, cross sections, gamma rays, incoherent scattering function, photoelectric effect, pair production, photons, x-rays)

Introduction

Dr. Ghose, Dr. Ramanna, Chairman Dr. Snyder, fellow Symposium participants ------ it is my pleasure to revisit on this occasion the city of Nobel laureate (literature, 1913), Rabindranath Tagore who in his Gitanjali[1] wrote:

"Where the mind is without fear and the head is held high;
Where knowledge is free;
Where the world has not been broken up into fragments by narrow domestic walls;
Where words come out from the depth of truth;
Where tireless striving stretches its arms towards perfection;
Where the clear stream of reason has not lost its way into the dreary desert sand of dead habit;
Where the mind is led forward by thee into ever-widening thought and action --
Into that heaven of freedom, my Father, let my country [or, my world] awake."

so appropriate to the spirit of this Symposium.

In this talk I will (1) touch briefly on some topics in photon cross sections and dosimetry which will be explored in much more depth and detail by other speakers in this and other sessions, (2) show some comparisons of present theoretical cross sections with available total and partial measurements, (3) look a little at Z-smoothness with its implications for Z-interpolation, and finally (4) make some estimates of how well we are converging toward "underlying reality" or the unique photon cross section set we would all like to have.

General Background

Any review of x-ray cross section data should start with Röntgen, whom we call to mind with figure 1. This picture, assumed to be of Frau Röntgen's hand, is reproduced from Röntgen's 1895 discovery paper[2], and should have a "familiar ring" to it.

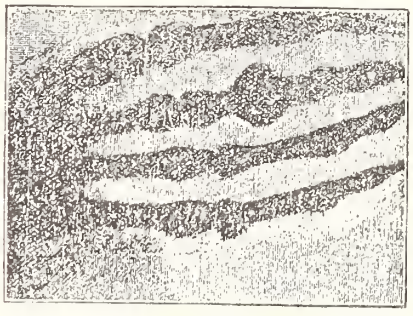

Fig. 1.

*Work supported by the NBS Office of Standard Reference Data.

As well as taking pictures of bones and other hidden objects, x-rays deposit energy, or "dose", in the media through which they pass, as illustrated in figure 2 by a radiation-sensitive dye solution developed by McLaughlin et al.[3]. The x-ray dose range 0-100 kilorads illustrated in figure 2 is important in a variety of practical applications including, as shown in figure 3, insect population control and food storage-life extension.

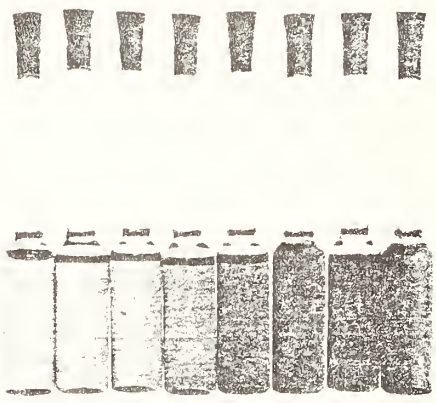

Fig. 2.

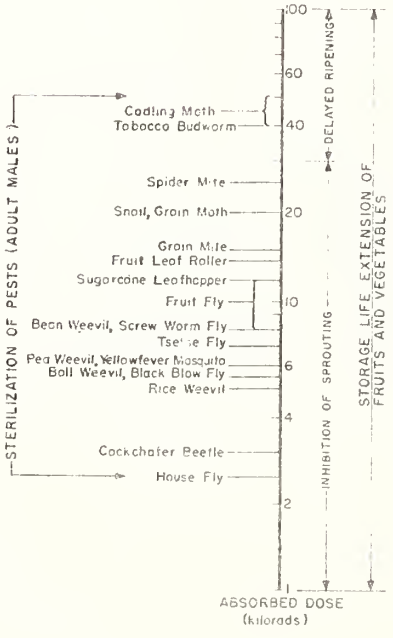

Fig. 3.

In figure 4 we indicate the principal photon interaction processes (see, e.g. ref.[4]): (a) κ, creation of electron-positron pairs, (b) τ, atomic photoeffect and (c) σ_{inc}, incoherent (Compton) scattering, contributing to the above "energy deposition", and the types of secondary radiations (annihilation radiation, bremsstrahlung, fluorescence and Compton scattered photons) which subtract from the energy deposited at a photon interaction site. Sums over various combinations of these cross sections, corrected for the escape of secondary radiation appropriate to a given problem, are the so-called "true absorption coefficient" μ_a/ρ, the "mass energy transfer coefficient" μ_K/ρ, and the "mass attenuation coefficient" μ_{en}/ρ (see ref.5 for a review of this nomenclature) as schematically shown in figure 4.

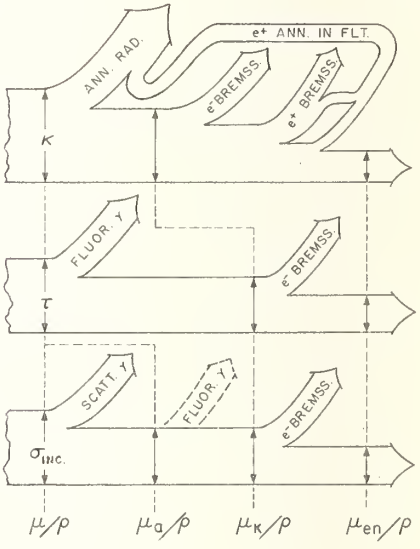

Fig. 4.

The "mass attenuation coefficient" μ/ρ which should include, in addition to the processes shown in figure 4, a contribution from coherent (Rayleigh) scattering $\sigma_{coh.}$, is usually defined for purposes of tabulations as (see, e.g.ref 4,6,7):

$$\mu/\rho = \frac{N_A}{M} \cdot \sigma_{tot} \qquad (1)$$

in which N_A = Avogadro's number (6.022045×10^{23} atoms/g-atom), M is the atomic weight (g/g-atom) and

$$\sigma_{tot} = \kappa + \tau + \sigma_{coh.} \quad (2)$$

The mass attenuation coefficient μ/ρ is obtained from narrow-beam measurements of monoenergetic photon beams transmitted by samples using the relations

$$I/I_o = e^{-\frac{\mu}{\rho} t} \quad (3)$$

or

$$\mu/\rho = -\ln(I/I_o)/t \quad (4)$$

where I and I_o are the beam intensities with and without the interposed sample, respectively, and t is the sample thickness in mass per unit area.

The relative magnitudes of the above interaction processes as a function of photon energy are shown in figure 5 for the case of copper, with the further addition of the photonuclear cross section $\sigma_{ph.\ n.}$ which has a broad peak, or "giant resonance" feature, centered at about 24 MeV for light nuclei, decreasing in energy with increasing mass number to about 12 MeV for the heaviest nuclei[8]. Experimental total cross sections σ_{tot} for copper, derived from existing μ/ρ measurements[9] using the above relations in equations (4) and (1), are shown in figure 5 as the small circles.

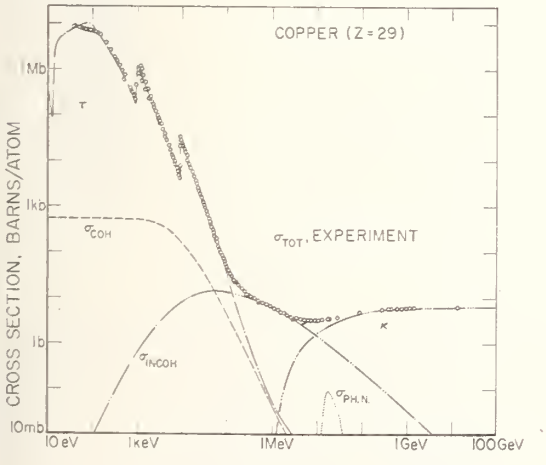

Fig. 5.

The coverage of total cross section measurements for other elements is shown in figure 6 in which the solid black bars indicate that we know σ_{tot} or μ/ρ to within a $\pm$ 2% uncertainty. A feature of interest in figure 6 is the gap in existing measurements in the neighborhood of 1 keV.

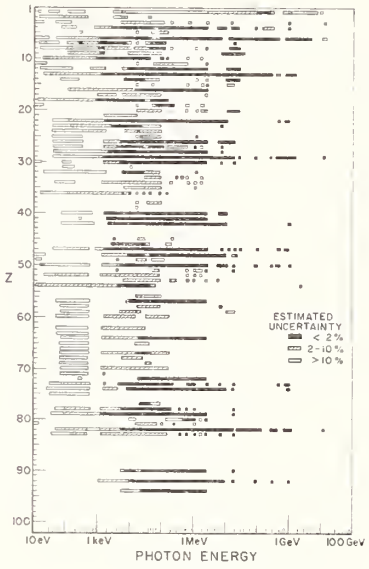

Fig. 6.

Comparisons of Theoretical with Experimental Total Cross Section Data

In the next series of figures we will compare some of the total cross section measurements indicated in figure 6 with some existing compilations of theoretical or smoothed data.

In figure 7 for hydrogen we see that the Henke et al. (67 He 01)[10]

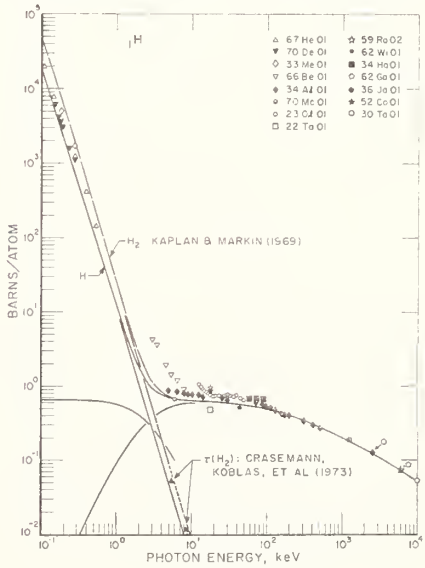

Fig. 7.

total cross section measurements and the Crasemann et al.[11] photoeffect measurements suggest, as discussed by Cooper[12] that the photoeffect cross section for molecular H_2 is roughly 40% higher than for atomic H for photon energies 0.5 to 10 keV. An even larger enhancement (as much as a factor of two) in the coherent scattering cross section for H_2 vs. H is predicted by Bentley and Stewart[13] (see also integral data in ref. 14). Hence, although cross section compilations (see, e.g. ref. 4,6,7) customarily present data only for the exactly-calculable isolated H-atom, for practical applications a table of molecular H_2 cross section data should perhaps also be included in subsequent compilations.

Figure 8 for lithium shows the gap in our experimental information around 1 keV mentioned earlier also the status of some of the calculated and fitted results. No significant difference is seen here between the Sandia (Biggs and

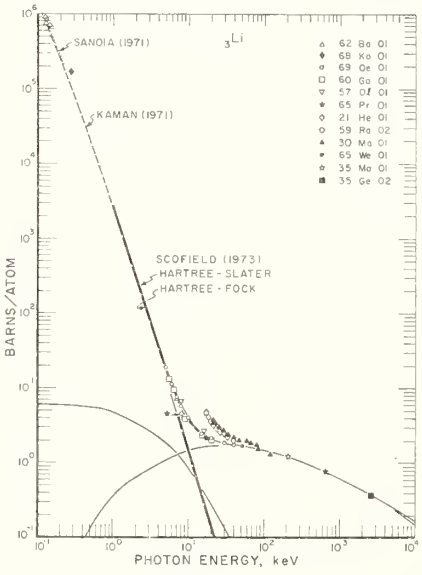

Fig. 8.

Lighthill[15] parametric fit and the Kaman (Veigele et al.[16]) calculated values. In Scofield's[17] recent photoeffect calculation, covering the range 1 keV to 1.5 MeV for all elements Z = 1 to 101, he has suggested that his Hartree-Slater results could be improved by renormalizing to the Hartree-Fock model. Lithium happens to be the element most affected in the K-shell by this renormalization, here shown to decrease by 7% .

In figure 9, moving up through the periodic table to nitrogen, we see the 1 keV region reasonably well measured, as gas targets lend themselves well to studies in this region. Above 100 keV we must still rely on either theory or interpolation across Z, although some data (not shown on this figure) for nitrogen in the range 0.66 - 1.33 MeV, deduced from measurements on carbon (in 11 hydrocarbons), boron carbide and boron nitride, were recently published by Goswami and Chaudhuri[18] .

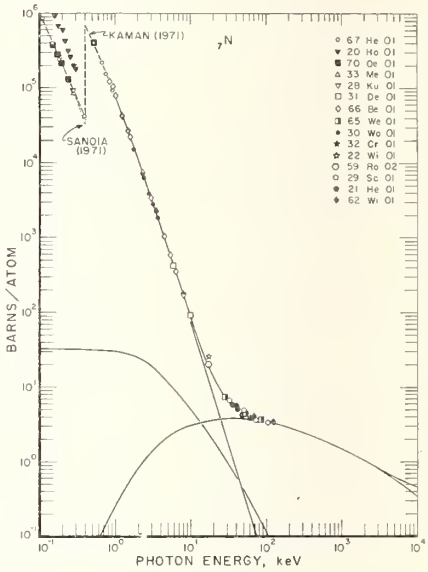

Fig. 9.

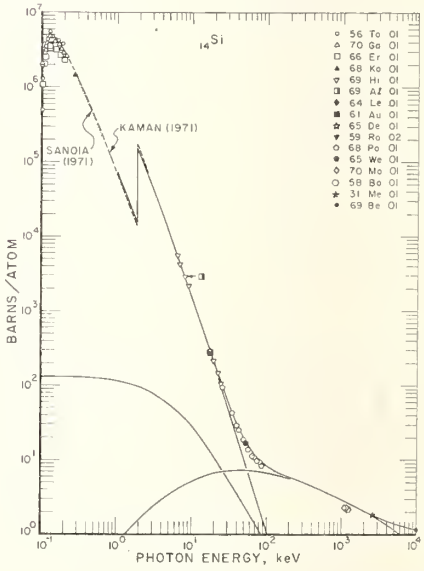

Fig. 10.

In figure 10 we see that silicon, an important detector material, again shows a wide gap in the experimental information in the vicinity of 1 keV and in this case the K absorption edge. Further measurements filling in the region around 1 keV would be useful. In the region around 1 MeV the recent silicon measurements by Goswami and Chaudhuri[18] (not shown in this figure) are in much better agreement with the theoretical curve than the indicated measurements by Mavroyannakis and Antoniades (70 Ma 01)[19] and by Boltaks et al. [58 Bo 01][20] .

In figure 11 we have germanium, another popular detector material. The region of interest to crystallographers from 4 to 30 keV and extending up to 100 keV is rather well mapped out, but down around the L edges (1.22, 1.25 and 1.41 keV) there are disagreements of the order of 10%. The (not shown) recent Goswami-Chaudhuri[18] .0.66 - 1.33 MeV measurements are in good agreement with the theoretical curve shown.

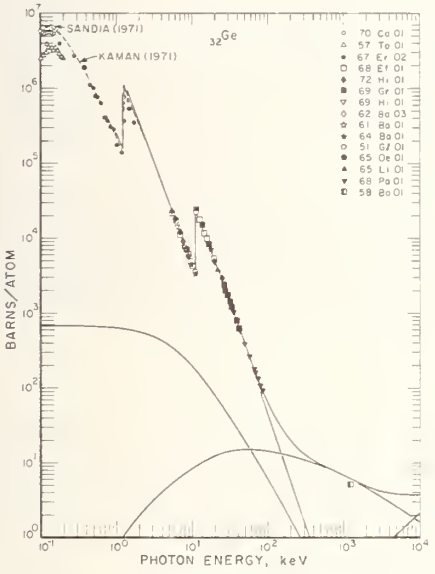

Fig. 11.

Figure 12 shows tin taken down on additional decade to 10 eV. Low-energy data reported by NBS (Codling et al. [66 Co 01][21] and DESY [Haensel et al. 68 Ha 01][22] synchrotron-light groups and by the Leningrad group (Lukirski et al. (66 Lu 02)[23]) are reasonably consistent, and can be compared with the McGuire[24] and Kaman[16] calculations, and with the parametric fit by the Sandia[15] group. Above 1 keV the LLL-NBS (McMaster et al.[25,26]) tabulation follows the 1936 data by Biermann (36 Bi 01[27]), which is 30% higher than the Scofield[17] or Kaman[16] calculations at 1 keV. Hence for tin, as for some elements previously mentioned, new measurements in the neighborhood of 1 keV would be useful.

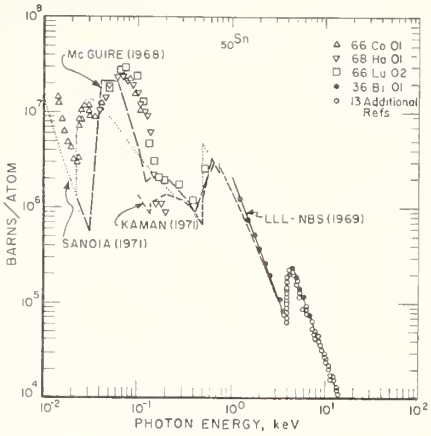

Fig. 12.

In figure 13 gadolinium is seen to have a good distribution of measurements, all of them more recent than 1967, all reasonably consistent. Below 1 keV the Kaman photoeffect calculation[16] is seen to agree within 20% with the measured points except for the absorption peak at 150 eV observed by Zimkina et al. (67 Zi 01)[28] .

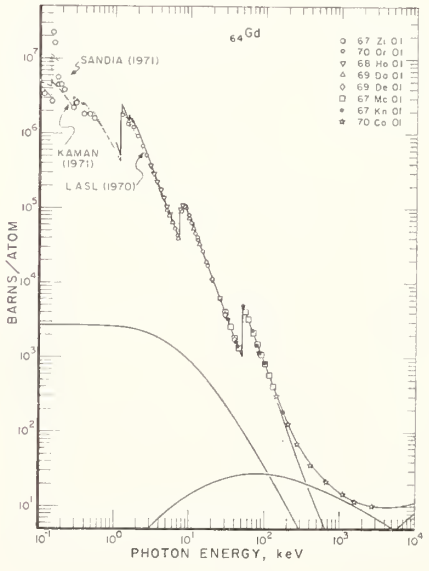

Fig. 13.

In figure 14 uranium measurements are gradually filling in toward lower energies. Where the Kaman[16] and Scofield[17] photoeffect calculations overlap in the range 1.0 - 2.5 keV, and disagree by 10% , the recent 1-10 keV measurements by Del Grande and Oliver (73 De 01)[29] favor the Kaman results. However at lower energies the new 130 - 450 eV uranium measurements by Cukier et al.[30] (not shown), although

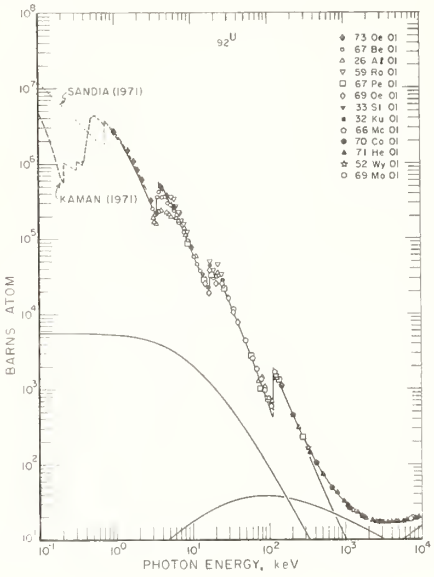

Fig. 14.

exhibiting a shape similar to that predicted by Veigele et al.[16] , are closer in magnitude to the Sandia (Biggs and Lighthill[15]) extrapolation down through this region. Further uranium measurements at and below 1 keV are in progress at the University of Hawaii[31] .

A More Explicit Look at Photoeffect

A more sensitive graphical comparison of measured total attenuation coefficients with calculated photoeffect cross sections can be achieved by subtracting calculated coherent and incoherent scattering cross sections from the measured totals, then multiplying these "photoeffect" differences by an appropriate power of photon energy. In figures 15 and 16 we see that the power E^2 is a convenient compromise for application to all elements Z = 1 to 100. Veigele and Briggs[32] have constructed these and similar plots for all elements having measured data in the Kaman file, for purposes of evaluating theoretical photoeffect cross sections shown as solid curves in figures 15 and 16 (Kaman[16] below ~1 keV; Scofield[17] above 1 keV).

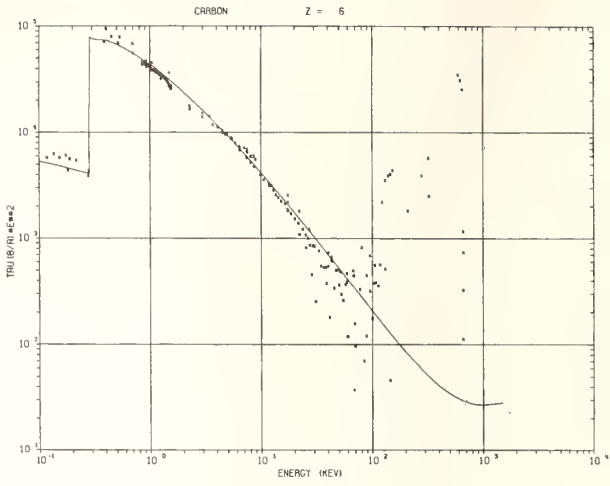

Fig. 15.

The principal features in figure 15 for carbon are (a) the slight systematic divergence of the "difference" photoeffect data points from Scofield[17] theory in range 10 to 30 keV, and (b) the complete breakdown above 30 keV of this method for experimentally determining the carbon photoeffect cross section.

In figure 16 for uranium we can now see more clearly the relation of the Del Grande and Oliver[29] measured points (open circles) to the Veigele et al.[16] calculation (0.1 to 2.5 keV for uranium) and to the Scofield[17] calculation (1 to 1500 keV).

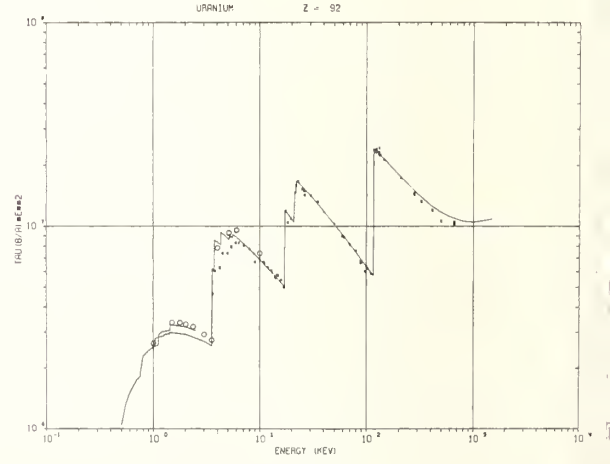

Fig. 16.

Scattering Data

This section of the talk is a brief summary of a recent extended-range tabulation and discussion of the atomic form factor F(x,Z) and the incoherent scattering function S(x,Z), to which reference can be made for further details[14] .

The atomic form factor for hydrogen is shown in figure 17 for (a) a neutral isolated hydrogen atom (solid curve) calculated using the simple closed-form "exact" formula given by Pirenne[33] , (b) the "floated sphere" (0.07 Å off the proton into the bond) Stewart et al. result[34] (circles useful for approximating terminally-bonded hydrogen, and (c) H in molecular H_2 as calculated by Bentley and Stewart[13] (triangles) using Kolos-Roothaan[35] wavefunctions.

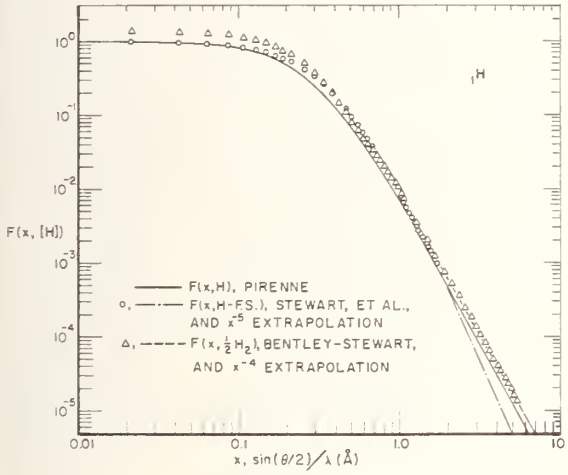

Fig. 17.

In figure 18 the ratios of the above Stewart et al.[34] and Bentley-Stewart[13] molecular-hydrogen results to the Pirenne atomic-hydrogen results suggest that H_2 molecule, at least for $x < 1.0$ Å^{-1}, strongly resembles the He atom. That is, the effective Bentley-Stewart ½ H_2 form factor ($\sim\sqrt{2}$ for x = 0) as used in calculating the coherent scattering cross section for H_2 would be of the form

$$2\left\{\left|F(\tfrac{1}{2}H_2)\right|_{x=0}\right\}^2 = 2\left\{\sqrt{2}^{\,2}\right\} = \sim 4 \qquad (5)$$

which can be compared with

$$\left\{\left|F(He)\right|_{x=0}^{\,2}\right\} = \left\{2\right\}^2 = 4 \qquad (6)$$

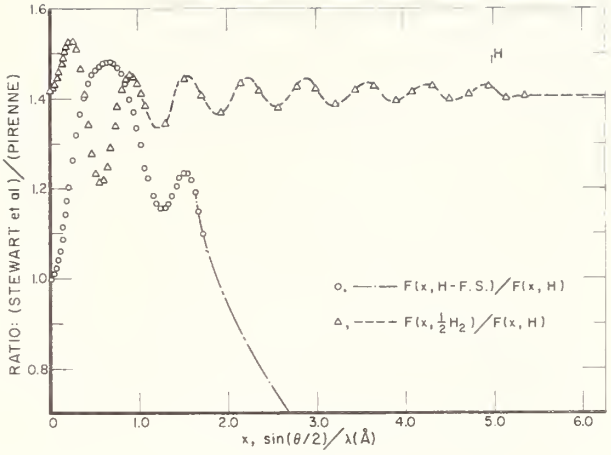

Fig. 18.

For elements other than hydrogen, the atomic form factor in the present tabulations[14] was pieced together from available numerical calculations by Brown[36] and by Cromer and Mann[37] , additional extended-range results supplied by Cromer to Veigele et al.[16] ,

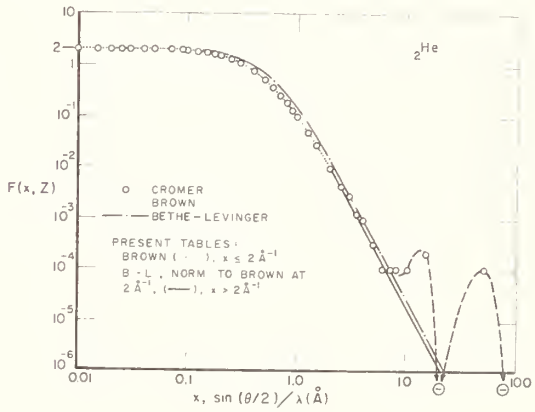

Fig. 19.

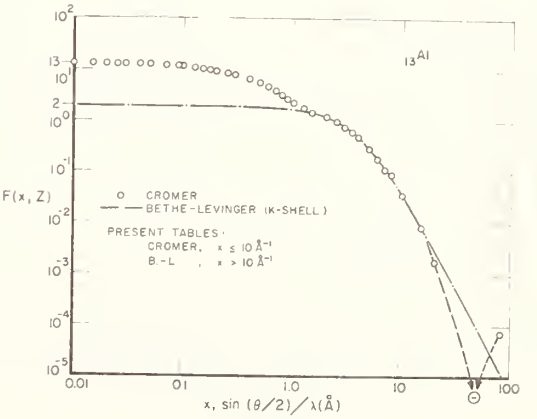

Fig. 20.

and from the Bethe-Levinger[38] closed-form expression for the asymptotic high-x region. The composition of the present tables from the above data-sources is indicated in figures 19, 20 and 21 for helium, aluminum and lead.

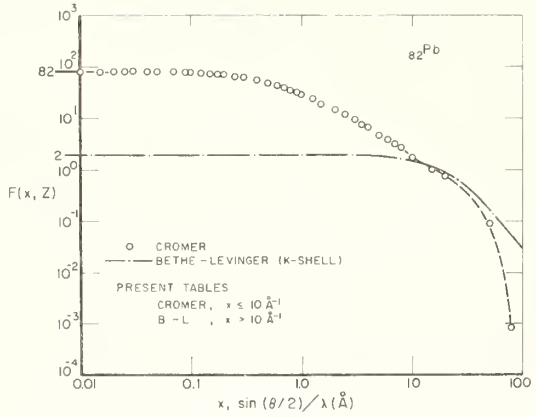

Fig. 21.

In figure 22 through 26 we compare the above theoretical form factor tabulation with available measurements for

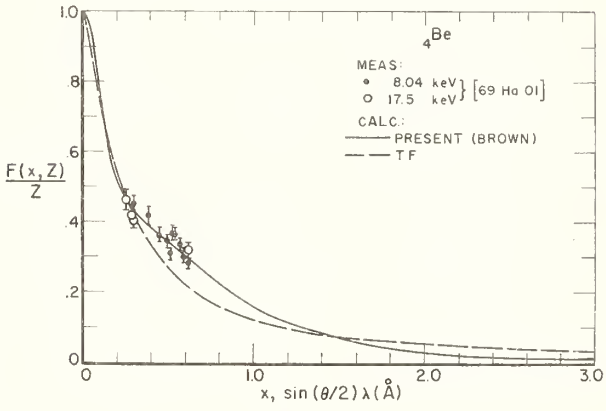

Fig. 22.

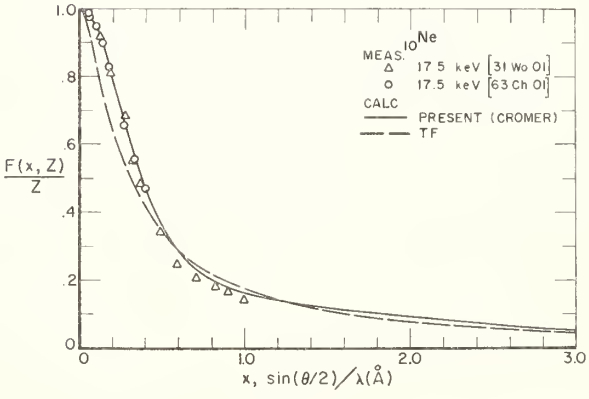

Fig. 23.

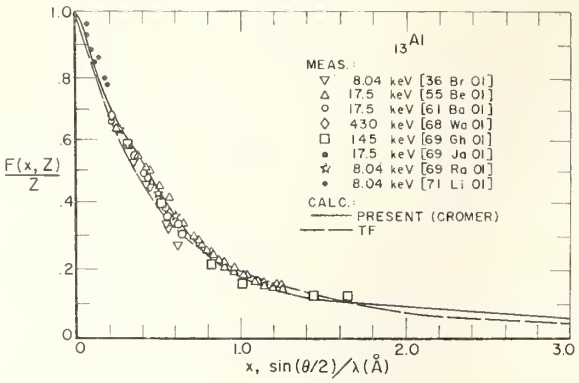

Fig. 24.

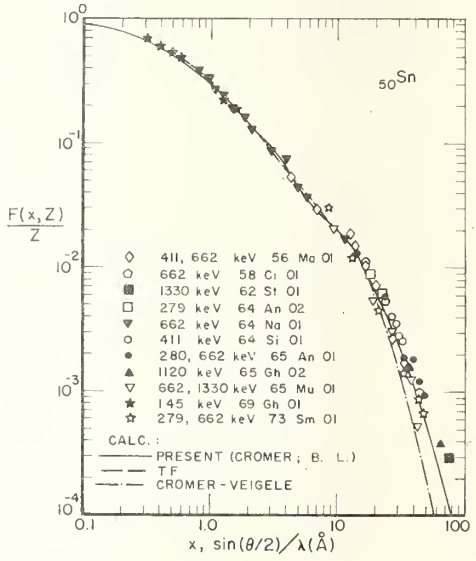

Fig. 25.

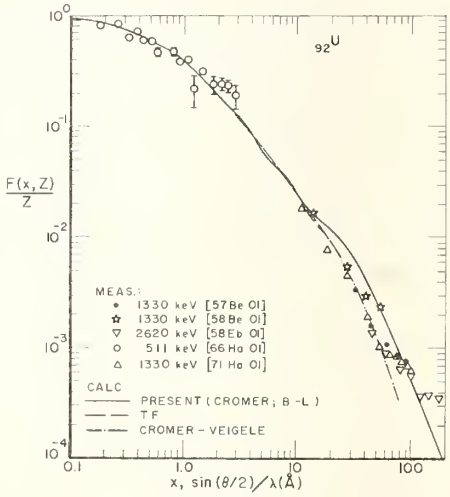

Fig. 26.

the elements beryllium, neon, aluminum, tin and uranium, also with form factors calculated using the Thomas-Fermi (TF) statistical model of the atom. In the measurement-reference symbols in figures 22-29, the first two digits refer to the year of publication and are followed by the first two letters of the first-author's last name and an additional number for uniqueness. For example, "[58 Eb 01]" stands for "Eberhard, P., Goldzahl, L. and Hara, E., J. Phys. Radium 19, 658-667 (1958)". A complete listing of measurement references for these and other elements is given in reference [14] of this paper.

Figures 27 to 29 show similar comparisons of the present theoretical tabulations[14] of the incoherent scattering function S(x,Z) with available measurements for carbon, aluminum and lead. For the elements helium through carbon we have used the configuration-interaction results of Brown[36] in preference to those of Cromer and Mann[39] for S(x,Z) [also for F(x,Z)]. As can be seen in figure 27 for carbon, the differences in S(x,Z) for Be, B and C between Brown and Cromer-Mann in the range x = 0 to 0.5 $Å^{-1}$ are substantial, resulting in 20% to 30% differences in the integrated incoherent scattering cross section at 1 keV.

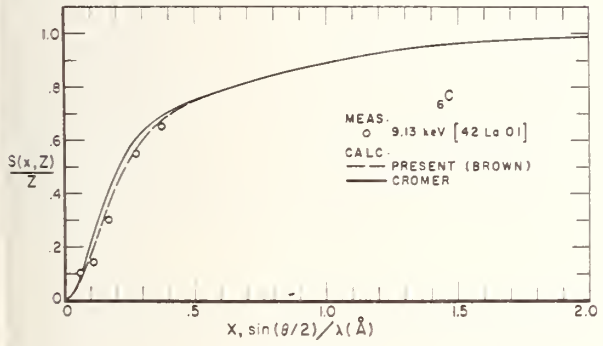

Fig. 27.

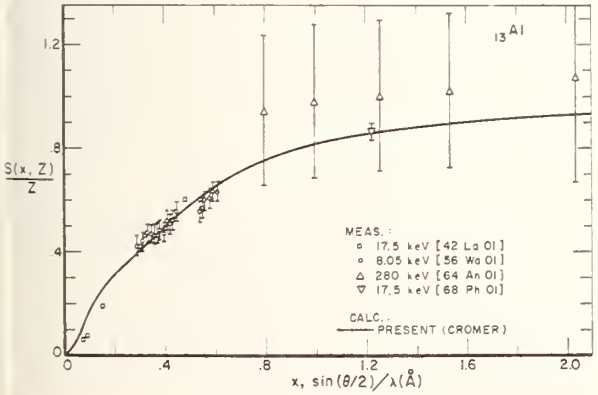

Fig. 28.

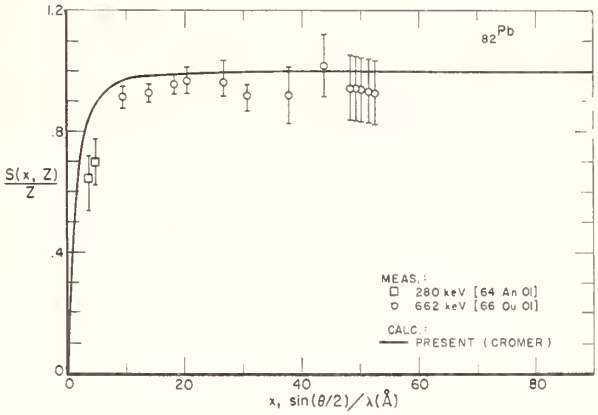

Fig. 29.

Pair Production

Recent total attenuation coefficient measurements by Ahrens et al.[40] suggest that calculated pair production cross sections in present tabulations[4, 6, 7, 15] may be too low by amounts shown in figure 30 of 0.8%, 2% and 4% for the elements copper, tin and lead at photon energies 10 to 11 MeV.

Since no theoretical treatment is yet available for this intermediate energy region, various semi-empirical schemes, as shown in figure 31, have been employed[4, 41, 42], to join the

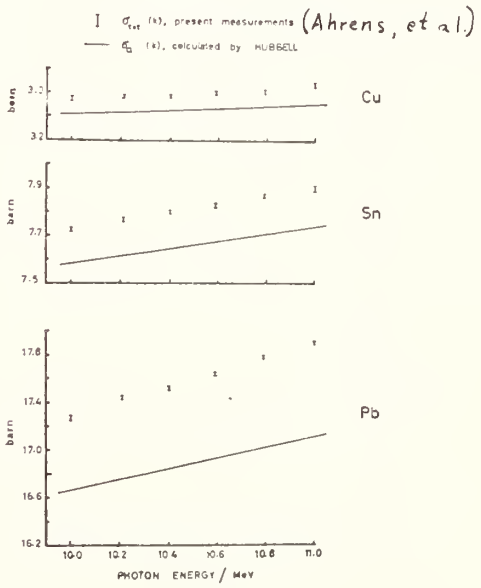

Fig. 30.

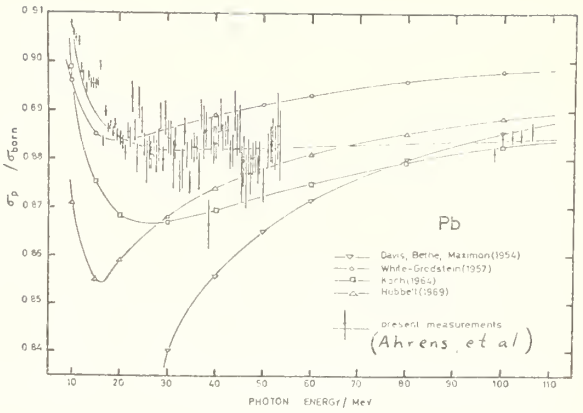

Fig. 31.

threshold-region (1.022 to 5 MeV) results to the high-energy asymptotic region. In these schemes the high-energy Davies-Bethe-Maximon[43] Coulomb correction is usually modified to prevent the cross section from going negative and, within the spread of available data-points, to smoothly join the threshold region. In subsequent tabulations, unless this gap in our theoretical understanding is bridged in the meantime, the empirical correction-function suggested by Ahrens et al. should be used in calculating pair-production cross section values.

Z-Smoothness

Rau and Fano[44] have suggested looking for breaks in Z-smoothness in the various interaction cross sections not only in crossing the rare gases but also in the vicinity of the "noble metals" copper, palladium and gold which mark the completion of the L, M and N d-electron shells.

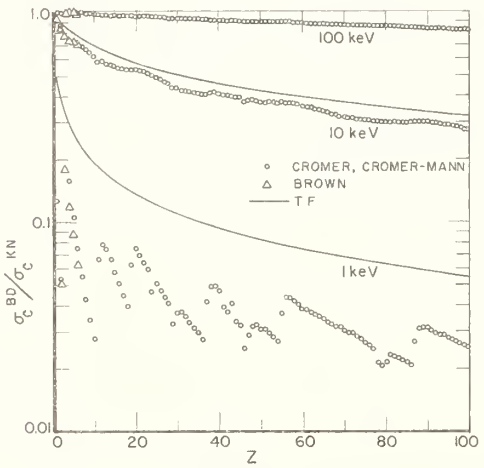

Fig. 32.

In figure 32 the ratios of various bound-electron incoherent (Compton) scattering σ_C^{BD} models to the free-electron Klein-Nishina model σ_C^{KN} are plotted vs. Z. Here we see that although the Thomas-Fermi (TF) statistical model predicts a smooth Z-dependence, the Cromer-Mann[39] Hartree-Fock and Brown[36] configuration-interaction models at 1 keV indeed display breaks where predicted by Rau and Fano[44].

On the other hand the coherent scattering cross section, plotted against Z in figure 33 for several constant energies, is seen to be insensitive not only to Z-discontinuities in atomic structure, but also to the choice of atomic model except for the lowest-Z elements.

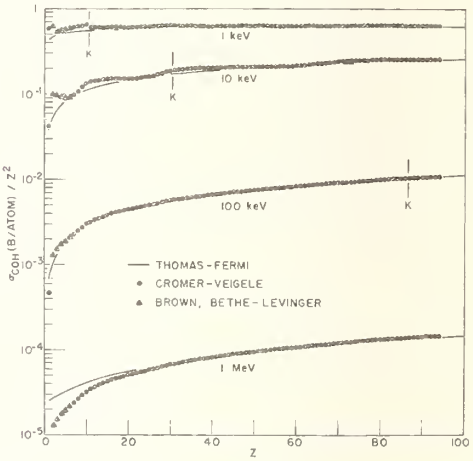

Fig. 33.

With the systematic all-Z photoeffect calculations by Veigele et al.[16] and Scofield[17] now available, it is also possible to look similarly at the photoeffect cross section τ for theoretical predictions of departures from Z-smoothness. In figure 34, based on the Scofield[17] results at 1 keV, the major Z-dependence between absorption edges is removed by dividing the cross section in barns/atom by Z^4, and here various multiples-of-ten factors have been applied to examine these regions side-by side.

Although argon, krypton, palladium and gold fall well-between edge-regions for 1 keV, the pronounced structure seen for incoherent scattering is not present. The Veigele et al.[16] calculated photoeffect results at 1 keV are qualitatively the same as in figure 34. Thus present theory, at least, would suggest that the photoeffect and total

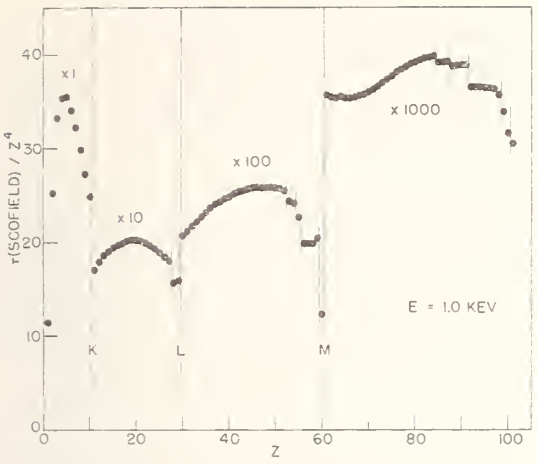

Fig. 34.

attenuation coefficient can be interpolated across Z (except across absorption edges) to 1 or 2%, although for the heavier elements larger errors could result if a gap between measured elements is too large.

Convergence in Time

In figure 35 one final means of examining and evaluating photon cross sections is shown. The attenuation coefficient for the 8.04 - keV copper K_α emission line in various materials has been remeasured over the years, following the 1909 measurements by Barkla and Sadler[45] . In this figure the measured values have been divided by the ENDF/B[7] [McMaster et al.[25,26]] compilation values, represented by the unit-value solid horizontal lines.

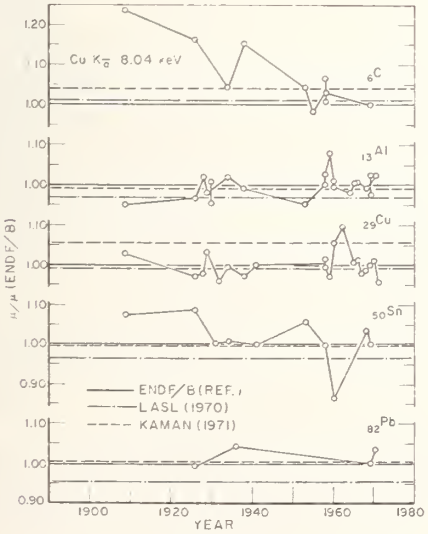

Fig. 35.

In addition to the experimental points and the ENDF/B library arbitrary baseline in figure 35 the dash-dot line represents the LASL [Storm and Israel[6]] theoretical compilation and the dotted line is the Kaman [Veigele et al.[16]] compilation which was fitted to experimental values. Such graphs indicate the rate of convergence (if any) of measurements and theory toward determining "underlying reality" in which the data-points and compilation-lines should coalesce to a single horizontal asymptote for each element as we proceed off to the right.

In figure 35 copper is interesting in that the experimentally-based Kaman compilation appears 5% higher than the bulk of the data points, even though the two high points, Dyer[46] and Ehrenfried and Dodds[47] were not given excessive weight in the fitting. This compilation assumed Z-smoothness, with five iterations fitting alternatively energy and on Z. Hence it is still possible that the "real world" is not as smooth in Z as suggested by the Scofield and Kaman calculated results.

Moving down to tin and lead we see that the LASL[6] values, which are here the Brysk-Zerby[48] theoretical photoeffect, are 3 - 4% lower than the measured values. The Scofield[17] values for uranium, as we have noted, are also a few percent lower than the recent Del Grande and Oliver[29] measurements in this region.

Conclusion

In summary, uncertainties in the available photon cross section information appear to be of the order of 20% or greater below 1 keV, 3 to 10% in the region 1 to 10 keV and 1 to 4% above 10 keV.

References

1. Tagore, R., Collected Poems and Plays, (MacMillan, N.Y., 1936).

2. Röntgen, W.C., Über eine neue Art von Strahlen, Sitzungsber. Würzburger Physik. - Medic. Gesellschaft. (1895).

3. McLaughlin, W.L., Hussmann, E.K., Eisenlohr, H.H., and Chalkley, L., A Chemical Dosimeter for Monitoring Gamma-Radiation Doses of 1-100 krad, Int. J. Appl. Radiat. Isot. 22, 135-140 (1971).

4. Hubbell, J.H., and Berger, M.J., Sections 4.1 and 4.2 in Jaeger, R. G. (Ed.): Engineering Compendium on Radiation Shielding (IAEA, Vienna), Vol. 1, Ch. 4, (Springer, Berlin 1968), pages 167-202. See also Hubbell, J.H., Photon Cross Sections, Attenuation Coefficients, and Energy Absorption Coefficients from 10 keV to 100 GeV, Natl. Stand. Ref. Data Ser. 29 (1969), 80 p.

5. Berger, R.T., The X- or Gamma-Ray Energy Absorption or Transfer Coefficient: Tabulations and Discussion, Rad. Res. 15, 1-29 (1961).

6. Storm, E., and Israel, H.I., Photon Cross Sections from 1 keV to 100 MeV for Elements Z=1 to Z=100, Nucl. Data Tables A7, 565-681 (1970).

7. Wright, J.B., and Roussin, R.W., ENDF (Evaluated Nuclear Data File) photon interaction data tape DLC-7E (Dec. 1974), available from RSIC (Radiation Shielding Information Center, Oak Ridge Nat. Lab.).

8. Fuller, E.G., Gerstenberg, H.M., VanderMolen, H., and Dunn, T.C., Photonuclear Reaction Data, 1973, NBS Spec. Publ. 380 (1973) 131 p.

9. Hubbell, J.H., Survey of Photon-Attenuation-Coefficient Measurements 10 eV to 100 GeV, Atomic Data 3, 241-297 (1971).

10. Henke, B.L., Elgin, R.L., Lent, R.E., and Ledingham, R.B., X-Ray Absorption in the 2-to-200 Å Region, Norelco Reporter 14, 112-131 (1967).

11. Crasemann, B., Koblas, P.E., Wang, T.C., Birdseye, H.E., and Chen, M.H., Measurement of the Photoelectric Cross Section of H_2 at 5.4 and 8.4 keV, Phys. Rev. A 9, 1143-1151 (1974).

12. Cooper, J.W., High-Energy Dependence of the Molecular-Hydrogen Photoionization Cross Section, Phys. Rev. A 9, 2236-2237 (1974).

13. Bentley, J., and Stewart, R.F., Two-Center Calculations for X-Ray Scattering, J. Comput. Phys. 11, 127-145 (1973). See also: Total X-Ray Scattering by H_2, J. Chem. Phys. 62, 875-878 (1975).

14. Hubbell, J.H., Veigele, Wm. J., Briggs, E.A., Brown, R.T., Cromer, D.T., and Howerton, R.J., Atomic Form Factors, Incoherent Scattering Functions, and Photon Scattering Cross Sections, J. Phys. Chem. Ref. Data 4, 471-538 (1975).

15. Biggs, F., and Lighthill, R., Analytical Approximations for X-Ray Cross Sections. II. Sandia Lab. (Albuquerque, N. Mex.) Report SC-RR-71-0507 (1971), 140 p. See also: Biggs, F., and Lighthill, R., Analytical Approximations for Total and Energy Absorption Cross Sections for Photon-Atom Scattering, SC-RR-72-0685 (1972), 131 p.

16. Veigele, Wm. J., Briggs, E., Bates, L., Henry, E.M., and Bracewell, B., X-Ray Cross Section Compilation from 0.1 keV to 1 MeV, Vol. 1 (225 p.) and 2(73 p.), Rev. 1, Kaman Sciences Corp. (Colorado Springs, Colo.) Report KN-71-431(R) (1971). See also: Veigele, Wm. J., Photon Cross Sections from 0.1 keV to 1 MeV for Elements Z=1 to Z=94, Atomic Data 5, 51-111 (1973).

17. Scofield, J.H., Theoretical Photoionization Cross Sections from 1 to 1500 keV, Lawrence Livermore Lab. (Livermore, Calif.) Report UCRL-51326 (1973), 373 p.

18. Goswami (now Sinha), B., and Chaudhuri, N., Measurements of Gamma-Ray Attenuation Coefficients, Phys. Rev. Z 7, 1912-1916 (1973).

19. Mavroyannakis, E., and Antoniades, J., Mesure du Coefficient d'Absorption Gamma par des Materiaux Utilises aux Constructions Nucleaires, Nucl. Res. Ctr. "Democritus" (Athens, Greece) Report DEMO-70/11 (1970) 12 p.

20. Boltaks, B.I., Plachenov, B.T., and Semenov, E.V., The Coefficient of Absorption of Co-60 γ-Rays by Semiconductors, Dokl. Akad. Nauk SSSR 123, 72-75 (1958).

21. Codling, K., Madden, R.P., Hunter, W.R., and Angel, D.W., Transmission of Tin Film in the Far Ultraviolet, J. Opt. Soc. Am. 56, 189-191 (1966).

22. Haensel, R., Kunz, C., Sasaki, T., and Sonntag, B., Absorption Measurements of Copper, Silver, Tin, Gold and Bismuth in the Far Ultraviolet, Appl. Opt. 7, 301-306 (1968). See also Phys. Lett. A 25, 205-206 (1967).

23. Lukirski, A.P., Zimkina, T.M., and Gribovski, S.A., Photoionization of d-Electrons in Te, Sn, Pb, PbTe and SnTe, Fiz. Tver. Tela 8, 1929-1931 (1966).

24. McGuire, E.J., Photo-Ionization Cross Sections of the Elements Helium to Xenon, Phys. Rev. 175, 20-30 (1968).

25. McMaster, W.H., Del Grande, N.K., Mallett, J.H., and Hubbell, J.H., Compilation of X-Ray Cross Sections, Lawrence Livermore Lab. (Livermore, Calif.) Report UCRL-50174, Sec. II, Rev. 1 (1969), 350 p.

26. Hubbell, J.H., McMaster, W.H., Del Grande, N.K., and Mallett, J.H., Sec. 2.1 in Ibers, J.A., and Hamilton, W.C. (eds.): International Tables for X-Ray Crystallography (IUCr), Vol. 4 (Kynoch Press, Birmingham, England 1974), pages 47-70.

27. Biermann, H.H., Die Massenschwächungskoeffizienten monochromatischer Röntgenstrahlen für Cellophan, Al, Se, Ag, Cd, Sn, Sb und Te bis 10 ÅE, Ann. Phys. 26, 740-760 (1936).

28. Zimkina, T.M., Fomichev, V.A., Gribovski, S.A., and Zhukova, I.I., Some Peculiarities in X-Ray Absorption by Lanthanum Group Rare Earth Metals, Fiz. Tver. Tela 9, 1447-1450 (1967). See also: Izv. Akad. Nauk SSSR Ser. Fiz. 31, 874-882 (1967). Also Zimkina, T.M., personal comm.

29. Del Grande, N.K., and Oliver, A.J., Soft X-Ray Cross Section Measurements for Uranium (Abstract), Bull. Am. Phys. Soc. 18, 635 (1973). Also Del Grande, N.K., personal comm.

30. Cukier, M., Dhez, P., Wuilleumier, F., and Jaegle, P., Photoionization Cross Section of Uranium in the Soft X-Ray Region, Phys. Lett. A 48, 307-308 (1974).

31. Henke, B.L., personal comm.

32. Veigele, Wm. J., and Briggs, E., personal comm. Also: Hubbell, J.H., and Veigele, Wm. J., Comparison of Theoretical and Experimental Photoeffect Data 0.1 keV to 1.5 MeV, NBS Tech. Note 901 (1976), 43 p.

33. Pirenne, M.H., The Diffraction of X-Rays and Electrons by Free Molecules, (Cambridge Univ. Press, London 1946), page 9.

34. Stewart, R.F., Davidson, E.R., and Simpson, W.T., Coherent X-Ray Scattering for the Hydrogen Atom in the Hydrogen Molecule, J.Chem.Phys. 42, 3175-3187 (1965).

35. Kolos, W., and Roothaan, C.C.J., Accurate Electronic Wave Functions for the H_2 Molecule, Rev. Mod. Phys. 32, 219-232 (1960).

36. Brown, R.T., Atomic Form Factor for Neutral Carbon, J.Chem.Phys. 55, 353-355 (1971); See also: Phys. Rev. A 1, 1342-1347 (1970) 2, 614-620 (1970); 5, 2141-2144 (1972) and 10, 438-439 (1974).

37. Cromer, D.T., and Mann, J.B., X-Ray Scattering Factors Computed from Numerical Hartree-Fock Wave Functions, Acta Crystallogr. A 24, Part 2, 321-324 (1968).

38. Levinger, J.S., Small Angle Scattering of Gammas by Bound Electrons, Phys. Rev. 87, 656-662 (1952).

39. Cromer, D.T., and Mann, J.B., Compton Scattering Factors for Spherically Symmetric Free Atoms, J. Chem. Phys. 47, 1892-1893 (1967). Also: Cromer, D.T., Compton Scattering Factors for Aspherical Free Atoms, J. Chem. Phys. 50, 4857-4859 (1969).

40. Ahrens, J., Borchert, H., Eppler, H.B., Gimm, H., Gundrum, H., Riehn, P., Ram, G.S., Zieger, A., and Ziegler, B., Photo-Nuclear Cross-Sections and Pair-Production Cross-Sections in the Range of 10-150 MeV, Proc. Electron Accel. Working Group Conf., Giessen, Germany (Sept. 1971), pp. 359-370.

41. Grodstein, G.W., X-Ray Attenuation Coefficients from 10 keV to 100 MeV, Natl. Bur. Stand. Circ. 583 (1957), 54 p.

42. Koch, H.W., Electromagnetic Cross Sections for Electron and Nuclear Research, Nucl. Instrum. Methods 28, 199-204 (1964).

43. Davies, H., Bethe, H.A., and Maximon, L.C., Theory of Bremsstrahlung and Pair Production. II. Integral Cross Section for Pair Production, Phys, Rev. 93, 788-795 (1954).

44. Rau, A.R.P., and Fano, U., Atomic Potential Wells and the Periodic Table, Phys. Rev. 167, 7-10 (1968).

45. Barkla, C.G., and Sadler, C.A., The Absorption of Röntgen Rays, Philos. Mag. 17, 739-760 (1909).

46. Dyer, G.R., The Determination of Low-Energy X-Ray Mass Absorption Coefficients for Copper, M.S. Thesis, Emory Univ. (1962), 80 p.

47. Ehrenfried, C.E., and Dodds, D.E., X-Ray Mass Attenuation Coefficients in the 1.49 to 11.9 keV Range, AFSWC-TN-59-33 (1960), 56 p.

48. Brysk, H., and Zerby, C.D., Photoelectric Cross Sections in the keV Range, Phys, Rev. 171, 292-298 (1968).

Discussion

W.S. Snyder

I refer to the figure showing the early calculated results of Jaeger and Hulme published in 1936. There were only three other calculations shown in the later years. Is it likely that more calculations would improve our knowledge of the photoelectric effect ?

J.H. Hubbell

The Jaeger-Hulme(1936) points were for pair production rather than atomic photoeffect. There are still some

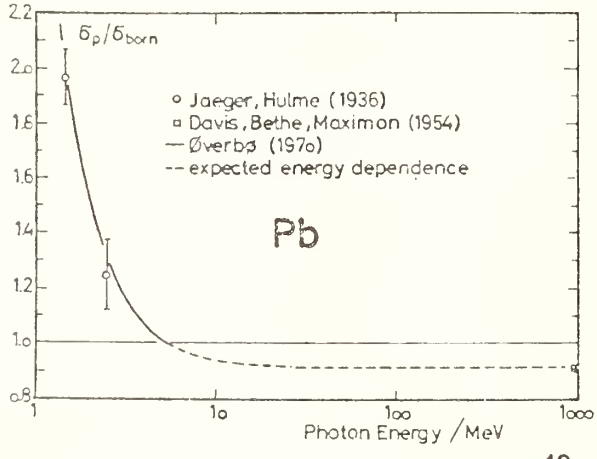

Additional figure from Ahrens et al.[40]

unresolved differences between experiment and present theory in the case of both photoeffect and pair production. Hence in either case further calculations based on improved atomic models would indeed be desirable.

A.M. Ghose

What would you consider to be the most useful areas to which experimental investigation should now be directed ?

J.H. Hubbell

In my opinion, one of the most urgent areas of need is the measurement of whole-atom incoherent scattering differential cross sections, from which one can derive values to check present theoretical incoherent scattering functions. Although the K-shell and some L-shell measurements are very valuable, we need the whole atom data for compilation purposes. Dr. J.W. Motz at N.B.S. plans to make some measurements, but more would also be useful.

SEMIEMPIRICAL FORMULATION OF COHERENT SCATTERING OF GAMMA RAYS

S.C. Roy and A.M. Ghose
Nuclear Physics Laboratory
Bose Institute, Calcutta-700009
India

An empirical formula to estimate Rayleigh scattering cross-section of gamma rays depending on photon energy and momentum transfer involved was first developed by Nath and Ghose by considering the available theoretical and experimental cross-section values. With availability of much accurate cross section values in recent times by using large volume Ge(Li) detectors [M.Schumacher et al, Nucl.Phys. A206, 531 (1973); Nucl.Phys. A213, 306 (1973)] it becomes necessary to recheck the existing formula. We observe reasonable difference in cross-section values in the region where theoretical calculations are not available due to the uncertainties in earlier measurements. In the present paper an analytical formula of coherent scattering cross-sections of photons valid for photon energy below 1.5 MeV and upto momentum transfer 2.0 in units of mc has been developed. The calculated values for different photon energies have been compared with experimental results and is in good agreement within experimental uncertainty.

(Analytical formula; coherent scattering; cross section; gamma rays; photons; Rayleigh scattering.)

Introduction

For photons of energy less than about 1.5 MeV and momentum transfer during collision below about 2.0 mc units [m is the mass of the electron, c the velocity of light] Rayleigh scattering is the most dominant of the processes constituting coherent scattering of gamma rays. Also, Rayleigh scattering, being one of the fundamental modes of interaction of radiation with matter, not only requires careful investigations on its own right but careful estimation of Rayleigh scattering is important in various radiation physics measurements and calculations. Unfortunately, theoretical computation of Rayleigh scattering is a complex problem and it is not practicable to compute the Rayleigh scattering intensity for all photon energy and for all scatterers. Therefore, a simple analytical formula, even if it is obtained semi-empirically, which can reproduce Rayleigh scattering cross section reasonably well is useful to radiation physicists. An attempt was made by Nath and Ghose[1] to develop such a formula on the basis of the then available theoretical and experimental cross section values. Recently more accurate cross section values have been reported[2,3] and it has become necessary to modify the above formula. In the present paper the development of an analytical formula of coherent cross section valid for photon energies below 1.5 MeV and up to momentum transfer 2.0 mc units will be described.

Derivation of the Empirical Formula

The empirical formula was proposed on the basis of the form factor approximation in the low energy limit. If the coherent scattering cross section $\sigma(\theta,Z)$ is expressed in the following form:

$$\sigma(\theta,Z) = \tfrac{1}{2}(1+\cos^2\theta)r_0^2\, Z^n f(q) \quad \ldots (1)$$

where, θ is the angle of scattering
Z is the atomic number of scatterer
$f(q)$ is a function of momentum transfer q
r_0 is the classical electron radius,

then $\sigma(\theta,Z)/\frac{1}{2}(1+\cos^2\theta)$ is a function of q only and has no explicit dependence either on the angle of scattering or on the energy of the photon. Such dependence is implicit through momentum transfer q. Nath and Ghose plotted $\sigma(q,Z) = \sigma(\theta,Z)/\frac{1}{2}(1+\cos^2\theta)$ as a function of q and observed it to be a smooth function of q for energies of the photon below 0.4 MeV, but above 0.4 MeV to be a family of curves falling systematically below one another as energy increases. Nath and

Ghose ascribed this trend to relativistic effects and proposed empirical corrections to make the above expression a smooth function of q for all values of photon energy. This was done by introducing a factor $\varphi(E,q)$ whose values is 1 for $0 < E \leq 0.4$ MeV and $(13.5\ E - 4.4)^{-0.35q}$ for $E > 0.4$ MeV. Using recent experimental value of cross sections measured by Schumacher et al, and by Roy, Nath and Ghose[4] we have now detected an explicit energy dependence of $\sigma(q,Z)$ for photon energies as small as 0.145 MeV for large angles of scattering. The plot of log $\sigma(q,Z)$ against q for different photon energies is shown in Figure 1. In general, it can be said that within the experimental uncertainty coherent scattering cross section is independent of energy for $q < 0.15$ mc.

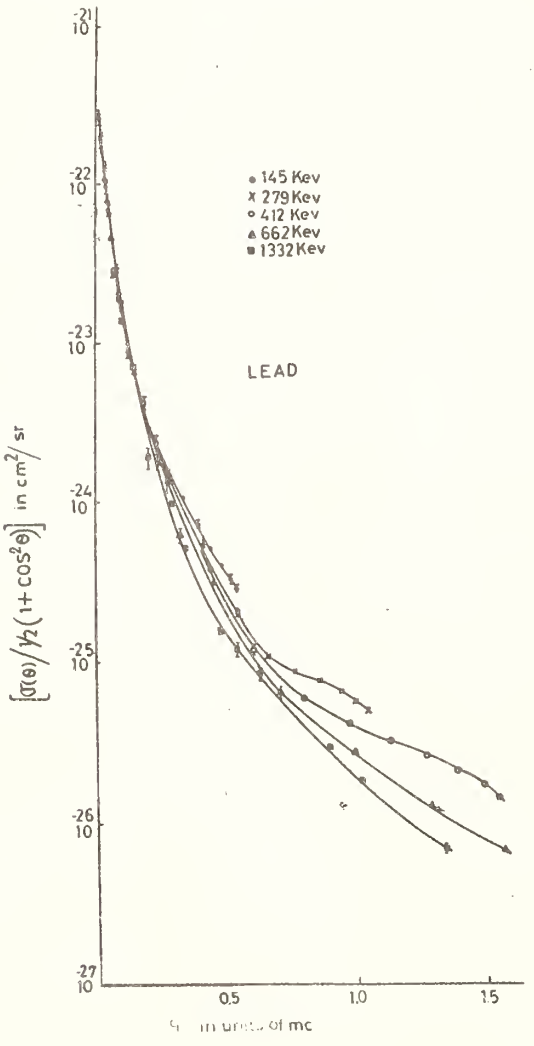

Fig. 1. Experimental $\sigma(q)$ data of lead for different photon energies plotted as a function of q.

In the present paper we shall derive the modified semi-empirical formula for a standard absorber which is taken as lead for obvious reasons and the estimation of cross section values for other elements will be taken up later. The equation (1) for a standard absorber of atomic number Z_o will be

$$\sigma(\theta,Z_o) = \tfrac{1}{2}(1+\cos^2\theta)r_o^2(Z_o)^{n(q)}f(q)$$

By plotting log $\sigma(q,Z_o)$ for standard absorber lead against 1/E for different values of momentum transfer involved we observe that it can be approximated by a straight line with varying slope and intercepts. Therefore the equation (1)

$$\sigma(\theta,Z_o) = \tfrac{1}{2}(1+\cos^2\theta)\ \exp[a(q)+b(q)/E].$$

The curves were fitted by least square fitting and values of 'a' and 'b' were thus derived. As expected 'a' varies very rapidly with q for smaller values of q and varies linearly with q for $q > 0.7$ mc. It has been observed that values of a for $q > 0.7$ mc can be fitted by a polynomial in q. Similarly values of b obtained for different values of q was plotted against q and an expression for the same has been obtained. The expressions for 'a' and 'b' are given below

$$a = 15.3395-44.4843q+127.5617q^2 -197.0323q^3+343.6817q^4$$

$$b = 0.2532q \qquad \text{for } 0 \leq q \leq 0.7 \text{ mc}$$

$$a = 3.9654-3.9848q$$

$$b = 0.0769+0.2731q^{2.5494} \qquad \text{for } q > 0.7 \text{ mc}$$

The general formula for the coherent scattering cross section of any element Z can be written as :

$$\sigma(\theta,Z)=\tfrac{1}{2}(1+\cos^2\theta)(Z/Z_o)^{n(q)}\exp[a+(b/E)]\times10^{-28}\text{cm}^2,$$

where index n(q) obtained by Nath and Ghose is given by

$$n(q)=2.90+0.08q+1.27^2-0.36q^3 \qquad q > 0.1 \text{ mc.}$$

for q below 0.1 mc an additional term $-0.90\ \exp(-500q^2)$ was found necessary.

Discussion

The coherent scattering cross section calculated on the basis of the present formula for lead was compared with the experimentally obtained values in Figure 2. Except for photon energies 1.17 and 1.33 MeV the cross section values for angles greater than 30^o were taken from the measurements

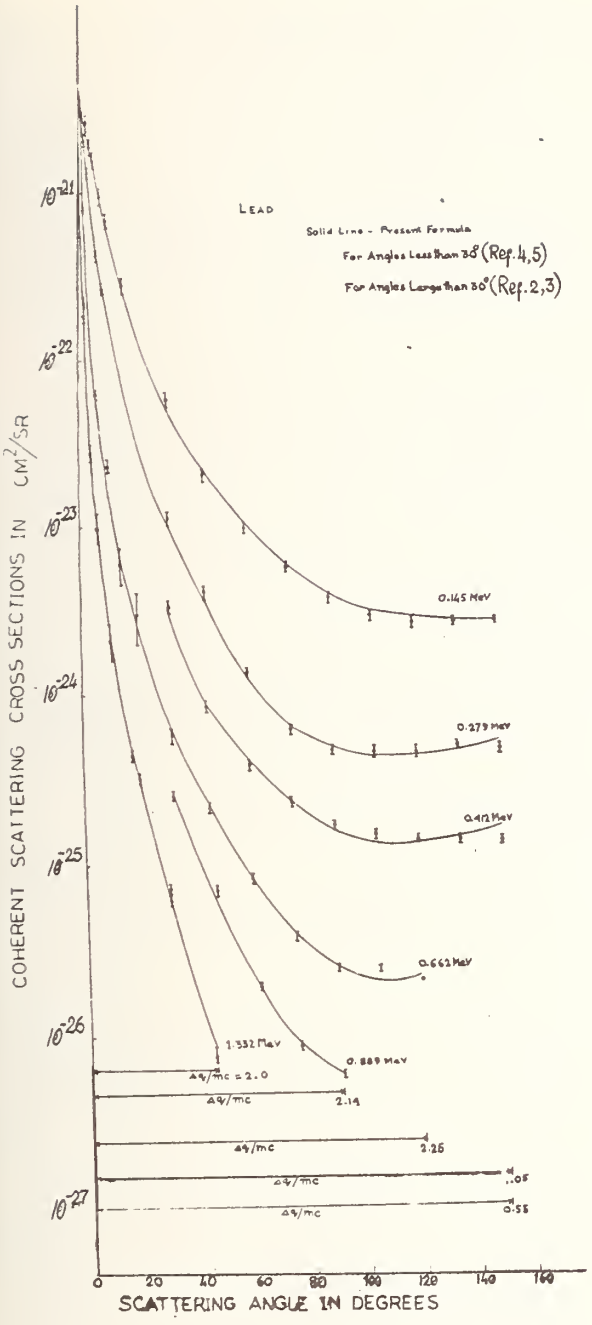

Fig. 2. Comparison of the empirical formula with the experimental data for different photon energies.

made by Schumacher. For angles less than 30°, except for 1.33 MeV, the cross section values are taken from the measurements made by Roy, Nath and Ghose[4] and Nath and Ghose[5]. The cross section values of 1.17 MeV for angles 30° onwards were taken from the measurements of Dixon and Storey[6]. The cross section values for photon energy 1.33 MeV and angles 30° onwards were compared with the measured data of Dixon, Storey and Hardie et al; whereas for angles less than 30° were compared with measured values of Nath and Ghose[5], Roy and Ghose[8] and Standing and Jovanovich[9]. The comparison shows that agreement is quite satisfactory within the experimental uncertainties. Schumacher[10] studied Z-dependence of coherent scattering cross sections in the intermediate to high Z region for a few elements and more accurate measurements covering wider range of elements are necessary to recheck the values of n as obtained by Nath and Ghose. The present formula will be utilised to study electronic charge density distributions of various elements and to recheck the earlier calculations by Roy and Ghose[11] for lead.

Our thanks are due to Prof. S.M. Sircar, Director, Bose Institute for his kind interest in the work.

References

1. Nath, A. and Ghose, A.M., NBS Technical Note 442 (1968).
2. Schumacher, M., Phys. Rev. 182, 7 (1969).
3. Schumacher, M, Smend, F. and Borchert, I., Nucl. Phys. A206, 531 (1973).
4. Roy, S.C., Nath, A. and Ghose, A.M., Nuclr. Instr. and Methods (accepted for publication.
5. Nath, A. and Ghose, A.M., Nucl. Phys. 57, 547 (1964).
6. Dixon, W.R. and Storey, R.S., Can. J. Phys. 46, 1153 (1968).
7. Hardie, G., Merrow, W.J. and Schwandt, D.R., Phys. Rev. C1, 714 (1970).
8. Roy, S.C. and Ghose, A.M., Ph.D. thesis of Roy (C.U. 1971).
9. Standing, K.G. and Jovanovich, J.V., Can. J. Phys. 40, (1962).
10. Smend, F., Schumacher, M. and Borchert, I., Nucl. Phys. A213, 309 (1973).
11. Roy, S.C. and Ghose, A.M., Phys. Rev. 8A, 2298 (1973).

EXPERIMENTAL PHOTOIONIZATION CROSS SECTIONS OF GAMMA RAY PHOTONS FOR LOW, MEDIUM AND HIGH Z ATOMS

B. Sinha (Goswami) and N. Chaudhuri
North Bengal University, Darjeeling
India

Direct measurements of subshell and total photoionization cross sections reported so far are relatively few. Total photoionization cross sections have been determined previously from the measured total photon attenuation cross sections using the available theoretical estimates of incoherent and coherent scattering cross sections and above 1.02 MeV the electron-positron pair production cross section. This method is suitable at an energy region for such atoms for which photo absorption contribution is larger than or at least comparable to other individual contributions to the total photon attenuation coefficient. Theoretical investigations have been continued to improve the accuracy of individual cross sections. J.H. Scofield has calculated screened relativistic photoionization cross sections for all 100 atoms (Z = 1 - 100) in the energy range from 1 keV to 1.5 MeV. Refined incoherent and coherent scattering calculations for all 100 elements over a wide energy range using SCF Hartree-Fock wave functions have been reported recently. Improved pair production cross sections are also available. In view of these accurate theoretical results and inadequacy of experimental information on photoionization in the energy from 10 to 100 keV and above, we have evaluated experimental total photoionization cross sections for low, medium and high Z elements in the range Z = 12 to 92, from the very accurately measured total cross sections using the accurate theoretical estimates of partial cross sections. An analysis of the experimental results has been made and interpreted in a comparison of the theoretical photoionization results recently published. The Z dependence and photon energy dependence of total cross sections have also been studied.

(Coherent scattering, cross sections, gamma ray, incoherent scattering, pair-production, photoionization.)

Introduction

Highly accurate relativistic treatment of the photoionization process in the Hartree-Slater screened potential model has recently been made by Scofield[1] for all atoms with Z from 1 to 101 in the photon energy range from 1 to 1500 keV. In this energy range the only other high-accuracy cross section calculations are those for 14 atoms in the range of Z from 13 to 92 by Schmickley and Pratt[2].

In view of these highly accurate theoretical results, we feel a need for reanalysis of the earlier measurements and to carry out accurate measurements of photoionization cross sections for low, medium and high Z atoms over a wide range of photon energies. The direct measurements of photoabsorption cross sections so far reported are relatively few, because of experimental difficulty in separating the photoelectric process from other processes involved. The other method is to measure the total attenuation of photons, from which photoionization cross sections can be obtained by subtraction of theoretical values for the scattering (coherent and incoherent) cross sections and pair production cross sections for photon energy above 1.02 MeV. This method gives sufficiently accurate results for such photon energies and atoms for which photoionization contribution is larger than or comparable to the scattering and pair production contributions. Further, these cross section values must be very accurately known. Highly accurate theoretical values of coherent scattering cross section and incoherent scattering cross section are now available from the compilations of Veigele et al[3] and of Hubbell et al[4]. These cross section data are based on Hartree-Fock atomic form-factor and incoherent scattering function calculated by Cromer and Mann[5] and Cromer[6]. In the compilation of

Hubbell et al, Bethe-Levinger[7] relativistic K-shell form factor was used for the atomic form factor above a momentum transfer of 0.5 mc. New theoretical results for pair production cross sections in the energy range from 1.02 - 5 MeV have been given by Øverbø[8] . Since the individual photon cross sections are very accurately known theoretically at present, the total attenuation method is well suited in the present energy range where available experimental data are found to be inadequate.

Method

The total attenuation method has been used to obtain photoionization cross sections for 34 elements from our own measurements[9] and the recent measurements of Conner et al[10] . The measurements of total attenuation were made at a level of accuracy of about 1% . All total attenuation data for each element were converted to attenuation cross sections using the recent data of physical constants[11]. Theoretical scattering (coherent and incoherent) and pair production cross sections at our photon energies were derived through interpolation of published cross section data mentioned in the section 1.

The total attenuation data analysed here have been obtained by excluding or minimizing a number of systematic errors which were present in many of the earlier attenuation measurements. The error in the final photoionization cross sections for each element and energy is a combination of errors of (i) the measured attenuation cross sections, (ii) theoretical scattering and pair production cross sections and (iii) interpolation of theoretical cross sections.

The measurement of transmission of photons through a spherical or a cylindrical absorber totally enclosing a point source of photons yields absorption cross sections of photons for absorber atoms. Owing to the circular symmetry of the source-absorber assembly, there is no preferred direction of photon scattering to a suitable photon detector and the transmission measurements by a uniform spectral sensitivity photon counter under the required geometric conditions give total absorption cross sections directly. Ghose[12] developed the sphere transmission method and measured photoelectric cross sections by employing a uniform spectral sensitivity photon counter. We have determined absorption cross section by measuring photon transmission through cylindrical lead absorbers in a procedure the same as that adopted by Ghose[12].

Results and Discussion

Accurate theoretical whole atom cross sections for photoionization process were not available in early sixties and the earlier experimental values of total atomic photo-absorption cross sections were compared with the calculated K-shell cross sections using the available values of total-to-K-shell cross section ratio. We have given in Table 1 the present experimental results and the new whole atom theoretical cross sections only for some atoms representing low, medium and high Z elements. The theoretical results are those obtained from tabulations given by Scofield[1] and Schmickley-Pratt[2]. The cross sections of Scofield are found to agree within about 1% with those of Schmickley - Pratt for the common elements in these two calculations. For a given element these cross sections were plotted against photon energy to obtain a smooth curve. The cross sections were read from these curves at energies for which cross sections were not directly calculated by Scofield[1] and Schmickley-Pratt[2]. It is seen from the table that the new whole atom photoionization cross sections are in fair agreement with the measured data except for the cross section for lead (Z = 82) at 88.1 keV which is almost the same as K-shell threshold energy of this element. By the method of least-squares, the Z^n variation of the experimental cross sections in the range of Z from 12 to 92 has been studied at fixed photon energies. The value of the exponent n has been found to increase from 4.2 to 4.6 in the energy range from 88 keV to 1.33 MeV. An analysis has also been made for the E^{-m} variation at fixed Z in the energy range above K-shell threshold energy of the element. The exponent m is found to decrease slowly from 2.8 to 2.5 in the range of Z between 16 and 30 and again from 2.5 to 2.3 in the range Z = 57 to 82.

The results of our cylindrically symmetric transmission method are in agreement with those obtained in the sphere transmission method by Ghose[12]. This indicates that perhaps there is not much practical distinction between two experimental arrangements.

Table 1

Total photoionization cross sections for some representative elements in the low, medium and high Z ranges. (The final error to the experimental cross section is shown in parentheses).

Photon energy (keV)	Z	Experimental photoionization cross section (barns/atom)	Theoretical values from calculations of Scofield[1], Schmickley and Pratt[2] (barns/atom).
	13	1.06(0.20)	1.21
	26	28.46(0.46)	28.8
	50	423.8 (3.50)	424.0
88.1	74	1783.1 (9.40)	1800.0
	82	2141.9 (9.70)	2500.0
	92	868.9 (5.60)	895.0
	22	2.95(0.10)	2.9
145.4	40	38.35(0.23)	3.7
	57	167.90(0.53)	165.0
	79	584.63(3.90)	580.0
	26	1.88(0.31)	1.8
208.4	50	33.80(0.64)	35.5
	74	174.1 (1.50)	179.0
	92	399.2 (2.00)	407.0
	26	0.66(0.28)	0.82
279	50	14.6 (0.50)	15.4
	74	80.1 (0.80)	80.3
	92	187.8 (1.40)	192.0
	50	4.87(0.50)	5.30
412	74	29.4 (0.70)	29.2
	92	73.4 (0.2)	73.6
	57	2.94(0.53)	2.92
662	64	5.06(0.60)	4.92
	82	a14.8 (0.40)	
		14.40(0.63)	14.9
	92	23.60(0.70)	23.9
	57	0.815(0.35)	0.952
1115.5	64	1.50(0.40)	1.6
	82	5.02(0.50)	4.97
	57	0.67(0.34)	0.87
1173	64	1.51(0.38)	1.50
	82	4.61(0.48)	4.52
1252 (mean value for Co-60 photons)	82	a3.85(0.50)	4.10
	57	0.663(0.32)	0.685
1332	64	1.23(0.36)	1.22
	82	3.54(0.45)	3.56

a - Results by the direct method.

References

1. Scofield, J.H. UCRL-51326(1973).
2. Schmickley, R.D. and Pratt, R.H., Phys. Rev. 164, 104 (1967).
3. Veigele et al., Kaman Sci. Rep., KN-71-431(R) (1971).
4. Hubbell et al., J. Phys. and Chem. Ref. Data 4, 471 (1975).
5. Cromer, D.T. and Mann, J., Chem. Phys. 47, 1892 (1967).
6. Cromer, D.T., J. Chem. Phys. 50, 4857 (1969).
7. Levinger, J.S., Phys. Rev. 87, 656 (1952).
8. Øverbø, I., Thesis Univ. of Trondheim (1970).
9. Goswami, B. and Chaudhuri, J., Phys. Rev. A7, 1912 (1973).
10. Conner, A.L., Atwater, H.F., Plassmann, E.H. and McCrary, J.H., Phys. Rev. A1, 3 (1970).
11. Hubbell, J.H., Nat. Stand. Ref. Data. Ser. NSRDS-NBS 29 (1969).
12. Ghose, A.M., Nucl. Phys. 75, 539(1966), Nucl. Inst. and Methods 35, 45(1965).

INNER BREMSSTRAHLUNG ACCOMPANYING ELECTRON CAPTURE IN ^{7}Be AND ^{51}Cr

H. Sanjeevaiah and B. Sanjeevaiah
Department of Physics, University of Mysore
Manasagangotri, Mysore-570006, India

The inner bremsstrahlung spectra accompanying electron capture in ^{7}Be and ^{51}Cr are studied in coincidence with the 477 and 325 keV gamma rays respectively. The random coincidence counts are subtracted from the true plus random coincidence counts to get the inner bremsstrahlung spectra. The disintegration energies of ^{7}Be and ^{51}Cr leading to the first excited states of ^{7}Li and ^{51}V respectively are determined from the Jauch plots. Using these values the total disintegration energies of ^{7}Be ^{7}Li and ^{51}Cr ^{51}V decay processes are calculated. The total disintegration energies are also measured directly by studying the inner bremsstrahlung spectra emitted in the ground-to-ground transitions. The results obtained by these methods will be presented and discussed.

(Coincidence; electron capture; excited state; gamma ray; ground state; inner bremsstrahlung; Jauch plot; spectrum; transition.)

Introduction

When a nucleus captures an orbital electron there is a small probability that this process is accompanied by the emission of electromagnetic radiation. This effect, known alternatively as radiative capture or inner bremsstrahlung (henceforth denoted as IB) was predicted by Morrison and Schiff[1]. The energy spectrum of the electromagnetic radiation was calculated to be continuous upto some maximum energy, the end-point, and to have a characteristic shape.

Most of the early experiments[2-4] performed to verify Morrison-Schiff theory showed an excess of low energy photons. This was explained in allowed captures by an improvement of the theory presented by Martin and Glauber[5,6] which included relativistic effects and the possibility of radiative capture from both S and P orbital states. However, the predictions of both the theories become nearly equal over a wide range of energy below the end point. Therefore it may be assumed that the shape of the IB spectrum in the higher energy region is essentially given by Morrison-Schiff theory. Then by constructing the Jauch-plot of the IB spectrum one can get the end-point energy. If the K-shell binding energy of the daughter nuclide is added to the IB end-point energy, one gets the disintegration energy of the process. The present experiments are performed to measure the disintegration energies of electron capture processes in ^{7}Be and ^{51}Cr.

Experiment

The IB spectra accompanying electron capture in ^{7}Be and ^{51}Cr to the first excited states in ^{7}Li and ^{51}V are measured in coincidence with the nuclear γ-rays from the de-excitation of these states. Two NaI(Tl) crystals 1"x $1\frac{1}{4}$" and $1\frac{3}{4}$" x 2" in size are used in a face-to-face geometry. The resolving time (2τ) of the coincidence circuit used in the measurement is 40 ns. The bigger crystal detects the IB photons and the signals from it are scanned in a single channel analyser. The smaller crystal detects the nuclear γ-rays and the single channel analyser which receives the signals from this crystal is set on the required photopeak. The IB detection assembly is housed in a lead chamber of 3" wall thickness. A lead plate of thickness 1.7 mm is placed in between the source and the smaller crystal. This is done with a view to reduce the spurious coincidences due to escape X-rays and cosmic rays.

The IB emitted in the ground-to-ground transitions is measured in each case in the energy region beyond the photopeak using the shielded NaI(Tl) crystal and the single channel analyser associated with it. The intensity of the sources used in these measurements are somewhat higher than those of the sources used in the coincidence measurements. The purity of the sources used in the present investigation is checked by recording the single spectrum over two half-lives in each case. No significant

impurity peaks are detected. ^{51}Cr was obtained from Bhabha Atomic Research Centre, Bombay, India in the form of $CrCl_2$ and ^{7}Be was obtained from the Radio Chemical Centre, Amersham, UK in the form of $BeCl_2$.

Results and Discussion

The IB spectrum emitted in coincidence with the nuclear γ-rays is obtained by subtracting the random coincidence counts at each channel from the corresponding true-plus-random coincidence counts. Corrections for Compton continuum, detection efficiency, energy resolution and K X-ray escape are considered following the method of Liden and Starfelt[7]. Correction for energy resolution and K X-ray escape are found to be insignificant in the energy range of present interest. A large contribution to the error comes from counting statistics. Jauch-plots of the corrected spectra are constructed to get the end-point energies. A typical Jauch plot for the IB from electron capture decay of ^{7}Be is shown in Fig. 1.

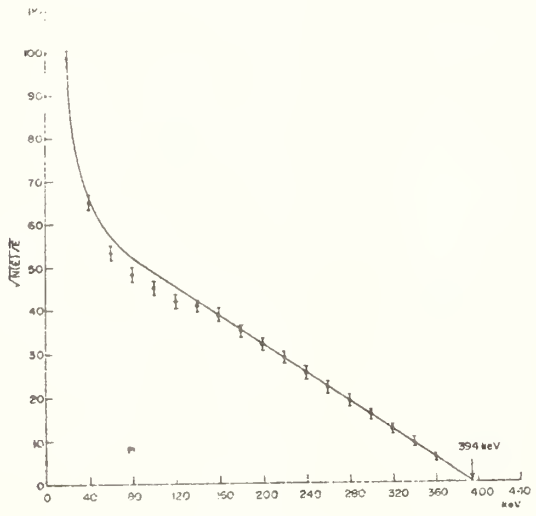

Fig. 1. Jauch plot $\sqrt{N(E)/E}$ in arbitrary units versus E in keV for the IB from electron capture decay of ^{7}Be to the first excited state in ^{7}Li.

The IB spectrum emitted in the ground-to-ground transition is obtained by subtracting the background counts at each channel from the corresponding total counts in each case. After considering the corrections as before the Jauch-plots are constructed. A typical Jauch plot for the IB from ground-to-ground transition $^{7}Be \rightarrow {}^{7}Li$ is shown in Fig. 2. [The results of the present measurements are given in Table 1 along with those of other workers in the field].

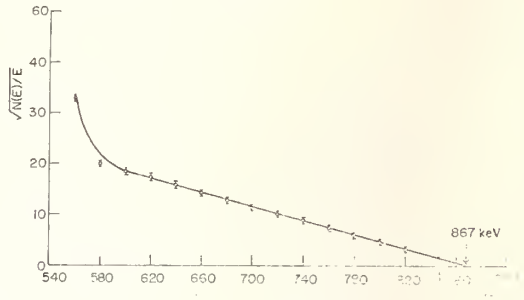

Fig. 2. Jauch plot $\sqrt{N(E)/E}$ in arbitrary units versus E in keV for the IB from ground-to-ground transition $^{7}Be \rightarrow {}^{7}Li$.

The end-point energy of the IB spectrum in ^{7}Be emitted in coincidence with 477 keV nuclear γ-rays is found to be 394 ± 16 keV. This is in good agreement with previously measured values[8,9]. The K-shell binding energy in ^{7}Li is very small. Therefore the disintegration energy of the process may be considered to be 394 ± 16 keV. The end-point energy of the IB emitted in the ground-to-ground transition is found to be 867 ± 10 keV. This agrees fairly well with that computed from the first measurement (394 ± 16 + 477 = 871 ± 16 keV).

Table-1

End-point energies of IB spectra

Transition		End-point energy (keV)	Reference
$^{7}Be \xrightarrow{E.C} {}^{7}Li^{*}$	(First excited state)	395±25 388± 8 394±16	8 9 Present
$^{7}Be \xrightarrow{E.C} {}^{7}Li$	(ground-to ground)	867±10	Present
$^{51}Cr \xrightarrow{E.C} {}^{51}V^{*}$	(First excited state)	424±16 427±14	10 Present
$^{51}Cr \xrightarrow{E.C} {}^{51}V$	(ground-to ground)	725±20 794±60 748±16	11 12 Present

The end-point energy of the IB spectrum in ^{51}Cr emitted in coincidence with 325 keV nuclear γ-rays is found to be 427 ± 14 keV. This is in good agreement with previously measured

value[10]. The disintegration energy corresponding to this transition is 433 ± 14 keV. The end-point energy of the IB emitted in the ground-to-ground transition is found to be 748 ± 16 keV. This is in good agreement with the value computed from the coincidence measurement (427 ± 14 + 325 = 752 ± 14 keV).

The results of the present experiments clearly show that the predictions of Morrison-Schiff and Martin-Glauber theories become nearly indentical with regard to the spectral distribution of the IB photons in the higher energy region. This is indicative of the fact that the major contribution to the IB spectrum in the higher energy region comes from radiative capture from LS orbital state. The deviation of the Jauch-plot from linearity in the low energy region, however, shows the contribution from the P orbital state as well. This is explained by Martin-Glauber theory. In addition, one might observe an interesting deviation in the energy interval 40-140 keV in Fig. 1. This may be attributed to the inadequacy of even the relativistic theory to account for the shape of the IB spectrum from ^{7}Be where it is expected to be quite accurate.

References

1. Morrison, P. and Schiff, L., Phys. Rev. 58, 24 (1940).
2. Saraf, B., Phys. Rev. 94, 642 (1954).
3. Madansky, L. and Rasetti, F., Phys. Rev. 94, 407 (1954).
4. Lindquist, T. and Wu, C.S., Phys. Rev. 100, 145 (1955).
5. Glauber, R.J. and Martin, P.C., Phys. Rev. 104, 158 (1956).
6. Martin, P.C. and Glauber, R.J., Phys. Rev. 109, 1307 (1958).
7. Liden, K. and Starfelt, N., Ark. f. Fys. 7, 427 (1954).
8. Lancman, H. and Lebowitz, J., Phys. Rev. C2, 465 (1971).
9. Borje, I, Persson and Steven, E. Koonin, Phys. Rev. C5, 1443 (1972).
10. Koonin, Steven E. and Persson, Broje I., Phys. Rev. C6, 1713 (1972).
11. Offer, S. and Wiener, R., Phys. Rev. 107, 1639 (1957).
12. Narsimha Murthy, K. and Jnanananda, Swami, Ind. J. Pure&Appl. Phys. 12, 557 (1967).

INELASTIC SCATTERING OF 279-KEV GAMMA RAYS BY BOUND ELECTRONS IN HEAVY ATOMS

D.S.R. Murty, V. Govinda Reddy, E. Narasimhacharyulu, and S.T.P.V.J. Swamy
Department of Physics, Osmania University
Hyderabad, India

The differential cross section for the inelastic scattering of 279-KeV photons by K-shell electrons of thorium was experimentally determined and expressed in terms of free electron scattering cross section at scattering angles of 30°, 50°, 70°, 105°, 125° and 150°. Two scintillation spectrometers and a fast-slow coincidence circuit were used. The differential cross section for the inelastic scattering vanishes as the scattering angle approaches zero and becomes larger than the free electron scattering cross-section at very large angles. The experimental results were compared with those computed on the basis of different theories. Total cross section for the bound electron scattering was also obtained by graphical method.

(Bound electrons; cross section; gamma rays; inelastic scattering; K-shell electron; photon; x-ray.)

Introduction

Among various types of interactions of gamma rays with matter, Compton effect is of considerable importance in the energy region of few hundreds of KeV. To study the effect of electron binding on Compton scattering especially at lower photon energy is of considerable interest and has been studied by several workers [1,2,3,4]. In this present investigation the differential cross section of 279 KeV gamma rays scattered by the K-shell electrons of thorium was measured in the angular range of 30°-150° in terms of free electron scattering cross section. The total cross section was also obtained from the differential cross section by graphical method.

Method

In the present investigation the number of gamma rays scattered inelastically by the K-shell electrons were measured in coincidence with the corresponding fluorescent x-rays. Both the scattered gamma rays, and the x-rays were detected using NaI(Tl) scintillation spectrometer. A fast-slow coincidence circuit with an effective resolution of 30 ns along with 20-channel pulse height analyser was employed. The false coincidence contribution was determined by using an equivalent aluminium foil and subtracted from the total coincidence counting rate. The thickness of the thorium scatterer used throughout observed angular range was 11.59 mg/cm^2. Another observation was made for scattering angle of 125° with a thinner thorium target of thickness 4.89 mg/cm^2. A 0.9Ci radioactive ^{203}Hg source was used as the source of 279 KeV gamma rays.

Results and Discussion

The differential cross section of 279 KeV gamma rays scattered by K-shell electrons of thorium was calculated in terms of free electron scattering. The ratio $d\sigma_K/d\sigma_F$ ($d\sigma_K$ represents differential scattering cross section for K-shell electrons $d\sigma_F$ represents the corresponding cross section considering the electrons as free) was presented in Fig. 1. The errors shown are standard deviations. The observation that the scattering ratio $d\sigma_K/d\sigma_F$ at 125° with two different thicknesses (11.59 and 4.89 mg/cm^2) of scatterers remained unaffected confirmed the findings of Krishna Reddy et al[5] that the effect of scatterer thickness is negligible on the bound electron scattering below 20 mg/cm^2 for photon energy of 662 KeV. The experimental values of $d\sigma_K/d\sigma_F$ increases from 0.264 at θ = 30° to 1.191 at θ = 150°. The increase of the ratio with increasing scattering angle can be easily understood from the fact that higher and higher momentum is transferred to the electrons at those angles and thereby increases the probability for the ejection of bound electrons. The ratio reaches unity beyond θ = 125° with 279 KeV gamma rays whereas the same ratio reaches unity below 70° for the same scatterer with photon energy of 662 KeV as observed by Krishna Reddy[6]. The general trend of the experimental curve as presented in Fig. 1 is that the ratio $d\sigma_K/d\sigma_F$ approaches zero as the scattering angle approaches zero. It may

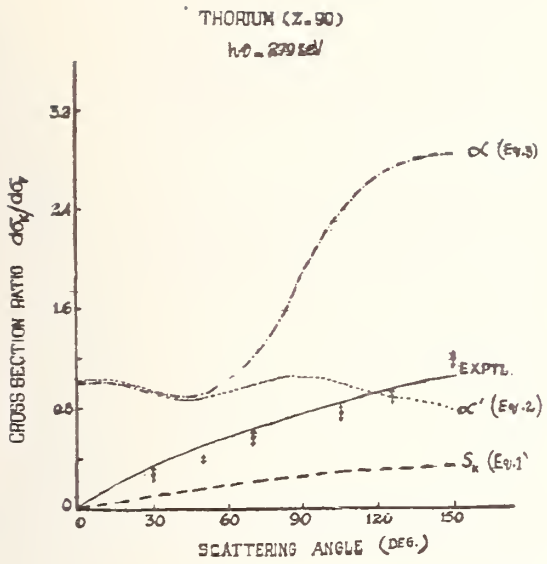

Fig. 1. Comparison of present values of $d\sigma_K/d\sigma_T$ with the values obtained from Eq. (1), Eq. (2) and Eq. (3).

however be pointed out in this connection that the exact relativistic calculation of Whittingham[7] for the incoherent scattering of 662 KeV photons from K-shell electrons of lead gave a non zero value even at zero angle. No relativistic calculations are available for direct comparison with the present experimental results.

The effect of electron binding on Compton scattering was usually taken into account by introducing a scattering function S as a correction to free electron cross section and may be expressed as:

$$\frac{d\sigma_K(k_o,\theta,Z)}{d\Omega} = S_k(k_o,\theta,Z)\,\frac{d\sigma_F}{d\Omega} \quad \ldots(1)$$

k_o is the incident photon energy, θ the angle of scattering, Z the atomic number of the element and S_k is the probability that the K-shell electrons receive a momentum k from the incident photon. Neglecting transitions to excited discrete states Shimizu et al[8] obtained an equation for S_k. The values of S_k obtained on the basis of this calculation was presented in Fig. 1. It is clear from the figure that excepting the general trend of the two curves there is no agreement between the experimental and calculated values.

Jauch and Rohrlich[9] developed the idea that in Compton scattering the initial electron is free but not stationary especially at large scattering angles when the momentum transfer is more than the momentum of the initial electron. Based on this idea they obtained an expression for the scattering of gamma rays by free electrons with non-zero velocity. From this the average cross-section $d\sigma_K/d\Omega$ which is a good approximation is given for any value of by the following expression

$$\left\langle\frac{d\sigma_k}{d\Omega}\right\rangle = \frac{\int_1^{-1}\int_1^{-1}\frac{d\sigma_k}{d\Omega}\,d(\cos\varphi)\,d(\cos\alpha)}{\int_1^{-1}\int_1^{-1}d(\cos\varphi)\,d(\cos\alpha)} \quad \ldots(2)$$

where φ is the angle between the planes formed by K, P and K,K- where K, K- are the three momentum vectors of the photon and P is that of the initial electron, α is the angle between the incident photon and initial electron; $\frac{d\sigma K}{d\Omega}$ is the differential cross section for a given value of φ and α.

The average differential cross-section using the above equation was obtained by computing $d\sigma_K/d\Omega$ for different values of φ and α using IBM 1620 computer and the mean value is determined for each scattering angle. The values thus obtained are shown in Figure 1 and are not in agreement with the experimental results even at large scattering angles. If one ignores the variation in φ and considers the variation in α alone as was pointed out by Motz and Missoni[10] the average cross section can be given

$$\left\langle\frac{d\sigma_K}{d\Omega}\right\rangle = \frac{\int_1^{-1}\frac{d\sigma_K}{d\Omega}\,d(\cos\alpha)}{\int_1^{-1}d(\cos\alpha)} \quad \ldots. (3)$$

The mean scattering cross section values for different scattering angles calculated on the basis of this equation was shown in Figure 1 for comparison with the experimentally obtained values. In this case also the calculated values are not in agreement with the experimental values. However the values obtained by the equation (2) and (3) agree fairly

well for scattering angles upto 50° and diverges violently beyond 50°.

From the above information we may conclude that the experimental results do not agree with any of the existing theories throughout the angular range of observation.

By multiplying the ratios $d\sigma_K/d\sigma_F$ with free electron (Klein-Nishina) cross sections the bound electron scattering cross sections were obtained and these were plotted in figure 2. The curve was extended to 0° on the lower angle side and to 180° on the higher angle side. The free electron cross section was also shown by dotted line in the same figure. The area under the bound electron curve represented the total cross section σ_K due to bound electron scattering while the area countered by the Klein Nishina values represented the total cross section σ_F due to free electron scattering and the ratio σ_K/σ_F came out as about 0.5. Parthasaradhi reported this ratio as 0.81 for lead.

The differential incoherent scattering cross sections have been computed on the basis of Thomas-Fermi bound electron model by Donaldson et al[12] for different elements and energies and the interpolated values pertinent to the present case are shown by dashed curve (Kaman Nuclear) in figure 2. These values pertain to all the bound electrons but not to k-shell electrons alone.

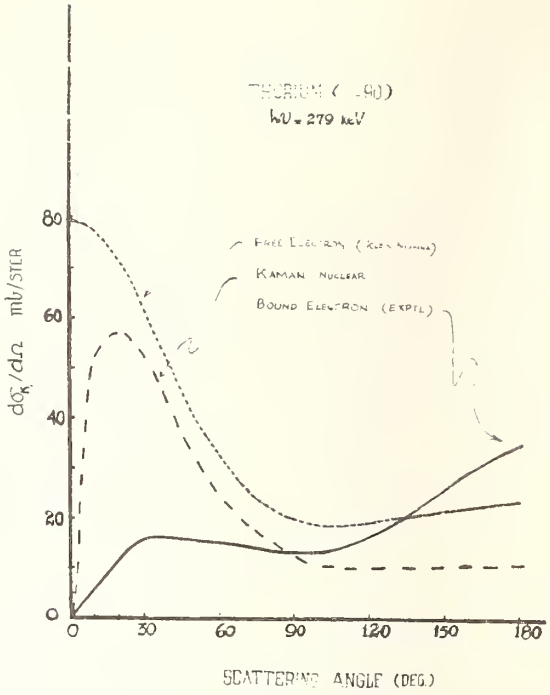

Fig. 2. Comparison of experimental differential incoherent scattering cross sections with calculated values from Klein-Nishina formula and Thomas-Fermi bound electron model.

Acknowledgements

The authors express their grateful thanks to the Department of Atomic Energy for generous financial assistance. The thorium foils were kindly supplied by the Atomic Fuels Division of the Bhabha Atomic Research Centre. Thanks are also due to the Head of the Physics Department for the facilities given.

References

1. Ramalinga Reddy, A., Lakshminarayana, V. and Jnanananda, S., Proc. Phys. Soc. 91, 71 (1967).
2. Pingot, O., Nucl. Phys. A 133, 334 (1969).
3. Pingot, O., Le Journal De Physique 33, 189 (1972).
4. Murty, D.S.R., Govinda Reddy, V. and Narasimhacharyulu, E., J. Phys. A (Gen. Phys.) 6, 265 (1973).
5. Krishna Reddy, D.V., Narasimhacharyulu, E. and Murty, D.S.R., Proc. Ind. Acad. Sci L XX 11, Sec. A, 185 (1971).
6. Krishna Reddy, D.V., Ph.D. Thesis, Osmania University, 1971.
7. Whittingham, I.B., J. Phys. A (Gen. Phys.) 4, 21 (1971).
8. Shimizu, S., Nakayama, Y. and Mukoyama, T., Phys. Rev. 140, A 806 (1965).
9. Jauch, J.M. and Rohrlich, F., The theory of photons and electrons Cambridge, Mass. Addison-Wesley 1955.
10. Motz, J.W. and Missoni, G., Phys. Rev. 124, 1458 (1961).
11. Parthasaradhi, K., J. Phys. A 1, 171 (1968).
12. Donaldson, M.E., Henry, E.M. and Veigele, Wm.J., Ray transport, Vol. 5, Kaman Nuclear, Colorado springs, Colorado, 1965.

GAMMA RAY ATTENUATION COEFFICIENT MEASUREMENTS AT 1115, 1173 AND 1332 KEV

S. Gopal and B. Sanjeevaiah
Department of Physics, University of Mysore
Manasagangotri, Mysore-570006, India

Gamma ray attenuation coefficients in C, Al, Cu, Zr, Sn and Pb were measured for gamma ray energies 1115, 1173 and 1330 keV using the technique employed earlier by the authors for similar measurements at lower energies. The results will be presented here and discussed.

(Attenuation coefficient; counting sequence; cross section; gamma ray; photon.)

Introduction

Studies on the interaction of gamma radiation with matter yield useful information for designing experimental arrangements for handling the isotopes decaying by gamma emission. The most important quantity characterising the penetration and diffusion of gamma radiation in extended media is the attenuation coefficient μ. This quantity depends on the photon energy E and the nature of the medium. Gamma ray attenuation coefficient measurements have been made from time to time using narrow-beam-collimated geometry[1-10]. In these experiments it is tacitly assumed that the energy-degraded photons due to multiple scattering in the sample do not reach the detector and hence the good geometry condition is preserved. But it may be expected that the number of multiple scattered photons reaching the detector would increase as the sample thickness increases. The recent investigations[11,12] indicated that the gamma ray attenuation coefficients would improve if one follows the counting sequence of Conner et al[8] together with the criterion $\mu t < 1$, where μ is the gamma ray attenuation coefficient and t is the thickness of the sample. In this paper we report the gamma ray attenuation coefficients measured in carbon, aluminum, copper, zirconium, tin and lead at gamma ray energies of 1115, 1173 and 1332 keV using the above criterion.

Experimental Method

The experimental set-up and the shape and size of the samples used in the present investigation are the same as those described by the authors earlier[11,12].

The gamma ray sources of 10 mCi ^{65}Zn (1115 keV) and 10 mCi ^{60}Co (1173 keV and 1332 keV) in the form of radiographic capsules (supplied by the Isotope Division, Bhabha Atomic Research Centre, Bombay, India) have been used. The gamma ray lines of 1173 and 1332 keV are resolved by the scintillation spectrometer.

The gamma ray attenuation coefficients are determined by following the counting sequence of Conner et al[8] choosing the sample thicknesses such that $\mu t = 0.2$ to 0.4 for 1115, 1173 and 1332 keV gamma ray energies in carbon, aluminum, copper, zirconium and lead. A sufficient number of counts was recorded so that counting statistics contributed less than 0.3% error. The background counts were taken by placing a 15 cm long lead cylinder of 1.5 cm diameter in the sample position. The errors associated with measured gamma ray attenuation coefficients have been calculated by the method described earlier[11,12].

Results and Discussion

The values of attenuation coefficients measured in this experiment are given in Table 1. Also the attenuation coefficients determined by Conner et al[8], Henry and Kennett[9] and Goswami and Chaudhuri[10] which are common to our measurements are given for comparison.

It can be seen from Table 1 that the present values are in general agreement with the results of Conner et al[8], Henry and Kennett[9] and Goswami and Chaudhuri[10] suggesting that the sample thicknesses used by them satisfy our criterion $\mu t < 1$. Also it can be observed that in some cases our values fill the gaps in the improved gamma ray attenuation coefficient measurements.

Table 1

Comparison of measured total attenuation coefficients (cm^2/m). (In parentheses is given the uncertainty in the last one or two places).

Element	Energy (keV)	Present work	Conner et al[8]	Henry and Kennett[9] (error 1%)	Goswami and Chaudhuri[10]
Carbon	1115	0.06025(26)	0.06043(27)	0.06017	0.0601(1)
	1173	0.05826(24)	-	-	0.0585(1)
	1332	0.05524(24)	-	-	0.0551(1)
Aluminium	1115	0.05842(31)	0.05807(45)	0.05781	0.0583(2)
	1173	0.05655(29)	-	-	0.0567(2)
	1332	0.05347(28)	-	-	0.0531(2)
Copper	1115	0.05586(28)	-	0.05573	-
	1173	0.05434(29)	-	-	-
	1332	0.05096(28)	-	-	-
Zirconium	1115	0.05407(27)	-	-	-
	1173	0.05295(26)	-	-	-
	1332	0.04965(28)	-	-	-
Tin	1115	0.05367(25)	-	-	-
	1173	0.05227(26)	-	-	-
	1332	0.04944(27)	-	-	-
Lead	1115	0.06384(28)	0.06324(32)	0.06413	0.0640(1)
	1173	0.06167(32)	-	-	0.0615(1)
	1332	0.05556(31)	-	-	0.0557(1)

References

1. Davisson, C.M. and Evans, R.D., Phys. Rev. 81, 404 (1951).
2. Colgate, S.A., Phys. Rev. 87, 592 (1952).
3. Wiedenbeck,M., Phys. Rev.126,1009 (1962).
4. Ramana Rao, P.V.,Rama Rao, J. and Lakshminarayana, V., Proc.Phys.Soc. 85, 1081 (1965).
5. Perkin, J.L. and Douglas,A.C., Proc. Phys. Soc. 92, 618 (1967).
6. McCrary, J.H., Plassmann, E.H., Puckett, J.M., Conner, A.L. and Zimmermann, G.W., Phys. Rev. 153, 307 (1967).
7. Carter,R.W., Rohrer, R.H.,Carlton, W.R. and Dyer, G.R., Health Phys. 13, 593 (1967).
8. Conner, A.L., Atwater, H.F.,Plassman, E.H. and McCrary,J.H., Phys. Rev. A1, 539 (1970).
9. Henry, L.C. and Kennett, T.J., Can.J. Phys. 49, 1167 (1971).
10. Goswami, B. and Chaudhuri, N., Phys. Rev. A7, 1912 (1973).
11. Gopal, S. and Sanjeevaiah, B., Nucl. Instr. and Meth. 107,221 (1973).
12. Gopal, S. and Sanjeevaiah, B., Phys. Rev. A8,2814 (1973).

Discussion

A.M.Ghose

I would like to know what special cares have been taken by you to improve the accuracy of your measurements?

S. Gopal

We have adopted the geometry of Davisson and Evans but the distance between the source and the detector is doubled and the diameters of the slits are halved. This makes the maximum angle for scattered photons (θ_{max}) to reach the detector equal to 16^{o} and therefore the contribution of coherently scattered photons on the measured attenuation coefficients is less than 0.05% . Also in our

geometry the sample position becomes insensitive to gamma ray attenuation coefficient measurements. Our investigations[11,12] indicate that the multiple scattered photons reaching the detector can be largely minimized by selecting the sample thicknesses less than $\mu t = 1$ where μ is the attenuation coefficient and t is the thickness of the material and thereby improving the measurements.

D.V.Gopinath

Has it not been recognized much earlier that the foil thickness should be much smaller than a mean-free-path for attenuation coefficient measurements ?

S. Gopal

I do not know why it was not recognized earlier in the measurements of gamma ray attenuation coefficients.

RADIATION PHYSICS AND NUCLEAR TECHNOLOGY

P.K. Iyengar
Bhabha Atomic Research Centre
Trombay, Bombay-400085
India

Understanding of basic interaction processes of radiations with atoms, nuclei and bulk matter contributes a lot towards the advances in nuclear technology. Yet it seems that more accurate and wide ranging measurements are required to make accurate predictions for the design of reactors, accelerators etc. The present article is a birds-eye view of the problems which need solution in new technologies - problems due to radiation effects, study and solution of which can arise from use of accelerators.

(Cross section; energy transfer; gamma rays; moderator; neutron; radiation damage; reactor; scattering; spectrometer).

Introduction

The subject of radiation physics is a very general one. Long before man understood the structure of matter and atoms and started theorizing interaction of radiation with matter, nature has been using it in various ways. For example, plants have been using optical radiation in photosynthesis, meterological phenomena are a result of interaction of radiation with bulk matter.

Confining our attention to nuclear technology, the radiations we are concerned with here are mainly γ-rays, neutrons and charged particles, that too in a small energy region. Parameters which govern their interaction with atoms, nuclei and bulk matter have been measured for several decades now, yet it seems that more accurate and wide ranging measurements are required to make accurate predictions for design of reactors, accelerators, in many of the applications. It is not my intention to cover all these, for there are several papers in this conference dealing with basic theories, experimental measurements and computer codes. I shall restrict myself to a few examples which to my mind have contributed significantly to nuclear technology. This also helps to remind us that research in understanding the basic interactions of radiations with both individual nuclei and collective systems can contribute a lot towards advances in nuclear technology.

Unique Moderating Properties of Zirconium Hydride

An interesting example of how a systematic study of interaction of slow neutrons with matter led to the development of a powerful new moderating material for use in nuclear research reactors, is the discovery of the unique thermalising properties of zirconium hydride. During the late fifties physicists were interested in understanding the effects of chemical binding on the scattering and thermalising properties of various hydrogen bearing compounds. The object of the studies was the difference in behaviour of the hydrogen atom when it is free and when it is bound in various chemical compounds such as water polyethylene, zirconium and other metallic hydrides. The emergence of powerful research reactors having high neutron fluxes and the concurrent development of sensitive new experimental techniques enabled the observation of phonons - by the inelastic energy transfers between incident neutrons and crystal lattices.

The tetrahedral structure of zirconium hydride wherein the hydrogen atom sits at the centre of a tetrahedron of zirconium atoms, performing nearly harmonic oscillations bestows this material with very interesting neutron scattering properties. The tightly bound proton is found to have quantized optical vibration levels spaced at equal intervals of ~ 0.14 eV. Although Fermi had predicted as early as 1936, while discussing neutron slowing down by hydrogenous moderators, that the bound proton would act as a simple harmonic oscillator bound to an infinitely heavy atom and have energy levels of $nh\omega$, the first experimental evidence of such a system was obtained only in 1957 in simple total transmission experiments with zirconium hydride[1]. Fig. 1 shows the total neutron cross section of the hydrogen in zirconium hydride obtained with a crystal spectrometer. The arrows indicate the excitation levels for

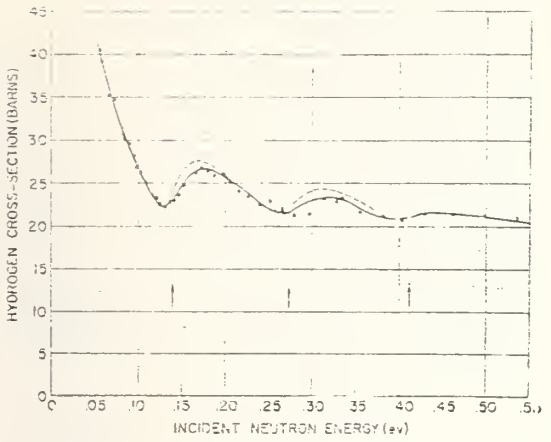

Fig. 1. Total neutron cross section of hydrogen in Zr H_2 as a function of neutron energy.

hydrogen vibration in zirconium lattice. Fig. 2 shows the energy distribution of neutrons scattered from zirconium hydride as measured[2] at 296°K. The peak at ~ 0.14eV corresponding to the first optical vibrational level is clearly visible. (Below .02 eV there is some indication of the acoustic modes and at .28 eV a double phonon scattering peak is just visible). Since these levels would be excited or de-excited by collisions with neutrons, energy transfers between slow neutrons and zirconium hydride can occur only in multiples of $h\nu \sim 0.14$eV, which is very large compared to kT (~C.25 eV), the thermal energy of the moderator.

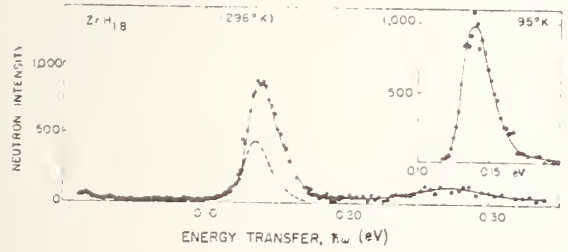

Fig. 2. Energy distribution of scattered neutrons from Zr H_2 at 296°K.

Because of the above characteristics low temperature zirconium hydride moderator exhibits an unusual neutron spectrum, significantly different from a Maxwellian distribution. During the slowing down process once the neutron energy becomes less than 0.14 eV it cannot transfer any more energy to the lattice. However collisions down to about 1 eV is as if it were with free hydrogen; hence the slowing down source into the 0-0.14 eV region is uniform (independent of energy) and is unaffected by molecular binding effects or moderator temperature. When the zirconium hydride moderator is heated, neutrons pick up energy from the vibrating protons in quanta of 0.14 eV; as at higher moderator temperatures, more number of vibrating protons are found in an excited state. The fraction of neutrons speeded up to the region $h\nu$ to $2\ h\nu$ is therefore proportional to $e^{-h\nu/kT}$.

This phenomenon has been very effectively exploited in the design of a research reactor possessing a strong prompt negative temperature coefficient of reactivity. The TRIGA research reactor as it is called, uses enriched uranium mixed intimately with zirconium hydride and fabricated into fuel rods. When this solid homogeneous fuel moderator rod gets heated following an accidental power excursion the average energy of the neutron spectrum quickly increases resulting in significant loss of reactivity, "instantly" shutting down the reactor. The prompt temperature coefficient of such reactor has been shown to be given by

$$\frac{dk}{dT} = a\frac{d}{dT}\, e^{-h\nu/kT}$$

$$= \frac{a}{T_o}\left(\frac{T_o}{T}\right)^2 e^{-T_o/T}$$

where $T_o = h\ /k \sim 1500^oK$

and $T \sim 300^oK$

a is a constant measuring the relative loss of importance of the speeded up neutron. The TRIGA class of reactors are very safe and have been operated successfully as Pulsed reactors producing strong pulses of thermal neutrons.

Slowing Down Time Lead Spectrometer

The Slowing Down Time (SDT) Lead Spectrometer[3] represents another example wherein certain special features of neutron interaction with matter have been exploited. Unlike zirconium hydride which is an efficient moderator by virtue of the presence of hydrogen, lead has a high mass number of 207 because of which the neutron loses on an average only 1% of its energy per collision. This, coupled with the fact that scattering cross section of lead is independent of energy, leads to a type of focussing with time during the slowing down of monoenergetic neutrons injected into a large lead assembly.

Neutrons undergoing elastic collisions thus gather into a comparatively narrow velocity group which as a whole gradually shifts towards lower velocities with increasing slowing down time. Fig. 3 depicts this behaviour schematically. By injecting short bursts of fast neutrons periodically into a large block of lead and by looking at events for a short interval of time Δt, delayed by time t with respect to the **initial** burst, approximately monoenergetic neutrons could be selected. The basic equations governing SDT spectrometer are given below:

$$t = M \lambda_s \left(\frac{1}{v} - \frac{1}{v_o}\right) \quad \ldots (1)$$

where t : time after neutron pulse
M : Mass Number
λ_s: scattering mean free path
v_o, v : neutron velocities at to, t

$$q_o(t) = \frac{Q}{abc} e^{-B_g^2 \tau} e^{-t/l} \quad \ldots (2)$$

q_o : Slowing down density at centre
Q : source intensity
abc : dimensions of the block
B_g^2 : geometrical buckling
τ : neutron age
l : neutron lifetime

Dispersion D is given by

$$D = \frac{2}{3M} + \frac{kT}{4E} \quad \ldots (3)$$

Equation 1 in this figure defines the relationship between the slowing down time t and the energy of neutrons corresponding to this time. Equation 2 give the slowing down density of neutrons at time t.

The velocity distribution of neutrons at any instant during slowing down is found to be a gaussian with a dispersion given by equation 3, where E is the neutron energy corresponding to time t.

The second term represents the additional spectral broadening caused by the thermal motion of the lead nuclei.

These characteristics enable a large block of lead together with a pulsed neutron source to be used as a neutron spectrometer having several useful applications. The main advantage of the slowing down time (SDT) lead spectrometer is the large gain in intensity by 3-4 orders of magnitude compared to conventional time-of-flight methods. It has been used in a wide energy range from 0.1eV to ~1 keV for the measurement of **cap**ture cross sections of a variety of nuclei.

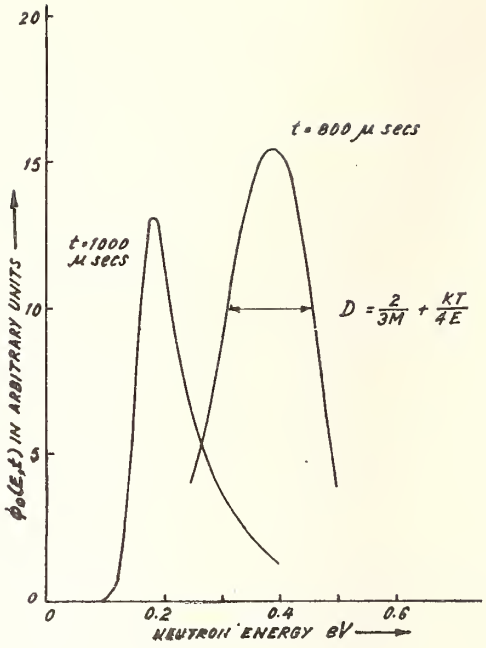

Fig.3. Slowing down spectrum in lead as a function of energy for various slowing down times.

Fig. 4 gives the capture cross-section of ^{108}Ag measured as a function of neutron energy, using an SDT spectrometer. A second application is for the determination of resonance parameters[4]. By measuring the capture gamma rays and using an area method of analysis, the resonance parameters of ^{108}Ag, ^{198}Au, ^{131}Ta, ^{165}Hg etc., have been obtained.

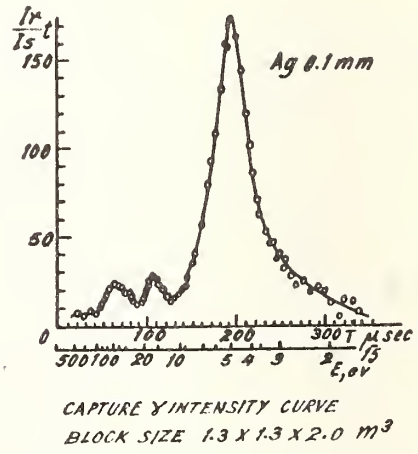

Fig.4. Variation of neutron capture cross section of Ag^{108} as a function of neutron energy.

An important application of the SDT spectrometer is in the non-destructive assay of Pu^{239} in irradiated fuel rods. In the energy region below 1 eV fission cross section of ^{235}U and ^{239}Pu are similar except at 0.3 eV where ^{239}Pu has a large resonance. This difference has been exploited to determine the ^{239}Pu content of irradiated fuel elements by measuring the fission yield as a function of neutron energy in the energy range 0.1 eV - 1 eV. Fig. 5 shows different behaviour of ^{239}Pu and ^{235}U samples obtained during a calibration experiment carried out at Trombay.

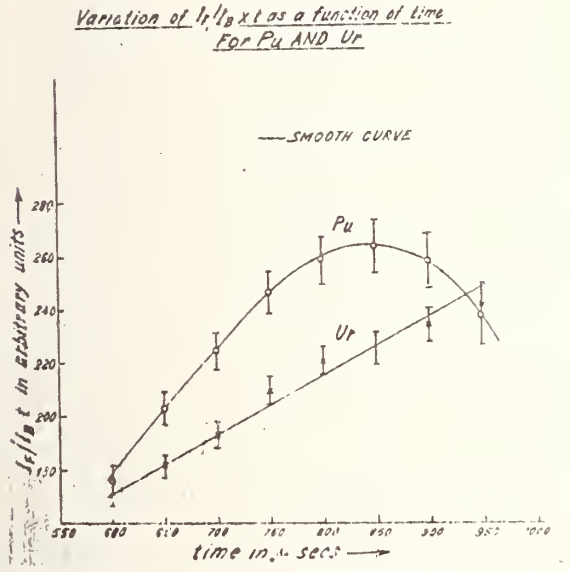

Fig.5. Variation of fission yield in U^{235} and Pu^{239} as a function of neutron energy.

Radiation Effects in Nuclear Technology

In the next few minutes, I would now like to deal with the effects of radiation bombardment on the physical and mechanical properties of materials. In the field of nuclear technology, one is concerned with these effects since they turn out to be major problems in the design and development of nuclear reactor systems. The nuclear reactor, as everyone knows, is a high intensity source of fast neutrons, heavy high energy fission fragments, charged particles and gamma rays. The energy contained in these various radiations gets deposited in various components of the reactor system like the fuel cladding and structural materials and ultimately we are interested in extracting this energy content in one form or another to produce electrical energy. Here I am not concerned about the extraction of energy but about the radiation effects that take place (in the process of energy deposition in the components and consequent behaviour of the components) over long periods of time (of the order of a few years).

On the microscopic scale, it is well-known that an energetic radiation bombarding a solid can impart sufficient kinetic energy to a lattice atom, resulting in the lattice atom being displaced from its normal position. This was suggested by Wigner about thirty years ago. Since then a large number of physicists have been studying phenomenon of radiation bombardment of solids. In particular the study of formation, combination and annealing of point defects in solids has been pursued in a number of laboratories. This forms a part of defect solid state studies. For example, materials like copper have been irradiated in nuclear reactors at very low temperatures of the order of 4°K and the resistivity of the samples has been measured, after bombardment, as a function of temperature. The recovery spectrum was studied to understand the kinetics of recovery and thereby the underlying atomic mechanisms. This kind of work is being pursued even after two decades; the recovery spectrum is rather complex particularly in alloys and there is a wealth of information to be unravelled. Similarly interest in optical properties of defects and other studies are well known. These studies are essentially of basic interest to understand the defect solid state and can be pursued only when the defect concentration is sufficiently low. When the defect concentration increases, although the radiation effects increase in their magnitude and importance theoretical understanding become difficult due to the complexity involved in taking account of the mutual interactions between various kinds of defects in the high concentration limit. On the otherhand, during the lifetime of a reactor, various components of the reactor get exposed to such large doses of radiation that they come to contain a large concentration of defects within a few years and consequently radiation effects begin changing certain physical properties that they become technologically important. It is in this region that physicists have begun taking interest in the last few years and my purpose in the rest of the talk is to high light this aspect of defect solid state. I shall review briefly the nature of radiation effects and how these studies are conducted.

Radiation Damage

(a) Fast Neutron Bombardment

To begin with let us consider the effect of fast neutron bombardment of a solid, in Fig. 6. Here the neutron of energy let us say 0.1 MeV enters the solid on the left side and collides with an atom of the lattice. The atom is knocked out of its 'official' position and moves in some direction. The neutron follows a different path. The atom knocked out by the neutron is called the Primary Knock-on Atom (PKA). The kinetics of the collision like the mass of the atom, angle of scattering determine the energy of the PKA. It can, in its turn, have elastic and 'inelastic' collisions with other atoms in the lattice. There can be excitation or ionisation of atoms in addition to other atoms in the lattice being knocked out of their sites. Hence the PKA produces secondaries in its path and secondaries tertiaries in their turn and so on. The net result is a cascade of collisions and atoms displaced from their lattice sites. This process goes on till the energy transfer in a collision falls below say 25 eV. This is the order of energy required to displace atoms from their sites. Below 25 eV, atoms cannot be removed from their sites but this energy gets transferred to a large number of atoms in the form of thermal energy - kind of 'hot-spot' in the material. In the literature these regions are known as 'thermal spikes', locally in such regions, the effective temperatures can exceed the melting point of the solid for short times and recrystallisation can take place. So, therefore a single PKA can create a lot of havoc as it ploughs through the lattice. Sites from where atoms are removed can lie vacant-vacancies - and dislodged atoms can come to rest at irregular points in the lattice - interstitials. Such PKA cascades occur in large numbers in a fast neutron bombardment till the neutron loses all its energy and comes to thermal equilibrium with the solid. Unless the neutron escapes from the lattice, it is absorbed by one of the atoms of the lattice resulting in formation of an 'impurity' atom. The net result of all this is that the order present in the lattice changes to disorder and the solid is said to be damaged due to radiation. What we have discussed so far applies to all materials be they elemental metals or alloys. In the case of fissile materials, in addition to 'radiation damage' as discussed above, we have the process of fission taking place, a source of fission fragments, γ-rays, more neutrons etc. The fission fragments carry enormous energies resulting in large scale localised damage. Secondly the fission fragments decay ending up in gaseous products like Kryton and Xenon. Another effect common to fissile and non-fissile materials is the formation of hydrogen and helium due to (n,p) and (n,α) reactions in the material.

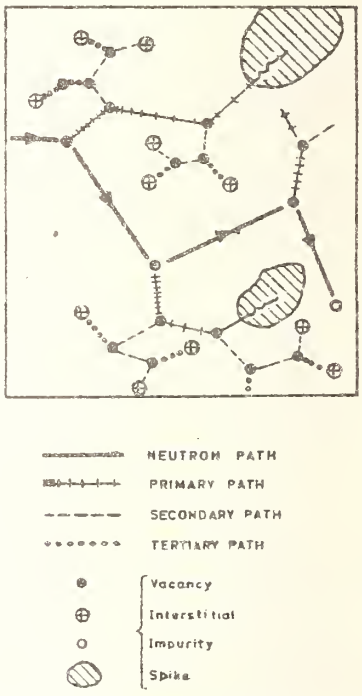

Fig.6. Typical damage pattern in fast neutron irradiation.

(b) Charged Particle Bombardment

In the case of a charged particle bombardment, shown schematically in Fig. 7, the nature of radiation damage is qualitatively and quantitatively different from that in neutron bombardment. In addition to phenomena like back-scattering sputtering etc., the essential characteristic is that the damage is rather dense and is confined to a thin surface layer because of the coulombic nature of the interaction. One does find however displaced atoms at larger distances because of focussed collisions. Impinging atoms can penetrate deeper if they are 'channelled'.

Certain components in nuclear reactors, controlled thermonuclear fusion reactors and space-vehicles are exposed to a high flux of radiations - neutrons, γ-rays, fission fragments and charged particles. Several radiation effects occur as a result of the materials being in this hostile environment.

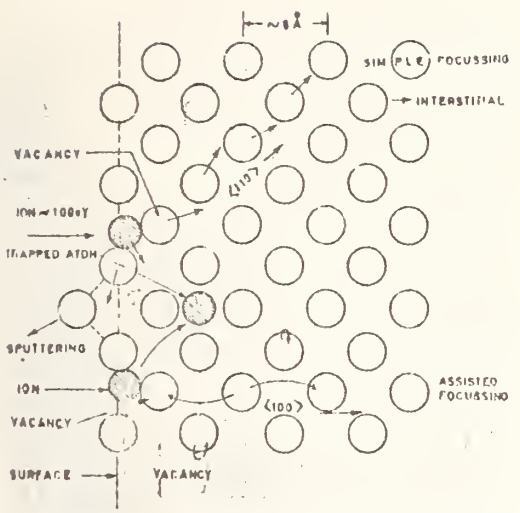

Fig.7. Typical damage pattern in charged particle irradiation.

Radiation Effects (Mechanical)

A few radiation effects particularly those that affect the mechanical properties of materials are: a) radiation growth in fissile materials like uranium, for example, at room temperature, when 1% atoms have undergone fission in monocrystal, the specimen increases in length by 400% .

(b) a similar effect on a reduced scale occurs in anisotropic, non-fissionable materials also when they are bombarded by fission products.

(c) radiation hardening - increases of the flow stress or yield stress of a crystal normally at low temperatures.

(d) change in the ductile-brittle transition temperature - I shall refer to this in greater detail in a few minutes.

(e) swelling due to gases - accumulation of fission products like Kr or Xe can, for example, cause swelling of the fuel when these gases are formed in sufficiently large concentrations. This phenomenon in uranium is known to result in 'frothing' of uranium.

(f) radiation creep - neutron irradiation produces a weaker material when the material is under load.

(g) swelling due to 'void' formation:

Recently Cawthorne and Fulton[8] of Harwell observed that certain fast reactor structural materials like stainless steel irradiated by neutrons exhibited nearly 6% increases in volume due to 'voids'. Void-swelling is believed to arise from nucleation and growth of three dimensional vacancy agglomerates, possibly originating and stabilised in the beginning by a few gas atoms particularly that of He. Void formation is an important radiation effect usually in the temperature range of 0.3 T_m to 0.5 T_m.

(h) loss of ductility at high temperatures above 0.5 T_m due to formation of gas bubbles when voids anneal out.

(i) blistering formation on surfaces due to gases inside materials.

Technological Consequences

I shall now pick up a few of the effects mentioned above and illustrate how these effects play an important role in the economy and technology of reactor systems.

(a) Change in NDT

I have already referred to the effect resulting in the change in ductile to brittle transition temperatures. The pressure vessels used to contain reactors are made of some kind of steel let us say. Steel as we all know is ductile above a certain temperature but brittle below this temperature. This characteristic temperature at which the materials goes over from ductile to brittle condition is referred to as NDT in literature (Nil-Ductility Transition). The important point to note is that a small flow like a hair-line crack can propagate at great velocities below the NDT. Above the NDT this does not happen. A very large number of cases in shipping are known wherein huge ships have just broken apart as a result of their temperature coming down below NDT in cold waters. Hence to remedy the situation the NDT must be as low as possible (much below normal operating temperatures) which can be achieved by suitable change in carbon content of steel or by alloying the steel with various elements. The pressure - vessels used in reactors also should therefore be made of such materials that its NDT must be below the operating temperature.

More than a decade earlier it was observed that due to radiation damage the NDT was found to shift to higher temperatures as a function of dosage. Fig. 8 shows this behaviour qualitatively. In other words, a pressure vessel designed properly out of a material having a low NDT was no longer suitable after operation of the reactor for a few years since its NDT could move into the

operating temperature range of the reactor or can even move up beyond this range. Technologically, therefore, a new situation arose wherein there can be a catastrophic failure of the pressure vessel itself. Several nuclear and non-nuclear solutions to this problem have been proposed from time to time. Suffice to say that a new element, namely change in NDT, has to be taken into account in the design and fabrication of reactor pressure vessels.

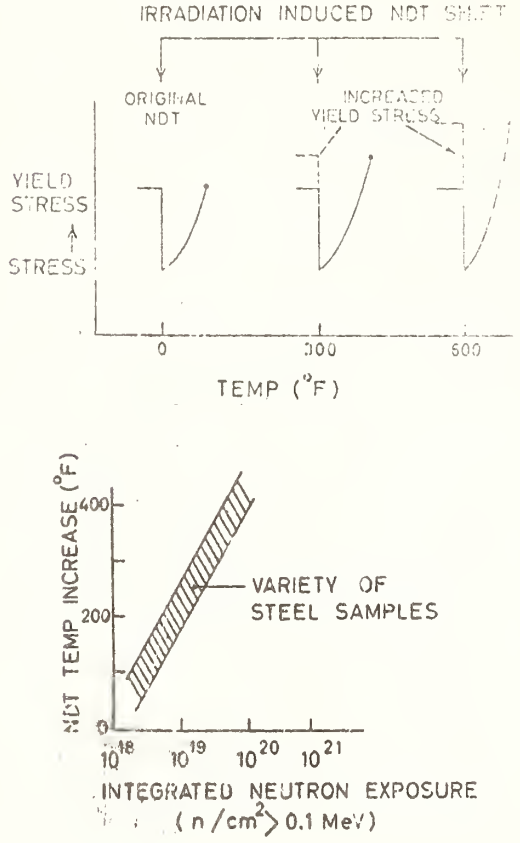

Fig.8. Qualitative features of change in NDT as a function of irradiation dose.

(b) Void Swelling

The fast breeder reactors which are currently under design are expected to provide fluences of order 10^{23} to 10^{24} to various reactor components like fuel cladding etc. during the life of the fuel. The void swelling in such cases could be 10% or more. Such swelling is expected to result in two important effects. It will decrease the breeding ratio (atoms of fissionable material generated per atom of fissionable material consumed) because additional free space must be provided in the core to accommodate the swelling. (Secondly other problems can arise from fuel pin buckling, core warping etc. due to non uniform temperature and flux distributions and consequent non-uniform void density distribution). Hence in fast reactor technology, void swelling has come to be looked upon as a greater bane compared to other problems such as low temperature hardening, high temperature embrittlement and the acceleration of diffusion controlled processes known earlier. Material assessment has become important. However in order to obtain this data through fast neutron irradiation one has to go through tedious and time consuming irradiations over ten or twenty years in fast neutron environment if one were to use the materials for such periods of time in the reactor. This is clearly an unsatisfactory situation. It is here a new breakthrough has been achieved by charged particle irradiation using accelerators. Charged particles, though limited in their range, interact through atomic interactions which have cross sections four to six orders of magnitude larger than the nuclear cross-sections of the neutron. The damage rate is several orders greater than the neutron damage rate. So in principle the damage density produced during many years irradiation within a reactor can be 'simulated' in a few hours using ion beams. Experimental studies involve irradiation of materials by light or medium heavy charged, particles like C, Al, Ni etc. accelerated to energies of order of a few tens of MeV. These irradiated materials are then examined using transmission electron microscopes and parameters like void density and void diameter are measured. It is observed that when specimens are irradiated for comparable damage doses as with fast neutrons, the micrographs reveal almost similar void patterns.

Fig. 9 shows comparison of 316 stainless steel which has been irradiated by neutrons and charged particles[9]. The figure on left corresponds to irradiation by fast neutrons (> 0.1 MeV) at EBR-II to a fluence of 3×10^{22} n/cm^2 for a duration of one year and that on the right hand side, the same material bombarded by 5 MeV nickel ions to a fluence of 3×10^{16} ions/cm^2 over a duration of 30 minutes. You can see the similarity in voidage. In this context I wish to point out that the Variable Energy Cyclotron that is being constructed by Bhabha Atomic Research Centre at Calcutta could prove to be a very powerful instrument for such studies. Physicists who are conversant with acceleration techniques and solid state physics can play a very important role in this effort of materials assessment

for fast reactors. Physics of void formation, void morphology, inter comparison of accelerator samples and reactor samples (to take into account accelerated damage rate in case of simulation experiments) are areas wherein physicists can contribute to our understanding.

(A)
Neutron irradiated at 585°C (1 year exposure)

(B)
Ni ion irradiated at 585°C (30 minutes exposure)

Fig.9. Voids in 316 stainless steel due to neutron and Ni bombardment.

(c) Blistering

Tremendous efforts are underway all over the world to make the controlled thermonuclear fusion a reality for meeting power needs of the future. One of the problems in this area has been containment of the plasma in a vessel for sufficiently long time. The vacuum wall of the chamber containing the plasma is expected to operate at temperatures of order of 700° to 1000°C and is exposed to bombardment of neutral atoms, neutrons, photons and charged particles. As a result of bombardment by these it is expected that the wall can undergo large scale erosion.

Typical parameters[7] of a chamber are given in Table-I and assuming very small sputtering coefficients of the order of less than 1% even, it is seen that the life time of such vessels could be very small indeed. In addition to this recently a new problem is expected to play a major role. The plasma is expected to contain H^+, He^+, T^+ etc. and these can bombard the wall. If radiation damage is caused by gaseous projectiles such as these, the impurity concentration due to these atoms builds up in the material as a function of dose. Secondly such products can accumulate due to (n,p) and (n,d) reactions also. Due to low solubility of the gases in the metal, the gaseous atoms can precipitate out of the metallic solution and create 'bubbles' in the interior or 'blisters' on the surface. Depending on the size of the blisters and metallic strength, the blisters can get ruptured and skin defoliation can take place. Fig. 10 shows the kind of blisters observed by Das and Kaminsky[10] is vanadium as a result of charged particle bombardment. Low energy accelerators (2-3 MeV) can be used for irradiating materials with protons, particles etc. and one can examine the surface using scanning electron microscopes. This figure shows a sample of one such study in which 0.5 MeV particles were used to bombard the surface of polycrystalline vanadium film at 600°C. Interesting results are obtained as a function of irradiation temperature, projectile energy, pre-irradiation treatment, micro-structure etc. on other metals and alloys also.

Table-I

500 MW(t) Fusion Reactor Parameters

Wall area	400 m^2
Radial loss	10^{23} IONS/SEC
Particle flux	2.6×10^{16} IONS/Cm^2/sec
Average Sputtering Coefficient	0.008 $\frac{\text{ATOM}}{\text{ION}}$
Erosion rate	1.2 mm/Year
Wall thickness	1 cm
Permitted loss	20%
Life-time	2 Years

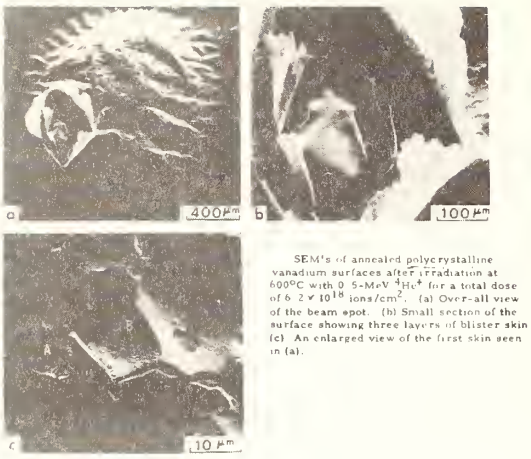

SEM's of annealed polycrystalline vanadium surfaces after irradiation at 600°C with 0.5-MeV $^4He^+$ for a total dose of 6.2×10^{18} ions/cm^2. (a) Over-all view of the beam spot. (b) Small section of the surface showing three layers of blister skin (c) An enlarged view of the first skin seen in (a).

Fig.10. Blisters in polycrystalline vanadium produced by charged particle bombardment.

Conclusion

I have tried to give a birds-eye view of new problems that need solution in new technologies - problems due to radiation effects, study and solution of which can arise from use of accelerators. Radiation Physics, in the broad sense of the word, has large scale implications in these new technologies.

References

1. Mc Reynolds, A.W., Nelkin, M.S., Rosenbluth, M.N. and Whittemore, W.L. PICG, 297 (1958).
2. Woods, A.D.B., Brockhouse, B.N., Sakamoto, M. and Sinclair, R.N., Inelastic Scattering of Neutrons in Solids and Liquids - (IAEA) p.487 (1961).
3. Bergmanm, A.A., Isacoff, A.I., Murin, I.D., Shapiro, F.L., Shtranikh, I.V. and Kazarnovsky, M.V., PICG, 135 (1956).
4. Chandramoleshwar, K., Navalkar, M.P., Ramakrishna, D.V.S., Nucl.Inst. and Methods 60, 113 (1968).
5. Chandramoleshwar, K., Navalkar, M.P., Ramakrishna, D.V.S., Ramanna, R. and Subramu, K.R., PICG (1964).
6. Radiation Damage in Reactor Materials, Proceedings of an IAEA meeting Vol.1 and Vol.II (1969).
7. Proceedings of the BNES Nuclear Fusion reactor Conference (1970).
8. Cawthorne, C. and Fulton, E.O., AERE-R 5269 (1966), p 446 and Nature 216, 575 (1967).
9. Kulcinski, G.L., Nucl.Inst. and Methods 94, 365 (1971).
10. Das, S.K. and Kaminsky, M., J.Appd. Phys. 44, 25 (1973).

VARIATION OF TOTAL TO K-SHELL PHOTOELECTRIC CROSS SECTION RATIOS WITH ATOMIC NUMBER AND PHOTON ENERGY

Ramakrishna Gowda and B. Sanjeevaiah
Department of Physics, University of Mysore
Manasagangotri, Mysore-570006, India

The total to K-shell photoelectric cross section ratios are calculated from the measured total and K-shell photoelectric cross sections (using a well type plastic scintillation spectrometer) in copper, zirconium, silver, tin, tantalum, gold, and lead for 145.4, 279.1, 411.8 and 661.6 keV gamma rays. The ratios are plotted against the atomic number and also the photon energy. The theoretical ratios obtained form the cross sections of Scofield [UCRL Report No. 51326] are also plotted and a comparison is made. The dependence of these ratios on the atomic number of the element and the photon energy is discussed.

(Atomic number; cross section; K-shell; measurement; photoelectric effect; photon)

Introduction

Until the 1960's the relativistic calculations gave only the cross sections for the K-shell. It was the practice to estimate the contribution of all other higher shells by using the ratio σ_t/σ_K, where σ_t and σ_K are the total and K-shell photoelectric cross sections respectively. The law of "five fourths" simply claimed that $\sigma_t/\sigma_K = 5/4$. This value holds good only for high Z materials above Hulme energy limit 0.35 MeV[1]. Davisson and Evans[2], Grodstein[3] and Davisson[4] tabulated the absolute photoelectric cross sections together with cross sections for the various gamma ray interaction processes contributing to the total. In the tabulation of Davisson and Evans[2] the total atomic cross section was obtained by applying the 5/4 law to the K-shell cross sections. Grodstein[3] also followed a similar method, but instead of using the 5/4 law she used the ratios σ_{K+L+M}/σ_K as calculated with Stobbe's formula[5] and similar formula of Hall[6], which corrects the overestimation of cross sections for the low Z values. In the later table of Davisson[4] she used Kirchner's experimental ratios[7] measured at the K-shell thresholds in which the Z-dependence of this ratio was found to vary monotonically from 1.09 for aluminium to 1.235 for uranium. Hubbell[8] gives an empirical fit to calculate the ratios σ_t/σ_K as a function of Z with an accuracy of ± 2 to 3 percent with Kirchner values. This fit does not take into consideration any possible energy dependence. Later calculations of Rakavy and Ron[9] showed that the ratio is slightly energy dependent especially at low energies. So the calculations using Kirchner's values are found to be under-estimated above K-shell threshold.

The total to K-shell photoelectric cross section ratios are measured by Hultberg[10] using magnetic beta ray spectrometer at the energies 1332, 662 and 412 keV gamma rays in uranium. Latyshev[11] gives the ratios for Z = 73 and Z = 82 at 2.62 MeV. Experimentally measured K-shell and L sub-shell ratios are tabulated in the recent review article of Pratt et al[12].

Results and Discussion

The total and K-shell photoelectric cross sections are measured using a well type plastic scintillation spectrometer previously described by the authors[13-17]. Using these measured total and K-shell photoelectric cross sections, the ratios are calculated in copper, zirconium, silver, tin, tantalum, gold, and lead for 145.4, 279.1, 411.8 and 661.6 keV gamma rays. The ratios are plotted against the atomic number (Z) in Fig. 1. and against the photon energy in Fig. 2. The theoretical ratios obtained from the cross sections of Scofield[18] are also plotted in the same figure for comparison. In the plot of total to K-shell ratios against the photon energy, one can observe the energy dependence at lower energies. Especially for high Z materials the dependence is found to be prominent. As the energy increases the dependence decreases. The total to

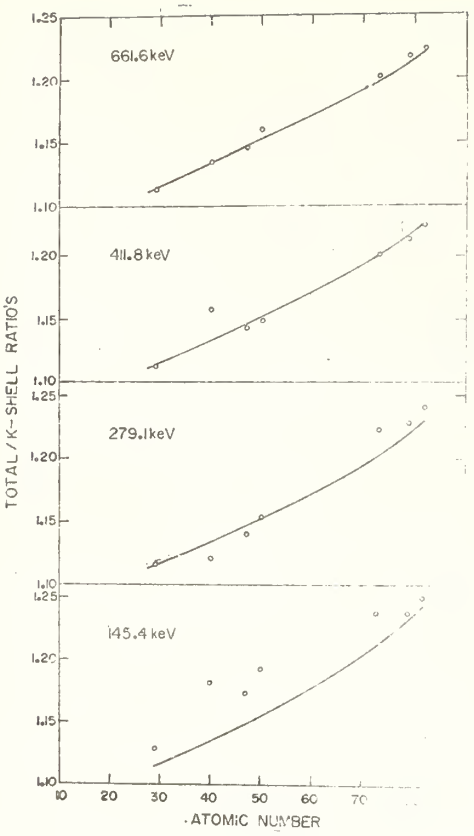

Fig. 1. Variation of total to K-shell Photoelectric cross section ratios with atomic number.

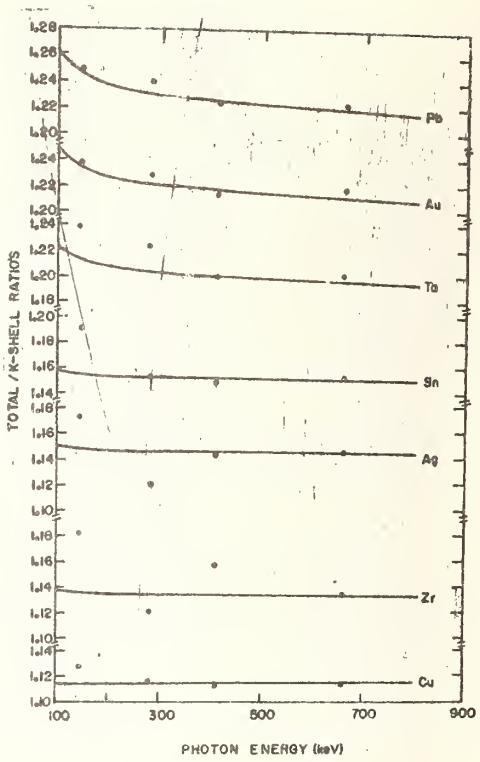

Fig. 2. Variation of total to K-shell Photoelectric cross section ratios with photon energy.

K-shell ratios obtained using the measured cross sections are found to be consistantly higher than those obtained from Scofield values at 145.4 keV, and as the energy increases the agreement becomes fair. These ratios are found to vary monotonically as Z increases. The errors on these ratios are found to be about 9% in the case of photon energy 145.4 keV and 6% at all other photon energies.

References

1. Hulme, H.R., McDougall, J., Buckingham, R.A. and Fowler, R.H., Proc. Roy Soc. (London) A149, 131 (1935).
2. Davisson, C.M. and Evans, R.D., Rev. Mod. Phys. 24, 79 (1952).
3. Grodstein, G. White, N.B.S. Circular No. 583 (1957).
4. Davisson, C.M., Alpha-Beta-Gamma Ray Spectroscopy, Ed. K. Siegbahn, Vol.1, Chap. 2 (1965) (North Holland, Amsterdam).
5. Stobbe, M. Ann. Physik 7, 661 (1930).
6. Hall, H. Rev. Mod. Phys. 8, 358 (1936).
7. Kirchner, F. 1930, Handbuch der Experimental Physik, Ed. W. Wien and F. Harms (Akademische, Verlagsgesllschaft, Leipzig).
8. Hubbell, J.H., Nat. Stand. Ref. Data. Ser. NSRDS-NBS 29, (1969).
9. Rakavy, G. and Ron, A. Phys. Rev. 159, 50 (1967).
10. Hultberg, S. Arkiv für Fysik 15, 307 (1959).
11. Latyshev, G.D., Rev. Mod. Phys. 19, 132 (1947).
12. Pratt, R.H., Ron, A. and Tseng, H.K. Rev. Mod. Phys. 45, 273 (1973).
13. Gowda, Ramakrishna and Sanjeevaiah, B. J. Phys. (GB) A6, 1041 (1973).
14. _____ Phys. Rev. A8, 2425 (1973).
15. _____ J. Phys. B (GB) 7, 1772 (1974).
16. _____ Phys. Rev. A6, 2569 (1974).
17. _____ Can. J. Phys. 53, 846 (1974).
18. Scofield, J.H., UCRL Report No.51326 (1973) (unpublished).

Discussion

Roy, S.C.

1. Have you measured τ_K or τ_{total} or both of them ?

2. Well, in case of measuring τ_K, how are you sure that you are considering K-electrons only ?

3. Next, is there anything new in the technique from the conventional measurements ?

4. Can you assign any reason for the large observed discrepancy for some of the elements ?

Gowda, R.

1. We have measured both total and K-shell cross sections.

2. For monoenergetic electrons the pulse height amplitude spectrum in the scintillators is mainly a Gaussian. The main peak in the photoelectron spectrum is attributed to the K-shell electrons and using the left portion of the peaks Gaussians were fit. The areas under these Gaussians would then give the number of K-shell photoelectrons. Also the plot of observed K-shell photoelectron peak energy against the pulse height amplitude gives a straight line.

3. Although the experimental technique is similar to the conventional methods we have introduced some modifications in the geometry and the detector size. We also observe the peak due to photoelectrons in aluminium at 145.4 keV, which was not observed in earlier experiments. This shows that our experimental set up is much better than the previous ones.

4. If we draw the error bars on the ratios there is agreement in the case of all the elements within the errors. The errors are about 6% at 279.1, 411.8 and 661.6 keV and 9% in the case of 145.4 keV.

OPTICAL MODEL ANALYSIS OF NONELASTIC INTERACTION OF 14.2 MEV NEUTRONS *

B. Pal, Arun Chatterjee and A.M. Ghose
Nuclear Physics Laboratory, Bose Institute
Calcutta-700009, INDIA

Non-elastic cross sections of several nuclei for 14.2 MeV neutrons have been measured using sphere transmission technique. The measured data together with the results of others have been analysed with optical model using a least square criteria over a wide range of mass number ($12 \leqslant A \leqslant 207$).

(Cross section; multiple bias; neutron; non-elastic; optical model; parameter; polynomial extrapolation; sphere transmission.)

Introduction

In the present work, the experimental and theoretical studies on neutron non-elastic interactions have been undertaken in the 14 MeV region. Efforts have been made here to find out an average set of mass-independent optical model parameters, utilizing essentially the non-elastic scattering cross section data measured by us. References 1 to 9 contain the works already carried out in this field.

Measurement of Non-elastic Cross Section for Different Nuclei

Non-elastic cross sections of seven nuclei for 14.2 MeV neutrons have been measured by using reciprocal sphere transmission technique. Two important correction factors arising from (a) the recoil energy loss suffered by elastically scattered neutrons and (b) the multiple scattering in the finite scatterer thickness have been estimated by multiple bias and polynomial extrapolation methods[10] respectively. The results obtained are presented in Table 1.

Table 1

Non-elastic Cross Sections σ_{ne} (barns) for 14.2 MeV Neutrons

Element	σ_{ne} in barns
O	0.82 ± .02
Al	0.94 ± .02
Cu	1.49 ± .03
Cd	1.90 ± .04
Sn	1.90 ± .03
W	2.40 ± .06
Pb	2.57 ± .05

Optical Model Analysis

Analysis of non-elastic data obtained from present measurement as well as from data obtained by others[10,11,12] was performed using the widely used nine parameter local optical potential given by the following form:

$$V(r) = -V_o \left[1 + \exp\left(\frac{r - r_o A^{1/3}}{a_o}\right)\right]^{-1}$$
$$+ 4ia_D W_D \frac{d}{dr}\left[1 + \exp\left(\frac{r - r_D A^{1/3}}{a_D}\right)\right]^{-1}$$
$$+ V_S \cdot \left(\frac{\hbar}{m_\pi c}\right)^2 \cdot \frac{1}{r} \cdot \frac{d}{dr}\left[1 + \exp\left(\frac{r - r_S A^{1/3}}{a_S}\right)\right]^{-1} \cdot \vec{\sigma} \cdot \vec{l}$$

where the symbols have their usual significance. Volume absorption term in the imaginary part of the potential has not been considered because of its negligible contribution[13] on the absorption of 14 MeV neutrons. The spin-orbit part of the potential has practically no effect on non-elastic cross section. Therefore, throughout our present analysis we have fixed the parameters V_S, r_S and a_S at their reasonably expected values, namely,

V_S=7.0 MeV, r_S=1.25 fm, a_S=0.65 fm

In the 14 MeV region the compound elastic cross section is negligibly small[14] and so we have disregarded this effect and compared the measured cross sections with the computed values directly.

The experimental cross sections σ_{exp} may be compared with those predicted by optical model, σ_{th}, simply by examining the sensitivity of σ's on parameters. The difference between these two cross sections denoted by σ_{error} may be then expressed as a summation of variation of cross section with each free parameter a_j of the model about a fixed initially chosen value a_j^0 i.e.

*Work carried out under a PL-480 Project sponsored by the National Bureau of Standards, U.S.A.

$$\sigma_{error} = \sigma_{exp} - \sigma_{th} = \sum_{j=1}^{6} \left(\frac{\delta\sigma}{\delta a_j}\right)_o . \delta a_j \quad \ldots (2)$$

We have started with an initial set of parameters chosen from the works of Perey and Buck[1] and Wilmore and Hodgson[9]. Non-elastic cross section data for several elements (seventeen) have been taken from different sources[10,11,12]. Each of the six parameters was varied arbitrarily by 2% from its initial value keeping others fixed. Thus partial derivative $\left(\frac{\delta\sigma_{th}}{\delta a_j}\right)_o$ corresponding to each parameter was obtained. Least square criteria was applied to eqn. 2. A mass-independent set of parameters which, in principle, should give optimum fit to the experimental data was then obtained. The parameter set thus obtained has been presented in Table 2.

Table 2

Optical Potential Parameters from Non-elastic Cross Sections Fitting.

V_o (MeV)	r_o (fm)	a_o (fm)	W_D (MeV)	r_D (fm)	a_D (fm)
40.225	1.261	0.618	9.795	1.477	0.452

A comparison of theoretically calculated values of cross section σ_{th}, with the new parameter set against the measured values of present investigation has been made in fig. 1. In table 3 we have compared the potential parameters with the average parameters obtained by Bjorklund and Fernbach[2], Rosen et al[5] and Cassola and Koshel[7].

Discussion

The amount of variations from set to set noted in the values of a particular parameter is not surprising; that different approaches of analysis would lead to sets of slightly varying values, is expected normally. The value of r_D obtained in our analysis is notably large compared to that of each set. However, this value though large, is not unrealistic. Optimum parameter searches for individual elements have quite often lead to values which vary over a wide range from element to element. For example[7], maximum and minimum values of r_D are found to be 1.49 (for K) and 1.04 (for Al) respectively.

It will be seen from fig. 1, that except for too low mass number elements,

Table 3

Comparison of the 14 MeV A-independent Average Parameters Obtained in the Present Investigation with those Reported by Other Authors.

Parameter	Bjorklund and Fernbach[2] (14 MeV)	Rosen et al[5] (14.5 MeV	Cassola and Koshel[7] (14.0 MeV)	Present work (14.2 MeV
V_o	44.0	44.5	43.4	40.24
r_o	1.25	1.25	1.25	1.26
a_o	0.65	0.65	0.63	0.62
W_D	11.0	5.75	8.20	9.8
r_D	1.25*	1.25	1.24	1.48
a_D	0.98*	0.70	0.47	0.45

(* indicates parameters pertaining to surface absorption potential of Gaussian form)

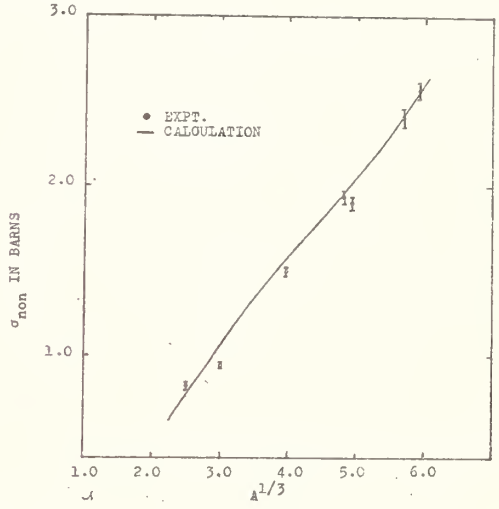

Fig.1. Experimental and theoretical nonelastic cross section of 14.2 MeV neutrons as a function of $A^{1/3}$.

the cross sections calculated with the new set of mass independent parameters agree well with the experimental results over a wide range of mass numbers. The variations for low A nuclei are not surprising since the optical model is not expected to be valid for low mass number elements. The parameters given in Table 2, thus represent, in the mass independent approximation, a set of reliable parameters for describing non-elastic scattering of 14 MeV neutrons from nuclei of mass number lying in the range $12 \leqslant A \leqslant 207$.

Since our next endeavour will be to make another approach to fit the non-elastic as well as elastic scattering data simultaneously, with a single set of parameters, we have not attempted multiple iterations for obtaining more accurate values of the parameters.

References

1. Perey, F.G. and Buck, B., Nucl. Phys. 32, 353 (1967).
2. Bjorklund, F.J. and Fernbach, S., Phys. Rev. 109, 1295 (1958).
3. Engelbrecht, C.A. and Fiedeldey, H., Ann. Phys. 42, 262 (1967).
4. Aver'Yanov, I.K. and Purtseladze, Z.Z., Sov. J. Nucl. Phys. 7, 193 (1968).
5. Rosen, L., Beery, J.G., Goldhaber, A.S. and Auerbach, E.H., Ann. Phys. 34, 96 (1965).
6. Becchetti, F.D. and Greenlees, G.W., Phys. Rev. 182, 1190 (1969).
7. Cassola, R.L. and Koshel, R.D., Nuovo Cim. 53B, 363, 1968.
8. Korzh, I.A., Kashuba, I.F., Kozin, B.D. and Pasechnik, M.V., Sov. J. Nucl. Phys. 7, 190 (1968).
9. Wilmore, D. and Hdgson, P.E., Nucl. Phys. 55, 673 (1964).
10. Chatterjee, A. and Ghose, A.M., Phys. Rev. 161, 1181 (1967).
11. MacGregor, M.H., Ball, W.P. and Booth, R., Phys. Rev. 108, 726 (1957).
12. Flerov, N.M. and Talyzin, V.M., J. Nucl. Energy 4, 529 (1957).
13. Hodgson, P.E., The Optical Model of Elastic Scattering (Lond.) (1963).
14. Lane, A.M., Rev. of Mod. Phys. 29, 191 (1957).

GEOMETRIC FACTORS IN RADIATION PHYSICS MEASUREMENTS *

A.M. Ghose
Department of Physics
Bose Institute
Calcutta-700009, India

Optimisation of geometrical factors through symmetry considerations is a powerful means of improving the accuracy of measurements in Radiation Physics. This has been illustrated for the cases of spherical and axial symmetries. Design of double scattering fast neutron polarimeters as well as of gamma ray linear polarimeter systems have been discussed. Applications of the surface of revolution geometries to various fields have also been considered.

(Absorption; accuracy; cross section; fast neutrons; geometric factors; photon; polarimeter; radiation physics; scattering; spectrometers.)

Introduction

One of the most important elements in the design of experiments in many areas of Radiation Physics is the spatial distribution of the component parts of the entire experimental arrangement comprising the source, the absorber and the detector. The purpose of the present paper is to indicate how the effective signal strength at the detector and hence the accuracy of the measurements can be increased, sometimes even by orders of magnitude, by making the distribution of the components symmetrical. The symmetries correspond naturally to those inherent in the quantities or processes under investigation. These considerations are particularly important when scattering cross sections are either being measured or differentiated from other interaction processes.

Spherical Symmetry

When total scattering from all directions is being measured (or discriminated) the inherent geometry is spherical. This is the basis of the well-known sphere transmission technique which can be used, at least in principle, to effect a separation of scattering and absorption processes (Fig. 1a). In practice, the application of the sphere transmission technique depends upon the validity of several implicit assumptions and the accuracy obtainable depends critically on how closely these assumptions are obeyed by the actual experimental arrangement. Since the method of spherical symmetry has been discussed elsewhere in other publications[1] we shall not discuss it further.

Axial Symmetry

When the phenomenon or the process under study shows no explicit dependence on the azimuthal angle, the symmetry natural to the experimental arrangement is axial (Fig. 1b). Thus in the measurement of the differential scattering cross sections $\sigma_s(\theta)$ of unpolarised radiations the symmetry is around the scatterer - detector axis. Other instances where axial symmetry is important includes simple angular correlation experiments, study of nuclear fluorescence radiation using Compton scattered gamma rays etc. Extensively used ring geometry is the simplest version of axially symmetric arrangement and it has the additional virtue of being adaptable to the time-of-flight technique. However, in plane geometry constant angle θ corresponds to an arc of a circle and this fact was utilised by Tandon and McIntyre[2] in their investigations on nuclear fluorescence radiation (Fig. 1c). Obviously a surface of revolution shaped geometry of the scatterer around the source-detector axis is a natural extension to the three dimensional case (Fig. 1d); in a separate paper[3] we have shown how this geometry has been utilised as the basis for the measurement of differential scattering cross sections of fast neutrons. A version of the arrangement proposed for the measurement of differential incoherent scattering cross section of gamma rays[4] is shown in Fig.2.

A possible use of the axial symmetry lies in the field of angular correlation experiments involving prompt radiations or radiations from short-lived nuclei emitted by a source, which, in turn, is produced by irradiation in a

*Work carried out under a PL 480 project sponsored by the National Bureau of Standards, U.S.A.

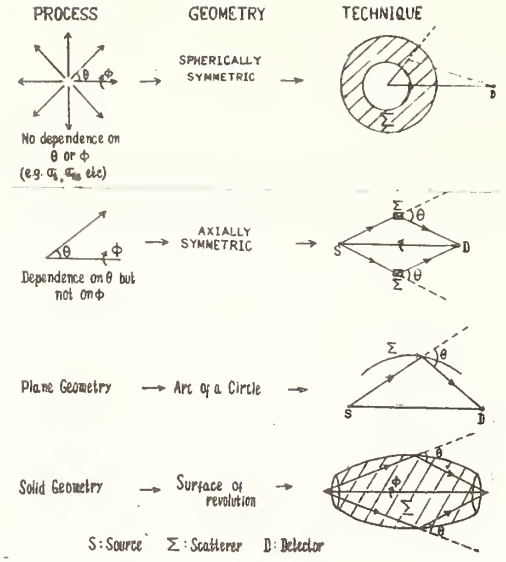

Fig.1. Geometrical arrangement for different types of symmetries.

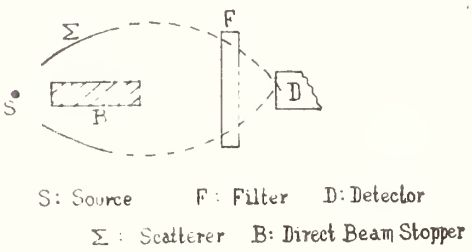

Fig.2. Geometrical arrangement for the measurement of differential incoherent scattering cross section of gamma rays.

wide beam. In the usual angular correlation arrangement, source absorption and scattering can be reduced only at the expense of intensity. In the arrangement shown in Fig. 3 the source has the shape of a surface of revolution about the line joining the two coincidence detectors as axis; since the extended source can be thin there is considerable gain in intensity over the usual point source geometry. The arrangement is also potentially useful for inner bremstrahlung experiments.

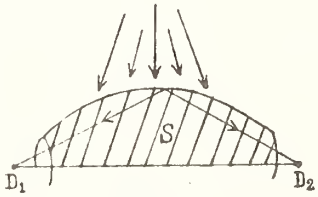

Fig.3. Proposed arrangement for angular correlation measurements.

Double Scattering Fast Neutron Polarimeter

In measurements involving linearly polarised radiations we come across symmetry considerations of a different type. We shall illustrate them first by considering the design we have proposed for a double scattering fast neutron polarimeter.

Fig. 4 shows the essential elements of a double interaction fast neutron polarimeter[5]. Unpolarised beam of neutrons incident on the polariser Σ_1 gets polarised after scattering through an angle θ_1. The flux of particles issuing out from the second target Σ_2 at a fixed angle of scattering θ_2, depends on the azimuthal angles φ through the relation

$$N(\theta_2,\varphi)=N_o(\theta_2)[1+P_1(\theta_1)P_2(\theta_2)\cos\varphi] \quad \ldots (1)$$

where N_o is the flux in absence of polarisation and P_1 is the polarisation vector in the initial interaction while P_2 is the polarisation that would result had an unpolarised beam been incident on Σ_2. Using the Basle convention[6], the differential cross sections for scatterings to the "left" ($\varphi=\pi$) and to the "right" ($\varphi=0$) in the common plane becomes respectively

$$\sigma_L = \sigma_o(\theta_2)[1-P_1(\theta_1)P_2(\theta_2)] \quad \ldots (2)$$

$$\sigma_R = \sigma_o(\theta_2)[1+P_1(\theta_1)P_2(\theta_2)] \quad \ldots (3)$$

Hence the asymmetry ratio $A(\theta_2)$, defined to be equal to σ_L/σ_R, becomes

$$A(\theta_2) = \frac{1-P_1(\theta_1)\ P_2(\theta_2)}{1+P_1(\theta_1)\ P_2(\theta_2)} \quad \ldots (4)$$

so that $$P_1(\theta_1)P_2(\theta_2)=\frac{1-A(\theta_2)}{1+A(\theta_2)} \quad \ldots (5)$$

Hence a measurement of $A(\theta_2)$ yields product $P_1(\theta_1)P_2(\theta_2)$, which, in turn, gives $P_1(\theta_1)$ or $P_2(\theta_2)$, when one of the two quantities is known.

The usual method for producing a polarised beam of fast neutrons is based on the polarisation during the production of neutrons e.g. by using d-t or d-d reactions well above their corresponding thresholds; $P_2(\theta_2)$ is usually obtained from phase-shift analysis if the second interaction consists of elastic scattering from a spinless target like He or C. Near the threshold (e.g. for "14" MeV t-d neutrons) $P_1(\theta_1)$ is very small and the above method is therefore difficult to apply.

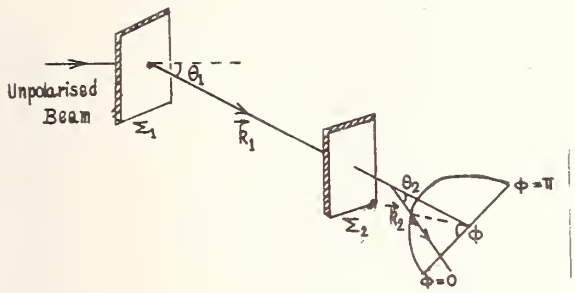

Fig.4. Elements of a double interaction fast neutron polarimeter.

An alternative method is to use the technique of double scattering. If the second reaction is again an elastic scattering from target nuclei which are not too light, the energy change during the scattering can be neglected and further if θ_1 is set equal to θ_2, we can write $P_1(\theta_1) = P_2(\theta_2)$ and hence

$$P_1(\theta_1) = \frac{1-A(\theta_2)^{\frac{1}{2}}}{1+A(\theta_2)} \qquad \ldots (6)$$

Thus a measurement of A yields P and once the polarimeter is calibrated, it can be used to analyse diverse polarisation processes.

In the conventional approach, without optimising geometry, the double scattered beam intensity is 10^{-12} to 10^{-15} of the primary total beam strength and this figure is too low to have any practical utility. A possible arrangement of double scattering fast neutron polarimeter based on the surface of revolution geometry is shown in Fig. 5. The neutrons are successively scattered by two sectors of angular width δ and forming a part of the surface of revolution. The number of neutrons detected by the neutron counters in the two symmetrical positions depend upon the polarisation induced in the first scatterer Σ_1. To get an estimate of the typical counting rate we note that the number N_1 of neutrons issuing out of Σ_1 and passing through a hole H of effective radius a is given by

$$N_1=\frac{\delta a^2\gamma N_o t}{2^{9/2}l^2}\left(\frac{d\sigma(\theta)}{d\Omega}\right)\tan^4\theta\,\sec\theta\int_{-f}^{+f} f(x,\theta)\,dx \qquad \ldots (7)$$

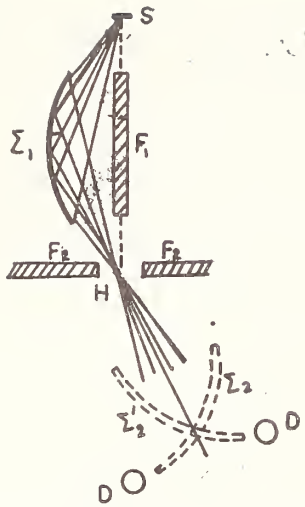

Fig.5. Double scattering fast neutron polarimeter.

where γ is the number of nuclei per c.c. of the scatterer, t is its normal thickness, N_o is the no. of neutrons emitted by the source S per sec., 2l is the length of the SH axis, θ is the scattering angle, $x = \frac{z}{l}$, z is the distance along the axis SH of the projection of an element of scatterer from the centre of the axis and where the integrand $f(x,\theta)$ which is taken over the scatterer Σ_1 is given by

$$f(x,\theta)=\frac{(1-x)\sqrt{1+(1-x^2)\tan^2\theta}-1}{1+(1+x)\tan^2\theta-\sqrt{1+(1-x^2)\tan^2\theta}}$$

$$x\frac{1}{[\sec^2\theta-x^2\tan^2\theta]^{\frac{1}{2}}}x\frac{1}{[1+(1-x)\tan^2\theta-\sqrt{1+(1-x^2)\tan^2\theta}]} \qquad \ldots (8)$$

The limits of the integral in Eqn. (7) correspond to the two extreme positions at the ends of the scatterer. In the above derivation we have assumed that the scatterer is "thin" enough to replace expressions of the type $\frac{\sigma_s}{\sigma_t}(1-e^{-\alpha\sigma_t\gamma t})$ by $\alpha\sigma_s\gamma t$ where α is a numerical factor of the order of unity. With this approximation the mean counting rate after double scattering becomes

$$C=\epsilon\frac{\delta\pi a^4\gamma^2t^2}{2^8l^4\Omega}\left[\frac{d\sigma(\theta)}{d\Omega}\right]^2\tan^8\sec^2\theta\left[\int_{-f}^{+f} f(x,\theta)\,dx\right]^2 \qquad \ldots (9)$$

where we have assumed that Σ_1 and Σ_2 have the same dimensions, ϵ is the efficiency of the detector and Ω is the solid angle subtended by at S. If Σ_1 and Σ_2 are made of sulphur, typical mean counting rates (neglecting the polarisation factor) obtainable by this method is shown in Fig. 6. It will be seen that C is several orders of magnitude more than the corresponding values using conventional geometry. In the calculations we have assumed the following parameters,

$$\delta = 0.1,\ \frac{a}{l} = 0.1,\ \epsilon = 0.01 \qquad \ldots (10)$$

$$t = 1 \text{ cm and } f = 0.75$$

If instead of ^{32}S one uses ^{208}Pb, the double scattered counts are even higher as shown in Fig. 7. In the calculations we have used the same set of parameters as given in (10).

The surface of revolution geometry thus promises to furnish us with a method for polarisation measurement of fast neutrons by double scattering. However the design of filters and slits poses a practical problem of some difficulty.

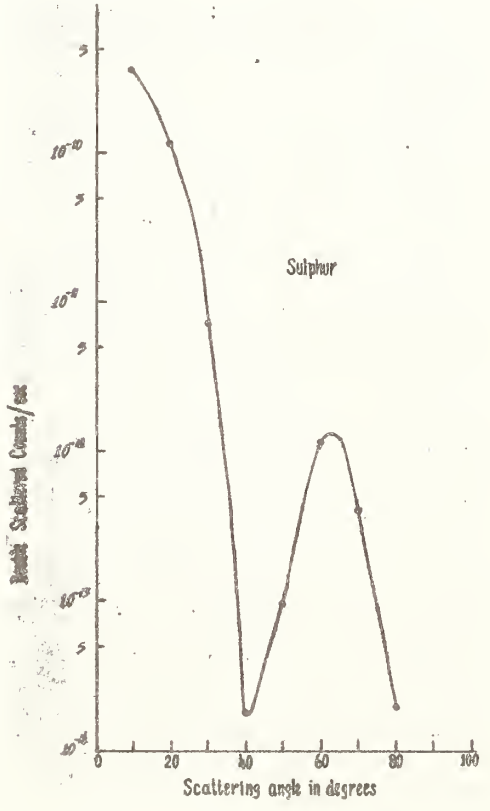

Fig.6. Expected mean double scattering counts for sulphur in a typical polarimetric arrangement.

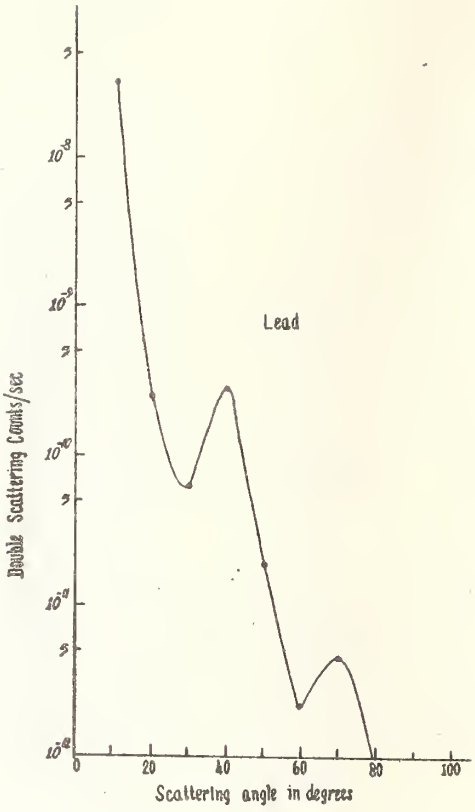

Fig.7. Expected mean double scattering counts for lead in a typical polarimetric arrangement.

Gamma Ray Polarimeter System

For gamma photons the linear polarisation is transverse rather than longitudinal and this, therefore, calls for different type of geometrical considerations. We shall briefly consider a polarimeter system proposed by Rudra and Ghose[7] consisting of a ring Σ_1 of scatterer (and partial polariser) followed by an analyser ring Σ_2 which scatters radiations through 90° to a specially shaped detector D in position I after channelling them through suitable filters. (Fig.8). The source of unpolarised photons S is placed on the axis of the system. Fig. 8 depicts the plane of the first scattering - the σ-plane. To measure the polarisation, it is also necessary to measure the intensity of photons scattered by Σ_2 through 90° in π - plane, which is normal to σ-plane. The detector D has now to be moved to the position II concentric with Σ to receive the photons. The path of typical ray in the π-plane is shown in Fig. 9. The cross section of D transverse to the axis of the system is ring - shaped and the path of a photon through the ring is inclined at an angle φ. In order that the

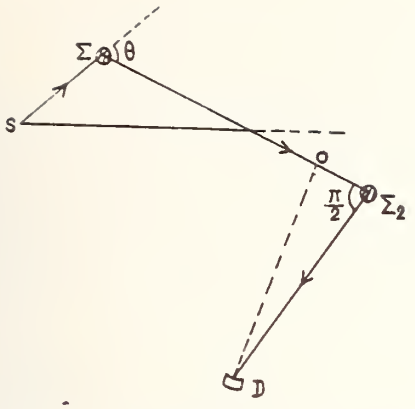

Fig.8. Basic elements of a double scattering polarimeter system for photons.

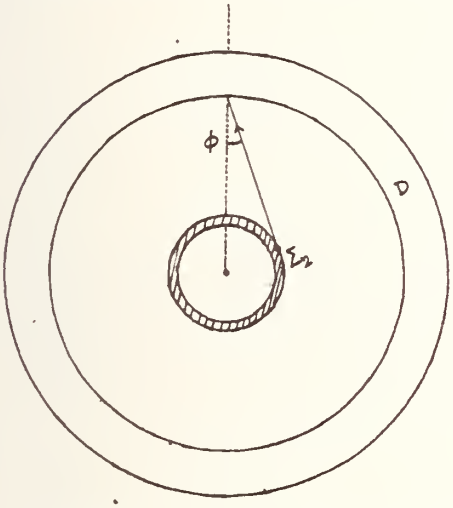

Fig. 9. Path of a typical ray in the π-plane.

geometry of paths in π and σ positions of the detector be symmetrical, the photons must traverse the detector in position I in a similar manner and the longitudinal cross section of D must be a section of a ring with the point O as centre. However if D has a large efficiency these considerations need not be enforced rigidly.

For a more extensive arrangement, it can be shown that if the points S and O are kept fixed, the locus of the projection of Σ_1 is a circle, while the points corresponding to Σ_2 and D lie on the same parabola. In fact, in Fig. 10, the locus of the projection of Σ_1 on the plane is determined by the equation:

$$D = X + (Y + h) \text{ Cot } \varphi, \quad \ldots \quad (11)$$

where (D,h) are the coordinates of O in the plane of the figure, with the source S situated at the origin and (X,Y) are coordinates of the projection of Σ_1. But

$$X = Y \text{ Cot } (\theta - \varphi), \quad \ldots \quad (12)$$

where θ is the angle of scattering in Σ_1. This makes

$$D = X + (Y+h) \frac{X \text{ Cot } \theta + Y}{X - Y \text{ Cot } \theta} \quad \ldots \quad (13)$$

and hence $[X-\frac{1}{2}(D-\alpha h)]^2+[Y+\frac{1}{2}(\alpha D+h)]^2$

$$= \tfrac{1}{4}(D^2+h^2)(\alpha^2+1) \quad \ldots \quad (14)$$

where $\alpha = \text{Cot } \theta$. This is arc of a circle, as expected from sec. 3. The loci of the projections of Σ_2 and D are given by the same eqn.

$$Y^2 = (x-D)^2 + (y-h)^2 \quad \ldots \quad (15)$$

Thus as the point (X,Y) moves over an arc of a circle, the coordinates of Σ_2 and D describe two branches of the same parabola. The complete arrangement in space is obtained by generating surfaces of revolution by rotating the arc and the parabola around the symmetry axis of the system, nearly conical parts of the latter being suitable for practical systems.

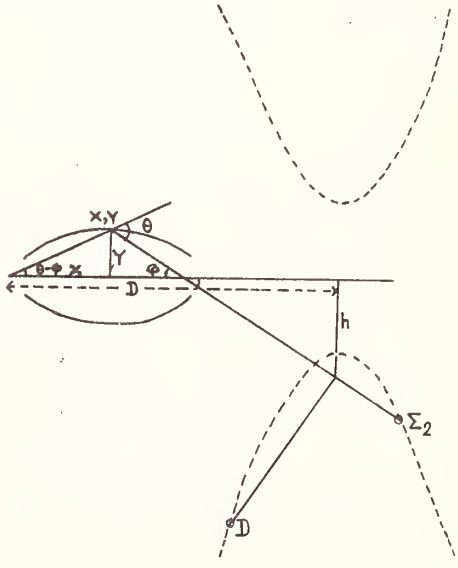

Fig. 10. Earlier version of proposed γ-ray linear polarisation.

A more elegant system[8] for linear transverse polarisation measurements can be derived from Fig. 11 which shows a section through the positions D_1 and D_2

of the detector in the σ and π planes respectively. If the scattering planes are distributed normally to the plane of the Fig. 11, the rays P_1D_1, P_2D_2 etc. are in the σ-plane while the corresponding rays P_1D_2, P_2D_2 are in the π-plane, where the points P_1, P_2, etc. on Σ_2, which now assumes the form of an arc of a circle. To find the form of the scatterer Σ_1, we consider the σ-plane $SQ_1P_1D_1$ corresponding to the point P_1 on Σ_2 (Fig. 12). The ray SQ_1 emerging from the source is scattered by Σ_1 at the point Q_1 through an angle θ; Q_1P_1 corresponds to the scattered ray which is further scattered by Σ_2 at Q_1.

Let the equation of Σ_1 be

i.e. $x^2 + y^2 = 2yR$ (Fig.11) ... (6)

It will be seen that the projection Z of Q_1 along SD_1 satisfies the equation

$$\cos\theta = \frac{Z}{\sqrt{x^2 + y^2 + z^2}} \quad \ldots (7)$$

since the points P_1 and Q_1 have identical x and y coordinates. From (6), we immediately have

$$z^2 = 2yR\,\mathrm{Cot}^2\theta \quad \ldots (8)$$

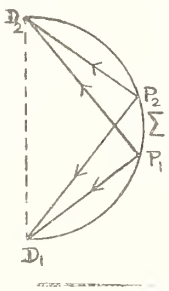

Fig.11. Improved version of the proposed γ-ray linear polarimeter.

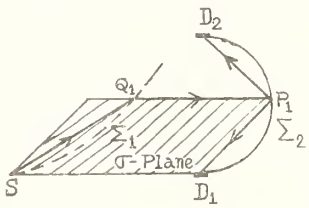

Fig. 12. Plane of polarimeter.

showing that for any given angle of scattering θ, the projection of the points on Σ_1 on y,z plane describes a parabola i.e. Σ_1 lies on the intersections of a parabolic cylinder with a right circular cylinder.

For this system it is relatively easy to design and fabricate systems of slits. Incidentally, gamma ray polarimeter systems of the type discussed above are going to be useful for estimating the individual contributions of different types of coherent processes to the total coherent scattering cross section of gamma rays.

Other Uses of Geometrical Factors

One of the early use of axial symmetry was made by Potenza and Rubbino[9] in their design of fast neutron spectrometer. Another important area where surface of revolution geometry can play an important role is the generation of neutrons of predetermined energy from a intense source of neutrons of higher energy (e.g. 7 to 14 MeV neutrons from t-d neutrons) by elastic scattering in a low z scattering. If the source neutrons have anisotropic energy distribution in the laboratory system, the scatterer might be shaped properly to take this account. For isotropic or nearly isotropic sources the arc of a circle geometry discussed in sec. 3 is adequate. For practical systems, the difference of counts with equivalent amounts of paraffin $(CH_2)_m$ and polythene $(CH)_n$ scatterers can be ascribed to elastic scattering from hydrogen

Acknowledgement

The author wishes to thank his students who have been associated with different phases of the programme outlined here. He wishes to thank Dr. S.M. Sircar, Director, Bose Institute, for his interest in the present work.

References

1. Bethe, H.A., Los Alamos Sci.Lab. Report LA-1428 (1952).
   Ghose, A.M. and Ganguly, N.K., Ind. Jour.Phys. 31, 285 (1956).
   Bethe, H.A., Beyester, J.R. and Carter, R.E., J.Nucl.Energy 3, 273 (1956).
   Fast Neutron Physics, Vol. II, Edited by J.B. Marion and J.L. Fowler; Interscience Publications, (1960) and references contained therein.
   Ghose, A.M., Nucl.Inst. and Methods 35, 45 (1965).
2. Tandon, G.K. and McIntyre, J.A. - Nuclr.Instr. and Methods 59, 181(1968).
3. Nath, S. Chatterjee, A and Ghose, A.M. paper presented in this Symposium.
4. Roy, S.C. and Ghose, A.M. (Private communication).

5. Elwyn, A.J. and Lane, R.O., Nucl. Phys. 31 78 (1962).
6. Proc. Int. Symp. Polarisation Phenomen of Neutrons (Basle 1970) ed. R. Huber and K.P. Meyer (Birkhäuser Verlag, Basle, 1961).
7. Rudra, N. and Ghose, A.M. Nucl. Phys. Solid State Phys. (India) 10, 581 (1967).
8. Ghose, A.M. (in press).
9. Potenza, R. and Rubino, A. Nucl. Inst. Methods 25, 77 (1963).

Discussion

P.K. Iyengar

I must congratulate Prof. Ghose for inventing these innovations, however I must stress that it is due to the situation of limited resources that he has been found to think of much clever tricks.

What will be the effect of non-uniform energy sensitivity and direction dependence of the detector on the over-all resolution?

A.M. Ghose

Optimisation of geometrical factors will not be effective unless suitable detectors are devised to exploit the full benefit which would result from this optimisation. In our laboratory we have developed suitable detectors for photons and neutrons which have the desirable properties. With conventional detectors the resolution will be poor indeed.

D.V. Gopinath

The spread in the angle and thereby the resolution of the system depends on the distances between the detector and source and their sizes. One can improve the resolution to the desired extent by increasing the distances but thus one has to use larger detectors for the same efficiency.

A.M. Ghose

In fact by increasing the sizes, one only gets a scaled up version of the same geometry and angular resolutions etc. are not improved thereby. It is essential that the improvement in detector quality must match the improvement in geometry.

B.B. Baliga

Is it necessary to shape the detectors for good geometry ? If so uniform efficiency of one detector is a real problem to achieve.

A.M. Ghose

It is not always necessary to shape the detector to improve their characteristics. For example uniformity of response in the gamma ray detectors can be achieved by incorporating a suitable detector in the system. For fast neutrons multiple bias method developed by us achieves the same purpose. In general the desired symmetry is also applicable to the corresponding detectors and their fabrications etc. is not necessarily difficult.

P.P. Kane

1. It is perhaps appropriate to point out that linear polarisation measurements with gamma rays can sometimes be made more accurately through the use of (p,pγ) reactions with selected targets such as magnesium. This has been done at 1.38 MeV for example.

2. There is a real problem with regular to Delbrück scattering amplitudes at large angles. On our work (Nucl. Phys. 1970) and that of Schumacher et al (Nucl. Phys. 1973) shows that empirically the Delbrück amplitude at an angle such as 120° interferes destructively with the Rayleigh amplitude. Theory, as known at present, predicts a constructive interferences between the two amplitudes at 120°.

Geometrical factors are important in all measurements.

A.M. Ghose

I fully agree with Dr. Kane that under suitable situations other methods might have the same order of efficiency; but here we have concentrated on general methods applicable to almost all situations. Delbrück scattering is indeed an important area which requires thorough investigation both theoretically and experimentally and polarisation measurements are expected to remove some of the uncertainties in this field.

K. Gopala

Have you taken into consideration the effects of multiple scattering amongst the various parts of the scatterer particularly in view of the large size and closed shape of the scatterer.

A.M. Ghose

Multiple scattering is an important problem. We have considered this aspect and one of the incentives for the

present investigation came from the desirability of using thin targets in an optimised geometry so that overall intensity remains at a reasonable value.

S. Gopal

Can we really discriminate experimentally the phase differences exist between Rayleigh scattering and Delbrück scattering ?

A.M. Ghose

I am afraid that experiments alone are not sufficient to settle the relative phase problem. However, at each angle of scattering, polarisation data will furnish additional data which are sensitive to the choice of phases. Hence a judicial mixture of theory and experiment will certainly lead to a better understanding of the coherent scattering phenomena.

MEASUREMENT OF ANGULAR DISTRIBUTION OF INCOHERENTLY SCATTERED GAMMA RAYS FROM ATOMS

B.Sinha (Goswami) and N. Chaudhuri
North Bengal University, Darjeeling
India

There has been comparatively little experimental investigation on the whole-atom incoherent scattering of photons in the x-ray and gamma-ray regions. A rigorous theoretical treatment of this type of scattering has not yet yielded enough results and the incoherent scattering function approach is taken to calculate the incoherent scattering cross section. Recently, Cromer and Mann calculated using SCF Hartree-Fock wave functions the incoherent scattering function over a wide range of momentum transfer in the photon scattering process. These data are more accurate than the earlier Hartree-Fock data in the low momentum transfer range and form the only available most comprehensive set of data over the range of momentum transfer upto 3.9 mc. In the present work, the angular distribution has been measured for incoherent scattering of 662 keV and 1.115 MeV photons by atoms with low, medium and high Z in the angular range from 1°to 165°. The experimental values of the incoherent scattering function have been interpreted on the basis of Cromer's theory.

(Angular distribution; cross section; gamma rays; photon; scattering, incoherent; x-rays.)

Introduction

The incoherent scattering of photons by electrons of different atoms is a topic of current interest. In absence of exact theoretical calculations the incoherent scattering function approach is taken in the calculation of incoherent scattering cross section. Highly accurate values of incoherent scattering function over a wide range of momentum transfer upto 4 mc are now available from the recent SCF Hartree-Fock calculations of Cromer and Mann[1] and Cromer[2,3]. Comparatively few experiments on the whole-atom incoherent scattering of photons have so far been reported. The data from the available experiments[4,5] cover only small ranges of momentum transfer, have large experimental errors and show considerable discrepancies at small and large scattering angles.

Method

The whole-atom incoherent scattering experiments[4] reported have been carried out by the auxiliary source method. This method requires a photon detector with efficiency independent of photon energy. Instead of using this method, we have compared, in the angular range 10° - 165°, the scattered counts from a given scatterer at each scattering angle with the scattered counts from an auxiliary aluminium scatterer of exactly the same size. The auxiliary aluminium scatterer provides a secondary (scattering target) source of photons of energy almost the same as the energy of photon scattered at a given angle from the given scattering target. The measurements were carried out with the main and the auxiliary aluminium scatterers under the same experimental conditions using multichannel analyzer with spectrum storage times in the range from 4 k secs to 100 k secs. Under the experimental conditions mentioned, the detector efficiency and the solid angle factors cancel out in the determination of the ratio of the differential scattering cross section for a given scatterer atom to that for a free electron in aluminium atom. This ratio was divided by the atomic number Z of the scatterer atom to obtain the incoherent scattering factor S.

The cylindrical scatterers used were of pure aluminium, copper, tin, mercury, tungsten and lead. The maximum value of μr (μ-photon attenuation coefficient, r-scatterer radius) for all the scatterers was 0.7. Even for such small scatterers, the corrections for absorption of primary and scattered photons in the scatterer target were necessary and made using Dixon's[6] results for calculating the self absorption correction in small gamma-ray sources. For angles 10° and 150° at which μr values were very small, S values were evaluated by extrapolating to zero scatterer radius a number of scattering measurements at slightly different scatterer radii. Measurements were made using a 150 mCi Zn-65

source collimated over a distance of 80 cm in iron block. The source, provided with adequate lead shielding, was at a distance of 130 cm from the scatterer. The detector, a 3" x 3". NaI(Tl) scintillator head shielded at sides, was coupled through a ND-52 PAD to a ND-1100 analyzer with 512 channels. The distance between the scatterer and the detector was 70 cm.

For measurements at angles less than 10^{o}, a shadow-cone type experimental arrangement was used. The Cs^{137} source in a conical shape collimator and the detector head, 1" x 1". NaI(Tl) scintillator, were provided with adequate lead shielding for reducing the background to a very low level. The scatterers of lead in the form of narrow width rings ($\sim$1 cm) were used for scattering measurements by the auxiliary source method. At a fixed source-to-detector distance of 3.3 m, the angle of scattering in the range 1^{o}- 5^{o} was chosen by taking scatterers of different radii. In the arrangement used, there was little background scattering material, except the shadow-cone, the light suspension threads for the shadow-cone, the air mass between the source and the detector, and the foam rubber scatterer holder. The detector pulses were recorded by the ND 1100 analyzer using 512 channels and storage times in the range 20 k secs to 100 k secs for a statistical precision near 1% . The total scattering cross section at each angle was determined and the incoherent scattering cross section was evaluated by subtracting from the total the accurate σ_{coh} theoretical value based on recent SCF Hartree-Fock calculations[1-3]. The results have been expressed as S.

Results and Errors

The scattered counts in the shadow-cone method were corrected for any difference in background counts with and without the scattering target. The experimental results for lead expressed as incoherent scattering factor S are given in the Table 1. The measurements on other elements mentioned above are not included in the Table. The measurements on all the elements studied give $S \leqslant 1$ in the angular range upto 165^{o}. The errors of the experimental S values have been computed by taking into consideration statistical errors in all the measured counts taken for evaluation of the experimental results and errors in other factors involved in the evaluation of results. At scattering angles less than 5^{o}, the energy change of the 662 keV photons in the inelastic incoherent scattering is negligibly small and no correction for this effect is necessary in very small angle measurements.

The theoretical values of S included in the Table are derived from the new work of Cromer[2] and Veigele et al[3]. Agreement between our results and Cromer values appears satisfactory at all values of momentum transfer studied. The earlier experiments[4] show greatest disagreement with theory at low values of momentum transfer.

Table 1

Experimental whole atom incoherent scattering factors for lead (Z = 82) with the corresponding Cromer-Veigele values. ($X = \sin[\theta/2]/\lambda$, θ - scattering angle, λ - photon wavelength in angstrom units. The experimental errors are in parentheses).

θ^{o}	$X(\text{Å}^{o-1})$	Experimental incoherent scattering factor S.	Cromer - Veigele values of S.
1.92	0.894	0.374(010)	0.46
2.65	1.232	0.558(010)	0.55
3.51	1.628	0.615(010)	0.63
4.64	2.161	0.669(010)	0.72
10	7.84	0.937(030)	0.95
15	11.67	0.942(032)	0.98
30	23.27	0.984(022)	0.995
45	34.42	0.984(022)	0.996
60	44.96	0.990(028)	0.998
75	54.76	0.978(030)	0.999
90	63.59	0.980(038)	0.999
105	71.36	0.976(055)	0.999
120	77.88	0.984(055)	0.999
135	83.10	0.990(051)	1
150	86.86	1.007(100)	1
165	89.17	0.999(098)	1

References

1. Cromer, D.T. and Mann, J.B.,J.Chem. Phys. 47, 1892 (1967).
2. Cromer, D.T., J.Chem. Phys. 50,4857 (1969).
3. Veigele, Wm. J. et al, Kaman Sciences Report, KN-71-431(R) (1971).
4. Sood, B.S. et al, Current Science,33, 139 (1964), Indian J. Pure and Appl. Phys. 1,305 (1963).
5. Quivy, R., Nucl.Phys.76,362 (1966).
6. Dixon, W.R., Nucleonics 8,68 (1951).

MEASUREMENT AND ANALYSIS OF A FEW 14 MEV NEUTRON CAPTURE CROSS SECTIONS

Manjushree Majumdar and B. Mitra
Bose Institute, Calcutta-700009
INDIA

Total 14 MeV neutron capture cross sections of seven representative nuclei have been measured by activation method, in a relative way. Data with an estimated error of ± 2% have been presented. Analysis of $\sigma(n,\gamma)$ total has been attempted with (a) Statistical evaporation type formula presented by Naguib and Lukyanov and (b) Direct reaction formula presented by Lane and Lynn. It has been shown that D.I. gives absolute estimate of values agreeing with experimental ones. Statistical model analysis with carefully adjusted neutron width function yields rather high radiative strength function.

(Activation; β-counting error; capture reaction; cross section; measurement; neutron)

Introduction

The Bose Institute 250 kV Cockcroft Walton accelerator has been used as a 14 MeV neutron generator for quite a few years in measuring cross sections of various nuclear reactions. We report here a few(n,γ) cross sections, with adequate stress on experimental methods of obtaining reliable results by activation method.

Method

The source of maximum error in activation results by β- counting has been tracked down to errors arising out of self-absorption and self-scattering of β-rays. In case of 14 MeV (n,γ) cross sections, additional trouble is in low counting rate of the relevant activity. Hence we propose to deal, in this report, with our method of minimising β- counting errors in activation. The result presented here are all relative measurements, i.e. cross sections relative to a standard cross section. This standard is (n,2n) cross section of ^{63}Cu nucleus and (n,α) cross section in ^{27}Al, the values of which are taken as 540 mb and 117 mb at 14.8 MeV respectively.

It has been reported previously from our laboratory that self-interaction errors in β- measurements can adequately be taken account of, even by using end window G.M. counting set up. Mitra and Ghose[1] proposed a semi empirical formula for preconstructing efficiency curves of such G.M. counters for different β-ray energies, where useful parameter referred to β-energies rather than maximum β-energies. For establishing such a relation they had to make very thin foils of elementary copper and aluminium, irradiate them for generation of suitable β-activity and draw efficiency curves for a realistic thickness of 20 mg/cm^2 samples, neglecting Z-dependence. We have tried to verify the same analytic relationship, viz

$$\eta_{rel} = 1 - exp(-b\bar{E}_\beta)$$

by going down to much lower values of sample thickness in which tracer activities are uniformly dispersed. For this, we first followed the method of physically pouring out in pots, a uniform suspension in solvent ether, of finest mesh metal dusts with tracer elements added. These tracers used were ^{35}S, ^{90}Sr, ^{204}Tl and ^{32}P, all in liquid chemical forms, to scan a β-energy range of $\bar{E}_\beta$ = .047 to 58 MeV.

We have assumed that, as in fig. 1, the efficiency is defined by

$$\eta = C_1/C_2 \quad \text{where } C_1 = \text{count}$$

rate at a minimum value of thickness of the sample achieved and C_2 = count rate at a standard thickness of 20 mg/cm^2. The results of obtaining (ct. rate vs thickness) curves in all the four above cases are shown in figs. 2-5.

Fig. 6 is the constructed (η_{rel} vs $\bar{E}_\beta$) curve. To construct this we determined the value of the constant 'b' from experimental η for ^{90}Sr. In fig. 6, the solid curve is the analytically constructed curve, and the experimentally obtained values for ^{35}S, ^{204}Tl and ^{32}P are plotted.

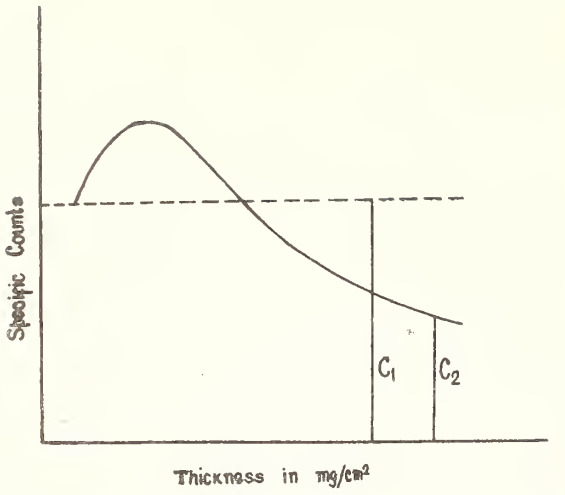
Specific Counts
C1
C2
Thickness in mg/cm²

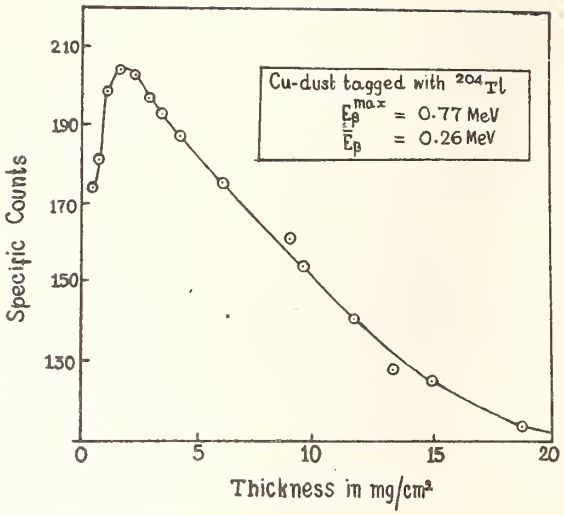
Cu-dust tagged with 204Tl
Eβ max = 0.77 MeV
Ēβ = 0.26 MeV
Specific Counts
Thickness in mg/cm²

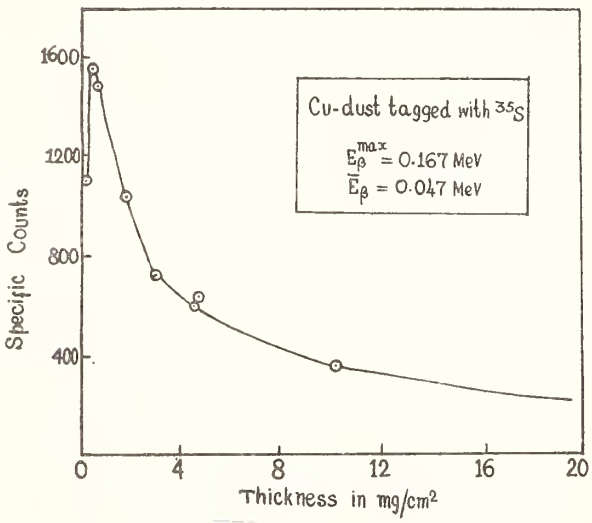
Cu-dust tagged with 35S
Eβ max = 0.167 MeV
Ēβ = 0.047 MeV
Specific Counts
Thickness in mg/cm²

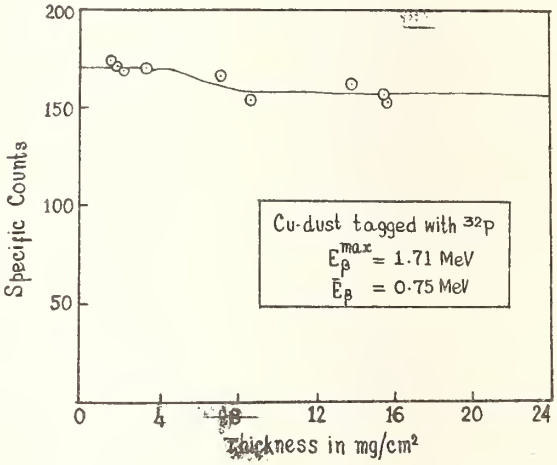
Cu-dust tagged with 32P
Eβ max = 1.71 MeV
Ēβ = 0.75 MeV
Specific Counts
Thickness in mg/cm²

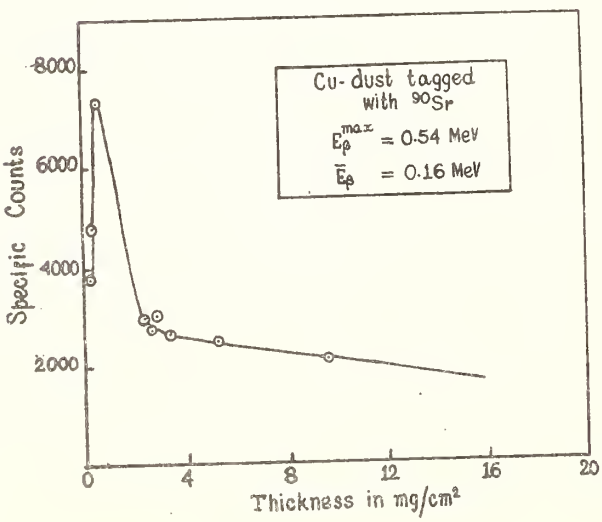
Cu-dust tagged with 90Sr
Eβ max = 0.54 MeV
Ēβ = 0.16 MeV
Specific Counts
Thickness in mg/cm²

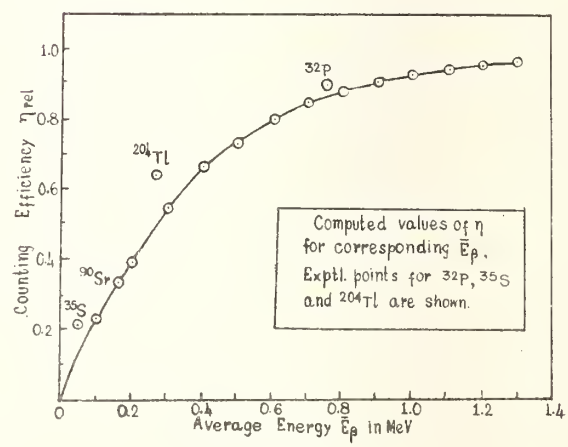
Counting Efficiency ηrel
Average Energy Ēβ in MeV
32P
204Tl
90Sr
35S
Computed values of η for corresponding Ēβ.
Exptl. points for 32P, 35S and 204Tl are shown.

Therefore it is seen that the analytically simple expression remains valid, within the limits of experimental error, for a range of $\bar{E}_\beta$ = 0.047 to 0.5, MeV.

Our sole assumption is that, in the (Sp. count vs Thickness) curve, the so called 'Zero-thickness' value is given by that actually obtained for the 'minimum' prepared thickness. To give more credence to the method, we are now producing very thin, doped samples by electrospraying. We assume albeit drastically, that going down to a thickness one order of magnitude smaller, will not appreciably alter the η values as defined. In electrospraying method, we can go down to few $\mu g/cm^2$ thickness. The (n,γ) reaction cross section of a few nuclei relative to $\sigma(n,2n)$ of ^{63}Cu = 540 mb. and to $\sigma(n,\alpha)$ of ^{27}Al = 117 mb, obtained in our laboratory, are shown in the Table 1.

In this table we have also presented cross section values as predicted by calculations according to a classical statistical model formula presented by Naguib and Lukyanov[2], also presented are the values from crude Direct Interaction (D.I.) model calculations according to Lane and Lynn[3], along with the experimental values. We have analysed the Naguib formula viz.

$$\sigma(n,\gamma)=K\sigma(c)E^{-1}U^{x}\exp[-2y\sqrt{aU}]$$

Table-I

14-MeV (n,γ) cross sections

Target	Exptal $\sigma n\gamma$ (mb)	Author	Calc. $\sigma_{n\gamma}$(mb) statistical model acc. to Naguib	Calc. $\sigma_{n\gamma}$ (mb) acc. D.I. model of Lane and Lynn
^{51}V	0.37 0.49	Csikai Present		.076
^{71}Ga	1.9 1.29	Perkin Present	1.44	0.2
^{75}As	1.39	Present	1.55	0.129
^{127}I	2.5 2.74	Perkin Present	1.20	0,19
^{138}Ba	1.3 1.12	Perkin Present	1.29	0.24
^{141}Pr	3.33 3.00 2.19	Perkin Csikai Present	2.727	0.6

and made a change in their method of obtaining the values of K and y. Naguib et al have proposed an arbitrary energy, E_B, of incident neutrons in the experimental σ vs E_n curve and the value of σ at the point so specified yields his K. But we have shown that it is not necessary to have arbitrary E_B values; instead, one could choose the exact E_B value at the point where the last bump in the σ vs E_n curve disappears for each nucleus, in their $\sigma(n,\gamma)$ vs E_n curves obtained from data accumulated in a single set of experiments of a single laboratory. For this, we have consulted BNL 325 data[4]. In general, Johnsrud et al data (1959) and Stavissky's (1959) data have been compared as instances of a single laboratory's single set of data in the neighbourhood of E_B. Presumably, E_B is a critical energy below which partial wave analysis is possible and at which point g-wave contribution comes in and the synthetic curve for that nucleus becomes exponentially decaying. Above E_B, the classical statistical formula with suitable level density parameter is applied.

Conclusion

We conclude from our comparison of values in Table that it is highly debatable whether at this high energy, $\sigma(n,\gamma)$ is quantitatively given by the classical statistical formula. Certainly the Naguib formula has the character of a statistical formula, but there is no way of checking it, since it contains constants, two of which, x and y are energy independent. Calculation from Perkin's estimation of Γ_γ and Γ_n - the respective width, the values of σ obtained were 10^{-4} orders lower than the experimental ones, while D.I. calculations yield values nearly of the same order of magnitude as the experimental ones, obtained by Perkin and the present author.

References

1. Mitra, B. and Ghose, A.M. - Nucl. Phys. 83, 157 (1966).
2. Naguib, K. and Lukyanov, A. - J. of Nucl.Energy 20, 373 (1966).
3. Lane, A.M. and Lynn, J.E. - 2nd Geneva Conf. Report, 15, 38 (1958).
4. Neutron Cross sections - BNL 325 published by Signa Center, Brookhaven National Laboratory, 2nd Edition (1966).
5. Johnsrud, A.E., Silbert, M.G. and Bnschall, H.H.-Phys.Rev. 116,927(1955).
6. Stavissky, Y.Y. - Atomnaya Energiga 7, 259 (1959).
7. Perkin, J.L., O'Connor, L.P. and Coleman, R.F.-Proc.Phys.Soc. 72,505(1958).
8. Csikai, J., Peto, G., BncZke, M., Milligy,Z, and Eissa, N.A.-Nucl.Phys. A95, 229 (1967)

INTERMEDIATE ENERGY APPROXIMATION OF THE BETHE-HEITLER FORMULA FOR THE BREMSSTRAHLUNG CROSS-SECTIONS

K. Gopala and B. Sanjeevaiah
Department of Physics
University of Mysore
Manasagangotri, Mysore-570006
INDIA

Bremsstrahlung cross section calculations are still attracting attention because of the inadequacy of the existing formulae. The Sommerfeld-Elwert formula holds good upto 0.1 MeV. Bethe and Heitler gave a relativistic expression for the bremsstrahlung cross sections using Dirac's electron theory and Born approximation. Coulomb and screening effects were not included in their calculations. Calculations of the bremsstrahlung cross sections using the B-H formula are tedious. Approximations of the B-H formula in the nonrelativistic and extreme relativistic regions exist. But no such approximation is available in the intermediate energy region. An attempt is made to obtain an approximation of the B-H formula in the intermediate energy region. Several approximations are made to reduce the B-H formula into a polynomial in x, the ratio of the photon energy to the total energy of the incident electron. The coefficients of the polynomial turn out to be a long series of terms which are functions of incident electron energy. The validity of the approximate formula in the intermediate energy region will be discussed.

(Approximation; bremsstrahlung; cross section; electron; intermediate energy; photons.)

Introduction

Calculation of the bremsstrahlung cross section using the Bethe-Heitler (B-H) formula is tedious. Approximations of the B-H formula in the nonrelativistic (NR) and extreme relativistic (ER) regions exist. But no such approximation is available in the intermediate energy regions.

The present paper attempts to arrive at a simple form of the B-H formula by affecting certain approximations to make it hold good in the intermediate energy region.

The B-H formula for the bremsstrahlung cross section, differential in photon energy is given by[1]

$$\frac{d\sigma}{dk} = \frac{\alpha}{x}(Zr_o)^2 \frac{p_2}{p_1}\left\{\frac{4}{3} - \frac{2}{\beta_1^2\beta_2^2}\left(\frac{\gamma_1^2+\gamma_2^2-2}{\gamma_1\gamma_2}\right) + \left(\frac{l_1\gamma_2}{\gamma_1^2-1} + \frac{l_2\gamma_1}{\gamma_2^2-1} + l_1l_2\right) + L\left[\frac{8}{3}+\frac{W^2}{\gamma_1\gamma_2}\left(\frac{1+\beta_1^2\beta_2^2}{\beta_1^2\beta_2^2}\right)+\frac{W}{2\gamma_1\gamma_2}\left(\frac{\gamma_2+\gamma_1\beta_1^2}{\gamma_1\beta_1^2}\right)l_1 - \frac{\gamma_1+\gamma_2\beta_2^2}{\gamma_2\beta_2^2}l_2 + \frac{2W}{\gamma_1\gamma_2\beta_1^2\beta_2^2}\right)\right]\right\} \quad \ldots\ldots (1)$$

where α = fine structure constant = 1/137

Z = atomic number

$r_o = e^2/m_oc^2$ = classical electron radius

$W = k/m_oc^2$ = photon energy in terms of the electron rest energy

$\beta_i = v_i/c$; (i = 1,2) is the velocity of the electron in units of c (subscript 1 refers to the incident electron and subscript 2 refers to the scattered electron)

$\gamma_i = (1 - \beta_i^2)^{-\frac{1}{2}}$; i = 1,2

p_i = momentum; i = 1,2

$$l_i = \frac{1}{\gamma_i\beta_i} \ln\left(\frac{1+\beta_i}{1-\beta_i}\right) ; \quad i = 1,2$$

$$L = \frac{2}{\beta_1\beta_2} \ln\left[\frac{\gamma_1\gamma_2(1+\beta_1\beta_2) - 1}{W}\right]$$

We now write

$$\gamma_2 = \gamma_1(1-x) \qquad \ldots\ldots(2)$$

where $x = W/\gamma_1 = k/E_o$ = photon energy in terms of the total energy of the incident electron

$$\frac{p_2}{p_1} = \frac{\beta_2}{\beta_1}(1-x) \qquad \ldots(3)$$

$$\ln\left[\frac{\gamma_1\gamma_2(1+\beta_1\beta_2)-1}{W}\right] \simeq K + 2\left(1 - \frac{2x}{a}\right) \qquad \ldots(4)$$

where $K = \ln(b)$

$$b = \gamma_1 + \gamma_1\beta_1 + (\beta_1/2\gamma_1)$$

$$a = \left(\gamma_1 + \gamma_1\beta_1 - \frac{1}{\gamma_1} - \frac{\beta_1}{2\gamma_1}\right)/b$$

and $$\ln\left(\frac{1+\beta_2}{1-\beta_2}\right) \simeq 2\left(\beta_2 + \frac{\beta_2^3}{3} + \frac{\beta_2^5}{5}\right) \qquad \ldots(5)$$

The approximation made in (4) underestimates the B-H cross sections in the low photon energy region and overestimates them in the higher photon energy regions. Calculations show that the overall effect of the approximation made in (5) is negligible. With the above relations, equation (1) becomes

$$\frac{k}{z^2}\frac{d\sigma}{dk} = \frac{\alpha r_o^2}{\beta_1}\left[a_o + a_1\beta_2 + a_2\beta_2^2 + a_3\beta_2^3 + a_4\beta_2^4 + a_5\beta_2^5 + \frac{a_6}{\beta_2} + \frac{a_7}{\beta_2^2}\right] \qquad \ldots(6)$$

where a_o, a_1 etc. are functions of β_1 and x i.e. functions of incident electron energy and fractional photon energy. β_2 can be written as,

$$\beta_2 = \left[1 - \frac{1}{\gamma_1^2(1-x)^2}\right]^{\frac{1}{2}} \qquad \ldots(7)$$

using (7), β_2, β_2^3 etc. being expanded binomially upto the term containing $\gamma_1^2(1-x)^6$. Further simplification limiting to the term involving x^4 leads to

$$\frac{k}{z^2}\frac{d\sigma}{dk} = \alpha r_o^2(A_o + A_1x + A_2x^2 + A_3x^3 + A_4x^4) \qquad \ldots(8)$$

where A_o, A_1 etc. are functions of incident energy of the electron only (each of A_o, A_1 etc. comes out to be a long series of terms involving 1_1 and γ_1 which are of course functions of incident electron energy only).

Calculation of the cross sections taking three, four and five terms in equation (8) for various incident electron energies in the region 0.05 to 4.54 MeV shows that the contribution of the fifth term is negligible. So,

$$\frac{k}{z^2}\frac{d\sigma}{dk} \simeq \alpha r_o^2(A_o + A_1x + A_2x^2 + A_3x^3) \qquad \ldots(9)$$

can be taken as the required approximation of the B-H formula in the intermediate energy regions. The coefficients A_o to A_3 vary with γ_1 as shown in Fig. 1. For values of $\gamma_1 \geq 3$ we can approximate the various coefficients as

$$\begin{aligned} A_o &= (18.5 + 0.55\ \gamma_1) \\ A_1 &= -(42 + 0.33\ \gamma_1) \\ A_2 &= (37 + 0.20\ \gamma_1) \\ A_3 &= -(18.0 - 0.20\ \gamma_1) \end{aligned} \qquad \ldots(10)$$

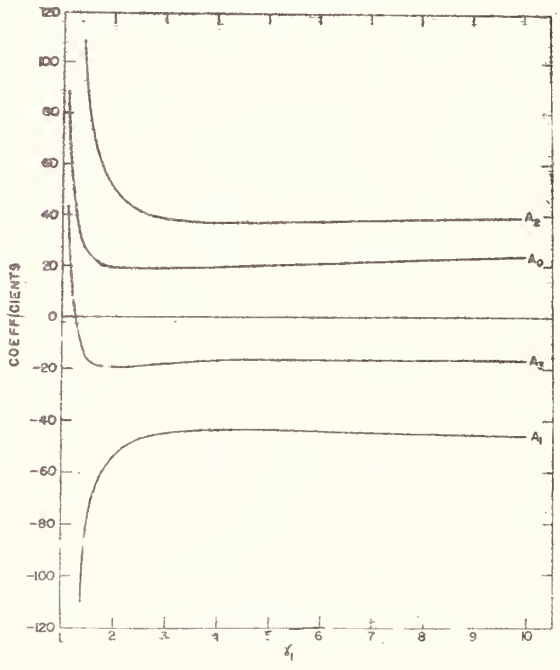

Fig. 1 Variation of the coefficients A_o to A_3 with γ_1.

The cross sections calculated using equation (9) with the coefficients given in (10) are plotted along with those of B-H formula (1) and the experimental results in Figs. 2. The experimental

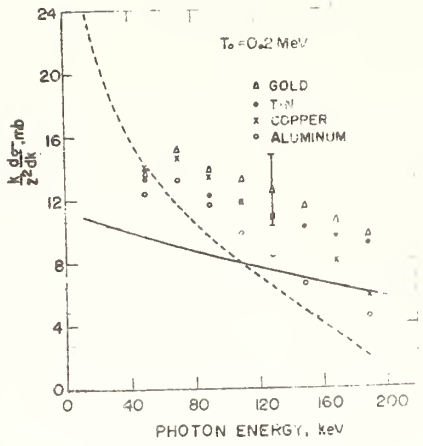

Fig. (a)

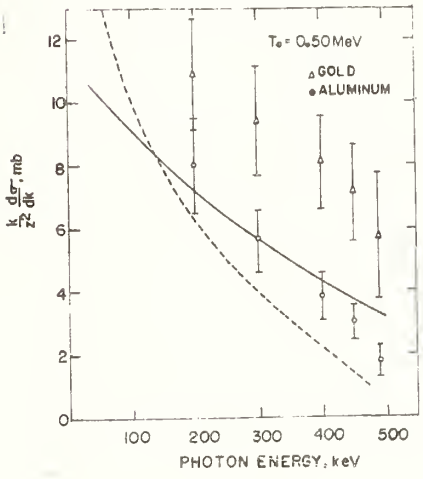

Fig. (b)

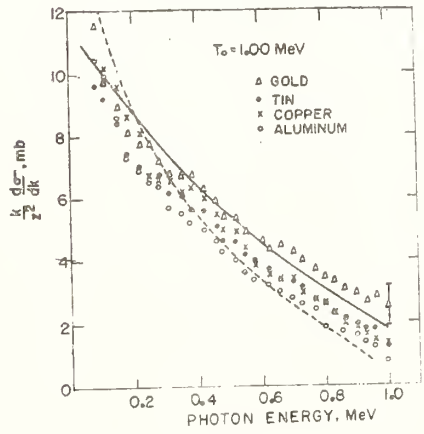

Fig. (c)

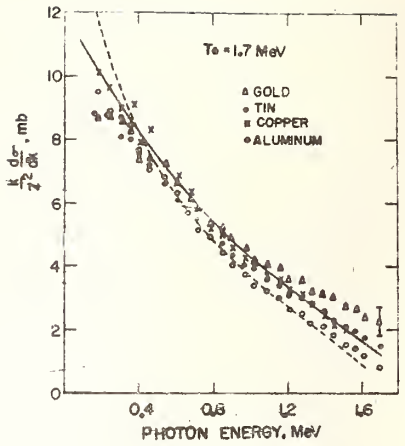

Fig. (d)

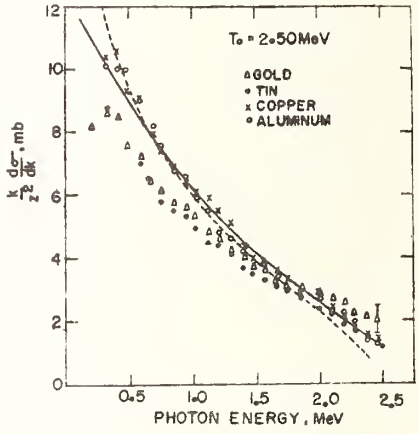

Fig. (e)

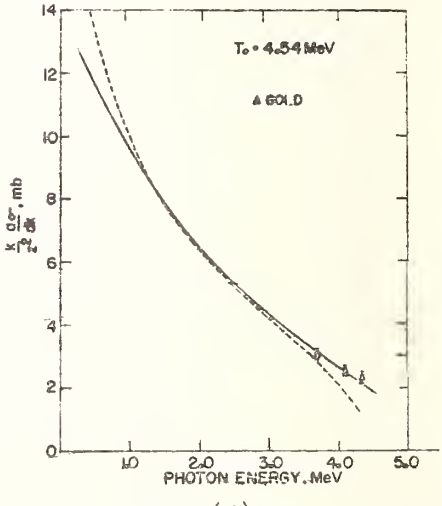

Fig. (f)

Figs.2a to 2f : Bremsstrahlung cross sections as a function of emitted photon energy for different incident electron kinetic energies (T_o). ---- Bethe-Heitler formula, ———— present approximate formula. The points are the experimental data.

results were taken from Motz[2] for 0.5 MeV electrons, from Dance et al[3] for 0.2, 1.0, 1.7 and 2.5 MeV electrons and from Starfelt and Koch[4] for 4.54 MeV electrons. It can be seen from the figures that the approximate formula (9) deviates considerably from the B-H formula for low energy electrons and in low photon energy regions of the spectra.

But the approximation is justified by the fact that it is closer to the experimental data.

References

1. Jauch, J.M. and Rohrlich, F., The Theory of Photons and Electrons, Addison-Wesley Co., Mass., U.S.A., 1955, p.369.
2. Motz, J.W., Phys. Rev. 100, 1560 (1955)
3. Dance, W.E., Rainwater, W.J. and Rester, D.H., Investigation of Electron Interaction in Matter, LTV Research Report No. 0-71000/SR-2 Feb. 1968; see also Rester, D.H. and Dance, W.E., Phys. Rev. 161, 85 (1967).
4. Starfelt, N. and Koch, H.W., Phys. Rev. 102, 1598 (1956).

A NEW METHOD FOR THE MEASUREMENT OF DIFFERENTIAL ELASTIC SCATTERING CROSS SECTIONS OF FAST NEUTRONS*

S. Nath, A. Chatterjee and A.M. Ghose
Nuclear Physics Laboratory
Bose Institute, Calcutta-700009, India

A new method has been described which successfully reduces the problem of low scattering intensity. The scatterer has been taken in the form of a spheriod. The elastically scattered neutrons have been discriminated from the inelastically scattered ones by using multiple bias technique. Experimentally measured values of differential elastic scattering cross sections for sulphur at four angles for 14 MeV neutrons have been presented. The results have also been compared with the optical model prediction.

(Cross section; differential; elastic; multiple bias technique; neutron; scattering).

Introduction

This paper deals with a new method suitable for the measurement of elastic scattering cross sections of fast neutrons over a wide range of incident energy. In the present method, emphasis has been laid on the geometric factors involved in the experimental arrangement[1] so as to avoid two limitations encountered in the usual measurements. The size and shape of the scatterer, predetermined by the design of the experimental set-up, sets out a limit to the intensity of the scattered count. This factor has been carefully considered in designing the experimental set-up. The method also gives an effective way to discriminate between the elastically scattered counts and the non-elastically scattered ones. The method described is an absolute one in the sense that it does not require knowledge of any other related cross section and the final cross section value can be derived from the data obtained in the present experiment alone.

Geometry and Underlying Theory

In this method, as mentioned earlier, the shape of the scatterer plays the most important role. The scatterer is shaped in the form of a surface of revolution obtained by rotating an arc of a circle about the corresponding chord as axis. Fig. 1. depicts section of such a surface truncated at sections AA' and BB', and the positions of the source and detector with respect to it. The distribution of a function directly related to the exposed area of the scatterer plotted against the length (measured along source - detector line) of the scatterer surface, has also been shown in Fig. 2. This function is obtained by theoretical evaluation of scattered intensity to be presented below The length of the scatterer is determined by the necessary aperture to be left to make the entire surface of the scatterer available to neutrons emitted from the target and by the intensity of the scattered beam desired. The length and position of the scatterer (symmetrically placed w.r.t. source and detector), in our set-up, have been confined to the central section of the scatterer intentionally; this is to avoid the steeply rising portion of the curve, inclusion of which would have otherwise made the scattering more critically dependent upon the scattering angle. Referring to fig.1, the number of neutrons scattered elastically towards the detector D can be shown to be,

$$H=\frac{\pi a^2 \nu N_o t}{2^{7/2}\, \ell^2}\cdot\frac{d\sigma_s(\psi)}{d\Omega}\cdot \mathrm{Sec}\psi \tan^4\psi \int_{-f}^{+f} f(x,\psi)\,dx$$

where

$$f(x,\psi)=\frac{(1-x)\left(\sqrt{1+(1-x^2)\tan^2\psi}-1\right)}{\left[1+(1+x)\tan^2\psi\sqrt{1+(1-x^2)\tan^2\psi}\right]}\cdot\frac{1}{\left[1+(1-x)\tan^2\psi-\sqrt{1+(1-x^2)\tan^2\psi}\right]^{3/2}}\cdot\frac{1}{(\sec^2\psi-x^2\tan^2\psi)^{1/2}}$$

*Work carried out under a PL-480 Project sponsored by the National Bureau of Standards, U.S.A.

and

$x = z/l$
$2l$ = source to detector distance
N_o = number of neutrons emitted/sec.
ν = number of scattering nuclei/c.c. of the scatterer
t = radial thickness of the scatterer
a = aperture of the detector
ψ = scattering angle

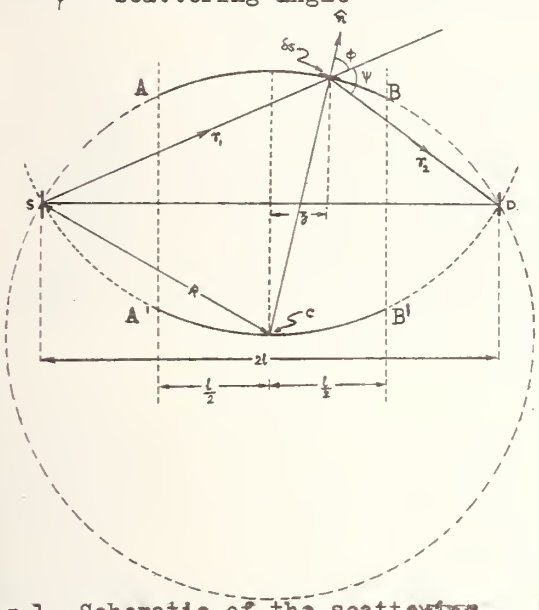

Fig.1. Schematic of the scattering geometry.

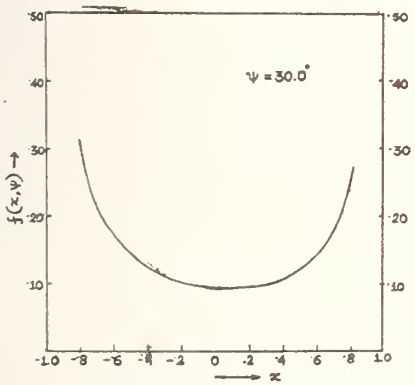

Fig. 2. The intensity function $f(x,\psi)$ between the source and the detector.

The counting rate registered by the detector D, is then given by

$$N = \epsilon \frac{\pi a^2 \nu N_o t}{2^{7/2} l^2} \cdot \frac{d\sigma_s(\psi)}{d\Omega} \tan^4\psi \, \mathrm{Sec}\psi \int_{-f}^{+f} f(x,\psi)\,dx$$

Here, the mean detector efficiency ϵ is assumed to be independent of the spectrum of elastically scattered neutrons (including distortion caused by the multiple scattering effects) while it is zero for neutrons of significantly lower energies. This scattered count is compared against the experimentally measured counts obtained as a difference of counts with and without the shadow bar in position.

Absolute knowledge of ϵ is not necessary, as the expression for the direct count also involves ϵ i.e.

$$n = \epsilon \cdot \frac{N_o}{4\pi} \cdot \frac{\pi a^2}{4 l^2}$$

and this ϵ can be eliminated out by taking the ratio of N to n i.e.

$$\frac{N}{n} = \nu t . \sqrt{2} . \pi . \frac{d\sigma_s(\psi)}{d\Omega} . \mathrm{Sec}\psi \tan^4\psi \int_{-f}^{+f} f(x,\psi)\,dx$$

The count recorded by the detector has to be corrected, as it contains contributions from both elastic and non-elastic events. This has been done by the double bias technique developed in our laboratory. The method consists of recording the counts at two bias levels simultaneously and utilising the relative efficiency vs. energy curves[2] for the corresponding set of biases.

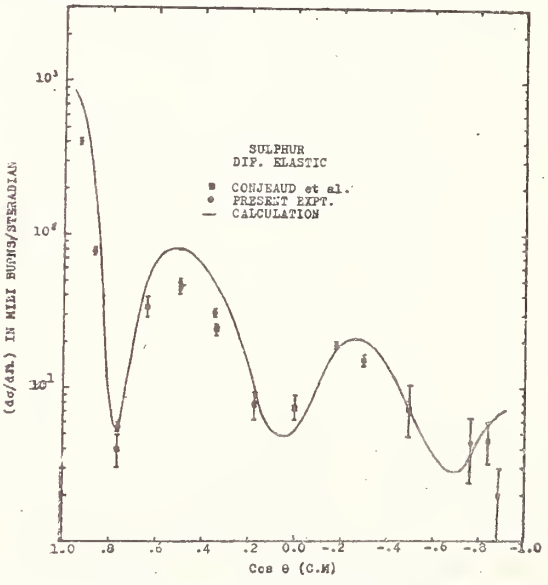

Fig. 3. Differential elastic spectrum of 14 MeV neutrons from sulphur.

Results and Discussions

The differential cross section of sulphur has been measured for 14.8 MeV neutrons at 4 scattering angles 30°, 40°, 60°, 70°. The results have been compared with the experimentally measured data of Conjeaud et al[3] in fig. 3. The experimental values have also been compared with the optical model prediction[4] (fig. 3). This set of average parameters has been obtained by simultaneously analysing all the experimentally measured non-elastic cross section data in our laboratory by Pal, Chatterjee and Ghose[4]. The measured values, though in fair agreement with the other experimentally measured ones, are not so close with the theoretical values obtained with the above mentioned set of parameters. This is probably due to the over-emphasis placed on the non-elastic set of data while arriving at the set of parameters. We are extending the measurements to large angles of scattering.

The authors wish to thank the Director, Bose Institute for his kind interest in this work. One of the authors (S.N.) wishes to thank the Council of Scientific and Industrial Research for awarding him a scholarship which enabled him to carry out this work.

References

1. Ghose, A.M.; Proc. Int. Symp. Rad. Phys., India, 1974 (in press).
2. Chatterjee, A. and Ghose, A.M.; Nucl. Inst. and Methods, 49, 1967.
3. Conjeaud, M.; Fernandez, B., Haror, S., Picord, J. and Souchere, G., Nucl. Phys. 62, 1965.
4. Pal, B., Chatterjee, A. and Ghose, A.M., Proc. Int. Symp. Rad. Phys., India, 1974 (in press).

COMPTON SCATTERING OF 1.12 MeV GAMMA RAYS BY K-SHELL ELECTRONS

P.N. Baba Prasad, G. Basavaraju and P.P. Kane
Physics Department, Indian Institute of Technology
Powai, Bombay-400076

Two sodium iodide counters in coincidence and a twenty channel pulse height analyzer have been used to determine the pulse height distribution of 1.12 MeV gamma rays which are Compton scattered by the K-shell electrons of gold, lead and thorium. The angular variations of the differential cross section ratio, $\frac{d\sigma_K}{d\sigma_F}$, have already been reported. The present measurements were made at 60° and 100° scattering angles. At 60°, lead targets of 30 mg/cm^2 and 143 mg/cm^2 were used. At 100°, targets of gold (13 mg/cm^2), lead (143 mg/cm^2) and thorium (14 mg/cm^2) were used. In all cases, pulse height distributions of false coincidence events were determined and subtracted from the measured distributions in order to obtain the true distributions. A broadening of the K-shell electron Compton peak has been observed. The results of these measurements are discussed.

(Compton scattering; differential cross section; electron binding; gamma rays; K-shell; photons.)

Introduction

In a recent paper[1] where references to the earlier works have been listed, a report has been given regarding the angular variation and the target-Z dependence of the energy integrated cross sections for the Compton scattering of 1.12 MeV gamma rays by K-shell electrons. The energy distributions of 0.662 MeV gamma rays Compton scattered by the K-shell electrons of thin targets have been studied in only a few of the earlier experiments. A broadening of the K-shell electron Compton peak and a peak shift of about 35 keV towards lower energies relative to the free Compton line were observed by Missoni et al[2]. The present work was undertaken in order to provide new information on Compton scattering by K-shell electrons at as high an energy as practicable.

Experimental Methods

Some of the details of our experimental arrangement have been given elsewhere[3]. The pulse height distributions of 1.12 MeV gamma rays Compton scattered by K-shell electrons have been measured at two scattering angles with a coincidence gated twenty channel analyser. At 100°, targets of gold (13 mg/cm^2), lead (143 mg/cm^2) and thorium (14 mg/cm^2) were used. At 60°, only thicker targets of lead (30 mg/cm^2 and 143 mg/cm^2) could be used on account of counting rate considerations. In all cases, pulse height distributions of false coincidence events were determined and subtracted from the measured distributions in order to obtain the true distributions. The usual procedure for the estimation of false events is to record a coincidence spectrum with an aluminium target of a thickness equivalent to that of the given target under consideration. Such a procedure assumes that Z-dependent false events are negligible. The reliability of this procedure has been examined experimentally at 60° as follows. Firstly, the false event spectra were measured with targets of aluminium and copper equivalent to 143 mg/cm^2 lead. For 1.12 MeV gamma rays, the binding energy of the copper K-shell electrons can be considered relatively small. Moreover, on account of the narrow pulse height window used with the x-ray counter, there was a negligible probability of true events due to the copper K-shell electrons being recorded. The integrated false coincidences per hour determined with aluminium and copper targets were 26.30 ± 0.85 and 38.20 ± 1.07 respectively. After subtracting the 'target out' coincidence rate from these numbers and assuming the

---

Work supported in part by a grant from the National Bureau of Standards under the Pl-480 programme.

differences to be proportional in each case to t^2, where t is the thickness of the target, we estimated the corresponding differences for the thinner targets of aluminium and copper equivalent to 30.3 mg/cm^2 lead. Then, with the addition of the 'target out' coincidence rate, the false coincidence rates were calculated to be 18.09 $\pm$ 0.97 and 18.54 $\pm$ 0.97 respectively and, further, were in agreement with the rate 17.83 $\pm$ 0.42 actually measured with a copper target equivalent to the 30.3 mg/cm^2 lead. In view of this agreement, the equivalent aluminium substitution procedure can be seen to be reliable to about 3% in the case of thin targets for the determination of the false coincidence rates. However, the above mentioned data show that the same procedure is unreliable in the case of thick targets. This is an important point to remember during any discussion of several early experiments.

The true pulse height distributions obtained at 60° with the lead (30 mg/cm^2) target and at 100° with the gold (13 mg/cm^2) target are shown in Figs. 1 and 2 respectively. The solid curve in each figure represents the pulse height distribution of single events corresponding practically to scattering from free electrons. There is a noticeable rise in the coincidence spectrum at lower pulse heights. A similar rise was also observed by Missoni et al with 0.662 MeV gamma rays. On the basis of an 'exact' non-relativistic calculation, Gavrila[4] has shown that such a rise is connected with the well-known infrared divergence in quantum electrodynamics. The present measurements also indicate a broadening of the K-shell electron Compton peak. In Fig. 2, a slight shift of the peak towards lower pulse heights is clearly seen. In each case, as expected, there is an appreciable number of scattered photons with energies considerably in excess of that corresponding to Compton scattering from free electrons at rest.

The response of the gamma detector has been determined for several known energies so as to enable the determination of the energy distribution, $d^2\sigma_K/d\,dE'$, of the scattered photons. 1.12 MeV is the highest photon energy at which electron binding effects have been studied so far.

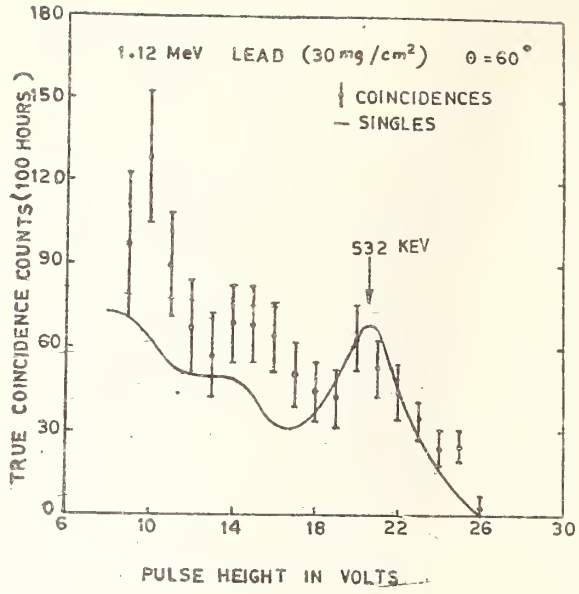

Fig. 1. Pulse height distributions obtained for 1.12 MeV gamma rays for lead at 60°.

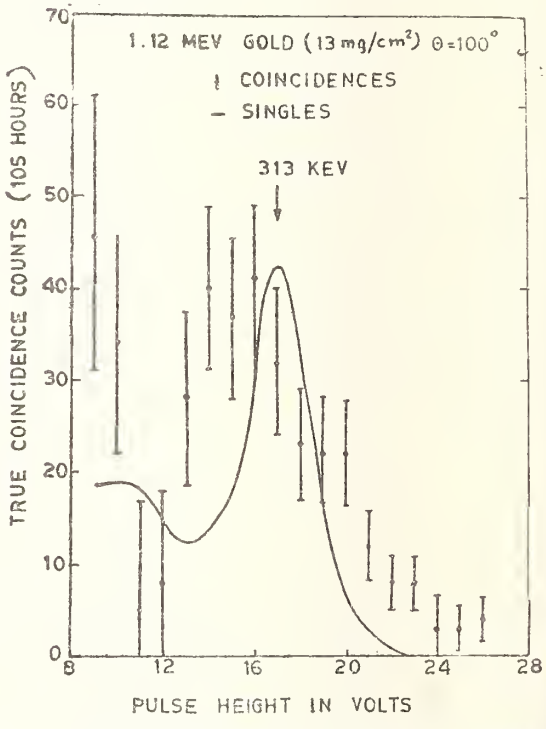

Fig. 2. Pulse height distribution obtained for 1.12 MeV gamma rays for gold at 100°.

References

1. Baba Prasad, P.N. and Kane, P.P. NBS J. Res. 78A, 15 (1974).
2. Missoni, G. and Di Lazzaro, M.A., Istituto Superiore Di Sanita Reports ISS-66/7 and 66/8 (1966) (unpublished).
3. Baba Prasad, P.N. and Kane, P.P., Nuclear Physics and Solid State Physics (India) 12B, 81 (1969) and 13B, 187 (1970).
4. Gavrila, M., Phys. Rev. A6, 1348 (1972).

Discussion

S. Gopal

Is it possible to measure K-shell incoherent scattering cross section at 0^{o} scattering angle in view of the theoretical prediction of non-zero cross section by Whittingham?

P.P. Kane

a) Firstly, it does not seem possible to do this actually at 0^{o}.

b) Gavrila et al have argued that this conclusion of Whittingham is probably an erroneous one.

NUCLEAR THEORY BASED CROSS SECTIONS OF TH-232, TH-233 AND U-233 AND THEIR APPLICATIONS IN REACTOR TECHNOLOGY.

S. B. Garg and Ashok Kumar
Bhabha Atomic Research Centre, Trombay,
Bombay, India.

Thorium fuel cycle is an active subject of research - more so for us since we have large deposits of thorium. Because of various reasons thorium has not found much favour with the reactor technologists and therefore its cross sections have not been studied with the desired accuracy. Cross sections make their impact on reactor design right from its inception to its completion and therefore a coherent study of the cross sections of thorium and uranium-233 has been made. In Reactor Physics studies emphasis is placed on total, fission, capture, elastic and inelastic scattering cross sections. Generally, the measured information on inelastic scattering cross section of heavy nuclides is not sufficient in the MeV energy range for reactor applications. In order to correctly predict the neutron spectrum and its effect on reactor parameters the inelastic cross sections have been evaluated with the local optical and statistical models. The total and elastic scattering cross sections have also been evaluated together with the angular distributions of elastically and inelastically scattered neutrons. Multigroup temperature dependent cross sections have also been generated for thorium and uranium-233 in the entire energy range extending upto 10 MeV.

(Calculation ; cross section ; optical model ; reactor technology; scattering - elastic , inelastic, total ; thorium ; uranium)

Introduction

Thorium fuel cycle is an active subject of research particularly for us since we have large deposits of thorium. Because of various reasons thorium has not found much favour with the reactor technologists and therefore its cross sections have not been studied with the desired accuracy. But, with the upcoming of fast reactor technology in this country thorium is bound to find a place as a fertile material to produce uranium-233. It is, therefore, imperative for us to estimate the cross sections of thorium-232, thorium-233 and uranium-233 in the MeV energy range based on nuclear theory.

In reactor physics studies emphasis is placed on total, fission, capture, elastic and inelastic scattering cross sections. In the high energy region the neutrons lose energy mainly by inelastic collisions and therefore the neutron spectrum, in a fast reactor, is very sensitive to inelastic cross sections. Generally, the measured information on inelastic scattering cross sections of heavy nuclides is not sufficient in the MeV energy range for reactor applications. This information can be generated with the optical and statistical models[1,2,3,4]. For short lived elements such as thorium-233, the fission cross section can be estimated with the channel theory of fission[5,6,7] and the capture cross section can be predicted either with the dipole radiation theory of the compound nucleus[8] or with the direct[9] or semi-direct[10] dispersion theories.

The reactor oriented studies of nuclear cross sections are concerned with the generation of group cross sections

from the basic energy point data. In order to adhere to the spirit of this symposium we shall not discuss this subject in this paper but only concentrate on the analysis of Th-232, Th-233 and U-233 cross sections in the energy range 0.1 MeV to 20.0 MeV.

Optical and Statistical Models

The local optical model with the Saxon-Woods form of the real part, Gaussian form of the imaginary part and Thomas form of the spin-orbit part of the potential has been used in these analyses. The Schrödinger equation is numerically solved to obtain the reflection coefficient which is then used to evaluate the transmission coefficients, shape elastic, compound nucleus and the total cross sections.

The statistical decay of the compound nucleus leads to the calculation of compound elastic, inelastic, (n,2n), (n,p), (n,α) and other energetically possible reaction cross sections. However, the customary application of the statistical model is in the calculation of inelastic cross sections. This model also yields the differential elastic and inelastic cross sections. The relevant formulae for these cross sections are given in reference 11.

The χ^2 Criterion

The six parameters of the optical model potential, namely, U, W, r, a, b and V_{so} are varied in such a way that a minimum value of χ^2 is obtained. A computer programme AUTO, which allows the simultaneous variation of five parameters, has been coupled to another programme ABACUS-2 and the search has been carried out for U, W and r. This search was terminated when the calculated elastic scattering cross sections matched with the measured ones. In this study it was, however, noticed that U and r did not show much variation with energy and therefore to save time they were not varied throughout the entire energy range. The values of V_{so}, a and b were fixed at 7.0 MeV, 0.6 f and 0.6 f respectively.

Calculations

a) Thorium-232 : The local optical model parameters have been derived by obtaining correctly the elastic scattering cross sections in the energy range 0.1 MeV to 15 MeV. Since no measurements have been reported beyond 15 MeV, the model predictions of total, elastic and inelastic cross sections have been extended upto 20 MeV and they are recorded in Table I. The optical model parameters are given below:

$U = 40$ MeV ; $r = 1.32$ f ;
$R_e = (1.32A^{1/3} + 2.0)$f.

(i) $W = 20$ MeV ; $0.1 \leq E \leq 6.0$ MeV.
(ii) $W = 26$ MeV ; $7.0 \leq E \leq 20.0$ MeV.

14 energy levels were used to obtain the level excitation cross sections, but due to space limitation these cross sections are not given in this paper.

b) Uranium-233 : In this case the energy dependence of the parameters was observed to be very weak. The following parameters were chosen for the entire energy range:

$U = 40$ MeV ; $W = 24$ MeV ; $r = 1.32$ f ;
$R_e = (1.32\ A^{1/3} + 2.5)$ f.

The total, elastic and inelastic cross sections are tabulated in Table II. The excitation cross sections were evaluated with 9 energy levels.

c) Thorium - 233 : Because of very short half-life of 22.2 minutes cross section of Th-233 have not been measured. Only the thermal neutron cross section is reported in the literature. The cross sections of Th-233 may be very significant in the production of U-233 when thorium is used as fertile material in high flux fast reactors. The situations in which the neutron captures in Th-233 occur at a faster rate than beta-decay would not be conducive to the production of U-233. Then the capture cross sections of Th-233, in the MeV energy range, assume a special significance. We have calculated the total, shape elastic and compound nucleus formation cross sections with the following optical model parameters:

$U = 40$ MeV ; $r = 1.32$ f ;
$R_e = (1.32\ A^{1/3} + 2.5)$ f.

(i) $W = 20$ MeV ; $0.1 \leq E \leq 6$ MeV.
(ii) $W = 26$ MeV ; $7.0 \leq E \leq 20$ MeV.

Capture and Fission Cross Sections:

The capture and fission cross sections can be estimated in terms of compound nucleus formation cross section by knowing Γ_γ, Γ_f and Γ. Γ_γ is given by the Weiskopf formula[8]. Using Newton's level spacing formula Cameron[12] recently obtained an expression for Γ_γ in terms of the effective total angular momenta of single particle states near the Fermi surface. These momenta are listed by

Newton[13]. Based on this formula and choosing the appropriate values of various parameters we have obtained Γ_γ for Th-233 at 0.1 MeV to be 22.5 MeV. In general, Γ_γ for even-odd nuclei ($Z \geqslant 90$) in the MeV energy region is negligibly small and for Th-233 Cramer and Britt[14] have neglected it in their recent evaluations.

Table I

Total, Elastic and Inelastic Scattering Cross Sections of Th-233.

E (MeV)	$\sigma_t^{(c)}$	$\sigma_t^{(m)}$	$\sigma_e^{(c)}$	$\sigma_e^{(m)}$	$\sigma_{in}^{(c)}$
0.1	10.72	11.65	10.12	10.89	0.34
0.57	6.91	7.29	5.37	5.41	1.36
1.5	6.61	6.55	4.06	3.96	2.37
3.0	7.35	7.60	4.62	4.63	2.54
4.0	7.18	8.00	4.61	5.00	2.40
7.0	5.93	6.25	3.38	3.37	2.20
15.2	5.44	5.70	2.92	2.95	0.98
17.0	5.58	-	3.06	-	0.97
19.0	5.75	-	3.23	-	0.98
20.0	5.82	-	3.30	-	0.98

Table II

Total, Elastic and Inelastic Scattering Cross Sections of U-233

E(MeV)	$\sigma_t^{(c)}$	$\sigma_t^{(m)}$	$\sigma_e^{(c)}$	$\sigma_e^{(m)}$	$\sigma_{in}^{(c)}$
0.1	10.63	11.03	8.06	8.24	0.15
0.5	7.23	7.66	4.82	5.04	0.40
1.0	6.44	6.41	4.81	3.71	0.74
3.0	7.12	7.67	4.35	4.12	1.01
5.0	6.67	7.34	4.16	4.23	1.03
7.0	5.98	6.51	3.36	3.05	0.43
9.0	5.49	5.95	2.85	2.91	0.39
10.0	5.37	5.78	2.75	2.90	0.45
12.0	5.33	5.85	2.71	2.98	0.40
15.0	5.41	5.99	2.87	3.01	0.13
18.0	5.69	-	3.16	-	0.12
20.0	5.89	-	3.34	-	0.13

Γ_f is given by Bohr and Wheeler[15] in terms of the exit fission channels and effective level spacing D. Making use of these expressions at 0.1 MeV, we get D = 0.46 eV and Γ_f = 0.18 eV.

Fujimoto and Yamagnchi[16] have derived an expression for Γ_n/Γ_f in terms of fission threshold and neutron binding energies. Based on these considerations we obtain $\Gamma_n/\Gamma_f \simeq 39$ so that Γ_γ/Γ = .003 and Γ_f/Γ = .024. We now assume that these ratios of reaction widths do not vary with energy and calculate the various reaction cross sections. These cross sections are given in Table III.

Table III.

Reaction Cross Sections of Th-233

E(MeV)	$\sigma_t^{(c)}$	$\sigma_{ce}^{(c)}$	$\sigma_{cn}^{(c)}$	$\sigma_f^{(c)}$	$\sigma_r^{(c)}$	$\sigma_{seat}^{(c)}$
0.1	10.85	7.07	2.88	0.069	0.0086	9.87
0.5	7.13	4.63	2.50	0.060	0.0075	7.06
1.0	6.30	3.57	2.73	0.066	0.0082	6.23
2.0	6.97	3.86	3.11	0.075	0.0093	6.89
3.0	7.33	4.39	2.94	0.071	0.0088	7.26
4.0	7.18	4.45	2.73	0.066	0.0082	7.12
5.0	6.82	4.18	2.64	0.063	0.0079	6.76
6.0	6.40	3.76	2.64	0.063	0.0079	6.34
7.0	5.97	3.28	2.69	0.065	0.0081	5.91
8.0	5.70	3.00	2.70	0.065	0.0081	5.64
9.0	5.51	2.81	2.70	0.065	0.0081	5.45
10.0	5.40	2.69	2.71	0.065	0.0081	5.34
12.0	5.34	2.69	2.65	0.064	0.0079	5.28
15.0	5.41	2.83	2.58	0.062	0.0077	5.35
17.0	5.57	3.00	2.57	0.062	0.0077	5.51
20.0	5.81	3.26	2.55	0.061	0.0076	5.75

Discussion

The simple approach of local optical model used in the cross section calculation of the deformed nuclides Th-232, Th-233 and U-233 appears to be reasonably good. The calculated elastic and total cross sections match with the measured ones at several energy points as can be seen in Tables I and II. The maximum deviation observed between them at some of the energy points is 10% or less which is well within the experimental error. This error can be minimized further if the potential is generated by fitting the experimental data on inelastic and differential elastic cross sections. This approach is quite time consuming and is feasible if there is no restraint on computer time.

The level excitation cross sections of these elements have not been measured in the entire energy range. These calcu-

lations serve to fill this void. The cross sections of Th-233 have not been measured and their evaluation based on various nuclear theories may be of some use in certain applications.

Acknowledgements

Our grateful thanks are due to Shri V.N.Meckoni, Director, Reactor Group for encouraging us throughout the course of this work. Also, we owe our sincere thanks to Dr. P.K. Iyengar, Director, Physics Group fcr suggesting to us to undertake the cross section study of Th-233.

References

1. Feshbach,H., Porter, C. and Weisskopf, V., Phys. Rev. 96, 448 (1952).
2. Hauser, W. and Feshbach, H., Phys. Rev. 87, 366 (1952).
3. Auerbach, E.H., BNL-6562.
4. Moldauer, P., Engelbrecht, C. and Duffy, G., ANL-6978 (1964).
5. Hill, D.L. and Wheeler, J.A., Phys. Rev. 89, 1102 (1953).
6. Strutinsky, V.M., Nucl. Phys. A95, 420 (1967).
7. Vandenbosh, R. and Huizenga, J.R., 2nd UN Intern. Conf. on Peaceful Uses of At. Energy, 15,284 (1958).
8. Blatt, J.M. and Weisskopf,V., Theoretical Nuclear Physics, John Wiley, New York (1952).
9. Lane, A.M. and Lynn, J.E., Nucl.Phys. 11, 646 (1959).
10. Brown, G.E., Nucl. Phys. 57, 339 (1964).
11. Garg, S.B. and Rastogi, B.P., Fast Reactor Physics (IAEA) 1, 339 (1967).
12. Cameron, A.G.W., Can. J. Phys. 37, 332 (1959).
13. Newton, T.D., Can. J. Phys. 34, 804 (1956).
14. Cramer, J.D. and Britt, H.C., Nucl. Sci. Eng. 41, 177 (1970).
15. Bohr, N. and Wheeler, J.A., Phys.Rev. 56, 426 (1939).
16. Fujimoto, Y. and Yamaguchi, Y., Progr. Theoret. Phys. 5, 76 (1950).

THE DEVELOPMENT OF RADIATION SHIELDING STANDARDS IN USA*

D.K. Trubey+
Radiation Shielding Information Center
Oak Ridge National Laboratory
Oak Ridge, Tennessee, 37830, U.S.A.

The American Nuclear Society (ANS) is a standards-writing organization-member of the American National Standards Institute (ANSI). The ANS Standards Committee has a subcommittee denoted ANS-6, Shielding, whose charge is to establish standards in connection with radiation shields, to provide shielding information to other standards writing groups, and to prepare recommended sets of shielding data and test problems. This paper is a progress report of this subcommittee.

(American Nuclear Society, radiation, shielding, standard).

By Standards, we mean voluntary Standards - sometimes called industry Standards - promulgated through the American National Standards Institute (ANSI) consensus procedure whereby all interested parties have an opportunity to comment on and contribute to the content in a manner avoiding any conflict of interest.

The purpose of a Standard is to set forth acceptable practices, procedures, dimensions, material properties, specifications, etc., which have been agreed upon by representatives of a broad segment of the subject activity.

The management organization of Nuclear Standards has accepted a definition propounded by an international standards organization as, first,

"Standardization: The process of formulating and applying rules for an orderly approach a specific activity for the benefit and with the cooperation of all concerned and in particular for the promotion of optimum overall economy taking due account of functional conditions and safety requirements.

It is based on the consolidated results of science, technique, and experience.

It determines not only the basis for the present but also for future development and it should keep pace with progress," and a Standard is "The result of a particular standardization effort approved by a recognized authority."

Our interest here, however, is primarily in American National Standards, of which about 5,000 exist. Perhaps the best known to the lay public are a few PH2 Standards defining the speed of photographic film and C1-1971 which, when given legal stature through adoption by a municipality, is the well-known electrical code.

The organization responsible for promulgating voluntary standards is ANSI. The Institute, a nonprofit corporation, is a federation of leading trade, technical and professional organizations, government agencies and consumer groups. ANSI's principle functions are to coordinate standards development, minimize duplication and overlap, and provide a neutral forum to consider and identify standards needs.

The Institute does not develop standards. It makes use of the combined technical talent and expertise of its member bodies: technical, professional, and trade organizations together with the companies and industrial firms that comprise the Institute. A standards writing organization, such as a technical society, having developed a standard and seeking approval by ANSI, prepares a list of the organizations, companies, and other groups with substantial concern and competence in the scope of the standard and then conducts a canvass of them on approval of the proposed standard. The final results are reported to the ANSI Board of Standards Review for determination that a consensus exists and declaration of the proposed standard as a

*Research sponsored jointly by the U.S. Atomic Energy Commission and Defense Nuclear Agency under contract with Union Carbide Corporation.

+Chairman Shielding Standards Subcommittee, ANS-6, Standards Committee, American Nuclear Society.

voluntary American National Standard.

The standards-writing organization of interest here is the American Nuclear Society (ANS). Among its several administrative committees is one on Standards composed of nearly 30 Subcommittees (see list below). Parenthetically, as presently constituted, the Committee consists of all individuals assigned to Standards tasks within the Society, some 800, and is, obviously, not a working or workable group. There is, therefore, an eleven-member Steering Committee. The ANS Standards Subcommittees are grouped along lines of common interest and assignments under supervision of a Steering Committee member. The Subcommittees, in turn, have established ad hoc Working Groups for preparation of individual Standards:

ANS-1 Performance of Critical Experiments
ANS-2 Site Evaluation
ANS-3 Reactor Operations
ANS-4 Reactor Dynamics and Control
ANS-5 Energy and Fission-Product Release
ANS-6 Shielding
ANS-8 Fissionable Materials Outside Reactors
ANS-9 Nuclear Terminology and Units
ANS-10 Mathematics and Computation
ANS-11 Radioactive Materials Handling Facility and Specialized Equipment
ANS-13 Fuel Assemblies Criteria
ANS-14 Operation of Pulse Nuclear Reactors
ANS-15 Operation of Research Reactors
ANS-16 Isotopes and Radiation
ANS-18 Environmental Impact Evaluation
ANS-19 Physics of Reactor Design
ANS-20 Systems Engineering
ANS-21 PWR Design Criteria
ANS-22 BWR Design Criteria
ANS-23 GCR Design Criteria
ANS-24 LMFBR Design Criteria
ANS-30 Nuclear Power Plant Systems
ANS-31 Engineered Safety Features
ANS-32 Reactor Plant Process Systems
ANS-33 Containment
ANS-34 Radioactive Waste Systems
ANS-35 Fuel Handling and Storage

The subcommittee on shielding standards, ANS-6, now composed of seven working groups, was established in 1964 with the sponsorship of what is now the Shielding and Dosimetry Division of the Society[1]. The standards development of the subcommittee is carried on within working groups composed of members from reactor vendors, architect-engineers, national laboratories, the Atomic Energy Commission, and universities. The goals and accomplishments of the working groups are briefly described below.

ANS-6.1: Shielding Cross Section Standards

Because of the changing state of knowledge of neutron cross sections, no standard is possible with anything near the time constant of the usual standard such as, for example, the classical ASTM code for unfired pressure vessels. At present it is better to think of recommended cross-section sets as reference sets rather than standards. Within ANS-6, "Shielding Cross Sections" has a broad interpretation, which includes neutron interaction cross sections for all common reactions, photon-production cross sections, photon interaction cross-sections, and secondary angular and energy distributions for all these interactions. Since the Evaluated Nuclear Data File (ENDF) represents current reference data, no action in this area seems to be required. The group did recommend in 1970 that the Lawrence Livermore Laboratory evaluated photon interaction cross section set be accepted as reference data and be distributed with the ENDF neutron data.

Current projects include standard flux-to-dose rate conversion factors and reference coupled neutron-gamma-ray multigroup cross sections for the elements normally found in concrete.

ANS-6.2: Benchmark Problems

The primary objective of the benchmark problems effort is to compile in convenient form a limited number of well-documented problems in radiation transport which will be useful in testing computational methods used in shielding.

The compilation and publication of solutions to benchmark problems are expected to accomplish several things: 1) attention will be focused on typical problems where careful work should produce solutions which are representative of the state-of-the-art in solving radiation transport problems, 2) specifications of standard configurations and data will make comparisons of different computational methods and theory-experiment comparisons more meaningful, 3) discrepancies between calculation and experiment may suggest refinements in the numerical approximations or nuclear data, or may suggest new experiments to resolve the disagreement, 4) reliable solutions by several methods will be made available to help judge the precision and efficiency of different computer codes, and to suggest if new codes ought to be developed, 5) newly acquired codes and codes

converted to new machines may be verified by duplication of the benchmark problem solution, and 6) mistakes in existing or new codes, or their options, can probably be detected by independent calculations of the benchmark problems.

Four problem solutions were published in 1969 in loose-leaf form in Ref. [2] by the Radiation Shielding Information Center. Revisions and a new problem were issued as a revision in 1970. Two new problems were recently issued as Suppl. 2 of Ref. [2] and are available from RSIC upon request. They are Neutron and Secondary Gamma Ray Fluence Transmitted Through a Slab of Borated Polyethylene by C.E. Burgart and A Benchmark Experiment and Calculation for Neutron Transport in Thick Sodium by R.E. Maerker et al. The work slowed for a period but now additional problems are being developed including several for typical reactor configurations.

ANS-6.3: Shield Performance Evaluation

The initial goal of this group was attained in 1972 with the publication of Ref. [3]. Shortly after publication, the U.S. Atomic Energy Commission issued a Regulatory Guide[4] based on this standard for research and training reactors. The current goal of the committee is to completely revise Ref. [3] to make it more applicable to current practices in the nuclear power industry.

ANS-6.4: Shield Materials

Initial efforts involving materials per se, e.g., lead as a shielding material, have failed. The current work has produced the draft of a standard, ANSI N403, on the Analysis and Design of Concrete Radiation Shielding for Nuclear Plants. The draft underwent balloting by ANS-6 in September of 1974. The standard is much more general, in many respects, than required for designing concrete shields only. That is, the approach to radiation analysis and the methods recommended can be applied to many shielding analysis problems.

ANS-6.5: Shielding Nomenclature

The effort of this group is directed to the preparation of a list of shielding terms and definitions and maintaining liaison with the Nuclear Terminology and Units Subcommittee (ANS-9). The latter subcommittee is assisting the Nuclear Terminology, Units, Symbols, Identification, and Signals Committee of the American National Standards Institute in the preparation of definitions for the ANSI Glossary of Terms in Nuclear Science and Technology. It is planned to have the special shielding terms and definitions prepared by the ANS-6.5 working group published separately since the list is sufficiently long and specialized to not be included in the glossary covering all of nuclear science. A draft glossary is presently being reviewed.

ANS-6.6: Calculation and Measurement of Direct and Scattered Radiation from Nuclear Power Plants

Organized in late 1973, the group has adopted the following scope:

"This standard will define calculational requirements and measurement techniques for estimates of exposures near nuclear power plants due to direct and scattered radiation from contained sources on site. On site locations outside plant buildings and locations in the offsite unrestricted area will be considered. All sources that contribute significantly to exposure levels will be identified and methods for calculating the source strength of each will be given. This standard specifically excludes radiation from gaseous and liquid effluents. The standard will review the considerations necessary to compute exposures, including component self-shielding, shielding afforded by walls and structures, and scattered radiation. Finally, the requirements for measurements and data interpretation of measurements will be given. This standard will include normal operation and shutdown conditions but will not address accidental or normal operational transient conditions. Nitrogen-16 gamma rays are a prime consideration.

ANS-6.7: Radiation Zoning for Design of Nuclear Power Plants

This group was organized in early 1974 to standardize radiation level zoning in power plants. The tentative goals were 1) definitions of radiation zone designations, 2) maximum and/or average dose rates in each zone, 3) methods for determination of access time to each zone, 4) precautions, posting, survey requirements, access control, and alarms, and 5) responsibility of issuing entry permits for admission to areas of limited access.

Related Standards Work

Most nuclear standards are listed in Ref. [5,6]. Two other organizations writing standards of direct interest to shielding specialists are:

1. American Society for Testing and Materials

ASTM, publisher of the world-renowned Book of ASTM Standards, is the world's largest source of voluntary consensus standards for materials, products, systems and services. Since 1898, the Society - mainly through the intensive activities of standards committees - has conducted vast numbers of investigations and researches leading to a better knowledge of the properties of materials and the development of more than 4400 widely used standards - specifications and methods of testing for materials.

Beginning with the 1974 edition of the Annual Book of ASTM Standards, the Society plans to provide a separate part of volume on ASTM's nuclear related standards. Part 45 of the 1974 Annual Book of ASTM Standards contains all ASTM standards dealing with nuclear materials and materials related to nuclear reactors. There are 104 standards in the book of which 159 are new, revised or changed in status since 1973. Sixty-six have also been approved by ANSI and a number of others by other organizations. The standards in Part 45 cover: concrete products for nuclear applications; graphite products for nuclear applications; metal products for nuclear applications (hafnium, nickel and nickel alloys, steel, tantalum, titanium and titanium alloys, zirconium and zirconium alloys); nuclear grade materials; radiation effects in organic materials; radioactivity; inorganic materials in water; analysis, dosimetry and radiation effects in metals; and temperature measurement.

The ASTM Headquarters staff of 150 is located at 1916 Race Street, Philadelphia, Pa. 19103; William T. Cavanaugh, Managing Director.

2. U.S. Atomic Energy Commission

Under the Atomic Energy Act, the Commission has the responsibility for establishing licensing procedures and regulatory functions for the control of materials and facilities essential to the atomic energy industry. These functions are carried out by a Director of Regulations who reports directly to the Commission. The Director is responsible for the Directorate of Regulatory Operations. The two basic reasons for the regulatory duties of the AEC are to protect the public health and safety, and to promote the common defense and security. Regulations of the AEC are included as parts of Title 10 of the Code of Federal Regulations, and are published in the Federal Register. Regulatory Guides are issued to describe and make available to the public methods acceptable to the AEC Regulatory staff of implementing specific parts of the Commissions's regulations, to delineate techniques used by the staff in evaluating specific problems or postulated accidents, or to provide guidance to applicants. Regulatory Guides are not substitutes for regulations and compliance with them is not required. Methods and solutions different from those set out in the guides will be acceptable if they provide a basis for the findings requisite to the issuance or continuance of a permit of license by the Commission.

Published guides will be revised periodically, as appropriate, to accommodate comments and to reflect new information or experience.

Copies of published guides may be obtained by request indicating the divisions desired to the U.S. Atomic Energy Commission, Washington, D.C. 20545, Attention: Director of Regulatory Standards. Comments and suggestions for improvements in these guides are encouraged and should be sent to the Secretary of the Commission, U.S. Atomic Energy Commission, Washington, D.C. 20545, Attention: Chief, Public Proceedings Staff.

The guides are issued in the following ten broad divisions:

1. Power Reactors
2. Research and Test Reactors
3. Fuels and Materials Facilities
4. Environmental and Siting
5. Materials and Plant Protection
6. Products
7. Transportation
8. Occupational Health
9. Antitrust Review
10. General

The USAEC Division of Reactor Research and Development (RRD) is responsible for the safe development of reactor technology in the U.S. Toward that end, they are concerned with the development of standards covering design, analytical methods, materials, equipment, systems, fabrication, construction, quality assurance, inspection, testing, operation, and maintenance for government-owned civilian water reactors. Toward this end, standards are being prepared, reviewed, reproduced, distributed and revised in order to incorporate latest developments, information, techniques, and experience. This work is being performed under contract to Oak Ridge National Laboratory (ORNL) with the assistance of other AEC offices and contractors as a continuing

activity in this program. The standards program will serve as a base on which to build current and future reactor programs with greater quality assurance and the attendant improvement in reactor reliability and safety. A thorough investigation of records, experience, knowledge, expertise, and evaluation from all available qualified sources is required for the successful attainment of the goals for the standards program. Initial efforts have been directed toward converting available standards into a form that may be used for engineering current (RRD) experimental activities and demonstration reactors and provide usable technical guides for the AEC Directorate of Engineering Standards, Directorate of Licensing, and the Advisory Committee of Reactor Safeguards. ORNL is responsible for overall management of the RDT Standards Program under direction from RRD. Standards are being prepared by ongoing development projects and by ORNL in its specific areas of expertise for which each writer is qualified. Such standards, designated as RDT standards, are also listed in Ref. [5].

References

1. Claiborne, H.C., Dudziak, D.J. and Schaeffer, N.M., Activities of the ANS-6 Subcommittee on Radiation Shielding Standards, ORNL-TM-3271 (1970) Oak Ridge National Laboratory.
2. Profio, A.E., Editor, Shielding Benchmark Problems, ORNL-RSIC-25 (ANS-SD-9) (1969; Suppl. 1, 1970; Suppl. 2, 1974), Oak Ridge National Laboratory.
3. Program for Testing Biological Shielding in Nuclear Power Plants, ANSI N18-9-1972 (1972), American Nuclear Society, 244 E. Ogden Avenue, Hinsdale, Ill., USA.
4. Shield Test Programs for Evaluation of Installed Biological Shielding in Research and Training Reactors, Regulatory Guide 2.1 (1973), U.S. Atomic Energy Commission, Washington D.C., USA.
5. Catalog of Nuclear Industry Standards (1974), American National Standards Institute, Inc., 1430 Broadway, New York, N.Y. 10018.
6. Standards in Nuclear Science and Technology, a Bibliography, TID-3336 (1973). Available from National Technical Information Service, Springfield, Va., 22151.
7. Part 45, Nuclear Standards, 1974 Annual Book of ASTM Standards, Publication Code No. 01-045074-35,

Discussion

Shanker Singh

The shielding requirements for the two types of Fast reactor concepts namely Loop type and Pool type reactor being different, are there any specific experiments being conducted or planned for either of these concepts and if so which concept is being pursued more vigorously?

D.K. Trubey

Experiments at Oak Ridge are in support of the US LMFBR program which employs the pool concept.

A.K. Gangully

1. Do you measure the scattered spectrum in open air below 0.21 MeV as given in the table?
2. Do you still have a programme of investigations on Multilayer shields?

D.K. Trubey

1. Not with sodium iodide detectors, but measurements at lower energies are made with Ge (Li) detectors.
2. Many of the experiments are with multilayer shields which mock-up particular systems. For example, iron-polyethylene and iron-sodium systems have been studied.

INTEGRAL EQUATION METHODS IN RADIATION TRANSPORT

D. V. Gopinath
Health Physics Division
Bhabha Atomic Research Centre
Bombay - 400085

This paper presents a review of the work done on the development of integral equation methods for different problems in radiation transport. The cases considered are:(i) Three-dimensional (XYZ) geometry and (ii) One dimensional time-dependent transport for the transport of (a) Charged particles and (b) Optical radiation. The methods are developed for arbitrary degree of anisotropy, and their simplification in the case of isotropic scattering are discussed. Few typical results are presented and the advantages of integral equation methods are discussed.

(Integral equation ; radiation ; semi-numerical ; scattering; transport)

Introduction

In this paper we present a semi-numerical technique for the solution of radiation transport problems. The methods developed here are applicable to energy dependent radiation transport with arbitrary degree of anisotropy in scattering. The purpose of the paper is to give a brief review of the work done in our group on integral equation methods for such problems. This is also intended to present a unified formulation for most problems in radiation transport and to show that any variation in the treatment for different types of problems are only marginal.

Mathematical Formulation

Basic equations:

The essential feature of the approach that is followed here is to separate the spatial and energy-angle transmission in radiation transport. Whence, the transport can be represented as

$$\phi(\vec{r},E,\vec{\Omega},t) = \iiint dt'd\Omega',dr' \; S(\vec{r}',E,\vec{\Omega}',t') \times T(E,\vec{\Omega}'\rightarrow\vec{\Omega},\vec{r}'\rightarrow\vec{r},t'\rightarrow t). \quad .. \quad (1)$$

$$S(\vec{r},E,\vec{\Omega},t) = \iint dE',d\Omega' \; \phi(\vec{r},E',\vec{\Omega}',t) \; G(\vec{r},E'\rightarrow E,\Omega'\rightarrow\Omega) + S'(\vec{r},E,\vec{\Omega},t) \quad .. \quad (2)$$

where

$\phi(\vec{r},E,\vec{\Omega},t)$ = radidation flux at $(\vec{r},E,\vec{\Omega},t)$

$S(\vec{r},E,\Omega,t)$ = radiation source at $(\vec{r},E,\Omega,t)$

$T(E,\vec{\Omega}'\rightarrow\vec{\Omega},\vec{r}'\rightarrow\vec{r},t'\rightarrow t)$ = spatial transmission kernel

$G(\vec{r},E'\rightarrow E,\vec{\Omega}'\rightarrow\vec{\Omega})$ = energy-angle transmission kernel

$S(\vec{r},E,\vec{\Omega},t)$ = external source.

In the above formulation, eqn.(1) represents transmission of radiation through space and eqn.(2) accounts for what happens at a spatial point during the collision. In obtaining the solution for the above equations, we have two options:(i) develop the solution for the most general case and obtain the simplifications for particular problems, (ii) obtain the solution for a simple system and introduce modifications for more general cases.

While the first approach is definitely more elegant and scholarly, the second method has the advantage of being simpler and easy to follow. We adopt the second approach.

The simplest case is that of time-independent radiation transport in one-dimensional slabs. This problem has already been worked out in detail and published elsewhere[1-3]. However for the sake of completeness and to introduce the broad principles of our approach, I start with this case. Further, in our formulation, we consider only gamma rays and neutrons. Towards the end we deal with the changes needed for other types of radiation.

One dimensional slabs:

In one dimensional slab geometry eqns.(1) and (2) simplify to (cf.Fig.1).

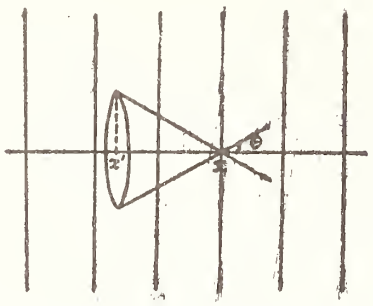

Fig.1. Pictorial representation of spatial transmission of radiation in one dimensional geometry.

$$\phi(x,E,\mu) = \int S(x',E,\mu)\ T\ (E,\mu,\vec{x}'\rightarrow x)dx' \qquad .. \quad (3)$$

$$S(x,E,\mu) = \iint \phi(x,E',\mu')\ G\ (x,E'\rightarrow E, \vec{\Omega}'\rightarrow\vec{\Omega})d\Omega',dE' + S'(x,E,\mu) \qquad .. \quad (4)$$

and

$$T(E,\mu,x'\rightarrow x) = \frac{e^{-\sum(E)(x-x')/\mu}}{|\mu|} \qquad (5)$$

$$G(x,E'\rightarrow E,\vec{\Omega}'\rightarrow\vec{\Omega}) = \sum_x(E'\rightarrow E)\delta\{\vec{\Omega}.\vec{\Omega}', \xi(E,E')\}$$

$$.. \quad (6)$$

where

$$\xi(E,E') = 1 - \frac{0.51}{E'} + \frac{0.51}{E} \quad \text{for } \gamma\text{-rays}$$

$$= \frac{M+1}{2}\sqrt{\frac{E}{E'}} - \frac{M-1}{2}\sqrt{\frac{E'}{E}} \quad \text{for neutron}$$

elastic scattering. M is the target mass. For inelastic scattering of neutrons

$$G(x,E'\rightarrow E,\vec{\Omega}'\rightarrow\vec{\Omega}) = \sum_x(E'\rightarrow E)\sum_n \sigma_n(x)P_n(\Omega'.\Omega)$$

Throughout our formulation we use discrete ordinate representation in μ' and x for spatial integration and legendre polynomial approximation in μ for the evaluation of collision integral[1]. Whence we obtain

$$\phi^k(x_i,E_g,\mu_e) = \sum_j S^k(x_j,E_g,\mu_e)T(g,l,j-i)$$

$$\phi_n^k(x_i,E_g) = \sum_l \phi^k(x_i,E_g,\mu_l)P_n(\mu_l)W_{nl}$$

$$S_n^{k+1}(x_i,E_g) = \sum_{g'}\phi_n^k(x_i,E_g)G(n,g'\rightarrow g) + S'_n(x_i,Eg)$$

$$S^{k+1}(x_i,E_g,\mu_l) = \sum_n S_n(x_i,E_g)P_n(\mu_l)$$

$$.. \quad (7)$$

where k is the iteration index. Starting with $S'(x_i,E_g,\mu_l)$, the set of equations are solved iteratively till they are self-consistent within a preset criterion.

Spherical Geometry

In this case, only the geometry differs from the earlier one. As such, equation describing the collision process remains unaltered.

Referring to fig. 2., the spatial transmission equation for spherical systems can be written as (for a given energy),

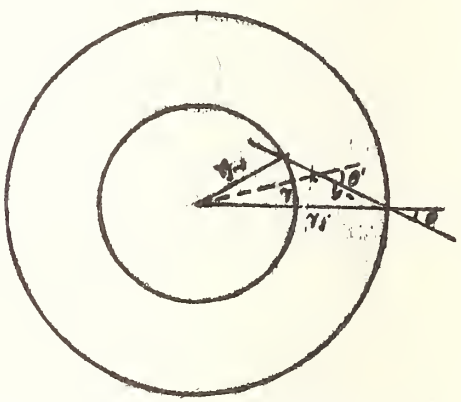

Fig.2. Pictorial representation of spatial transmission of radiation for spherical system.

$$\phi(r_j,\mu_l) = \iint S(r',\mu')\ T\ (r'\rightarrow r,\mu'\rightarrow\mu_l)\ d\mu',dr'. \qquad .. \quad (8)$$

and $T(r' \to r,\ \mu' \to \mu_1) = e^{-\Sigma y(r)}$

$$\left(-\frac{dy}{dr}\right)\delta\left\{\mu', \sqrt{1-r_j^2/r^2(1-\mu_1^2)}\right\} \quad ..(9)$$

where

$$y(r) = r_j\mu_1 \pm \sqrt{r^2 - r_j^2\,(1-\mu_1^2)} \quad \text{for } \mp\,\mu \qquad ..(10)$$

using exp.(9) in exp.(8) and with the discretization of space as in the slab case exp.(8) becomes, for

$$\phi(r_j,\mu_1) = \phi(r_{j-1},\mu(r_{j-1}))e^{-\Sigma y(r_{j-1})} + \int_0^{y(r_{j-1})} S(r,\mu(r))e^{-\Sigma y}\,dy \quad ..(11)$$

Writing

$$S(r,\mu(r))\Big|_{j,j-1} = S(r,\mu(r_{j-1})) + \frac{\Delta S}{\Delta r}\Big|_{j,j-1}(r-r_{j-1})$$

the integral in exp.(11) will be

$$\frac{1}{\Sigma}\left\{S(r_j,\mu_1) - S(r_{j-1},\mu(r_{j-1}))e^{-\Sigma y(r_{j-1})}\right\} + \frac{\Delta S}{\Sigma\Delta r}\int_0^{y(r_{j-1})} \frac{y-r_j\mu_1}{\sqrt{y^2-2yr_j\cdot\mu_1+r_j^2}}\,e^{-\Sigma y}\,dy \qquad .. (12)$$

The integral in exp.(12) cannot be integrated analytically. However one can note that the integrand contains the generating function for Legendre polynomials. Hence, expanding this, the integral can be obtained as fast converging series. Denoting this integral as g and combining exp.(11) and (12) (for μ + ve)

$$\phi(r_j,\mu_1) = \frac{S(r_j,\mu_1)}{\Sigma} + \left\{\phi(r_{j-1},\mu(r_{j-1})) - \frac{S(r_{j-1},\mu(r_{j-1}))}{\Sigma}\right\}e^{-\Sigma y(r_{j-1})} + \frac{\Delta S}{\Sigma\Delta r}\Big|_{j,j-1}\cdot g \qquad .. (13)$$

On exactly same lines it can be shown that for μ - ve

$$\phi(r_j,-\mu_1) = \frac{S(r_j,\mu_1)}{\Sigma} + \left\{\phi(r_{j+1},\mu(r_{j+1})) - \frac{S(r_{j+1},\mu(r_{j+1}))}{\Sigma}\right\}e^{-\Sigma y(r_{j+1})} + \frac{\Delta S}{\Sigma\Delta r}\Big|_{j,j+1}\cdot g \qquad .. (14)$$

Having thus obtained expressions for flux in terms of source, further procedure is the same as that of slab geometry. We go through the same iterative scheme till the final solution is obtained.

Next, before going to multi-dimensional geometry, we shall discuss one-dimensional time-dependent radiation transport. Of these the slab case is of little practical interest and only the spherical case is presented here.

Time-dependent Radiation Transport in Spherical Systems.

As in the stationary case, even here the equation accounting for the change during collision does not alter. (This is strictly true only if we neglect metastable states of target nuclei and delayed neutron emission. However this assumption is not a serious restriction). The spatial transmission equation will be (cf.Fig.3):

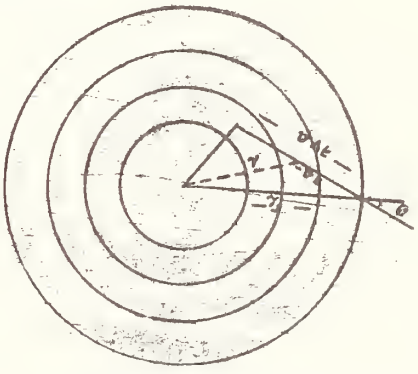

Fig. 3. Pictorial representation of time-dependence of radiation transport in spherical systems.

$$\phi(r_j,\mu_1,t_k) = \iiint dt,d\mu,dr.\,S(r,\mu,t)\ x\ T(r\to r_j,\ \mu\to\mu_1,\ t\to t_k) \qquad .. (15)$$

and

$$T(r\to r_j,\mu\to\mu_1,t\to t_k) = e^{-\sum y}\left(-\frac{dy}{dr}\right)\cdot$$

$$\delta\left\{\mu,\sqrt{1-r_j^2/r^2(1-\mu_1^2)}\right\}\delta\left\{t-t_k\cdot\frac{y(r)}{v}\right\} \quad ..(16)$$

where y(r) is, as before, given by eqn.(10).

Introducing exp.(16) in (15), because of the 'δ' functions in exp.(16), we can either integrate over μ and t and obtain the final expression as an integral over r or integrate over r and μ to have the final expression as an integral over t. Integrating exp.(15) over t and μ

$$\phi(r_j,\mu_1,t_k) = \int_0^{y(r_{j-1})} S(r,\mu(r),t_k-\frac{y(r)}{v})e^{-\sum y(r)}dy$$

$$+ \phi(r_{j-1},\mu(r_{j-1}),t_k-\frac{y(r_{j-1})}{v})e^{-\sum y(r_{j-1})} \quad .. \quad (17)$$

Alternately, integrating exp.(15) over r and μ

$$\phi(r_j,\mu_1,t_k) = \int_{t_k}^{t_{k-1}} S(r(t),\mu(t),t)e^{-\sum v(t_k-t)}$$

$$d(t_k-t) + \phi\left\{r(t_k-1),\mu(t_k-1),t_{k-1}\right\}$$

$$e^{-\sum v(t_k-t_{k-1})} \quad ... \quad (18)$$

where

$$r(t)=\sqrt{v^2(t_k-t)^2-2v(t_k-t)r_j\mu+r_j^2} \quad ... \quad (19)$$

$$\mu(t)=\frac{v(t_k-t)-r_j\mu_1}{r(t)}$$

Expressions (17) and (18) are exactly equivalent. However in evaluating exp. (17) one has to remember fluxes at all points for times earlier than t_{k-1}. In case of exp.(18), it is necessary to know the fluxes and sources only at t_{k-1}. Purely from the causal considerations, this is also the necessary and sufficient information to compute the fluxes and sources at t_k. Hence we deal only with exp.(18) in the sequel.

Making the transformation $t' = t_k - t$, the integral in exp.(18) becomes

$$\int_0^{\Delta t} S\left\{r(t_k-t'),\mu(t_k-t'),t_k-t\right\} e^{-\sum vt'}dt'$$

.. (20)

To evaluate exp.(20), as before we use linear interpolation between spatial, directional and time modal values of source. Within the range of integration o to Δt, r(t) in exp.(20) may not be within r_j and r_{j-1} but may fall between different spatial nodes. Hence the range of time integration is subdivided at t_1, t_2 etc. such that (cf.exp.6).

$$vt_i^2 - 2vt_i\, r_j\, \mu_1 + r_j^2 = r_{j-1}^2$$

$$\text{or} \quad t_i = \frac{1}{v}\left\{r_j\mu_1 \mp \sqrt{r_{j+i}^2 - r_j^2(1-\mu_1^2)}\right\} \text{ for } \pm\mu_1$$

.. (21)

and the maximum of i given by

$$I_{max} = \frac{r_j\mu_1 \pm \sqrt{v^2\Delta t^2 - r_j^2(1-\mu_1^2)}}{\Delta r} \text{ for } \mp\mu_1$$

.. (22)

With this subdivision, S in exp.(20) in the interval t_i and t_{i+1} can be written as

$$S_{j-i,\mu k} - \frac{\Delta S}{\Delta t}\Big|_{k,k-1}^{j-i}.t' + \frac{\Delta S}{\Delta r}\Big|_{j-i,j-i+1}^{k}.\left\{r(t_k-t') - r_{j-i}\right\}$$

$$- \frac{\Delta^2 S}{\Delta t.\Delta r}\Big|_{j-i,j-i+1}^{k,k-1}.t'\left\{r(t_k-t')-r_{j-i}\right\}$$

.. (23)

Taking only upto first order differential terms of exp.(23) in (20), completing the integration and using it in exp.(18)

$$\phi(r_j,\mu_1,t_k) = \phi\{r(t_{k-1}),\mu(t_{k-1}),t_{k-1}\} \cdot e^{-\sum v.\Delta t}$$

$$+\sum_i \left[\left\{ \frac{S_{j-i,\mu',k}}{\sum} + \frac{S_{j-i+1,\mu',k} - S_{j-i,\mu',k}}{\sum^2} (e^{-\sum y_i} - e^{-\sum y_{i+1}})\right\}\right.$$

$$- \frac{\Delta s}{\Delta t}\int_{k,k-1}^{j-i} (\frac{y_i}{\sum} + \frac{1}{\sum^2})e^{-\sum.y_i}$$

$$\left. - (\frac{y_{i+1}}{\sum} + \frac{1}{\sum^2}) e^{-\sum y_{i+1}}\right\}\Big] \quad .. (24)$$

where

$$y_i = r_j\mu_1 \pm \sqrt{r_{j\pm i} - r_j^2(1-\mu_1^2)} \text{ for } \mp \mu_1 \quad .. (25)$$

Having thus obtained the expression for flux in terms of source, we go back to the main iteration scheme. One difference to be noted in this case would be that the index k in eqn.(7) refers to time and not the iteration number.

Next, we consider the multi-dimensional systems. In this, the two dimensional case (finite cylinder) will be discussed in detail by my colleague in another paper in this symposium. Hence, I will skip that case and go directly to three- dimensional systems.

Stationary Radiation Transport in three dimensional systems.

Here we discuss only 3-dimensional cartesian systems and as before we assume discrete ordinate representation in X,Y,Z cordinates. The basic equations in this case would be

$$\phi(R,E,\vec{\Omega}) = \int S(R;E,\vec{\Omega}\,)\, T(\vec{\Omega},R'\rightarrow R)dR \quad .. (26)$$

$$S(R,E,\vec{\Omega}) = \iint \phi(R,E;\Omega')G(R,E'\rightarrow E,\vec{\Omega}'\rightarrow\vec{\Omega}) \cdot dE'd\Omega' + S'(R,E,\Omega) \quad .. (27)$$

where $R \rightarrow R(x,y,z)$

Referring to Fig.4, the flux at a given space point will be computed in 26 directions corresponding to 26 adjacent modal points. Thus flux at k,j,k due to sources

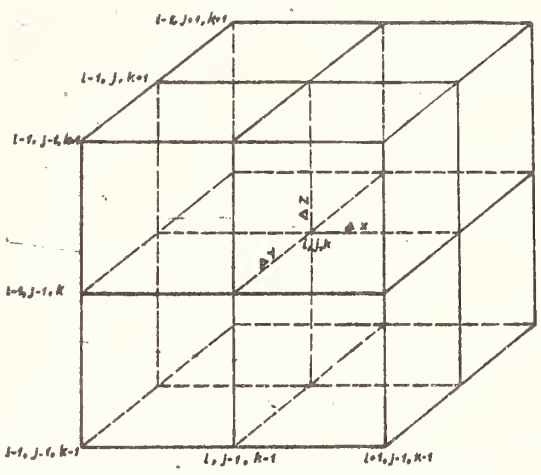

Fig.4. Pictorial representation of radiation transport in three dimensional cartesian system.

along x axis is

$$\phi_{i-1,j,k}.e^{-\sum.\Delta x} + \int_{(i-1)\Delta x}^{i.\Delta x} S(x',y_j,z_k)e^{-\sum.(x_j-x')}\,dx'$$

$$= (\phi_{i-1,j,k} - \frac{S_{i-1,j,k}}{\sum} e^{-\sum.\Delta x} + \frac{S_{i,j,k}}{\sum} + \frac{\Delta s}{\sum^2 \Delta x}\Big|_{i,i-1}^{j,k} (1-e^{-\sum.\Delta x}) \quad .. (28)$$

and this flux will be in the direction

$$\mu = o, \quad = \cos^{-1}\frac{\Delta x}{\sqrt{\Delta x^2 + \Delta y^2}}$$

Similarly flux due to sources along y axis is

$$(\phi_{i,j-1,k} - \frac{S_{i,j-1,k}}{\sum}) e^{-\sum.\Delta x} + \frac{S_{i,j,k}}{\sum} + \frac{\Delta s}{\sum^2.\Delta y}\Big|_{j,j-1}^{i,k} (1-e^{-\sum\Delta y}) \quad .. (29)$$

and so on.

In general, we can represent the flux equation as

$$\phi_{i,j,k}\left\{\frac{k'\Delta z}{\Delta R}, \frac{i'\Delta x}{\sqrt{\Delta x^2+\Delta y^2}}\right.$$

$$=\phi_{i-i',j-j',k-k'}\left\{\frac{k'\Delta z}{\Delta R}, \frac{i'\Delta y}{\sqrt{\Delta x^2+\Delta y^2}^2}\right\} e^{-\Sigma r}$$

$$+\sum^{i'}\left\{S_{i,j,k} - S_{i-i',j',k'}.e^{-\Sigma\Delta x} + \frac{\Delta s}{\Sigma\Delta x}\Big|_{i,i-i'}^{k,j}(1-e^{-\Sigma\Delta x})\right\}$$

$$+\sum^{j'}\left\{S_{i,j,k} - S_{i,j-j',k}.e^{-\Sigma\Delta y} + \frac{\Delta s}{\Sigma\Delta y}\Big|_{j,j-j'}^{i,k}(1-e^{-\Sigma\Delta y})\right\}$$

$$+\sum^{k'}\left\{S_{i,j,k} - S_{i,j,k-k'}e^{-\Sigma\Delta z} + \frac{\Delta s}{\Sigma\Delta z}\Big|_{k,k-k'}^{i,j}(1-e^{-\Sigma.\Delta z})\right. \quad .. (30)$$

where

$$\Delta R = \sqrt{\Delta x^2+\Delta y^2+\Delta z^2}^2 \;;$$

$$r = \sqrt{i'.\Delta x^2+j'.\Delta y^2+k'.\Delta z^2} \quad .. (31)$$

and i',j',k' can have values 1,0 or -1. It is evident that in this case the flux will not have any azimuthal symmetry. Hence, to evaluate the collision integral we express the angular dependence of the flux in terms of Associated Legendre polynomials. Writing

$$\phi(x_i,y_i,z_k,\Omega,E_g) = \sum_m \sum_n \phi_n^m(i,j,k,g)P_n^m(\mu)\text{Cos } m\varphi \quad .. (32a)$$

$$S(x_i,y_j,z_k,\Omega, E_g) = \sum_n \sum_m S_n^m(i,j,k,g)P_n^m(\mu)\text{Cos } m\varphi \quad ..(32b)$$

the main iteration scheme described in eqn.(5) get modified, as :

$$\phi_{i,j,k,g}(\mu,\varphi) = \sum_{i',j',k'} S_{i',j',k',g}(\mu,\varphi) \cdot T(\mu,\varphi,i'\to i,j'\to j,k'\to k) \quad ..(33a)$$

$$\phi_n^m(i,j,k,g) = \sum_{m'}\sum_{n'}\phi_{i,j,k,g}(\mu_{n'},\varphi_{m'}) P_n^m(\mu')\text{Cos } m\varphi_{m'} \times w_{m,n,m;n'} \quad ..(33b)$$

$$S_n^m(i,j,k,g)=\sum_{g'}\phi_n^m(i,j,k,g)G(n,g'\to g) \quad ..(33c)$$

$$S_{i,j,k,g}(\mu,\varphi)=\sum_n\sum_m S_n^m(i,j,k,g) P_n^m(\mu)\text{Cos } m\varphi \quad ..(33d)$$

It may be noted that ϕ and S in eqn.(32) with their 6 subscripts would need enormous computer memory even for modest mesh number. However in actual computation the angular fluxes and sources need to be remembered only at two space points at a time and the information is actually retained in S_n^m and ϕ_n^m.

Charged particles

As charged particle transport will be discussed in detail in another paper by my colleague in this symposium, I will only briefly outline the major differences.

In the case of charged particles we consider two types of interaction with the media:

1) Coulomb
2) Catastrophic collisions

Though Coulomb interaction can also be considered as collision, because very

small angle and energy change per such collision and very large number of such collisions per unit track length, it is better to treat this phenomenon as to continuous process. Thus, the charged particle can change its direction and lose energy continuously along its track even without any collision. To take into account such changes in energy and direction our first equation describing the spatial transmission modifies to

$$\phi(R,E,\vec{\Omega},) = \int_{\Omega}\int_{R}\int_{E'} S(R',E,\Omega')$$

$$T(E'\rightarrow E,\Omega'\rightarrow\Omega,R'\rightarrow R)dR'd\Omega',dE' \quad ..(34)$$

However if we are considering heavy particles the directional change is negligible and the eqn.(34) simplifies to

$$\phi(R,E,\vec{\Omega}) = \int_{R}\int_{E} S(R',E',\vec{\Omega})$$

$$T(\vec{\Omega},R'\rightarrow R,E'\rightarrow E)dR'dE' \quad ..(35)$$

where

$$T(\Omega,E'\rightarrow E,R'\rightarrow R) = e^{-\Sigma(R-R')}$$

$$\delta\{R-R',\ \xi(E,E') \quad ..(36)$$

The function $\xi(E,E')$ in exp.(36) is obtained by the relation

$$R - R' = \int_{E'}^{E} \frac{1}{dE/dx}\, dE$$

Because of the δ function in exp.(36), eqn.(35) can again be expressed as an integral over space only. Beyond this point, the treatment is essentially the same as in the case of non-charged radiation. As I mentioned earlier, the details will be discussed in another paper.

Optical Radiation

The three characteristics that make optical radiation transport different from others are:

1) Energy decoupling in the collision,
2) non-linearity of the system,
3) polarisation status of the radiation.

In optical radiation we are mostly concerned with Rayleigh scattering which is coherent. That is, energy (or wavelength) of the radiation does not change during scattering. Hence our second equation which accounts for the collision process reduces to

$$S(x,E,\mu) = \int\phi(x,E,\mu')\sigma(\Omega'\rightarrow\Omega)d\Omega'+S'(x,E,\mu) \quad .. (38)$$

Of course, to be exact there is an indirect energy coupling in exp.(38) through S'. S'(x,E,μ), which accounts for the emission of radiation is a function of temperature at x, which in turn depends on the absorption of radiation of all energies. However for the case planetary radiation, with which we are interested S' does not contribute to the wavelengths of our interest.

Further, for Rayleigh scattering

$$\sigma(\Omega'\rightarrow\Omega) = \sigma(\mu_o) = \sigma_o + \sigma_2 p_2(\mu_o) \quad ..(39)$$

using exp.(39) in exp.(38), in our formulation, the source eqn. further reduces to

$$S_o(x,E) = \sigma_o \phi_o(x,E)$$

$$S_1(x,E) = o$$

$$S_2(x,E) = \sigma_2 \phi_2(x,E) \quad .. (40)$$

For the intensities of our interest, the system could be non-linear. That is the radiation intensity may be sufficient to change the characteristics of transport medium while this may pose a serious problem in other methods, in the present approach it is handled in a natural way. In our main iteration scheme (cf.eqn.5) each iteration corresponds to a collision generation. Hence the only change necessary would be to have T and G matrices, which are dependent on medium properties, as a function iteration number. Of course, evaluation of the change in the media can be very much involved but that is an input for this problem.

Any analysis of optical radiation transport is not complete unless we consider the polarisation status of the radiation. Even in this case, equation governing the spatial transmission does not change. But equation governing the collision process does alter. Following Chandrasekhar[4], we specify the polarisation status of the radiation by the vectors

$$\bar{S} \rightarrow \bar{S}\ (S_l, S_r, u_1, v_1)$$

$$\bar{\phi} \rightarrow \bar{\phi}(\phi_l, \phi_r, u_2, v_2)$$

Then, to take into account the change in polarisation during scattering, instead of eqn.(40) we will have the matrix eqn.

$$\bar{S} = |P|.\bar{\phi}.$$

where the elements of the matrix $|P|$ are given by Chandrasekhar[4].

References

1. Gopinath, D.V. and Santhanam,K., Nucl.Sci.Eng.,43, 186 (1971).
2. Gopinath,D.V. and Santhanam, K., Nucl.Sci.Eng.,43, 197 (1971).
3. Gopinath, D.V., Santhanam, K. and Burte, D.P., Nucl.Sci.Eng.,52,494 (1973).
4. Chandrasekhar,S., Radiative Transfer, Dover (1948) P.25-42.

NEUTRON TRANSPORT PROBLEMS IN SPHERICAL GEOMETRY

D. C. Sahni
Reactor Engineering Division
Bhabha Atomic Research Centre
Bombay - 400085

The density transform method has been extended to cover spherically symmetric neutron transport problems. The density transform is expanded in plane geometry normal modes and explicit singular integral equations are derived for the expansion coefficients. The method is thus an extension of Case's method of singular eigen-functions to spherical geometry problems. The Green's function approach for transport problems in spherical geometry has been considered. It is shown that the reduction operators used in this method can solve only some of the problems in the interior of a solid homogeneous sphere.

(Density transform ; expansion coefficient ; Green's function ; neutron ; spherical ; symmetric ; transport)

Introduction

Analytical solutions of neutron transport equation have been obtained only for the narrow class of one dimensional plane geometry problems by using singular eigen-function technique of Case[1]. Straight forward extension of Case method to spherical and cylindrical geometries is not possible because in these cases Boltzmann equation is not translationally invariant.

In this paper we present a generalization of the density transform method for solving one speed spherically symmetric transport problems with isotropic scattering. The method consists of defining suitable integral transforms of the total flux (density) which satisfy the plane geometry transport equation in transform variables. This gives an expression for the total flux (and hence the angular flux) in terms of plane geometry singular eigen-functions, the expansion coefficients being determined as the solution of a singular integral equation. Finally we examine the Green's function approach for spherical geometry problems as given by Case et al[2]. These authors have introduced the expansion coefficients which are related to ones arising in the density transform method. However, the singular integral equations derived by them are not correct because of the use of reduction operator. This can be seen most readily from their expression of linear extrapolation distance in spherical Milne problem which is independent of the radius of the black sphere, contrary to the well known result of Davison[3]. We indicate the procedure for deriving the correct equations using the boundary values of a sectionally holomorphic function related to their definition of expansion coefficients.

Density transform method

We consider one speed spherically symmetric Boltzmann equation with isotropic scattering and isotropic source density $Q(r)$, in which angular flux $\Psi(r,\mu)$ depends only on the radial distance 'r', measured in units of mean-free-path, and 'μ' the cosine of the angle between the position vector $\vec{r}$ and the direction of motion of the neutron.

$$\mu \frac{\delta\Psi(r,\mu)}{\delta r} + \frac{1-\mu^2}{r} \frac{\delta\Psi}{\delta\mu} + \Psi(r,\mu) = \frac{c}{2}\rho(r) + \frac{Q(r)}{2} \quad .. (1)$$

'c' is the mean number of secondaries per collision and the total flux (density) $\rho(r)$ is given by

$$\rho(r) = \int_{-1}^{1} \Psi(r,\mu)\, d\mu \quad .. (2)$$

The transport equation (1) is to be solved for range $a \leq r \leq b$ and $-1 \leq \mu \leq 1$, subject to the prescribed incoming distributions $\Psi(a,\mu)$; $o \leq \mu \leq 1$ and $\Psi(b,\mu)$; $-1 \leq \mu \leq o$. It is seen that equation (1) can be integrated to the following form

$$\Psi(r,\mu) = \Psi\left(a, \sqrt{1-r^2(1-\mu^2)/a^2}\right)\exp\left(-\mu r + \sqrt{a^2-r^2(1-\mu^2)}\right) + \frac{1}{2}\int_a^r \frac{y[c\rho(y)+Q(y)]dy}{\sqrt{y^2-r^2(1-\mu^2)}} \cdot \exp\left(-\mu r + \sqrt{y^2-r^2(1-\mu^2)}\right) \quad .. (3a)$$

$$\text{if } \sqrt{1-a^2}/r \leq \mu \leq 1$$

and $\Psi(r,\mu) = \Psi(b, -\sqrt{1-r^2(1-\mu^2)/b^2})$.

$$\exp\left(-\mu r - \sqrt{b^2-r^2-(1-\mu^2)}\right)$$

$$+ \frac{1}{2} \int_r^b \frac{y[c\,f(y) + Q(y)]dy}{\sqrt{y^2 - r^2(1-\mu^2)}} \exp\left(-\mu r - \sqrt{y^2-r^2(1-\mu^2)}\right) + \Psi(\mu) \exp(-\mu r)$$

$$\int_r^r \frac{y[c\,f(y) + Q(y)]dy}{\sqrt{y^2-r^2(1-\mu^2)}} \operatorname{Cosh}\left(\sqrt{y^2-r^2(1-\mu^2)}\right) \qquad \text{.. (3b)}$$

Thus $\Psi(r,\mu)$ can be determined once the density $f(r)$ is determined. Integrating equations (3a) and (3b) we find that $f(r)$ is the solution of the integral equation

$$r\,f(r) = \frac{1}{2} \int_1^\infty \frac{ds}{s} \int_a^b y[c\,f(y) + Q(y)] \cdot$$

$$[\exp(-s|y-r|) - \exp(-s\sqrt{y^2-a^2} - s\sqrt{r^2-a^2})]dy$$

$$+ a^2 \int_o^1 \mu' \Psi(a,\mu') \exp\left(a\mu' - \sqrt{r^2-a^2-(1-\mu^2)}\right) d\mu' -$$

$$b^2 \int_{\sqrt{1-a^2/b^2}}^1 \mu' \Psi(b,-\mu') \frac{\exp(-b\mu' - \sqrt{r^2-b^2(1-\mu'^2)})}{\sqrt{r^2-b^2(1-\mu'^2)}} d\mu' +$$

$$2 \int_1^\infty \frac{ds}{s} \operatorname{Cosh}(sr) \int_b^\infty x(r') r' \exp(-sr') dr'$$

.. (4)

where the function $x(r)$ is related to the incoming angular flux $\Psi(b,-\mu)$; $\mu > o$ at the outer surface of the shell $a \leq r \leq b$ by the equation

$$\Psi(b,-\mu) = \int_b^\infty \frac{x(r')r'dr'}{\sqrt{r'^2 - b^2(1-\mu)}} \exp(-b\mu - \sqrt{r'^2 - b^2(1-\mu^2)}) \qquad \text{.. (5)}$$

We define the density transforms $\phi(r,\mu)$; $r \in (a, b)$; $\mu \in (-1,1)$ by the equation for $\mu > o$

$$\phi(r,\mu) \exp(r/\mu) = \frac{1}{2\mu} \int_a^r y[c\,f(y) + Q(y)] \exp(y/\mu)\, dy + \frac{a^2}{\mu^2} \int_o^1 \mu' \Psi(a,\mu') \exp(a\mu') I_o\left(\frac{a}{\mu}\sqrt{1-\mu^2}\sqrt{1-\mu'^2}\right) d\mu'$$

$$- \frac{1}{2} \int_a^b K(\mu,y)\, y[c\,f(y) + Q(y)]\, dy - \frac{1}{\mu} \int x(r')\, r' \exp(-r'/\mu)\, dr' - \frac{b^2}{\mu^2} \int_{\sqrt{1-a^2/b^2}}^1 \Psi(b,-\mu') \exp(-b\mu') I_o\left(\frac{b}{\mu}\sqrt{1-\mu^2}\sqrt{1-\mu'^2}\right) \mu'\, d\mu'$$

.. (6a)

while for $\mu < o$

$$\phi(r,\mu) \exp(r/\mu) = -\frac{1}{2\mu} \int_r^b y[c\,f(y) + Q(y)] \exp(y/\mu)\, dy - \frac{1}{\mu} \int_b^\infty x(r')\, r' \exp(r'/\mu)\, dr'$$

.. (6b)

where

$$K(\mu,y) = \frac{1}{\mu^2}\int_{\mu}^{1}\frac{d\mu'}{\mu'^2}\left[\mu^2\delta(\mu'-\mu) + \frac{a\mu\, I_1\left(a\sqrt{1/\mu^2 - 1/\mu'^2}\right)}{\sqrt{\mu'^2-\mu^2}}\right]\exp\left(-\sqrt{y^2-a^2}/\mu'\right) \quad .. (7)$$

Then it is seen from equation (4) that

$$r\,\rho(r) = \int_{-1}^{1}\phi(r,\mu)\,d\mu \quad .. (8)$$

From the equation (6a),(6b) and (8) it can be shown that $\phi(r,\mu)$ satisfies plane geometry transport equation

$$\mu\frac{\delta\phi}{\delta r} + \phi(r,\mu) = \frac{c}{2}\int_{-1}^{1}\phi(r,\mu)d\mu + \frac{rQ(r)}{2} \quad .. (9)$$

Thus $\phi(r,\mu)$ and hence $\rho(r)$ can be obtained by carrying out an expansion in terms of full range $\pm\nu_0$; $-1 \leqslant \nu \leqslant 1$ Case's singular eigen functions. This gives the following representation for $\rho(r)$.

$$r\,\rho(r) = a_{o+}\exp(-r/\nu_0) + a_{o-}\exp(r/\nu_0) + \int_{-1}^{1}A(\nu)\exp(-r/\nu)d\nu + \frac{1}{2N_{o+}}\int_a^b r'Q(r')dr'\left[\exp(-|r-r'|/\nu_0) - \exp(-|r+r'|/\nu_0)\right] + \int_0^1\frac{d\nu}{2N_\nu}\int_a^b r'Q(r')dr'\left[\exp(-|r-r'|/\nu) - \exp(-|r+r'|/\nu)\right] \quad .. (10)$$

$N_{o\pm}$ and N_ν are the normalization constants while the unknown coefficients $a_{o\pm}$ and $A(\nu)$ have to be determined by applying the following boundary conditions ; $\mu > 0$

i) $$\phi(a,\mu)\exp(a/\mu) = \frac{1}{2}\int_a^b K(\mu,y)y\left[c\rho(y)+Q(y)\right]dy - \frac{1}{\mu}\int_b^\infty x(r')r'\exp(-r'/\mu)dr' + \frac{a^2}{\mu^2}\int_0^1\mu'\psi(a,\mu')\exp(a\mu')I_o\left(\frac{a}{\mu}\sqrt{1-\mu^2}\sqrt{1-\mu'^2}\right)d\mu' - \frac{b^2}{\mu^2}\int_{\sqrt{1-a^2/b^2}}^1\mu'\,\psi(b,-\mu')\exp(-b\mu')I_o\left(\frac{b}{\mu}\sqrt{1-\mu^2}\sqrt{1-\mu'^2}\right)d\mu'$$

ii) $$\phi(b,-\mu)\exp(-b/\mu) = \frac{1}{\mu}\int_b^\infty x(r')r'\exp(-r'/\mu)dr' \quad .. (11)$$

This gives the following singular integral equations for determining the coefficients $a_{o\pm}$ and $A(\nu)$. For $\nu\varepsilon(o,1)$.

$$\left[1-\frac{c\nu}{2}\int_{-1}^{1}\frac{dt}{\nu-t}\right]A(\nu)e^{-a/\nu} + \frac{c\nu}{2}\int_{-1}^{1}\frac{\nu'A(\nu')e^{-a/\nu'}}{\nu'-\nu}d\nu' = \phi(a,\nu) - \frac{c\nu_0}{2}\left[\frac{a_{o+}e^{-a/\nu_0}}{\nu_0-\nu} + \frac{a_{o-}e^{a/\nu_0}}{\nu_0+\nu}\right] + \frac{c\nu_0}{4N_{o+}}\int_a^b r'Q(r')e^{-r'/\nu_0}dr'\left[\frac{e^{-a/\nu_0}}{\nu_0-\nu} - \frac{e^{a/\nu_0}}{\nu'+\nu}\right] - \int_0^1\frac{c\nu'd\nu'}{4N_{\nu'}}\int_a^b r'Q(r')e^{-r'/\nu'}dr' \times\left[\frac{e^{-a/\nu'}}{\nu'-\nu} - \frac{e^{a/\nu'}}{\nu'+\nu}\right] \quad ... (12)$$

while for $\nu \in (-1,0)$

$$\left[1-\frac{c\nu}{2}\int_{-1}^{1}\frac{dt}{\nu-t}\right]A(\nu)e^{-b/\nu}+\frac{c\nu}{2}\int_{-1}^{1}\frac{\nu' A(\nu')e^{-b/\nu'}}{\nu'-\nu}d\nu'$$

$$=\phi(b,\nu)-\frac{1}{2}\left[a_{0+}+\frac{1}{N_{0+}}\int_{a}^{b}r'Q(r')\sinh(r'/\nu_0)\right]\times\frac{c\nu_0 e^{-b/\nu_0}}{\nu_0-\nu}$$

$$-\frac{c\nu_0 a_{0-}e^{b/\nu_0}}{2(\nu_0+\nu)}-\int_{0}^{1}\frac{c\nu' e^{-b/\nu'}}{2(\nu'-\nu)}\frac{d\nu'}{N_{\nu'}}\times\int_{a}^{b}r'Q(r')\sinh(r'/\nu')\,dr' \qquad \ldots (13)$$

These equations can also be derived from the Green's function approach of Case et al. They have shown that for interior problem (when a = 0) the angular flux $\psi(r,\mu)$ in the sphere of radius 'b' is given by

$$\Psi(r,\mu)=\psi_q(r,\mu)+\frac{a^{<}_{0+}}{\nu_0}\phi(i/\nu_0,r,\mu)+\int_{0}^{1}A_{<}(\nu)\,\phi(i/\nu,r,\mu)\,d\nu/\nu \qquad .. (14)$$

where

$$\phi(i/\nu,r,\mu)=\int_{-1}^{1}\left[P\frac{c\gamma}{2(\gamma-t)}+\lambda(\gamma)\delta(\gamma-t)\right]e^{-\frac{r}{\nu}\mu t}\,I_0\left(\frac{r}{\nu}\sqrt{1-\mu^2}\sqrt{1-t^2}\right)dt \qquad .. (15)$$

$$\lambda(\gamma)=1-\frac{c\gamma}{2}\int_{-1}^{1}P\frac{dt}{\gamma-t} \qquad .. (16)$$

and

$$A_{<}(\nu)=\frac{i}{4\pi\nu^3}\left[\frac{T_1^{*}(i/\nu)}{\Lambda^{-}(i/\nu)}-\frac{T_1^{+}(i/\nu)}{\Lambda^{+}(i/\gamma)}\right] \qquad .. (17)$$

$$a^{<}_{0+}=\frac{iT_1(i/\nu_0)}{2\nu_0\Lambda^{-}(i/\nu_0)}\;;\;a^{<}_{0-}=\frac{i\,T_1(-i/\nu_0)}{2\gamma_0\Lambda^{+}(-i/\nu_0)} \qquad .. (18)$$

i.e. the expansion coefficients of equation (14) are related to the difference in the boundary values of the sectionally holomorphic functions $T_1(k)$ and $\Lambda(k)$ of the complex variable k having branch cuts from $(-i\infty, -i) \cup (i, i\infty)$. $\Lambda(k)$ in addition, has two simple poles at $\pm i/\nu_0$. The function $T_1(k)$ depends upon the angular flux $\Psi(b,\mu)$ on the surface r = b

$$T_1(k)=-b^2\int_{-1}^{1}\mu'\,\Psi(b,\mu')d\mu'\sum_{n=0}^{\infty}1^n(2n+1)P_n(\mu')\,\xi_n^{(1)}(kb)\int_{-1}^{1}\frac{P_n(t)dt}{1+ikt} \qquad .. (19)$$

$\xi_n^{(1)}(kb)$ being the Hankel functions of of first kind. By proving that the function $\varphi_{<}(k)$

$$\varphi_{<}(k)=\frac{2i}{k}\left[\int_{-1}^{1}\frac{\nu'A(\nu')e^{b/\nu'}d\nu'}{1+ik\nu'}+\frac{\nu_0 a^{<}_{0+}e^{b/\nu_0}}{1+ik\nu_0}+\frac{\gamma_0 a^{<}_{0-}e^{-b/\nu_0}}{1-ik\nu_0}\right]-\frac{T_1(k)e^{-ikb}}{\Lambda(k)} \qquad \ldots (20)$$

vanishes everywhere and using Plamely formulae[4] for the boundary values of a sectionally holomorphic function we obtain the same equation as obtained by the density transform method above. Similarly we have also treated the other problem, considered by Case et al, the exterior problem ($b\to\infty$) with same conclusions.

References

1. Case, K.M., Ann. Phys.(N.Y.)2,1(1960).
2. Case, K.M., Zelazny, R. and Kanal, M., J.Math. Phys., 11 223(1970).
3. Davison, B., Proc.Phys. Soc.Lond., 64, 981 (1951).
4. Muskhelishvilli, N.I., Singular Integral Equations; Noordhoff, Groningen, Holland.

TRANSPORT OF NEUTRONS DURING REACTOR TRANSIENTS

Sushil K.Kapil
Reactor Engineering Division
Bhabha Atomic Research Centre
Bombay-400085,
INDIA

The study of time dependent behaviour of nuclear reactors is important from operational and safety considerations. In this paper, situations requiring an explicit time dependent solution of the transport equation are identified. The range of validity of the approximation methods in different situations is discussed. Finally, severe transients in a Fast-Thermal coupled reactor are computed with various commonly used approximations and also by an explicit time-dependent solution of the Boltzmann equation, using a set of computer codes which were specially developed for the purpose. It is shown that the commonly used approximate methods can lead to erroneous results. The reasons for the deviation of the solutions for the different approximations from the correct behaviour of the reactor under transient are discussed.

(Approximations ; fast-thermal couple reactor ; neutron ;reactor transients ; solution ; time-dependent ; transport ; transport equation).

Introduction

The behaviour of neutrons in a reactor is described in detail by the linearised Boltzmann equation. Analytical solution of this equation for situations of practical interest is not possible at present and various approximations have to be used. Time dependent Diffusion Equation is one of the most commonly used approximations. It is quite satisfactory for most situations encountered in the dynamic studies with spatial effects.But a consequence of this approximation is that the effect of a disturbance anywhere in the reactor is instantaneously felt at all points i.e. the transport time for neutrons is zero (though the diffusion time is not). Diffusion approximation is therefore satisfactory for power excursions where neutron transport delays do not play a significant role.

Approximate Methods

Some of the other commonly used approximations are given below:

Point Kinetics

In the 'point' approximation[3] the parameters for use in the equation determining power variation are obtained on the basis of initial flux and adjoint distributions. During an excursion in a large or coupled reactor appreciable change in flux and adjoint distributions can take place. The integral quantities defined in terms of initial distributions would be inaccurate. In such a system point kinetics equation cannot be expected to be accurate.

Adiabatic Approximation

In this approximation[1,2] the flux is factorised into shape and time functions, the shape function is taken to be step wise constant in time. Although this is more accurate than the point kinetics approach the use of a static calculation for shape function involves the assumption that the flux changes adjust instantaneously everywhere to all perturbations made in the system. This could be valid only if the time derivative of shape function is small and the flux distribution reaches its asymptotic value within a span short compared to that for any significant change in power level. Furthermore, this approximation does not distinguish between the shapes of prompt and delayed neutron sources and thus neglects the time lag in the adjustment of the delayed neutron precursor distribution. If the power excursion produces any variations in spatial flux distribution, the adiabatic approximation cannot account for it. Spatial dependence of this type has been studied elsewhere and is not considered here.

Quasi-static Method

This method[3] lies between the time dependent diffusion equation and the adiabatic approximation since it includes a term for time derivative by

first order backward difference. This method also avoids the error due to the neglect of the lag in delayed neutron precursor distribution which is found directly from flux history.

Exact Method

It is 'exact' to the extent that the Boltzmann equation is solved without any of the above assumptions and it can be used as a touch-stone for validity of these assumptions. A DS_n solution of the time-dependent Boltzmann equation is taken as 'exact' here.

Computer Codes

A system of computer codes was developed[4] which permits solution of the time-dependent neutron transport equation in various approximations discussed above as well as by the 'exact' method. The delayed neutron effect and feedbacks have not been utilised in the present study because it is intended to study only the space dependent effects arising mainly due to the neutron transport.

System Model

The system chosen for this study is similar to the one described by Avery and Toppel[5] for a coupled fast-thermal steam superheating reactor. It consists of a central steam cooled fast core and surrounded by a water cooled and moderated thermal region. To prevent thermal peaking at the boundary of the fast core the two are separated by a buffer region. The thermal region is then surrounded by a thermal blanket and a high density uranium blanket. The region dimensions and core compositions are shown in Table I.

The calculations are performed in spherical geometry with an appropriately derived four energy group structure.

Calculation of Reactor Transients

The transient is induced in the fast core by a linear increase in the number of neutrons emitted per fission and totalling 5% over a period of 0.1 msec, after which it stabilises at the final value. Total reactivity change caused by this is 4.66% .

Rather than applying various approximations in the conventional manner, the effects of these approximations are simulated directly as discussed below:

A. Basic assumption of 'point' kinetics is that all the subsequent behaviour of the system can be described in terms of the initial flux and adjoint distribution. In Fig.1, Curve A shows the inverse of the

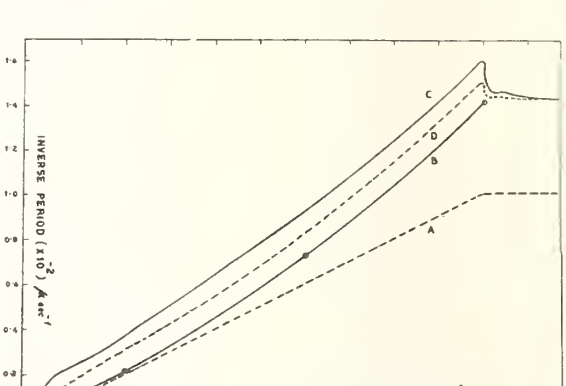

Fig.1. Plot of inverse of the period of power rise against the fraction of the ramp obtained from various approximation methods.

Table 1

Region No.	1	2	3	4	5
Region	Fast Core	Buffer	Thermal Core	Thermal Blanket	Uranium Blanket
Outer Radii	35 cm.	40 cm.	52 cm.	58 cm.	98 cm.
Material					
PuO_2	.08556	-	-	-	-
$U^{238}O_2$	.37369	.42016	.29456	.29611	-
$U^{235}O_2$	.00075	.00084	.00214	.00059	-
Depleted U	-	-	-	-	.3715
Fe	.156	.157	-	-	-
Zr	-	-	.4151	.4151	.4372
H_2O	.014131	.01553	.2087	.2087	.1350

period of the power rise against the fraction of total addition due to the ramp, for this situation.

B. For adiabatic approximation sequential shape calculations are made in w-mode (solution of Boltzmann equation with inverse period as an eigen-value). The results are shown by Curve B. The circles on the curve are the check points calculated by a statics code. The ramp insertion in fast region reduces its dependence on thermal region for criticality and the effective prompt neutron lifetime for the system reduces[6]. Therefore, the inverse period curve deviates from Curve A as more and more reactivity is added to the fast part. Curve A does not take account of this fact and is significantly wrong as the excursion proceeds.

C. The curve marked C shows the 'exact' space-time solution for the transient. The curve shows the upward curvature as in Curve B but the inverse period is significantly higher.

During the ramp the inverse period is higher for Curve C than for Curve B due to the 'bottling' of low energy neutrons in the thermal core. They are produced in the thermal core by moderation of fast neutrons created in fission and by those coming from the fast core. Fast neutrons from the fast core can travel to the thermal region in time short compared to that for significant rise in power. On the other hand, the low speed neutrons cannot travel far out from their place of birth in the corresponding time. Thus finally a dynamic equilibrium is reached with the neutron density higher in the thermal region compared to what it would have been under the adiabatic assumption (Curve B). A plot of the difference in the fission density distribution between the adiabatic approximation (Case B) and the space-time (Case C) calculations also shows that thermal neutrons which are dynamically trapped in the thermal region during the transient, are permitted to spread (majority of which are lost by capture in surrounding region) in the adiabatic approximation. The same fact is shown by a softer spectrum in the thermal region for Case C during the ramp than for Case B. In the 'exact' calculation this trapping leads to higher fission density in the thermal part and a higher contribution to reactivity due to it. On the other hand, feed back of the thermal neutrons to the fast core is reduced leading to some loss in over-all reactivity. Since in this system the fast core contributes most of the reactivity and drives the thermal core, this loss is small and there is a net over-all gain. In a system where the return of thermal neutrons to the fast core is very important for maintaining the chain reaction, the effect could be opposite. When reactivity becomes constant and flux transients have died, it is known that the asymptotic inverse period would be the w-mode solution of the Boltzmann equation. Therefore, at the end of the ramp, the inverse period quickly drops to that for the adiabatic case. Physically, it corresponds to a redistribution of neutrons.

D. Finally, if the reactivity is added to the system infinitely slowly so that at any time the flux distribution in space is in quasi-static equilibrium for the reactivity at that instant the adiabatic approximation and the 'exact' method should coincide. To check this, the same reactivity is added at half the ramp rate in the 'exact' calculation. The result of the calculation is Curve D in Figure 1. It is seen that for a lower ramp rate the inverse periods are closer to the adiabatic case curve. A plot of fission density distribution for this case confirms that the differences observed between Curves B and C are due to the reasons mentioned.

Conclusions

The spatial effects in reactor power transients may arise due to changes in region and spectral coupling, delayed neutron precursors' lag, loose coupling in parts of a large reactor and neutron transport effects. For the particular case of neutrons transport/diffusion effect it is found that an accurate space-time calculation may be required under certain conditions. Depending on the importance of various effects care must be exercised in the use of different approximations.

References

1. Henry : Nucl. Sc. Engg., 3, 52, 1958.
2. Henry and Curlee: Nucl. Sc. Engg., 22, 171, 1965.
3. Ott : Nucl. Sc. Engg., 26, 563, 1966.
4. Kapil : SPURT series of Codes, Report to be published.
5. Toppel and Avery: IAEA Seminar on Physics of Fast and Intermediate reactors, Vienna, 1962.
6. Avery : Second Geneva Conf., P/1858, 1958.

CRITICALITY CALCULATIONS BY SOURCE-COLLISION ITERATION TECHNIQUE FOR CYLINDRICAL SYSTEMS

V.K.Sundaram and D.V.Gopinath
Health Physics Division
Bhabha Atomic Research Centre
Bombay-400085

This paper presents a fast-converging iterative technique using first collision probabilities developed for obtaining criticality parameters in two-region cylindrical systems with multigroup structure in energy of the neutrons. The space transmission matrix is obtained part analytically and part numerically through evaluation of a single-fold integral. Critical dimensions for condensed systems of uranium and plutonium computed using this method are presented and compared with published values.

(Criticality; collision; cylindrical; energy; integral; iterative; neutron; transmission matrix.)

Introduction

An analytic treatment of integral equations for neutron transport in infinite, homogeneous, isotropic media on the one-velocity model is possible. Beardwood et al[1] have used first collision probabilities along with successive over-relaxation for the solution of group fluxes in their computer code for calculations in finite systems with multigroup structure for neutron energy. Gaussian quadrature has been employed in the Swedish code Flurig[2] to obtain the same probabilities.

A fast-converging iterative technique for criticality calculations in two-region spherical systems with multigroup structure has been reported by Gopinath et al[3]. This paper presents an extension of this technique to finite two region cylindrical systems. The collision probabilities are obtained numerically through evaluation of a single-fold integral.

Mathematical Formulation

Finite Difference Equations

In an isotropic medium, the collision density $C(E,\underline{r})$ per unit energy E and at space point $\underline{r}$ is given by

$$C(E,\underline{r}) = \int_V S(E,\underline{r}')K(E,\underline{r}'\rightarrow\underline{r})\, d\,\underline{r}' \qquad \ldots\ldots (1)$$

Where $K(E,\underline{r}'\rightarrow\underline{r})$ is the first collision density kernel for neutrons of energy E and represents the collision rate at $\underline{r}$ due to unit neutron source at $\underline{r}'$. $S(E,\underline{r}')$ is the source density per unit energy interval for neutrons of energy E and at space point $\underline{r}$! Given $C(E,\underline{r})$ for all energies, $S(E,\underline{r})$ is obtained as

$$S(E,\underline{r}) = \int_{E'} C(E',\underline{r})G(\underline{r},E'\rightarrow E)\, dE' \qquad \ldots\ldots (2)$$

Where $G(\underline{r}, E'\rightarrow E)$ is the mean number of secondary neutrons generated per unit energy interval at E and space point $\underline{r}$ due to the collision of a neutron with energy E'. $S(E,\underline{r})$ and $C(E,\underline{r})$ are uniquely determined by $K(E, \underline{r}'\rightarrow\underline{r})$ and $G(\underline{r}, E'\rightarrow E)$. Knowing K and G and starting with an arbitrary distribution of $S(E,\underline{r})$, the true values of S and C can be obtained iteratively.

For a cylindrical system, dividing the cylinder into a finite number of coaxial annular discs and the neutron energy range into finite energy groups, Eqs. (1) and (2) are transformed to

$$C_{g,n,l} = \sum_{n'}\sum_{l'} S_{g,n',l'}\, K_{g,n'\rightarrow n,l'\rightarrow l} \qquad \ldots.(3)$$

$$S_{g,n,l} = \sum_{g'} C_{g',n,l}\, G_{n,l,g'\rightarrow g} \qquad \ldots.(4)$$

Where $C_{g,n,l}$ and $S_{g,n,l}$ are the total first collision rate and total birth rate respectively for neutrons of g^{th} energy group in the $(n,l)^{th}$ coaxial annular disc (n referring to the number of the cylindrical shell in the radial direction and l the number of the axial segment), and $K_{g,n'\rightarrow n,l'\rightarrow l}$ is the total first collision rate of neutrons in the $(n,l)^{th}$ coaxial annular disc due to a unit source of neutrons of g^{th}

energy group in the $(n',l')^{th}$ disc. $G_{n,l\ g'\to g}$ is the number of neutrons born in the g^{th} energy group due to the collision of a neutron of group g' in the $(n,l)^{th}$ disc. It is given by[3]

$$G_{n,l,g'\to g}=\frac{(\sum^{f}_{n,l,g'}\nu_{n,l,g'})\alpha_{n,l,g}+\sum^{s}_{n,l,g'\to g}}{\sum^{t}_{n,l,g'}} \quad .... (5)$$

Calculation of $K_{g,n'\to n,l'\to l}$

If the uncollided flux integrated over a (receptor) disc of radius r_n and thickness (Z_l-Z_{l-1}) due to a unit source of neutrons of g^{th} energy group distributed uniformly over a cylindrical (source) surface of radius r_n, and situated at an average height, $(Z_l-Z_{l-1}-2Z_{l'})/2$, from the disc is denoted by $\phi_g(r_{n'},Z_{l'},r_n,Z_l)$, the uncollided neutron flux integrated over a coaxial annular disc with inner and outer radii r_{n-1} and r_n respectively is given by

$$\phi_g(r_{n'},Z_{l'},r_n,Z_l)-\phi_g(r_{n'},Z_{l'},r_{n-1},Z_l)$$

The total number of first collisions in the annular disc is then

$$\sum^{t}_{n,l,g}[\phi_g(r_{n'},Z_{l'},r_n,Z_l)-\phi_g(r_{n'},Z_{l'},r_{n-1},Z_l)]$$

In the above, $Z_{l'}$ and Z_l are the axial distances of the source and receptor discs from the base of the cylinder. Lumping the total source in each disc over a cylindrical surface of radius equal to the mid radius of the disc $(\bar{r}_{n'})$ and of height equal to the mid-height of the disc $(\bar{Z}_{l'})$,

$$K_{g,n'\to n,l'\to l}=\sum^{t}_{n,l,g}[\phi_g(\bar{r}_{n'},\bar{Z}_{l'},r_n,Z_l)-\phi_g(\bar{r}_{n'},\bar{Z}_{l'},r_{n-1},Z_l)] \quad .... (6)$$

$\phi_g(r_{n'},Z_{l'},r_n,Z_l)$ has different forms depending on the position of $r_{n'},Z_{l'},r_n$ and Z_l.

Computational Procedure

On the basis of the formulation in Section 2, a computer programme has been written for BESM-6. The scheme of computation is the same as given in[3]. Using the code, calculations have been done to obtain the critical dimensions of condensed bare as well as reflected cylindrical systems. The results are presented in Table - 1, which include the published values[4] for comparison.

Table - 1

System	Density gm/cc	Radius cms	Critical height cms	Critical mass (core bulk mass) kgs	Published values of critical parameters[4] Radius cms	Height cms	(core bulk mass) kgs
93.4% enriched uranium	17.7	19.05	8.269	166.9	19.05	8.26	166.7
		19.05*	8.259*	166.7*			
93.5% enriched uranium	18.8	9.434	11.52	60.56	9.434	11.509	60.5
		9.434*	11.533*	60.6*			
46% enriched uranium	18.44	21.49	13.742	367.6	21.49	13.89	371.5
		21.49*	13.720*	367.1*			
Plutonium	14.27	7.588	8.596	22.19	7.588	8.286	21.39
		7.588*	8.579*	22.14*			

*Values obtained by treating the system as two regions.

References

1. Beadwood, J.E., Clayton, A.J. and Pull, I.C., ANL-7050 (1965).
2. Carlvik, I., Nukleonik, 8 Band, S. 226 (1966).
3. Gopinath, D.V., Sundaram, V.K., Krishnan, L.V. and Santhanam, K., Nukleonik, 9 Band, 5 Heft, S. 252-256 (1967).
4. Reactor Physics Constants, ANL-5800 (1963).

STOCHASTIC METHOD OF CALCULATIONS FOR FAST SYSTEMS

B.K. Godwal and M.P. Navalkar
Bhabha Atomic Research Centre, Trombay, Bombay
INDIA

Neutron slowing down is a Markov process in which the probability for being in a certain volume element in phase space (space-time-energy) at some future time depends only on the present state of the system and not on the past. The process has been approximated to a discrete time, discrete state by Williamson et al to determine state transition probabilities. In this paper, this approach has been extended to calculate Rossi-α which is an important dynamic parameter of the system. The values of K_{eff} as a function of B^2 for the bare core of Zero Energy Fast Critical Facility, PURNIMA calculated from this method showed good agreement with the bare critical experimental parameters obtained from fission rate distribution. A method to extend this method of calculations to reflected system has also been described.

(BESM-6; JEZEBEL; Markov process; neutron; PURNIMA; Rossi-α; slowing down; stochastic.)

Introduction

Multi-group calculations for fast systems are basically static in character. Apart from the cross-sectional uncertainties as well as errors arising due to averaging over broad energy groups, the multigroup method does not describe adequately the physics of the slowing down in fast systems.

An approach based on Markov chain process to calculate temporal and integral properties of fast reactors has been proposed by T.J. Williamson et al[1]. In this approach, the neutron slowing down process is treated approximately as a discrete time, discrete state Markov process from which state transition probabilities based on collision physics are determined. The matrix is then applied to evolve the time dependence of a pulse of neutrons on a discrete time-energy mesh from which integral parameters of the system are obtained.

In the present paper we have extended the earlier work to calculate Rossi-α which is a dynamic and important parameter for the fast systems. In addition, we obtain the neutron density as a function of time due to a pulse of neutrons introduced in the system. The calculations using 26 group cross-section library have been performed on BESM-6 to determine Rossi-α as a function of subcriticality for JEZEBEL system which show good agreement with the experimental data.

Method Of Calculation

When a pulse of neutrons having fission energy distribution is injected in a finite multiplying assembly, the following processes take place:

(a) Scattering, elastic and inelastic, (b) Non fission capture, (c) Fission, (d) Leakage, (e) n,2n etc.

The flux $\phi(E,t)$ for the source neutrons can be obtained by operating the transition probability matrix on the initial pulse. The source of first generation fission neutrons is given by

$$k(t) = \int \nu(E)\ \Sigma_f(E)\ \phi_{in}(E,t)dE \quad ...(1)$$

where symbols have the usual meaning. The term k(t) can then be used to calculate the relationship between the nth generation fission source S_n and (n-1)th generation source, S_{n-1}.

$$S_n(t) = \int_0^\infty S_{n-1}(t)\ K(t-t')dt' \quad ...(2)$$

The Laplace Transform of K(t) is related to the Laplace Transform of a function G(t) by

$$G(s) = \frac{K(s)}{1-K(s)} \quad ... (3)$$

This can be inverted by using convolution theorem in Inverse Laplace Transform to give the function G(t) as

$$G(t) = k(t) + \int_0^t k(u)k(t-u)du + \int_0^t k(t-u')du' \int_0^{u'} k(u)k(u'-u)du + \int_0^t k(t-u'')du'' \int_0^{u''} k(u-u')du' \int_0^u k(u)du$$

$$\approx \nu \Sigma_f \phi(t) \quad ... (4)$$

Thus G(t) gives total number of fission neutrons of all generation at time t.

Hence the slope of the logarithm of G(t) gives Rossi-α.

We have applied above method to calculate Rossi-α as a function of sub-criticality for JEZEBEL for which the results are shown in Fig. 1. It is seen that Rossi-α varies linearly with reactivity and intercepts the reactivity axis at prompt critical, thereby indicating the self consistency in calculation of sub-criticality α. The delayed critical Rossi-α agrees fairly well with the quoted experimental results[2].

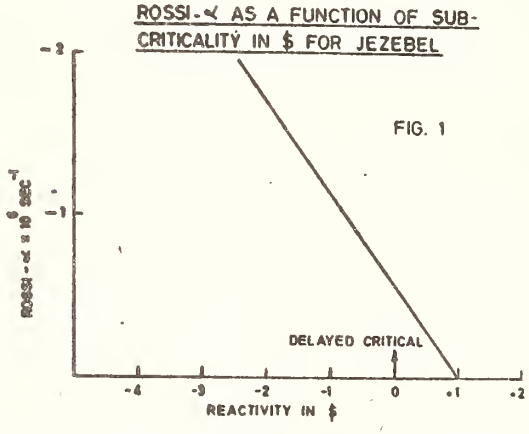

Fig. 1. Rossi-α as a function of sub-criticality in $ for JEZEBEL.

We have also done calculations of K_{eff} for bare case of Zero Energy Fast Critical Facility, PURNIMA. The details of the critical facility have been described by Iyengar et al[3]. It consists of six zones, the innermost being PuO_2 core whereas the outer most zone is mild steel. Other reflectors such as molybdenum, stainless steel, copper are employed between the first and the last zone. Fig. 2 shows $1-K_{eff}$ as a function of fuel pins for bare core (PuO_2 only) and gives a bare critical loading of 405 fuel pins. Using the axial reflector savings as measured by Ramakrishna et al[4], a critical loading of 360 fuel pins is obtained which is in agreement with the reported value[5] for core consisting of PuO_2 and molybdenum reflector.

The stochastic method has been applied to the bare fast system. In order to apply it to the reflected system, a combined Stochastic-Monte Carlo approach is proposed. In this, the leakage term for the bare core which gets modified due to reflector is calculated using Monte Carlo method.

The leakage for bare core is given by

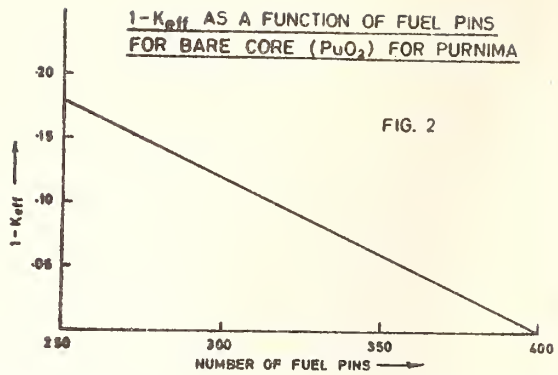

Fig. 2. $1-K_{eff}$ as a function of fuel pins for bare core (PuO_2) for PURNIMA.

$$P_{LB}(E) = \frac{D(E)B^2}{\Sigma_T(E)+D(E)B'^2} \qquad \ldots (5)$$

The leakage in presence of reflector is given by

$$P_{LR}(E) = \frac{D(E)B'^2}{\Sigma_T(E)+D(E)B'^2} \qquad \ldots (6)$$

Using Monte Carlo method and the leakage distribution given by stochastic for bare system, $P_{LR}(E)$ is calculated. This $P_{LR}(E)$ gives us equivalent $D(E)B'^2$ which is used in the bare stochastic model. The advantage of using Stochastic-Monte Carlo approach is the saving in the computational time as well as increasing the accuracy over the conventional Monte Carlo method. This is due to the fact that the neutron history is traced in the reflector only in the Stochastic-Monte Carlo approach unlike the complete history traced in pure Monte Carlo method.

References

1. Williamson, T.J. and Alberecht, R.W., Stochastic Calculation of Fast Reactor Generation Times, Fast Reactor Physics Vol. I.p.513 (IAEA, Vienna, 1968).
2. Reactor Physics Constants, ANL. 5800, Prepared by Argonne National Laboratory, Second Edition, July 1963.
3. Iyengar, P.K., Chandramoleshwar, K., Kapil, S.K., Krishnamurthy, T.N., Nargundkar, V.R., Pasupathy, C.S., Raj A.K., Seshadri, S.N., Srinivasan, M., Subba Rao, K., Preliminary Safety Analysis Report for Critical Facility of Pulsed Fast Reactor, B.A.R.C./I-134 - 1971.
4. Ramakrishna, D.V.S. and Navalkar, M.P Power Calibration for Purnima Proceedings of the Symposium on Nuclear

Science and Engineering, Bombay, India (1973).
5. Nargundkar, V.R., Basu, T.K., Chandramoleshwar, K., Job, P.K., Subba Rao, K., Pasupathy, C.S., Srinivasan, M. and Paramsivan, C. - Internal Note No. 071 BARC - (1974).

A RANDOM SAMPLING TECHNIQUE FOR CHOOSING SCATTERING ANGLES FROM ARBITRARY ANGULAR DISTRIBUTIONS IN DOSIMETRIC AND SHIELDING COMPUTATIONS

P.S. Nagarajan, C.P. Raghavendran, P. Sethulakshmi and D.P. Bhatia

Division of Radiological Protection
Bhabha Atomic Research Centre
Trombay, Bombay-400085

A random sampling technique has been developed for sampling the cosine of the scattering angle of the neutron in the centre of mass system. This technique could be incorporated in existing shielding and dosimetry codes. Recent differential scattering cross section data (from BNL-400 (1970)) is expanded in double Legendre polynomials of incident neutron-energy and a random number. The necessary coefficients for the elements C, N, O, Si, Ca, Fe and Pb for incident neutron energies upto 15 MeV have been obtained and the same are presented along with typical results, checking the method and coefficients.

(Angle; centre of mass; coefficients; computations, cross-section; Legendre polynomial; neutron; random sampling; scattering; shielding)

Introduction

In shielding and dosimetric computations it is necessary to take the anisotropy of neutron scattering from nuclei such as C, N, O, Si, Ca, Fe and Pb. In the course of our Monte Carlo work for the computation of leakage spectra through shields and in dosimetry we have developed certain data and procedures to sample the scattering angle of the neutron in the centre of mass system, using available data[1,2]. If sampling is needed from a unique angular distribution, i.e., just for one angular distribution, $f(\mu)$, simple schemes can be thought of, including the one due to Coveyou[3]. However, the distributions are functions of energy too.

Method

Garber et al[1] provide $d\sigma/d\Omega$ as a function of $\cos\theta_{cm}$ for various incident neutron energies. From this $f(\mu,E)$ the probability density function in μ is obtained at neutron energy E, as given by

$$f(\mu,E) = 2\pi \frac{d\sigma(E)}{d\Omega} \Big/ \int_0^{4\pi} \frac{d\sigma(E)}{d\Omega}.d\Omega$$

where $\mu = \cos\theta_{cm}$ and $-1 \leqslant \mu \leqslant +1$

Graphically, the $f(\mu,E)$ data was interpolated to obtain $f(\mu,E)$ at uniform intervals in E, from 0.5 MeV to 15 MeV. The usual procedure of sampling of value μ by solving

$$F(\mu_1,E) = \int_{-1}^{\mu_1} f(\mu,E)d\mu = R_1$$

for μ_1 (where R_1 is a random number and F is the distribution of f) is almost impossible because F is usually a high order polynomial in μ_1. To overcome this we have done the inverse interpolation to obtain

$$\mu = \mu(R,E)$$

Among the many choices for least square interpolation in R and E, it was found that the coefficients of a double normal polynomial expansion in R and E do not lend themselves convenient and required a large number of terms. Hence a double legendre expansion in R and E was resorted to, giving,

$$\mu = \sum_{i:o}^{m} \sum_{j:o}^{m} a_{ij} P_i(E') P_j(R)$$

where P's are the legendre functions

$$E' = (E-7.5)/7.5$$

and; R, a random number in the interval (-1, +1).

Results

The coefficients a_{ij}'s were obtained for seven elements of interest in shielding and dosimetry C,N,O,Si,Ca,Fe and Pb using data from ref.1 and in the case of lead data from Langley[4] was also used.

To increase the speed of sampling, coefficients b_{ij}'s were derived from a_{ij}'s, thus enabling sampling as

$$\mu = \sum_j \sum_i b_{ij} E'^i P_j(R)$$

Table 1 gives the coefficients b_{ij}'s. Sample results for carbon are given in Figs. 1 and 2 to illustrate the efficacy of the method. The histograms are the sampled data and the dotted lines are the original data used. Complete check results of this nature for all the seven elements and over the range of energies from 0.5 MeV to 15 MeV are available elsewhere[5].

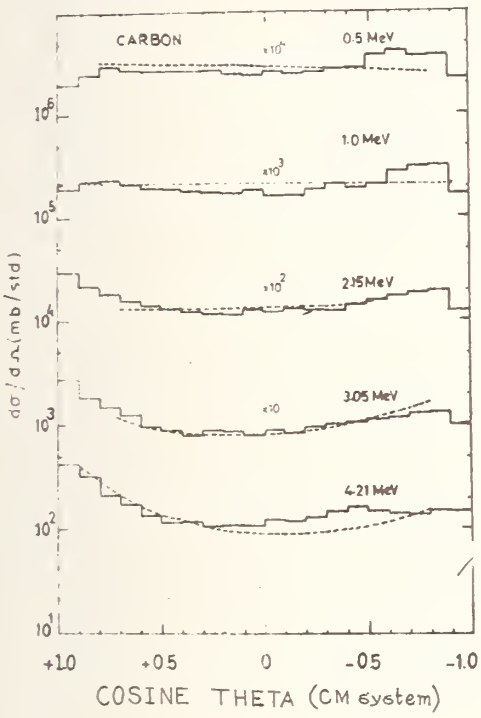

Fig. 1. Comparison of BNL-400 data and sampled results.

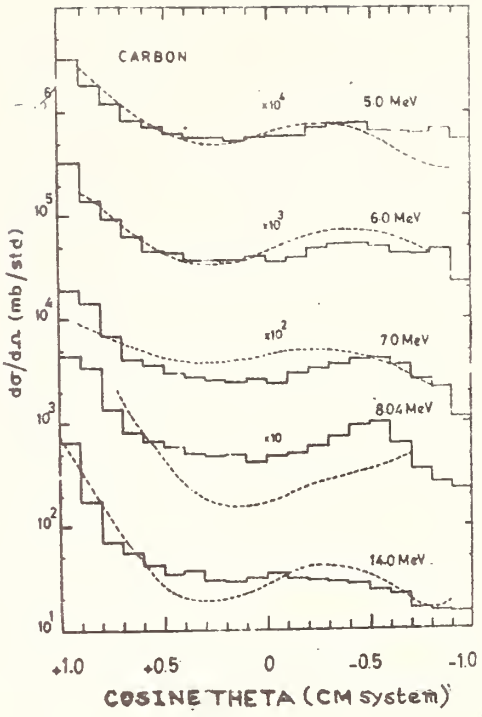

Fig. 2. Comparison of BNL-400 data and sampled results.

Table-1

NORMAL LEGENDRE COEFFICIENTS b_{ij}

CARBON

j \ i	0	1	2	3
0	4.50501400894-001	4.34897507829-001	-3.60518181658-001	-7.06348637003-002
1	-9.87239221686-001	3.34566944151-001	-1.09709837609-001	-2.53021085634-001
2	-4.82758167105-001	-4.62190415704-001	4.74898584566-001	1.11818118210-001
3	2.77740660495-002	-4.35186149663-001	-1.78755311314-001	4.89405090197-001
4	1.41103977613-001	1.28214626067-001	-4.61694986644-001	-3.08714596571-001
5	3.87079647265-002	4.16848722339-001	-7.27190210047-002	-1.33865834776+000
6	-7.91016890115-002	1.04642761832-001	1.04085643497+000	-1.63937627586+001
7	-1.09910491952-001	-3.82783285910-001	6.82361848404-001	1.36778067023+000
8	2.38796576455-002	-3.27382511153-001	-6.77004748027-001	1.27969383829+000

j \ i	4	5	6	7
0	2.82873281502-001	2.82285132430+002	-1.26081671612-001	-3.29610352200-002
1	6.93408923090-001	-4.29245072303-003	-7.05245659191-001	1.34832057746-002
2	-1.83586398673-001	-1.17201211537-001	-1.91732776638-001	1.15156202639-001
3	-9.12462587760-003	-3.23386041389-001	4.22680224343-002	1.17717243261-001
4	2.05626198255-001	2.03102045040-001	4.01670464112-001	-4.99507340693-002
5	3.08017261681-001	1.72401222232+000	-3.93975467854-001	-7.56500232726-001
6	-3.38610700524+000	-3.96070324611-001	3.85875155299+000	5.33729467946-001
7	-2.09797895839+000	-1.60037377408+000	2.73164727438+000	6.70039653361-001
8	1.92046615110+000	-1.85855555455+000	-2.08131151038+000	8.86103324505-001

j \ i	8
0	1.73098341147-002
1	2.36574371422-001
2	1.27179603514-001
3	-5.47183507695-003
4	-3.13161449435-001
5	1.39128934214-001
6	-1.37125207512+000
7	-1.20887607770+000
8	8.09035338239-001

NITROGEN

j \ i	0	1	2	3
0	3.41657850420-001	1.35599259400-001	3.75753298490-002	1.86433332547+000
1	-1.02760569029+000	1.10279115609-001	-2.20311381148-001	2.50699716537+000
2	-3.09629429720-001	6.46759831607-002	-1.42257096682+000	-2.70521262012+000
3	1.11629680701-001	-1.10612681247-001	4.81575442013-001	-1.29724016087+000
4	2.21010227498-002	-1.74883286518-001	9.21240956462-001	9.87740448172-001
5	-1.35124500984-001	-2.59829197126-001	4.62338324974-001	1.75597754812+000
6	-6.50246018187-002	-2.34100439197-002	-3.46876597603-001	-6.30258550513-001
7	4.92843881325-002	1.34369401035-001	-5.26102605959-001	-1.42227999244+000

j \ i	4	5	6	7
0	-1.71719805400+000	-3.51622420442+000	3.99887611047+000	1.70117466471+000
1	-9.09583675308-001	-9.27000057435+000	8.73287795350+000	1.17006035143+001
2	1.21504456271+001	4.14530576156+000	-3.07181128753+001	-6.21566179594-001
3	-2.08584552778+000	3.28206930018+000	1.39343388752+000	-2.14870996706+000
4	-4.55825559139+000	-3.53154886445-001	6.70878898715+000	-2.08038322972+000
5	-1.27674813112+000	-3.08016733910+000	2.11536264054+000	1.58313672158+000
6	1.67488395113+000	1.69154169450+000	-2.33429546056+000	-1.41777348517+000
7	1.94388059790+000	3.17833942308+000	-4.50697506090+000	-2.82364293850+000

j \ i	8	9	10
0	-2.10917502586+000	0.00000000000+000	0.00000000000+000
1	-1.35662431861+001	-4.78957183066+000	6.14955927899+000
2	3.06970847500+001	-1.01616754772+000	-1.08636268192+001
3	0.00000000000+000	0.00000000000+000	0.00000000000+000
4	-3.13322071371+000	1.53852849657+000	0.00000000000+000
5	-1.21037305813+000	0.00000000000+000	0.00000000000+000
6	1.05087059879+000	3.51166275844-001	0.00000000000+000
7	4.91016553820+000	9.30600236660-001	-1.88826998151+000

Oxygen

J \ i	0	1	2	3
0	3.35370477362-001	1.85071586259-001	2.09751228070-002	1.88937996427-001
1	-1.06247154837+000	9.79104316542-002	3.67167830906-002	1.16503260199-001
2	-3.81376480061-001	-2.79610738279-001	-1.36974464230-002	-6.17625047499-002
3	9.90547264895-002	-2.06756294478-001	-1.18517939920-001	4.59849475966-002
4	9.87178739255-002	3.24071284148-002	-2.04424503159-001	1.41367429724-002
5	-3.41400467835-002	1.98288564661-001	-9.54114407174-002	-4.52440496190-001
6	-7.34387851888-002	1.44825467291-001	2.42426167153-001	-5.04054495856-001
7	-3.14617860690-002	-7.66603269083-002	3.71353289613-001	1.62227645946-001

J \ i	4	5	6
0	-8.35270571440-002	-1.08570901774-001	3.74007723628-002
1	2.18643886658-001	-1.10051404381-001	-1.09312413580-001
2	3.43851570651-001	7.92949923351-002	-2.18116104162-001
3	-1.15534732674-003	8.20885452888-002	-5.39018263208-002
4	1.35757984759-002	-7.71117657259-003	4.54379671388-002
5	1.05710019042-001	2.23601373890-001	2.84792620754-002
6	-3.11326424355-001	3.35227289889-001	1.01120118192-001
7	-7.53441614690-001	-9.37861126462-002	3.7521581103 -001

Silicon

J \ i	0	1	2	3
0	5.22462054030-001	7.65124013693-002	-1.68939193775-001	-4.98708555384-001
1	-9.01448525670-001	-4.65451027651-002	-1.27119158331-002	8.56861430372-002
2	-5.80513048824-001	-7.67928985787-002	4.83001593641-002	4.14426240823-001
3	-1.72562131801-001	3.91020394728-002	6.10062390637-002	1.67950396449-001
4	2.40181973518-002	5.89320374255-002	-1.5747[illegible]074943-002	-1.78062182083-003
5	6.02660595857-002	-2.85896935235-002	1.59260580761-002	-9.00799205425-003
6	5.19110072705-002	-2.38001151465-002	-3.58919639023-002	-6.24451547305-002

J \ i	4	5	6
0	7.88661923908-001	6.70325888003-001	-8.86419619780-001
1	2.13981849040-002	-1.52791818403-001	7.78726239960-002
2	-3.40182993702-001	-6.49562890205-001	5.98613827770-001
3	-2.78242783528-001	-2.54519480357-001	3.38160261774-001
4	-6.35860644949-003	1.29769359988-002	-2.19898160610-003
5	-6.45362630966-002	6.38237376291-002	-8.75577729794-003
6	8.94145873542-002	9.19895269411-002	-1.12909557424-001

Calcium

J \ i	0	1	2	3
0	7.47266800399-001	1.61220486583-001	-5.05591059705-001	3.25544583980-001
1	-5.55956868051-001	2.22767223185-001	-8.61305029313-001	4.09456231575-001
2	-5.81866411349-001	-2.60985675694-002	-2.61798939426-001	3.65295994232-001
3	-4.49863468643-001	-1.45211936000-001	3.72295613238-001	-3.95261936533-001
4	-2.94447125693-001	-1.14762467907-001	8.07424143091-001	-8.14226421935-001
5	-1.12766947987-001	-7.00219048902-002	9.39602681007-001	-7.47027808021-001
6	4.90799606603-002	-7.76404262408-002	4.69754734617-001	1.90784759083-001
7	1.07096060186-001	-1.10022044290-002	-1.91186454778-001	6.01389617215-001
8	1.16031372207-001	5.58181296054-002	-5.60228721484-001	4.40401038197-001

J \ i	4	5	6	7
0	1.86155285530-001	-3.68393480781-001	1.52431856175-002	1.00491833804-001
1	6.87708318650-001	-7.84330901691-001	-1.51753809959-001	3.06047731226-001
2	8.04315903796-001	-1.28511159843+000	-3.42150381158-001	7.27893704031-001
3	1.05409295139-001	5.94317202982-001	-1.41168496952-001	-2.46152949138-001
4	-3.66510691115-001	1.53925545453+000	-2.18461486519-001	-5.80767138983-001
5	-1.27116817593+000	1.78803967427+000	4.04177826504-001	-9.26060883471-001
6	-1.16537853039+000	-5.34694873458-002	6.45475837173-001	-5.01785539337-002
7	-2.69780057237-001	-1.10042587287+000	3.63688053305-001	4.72211067388-001
8	5.33838376356-001	-1.09144711327+000	-3.27096488759-002	5.72476013186-001

Iron

J \ i	0	1	2	3
0	8.40255885231-001	1.26411432615-001	-3.04327547093-001	4.21033283580-001
1	-3.69321445133-001	2.26459347492-001	-7.99174293946-001	8.47868444110-001
2	-4.05689188612-001	1.21858716138-001	-6.62218767137-001	6.42328999038-001
3	-3.68872294181-001	2.34200425865-002	-3.91119839944-001	3.29832775875-001
4	-3.19087294703-001	1.46701197991-003	-5.79152336582-002	-1.46248586727+000
5	-2.48103982359-001	-7.43438899410-002	6.59643025377-001	-2.19997076862+000
6	-1.58233954105-001	-1.70373859276-001	1.18676973935+000	-1.55950682381+000
7	-6.07773368142-002	-2.10848675603-001	8.73372665333-001	6.49474293685-001

J \ i	4	5	6	7
0	-7.74259220164-001	2.93258558519-001	1.54476268036+000	-9.52074161203-001
1	2.48367543723-001	-2.41930893920-001	-9.36254432934-001	-1.43250096141+000
2	1.06665137304+000	-2.18294996569+000	-4.87092249911-001	1.50484340664+000
3	2.17817419252+000	-5.12906926980+000	-1.66547331886-001	8.27618644782+000
4	4.64103069095+000	1.31802031076+000	-1.15688311738+001	7.67828808236-001
5	1.54991841523+000	6.53985461804+000	-8.02723840291+000	-7.00496565413+000
6	-3.49760460400+000	7.71256462277+000	2.80651376136+000	-1.04150561367+001
7	-4.98378859545+000	1.57768205341-001	1.07467323530+001	-1.49816731644+000

J \ i	8	9	10
0	-1.22077952463+000	5.04886833576-001	3.63176881744-001
1	2.60478381761+000	8.57870880861-001	-1.41726069692+000
2	7.01780079029-001	-3.59205249544-001	-4.43221499453-001
3	-3.96543002594+000	-3.67678286931+000	2.45704759331+000
4	1.07894814322+001	-6.54543426954-001	-3.72953458369+000
5	1.00857927382+001	2.69514144915+000	-4.13437288543+000
6	7.02475319022-001	4.39042106050+000	-1.03119563277+000
7	-9.99590804709+000	8.98700872905-001	3.43652030775+000

Lead

J \ i	0	1	2	3
0	8.49084747195-001	6.85971275560-002	1.25927916866-001	2.46954139293-002
1	-3.74188789102-001	6.19285085859-002	-4.38710241861-001	1.76464212957+000
2	-4.65839348813-001	-3.69211586883-002	-2.27372826397-001	3.17455932633+000
3	-4.15466878216-001	-6.15370937410-002	-5.74703725292-001	1.93059943593+000
4	-3.19530261120-001	7.98274309213-002	5.22765643786-001	-2.84057956905+000
5	-1.97440078505-001	1.10630342821-001	6.28682178094-001	-4.29525940144+000
6	-9.77691056459-002	-8.72715248963-002	6.78567305693-001	-7.98989690440-001
7	-3.29769049646-002	-2.20078058989-002	5.73859547587-002	-1.31757324590-001
8	-1.00000000000-002	0.00000000000+000	0.00000000000+000	0.00000000000+000
9	-1.07711311510-003	3.53759775615-002	-9.93429086865-002	-2.21595353170-001

J \ i	4	5	6	7
0	-3.10675105422+000	4.12506579131+000	4.37200112054+000	-7.64290955646+000
1	-1.37559359632+000	-2.20435439558-001	4.59716101424-001	-4.57144248024+000
2	-3.48298531943+000	-1.27925833352+001	1.81348183401+001	1.50439243999+001
3	4.73610592345+000	-1.40018342792+001	5.13289277708+000	2.26194363191+001
4	1.12185864044+000	6.04213270381+000	-3.68680814062+000	-3.35127039409+000
5	1.01832417194+000	1.61948275267+001	-9.80872246515+000	-2.09568251869+001
6	-1.91226878005+000	3.53451119455+000	2.11898631719+000	-4.49071976442+000
7	1.55969170716-001	-9.23544498937-003	-2.04426284516-001	2.01432767918-001
8	0.00000000000+000	0.00000000000+000	0.00000000000+000	0.00000000000+000
9	7.81712624445-001	1.08007733182-001	-1.52968764626+000	5.73690037485-001

J \ i	8	9	10
0	-1.92189801704+000	3.63858087309+000	0.00000000000+000
1	3.06878676518+000	3.00782056613+000	-2.30790402168+000
2	-2.49100713465+001	-5.49632436672+000	1.04522643326+001
3	-5.68579697268-001	-1.02568561578+001	1.80859492875+000
4	2.42539970329+000	0.00000000000+000	0.00000000000+000
5	1.54240453992+001	8.96781494046+000	-6.97815900783+000
6	-7.97566059833-001	1.90057056135+000	0.00000000000+000
7	0.00000000000+000	0.00000000000+000	0.00000000000+000
8	0.00000000000+000	0.00000000000+000	0.00000000000+000
9	8.24826400693-001	-4.71070687343-001	0.00000000000+000

References

1. Garber, D.I., Stromberg, L.G., Goldberg, M.D., Cullen, D.E. and May, V.M., "Angular distributions in neutron-induced reactions". BNL-400, 3rd Edn. Vol. I (Jan 1970) and Vol.II June (1970).
2. Langner, I., Schmidt, J.J. and Woll, D.,"Tables of evaluated neutron cross sections for fast reactor materials"- KFK-750 (Jan 1968).
3. As reported by D.C. Irving, R.M. Freestone and F.B.K.Kam, "The Coveyou technique for selecting neutron scattering angles from anisotropic distributions" in Appendix 1 of 05 R - A general purpose Monte Carlo neutron transport code ORNL-3622 (1965).
4. Langley, H.J., "Neutron cross sections" - LA-2016 (1956).
5. Nagarajan, P.S., Sethulakshmi, P., Raghvendran, C.P. and Bhatia, D.P., "A random sampling procedure for anisotropic distributions"BARC report (to be published).

Discussion

Godwal, B.K.

Can the Coveyou technique be used for taking into account the anisotropic scattering in hydrogen due to neutrons ? How is it at Legendre Polynomial preferred ?

Nagarajan, P.S.

In the energy range of interest to us i.e. upto 15 MeV, assumption of isotropic acattering in the c.m. system is valid. Hence the cosine of θ_{lab} [cos θ_{lab}] can be directly sampled as the larger of a pair of random numbers. At thermal energies I have not developed any sampling scheme. Perhaps one could assume an isotropic law.

Makra, S.

Are the differential cross sections data available for all the materials and energies and if so from which library ?

Nagarajan, P.S.

The reports BNL-400 (1970) and KFK-750 (1968) yield the required data for all the elements C,N,O,Ca,Si,Fe and Pb. But in the case of Pb there is an energy gap where no data is available. We took the data from an old reference of 1956.

MONTE CARLO CALCULATIONS ON DOSE DISTRIBUTIONS FROM PLANE INFINITE OBLIQUE ELECTRON SOURCES

C.R. Gopalakrishnan and V.Sundararaman
Division of Radiological Protection
Bhabha Atomic Research Centre
Trombay,Bombay-400 085, India

A modified Monte Carlo method has been developed for tracking electrons. In this method individual collisions wherein the electron suffers a large deflection or loses large fraction of its energy (denoted as catastrophic) are treated separately. The history of the particle is divided into sections, within which no catastrophic collisions occur and in which continuous-slowing down is assumed. The angular distribution at the end of a section follows a Gaussian distribution. In this method the correlation between energy-loss fluctuations and multiple scattering deflections is preserved more faithfully. Dose distributions for electrons in carbon, aluminium and copper have been calculated for oblique incidence using this method. Data have been obtained for five different initial angles and covering a range of energies from 0.05 to 10 MeV electrons.

(Aluminium ; carbon ; copper ; collision ; dose ; distribution ; electron ; Gaussian ; Monte Carlo ; scattering)

Introduction

In this paper, we have reported some of the results on electron dose distributions obtained by Monte Carlo Methods. First, dose distribution functions have been computed for infinite plane oblique sources of different energies from 0.05 MeV to 10 MeV. These have been obtained in Carbon, Aluminium and Copper for cosines of the angles varying from 0.2 to 1.0. Spencer[1] has calculated dose distribution functions for plane perpendicular and point isotropic sources using the moments method with the continuous slowing down approximation. Berger[2] has calculated these distribution functions using the Monte Carlo method. However,no results are available for plane oblique sources. These are of some importance in calculating doses in non-electronic equilibrium conditions on X or gamma ray irradiation. Secondly, we have calculated depth dose curves for high energy electrons. These are required in treatment planning for high energy electron beams from accelerators. Also the perturbation in the depth dose curves due to the presence of cavity has been computed.

Method

Two Monte Carlo methods were used. The first one, for electrons of energy less than 2 MeV, was similar to the one used by Berger[2]. In this method, the electron track is divided into predetermined sections, section size corresponding to a distance in which the electron loses energy by a fraction 2^{-16}, on an average. The energy and angle at the end of each section are sampled from the Landau[3] straggling distribution and Goudsmit and Saunderson[4] multiple scattering distribution respectively. Since the computations are for infinite plane sources,the problem is one of one dimensional transport. The details of the method are presented elsewhere[5]. The range of electron was divided into forty slabs and the energy absorbed in each block was computed. 2000 histories were used in the calculation. The effect of secondary electrons was ignored.

For higher energies we have used a modified Monte Carlo Method. This is a mixed procedure in which one excludes from the grouping individual collisions denoted as major or catastrophic in which either the electron loses a very large fraction of its energy in an inelastic process or suffers a large change in angle due to elastic scattering. Here again the electron track is divided into sections. However, the section size is not fixed earlier but is decided by the probability for catastrophic collisions. No catastrophic collision occurs in each section and each section is terminated by a catastrophic collision. The section size is sampled from the probability distribution function,

$$P(s)ds = \exp\left\{-\int_0^s \sum_{\text{total}} (s')ds'\right\} \sum_{\text{total}} (s)ds$$

where $\sum_{\text{total}}(s) = \sum_{\text{elastic}}(s) + \sum_{\text{inelastic}}(s)$

$$\sum_{\text{elastic}}(s) = \int_{-1}^{\text{Cos}\theta_c} \sigma_{\text{elastic}}(\mu, s)\, d\mu$$

and $$\sum_{\text{inelastic}}(s) = \int_{\epsilon_c}^{0.5} \sigma_{\text{inelastic}}(\epsilon, s)\, d\epsilon$$

where Cos θ_c is the cut off angle and ϵ_c is the fractional energy of the incident electron above which the collision is considered to be catastrophic.

In each section energy loss was computed using a continuous slowing down model. The change in the angle was computed using a Gaussian distribution,

$$P(\omega)\, d\omega = \frac{2\omega}{\overline{\omega^2}} \exp\left\{-\omega^2 / \overline{\omega^2}\right\} d\omega$$

$\overline{\omega^2}$ was derived from the Moliere[6] multiple scattering theory as

$$\overline{\omega^2} = 2\pi NS \int_{\text{Cos}\,\theta_c}^{1} \omega^2\, \sigma(u)\, du$$

where N is the number of atoms per gram, S is the step size. The actual distribution was also obtained using Goudsmit and Saunderson[4] theory. It was found that the Gaussian approximation agreed well with the exact calculation. The catastrophic collision results in either a large angle scattering or production of a δ-ray. The large angle scattering was sampled from Mckinley-Feshbach[7] multiple scattering distribution and δ-ray distribution from the Møller[8] cross section. δ-rays above a certain cut off energy (100 keV) were tracked separately.

Photons produced can also be tracked separately. In the present calculations, however, bremsstrahlung losses have been added to the stopping power. This is because, the total radiation yield for a 10 MeV electron in carbon is only 4%. This method has the advantage that the correlation between energy loss fluctuations and production of δ-rays is preserved faithfully. The spatial location of the particle is also more accurate because large angle collisions have been excluded from the sections. Calculations for depth doses were carried out by tracking electrons in all the three co-ordinates. 10,000 histories were used in these calculations.

Results and Discussion

Fig.1 gives the energy dissipation function for 2 MeV electrons in three materials, viz., Carbon, Aluminium and Copper, the obliquity of the angle being Cos θ = 0.6. As atomic number of the material increases, peak of the distribution increases due to the increase in backscattering. Fig.2 gives the energy dissipation function for different energies from 0.1 MeV to 10 MeV in Aluminium, incident direction cosine being 0.8.

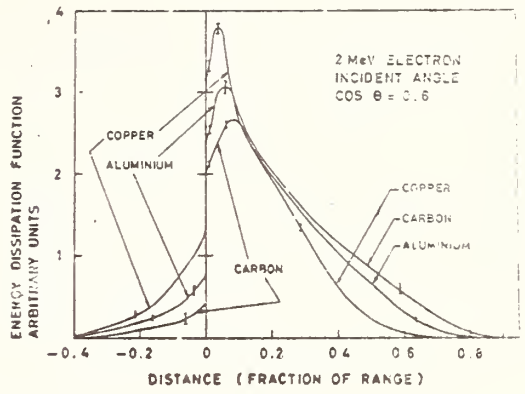

Fig.1. Energy dissipation distribution for infinite plane oblique (Cos θ = 0.6) sources of initial energy 2 MeV in different materials.

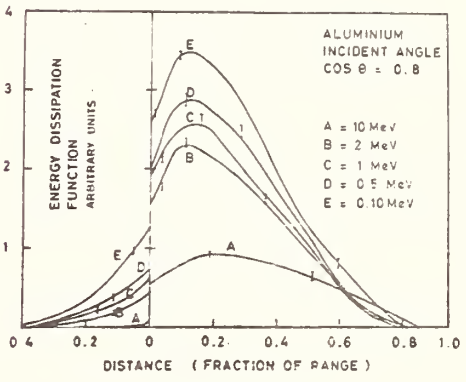

Fig.2. Energy dissipation distribution for infinite plane oblique (Cos θ = 0.8) electron sources of different initial energies in Aluminium.

Figs. 3a,b show the energy dissipation function in Carbon for 0.05 MeV electrons for 5 different angles. (Cos Θ=0.2, 0.4, 0.6, 0.8, 1.0). Here again, the peak increases for higher obliquity.

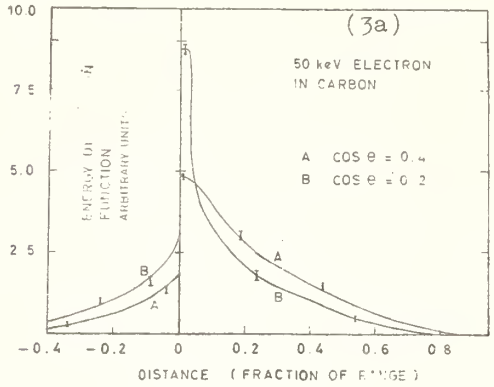

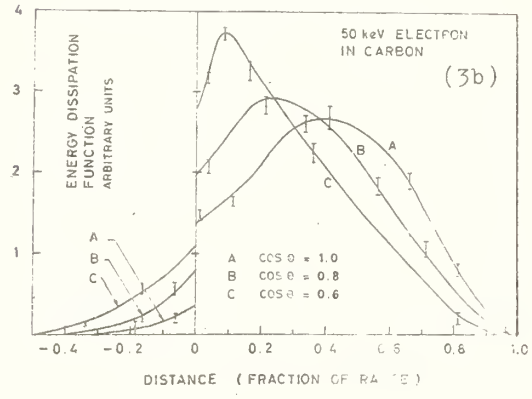

Figs. 3a,b : Energy dissipation distribution for infinite plane oblique electron sources of initial energy 50 keV in Carbon.

a) for incidence angles cos Θ = 0.2, 0.4.

b) for cos Θ = 0.6, 0.8 and 1.0.

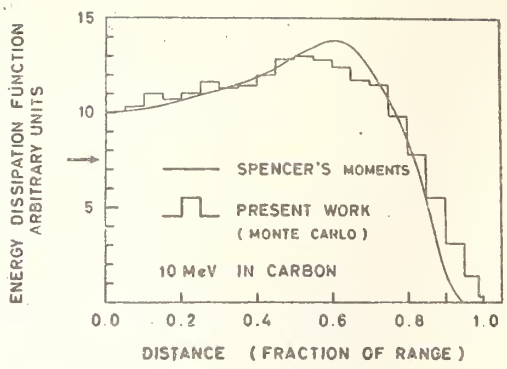

Fig. 4. Comparison of central axis depth dose data for a 10 MeV electron beam in Carbon.

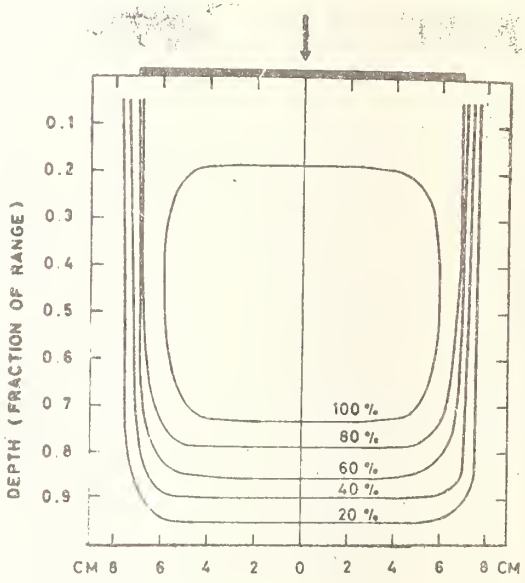

Fig. 5. Isodose curves for a 10 MeV electron beam in Carbon for a circular field (14 cm dia).

Fig.4 gives the central axis depth dose distribution in Carbon for a 10 MeV electron beam for a circular field of 14 cms. diameter. The central axis depth dose data for this field size, of course, corresponds to the data for an infinite plane perpendicular source. This agrees well with Spencer's[1] data. The higher peak and lower doses at large distances obtained by Spencer[1] are due to the fact that straggling has been neglected in his calculations. Fig.5 shows isodose curves for a 10 MeV electron beam for the same field size.

The perturbation due to an air cavity in the beam has been given in Fig.6. It can be seen that the depth dose curves are shifted downwards under the cavity. Another effect is the presence of a region of overdosage under the cavity (150%) This is because of 'focussing effect' associated with electron beams, i.e., electrons scattered into the cavity tend to stay there,

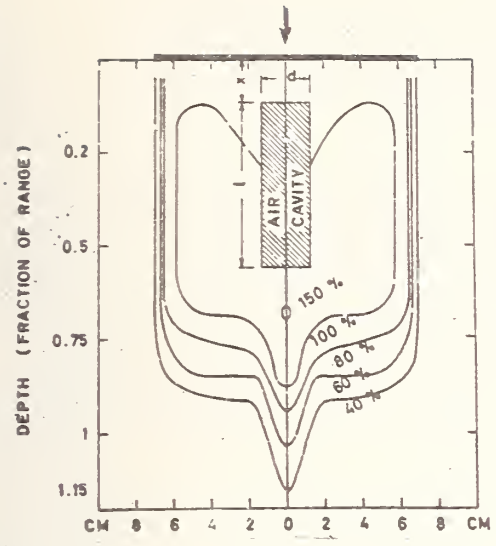

Fig. 6. Isodose curves for a 10 MeV electron beam in Carbon in the presence of a cylindrical cavity (2.5 cm length, 2.5 cm diameter) at a depth of 0.64 cm.

whereas no electrons are scattered out from the cavity. This has been observed experimentally also. (Starchman and Jen-Hung Chao[9]). However, there is quite a large disagreement between our results and those of Starchman and Jen-Hung Chao[9]. We are investigating the reasons for this discrepancy. It may be because of the bremsstrahlung contamination in the electron beam. Also the experimental measurements were made with photographic films - the Cerenkov radiation produced in the phantom material would have contributed significantly to the blackening of the film. Attempts are being made to correct for this.

Acknowledgements

The authors are grateful to M.A. Prasad and P.S. Iyer for the many useful discussions and help during the course of this work. Thanks are also due to K.G. Vohra for his keen interest in the work.

References

1. Spencer, L.V., Energy dissipation by fast electrons, NBS Monograph 1(1959).
2. Berger, M.J., Methods in Computational Physics Vol.1., ed. B. Adler, S. Fernbach and M. Rotenberg (New York and London Academic Press), pp 135-215 (1963).
3. Landau, L., J.Phys. USSR, 8, 201(1944).
4. Goudsmit, S. and Saunderson, J.L., Phys. Rev., 57, 24(1940).
5. Sundararaman, V., Prasad, M.A. and Vora, R.B., Phys.Med.Biol., 18, 208 (1973).
6. Moliere, G., Z. Naturf., 3A, 78(1948).
7. Mckinley, W.A. and Feshbach, H., Phys. Rev. 74, 1759(1948).
8. Møller, Zeits.f.Physik, 70, 786(1931).
9. Starchman, D.E. and Jen-Hung Chao, Radiology, 104, 177(1972).

BACKSCATTERING OF GAMMA RAYS

Tomonori Hyodo
Department of Nuclear Engineering
Kyoto University
Sakyo-ku, Kyoto
Japan

A survey of principal research on the backscattering of gamma rays is described. This is a macroscopic phenomena composing many photons scattered backward from a surface of material. After a historical survey as an introduction, principal theme of research is described; nomenclature of albedo, Monte Carlo calculation, measurement of albedos, semi-empirical formula of the differential albedo, exposure dose rate distribution outside a scatterer, distribution of scattered gamma rays on the surface.

(Albedo, backscattering, distribution, dose rate, gamma rays, Monte Carlo, photon.)

Introduction

During last 20 years much progress has been made toward the calculation and measurement of multiple scattering of gamma rays backward from the surface of material, namely backscattering of gamma rays. It may be said that the details of this type of interactions are now known to considerable accuracy. Most of papers are published in ten years, from 1959 to 1968. Review articles and books covering this field were published in the end of this period.[1-5] This paper is a survey of works in this field adding recent progress.

There are two large groups of published papers in this field. One concerns on the reflection characteristics of material, such as total albedo, differential albedo, reflection build up factors, and the other concerns exposure rate field distribution outside and on a scatterer.

Hine and McCall[6], Hayward and Hubbell[7] measured backscattering of gamma rays as a macroscopic phenomenon and they knew considerable amount of gamma rays were scattered backward. Bulatov and Garusov[8-10] used a small dosimeter without a collimator, Hyodo[11] used a small point isotropic source on the surface of a scatterer and a NaI(Tl) scintillator without a collimator. After these experiments measurements of total albedos have been continued.[12-22]

Monte Carlo method has been applied successfully for simulation of multiple scattering phenomena of gamma rays in material with the development of computers. Hayward and Hubbell[23] calculated albedos by a desk computer, Perkins[24], Berger and Doggett[25] and other workers[26-32] calculated total albedos using electronic computers. Total albedos and reflection build-up factors were calculated using invariant imbedding method[33], Moments Method[34], and semi-analytical method.[105-106]

For the necessity of estimation of exposure dose rate distribution outside a scatterer and estimation of duct streaming gamma rays several Monte Carlo calculations of differential albedos have been carried out with increasing of calculation speed[35-41]. Many experimental works measured differential albedos to obtain total albedos by integration[8,9,11-12]. Precise measurements of differential albedos have an utility to compare calculated values. Steyn and Andrews[42] and other workers[43-48] measured them. Bulatov[49] compiled these data in a form having good availability to calculate exposure dose rate distribution. Chilton and Huddleston[50-52] derived a semi-empirical formula for the differential albedo of concrete and applied for the estimation of the distribution. Shoemaker and Huddleston[54] proposed an approximation method to reduce the number of necessary angles for the calculation and experiment.

Backscattered radiation of bremsstrahlung of betatrons was measured by Pruitt[54] and other workers[55-57].

Berger[58] calculated energy dissipation in a medium with the scattering properties of water which consists of two semi-infinite regions, one of which is much denser than the other. Titus[59]

simulated experimentally with iron. Clarke and Batter[60] and other workers[61-63] measured scattered gamma ray exposure dose rate distribution. Chilton[64-65] and other workers[66-67] proposed calculation methods for the distribution and compared to the experimental results.

Propagation of gamma rays at or near an air-ground interface was measured by many workers[68-79] and a review article was written by Clarke[80]. Garrett[81] proposed a shielding benchmark problem and call for theoretical calculations and experiments.

Emergent gamma rays at an interface with point source placed on the interface was investigated by Bulatov[9], Hyodo[11], Davisson and Beach[82] and other workers[83-90].

Scattered gamma rays at an air-ground interface from air atoms is sky-shine. Several works has been published on this problem[91-94].

Several works[95-98] were published on the backscattering from room walls, a spherical shell and complicated configurations.

As an example of application of albedo concept, calculation of duct streaming[99-100] is shown.

Definition of Albedos

The quantities that characterized the reflection probability of material are called albedo. The definition of the albedo is described in many books and papers[3-5,35,65]. Traditionally, the albedo refers the ratio of the radiation entering in and leaving from a small area dS of the surface of a scatterer. In this usage the albedo is a ratio of current passing through dS and not of flux density. Several papers[3,35,65] discussed on this point in details.

Consider, for example, a monodirectional source of radiation of energy E_0 incident on a surface at polar angle θ_0 as shown in Fig. 1. The reflected current of energy E per unit energy per unit solid angle at polar angle θ and azimuthal angle ϕ is given by,

$$J(E,\theta,\phi) = J(E_0,\theta_0)\ \alpha(E_0,\theta_0;\ E,\theta,\phi) \quad ..(1)$$

where $J(E_0,\theta_0)$ is the incident current and $\alpha(E_0,\theta_0;\ \theta,\ \phi)$ is called (double) differential albedo or energy-angular distribution passing through the surface. The quantities of current incident and outgoing was measured by photon number, energy, and exposure dose rate are written by J_{ON}, J_N; J_{OE}, J_E; J_{OD}, J_D, respectively. Number differential albedo α_N, energy differential albedo α_E, dose differential albedo α_D is defined as follows:

$$\begin{aligned} J_N &= J_{ON}\ \alpha_N(E_0,\ \theta_0;\ \theta,\ \phi) = \\ &\quad J_{ON}\int\alpha_N(E_0,\ \theta_0;\ E,\ \theta,\ \phi)dE \\ J_E &= J_{OE}\ \alpha_E(E_0,\ \theta_0;\ \theta,\ \phi) = \\ &\quad J_{OE}\int\alpha_E(E_0,\ \theta_0;\ E,\ \theta,\ \phi)dE \\ J_D &= J_{OD}\ \alpha_D(E_0,\ \theta_0;\ \theta,\ \phi) = \\ &\quad J_{OD}\int\alpha_D(E_0,\ \theta_0;\ E,\ \theta,\phi)dE \end{aligned} \quad ..(2)$$

Total number albedo A_N, total energy albedo A_E, and total dose albedo A_D is obtained by integration of differential albedos,

$$\begin{aligned} A_N &= \int_0^{2\pi} d\phi \int_0^{\pi/2}\alpha_N(E_0,\ \theta_0;\ \theta,\ \phi)\ \sin\theta\ d\theta \\ A_E &= \int_0^{2\pi} d\phi \int_0^{\pi/2}\alpha_E(E_0,\ \theta_0;\ \theta,\ \phi)\ \sin\theta\ d\theta \\ A_D &= \int_0^{2\pi} d\phi \int_0^{\pi/2}\alpha_D(E_0,\ \theta_0;\ \theta,\ \phi)\ \sin\theta\ d\theta \end{aligned} \quad ... (3)$$

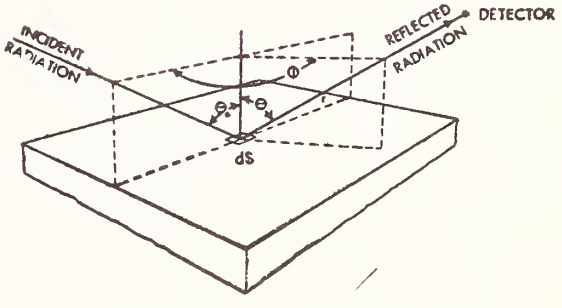

Fig. 1. Reflection geometry.

Scattered radiation flux and exposure dose rate outside a scatterer can be estimated if the value of differential albedo is known for every emerging angle of θ and o.

For the case of uniform monodirectional gamma rays are incident to a scatterer as shown in Fig. 2 a. The number and energy flux and exposure dose rate at a detector caused by photons emerging from an incremental area dS is

$$d\Phi_N = \frac{n_0 \cos\theta_0 \alpha_N dS}{r^2}$$

$$d\Phi_E = \frac{n_0 E_0 \cos\theta_0 \alpha_E dS}{r^2} \qquad \ldots(4)$$

$$dD = \frac{n_0 E_0 \eta \cos\theta_0 \alpha_D dS}{r^2}$$

where n_0 is photon flux at dS, r is the distance between the center of dS and the detector, η is the conversion constant from photon intensity to exposure rate.

For the case of a point isotropic source emitting Q photons/sec placed at r_0 from dS as shown in Fig. 2 b, formulas are,

$$d\Phi_N = \frac{Q \cos\theta_0 \alpha_N dS}{4\pi r_0^2 r^2}$$

$$d\Phi_E = \frac{Q E_0 \cos\theta_0 \alpha_E dS}{4\pi r_0^2 r^2} \qquad \ldots(5)$$

$$dD = \frac{Q E_0 \eta \cos\theta_0 \alpha_D dS}{4\pi r_0^2 r^2}$$

Monte Carlo Method

The backscattering of gamma rays has been the subject of a number of Monte Carlo calculations and got great success. Practical methods of the application are described in several books.[101-104]

The reason of success is following. Cross section of the interaction of gamma rays with matter is well known and monotonic functions with energy. The standard deviation is given by[26]

$$\sigma = \sqrt{\frac{A(1-A)}{N-1}} \qquad \ldots(6)$$

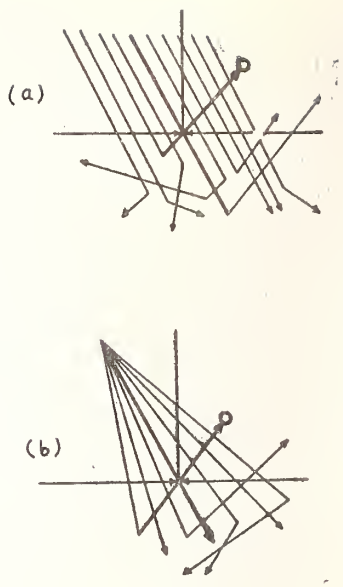

Fig. 2. Geometry of scattered gamma-ray calculation. a. Plane monodirectional source. b. Point isotropic source.

where A is the value of albedo and N the number of histories. The value of A is between 0.01 to 0.6, so small value of standard deviation σ is obtained.

The earlier works using Monte Carlo method were calculation of total albedos and reflection build up factors for uniform materials having plane surfaces and spherical shell[24-32]. After these works sufficient histories for the calculation of differential albedo have been available since ten years ago with increasing of calculation speed of digital computers. Numerical tables and graphs were published on several papers and books.[5,35-41] These calculated results are shown in the following paragraphs.

Measurement of Albedos

Measurement of differential albedos has been carried out by many workers. Most of these works had a purpose partially to obtain total albedos by integration of differential albedos, but several works had not the purpose because data of differential albedos were very important to get an information of scattered gamma rays in a definite direction and to compare calculated results as a benchmark experiment.

Measurement of photon current incident to and emergent from a small

area dS on the surface of a scatterer, truly to the definition, is difficult, because most of the photons incident to dS emerge from outside of dS or captured in the scatterer. Following three geometries are approximately possible to the measurement.

The first geometry is a narrow, well-collimated beam of gamma rays incident on a scatterer at a desired angle, together with isotropic detectors around on a hemispheric shell centered around the irradiation area as shown in Fig.3a. Bulatov and Garusov[8], Efimenko[40], Clifford[43], and Elias et al[48] measured scattered gamma rays with this well-collimated-beam geometry.

The second geometry is the irradiation of large scattering medium with a wide beam of gamma rays to simulate an infinite plane monodirectional source of gamma rays and use a well-collimated detector to observe the angular dependence of the scattered radiation emitted from a small surface region near the center of the irradiated area as shown in Fig. 3 b. Steyn and Andrews[42], Haggmark et al[44], and Barran et al[47] measured scattered gamma rays using well collimated detectors.

Both case has a dead space of measurements caused by beam of radiation, shadow of collimator or shield. The third geometry Fig. 3 c, is rather special case, but it has not any dead space of measurement. A small point isotropic source placed on the surface of a scatterer and a detector without a collimator moves on a hemisphere of sufficiently large radii. Bulatov[9], Hyodo and his coworkers[11-14], and Pozdneev[17-19] measured scattered gamma rays with this geometry.

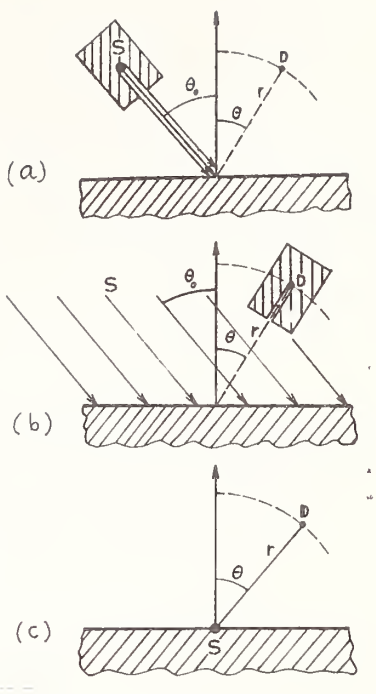

Fig. 3. Geometry of measurement for back-scattered gamma rays.

Albedo Data

Figure 4 shows Monte Carlo results of the total energy albedo for several elements as a function of energy. In high energy region, the albedo value decreases with increasing of energy because the differential cross-section of large angle scattering decrease with increase of energy. Figure 5 shows the total energy albedo value obtained by experiment. The figure shows the albedo value increase with increasing of scatterer thickness. Bulatov and Garusov[8] derived following experimental formula

$$A_E(d) = A_E(\infty)(1 - e^{-d/a}) \qquad \ldots(7)$$

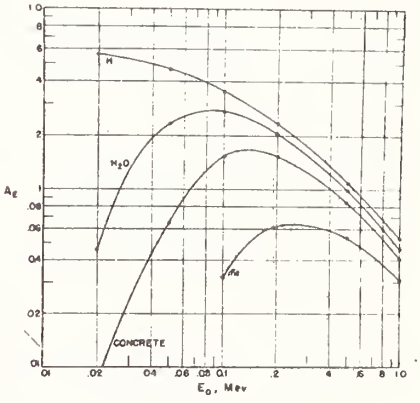

Fig. 4. Energy albedo as function of the source energy (perpendicular incidence, θ=0). (ref. 26)

where d is thickness of the scatterer and a is a constant. Figure 6 shows the total energy albedo obtained by third geometry. Figure 7 shows the value of differential albedo. There is two distinct group of curves in the figure. Upper two curves obtained by third geometry and lower group obtained by first geometry.

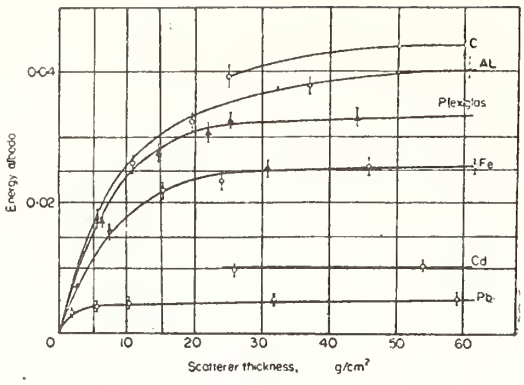

Fig. 5. Energy albedo as function of scatterer thickness (^{60}Co,θ_0=0). (ref.8)

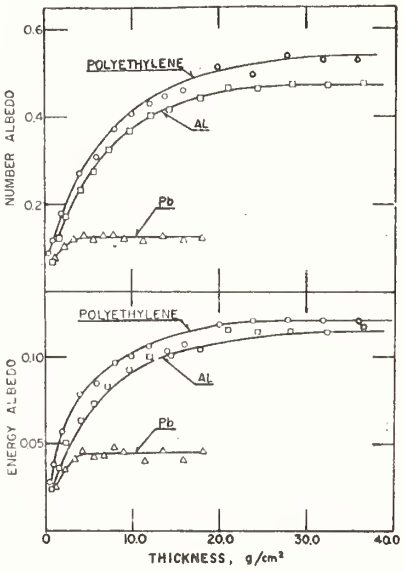

Fig. 6. Number and energy albedos as function of scatterer thickness (^{60}Co, point isotropic source placed on the surface). (ref.13)

Study of back scattered radiation caused by high-energy bremsstrahlung from a betatron and a linear accelerator is very important for the estimation of exposure distribution and for the understanding of scattering phenomena of high energy photons.

Figure 8 shows energy spectra of photons back scattered from aluminium scatterer, incident and emerging angles (θ_0, θ) = (0^o, 20^o). The energy of photons in the spectra is less than 0.5 MeV or annihilation radiation because of

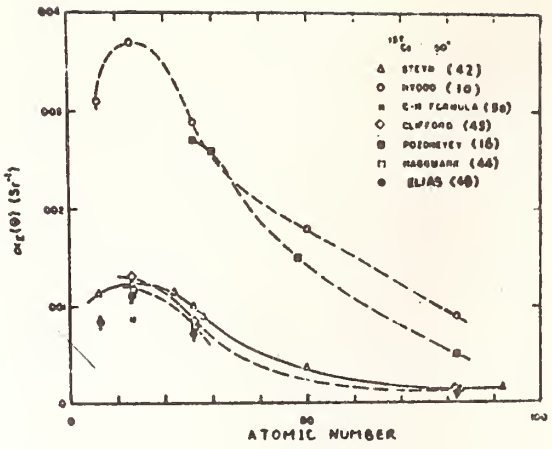

Fig. 7. Differential energy albedo as function of scattering angle (ref.48).

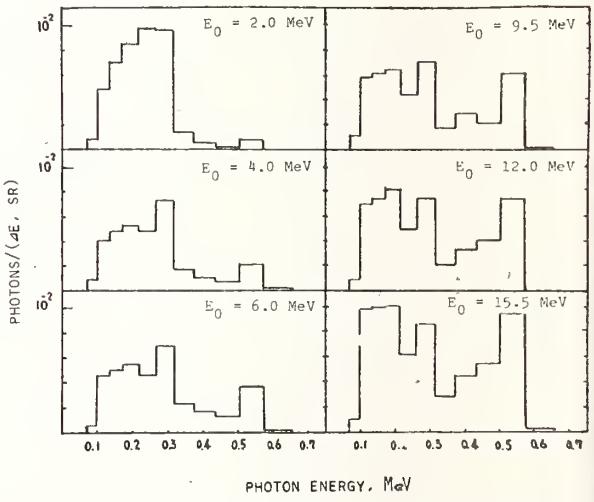

Fig. 8. Energy spectra of scattered radiation from aluminium. (ref.56

singly scattered gamma rays. Figure 9 shows the differential dose albedo for aluminium.

SEMIEMPIRICAL FORMULA OF DIFFERENTIAL ALBEDO

For the application of albedo concep for the calculation of duct streaming of gamma rays, scattered gamma ray exposure rate field, albedo values for many directions of emerging are necessary. A semi-empirical formula is very useful to interpolate albedo values from calculate and experimental data.

Chilton and Huddleston[50] derived a semi-empirical formula for the differ-

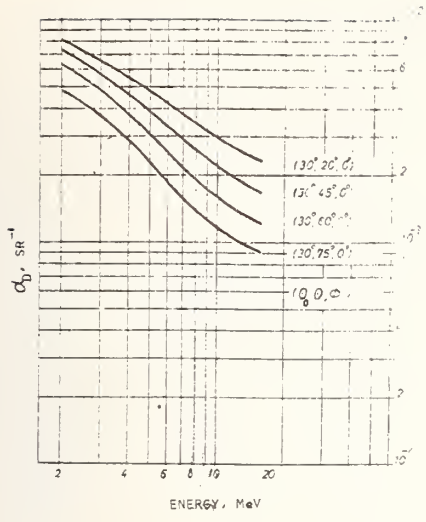

Fig. 9. Differential dose albedo as function of electron energy. (ref. 56)

ential dose albedo of concrete on the assumption: Scattered radiation can be broken down into two parts, one is proportional to single Compton scattering and the other is isotropically scattered; the effective attenuation coefficient $\bar{\mu}$ does not vary greatly during a scattering history. The differential dose albedo α_D is

$$\alpha_D = \frac{C.10^{26}.\ K_e(E_0,\ \theta_s) + C'}{1 + \frac{\cos\theta_0}{\cos\theta}} \qquad ...(8)$$

where θ_s is the scattering angle between the incident and outgoing ray, given by following formula,

$$\cos\theta_s = \sin\theta_0 \sin\theta \cos\phi - \cos\theta_0 \cos\theta \qquad ...(9)$$

and $K_e(E_0, \theta_s)$ is the energy scattering Klein-Nishina crosssection per electron, and C and C' are constants.

The value of differential albedos depends on the incident gamma ray energy and three angles θ_0, θ, ϕ, excluding axial symmetry case, $\theta_0 = 0$ or point isotropic source placed on the surface of a scatterer. Shoemaker and Huddleston[53] demonstrated a interpolation method to obtain the differential albedo for the direction (θ, ϕ) from those of $(\theta, 0^o)$ and $(\theta, 180^o)$.

EXPOSURE DOSE RATE DISTRIBUTION OUTSIDE A SCATTERER

It is necessary very often to estimate exposure dose rate distribution outside a scatterer as shown in Fig. 10. The exposure dose rate at the detector is superposition of those primary gamma rays from the source and those of scattered gamma rays from the scatterer.

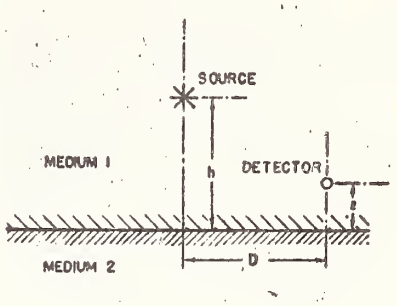

Fig. 10. Geometry of measurement.

Figures 11 and 12 show exposure dose rate distribution in the case h = z in Fig. 10. Medium 1 was air and medium 2 concrete. As shown in these figures the ratios between the exposure dose rate caused by gamma rays scattered from concrete and those of primary gamma rays are fair agreement at the same h/D values.

Chilton[64,65] calculated scattered gamma-ray exposure dose rate using formulas (5) and (8). The calculated value is shown in Fig. 11. The curve shows fair agreement with experimental data.

Kitazume[67] proposed a calculation method. The scattered gamma rays to the detector was calculated following formula,

$$D = \frac{Q.\eta}{2\pi} \int \frac{N_e\ d\sigma/d\Omega\ \exp(-\mu_1\rho_1 - \mu_2\rho_2)\ B(\rho_2)}{4\pi\ r_0^2\ r^2} dv \qquad ...(10)$$

where N_e is electron number per cm^3, $d\sigma/d\Omega$ is Compton scattering cross section, ρ_1 and ρ_2 is path length of primary and secondary gamma rays in the scatterer, and $B(\rho_2)$ is the build up factor for scattered gamma rays. Calculated results are shown in Figs. 11 and 12.

Hendee and Ellis[62] calculated on the assumption of isotropic scattering and showed good fit for the experimental value

in the range of the ratio h/D is more than 0.5 as shown in Fig. 12

A review article on the propagation of gamma rays at or near an air-ground interface was written by Clarke[82].

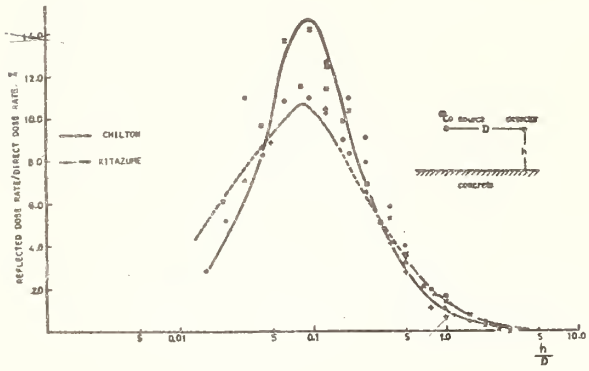

Fig. 11. Ratio of scattered to direct ^{60}Co exposure dose rate as function of h/D. (ref. 60)

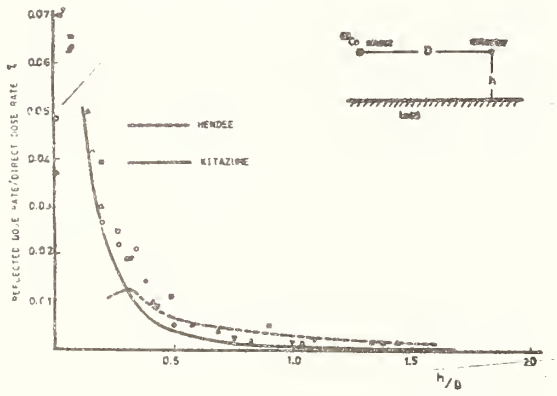

Fig. 12. Ratio of scattered to direct ^{60}Co exposure dose rate as function of h/D. (ref.62)

DISTRIBUTION OF SCATTERED GAMMA RAYS ON THE SURFACE

Scattered gamma ray distribution on the surface of a scatterer was measured and calculated by several workers on the case of a point isotropic source was placed on the surface.

Figure 13 shows the distribution of emergent energy or the intensity of photons emerging in an annulus of unit width at radius r calculated by Monte Carlo method together with experimental data. The experimental data were measured emergent photons normally to the surface.

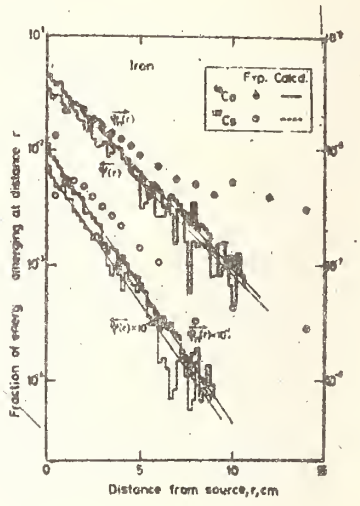

Fig. 13. Radial distribution of energy back scattered from within

These data show that emergent energy Ψ is fitted by following formula,

$$\Psi = \Psi_0 e^{-br} \qquad \ldots (11)$$

where Ψ_0 and b are constants. Differentiating this formula, we can get I(r) as emerging energy an unit area at r,

$$I(r) = C \frac{e^{-ar}}{r} \qquad \ldots (12)$$

where C and a are constants.

References

1. Bulatov, B.P. et al., Vop. Doz. Zash. Izluch. Vol. 5, pp. 5-35, 1966 (in Russian).
2. Hyodo, T. Nippon Genshi-Ryoku Gakkaishi 8, 371 (1966) (in Japanese); ORNL-TR-1670 (English translation).
3. Selph, W.E. Neutron and gamma ray albedos, ORNL-RSIC-21, (DASA-1892-2), 1968.
4. Leimdörfer, The back scattering of photons, in R.G. Jaeger ed., Engineering Compendium on Radiation Shielding, Vol. 1, pp. 233-245, Springer-Verlag, Berlin, 1968.
5. Bulatov B.P. et al., Al'bedo gamma-izlucheniya, Atomizdat, Moscow, 1968.
6. Hine, G.J. and McCall, R.C., J.Appl. Phys. 25, 506 (1954).
7. Hayward, H. and Hubbell, J.H., J. Appl. Phys. 25, 506 (1954).

8. Bulatov, B.P. and Garusov, E.A., At. Energ. 5, 631 (1958); Reactor Sci. 11, 159 (1960).
9. Bulatov, B.P., At. Energ. 7, 369 (1959); Sov. At. Energ. 7, 847 (1961).
10. Bulatov, B.P. and Leipunskii, O.I., At. Energ. 551 (1959); Soc. At. Energ. 7, 1015 (1961).
11. Hyodo, T., Nucl. Sci. Eng. 12, 178 (1962).
12. Fujita, H., Kobayashi, K. and Hyodo, T., Nucl. Sci. Eng. 19, 437 (1964).
13. Mizukami, K. et al., J. Nucl. Sci. Tech. 4, 607 (1967).
14. Nishi, M. et al., Memo. Faculty of Eng., Kyoto Univ., 29, 474 (1967).
15. Bulatov, B.P. and Andryushin, N.F., At. Energ. 22, 307 (1967); Sov. At. Energ. 22, 383 (1967).
16. Pozdneev, D.B., At Energ. 20, 317 (1966); Sov. At. Energ. 20 (1966).
17. Pozdneev, D.B., At. Energ. 20, 317 (1966); Sov. At. Energ. 20, 354 (1966).
18. Pozdneev, D.B. et al., At. Energ. 22, 358 (1967); Sov. At. Energ. 22, 358 (1967).
19. Pozdneev, D.B., At Energ. 22, 308 (1967); Sov. At. Energ. 22, 358 (1967).
20. Skvortsov, B.M. et al., At. Energ. 22, 404 (1967); Sov. At Energ. 22, 505 (1967).
21. Nakamura, T. and Hyodo, T., J. Nucl. Sci. Tech. 5, 458 (1968).
22. Nakamura, T. and Hyodo, T., Nucl. Sci. Eng. 36, 246 (1969).
23. Hayward, E. and Hubbell, J.H., Phys. Rev. 93, (1954).
24. Perkins, J.F., J. Appl. Phys. 26, 655 (1955).
25. Berger, M.J. and Doggett, J., J.Res. NBS 56, 89 (1956).
26. Berger, M.J.and Raso, D.J., Rad. Res. 12, 20 (1960).
27. Davisson, C.M. and Beach, L.A., Gamma-ray albedo of iron, NRL Quarterly of Nucl. Sci. and Tech. Progress Rep. for the period Oct.-Dec. 1959 (1960).
28. Berger, M.J., J.Res. NBS 55, 343(1955).
29. Raso, D.J., Rad. REs. 19, 384 (1963).
30. Leidörfer, M., Nucl.Sci.Eng.17, 345 (1963).
31. Leimdörfer, M., Nucl.Sci.Eng.17, 352 (1963).
32. Leimdörger, M., Nucl.Sci.Eng.17, 357 (1963).
33. Shimizu, A. and Mizuta, H., J.Nucl. Sci. Tech. 3, 57 (1966).
34. Smith, C.V. and Scofield, N.E., Nucl. Sci. Eng.47, 1 (1972).
35. Raso, D.J., Nucl.Sci.Eng.17, 411(1963).
36. Raso, D.J, Monte Carlo calculations on the reflection and transmission of scattered radiation, Technical Operations, Inc.Rep.No.TO-B-61-39.1961.
37. Raso, D.J, Monte Carlo codes to investigate the reflection and transmission of gamma rays and neutrons in homogeneous slabs, Final Report, Vol.III, results, Technical Operations Rep. No. TO-B-63-83, 1963.
38. Wells, M.B. Differential dose albedos for calculation of gamma-ray reflection from concrete, AD 615 598, RRA-T 46, 1964.
39. Berger, M.J. and Morris, E.E., Dose albedo and transmission coefficients for cobalt-60 and cesium-137 gamma ray incident on concrete slabs, NBS Report 9071, 1966.
40. Efimenko, B.A. et al., Vop.Doz.Zash. Izuch. Vol.5, 36 (1966).
41. Viktorov, A.A., At.Energ.23, 187(1967); Sov.At.Energ.23, 907 (1967).
42. Steyn, J.J. and Andrews, D.G., Nucl.Sci. Eng.27, 318 (1967).
43. Clifford, C.E., Can.J.Phys.42, 957 (1964).
44. Haggmark, L.G. et al., Nucl.Sci.Eng. 23, 138 (1965).
45. Pozdneev, D.B. and Churin, S.A., At. Energ. 20, 352 (1966); Sov. At. Energ.407 (1966).
46. Viktorov, A.A. et al., Vop.Doz.Zash. Izluch. Vol.6, 66 (1967)(in Russian).
47. Baran, J.A.et al., Nucl.Instr.Methods 75, 141 (1969).
48. Elias, E., J.Nucl. Energy. 27, 351 (1973).
49. Bulatov, B.P., At. Energ. 21, 345 (1966); Sov. At.Energ. 21, 345(1966).
50. Chilton, A.B. and Huddleston, C.M., Nucl. Sci. Eng. 17, 419 (1963).
51. Chilton, A.B. et al., Trans.American Nucl. Soc. 8, No.2, 656 (1965).
52. Chilton, A.B., Nucl. Sci. Eng.27, 481 (1967).
53. Shoemaker, N.F. and Huddleston, C.M., Nucl. Sci. Eng. 18, 113 (1964).
54. Pruitt, J.S., Nucl. Instr.Methods 27, 23-28 (1964).
55. Sugiyama, S. and Tomimasu, T., Nucl. Instr. Methods 53, 346 (1967).
56. Vogt, H.G., Nucl. Eng.Design 22, 138 (1972).
57. Maruyama, T. et al., Shimazu Hyoron 31, 39 (1974) (in Japanese).
58. Berger, M.J., J.Appl. Phys. 28, 1502 (1957).
59. Titus, F., Nucl. Sci.Eng.3, 609 (1958).
60. Clarke, E.T. and Batter, J.F., Nucl. Sci. Eng. 17, 125 (1963).
61. Henry, W.H. and Garrett, C., Acta Radiologica 2, 353 (1964).
62. Hendee, W.R. and Ellis, J.L., Health Phys. 12, 673 (1966).
63. Bozoky, L., Health Phys.20, 467-473 (1971).
64. Chilton, A.B., Nucl.Sci.Eng.21, 194 (1965).
65. Chilton, A.B., Backscattering for gamma rays from a point source near a concrete plane source, Univ. Illinois, College of Eng.Bulletin 471.
66. Eisenhauer, C., Health Phys.11, 1145 (1965).
67. Kitazume, M., J.Nucl.Sci.Eng.5, 98 (1969).

68. Clifford,C.E. et al.,Can.J.Phys. 38, 504 (1960).
69. Kukhtevich,V.I.et al., At. Energ. 8, 66 (1960); Sov. At.Energ.8,66 (1960).
70. Bulatov,B.P.,At.Energ.13, 440 (1962); Sov.At.Energ. 13, 1058 (1962).
71. Clifford,C.E., Can. J. Phys.42,2373 (1964).
72. Ermakov,S.M. et al.,At. Energ. 18, 534 (1964); Sov. At.Energ. 18, 416 (1965).
73. Vasil'ev,M.B., At. Energ. 21, 121 (1966); Sov. At. Energ.754 (1966).
74. Vasil'ev, M.B. and Merkel',M.A., At. Energ.21,134 (1966); Sov.At. Energ. 21,775 (1966).
75. Vasil'ev,M.B.,At. Energ.21,135 (1966); Sov.At. Energ.21,777(1966).
76. Kolebatov,Yu.I. et al., Vop.Phys. Zasch.React.Vol.2,pp.216-225(1966).
77. Andryshin,N.F. and Bulatov,B.P., At. Energ. 22,404 (1967).
78. Chilton,A.B.,Nucl. Sci.Eng.27,403 (1967).
79. Clifford,C.E. and Wait,C.D., Nucl. Sci.Eng. 27,483 (1967).
80. Clarke,E.T.,Nucl. Sci.Eng.27,394 (1967).
81. Garrett,C.W., Gamma-ray dose above a plane source of ^{60}Co on an air/ ground interface,Shielding Benchmark Problem 4.0,ORNL-RSIC-25 (ANS-SD-9) pp.4.0-1 - 22 (1969).
82. Davisson, C.M. and Beach,L.A., ANS Trasn.No.2,391 (1962).
83. Nakamura,T. and Hyodo,T.,Trans. 3rd Robutsuri Bunkakai,p.34 (1963) (in Japanese).
84. Marenkov,O.S.,At.Energ.21,297(1966).
85. Waechter,K.H.,Kerntechnik 9,62-64 (1967).
86. Andryushin,N.F. et al.,At.Energ. 23,110 (1967); Sov.At.Energ. 23, 802 (1967).
87. Nakamura,T. and Hyodo,T.,J.Nucl. Sci.Tech.6,143 (1969).
88. Wechselberger,E.,Atomkernenergie 16, 64 (1970).
89. Preiss,K. and Livnat,R.,Nucl.Eng. Design 24,258 (1973).
90. Pozdneev,D.B. and Faddeev,M.A., Kernenergie 16, 105 (1973).
91. Lynch,R.E. et al.,A Monte Carlo calculation of air-scattered gamma-rays, ORNL-2291, Vol.I,1958.
92. Trubey,D.K., Nucl.Sci.Eng.10,102 (1961).
93. Shimamura,A.,J.Nucl.Sci.Tech. 3, 300 (1966).
94. Kitazume,M.,J.Nucl. Sci.Tech. 5, 464 (1968).
95. Andryushin,N.F. and Bulatov,B.P., At.Energ.At.Energ.19,392 (1965).
96. Andryushin,N.F.et al.,At.Energ. 21, 298 (1966).
97. Bulatov,B.P. et al., At. Energ. 23, 240 (1967); Sov. At. Energ.23, 965 (1967).
98. Birchall Ivan.,Health Phys.16, 47 (1969).
99. LeDoux,J.C. and Chilton,A.B., Nucl. Sci.Eng. 11,362 (1961).
100. Zolotukhin,V.G. et al.,Radiation Transmission through inhomogeneities in Shields,Atomizdat,Moscva,1968 (translation in English,AEC-tr-7175).
101. Goertzel,G. and Kalos,M.H., Monte Carlo Methods in Transport Problems, Progress in Nucl. Energ. Series 1, Vol.2,pp.315-375, Pergamon Press, London,1958.
102. Cashwell,E.D. and Everett,C.J., A Practical Manual on the Monte Carlo Method for Random Work Problems, Pergamon Press, London, 1959.
103. Leipunskii,O.I. et al.,The Propagation of Gamma Quanta in Matter (translated from Russian),Pergamon Press, London, 1965, (original, Atomizdat, Moscwa, 1960).
104. Biro,G.G. 3.1. Application of the Monte Carlo Method to Shielding, Engineering Compendium on Radiation Shielding, Vol.I,pp.101-124, Springer-Verlag,Berlin,1968.
105. Gopinath, D.V. and Santhanam,K., Nucl. Sci. Eng. 43,186 (1971).
106. Gopinath, D.V. and Santhanam,K., Nucl. Sci. Eng. 43,197 (1971).

TRANSMISSION OF ^{252}CF FISSION NEUTRONS THROUGH VARIOUS SHIELDS

Yo Taik Song
Nuclear Physics Division
U.S. Naval Surface Weapons Center
White Oak, Silver Spring, Maryland,
U. S. A.

Measurements have been made of neutron transmission through various shield configurations. A ^{252}Cf source, having a neutron yield of 1.02 x 10^6 n/sec was used with a US Navy neutron dosimeter, AN/PDR-70. This detector was used to measure the integrated neutron dose equivalent (DE). 3 by 5 ft. slab shields of various materials were used, such as iron, lead, polyethylene, combinations of iron-polyethylene, lead-polyethylene, and iron polyethylene-iron. The measured data were corrected for room-scattered contributions. The scattered neutron DE was calculated using the differential dose albedo formula of Song, et al[1]. The experimental data thus obtained were compared with calculated values. The one-dimensionsal discrete ordinates neutron transport code, ANISN, with 40 energy groups, 22 groups for neutron and 18 groups for γ-rays, was used for the transmission calculations. Comparisons were made in terms of attenuation factors, the ratio of transmitted neutron DE to free-field neutron DE at the detector point. Agreement was within the expected dosimeter range of 20% for all cases. For the case of two inches of iron and five inches of polyethylene, placing the iron on the source side was more effective than placing it on the opposite side.

(ANISN ; ^{252}Cf ; code ; configuration ; dose equivalent ; energy ; gamma rays; neutron ; scattering; shield ; transmission)

Introduction

The transmission of neutrons from the ^{252}Cf source through various shields was measured by a neutron dosimeter, AN/PDR-70. The ^{252}Cf source is a small cylinder of about 0.25 inches in diameter and 2.5 inches long, and has a relatively high neutron yield of $\sim 10^6$ neutrons/sec. The AN/PDR-70[2] is a U.S. Navy standard neutron dosimeter of a modified Anderson Brown type, that measures thermal neutron flux with a BF_3 tube surrounded by cylindrical polyethylene moderator. The moderator is 8.5 inches in diameter and 9.4 inches in height.+

The purpose of the study is to find out the effectiveness of steel and other materials for shielding fission neutrons. The steel is commonly used as structural material in conjunction with neutron moderating materials such as the polyethylene. The experiment is simulated by the one dimensional discrete ordinate radiation transport code ANISN[3,4]. The ANISN results are compared with experimental results of various shield configurations. If the agreement between experiment and computational results is favourable, the effective attenuation kernel for further shielding calculations involving other shield configurations with other materials can be obtained and the confidence level in the computational results can be established. Furthermore, the choice of group structure and multigroup cross sections used in ANISN may be evaluated by comparing the experiment and computational results.

Experiments

The experiments were performed in a room about 28 ft. by 30 ft. in area and about 20 ft. high. The walls, floor and ceiling are concrete slabs. The source and detector were about 10 ft. above the

+ This dosimeter is calibrated to read dose-equivalent with units rem or millirem per hr. Hereafter, whenever neutron dose is used it will be understood to mean dose-equivalent.

floor. The shields were 3 ft. by 10 ft. with various thickness and placed on the rack so that the centers of the shield faces lie on the source detector line and the faces are normal to it. The source-detector distance in transmission measurements was kept constant at 2.5 ft. Various shields were placed on the rack and the distance from the source to source side face of the shield was kept at 10 inches. In Table I, the various shields used in the experiments are given. The left hand side material in this table was facing the source.

In order to aid in determining the component of the neutrons scattered from walls, ceiling and floor, the neutron dose rates were measured for various distances from the source. Results are shown in Figure 1. All data presented in this paper were corrected for natural background and have fractional standard deviations less than or equal to 5% of the measured values. The possible error in measurements of distance between source and detector is no greater than 3% of the measured values.

Analysis

In the calculation an S16 quadrature with 22 neutron and 18 gamma ray groups was utilized. The group structure, ^{252}Cf source spectrum, and DE conversion factors used in ANISN, are given in Table II. The ^{252}Cf source spectrum in 22 neutron groups is based on the data by Stoddard[5]. Basic cross sections are derived from the ENDF/B library, and edited into ANISN Format by Radiation Shielding Information Center. Cross sections for polymers, (polyethylene) were obtained by mixing carbon and hydrogen cross sections with the MACROMIX code. The basic cross sections have upto P_3 components in 22 neutron and 18 gamma energy groups. Monodirectional parallel beams of neutrons nearly normal to the shields were assumed in calculations. Based on the spectrum in Table II, the neutron DE at 2.5 ft. from the source was estimated to 1.69 mrem/hr, while the measured value was 1.64 mrem/hr with corrections for neutrons scattered from walls, ceiling and floor. The neutron yield at the time of the experiment was estimated to be 1.02×10^6 neutron/sec.

The room scattered neutrons reaching the detector were calculated by the method described by Song et al[1]. Utilizing the differential dose albedo concept with energy dependent parameters for the differential dose albedo formula, the scattered neutron DE was estimated to be 0.05 mrem/hr at the source-detector separation distance of 2.5 ft, the experimental detector location. When the shields were placed between the source and detector, the scattered neutron DE was estimated to be 0.026 mrem/hr. In Figure 1, the measured DE, measured DE with corrections for room scattered neutrons and the inverse square line fit to the corrected data by the least squares method are presented. From Figure 1, the room scattered corrections result in a good agreement between experimentally observed data and calculations. Therefore the room scattered data, 0.026 mrem/hr with shield in between source and detector, was subtracted to correct all

Table I

Shielding Material and Configurations

Materials	Thickness (inches)	Materials	Thickness (inches)
Iron	1	Polyethylene + Lead	6 + 1/2
Iron	2		
Iron	3	Iron + Polyethylene	1/2 + 5
Iron	4	Iron + Polyethylene	1 + 5
		Iron + Polyethylene	2 + 5
Lead	1/8		
Lead	1/4	Polyethylene + Iron	5 + 1/2
Lead	3/8	Polyethylene + Iron	5 + 1
Lead	1/2	Polyethylene + Iron	5 + 2
Polyethylene	2	Iron + Polyethylene + Iron	1 + 5 + 2
Polyethylene	4		
Polyethylene	6		
Polyethylene	8		

the shield transmission data. In Table III, the experimental results and calculated data for neutron transmission through various shields are given. In this Table, the results are given in terms of the attenuation factors, the ratio of transmitted neutron dose to free field neutron dose at the detector point. Further, comparison of the experimental results and theoretical results are presented in terms of the ratios of the calculated attenuation factor to the experimental attenuation factor.

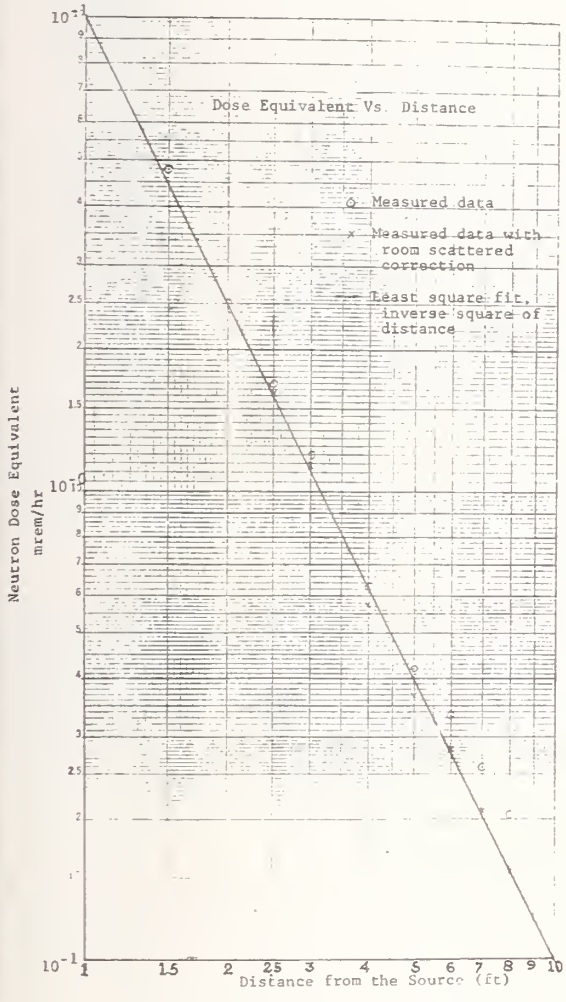

Fig. 1. Dose Equivalent Vs. Distance.

Discussion

From Table III, it is seen that the experiment and the calculated results are in good agreement. The agreement is generally better for thin shields than for thick shields as expected.

There are differences in the representation of the experimental geometry by ANISN. In the experiment, the source is a small cylinder, the shield is a finite slab and the detector is a cylinder. In ANISN, the source was assumed to be plane-monodirectional beam normally incident upon a semi-infinite slab shield and the detector to have an isotropic response. Therefore, neutrons scattered from beyond the actual geometry of the shield in ANISN were not detected in experiment. Further, in experiment, the scattering angle of neutrons reaching the detector by a single scattering in the shield is larger than those in ANISN. Therefore, the expected neutron dose reaching the detector by a single scattering in the shield will be larger in ANISN than those in experiment. Consequently, the thicker the shield, the greater the discrepancies between ANISN and experiment, as seen in Table III. It is also seen in Table III that iron is effective in neutron shielding if used with a moderating material such as polyethylene. Furthermore, the sandwich shield, iron + polyethylene + iron, was much more effective compared to the shield configuration of the same total amount of iron followed by polyethylene or polyethylene followed by iron, by about 25% . The attenuation afforded by one inch of iron followed by five inches of polyethylene was almost the same as five inches of polyethylene followed by two inches of iron.

That is, if iron and five inches of polyethylene are to be used for shielding of fission neutrons, place the iron on the source side. This conclusion can be drawn from both experimental and ANISN results. In Figure 2, the leakage spectrum from three different shields, one inch iron followed by five inches of polyethylene, five inches of polyethylene followed by two inches of iron and the sandwich shielding, are presented. Between about 0.1 to 1 MeV, there seems to be a window in the iron cross section that permits the neutrons to pass through. The contribution of a neutron to dose equivalent in the energy of 0.1 to about 1 MeV is about a factor of 3.5 higher than that of a thermal neutron. Although the iron behind the polyethylene is more effective in removing thermal neutrons, placing the iron in front of polyethylene is more effective in reducing the total neutron dose.

Acknowledgements

Assistance provided by D.C. Hugus and his group at PANTEX Plant in experimental work, technical consultation by D.E. Hankins at the Los Alamos Scientific Laboratory, C.M. Huddleston and N.E.

Table-II

Energy Group Structure, Cf^{252} Spectrum and DE Factors

Energy Group	Upper Energy (Mev)	NEUTRON DE* Factors	Source Spectrum (Fraction/Group)	Energy Group	GAMMA RAYS Upper Energy (Mev)	Dose+ Factor
1	15.0	5.8(-8)	0.0			
2	12.2	4.6	0.0			
3	10.0	4.1	2.70-3	23	10.0	2.72(-9)
4	8.18	4.1	1.57-2	24	8.0	2.30
5	6.36	3.9	3.83-2	25	6.5	1.90
6	4.97	3.7	4.94-2	26	5.0	1.60
7	4.07	3.6	1.19-1	27	4.0	1.32
8	3.01	3.5	9.05-2	28	3.0	1.10
9	2.46	3.5	2.27-2	29	2.5	.97
10	2.35	3.6	1.19-1	30	2.0	.83
11	1.83	3.7	2.30-1	31	1.66	.67
12	1.11	3.3	2.14-1	32	1.33	.53
13	5.50-1	1.5	9.87-2	33	1.00	.445
14	1.11-1	.18	0	34	.80	.35
15	3.35-3	.12	0	35	.60	.256
16	5.83-4	.13	0	36	.40	.177
17	1.01-4	.13	0	37	.30	.122
18	2.90-5	.125	0	38	.20	.066
19	1.07-5	.12	0	39	.10	.039
20	3.06-6	.115	0	40	.05	.084
21	1.12-6	.110	0			
22	4.14-7	.105	0			

* rem/neutron/cm^2

\+ rem/gamma ray/cm^2

Table-III

Dose Attenuation For Cf^{252} Neutrons Through Various Shields

Shield Material	Thickness (inches)	Dose Attenuation (D/D_o) ANISN	Experiment	D/D_o Ratio (ANISN/Exp)
	0	1.000	1.000	1.000
Iron	1	.992	.890	1.115
Iron	2	.878	.793	1.108
Iron	3	.749	.663	1.130
Iron	4	.624	.588	1.061
Polyethylene	2	.568	.529	1.073
Polyethylene	4	.235	.225	1.044
Polyethylene	6	.096	.083	1.156
Polyethylene	8	.040	.033	1.212
Lead	1/8	1.005	.929	1.082
Lead	1/4	1.009	1.007	1.002
Lead	3/8	1.011	.953	1.061
Lead	1/2	1.011	.949	1.065
Poly.+ Lead	6 + 1/2	.083	.083	1.000
Iron + Poly.	1/2 + 5	.122	.109	1.119
Iron + Poly.	1 + 5	.099	.089	1.112
Iron + Poly.	2 + 5	.065	.051	1.275
Iron + Poly.	5 + 1/2	.137	.114	1.202
Iron + Poly.	5 + 1	.123	.092	1.337
Iron + Poly.	5 + 2	.099	.082	1.207
Iron + Poly. + Iron	1 + 5 + 2	.064	.057	1.123

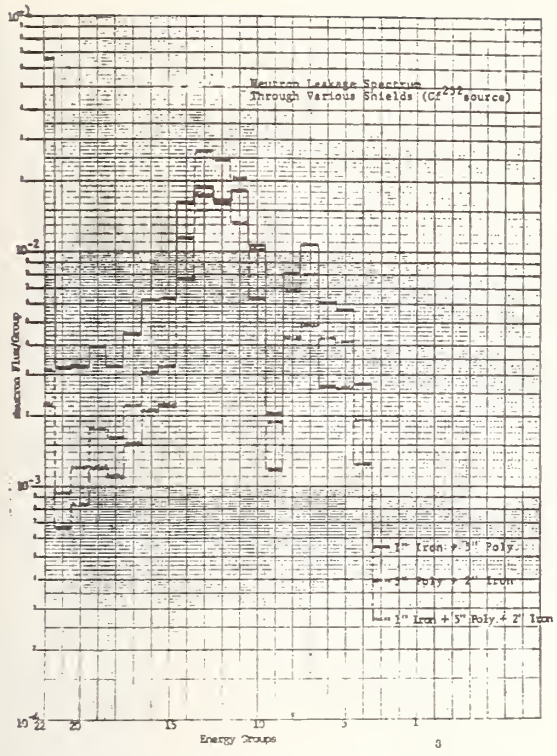

Fig. 2. Neutron Leakage Spectrum Through Various Shields (Cf^{252} source).

Scofield at the Naval Surface Weapons Center for their guidance and helpful assistance, and Jack Finkel at the Naval Surface Weapons Center for his numerical calculation of room scattered neutron dose, are all greatfully acknowledged.

References

1. Song, Y.T., Huddleston, C.M., & Chilton, A.B., Nucl. Sci. Eng. 35, 401 (1969).
2. Technical Manual, Set AN/PDR-70. NAVSHIPS 0967-871-5220, Nov.1969.
3. WANL-PR(LL)-034, Nuclear Rocket Shielding Methods, Modification, Updating, and Input data preparation, Volume 4, One-Dimensional, Discrete Ordinate Transport Technique, August 1970.
4. Engle,Jr., W.W., "A User's Manual for ANISN, A One-Dimensional Discrete Ordinate Transport Code with Anisotropic Scattering".
5. DP-939 Savannah River (Dupont) Radiation Properties of Cm^{244} Produced for Isotopic Power Generators, Savannah River Laboratory, Aiken, S.C., Nov. 1969 by D.H. Stoddard.

Discussion

S. Makra

Could you give me the exact difference in attenuation when reversing the sequence of the shield layers?

Y.T. Song

It will be shown in proceedings of this symposium. However, the following is one of the results of your interest.

2 in. Iron + 5 in. Poly	ANISN	0.065
	Exp.	0.051
5 in. Poly + 2 in. Iron	ANISN	0.099
	Exp.	0.082

As you see reversing the order, it gives as much as about 30% difference.

D.V. Gopinath

ANISN is a one-dimensional code and your experimental system seems to be away from one-dimensional geometry.Still the agreement between theory and experimental seems to be very good. Will you please comment ?

Y.T. Song

Mock up of experiment depends largely on how you use the facilities. ANISN results and experimental results should agree very well for a thin shield if you use ANISN properly. However, for thick shield, agreements expected are poorer. Note for the shield arrangements of my paper within this range of shield thickness, rather good agreement in terms of D/D_o is expected and we have it.

BACK-SCATTERING (SKY-SHINE) OF GAMMA-RAYS FROM A 650 CURIE COBALT-60 SOURCE BY INFINITE AIR

J. Swarup and A.K. Ganguly
Health Physics Division
Bhabha Atomic Research Centre
Trombay, Bombay-400 085

The paper reports the preliminary results obtained on the sky-shine spectra from a 650 Ci ^{60}Co source located at the centre of a gamma irradiation field of radius 90 m. fenced by a stone wall of thickness ~75 cm and height 3.66 m. The source is in the form of small pellet. The height of the source when raised for irradiation is 1.2 m above ground level and it is shielded on top by a lead cylinder of 10 cm diameter and 25 cm length. Thus, only the scattered radiation can reach the ground level beyond the fencing wall. There is a field of 100 mR/hr on the inner side and 2 mR/hr on the outer side of the wall with the source raised. Experiments are carried out for the measurement of sky-shine with a well-shielded NaI detector assembly coupled to a 400-channel analyser. The detector is placed 55 cm above ground looking vertically up through a lead collimator of diameter 12 mm (or 20 mm) at distances from 150 m to 325 m away from the source. Energy calibrations of the spectra have been carried out before and after each experiment using standard sources of gamma-energy ranging from 60 keV to 662 keV. It is found that the spectrum extends upto 400 keV with a pronounced peak at 72 keV for all the distances. There is no evidence of the presence of primary gamma-photons in the spectra. Total counts under the sky-shine are observed to follow an exponential decline with distance, with a slope of -0.50 ± 0.02 for both the collimators used. The ratio of peak counts (72 keV) to total sky-shine is 0.24 ± 0.02 for both the collimators. Also, the nature and intensity of the spectra remain unchanged when the lead shield around the detector is provided with an internal lining of 2.5 cm thick aluminium.

(Back scattering; ^{60}Co; gamma rays; sky-shine; spectrum)

Introduction

Swarup[1] has investigated the back-scattering of gamma rays obtained from ^{137}Cs inside a large room for different source-to-detector distances. The present work is a preliminary report on an extension of the same work in the open, to study the back-scattering of cobalt-60 gamma, at different source-to-detector distances, by infinite air above the source. This back scattering is also known in literature as sky-shine.

Field Description and Experimental Arrangements

The cobalt source for these observations is located at the centre of a large (90 m radius) circular gamma irradiation field and has a calculated strength of 650 Ci. The active material is in the form of small pellets of 1 mm diameter x 1 mm height filled in an annular stainless steel container of 18.5 mm outer diameter, 11.5 mm inner diameter and 40 mm length. Thus, it is effectively a point source when viewed from distances beyond 100 m.

The height of the source when raised for irradiation is 1.2 m above the ground level. It is shielded on the top by a plug of lead cylinder of 10 cm diameter and 25 cm length.

The gamma irradiation field is fenced by a stone masonry wall of height 3.66 m, and thickness 1 m at the base tapering to 75 cm at the top. There is a field of 100 mR/hr on the inner side and 2 mR/hr on the outer side of this wall when the source is raised. Because of this wall, only the scattered radiations, scattered by the air above the source, can reach the ground level beyond the fencing wall.

Observations on the sky-shine spectra are taken with a 5.08 cm x 5.08 cm NaI (Tl) Harshaw integral assembly coupled to a 400-channel analyser. The detector is placed inside a cylindrical (50 cm high) lead shield made of inter-locking rings of 5 cm thickness, 5 cm height and 15 cm inner diameter (Fig. 1). In the central hole of the top ring, a lead collimator or a lead plug to close it as the case may be, could be placed.

This whole assembly is mounted on a trolley of mild-steel 25 mm thick, for easy movement. Height of the detector head in this position is 55 cm above ground.

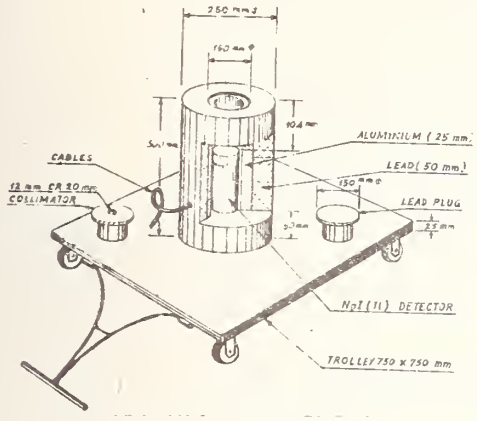

Fig. 1. Detector assembly inside the Pb shield with Al-lining.

Whereas the detector is kept in the open at atmospheric temperature, the analyser is located inside an air-conditioned room of constant (~25°C) temperature. This necessitated long cables of 100 m length to couple the two. For driving the pulses through such a length, the emitter follower of the pre-amplifier is fitted with a driver for coaxial cables which are appropriately terminated.

To avoid large changes in temperature of the detector in shade and sunshine, the entire set of observations are taken in the night. Changes in the gain of photomultiplier with temperature variations are discussed by Kinard[2]. E.H.T. of the photomultiplier is adjusted to less than the optimum working potential. This helped in keeping the gain constant throughout the interval of about five hours of one set of observations. By reducing the E.H.T., sensitivity of the photomultiplier is reduced and inspite of temperature changes of upto 8°C during one set, the spectra from 0.662 MeV to 0.060 MeV remained reproducible.

To take the observations at different distances from the source, a road radial to the source is used. This road, being inside the premises of Radioactive Solid Management Site used for burying radioactive wastes, however, has a significant background of its own (0.5 mR/hr) and therefore its own area-skyshine. This area-skyshine is measured and subtracted from the sky-shine obtained with ^{60}Co source raised. The spectra are taken with the detector looking vertically up for distances from 150 m to 325 m from the source at intervals of 10 m.

On the side of the experimental field is the sea and on the other side well beyond 400 m from the source, a vegetation covered hill gradually rising to a maximum height of about 75 m above the sea level. The contribution to the sky-shine from the hill is negligible as the observations have been taken in a narrow collimated vertically upward direction.

For taking the sky-shine spectra for distances between 325 m and 255 m collimator of 12 mm diameter and 5 cm length is used. The spectra with 20 mm collimator have also been recorded for distances of 150 m and 155 m.

Recording of Spectra

The procedure for recording the spectra is as follows:

i) First the detector is calibrated with thin standard sources of gamma energy ranging from 60 KeV to 662 KeV kept at the opening of the collimator (with the ^{60}Co source down). The strengths of these sources are known to a confidence level of 95% . The sources used are ^{241}Am, ^{109}Cd, ^{57}Co, ^{141}Ce, ^{203}Hg, ^{51}Cr, ^{198}Au, ^{85}Sr, ^{137}Cs.

ii) Keeping the ^{60}Co source down, the area-skyshine is determined for 30 mins. This shine is subtracted from the spectra of the standard sources. Then, by plugging the collimator, the background spectrum in the shield is determined. Subtracting this from the area-skyshine, true area-skyshine is obtained. As the area-skyshine could not be determined for all the individual experimental points, it is measured at one point and assumed to be the same throughout.

iii) The source is raised. First the spectrum is taken for 30 mins. with the lead-plug in position. This spectrum is termed the back-ground spectrum in this work.

(iv) Finally, the plug is replaced with an appropriate collimator and the sky-shine spectrum is recorded for 30 mins. The channel calibration is tested again with standard sources. From this sky-shine the sum of the spectra of back-ground and the true area-skyshine is subtracted to get the true sky-shine spectrum due to ^{60}Co source.

Typical spectra of sky-shine and area-skyshine with their respective back-grounds are shown in Fig. 2.

It is observed that the background continued upto almost the ^{60}Co energy

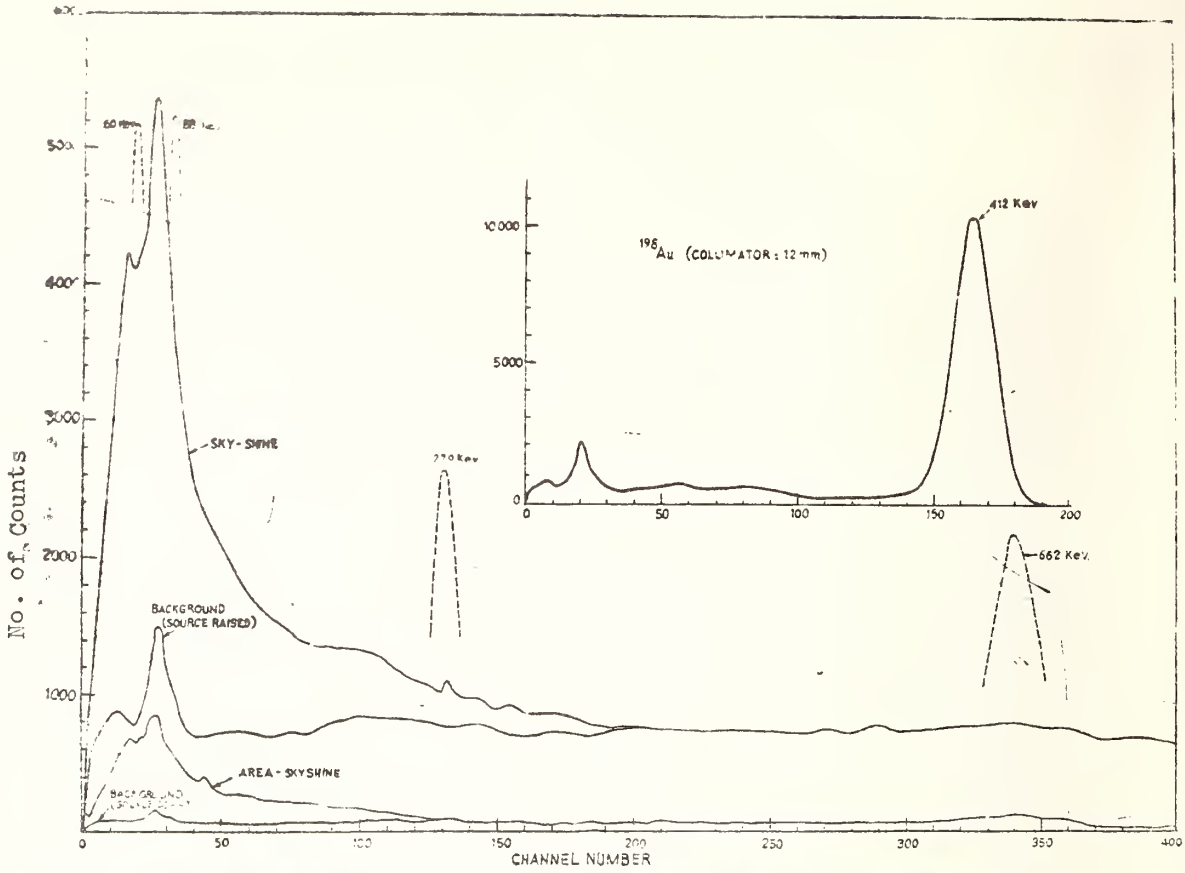

Fig. 2. **Sky shine spectrum at 255 m. source distance (Collimator:20 mm).**

without any peaking at that energy and increased continuously with decreasing source distance. A five-hours counting at 150 m source-distance did not show any ^{60}Co peak. At the distance of 255 m the back ground increased considerably (about 25% of the sky-shine at 72 keV) and it is reduced to 8% when the shield is provided with a single layer castling of 5 cm thick lead bricks all around. But the back ground subtracted sky-shine spectrum remained unaffected by castling. The remaining sky shine spectra upto 150 m are recorded with this 10 cm lead shielding arrangement.

Discussions

There is no data available in the literature for the measurement of spectra of sky shine of ^{60}Co source in the geometry used in the present work. Mary Alberg et al[3] have measured the spectra of scattering of ^{137}Cs gamma by water and have inferred the scattering by air (sky shine). But because of the lead plug (10 cm. diameter x 25 cm length) on the source in the present work, the geometries of the two works are different.

As a preliminary assessment of the spectra, the following important points are observed.

i) the counts of the true skyshine spectra extend upto 400 keV on energy scale for all the distances of observations.

The geometry of this set-up (Fig. 3) is such that all photons from the source and scattered ones from the lead-plug emanated below the horizontal plane passing through the source, strike the gamma field ground or its fencing wall i.e. photons in a solid angle 2π do not give any sky-shine directly. Only those source photons go straight out which are emanated from its near ground periphery and have their azimuthal angle, ϕ between 45° and 88.5°. The source points successively higher than this have less and less range of angles to emanate photons clearly into the sky. Source photons other than the above are obstructed by the lead plug.

For the photon with ϕ equal to 88.5° which goes out just above the fencing wall, to be detected, it should be

scattered vertically down by air to come in "the field of view" of the detector i.e. scattered to $\sim 90^{o}$ with an energy of 363 keV, as obtained from the Compton formula.

$$E_{scattered} = \frac{E_o}{1 + \frac{E_o}{mc^2}(1-\cos\theta)}$$

This is the high energy limit of sky shine spectrum and due to poor resolution of the detector in this energy region, the counts extend upto the channel corresponding to $\sim$ 400 keV.

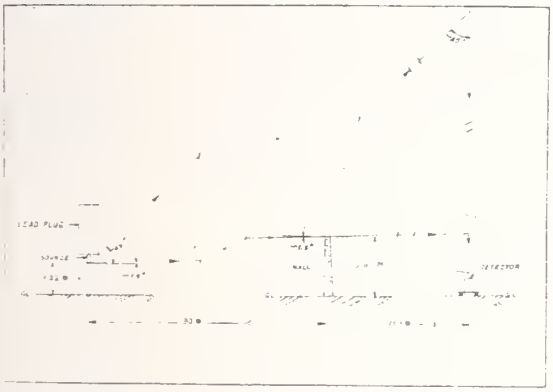

Fig. 3. Geometry of photon scattering by air.

The photon with ϕ equal to 45^{o} needs to be scattered by 135^{o} to strike the detector from a minimum height of 150 m. above it, and the scattered photon has 240 KeV of energy. The mean free-path[4], for 240 KeV gamma in air is $\sim$ 70 m. This scattered gamma, therefore, travels more than two mean free-paths for 150 m, and more than four mean free-paths for 325 m source distance to be detected. The photons with angles between 88.5^{o} and 45^{o} when scattered at appropriate heights by angles between 90^{o} and 135^{o} are detected.

ii) At all distances from the source the nature of the spectrum remains the same. There is a peak corresponding to the channel of 72 KeV. The ratio of counts in the range 64 KeV to 80 KeV (taken as 72 keV peak) with the total counts of sky shine (Fig. 4), for both the collimators is obtained as 0.24 $\pm$ 0.02 for all the distances; however the effect of source distance is felt only in the count rates.

The 72 KeV peak obtained in the sky shine is very close to the Pb x-rays (K_{α}; 75 KeV). The spectra were taken with and without 2.5 cm of Al-lining inside the detector shield at 155 m source distance. Differences observed are well within the limits of experimental errors. Thus, the true sky shine spectrum observed in the present work with a pronounced peak at 72 keV is not related in any way to the scattering from Pb-shield.

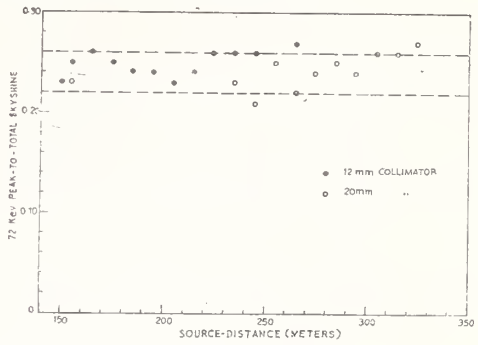

Fig. 4. 72 keV peak-to-total sky shine vs. source distance.

The inset in Fig. 2 shows spectrum obtained with ^{198}Au. The 412 keV photon in the present set-up does not contribute significantly to the Compton continuum in comparison to its photopeak. The contributions to the respective Compton portions of lesser energy photons are insignificant. If, therefore, as a first approximation, the Compton portion be neglected, about one-fourth of the intensity of sky-shine in vertical direction comprises of 72 keV photons.

iii) The total counts under the sky-shine (the intensity of the scattered photons) follow an exponential decline with distance from the source (Fig. 5). The following relationship gives the best fit with the recorded counts:

$$I = I_o e^{-1.15\ x}$$

where x is the source distance in meters and I_o is the intensity of a virtual source, the value of which depends on the diameter of the collimator.

iv) It is also found that the counts spectrum of the area-skyshine (Fig. 2), too shows a peak at 72 keV, but ends at $\sim$ 275 KeV. In the experimental field wastes containing different radioactive substances of varying strengths are buried deep in the ground about 50 m away from the detector, in about 30 cm thick concrete cells which are covered also with the same thickness of concrete. These sources also give sky shine with a peak at the same energy.

Further work is in progress.

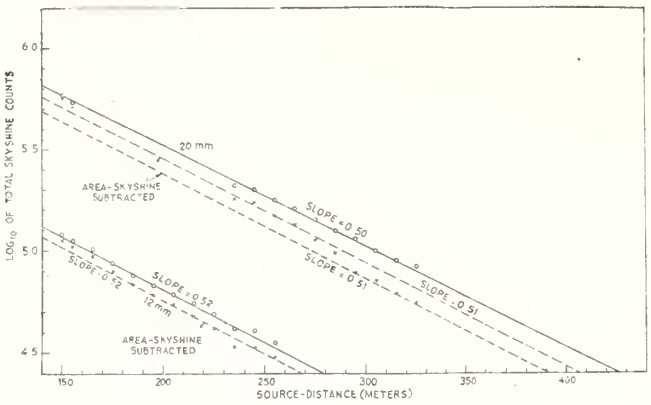

Fig. 5. Total sky-shine counts vs. source distance.

Acknowledgements

The authors wish to thank Mr. G.H. Vaze, Head, Electronics Division for the help given by his staff; Mr. R.K. Balani supplied the 400-channel analyser, Mr. C. G. Chatur developed and assembled the Pre-amplifier and matched it with the analyser through 100 m cables. The help in the experimentation given by M/s D.T. Khatri, A.R. Kamath, S.H. Shirke and K. Somanathan is gratefully acknowledged; the latter helped in calculations also. The facility of the source was kindly provided by Dr. B.M. Desai, in-charge, Experimental Gamma-Field Station.

References

1. Swarup, Indian J. Pure Appl. Phys. 11, 331 (1973)
2. Kinard, F.E., Nucleonics 15 (No. 4), 92 (1957).
3. Alberg, M., Beck, H., O'Brien, K. and McLaughlin, Nucl. Sci. Engg. 30, 65 (1967). [See also, E.T. Clarke, Nucl. Sci. Engg. 27, 394 (1967) and Chilton, A.B., ibid, 403 (1967)].
4. Hubbell, J.H., "Photon Cross Sections, Attenuation Coefficients and Energy Absorption Coefficients from 10 KeV to 100 GeV" NSRDS - NBS, 29 (Aug.1969).

BACKSCATTERING OF GAMMA RAYS BY BARRIERS FROM VARIOUS MEDIA *

D. B. Pozdneyev
Gorki State University, Gorki, USSR

Quantitative data about albedo of gamma radiation must be known to solve some problems of radiation shielding, radiometry, nuclear instruments. Spatial - energy, differential and integral characteristics of gamma rays albedo for the case of the barriers of different thicknesses from beryllium, graphite, aluminium, concrete, iron, tin, and lead were determined both experimentally and by means of Monte Carlo method. Energies of gamma rays from the point isotropic source and of monodirectional beam were 145, 279, 511, 662, 1000 and 1250 keV. Spectral - angular distribution of back-scattered gamma rays escaping from various portions of the barrier surface as a function of thickness and material of barrier, distance from the source, geometry of the source and energy of primary gamma radiation was also investigated. Systematized data about differential and integral albedo of gamma rays of various energies for the case of barriers of different thickness from various media are presented in the form convenient for practical uses.

(Albedo; angular; backscattering; barrier; differentials; distribution; gamma rays; integral; medium; Monte Carlo)

Introduction

The quantitative data about the backscattering of gamma rays from barriers of various media must be known for the solution of some problems of radiation shielding, in radiometry and dosimetry, in the elaboration and exploitation of some instruments detecting backscattered gamma radiation (such as thickness gauge, density gauge etc.)

Method

Let us introduce the following current characteristics of gamma rays albedo.

$\alpha(E_o, \Psi\ ;\ E,\ \theta, \varphi, X\ ,\ y,\ d)$ is the probability (per one quantum with the energy E_o and angle of incidence Ψ to normal to the plane barrier with the thickness d) of gamma radiation escaping from the reflector at the point with the Cartesian coordinates (x,y,z=0) in the direction (θ ,φ) (θ is polar and φ is azimuthal angle) within the unit solid angle (the energy of such radiation is equal to E). In the cases of point isotropic primary source with the reflecting barrier, and the monodirectional beam with $\Psi = 0^o$, it is convenient to introduce the γ - coordinate characterizing the distance between the source and the studying region of the reflector surface. Therefore we can write the function

$$\alpha(E_o, \Psi\ ;\ E,\ \theta, \varphi,\ x,\ y,\ d) \text{ as}$$

$$\alpha(E_o, \Psi\ ;\ E,\ \theta, \varphi, \gamma,\ d)$$

The spatial spectral albedo

$$\alpha_s(E_o, \Psi\ ;\ E,\ \gamma\ ,\ d) = \int_0^{2\pi} d\varphi \int_0^{\pi/2} \alpha(E_o, \Psi; E, \theta, \varphi, \gamma, d) \sin\theta\, d\theta$$

characterizes the integrated energy spectrum of backscattered gamma quanta escaped from various portions of the reflector surface.

The spatial number albedo (distribution of reflected gamma quanta along the barrier surface) is characterized by the value

$$\alpha_N(E_o, \Psi; \gamma, d) = \int_0^{E_o} dE \int_0^{2\pi} d\varphi \int_0^{\pi/2} \alpha(E_o, \Psi; E, \theta, \varphi, \gamma, d) \sin\theta d\theta$$

Characteristics of backscattered gamma rays were determined by us experimentally and by means of Monte Carlo method.

Some examples of $\alpha_s(E_o, \Psi; E, \Delta\gamma, d)$ for E_o = 1,25 MeV are presented in fig. 1. For the sake of clearness all

*Presented by Mr. J.H. Hubbell

the functions $\alpha_s(E_o,\Psi;E,\Delta r, d)$ are normalized on $1cm^2$ of the reflector surface.

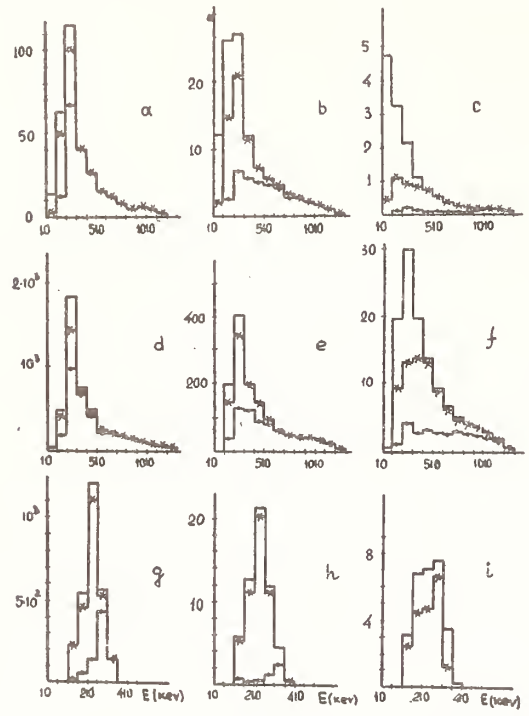

Fig. 1. Energy spectra of backscattered photons escaped from various portions of reflector surface. E_o=1,25MeV.
a,b,c, - graphite point isotropic source
d,e,f - iron
g,h,i - iron, monodirectional source (=0°) d=0, 1mfp
d=0, 4mfp d=2, 5mfp

While comparing spectra for various Δr there can be noted the following points of principal importance: the portion of backscattered gamma quanta decreases with the increase of r, the dependence of albedo on d becomes less sharp with increase of r. With light reflectors the increase of radius r is followed by the enrichment of the energy spectra with the low energy gamma quanta owing to multiple scattering in the barrier matter. It is easy to understand the deformation of spectra with r increasing (fig. 1a,1b,1c) taking into consideration the small role of photoabsorption in such materials as beryllium and graphite. With gamma quanta scattered at the angles nearing 180° essential contribution to albedo was observed in the region near the primary source[Δr=(0-0, 1)mfp - fig. 1a] (and in this situation the clearly expressed peak took place in energy interval (200-300)keV). With the thick scatterer essential contribution to albedo was rendered by the multiple scattered quanta issued from the depth of the reflector. Albedo from the thin barrier is conditioned by gamma quanta penetrating along the reflecting surface of the barrier and scattering at small angles (therefore they throw down their energy insignificantly see instance the spectra for d = 0, 1mfp).

The low-energy quanta corresponding to the multiple scattering are more intensively absorbed in the material of the barrier. Spectra $\alpha_s(E_o,\Psi;E,\Delta r, d)$ for the case of normal incidence of primary gamma rays beam are characterized by more finite energy field than in the geometry of point isotropic source. This is particularly characteristic for heavier media. Gamma quanta with energy lower than 110keV (for lead lower than 160keV) are absent in the spectrum due to photoabsorption. The mean energy of the spectra of backscattered gamma radiation for the monodirectional source (normal incidence) is lower.

In order to determine the meaning of albedo from the local portion of the barrier surface Δr (thickness of the reflector equals d) - $\alpha_N(E_o,\Psi;\Delta r, d)$ the relative change of this value with d $\frac{\alpha_N(E_o,\Psi;\Delta r,d)}{\alpha_N(E_o,\Psi;\Delta r,\infty)}$ and $\alpha_N(E_o,\Psi;\Delta r,\infty)$ must be known. Example of dependence on d of the ratio $\frac{\alpha_N(E_o,\Psi;\Delta r,d)}{\alpha_N(E_o,\Psi;\Delta r,\infty)}$ for concrete and isotropic source of primary gamma rays is presented in fig. 2a. Fig. 2b characterizes the change of spatial spectral albedo $\alpha_s(E_o,\Psi;E,\Delta r,d)$ for E = (10-160) keV with thickness of barrier d. The accumulation of low-energy gamma quanta due to multiple scattering extends the range of change of the value $\alpha_s(E_o,\Psi;E,\Delta r,d)/\alpha_s(E_o,\Psi;E,\Delta r,\infty)$. with d for greater distances r.

The analysis of the received data shows that the dependence of albedo on the circular regions of the semi-infinite reflector surface $\alpha_{NC}(E_o,\Psi;r,\infty)$ on r can be described by the following empirical formula (with accuracy ± 5%):

$$\alpha_{NC}(E_o,\Psi;r,\infty) = \alpha_N(E_o,\Psi;\infty,\infty)(1-e^{\beta r}) \quad (1)$$

where $\alpha_N(E_o,\Psi;\infty,\infty)$ is the number albedo from semiinfinite ($d\to\infty$) scatterer with an unlimited area of the surface ($r\to\infty$). The values of $\alpha_N(E_o,\Psi;\infty,\infty)$

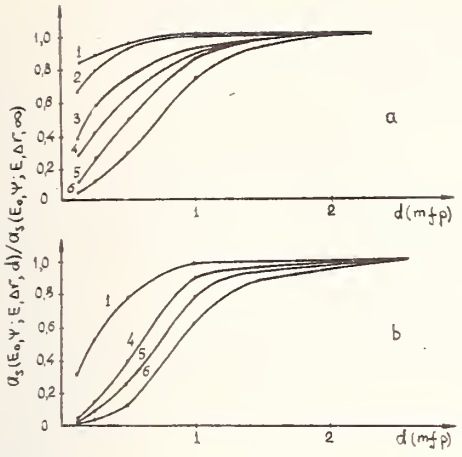

Fig. 2a and 2b. Albedo from local portion of reflector surface (in arbitrary units) as function of barrier thickness d. Cs point isotropic source

a - E = (10-662)keV, b - E=(10-160)keV.
1 - r=(0-0,1)mfp, 4 - r=(0,5-1,0)mfp,
2 - r=(0,1-0,2)mfp, 5 - r=(1-2)mfp,
3 - r=(0,3-0,5)mfp, 6 - r=(2-5)mfp.

Table 1

Values $\alpha_N(E_0, \Psi; \infty, \infty)$ and β for concrete (aluminium) and E_0=0,662Mev.

Source geometry	Point isotropic	Monodirectional ($\Psi = 0°$)
$\alpha_N(E_0, \Psi; \infty, \infty)$	0,436±0,002 0,42±0,04 (exp)	0,242±0,002
β (mfp)$^{-1}$	0,83	1,06

are given in Table 1 for concrete (aluminium) according to the results of the experiments and of our calculation by Monte Carlo method. The values β for the calculation of $\alpha_{NC}(E_0, \Psi; r, \infty)$ according to the formula (1) are given in the same table. It is easy to see that $\alpha_N(E_0, \Psi; \Delta r, \infty)$ ($\Delta r = r_2 - r_1$) can be found as

$$\alpha_N(E_0, \Psi; \Delta r, \infty) = \frac{\alpha_N(E_0, \Psi; \infty, \infty)}{\pi(r_2^2 - r_1^2)} \left(e^{-\beta r_1} - e^{-\beta r_2}\right) \quad \ldots (2)$$

The joint use of the formula (2) and graphs which are analogous to those on fig. 2 permitted to determine the dependence of albedo from local portion of reflector surface on the thickness of the barrier.

GAMMA RAY STREAMING THROUGH ANNULAR CYLINDRICAL DUCT

K.P.N. Murty, R. Vaidyanathan and
R. Shankar Singh
Reactor Research Centre
Kalpakkam-603102
Madras, India

In this paper we present the study of gamma ray streaming through an annular cylindrical duct from an infinite plane source. A rigorous formulation based on the ray-analysis procedure has been developed to compute the resultant dose in the vicinity of the duct exit. A parametric study has been carried out to evaluate the accuracies obtained with the present rigorous treatment as compared to the simple formula developed for hand-calculations. Attempts are being made to incorporate the scattering component to the dose at the exit, in our present study.

(Annular; computation; duct; gamma ray; integration; kernel; radiation; streaming)

Introduction

Radiation streaming through ducts is an important and difficult problem in nuclear reactor shielding. Methods of computing the streaming flux through straight cylindrical ducts have been reviewed profusely by many people[1-5]. Only a few attempts have been made in the study of radiation streaming through annular cylindrical ducts. This problem is of importance in reactor shielding, where one encounters cylindrical plugs with annular gaps all around. We present here a rigorous analysis of the problem of gamma streaming through annular cylindrical ducts using Ray-tracing procedure coupled with point-kernel integration.

Formulas for Uncollided Flux

Figure 1 shows the configuration of the duct with an infinite plane source perpendicular to the Z axis at the duct entry. The source is divided into 3 regions. Region 2 is further divided into two sub-regions, 2A and 2B. Region 3 is divided into 4 sub-regions 3A, 3B, 3C and 3D. Let the uncollided flux from each region be $\phi_i (i = 1,2,3)$. The total uncollided flux is then $\phi = \sum_{i=1}^{3} \phi_i$

Assume an axis passing through the dose point and parallel to the central axis of the duct. Let the separation of the two axes be 'a', the inner radius of the duct RI, the outer radius of the duct RE and the duct length L. Let the angular distribution of the gammas from the source be given by, $S = (n+1)\cos^n\psi/4\pi$ where ψ is the angle between the direction of the photon and the Z axis. The spatial distribution of the uncollided flux at the duct exit is evaluated as follows:

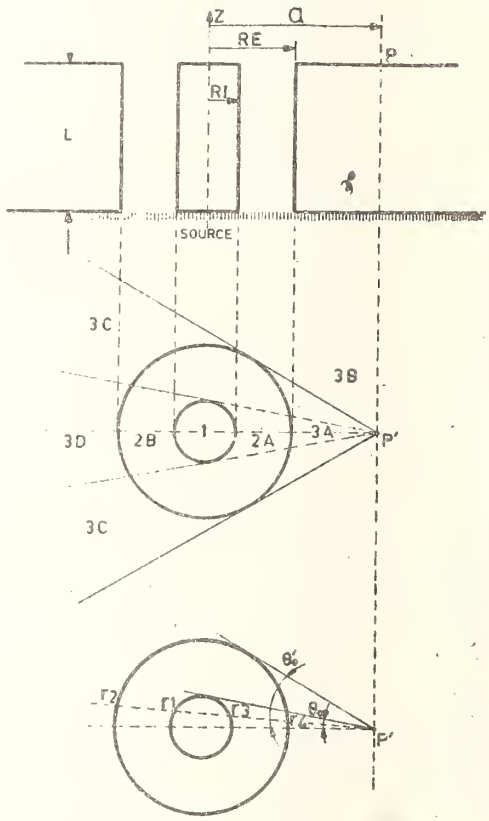

Fig.1. Annular cylindrical duct and the source regions.

Case 1 a = 0

$$\phi_1 = \frac{n+1}{2} \int_0^{R_I} \frac{L^n \exp\{-\mu(r^2+L^2)^{\frac{1}{2}}\}}{(r^2+L^2)^{1+n/2}} \, rdr$$

$$\phi_2=\frac{n+1}{2}\int_{R_I}^{R_E}\frac{L^n\exp\{-\mu(r^2+L^2)^{\frac{1}{2}}(RI/r)\}}{(r^2+L^2)^{1+n/2}}\,rdr$$

$$\phi_3=\frac{n+1}{2}\int_{R_E}^{\infty}\frac{L^n\exp\{-\mu(r^2+L^2)^{\frac{1}{2}}(1+\frac{RI-RE}{r})\}}{(r^2+L^2)^{1+n/2}}\,rdr$$

Case 2 $a \leqslant R_I$

$$\phi_1=\frac{n+1}{2\pi}\int_0^{\pi}d\theta\int_0^{r_1}\frac{L^n\exp\{-\mu(r^2+L^2)^{\frac{1}{2}}\}}{(r^2+L^2)^{1+n/2}}\,rdr$$

$$\phi_2=\frac{n+1}{2\pi}\int_0^{\pi}d\theta\int_{r_1}^{r_2}\frac{L^n\exp\{-\mu(r^2+L^2)^{\frac{1}{2}}(r_1/r)\}}{(r^2+L^2)^{1+n/2}}rdr$$

$$\phi_3=\frac{n+1}{2\pi}\int_0^{\pi}d\theta\;\frac{L^n\exp\{-\mu(r^2+L^2)^{\frac{1}{2}}(1+\frac{r_1-r_2}{r})\}}{(r^2+L^2)^{1+n/2}}$$

Case 3 $R_I < a \leqslant R_E$

$$\phi_1=\frac{n+1}{2\pi}\int_0^{\theta_o}d\theta\;\frac{L^n\exp\{-\mu(r^2+L^2)^{\frac{1}{2}}(1-r_3/r)\}}{(r^2+L^2)^{1+n/2}}rdr$$

$$\phi_{2A}=\frac{n+1}{2\pi n}\int_0^{\pi}d\theta\left(1-\frac{1}{\{1+(r'/L)^2\}^{n/2}}\right)\quad n\neq 0$$

$$=\frac{1}{4\pi}\int_0^{\pi}d\theta\,\ln(1+(r'/L)^2\qquad n=0$$

Where $r' = r_3$ when $0 \leqslant \theta < \theta_o$

$r' = r_2$ when $\theta \geqslant \theta_o$

$$\phi_{2B}=\frac{n+1}{2\pi}\int_0^{\theta_o}d\theta\int_{r_1}^{r_2}\frac{L^n\exp\{-\mu(r^2+L^2)^{\frac{1}{2}}(2/[R_E^2-a^2\sin^2\theta]\}}{(r^2+L^2)^{1+n/2}}$$

$$\phi_{3C}=\frac{n+1}{2\pi}\int_{\theta_o}^{\pi}d\theta\int_{r_2}^{\infty}\frac{L^n\exp\{-\mu(r^2+L^2)^{\frac{1}{2}}(1-r_2/r)\}}{(r^2+L^2)^{1+n/2}}rdr$$

$$\phi_{3D}=\frac{n+1}{2\pi}\int_0^{\theta_o}d\theta\int_{r_2}^{\infty}\frac{L^n\exp\{-\mu(r^2+L^2)^{\frac{1}{2}}(1+\frac{r_1-r_2-r_3}{r})\}}{(r^2+L^2)^{1+n/2}}rdr$$

case 4 a R_E

$$\phi_1=\frac{n+1}{2\pi}\int_0^{\theta_o}d\theta\int_{r_3}^{r_1}\frac{L^n\exp\{-\mu(r^2+L^2)^{\frac{1}{2}}(1+\frac{r_4-r_3}{r})\}}{(r^2+L^2)^{1+n/2}}rdr$$

$$\phi_{2A}=\frac{n+1}{2\pi}\int_0^{\theta_o}d\theta\int_{r_4}^{r'}\frac{L^n\exp\{-\mu(r^2+L^2)^{\frac{1}{2}}(r_4/r)\}}{(r^2+L^2)^{1+n/2}}\,rdr$$

Where $r' = r_3$ when $\theta < \theta_o$

$r' = r_2$ when $\theta \geqslant \theta_o$

$$\phi_{2B}=\frac{n+1}{2\pi}\int_0^{\theta_o}d\theta\int_{r_1}^{r_2}\frac{L^n\exp\{-\mu(r^2+L^2)^{\frac{1}{2}}(\frac{r_1-r_3+r_4)}{r}\}}{(r^2+L^2)^{1+n/2}}\,rdr$$

$$\phi_{3A}=\frac{n+1}{2\pi}\int_0^{\theta_o'}d\theta\int_0^{r_4}\frac{L^n\exp-\mu(r^2+L^2)^{\frac{1}{2}}}{(r^2+L^2)^{1+n/2}}\,rdr$$

$$\phi_{3B}=\frac{n+1}{2\pi}\int_{\theta_o'}^{\pi}d\theta\int_0^{\infty}\frac{L^n\exp-\mu(r^2+L^2)^{\frac{1}{2}}}{(r^2+L^2)^{1+n/2}}\,rdr$$

$$\phi_{3C}=\frac{n+1}{2\pi}\int_{\theta_o}^{\theta_o'}d\theta\int_{r_2}^{\infty}\frac{L^n\exp-\mu(r^2+L^2)^{\frac{1}{2}}(1+\frac{r_4-r_2}{r})}{(r^2+L^2)^{1+n/2}}\,rdr$$

$$\phi_{3D}=\frac{n+1}{2\pi}\int_0^{\theta_o}d\theta\int_{r_2}^{\infty}\frac{L^n\exp-\mu(r^2+L^2)^{\frac{1}{2}}(1+\frac{r_1-r_2-r_3+r_4}{r})}{(r^2+L^2)^{1+n/2}}rdr$$

In the above formulas,

$r_1 = a\cos\theta + (R_I^2-a^2\sin^2\theta)^{\frac{1}{2}}$

$r_2 = a\cos\theta + (R_E^2-a^2\sin^2\theta)^{\frac{1}{2}}$

$r_3 = a\cos\theta - (R_I^2-a^2\sin^2\theta)^{\frac{1}{2}}$

$r_4 = a\cos\theta - (R_E^2-a^2\sin^2\theta)^{\frac{1}{2}}$

$\theta_o = \sin^{-1}(R_I/a)$ $\theta_o^1 = \sin^{-1}(R_E/a)$

Refer to the 2A component of the total uncollided flux at $a = R_E$ in the duct exit plane considered in case 3. For an isotropic source (n=0), this component can be approximated as follows:

$$\phi_{2A}=\frac{1}{4\pi}\left[\int_0^{\theta_o}\ln(1+r_3^2/L^2)d\theta+\int_{\theta_o}^{\pi/2}\ln(1+r_2^2/L^2)\,d\theta\right.$$

For a duct whose radial dimensions are small compared to its length, $\ln(1+r_3^2/L^2) \approx r_3^2/L^2$ and $\ln(1+r_2^2/L^2)\approx r_2^2/L^2$. Substituting the expresions for r_2 and r_3 and integrating, we get

$$\phi_{2A}=\frac{1}{4\pi L^2}\left\{(2R_E^2-R_I^2)\,\mathrm{Cos}^{-1}(R_I/R_E)\right.$$

$$-R_I\sqrt{R_E^2-R_I^2}$$

Calculations and Results

Calculations were performed using the formulas derived in section 1. The source considered was ^{60}Co and the source angular distribution was considered to be isotropic (n=0). Various ducts in lead shields were studied. A part of the results obtained is presented in Fig. 2.

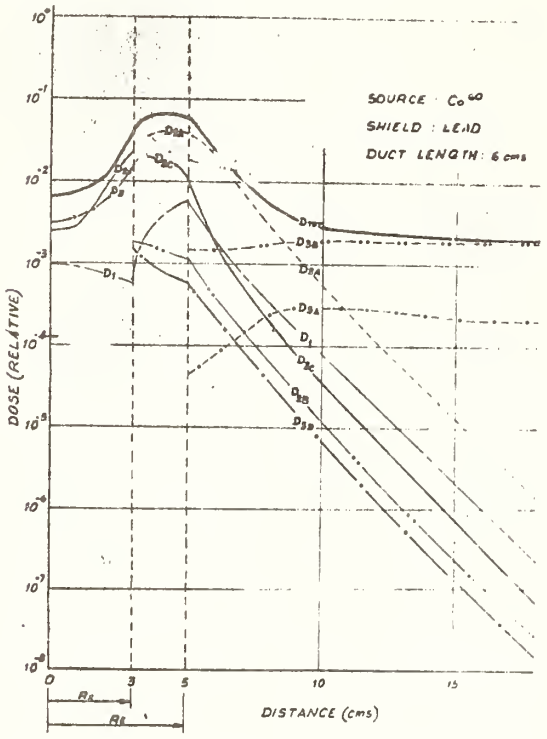

Fig. 2. Total dose-rate distribution in the duct exit plane.

Fig. 2 shows the total dose distribution in the duct exit plane for a duct with the parameters as follows: R_I = 3 cms, R_E = 5 cms, L = 6 to 60 cms. From a = 0 to a = R_I, the total dose increases; the increase is steeper for longer ducts. It remains practically constant in the annular region and falls down rapidly for longer ducts beyond a = R_E, reaching a constant value, given by infinite plane source and slab shield of thickness of L cms. In the annular region, the dose is approximately proportional to $1/L^2$.

Fig. 3 depicts the relative contribution of the various components to the total dose for a duct of R_I = 3 cms, R_E = 5 cms, L = 6 cms. These components are denoted by D1, D2A, D2B etc. At a = 0, D3 predominates. This accounts for 50% of the total dose for L = 6 cms and 64% for L = 60 cms. D2 contributes approximately the same fraction of the total dose (25% to 35%) for all duct lengths. D1 contribution falls down rapidly with increase of duct length (14.3% for L = 6 cms to less than .001% for L = 60 cms).

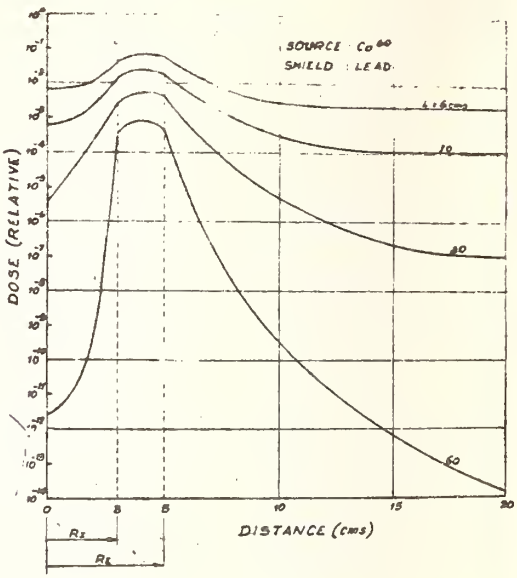

Fig. 3. Contribution of the components to the total dose.

When 'a' increases from 0 to R_I, D1 decreases while D2 and D3 increase - D2 increasing more steeply. For longer ducts D2 increases more rapidly with 'a'.

In the annular region D2A is the most predominant component. This component alone accounts for about 65% of the total dose for a duct of length = 6 cms. For a duct of length = 60 cms, it accounts for about 99% of the total dose. For longer ducts, the simple formula in section 1 which approximates the 2A component will provide a good estimate of the streaming flux. For shorter ducts components 2A and 3C together, will provide a good estimate of the streaming flux. For a $\gg R_E$, D1, D2A, D2B, D3C and D3D decrease with distance; D3A increases slowly and reaches a constant value. D3B also increases and reaches a constant value. Of these two components D3B is the predominant one. It accounts for 92% of the total dose while D3A accounts for about 8% for longer distances (L = 6 cms). This shows that for 'a' $\gg R_E$, the presence of the duct has little influence on the total dose.

References

1. Rockwell, III:Reactor Shielding Design Manual, McGraw Hill Book Co., New York (1956).

2. Price, B.T., Horton, C.C. and Spinney, K.T., Radiation Shielding, Pergamon Press, New York (1957).
3. Tsuruo, Akira; Shindo, Mitsuo; Kawabata, Masahiro, Journal of Nuclear Science and Technology, 2 (4) P. 121 - 126 (April 1965).
4. Tsuruo, A., Shindo, M. and Kawabata, Journal of Nuclear Science and Technology, 2 (9), P.325-330 (Sept. 1965).
5. Shindo, M. Tsuruo, A., Miyasaka, Shunichi et al, Nuclear Science and Engineering 27, 450-463 (1967).

MULTIPLE SCATTERING OF 12 TO 40 MeV HEAVY IONS THROUGH SMALL ANGLES

B.W. Hooton and J.M. Freeman
Nuclear Physics Division
AERE, Harwell, Didcot, U.K.

and

P.P. Kane

Physics Department
Indian Institute of Technology
Powai, Bombay-400076 and AERE, U.K.

Collimated beams of heavy ions were allowed to pass through thin foils. The angular distributions of the transmitted beams were measured with a position sensitive silicon detector. Oxygen, chlorine and iron ions of energy between 12 to 40 MeV were used in conjunction with carbon, aluminium, nickel and gold foils of thicknesses between 12 to 250 $\mu g/cm^2$. Values obtained for the half-angles of the distributions at half height are in fair agreement with the recent theoretical predictions of Meyer (1971). The data deviate substantially from the values calculated on the basis of the Moliere theory (1948) and even more markedly from those based on the theory of Nigam, Sundaresan and Wu (1959). Reasons for the success of the recent Meyer theory in the interpretation of the new data will be clarified.

(Angular distribution; foils; ions; chlorine; iron, oxygen; measurement; moliere theory; scattering; multiple.)

Introduction

An experimental investigation of multiple scattering of heavy ions in foils is important not only for the basic atomic physics interest, but also from the point of view of a detailed understanding of the behaviour of ion beams in targets used in nuclear reaction studies. Further, since foils are used for stripping in the high voltage terminals of tandem accelerators, and terminal voltages of twenty or even thirty million volts are now considered possible, such an investigation is likely to be useful in the estimation of beam emittance in future accelerators. We are not aware of any published work in relation to heavy ion multiple scattering in the energy range from about 5 MeV to 70 MeV. In the literature a study[1] on multiple scattering has been found at around 4 to 5 MeV. An investigation[2] with a photographic plate has been made of the multiple scattering of fission fragments with kinetic energies of about 81 MeV. 164 MeV oxygen ic 3 and 400 MeV argon ions have also been used in another experiment[3] using a similar technique.

Experimental Details

The experimental arrangement is shown in Fig. 1. An analysed beam from the tandem, after passing (in some of th experiments) through a 0.5 μm Ni foil to produce a uniform and adequately attenuated forward beam, was collimated by two rectangular apertures 4 mm high and 1 mm wide, with a spacing of 124 cm. The beam then passed through a target foil mounted in a scattering chamber on a moveable arm which could carry upto three foils at a time. After multiple scattering in the foil, the diverging beam passed through a 202 cm length of beam pipe to a position sensitive silicon detector (PSD) with an active surface of 5.0 cm by 0.75 cm mounted wit its long axis horizontal. The amplitude of a pulse taken from the end of the resistive surface layer of the detector was a measure of the position along the detector at which an individual ion impinged. From the distribution of the scattered beam along the line normal to the beam direction and the measured distance from the foil to the detector, the angular distribution due to multiple

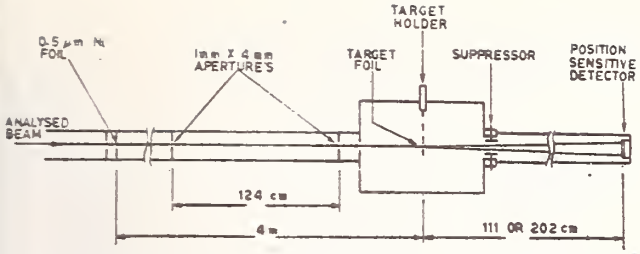

Fig. 1. Schematic plan view of apparatus.

scattering in the foil was simply obtained. In order to prevent pile-up distortion and damage in the PSD, total counting rates were limited to 500 per second or less. The target foil could be rotated about a horizontal axis so that its normal moved from the direction of the beam through an angle upto 70°. Thus the effective foil thickness seen by the beam could be varied from the actual thickness t to a value of almost 3t. The thickness of the target foils were measured in a separate Rutherford type scattering experiment. The mean thicknesses of the scattering foils in $\mu g/cm^2$ turned out to be 12 for carbon, 41 for aluminium, 45 for nickel and 127 for gold.

Figures 2 and 3 show typical spectra obtained with the PSD detector. In Fig. 2, we see spectra obtained with a 12 $\mu g/cm^2$ carbon foil and an Fe beam

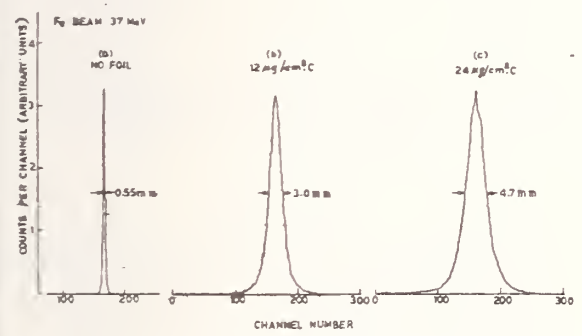

Fig. 2. Scattered spectrum obtained for 37 MeV Fe beam with a) no scatterer b) carbon foil placed normal to the incident beam c) carbon foil rotated through 60°.

of 37 MeV (calculated energy at the center of the foil). Fig. 3 shows the PSD spectrum obtained with 12.5 MeV oxygen ions on 50 $\mu g/cm^2$ aluminium and a Gaussian fit attempted near the central peak. Fig. 2(a) in fact shows the natural width of the beam obtained in this experiment without any foil scatterer. The half width at half height of

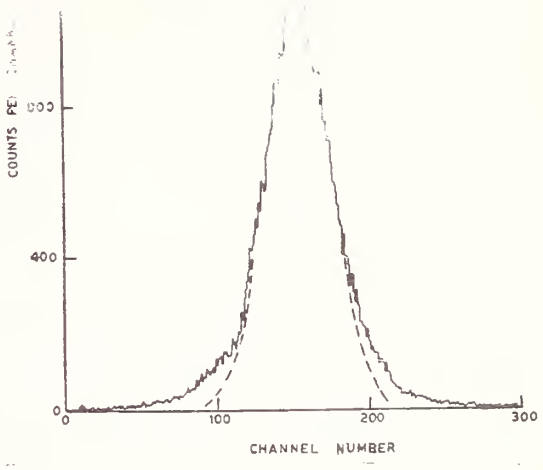

Fig. 3. PSD spectrum obtained with 12.5 MeV oxygen ions on Aluminium with an attempt for Gaussian fit at the centre of the peak.

this peak is around 1/4 mm. The spectrum in Fig. 2(b) was obtained with the plane of the carbon foil normal to the beam. The width due to multiple scattering in the scatterer was obtained by subtracting quadratically the 'foil out' width from the observed width. Fig. 2(c) shows the distribution obtained with the foil rotated through 60° so that the effective thickness seen by the beam was doubled. The half angle of scattering $\theta_{1/2}$ is defined as that corresponding to the half width at half height of the observed distribution, after correction for the 'foil out' width.

The overall uncertainties in the half-angle results are estimated to lie between $\pm$ 5% and $\pm$ 20% . The accuracy of the target thickness measurements was estimated to be $\pm$ 5% for aluminium, nickel and gold foils, and $\pm$ 10% for the carbon foils.

Discussion and Conclusions

A comparison of a few typical values of measured half-widths with those calculated on the basis of Moliere[4] and NSW[5] theories is presented in Table I. The NSW calculated widths are larger than the measured values by more than a factor of two in most cases. The Moliere widths

Table I

A comparison of measured values of $\theta_{1/2}$ with those computed on the basis of the Moliere and the NSW theories.

Ion	Energy (MeV)	Target foil	Target thickness ($\mu g/cm^2$)	Moliere calculated $\theta_{1/2}$ (degrees)	NSW calculated $\theta_{1/2}$ (degrees)	Measured $\theta_{1/2}$ (degrees)
O	12.6	C	12	0.0782	0.110	0.054
O	12.6	C	35	0.142	0.200	0.110
O	12.6	Ni	45		0.470	0.162
O	21.8	Ni	45		0.262	0.099
Cl	13.0	C	12	0.175	0.260	0.100
Cl	21.8	C	12	0.104	0.155	0.066
Fe	37.3	C	12	0.096	0.140	0.043
Fe	37.3	Ni	90	0.361	0.820	0.241

are closer to, but substantially larger than, the measured values. Serious disagreement with the NSW theory had previously been noted by Kerr et al[2] in their studies of multiple scattering of fission fragments of 81 MeV energy from silver and gold targets ($94 \leqslant \alpha \leqslant 848$). These authors had tried successfully to restore agreement with the Moliere theory by the replacement, in the theoretical formulae, of the primary nuclear charges of the ions with their effective charges. Bednyakov et al[1] had made a similar attempt in the course of the analysis of their experiments with 4 to 5 MeV nitrogen and oxygen ions on aluminium ($\alpha \simeq 30$). In a study of the scattering of 164 MeV oxygen ions and 400 MeV argon ions from zapon, aluminium, nickel and gold ($2.9 \leqslant \alpha \leqslant 30.8$), Simon[3] had noted that the NSW theory gave widths that were upto 60% too large.

In order to compare our data with the Meyer theory, the experimental $\theta_{1/2}$ and t values were converted to $\bar{\theta}_{1/2}$ and τ values. The resulting values are plotted in Fig. 4. The full curve represents Meyer's[6] theoretical calculations. The error bar shown on one of the oxygen on carbon points is an estimate of the total experimental error, which was larger for carbon than for the other foils. The overall agreement with the theoretical curve can be considered to be satisfactory, within the experimental uncertainties. However, the possibility of a z_1 dependence is not excluded, since the iron widths tend to lie slightly below the theoretical curve and the oxygen points are mostly above it.

A more detailed report will appear elsewhere.

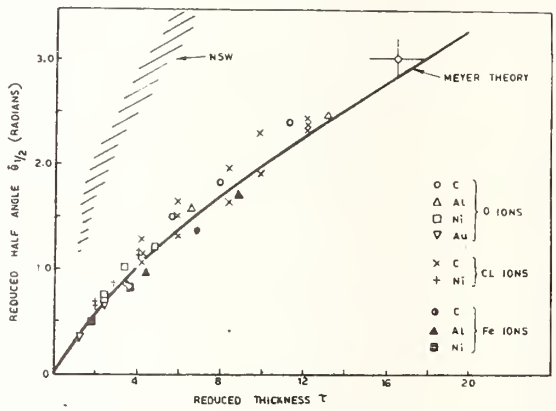

Fig. 4. Comparison of experimental values with theoretical calculations.

References

1. Bednyakov, A.A. et al., Zh. Eksperim i Teor. Fiz. 50, 589 (1966); Soviet Phys. JETP 23, 391 (1966).
2. Kerr, D. et al, Zeit. Naturf. 22a, 1799, (1967).
3. Simon, W.G., Phys. Rev. 136, 410, (1964).
4. Molière, G., Z. Naturforsch. 2a, 133 (1947).
5. Nigam, B. P., Sunderasan, M. K. and Wu, T. Y., Phys. Rev. 115, 491 (1959)
6. Meyer, L., Phys. Stat. Sol. 44b, 253 (1971).

Discussion

B.K. Godwal

How do the quantum mechanical effects appear only after a certain energy ?

P.K. Kane

The important parameter is the ratio of the de-Broglie (reduced) wavelength to the significant dimension i.e. collision radius in this case. When this ratio exceeds unity, quantum mechanical theory of scattering has to be applied of course, there is no sudden transition from the semi-classical to the quantum mechanical situation. When the above mentioned ratio is comparable to unity, the problem is quite complicated.

S. Mukherjee

1) has the scattering been considered on the basis of unscreened or screened Coulomb field ?

2) How is the effective charge of the ion taken into account ?

P.P. Kane

1) The ion-atom interaction includes a screening factor.

2) The Lindhard prescription for calculating the parameter a, the screening distance, is supposed to take into account the ion-atom interaction fairly well.

CHARGED PARTICLE TRANSPORT IN ONE-DIMENSIONAL FINITE SYSTEMS

G. Muthukrishnan*, K. Santhanam and D.V. Gopinath
Health Physics Division
Bhabha Atomic Research Centre
Bombay-400 085
India

A semi-analytical technique for the charged particle transport in one-dimensional finite media is developed which can be applied to multi-energy multi-region systems with arbitrary degree of anisotropy in scattering. For this purpose the transport equation is cast in the form of coupled integral equations separating spatial and energy-angle transmission. The spatial transmission is evaluated using discrete ordinate representation in space, energy and direction cosine for the particle source and flux. The collision integral is evaluated using discrete ordinate representation in energy and legendre polynomial approximation in the direction cosine. A computer code based on the above formulation is described.

(Anisotropy; charged particle; computer code; energy-angle; integral; legendre polynomial; scattering; semi analytical; spatial; transmission)

Introduction

The popular method for the study of charged particle transport is the MonteCarlo method in which the history of each particle is traced from the point of its origin to the point where it is absorbed or till it comes out of the medium. Because of the many kinds of interactions involved, computer time needed will be quite considerable. To save computer time, condensed[1] case histories are studied where a random walk takes into account the combined effect of many collisions.

By solving the transport equations, one can study the particle transport. Barish et al[2] have studied the transport of alpha particles and protons by solving the transport equations. In their study nuclear reaction products are neglected.

This paper describes a method of solving the transport equations for the charged particles. This is mainly based on the method developed for gamma ray and neutron transport studies[3]. To solve the equations, discrete ordinate representation in energy and spatial transmission and Legendre Polynomial approximation in direction cosines are used. Source and flux terms are calculated at discrete angles but for evaluating collision integral, Legendre polynomial approximation is used. Continuous slowing down approximation is used to fix the meshwidths which correspond to different energy losses of the incident particles as they traverse through the medium. Angular straggling is neglected in the studies.

Mathematical Formulation

Let $S(x,E,\mu)$ and $\phi(x,E,\mu)$ represent respectively the source and flux at position x with energy E and direction cosine μ.

At equilibrium,

$$\phi(x,E,\mu) = \int\int S(x',E',\mu)\,T(x' \to x,\ E' \to E,\mu)\,dE'dx' \qquad \ldots (1)$$

$$S(x,E,\mu) = \int\int \phi(x,E',\mu')\,G(x,E' \to E,\ \Omega' \to \Omega)\,dE'd\Omega' \qquad \ldots (2)$$

$$T(x' \to x, E' \to E, \mu) = \frac{e^{-\frac{\Sigma(x-x')}{\mu}}}{\mu}\,\delta\left(\frac{x-x'}{\mu}, f(E',E)\right) \qquad \ldots (2a)$$

*Present Address: VEC Project, Bidhan Nagar, Calcutta-700 064.

G and T represent the energy-angle and space transmission kernels respectively. The δ function in equation (2a) represents the reduction in energy corresponding to the distance travelled. Because of this relationship, eqn. (1), after spatial integration reduces to

$$\phi(x,E,\mu) = \int S(f(E'),E',\mu)\, e^{\frac{-\Sigma(x-x')}{\mu}} \frac{dE'}{\mu} \quad \ldots (3)$$

$e^{\frac{-\Sigma(x-x)}{\mu}}$ represents the space transmission kernel. In the transport study the mesh widths are so chosen that the delta function conditions are always satisfied; in other words, one can always find a source at x' with energy E' such that by the time the particle reaches the position x without catastrophic collision its energy would have been reduced to E. If x' and E' are the initial position and energy of the charged particle and x and E are the corresponding final values, then

$$\frac{x-x'}{\mu} = \int_{E'}^{E} \frac{1}{dE/dx}\, dE \quad \ldots (4)$$

$$-\frac{dE}{dx} = \frac{4\pi e^4 N Z}{m_0 v^2} \ln(2m_0v^2/I) \quad \ldots (5)$$

where the various notations have the usual meaning. Equation 5 can also be rewritten as

$$-\frac{dE}{dx} = \frac{K}{E'} \ln(K'E') \quad \ldots (6)$$

substituting this in equation 4,

$$\frac{x-x'}{\mu} = \frac{1}{K} \int_{E}^{E'} \frac{E'}{\ln K'E'}\, dE'$$

$$= \frac{1}{KK'^2} \left\{ E_i(2\ln K'E') - E_i(2\ln K'E) \right\} \quad \ldots (7)$$

As stated earlier we make discrete ordinate representation in E and Legendre Polynomial representation in μ as follows:

$$S(x_i,E_i,\mu) = \sum_l S_l(x_i,E_i) P_l(\mu)$$

$$\phi(x_i,E_i,\mu) = \sum_l \phi_l(x_i,E_i) P_l(\mu) \quad \ldots (8)$$

$S_l(x_i,E_i)$ and $\phi_l(x_i,E_i)$ are the Legendre coefficients of the source and flux respectively corresponding to the spatial position i and energy group i

$$\phi_l(x_i,E') = \phi_l(x_i,E_i) + \frac{\Delta\phi_l}{\Delta E}\Big|_{E_i,E_{i+1}}^{x_i} (E'-E_i) \quad \ldots (9)$$

Evaluation of the Flux Terms

The flux $\phi(x_j,E_g,\mu)$ is given by

$$\phi(x_j,E_g,\mu) = \int S(x',E',\mu)\, e^{-\Sigma(x_j-x')/\mu} \frac{dE}{\mu}$$

$$= \sum_{g'=0}^{G} \int_{E_{g'}}^{E_{g'+1}} S(x',E',\mu)\, e^{-\Sigma f(E',E_g)} \frac{dE}{\mu} \quad \ldots (10)$$

where

$$f(E',E_g) = \frac{1}{KK'^2} \left\{ E_i(2\ln K'E') - E_i(2\ln K'E_g) \right\} \quad \ldots (11)$$

Here Σ represents the macroscopic non-elastic scattering cross section. f(E', E_g) can be linearly interpolated between E_g's as

$$f(E',E_g) = a + bE' \quad \ldots (12)$$

$$a = \frac{1}{KK'^2} \left\{ E_i(2\ln K'E'_{g'}) - E_i(2\ln K'E_g) - \frac{\Delta E_i}{\Delta E}\Big|_{E_{g'},E_{g'+1}} \cdot E_{g'} \right\} \quad \ldots (13)$$

$$b = \frac{1}{KK'^2} \frac{\Delta E_i}{\Delta E}\Big|_{E_{g'},E_{g'+1}} \quad \ldots (14)$$

To start with, while computing, the medium is divided into various energy bins and into corresponding meshes for one particular direction cosine of say μ = 1. Thus there will be one to one correspondence between the energy bins and the mesh widths, when the source term is interpolated linearly for energy and space transmission in that direction. But this no longer holds good at other direction cosines. Hence the following procedure is adopted. Fixing the energy groups say Eg' and Eg' + 1 for contributing to the flux at x_j, the minimum and maximum distances that particles have to travel so that the delta function condition will be satisfied, are computed using equation 7.

Thus the locations of the particles can be calculated. They may be either in one mesh group or in two adjacent groups. Taking a general picture, let us assume that the locations are in the adjacent mesh groups say between $x_{j'}$ and $x_{j'+1}$ and $X_{j'+1}$ and $X_{j'+2}$ corresponding respectively to the two energy limits Eg' and Eg' + 1. Then the linear interpolation of the source term can be carried out follows :

$$S(x',E',\mu) = S(x',E_{g'},\mu) + \frac{S(x',E_{g'+1},\mu) - S(E_{g'},x',\mu)}{E_{g'+1} - E_{g'}} \quad \ldots (15)$$

Using linear interpolation of $S(x',Eg'_{+1},\mu)$ and $S(x',Eg',\mu)$ in spatial co-ordinate and converting spatial parameters into energy parameters using 12 and after substitution in (10) and integrating we get

$$\phi(x_j,E_g,\mu)=\frac{1}{\mu\Sigma b}\sum_{g'=0}^{G}\Big[\Big\{A+B\Big(E_{g'}+\frac{1}{\Sigma b}\Big)+C\Big(E_{g'}^2+2\frac{E_{g'}}{\Sigma b}+\frac{2}{\Sigma^2 b^2}\Big)\Big\}e^{-\Sigma(a+bE_{g'})}-\Big\{A+B\Big(E_{g'+1}+\frac{1}{\Sigma b}\Big)+C\Big(E_{g'+1}^2+\frac{2E_{g'+1}}{\Sigma b}+\frac{2}{\Sigma^2 b^2}\Big)\Big\}e^{-\Sigma(a+bE_{g'+1})}\Big] \quad \ldots (16)$$

where A, B and C are constants, depending on Eg's.

Calculation of Source Terms

$$S(x_j,Eg,\mu)=\iint\phi(x,E',\mu')G(x_j,E'\rightarrow E_g,\Omega'\rightarrow\Omega)\,dE'd\Omega' \quad \ldots (17)$$

Where G is the energy-angle transmission kernel. G can be split up into two terms F_1 and F_2, F_1 representing the probability that the energy of the particle changes from E' to Eg as a result of scattering and F_2 representing the probability of the direction changing from Ω' to Ω due to scattering.

$$\therefore G(x_j,E'\rightarrow Eg,\Omega'\rightarrow\Omega)=F_1(E'\rightarrow E_g)F_2(\Omega'\rightarrow\Omega) \quad \ldots (18)$$

After Yucker[4],

$$F_1(E'\rightarrow Eg)=\Sigma_{ne}\frac{dN}{dE} \quad \ldots (19)$$

$$F_2(\Omega'\rightarrow\Omega)=0.47865e^{3(\mu_o-1)} \quad \ldots (20)$$

Where $\frac{dN}{dE}$ is the energy spectre of the secondary particles and μ_o is the cosine of the angle between the emitted and the incident particles, that is between Ω and Ω'. Σ_{ne} is the non elastic scattering cross section. Equations 19 and 20 together give the differential spectra of the cascade particles. The evaporation process is not considered.

The angular distribution can be represented by

$$e^{3(\mu_o-1)}=\sum_{l=o}^{l}a_l P_l(\mu_o) \quad \ldots (21)$$

where a_l is the Legendre coefficient and is given by

$$a_l=\frac{2l+1}{2}\int_{-1}^{+1}e^{3(\mu_o-1)}P_l(\mu_o)\,d\mu_o \quad \ldots (22)$$

substituting 19, 20 and 21 in 17 and replacing $\phi(x_j,E',\mu')$ by $\sum_n\phi_n(x_j,E')\,P_n(\mu')$ we get

$$S(x_j,E_g,\mu)=0.47865\sum_{n=0}^{N}\sum_{l=0}^{l}a_l\iint\phi_n(x_j,E')P_n(\mu')P_l(\mu_o)\times\Sigma_{ne}\frac{dN}{dE}\,dE'd\mu' \quad \ldots (23)$$

$$Pl(\mu_o)=Pl(\mu').Pl(\mu) \quad \ldots (24)$$

Expressing $S(x_j,Eg,\mu)$ in terms of Legendre coefficients, we get

$$\sum_m S_m(x_j,E_g)P_m(\mu)=0.47865\sum_l a_l\iint\phi_n(x_j,E').P_n(\mu')P_l(\mu)P_l(\mu')\Sigma_{ne}\frac{dN}{dE}(E')\,dE'd\mu' \quad \ldots (25)$$

Multiplying 25 by $P_j(\mu)$ and integrating over μ

$$S_j(x_j,Eg)=0.47865\,\Sigma_l a_l\iint\phi_n(x_j,E')\times\sum_{ne}\frac{dN}{dE}(E')xP_l(\mu')P_j(\mu')dE'd\mu' \quad \ldots (26)$$

$$=0.47865\,\frac{2a_l}{2l+1}\sum_{g'=0}^{G}\int_{E_{g'}}^{E_{g'+1}}\phi_n(x_j,E')\Sigma_{ne}\frac{dN}{dE}(E').dE' \quad \ldots (27)$$

$\phi_n(x_j,E')$ and $\frac{dN}{dE}(E')$ can be linearly interpolated between Eg' and Eg'+1. The cross section is assumed to be constant between Eg' and Eg'+1.

$$\phi_n(x_j,E')=\phi_n(x_j,E_{g'})+\frac{\Delta\phi_n}{\Delta E}\Big|_{E_{g'},E_{g'+1}}(E'-E_{g'}) \quad \ldots (28)$$

$$\frac{dN}{dE}(E')=\frac{dN}{dE}(E_{g'})+\frac{\Delta\left(\frac{dN}{dE}\right)}{\Delta E}\Big|_{E_{g'},E_{g'+1}}(E'-E_g)$$

Substituting for $\phi_n(x_j,E')$ and $\frac{dN}{dE}(E')$ and integrating over Eg's, we get

$$S_j(x_j,E_g)=0.47865\,\frac{2a_l}{2l+1}\sum_{g'=0}^{G}\Sigma_{ne}(\bar{E}_{g'})\Big\{C_1(E'_{g'+1}-E_{g'})+\frac{C_2}{2}(E_{g'+1}-E_g)^2+\frac{C_3}{3}(E_{g'+1}-E_{g'})^3\Big\} \quad \ldots (28)$$

$$\bar{E}_{g'}=E_{g'}+E_{g'+1}/2 \quad \ldots (30a)$$

$$C_1=\phi_n(x_j,E_{g'})\frac{dN}{dE}(E_{g'}) \quad \ldots (30b)$$

$$C_2 = \phi_n(x_j, E_{g'}) \left.\frac{\Delta(dN/dE)}{\Delta E}\right|_{E_{g'}, E_{g'+1}}$$

$$+ \frac{dN}{dE}(E_{g'}) \cdot \frac{\Delta \phi_n}{\Delta E} \quad \ldots (30c)$$

$$C_3 = \left.\frac{\Delta \phi_n}{\Delta E}\right|_{E_{g'}, E_{g'+1}} \left.\frac{\Delta(dN/dE)}{\Delta E}\right|_{E_{g'}, E_{g'+1}} \quad \ldots (30d)$$

Method of Computation

Dividing the medium into various meshes, such that the variation in $2 \ln(K'E_g)$ is uniform, the transmitted flux is calculated at various meshpoints. The angular straggling is neglected in this case. Having computed the uncollided flux, at various mesh points the first collision source terms are computed analytically at these mesh points for various direction cosines. Then iteration is carried out .

In integrating the right hand side of equation(4), the relativistic correction to the dE/dx formula is not included; however this correction also can be incorporated in which case also the integral can be carried out analytically.

Conclusion

This paper describes a method that is being developed to study the proton transport through various media. A computer programme is being developed for this method.

References

1. Adler and Fernbach, "Methods in computational Physics".
2. Barish, J., Santoro, R.T., Alsmiller, F.S. and Alsmiller, R.G., Jr. "Trapp, a computer Program for the transport of alpha particles and protons with all nuclear reaction products neglected"ORNL-4763 (1972).
3. Gopinath, D.V. and Santhanam, K., Nuclear Science and Engineering 43, 186 (1971).
4. Yucker, W.R., "Empirical formulae for secondary nuclear production cross sections" Proceedings of the special sessions of Accelerator shielding. Presented at the 1965 winter meeting of the American Nuclear Society ANS-SD-3(1965).

PASSAGE OF HEAVY CHARGED PARTICLES THROUGH MATTER

Shankar Mukherji and Brijesh K. Srivastava
Department of Chemistry
Indian Institute of Technology
Kanpur-16, U.P., India

The energy loss of charged particles (much heavier than electrons) at energies where electronic collision predominates may be studied conveniently by separating the particles into two groups : completely stripped particles and partially stripped particles. Bethe's quantum mechanical stopping power equation is of limited applicability for the first group of particles and inapplicable for the second group. A general stopping equation valid for all ions upto relativistic energies has been developed which predicts the experimentally measured stopping powers and ranges of partially stripped heavy ions accurately. From the detailed analysis of the equation a simple formula to predict the number of orbital electrons with velocity less than a given velocity in an element of atomic number Z has been developed. Assuming the above equation to be valid for all the orbital electrons except the two K-shell electrons, it has been possible to calculate the mean excitation potential for any medium.

(Charge; charged particle; collision; electron; ionic charge; ionisation potential; stopping power; stripped particle; velocity)

Introduction

For a completely stripped and comparatively light ion like a proton or an alpha particle moving with velocity V the energy loss per unit path length in a medium containing n atoms per unit volume is given by Bethe's[1] equation:

$$\frac{dE}{dx} = \frac{4\pi Z_1^2 e^4 n}{mV^2} Z_2 \ln \frac{2mV^2}{I} \quad \ldots (1)$$

In the above equation, I, m and e signify, respectively, the mean excitation potential of the medium of atomic number Z_2, the mass and the charge of the electron, and Z_1 is the atomic number of the moving ion. Mukherji and Srivastava[2] have shown that modification of a semi-classical stopping-power equation of Bohr[3] leads to a general stopping-power equation valid for partially-stripped heavy ions like the fission fragments. However, neither of these equations holds for many ions which are heavier than alpha particles (i.e., ^{32}S, ^{16}O etc.) at energies which are too low for the use of Eq. (1) and too high for the equation of Mukherji and Srivastava[2]. This work attempts to present general stopping-power equations appropriate for different ions at energies at which electronic collision is the predominant mode of energy loss.

Formulation

Bohr's[3] semi-classical stopping-power equation is

$$\frac{dE}{dx} = n\beta_\varepsilon \left\{ \sum_s (\ln \eta_s^2 \lfloor x \rfloor^{-2} + \sum_s (\ln \eta_s^2 \lfloor \frac{x}{\eta_s} \rfloor^{-1} \right\} \quad \ldots (2)$$

in which the symbols stand for:

$$\beta_\varepsilon = \frac{2\pi z^2 e^4}{mV^2} \; ; \; \eta_s = \frac{2V}{U_s} \text{ and } x = 2z\frac{V_o}{V} \quad \ldots (3)$$

Further, ze is the charge of the particle, V its velocity, U_s is the orbital velocity of the s^{th} electron of the medium and $V_o = e^2/\hbar$; m and e are the electronic mass and charge. The terms within the square brackets, if less than unity, should be replaced by unity. The summations were replaced by Bohr[3] with integrals

$$\sum_s (\ln \eta_s^2 \lfloor x \rfloor^{-2}) + \sum_s (\ln \eta_s^2 \lfloor \frac{x}{\eta_s} \rfloor^{-1}) = \int_{U_s} (\ln \eta_s^2 \lfloor x \rfloor^{-2}) dn(U_s) + \int_{U_s} (\ln \eta_s^2 \lfloor \frac{x}{\eta_s} \rfloor^{-1}) dn(U_s) \quad \ldots (4)$$

where $n(U_s)$ is the number of orbital electrons of the medium with velocity less than U_s. It has been shown[2] that in general, for a medium of atomic number Z_2, $n(U_s)$ is given by

$$n(U_s) = f(Z_2)\, U_s/V_o \qquad \ldots(5)$$

where $f(Z_2) = 0.28\, Z_2^{2/3}$ for $Z_2 \leqslant 45.5$, ...(6)

and $f(Z_2) = Z_2^{2/3}$ for $Z_2 \geqslant 45.5$. ...(7)

The integrals in Eq.(3) may be written as three integrals keeping in mind that $[x/\eta_s]^{-1} = 1$ for $(x/\eta_s) < 1$,

$$\int_{U_s}(\ln \eta_s^2 [x]^{-2})\, dn(U_s) + \int_{U_s}(\ln \eta_s^2 \cdot [\tfrac{x}{\eta_s}]^{-1})\, dn(U_s) =$$

$$\frac{f(Z_2)}{V_o}\left[\int_o^{U_s'}(\ln \eta_s^2 [x]^{-2})\, dU_s + \int_o^{2Vx^{-1}} (\ln \eta_s^2)\, dU_s + \int_{2Vx^{-1}}^{U_s''} \ln(\eta_s^3 x^{-1})\, dU_s\right] \qquad \ldots(8)$$

Designating $J_1 = \int_o^{U_s'} (\ln \eta_s^2 [x]^{-2})\, dU_s$,

$$J_2 = \int_o^{2Vx^{-1}} (\ln \eta_s^2)\, dU_s$$

and $J_3 = \int_{2Vx^{-1}}^{U_s''} (\ln \eta_s^3 x^{-1})\, dU_s$, Eq.(2)

becomes:

$$\frac{dE}{dx} = \frac{2\pi z^2 e^4 n}{mV^2} \cdot \frac{f(Z_2)}{V_o}\,(J_1 + J_2 + J_3) \qquad \ldots(9)$$

The upper limits U_s' and U_s'' must be fixed corresponding to the actual physical situations so that the integrals make only positive contributions towards the energy-loss. The following cases may be considered:

A. $x > 1$

(a) $V > \frac{Z_2 V_o x}{2}$

Since $x > 1$, for $V > \frac{Z_2 V_o x}{2}$, J_1 would include all values of U_s upto the velocity of the K-shell electron which may be taken as $Z_2 V_o$. Since $(\frac{2V}{U_s})^2 = \frac{2mV^2}{I_s}$ where I_s is the ionization potential of the $s^{\underline{th}}$ electron, one obtains:

$$J_1 = \int_{U_s=o}^{U_s=Z_2V_o} \left\{\ln(\frac{2V}{U_s})^2\right\} dU_s = \frac{Z_2 V_o}{f(Z_2)} \ln \frac{2mV^2}{\bar{I}x^2} \qquad \ldots(10)$$

in which $\bar{I}$ stands for the mean ionization potential of the medium of atomic number Z_2 and is defined by

$$Z_2 \ln \bar{I} = \sum_{s=1}^{s=Z_2} \ln I_s \qquad \ldots(11)$$

As for J_2, since $V > \frac{Z_2 V_o}{2}$, $\ln (\frac{2V}{U_s})^2$ would be positive for all possible values of U_s. Further, since the lower limit for U_s in J_3 is $2Vx^{-1}$ and this already corresponds to the highest possible value for $U_s (= Z_2 V_o)$, J_3 becomes redundant. Thus,

$$J_2 = \int_o^{2Vx^{-1}} \left\{\ln(\frac{2V}{U_s})^2\right\} dU_s = \frac{Z_2 V_o}{f(Z_2)} \ln \frac{2mV^2}{\bar{I}} \qquad \ldots(12)$$

$J_3 = 0$

(b) $\frac{Z_2 V_o x}{2} > V \gg \frac{Z_2 V_o x^{1/3}}{2}$

Since $x > 1$, $\frac{Z_2 V_o x}{2} > \frac{Z_2 V_o x^{1/3}}{2} > \frac{Z_2 V_o}{2}$ one needs to consider all the three integrals. In the case of J_1, for a given V the term $\ln(\frac{2V}{U_s x})^2$ would be negative for all values of U_s lying between $2Vx^{-1}$ and $Z_2 V_o$. Hence one must use $U_s' = 2Vx^{-1}$

and get

$$J_1 = \int_0^{U_s'} \ln\left(\frac{2V}{U_s}\right)^2 dU_s = 4Vx^{-1} \quad \ldots(13)$$

Since $2Vx^{-1} < Z_2V_o$, J_2 does not include all possible values of U_s. Hence,

$$J_2 = \int_0^{2Vx^{-1}} \left\{\ln\left(\frac{2V}{U_s}\right)^2\right\} dU_s = 4Vx^{-1}(1+\ln x) \quad \ldots(14)$$

In the case of J_3, one finds that $U_s'' = Z_2V_o$ if $V = \frac{Z_2V_o x^{1/3}}{2}$.

Hence,

$$J_3 = \int_{2Vx^{-1}}^{U_s''=Z_2V_o} \left\{\ln \eta_s^3 x^{-1}\right\} dU_s \quad \ldots(15)$$

In the actual evaluation of J_3 it is convenient to consider separately the contribution of the two K-shell electrons from that of other electrons with velocities $U_s > 2Vx^{-1}$. Thus,

$$J_3 = \int_{2Vx^{-1}}^{\frac{(Z_2-2)V_o}{f(Z_2)}} \left\{\ln\left(\frac{2V}{U_s}\right)^3 x^{-1}\right\} dU_s + 2\ln\left\{\left(\frac{2V}{Z_2V_o}\right)^3 x^{-1}\right\} \quad \ldots(16)$$

where the velocity of the $(Z_2 - 2)$th electron, counting the outermost electron as the first one, is given by $U_s = \frac{(Z_2-2)V_o}{f(Z_2)}$ as obtained from Eq. (5).

(c) $V < \frac{Z_2V_o}{2}$

In this case both J_1 and J_3 would require upper cut-off values for U_s and has been considered by Mukherji and Srivastava:[2]

$$\frac{dE}{dx} = \frac{4\pi z^2e^4n}{mV^2} \frac{f(Z_2)}{V_o} (3x^{-1/3}+x^{-1}) \quad \ldots(17)$$

B. $x < 1$, (a) $V \gg \frac{Z_2V_o}{2}$

For $x < 1$, J_3 becomes superfluous, while J_1 and J_3 become identical.

$$J_1 = J_2 = \int \ln\left(\frac{2V}{U_s}\right)^2 dU_s = \frac{Z_2V_o}{f(Z_2)} \ln\frac{2mV^2}{\bar{I}} \quad \ldots(18)$$

(b) $V < \frac{Z_2V_o}{2}$

In this case J_1 or J_2 requires an appropriate upper cut-off value for U_s which makes the logarithmic term zero. Thus,

$$J_1 = J_2 = \int_0^{U_s'} \left\{\ln\left(\frac{2V}{U_s}\right)^2\right\} dU_s = 4V \quad \ldots(20)$$

Comparison with Experimental Stopping-power Data

For convenience, the various stopping-power equations obtained by putting the values of J_1, J_2 and J_3 in Eq.(9) are shown below:

A. $x > 1$

(a) $V \gg \frac{Z_2V_o x}{2}$: $\frac{dE}{dx} = \frac{4\pi z^2e^4nZ_2}{mV^2} \ln\frac{2mV^2}{\bar{I}}$ ... (21)

(b) $\frac{Z_2V_o x}{2} > V \gg \frac{Z_2V_o x^{1/3}}{2}$:

$$\frac{dE}{dx} = \frac{2\pi z^2e^4n}{mV^2} \left[3(Z_2-2)+3(Z_2-2)\ln\frac{f(Z_2)}{V_o(Z_2-2)} - 6\ln(Z_2V_o) - Z_2\ln x + \frac{2f(Z_2)V}{V_o x} + 3Z_2\ln(2V)\right] \quad \ldots (22)$$

(c) $V < \frac{Z_2V_o}{2}$: $\frac{dE}{dx} = \frac{4\pi z^2e^4n}{mV^2} \frac{f(Z_2)}{V_o} \cdot (3x^{-1/3}+x^{-1})$ ...(17)

A. $x < 1$

(a) $V > \frac{Z_2V_o}{2}$: $\frac{dE}{dx} = \frac{4\pi z^2e^4n}{mV^2} Z_2 \ln\frac{2mV^2}{\bar{I}}$ ...(23)

(b) $V < \frac{Z_2 V_o}{2} : \frac{dE}{dx} = \frac{16\, z^2 e^4 n}{mV^2 V_o} f(Z_2)$ ...(24)

The term z which figures in these equations explicitly as also implicitly through the parameter x stands for the "effective charge" Z^{eff} if the ion is partially-stripped and equals Z_1 if the ion is completely stripped. If has been shown[2] that

$$Z^{eff} = f(Z_1) \frac{V}{V_o} , \qquad ...(25)$$

where $f(Z_1) = 0.28\, Z^{2/3}$ for $Z_1 \gg 45.5$ and $f(Z_1) = Z_1^{1/3}$ for $Z_1 \gg 45.5$. Thus, the criterion for complete stripping is

$$Z^{eff} = Z_1 = f(Z_1) \frac{V}{V_o} , \qquad ...(26)$$

from which it follows that the velocity V_m above which the ion remains completely stripped is

$$V_m = \frac{Z_1 V_o}{f(Z_1)} \qquad ...(27)$$

Hence, at ion velocities above V_m z in the above equations and in Eq.(3c) must be replaced by Z_1 while below this it should be replaced by Z^{eff} as given by Eq.(25). Eqs(21) and (23) contain the term $\bar{I}$ which needs to be known for the various media. Mukherji[4] has shown that $\bar{I}$ in eV is obtainable from

$$Z_2 \ln \bar{I} = \iint \ln\left(\tfrac{1}{2} m U_s^2\right) dn(U_s) =$$

$$\frac{f(Z_2)}{V_o} \left[\int_o^{\frac{(Z_2-2)V_o}{f(Z_2)}} \left\{ \ln\left(\tfrac{1}{2} m U_s^2\right) \right\} dU_s \right.$$

$$\left. + 2 \ln(13.6\, Z_2^2) \right] \qquad ...(28)$$

Further, it is found that the values of $\bar{I}$ calculated from Eq.(28) are well represented by the expressions

$$\bar{I}_{Z_2} = (28\, Z_2^{2/3} - 6), \text{ for } Z_2 \leqslant 45.5 \qquad ...(29)$$

$$\bar{I}_{Z_2} = (323 + 10.33(Z-45)) \text{ for } Z_2 \gg 45.5 \qquad ...(30)$$

where $\bar{I}_{Z_2}$ is the mean ionization potential of a medium of atomic number Z_2.

Table I shows a comparison between the experimental values of the stopping powers of ^{19}F ions in Al from Northcliffe[5] along with the corresponding calculated values using Eqs.(21), (22) and (23) in appropriate cases. A similar comparison is shown in Table II with the experimental data for ^{20}Ne ion in Al from Northcliffe[5] and calculated values using Eq.(21). Further, it is found that the energy-loss data of Hower and Fairhall[6] for completely stripped ^{9}Be ion in Au and Al foils are in good agreement with our calculated values, as also Northcliffe's[5] values for ^{14}N and ^{16}O ions in Al. The experimental stopping-power data of Kelley et al.[7] are also in good agreement with the corresponding calculated values of ours in the case of ^{12}C, ^{14}N and ^{16}O ions in 94.6 μm thick silicon.

Table I

Calculated and Experimental[5] Stopping powers for ^{19}F Ions in Al

Ion Energy (MeV/amu)	$(\frac{dE}{dx})_{exp}$ $(\frac{MeV\ cm^2}{mg})$	$(\frac{dE}{dx})_{calc}$ $(\frac{MeV\ cm^2}{mg})$	Appropriate equation
9.60	2.85	2.89	Eq. (23)
9.04	2.98	3.08	Eq. (23)
7.92	3.14	3.35	Eq. (21)
7.40	3.49	3.51	Eq. (21)
2.48	6.60	6.82	Eq. (22)

Table II

Calculated and Experimental[5] Stopping powers for ^{20}Ne in Al

Ion Energy (MeV/amu)	$(\frac{dE}{dx})_{exp}$ $(\frac{MeV\ cm^2}{mg})$	$(\frac{dE}{dx})_{calc}$ $(\frac{MeV\ cm^2}{mg})$	Appropriate equation
9.92	3.51	3.46	Eq. (21)
9.23	3.86	3.65	"
8.13	4.00	3.98	"
7.19	4.21	4.32	"
6.20	4.86	5.02	"
5.38	5.04	5.22	"
3.50	6.51	6.74	"

References

1. Bethe, H.A., Ann. Phys., 5, 325 (1930).
2. Mukherji, S. and Srivastava, B.K., Phys. Rev., B9, 3708 (1974).
3. Bohr, N., K. Danske Vidensk. Selsk. Mat. Fys. Medd., 18, 8 (1948).
4. Mukherji, S., Phys. Rev. B12, 3530 (1975).
5. Northcliffe, L.C., Phys. Rev., 120, 1744 (1960).
6. Hower, C.O. and Fairhall, A.W., Phys. Rev., 128, 1163 (1962).
7. Kelley, J.G., Sellers, B. and Hanser, F.A. Phys. Rev., B8, 103 (1973).

NEUTRON THERMALIZATION IN HYDROGENOUS MODERATORS

L.S. Kothari
Department of Physics and Astrophysics
University of Delhi, Delhi-110007, India

The mechanism of neutron scattering from various moderators is a poorly understood subject. Exact calculations of neutron scattering properties of commonly used moderators namely light and heavy water and graphite are extermely difficult. Calculations of neutron scattering from light and heavy water are complicated because of our imperfect understanding of liquid structures. Therefore one has to depend on various approximations or models for such calculations. This paper first stresses on investigations carried out in this field for hydrogenous moderators. A scattering kernel for light and heavy water and its mixtures developed by us considering the low-frequency collective oscillations in the quasicrystalline approximation using Debye distribution has then been described. The total scattering cross section, diffusion coefficient and various other physical parameters calculated on the basis of this kernel has been presented and compared with the available experimental and theoretical results.

(Cross section, diffusion, kernel, lattice vibration, model, moderator, neutron, scattering, thermalization)

Introduction

Light and heavy water, along with graphite are the three important moderators. As it happens, neutron scattering from all these three is poorly understood. Graphite has a layer structure and its lattice dynamics is quite different from that of more isotropic solids. Because of this, considerable difficulties arise when one wants to calculate neutron scattering cross section of this material, and the problem is still far from being closed[1]. For light and heavy water, or mixtures, it is again difficult to calculate neutron scattering cross section precisely, because of our imperfect understanding of the liquid state. However, a number of models have been developed to explain neutron scattering from these materials and we will consider them first. Later we will consider some other hydrogenous moderators.

To study neutron thermalization, one needs information about the scattering kernel, i.e. the scattering cross section for a neutron of energy E being scattered into a unit energy interval about some other energy E'. Calculating this is a major problem in itself. For water three different approaches have been adopted: (i) gas model, (ii) scattering kernel based on experimental data of the scattering law and (iii) quasicrystalline model.

Gas Model

This model for solids and liquids was first developed by Wigner and Wilkins Jr.[2] around 1944, and has been very widely used. This model implies the complete neglect of chemical binding. Radkowsky[3] suggested that one could partially take account of the chemical binding in liquids by treating the mass of the scattering unit as a free parameter, and fixing its value by adjusting the calculated values of the total scattering cross section to agree with the observed data. Nelkin[4] developed another scattering kernel in which he included the contributions of hindered rotation and intramolecular vibrational modes of the water molecules in the harmonic approximation. The translational motion was treated on the basis of gas model. To obtain an agreement between the calculated values of the total scattering cross section and the observed data, he had to divide the energy range into three regions and choose different numerical values for the parameters involved in each energy region. This kernel, which is now referred to as the Nelkin kernel, has been very widely used for thermalization and diffusion studies in water and is able to explain the results of pulsed neutron experiments very satisfactorily.

Recent pulsed neutron experiments by Fujino and his co-workers[5] in water

poisoned with non-1/v absorbers and the measurements of temperature coefficient of water moderated thermal reactors has brought out the inadequacy of the Nelkin kernel[6]. It is now generally recognized that Nelkin kernel works satisfactorily in cases where equilibrium neutron spectrum does not differ appreciably from a Maxwellian - but in such cases the calculated results are insensitive to the scattering kernel, provided of course that it satisfies the detailed balance condition.

Many modifications of the Nelkin kernel have been suggested, among others by Kosaly and Valko[7], Ardente and Gallus[8], Esch et al[9], Gotoh and Takahashi[10]. Using an approach very similar to that of Nelkin, Honeck[11] worked out a scattering kernel for heavy water which has also been very widely used for thermalization and diffusion studies.

Scattering kernel based on Experimental Data

Egelstaff and Schofield[12] were amongest the first to develop a scattering kernel for water based on the experimental data on scattering law. Koppel[13] and also Haywood[14] have done considerable work in the direction. However, scattering kernels generated by this method depend strongly upon the accuracy of the experimental data and have only been rarely used for thermalization or diffusion studies.

Quasi-crystalline Model

Quasi-crystalline model for water was proposed as early as 1933 by Bernal and Fowler[15]. Such a model is based on the idea that liquids behave as disordered crystals for times shorter than the diffusive time. In the early 60s considerable work, both theoretical and experimental, was done which lent support to this model. Larsson and Dahlborg[16] found that the frequency spectrum of water at - 3°C was very similar to that of water at +2°C. Some differences have later been reported by Burgmann[17] and others[18,19].

Following these and similar other studies, a number of workers have tried to explain neutron scattering in H_2O and D_2O, particularly the quasi-elastic scattering, on the basis of quasi-crystalline model for these liquids. Total neutron scattering cross section as well as the average cosine of the scattering angle in the laboratory frame of reference has been calculated. However, till recently no attempt seems to have been made to study neutron thermalization and diffusion using a scattering kernel based on this model.

We[20-22] have recently developed scattering kernels for light and heavy water and mixtures. We treat the low frequency collective oscillations in the quasi-crystalline approximation using a Debye distribution function. The rotational and intramolecular vibrational modes are taken as discrete levels and are treated in the harmonic approximation. Using these kernels we have calculated the total scattering cross section and have studied the pulsed neutron problem in H_2O, D_2O and in H_2O poisoned with non-1/v absorbers.

The total neutron scattering cross section for H_2O and D_2O are shown in Figs. 1 and 2 respectively. Also shown for comparision are cross sections based on a pure Debye model with θ_D = 200 K (case A) and θ_D = 250 K (case B) and experimental results due to Hughes and Schwartz[23], Neill et al[24] and McReynolds et al[25].

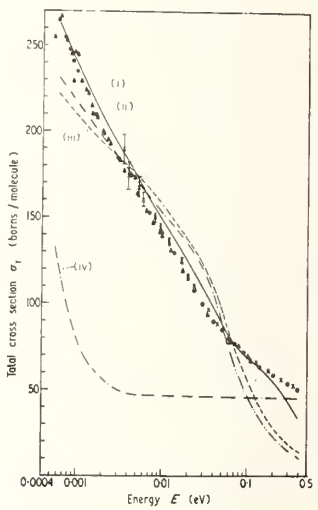

Fig. 1. Total neutron scattering cross section for water at T=20°C. Curves (i), (ii) and (iii) represent respectively the results of present calculations based on our model and cases A and B. Curve (iv) represents the values obtained using the gas model with mass 18. ●, X denote the experimental values of Hughes and Schwartz[23] and Neill et al[24] respectively. For comparison, the experimental values (▲) of Whittemore and McReynolds[25] for 5°C are also shown.

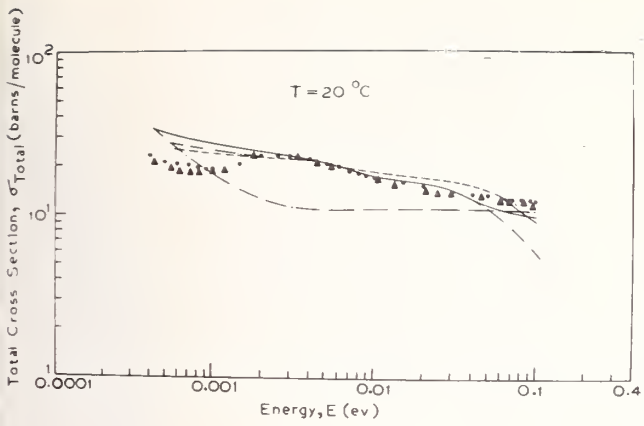

Fig. 2. Total neutron scattering cross section for heavy water at T= 20°C. Curves _____, _____..._____.. _____..._____, ------ represent respectively the results of present calculations based on our kernel and cases A and B. Curve _____._____._____, represent the values obtained using the gas model with mass 20. • denote the experimental values of Hughes and Schwartz[23]. For comparison the experimental values (▲) of Whittemore and McReynolds[25] at 9°C are also shown.

Pulsed Neutron Problem

The pulsed technique for measuring neutron diffusion parameters in moderating materials was first introduced by von Dardel[26] around 1954. Because of its simplicity, it is still very widely used. The experiment consists in introducing a burst of high energy neutrons inside a medium and studying how it decays in time. If one waits for a sufficiently long time, the decay becomes exponential and one can determine the asymptotic decay constant for the pulse. (For small assemblies the problem is more complicated and we will not go into those details here[27,28]. This decay constant λ_o is measured for assemblies of different sizes and the results are usually analysed in terms of a series expansion[29,30]

$$\lambda_o = v \sum_a (v) + D_o B^2 - C B^4 + \cdots \qquad (1)$$

where B^2, called the buckling of the assembly, is a measure of its size. $B^2 = 0$ corresponds to infinity assembly and larger values of B^2 correspond to smaller sizes. $\Sigma_a(v)$ is the macroscopic absorbtion cross section for neutrons of velocity v. It is assumed to vary as 1/v with velocity. D_o is the diffusion coefficient and C is the diffusion cooling coefficient.

The value of λ_o can be calculated by solving the integro-differential equation[29,30]

$$\left(-\frac{\lambda_o}{v} + \sum_s + \sum_a - D(E)\nabla^2\right)\varphi(\underset{\sim}{r}, E) = \int \sum_s (E' \to E)\, \varphi(\underset{\sim}{r}, E')\, dE' \qquad (2)$$

where Σ_s is the macroscopic scattering cross section, D(E) is the diffusion coefficient for neutrons of energy E, $\Sigma_s(E' \to E)$ is the scattering kernel and $\varphi(\underset{\sim}{r}, E)$ is the neutron flux at $\underset{\sim}{r}$ corresponding to energy E.

As an example we report in Fig. 3, calculated values of λ_o (curve i) as a function of B^2 in D_2O at 20°C, along with the experimental data[31-33]. Curve (iv) represents calculations based on Honeck kernel whereas curves (ii) and (iii) are based on pure Debye model with θ_D = 200 (case A) and 250 K (case B) respectively.

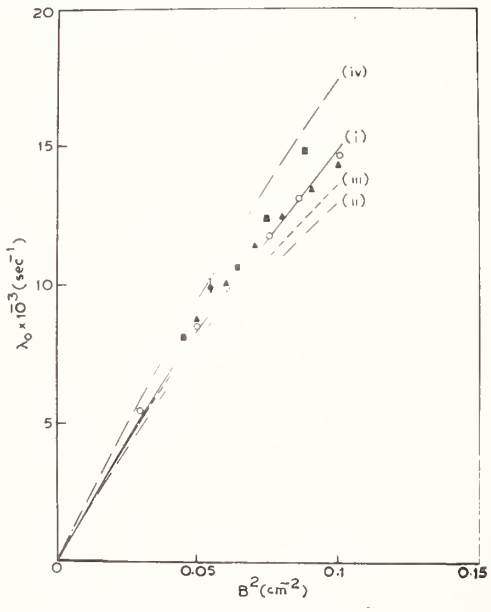

Fig. 3. Dependence of λ_o on buckling, B^2 for heavy water at 20°C ($v\Sigma_a$ = 19 sec^{-1}). Curve (i) is based on our kernel. Curves (ii) and (iii) are for cases A and B respectively. Experimental data are due to Kussmaul and Meister[31] (○), Jones[32] (◐) and Parks et al[33] (▲). Theoretical results using the Honeck kernel (curve (iv)) are also shown for comparison.

By fitting a polynomial in B^2 (eq. 1) to the calculated or the experimental data on λ_o, one can determine the values of D_o and C. In figure 4a are given the experimental values of D_o at various temperatures measured by different groups, along with our calculated temperature variation of D_o. It will be observed that the temperature variation of D_o calculated on the basis of the Nelkin kernel can not satisfactorily account for the experimental results. In general the values based on the Nelkin kernel are larger than the measured values. On the other hand, the calculated values of C that are based on the Nelkin kernel are smaller than the measured values in figure 4b.

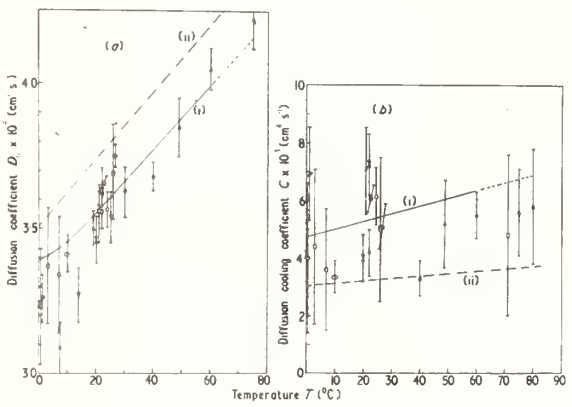

Fig. 4. Temperature variation of (a) the diffusion coefficient D_o and (b) the diffusion cooling coefficient C for water: (i) present model; (ii) Nelkin kernel Clendenin[34]. ⧗ von Dardel and Sjostrand[35]; ▲ Kuchle[36]; □ Antonov et al[37]; ○ Meadows and Whalen[38]; ● Lopez and Beyster[39]; ⧖ Dloughy and Kvitek[40]; △ Dio and Schopper[41]; ∞ Kobayashi et al[42]; ■ Paiano and Paiano[43]; ◢ Salaita and Robeson[44]; X Jones[32]; ▼ Williams and Munno[45]; 8 Bretscher[46].

The temperature variation of D_o and C for heavy water is shown in figures 5 and 6 respectively. Curves (ii) are based on Honeck kernel whereas solid curves are results based on our kernel. It will be observed that the variation in the measured values of C is very large. This is because, to determine accurately the value of C one must extend measurements to large values of B^2, but [29,30] in such assemblies interpretation of results becomes difficult.

We[20,21] have also calculated neutron spectra at different times following a burst of fast neutrons in various H_2O and D_2O assemblies at different

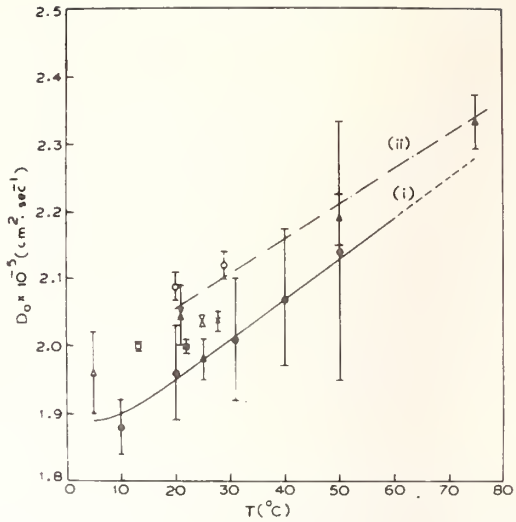

Fig.5. Temperature variation of diffusion coefficient D_o: (i) present model; (ii) Honeck kernel (Honeck and Michael[47]). In this figure the experimental results shown are of the following workers: ◖ Ganguly et al[48]; ◊ Parks et al[33]; ◭ Salaita and Robeson[44]; ⧗ Westfall and Waltner[49]; ⧗ Mala viya and Profio[50]; ◆ Kussmaul and Meister[51]; ⊡ Raiavski and Horowitz[51]; ⧖ Silk and Wade[52]; ◭ Daughtry and Waltner[53].

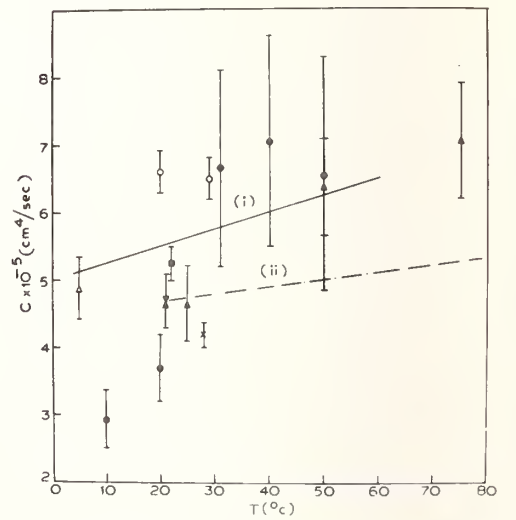

Fig.6. Temperature variation of the diffusion cooling coefficient C for heavy water: (i) present model; (ii) Honeck kernel (Honeck and Michael[47]). In this figure the experimental points are of the following workers: ◖ Ganguly et al[48]; ◊ Parks et al[33]; ◭ Salaita and Robeson[44]; ⧗ Westfall and Waltner[49]; ⧗ Malaviya and Profio[50]; ◆ Kussmaul and Meister[51].

temperatures. Some typical results for H_2O are shown in figures 7 and 8 for D_2O in figures 9 and 10. Ishmaev et al[54], measured time-dependent spectra in water assembly (30x30x45 cm^3) at 35°C. In figure 7 is plotted the time evolution of the neutron flux at a few typical energies. The calculated results account fairly well for the approach to equilibrium of the neutron pulse. The experimental results of Menzel and his group[55] in water assembly(7.16 x 25.02 x 25.4 cm^3) at 37.8°C are shown in figure 8 along with the calculated results. The agreement between the two sets of data is good.

Menzel et al[55] found that the neutron spectrum after 23 μs of the introduction of the pulse inside the assembly was a Maxwellian at 37.8°C. From this they concluded that the thermalization was complete in 23 μs. However, as our study shows for this large buckling that they have used, the asymptotic spectrum is not a Maxwellian at the temperature of the medium and it takes about 60 μs for the equilibrium to be established.

Time-dependent spectra in D_2O assembly with $B^2 = 5.78 \times 10^{-3}$ cm^{-2} at 20°C were measured by Poole and Wydler[56] and Wydler[57] and their results are shown in figure 9. Our calculated results are also shown for comparison. In fig. 10 are shown the results in D_2O assembly at 43.3°C for a 50 cm cube assembly ($B^2 = 0.0108$ cm^{-2}) and experimental results of Kryter et al[58]. In pulsed neutron experiments, the effect of adding 1/v poison to the medium is only to increase the decay constant by a constant amount, $v\Sigma_a$. However, if the assembly is poisoned by a non-1/v absorber, then the asymptotic neutron energy spectrum is modified and one has to solve the Boltzmann equation for each poison concentration separately. Fujino and his coworkers[5] have measured, as a function of time the reaction rate R(t) in water poisoned with various concentrations of cadmium: where

$$R(t) = \int \Sigma_a(E)\,\varphi(E,t)\,dE$$

The experimental data along with our calculated results are shown in Fig. 11. As is to be expected, for larger concentration the Nelkin kernel gives results which are markedly different from the experimental data.

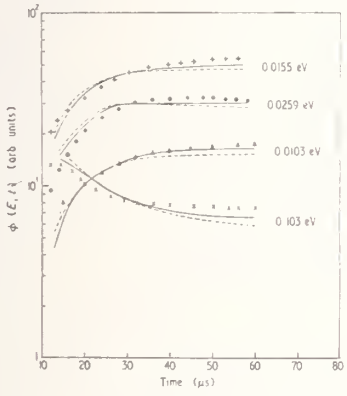

Fig. 7. Neutron spectra $\varphi(E,t)$ for $B^2 = 0.0256$ cm^{-2} for water at 35°C as a function of time: —— present model calculations; – – – case B calculations. The experimental results of Ishmaev et al[54] for various energy groups are also shown for comparison: (▲) 0.010 ev; (+) 0.015 ev; (●) 0.025 ev; (X) 0.100 ev. (The normalization is arbitrary and is different for different energy groups.)

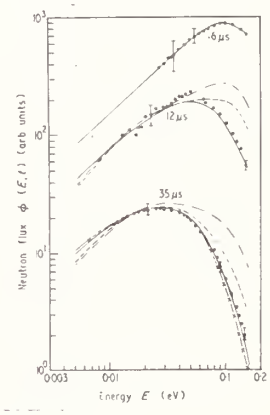

Fig. 8. Neutron spectra $\varphi(E,t)$ for $B^2 = 0.2238$ cm^{-2} for water at 37.8°C and at different times. The experimental data of Menzel et al[35] (●) are also shown for comparison. Curves ——, ——·——·——, – – – –respectively represent results based on our model, case A and B. Curve ..... is Maxwellian at 37.8°C. Curve —— X —— X —— is the asymptotic spectrum corresponding to $B^2 = 0.2238$ cm^{-2}. (The normalization at different times is arbitrary).

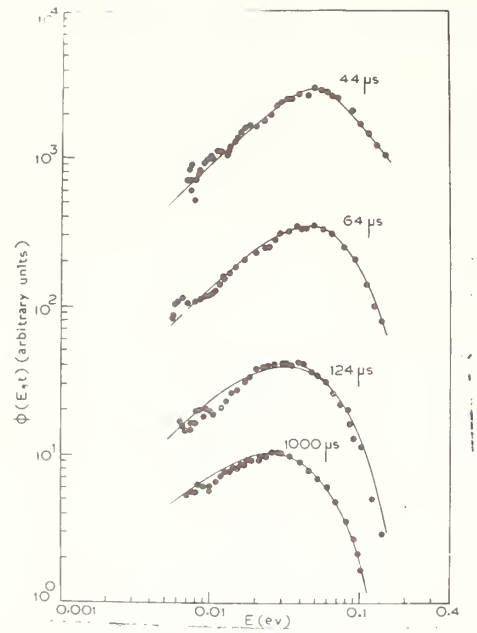

Fig. 9. Neutron spectra $\varphi(E,t)$ for $B^2 = 5.78 \times 10^{-3}$ cm^{-2} for heavy water at 20°C and at different times. (●) the experimental data of Poole and Wydler[56]. Curve ——is based on our kernel. (The normalization at different times is arbitrary).

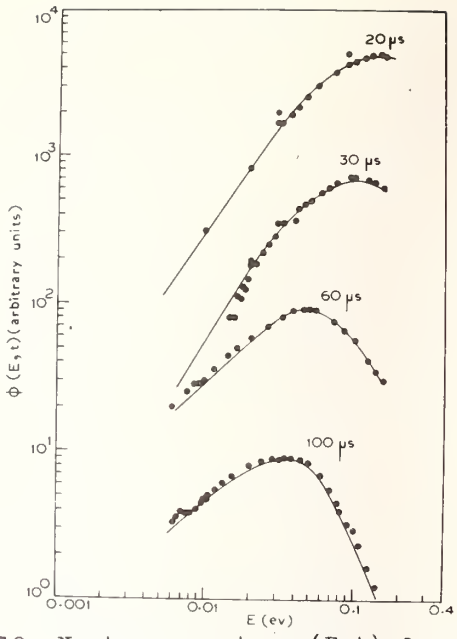

Fig. 10. Neutron spectra $\varphi(E,t)$ for $B^2 = 0.0102$ cm^{-2} for heavy water at T = 43.3°C and at different times. (●) the experimental data of Kryter et al[58]. Curve —— present kernel. (The normalization at different times is arbitrary).

In Fig. 12 we have plotted $(\lambda(t)-\lambda_{oo})/v_o N$ as a function of cadmium concentration, N, at various times, where λ_{oo} is the fundamental mode decay constant for the unpoisoned assembly and v_o is the neutron velocity corresponding to an energy $k_B T$. Experimental results of Meadows and Whalen[59] and Larsson and Moller[60] are also shown. For comparison results based on Nelkin kernel are also given. In almost the entire concentration range studied, the agreement between our calculations and the experimental results is very satisfactory, whereas Nelkin kernel gives rather low values for $(\lambda(t)-\lambda_{oo})/v_o N$.

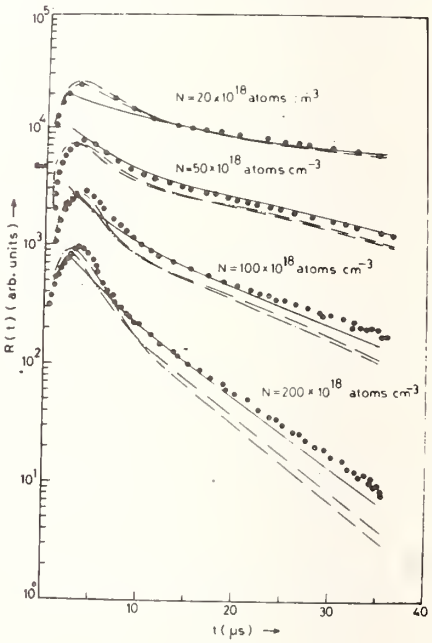

Fig. 11. Reaction rate R(t) as a function of time for water assembly (B^2 = 0) for various concentrations of cadmium. Experimental data of Fujino et al[5], ——..——..—— free gas kernel (mass = 1); ——.——.——., Nelkin kernel; ——— , present kernel.

Ice

Recently there has been increased interest in studying neutron thermalization in cold moderators, with a view of producing large flux of cold neutrons. Moderators like graphite or beryllium are completely useless for this purpose since they are almost transparent to low energy neutrons more so at low temperatures. Hence one has to rely only on hydrogenous moderators. Lot of work, both experimental and theoretical, has been done to study neutron thermalization in H_2O, D_2O ice and also liquid H_2 and D_2. Because of possible hazards of explosion, some countries do not permit the use of liquid H_2 in or near

reactor cores. Further in many ways, $H_2O + D_2O$ ice is almost as good as liquid H_2 (D_2 or mixtures), and the study of neutron thermalization in ice, which had been neglected for sometime, is again gaining importance.

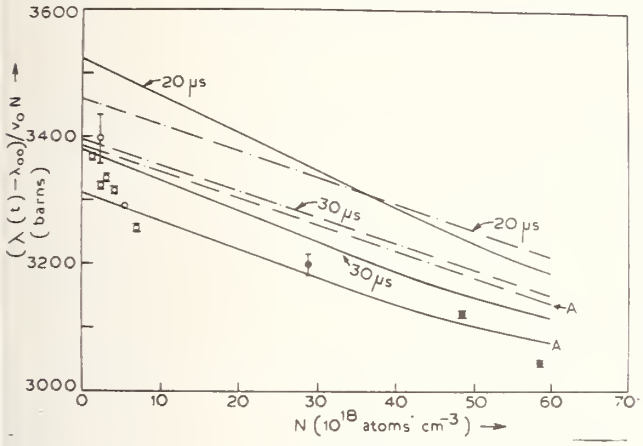

Fig. 12. $(\lambda(t) - \lambda_{\infty})/v_0 N$ as a function of cadmium concentration, at various times. Experimental results, ○ Meadows and Whalen[38]; ● Larsson and Möller[60]. Theoretical results, curve ———, present kernel calculations; curve ——.——.——, Nelkin kernel, curves marked A represent asymptotic values.

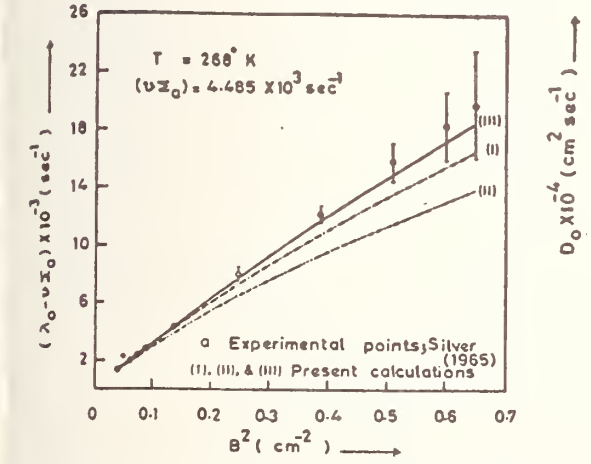

Fig. 13. $(\lambda_c - \upsilon\Sigma_a)$ vs B^2 for ice at T=268°K ($\upsilon\Sigma_a = 4.485 \times 10^3 B^{-1}$) for different frequency distributions: curve (i)—·—Debye frequency (one phonon kernel): curve (ii)----Larsson and Dahlborg[16] which includes rotational modes (one-phonon kernel): curve (iii) ———Debye frequency distribution (one-phonon plus two-phonon kernel).

Using the Debye model for lattice vibrations of ice with suitably chosen Debye temperature we[61] have studied neutron thermalization in ice down to 4° K. The results of pulsed neutron experiments at 268°K are shown in fig. 13. In fig. 14 is shown the calculated temperature variation of the diffusion coefficient D_0 in ice, along with some experimental values[62-66].

Time -dependent spectra in ice assemblies at 77° and 21° K were measured by Reichardt[65] and these are shown in figures 15 and 16 respectively. Our calculated spectra are also shown. The equilibrium spectrum at 77°K is slightly cooler than Maxwellian at 77°K. Further, equilibrium is established in around 450 μs. When ice temperature is below about 50°K, it takes unusally long for the equilibrium to be reached. At 21°K, even after 2 ms equilibrium is not reached.

Of particular interest is the equilibrium spectrum of neutrons in the presence of a 1/E source. This, the so called, steady state spectrum is what one would observe in a moderator block placed near a reactor core. We have calculated[66-68] steady state spectra in ice (H_2O, D_2O and mixtures) at various temperatures down to 4° K and in assemblies of various dimensions. Results for ice assemblies at 77°, 21° and 4° K of $B^2 = 0.1113$ cm^{-2}

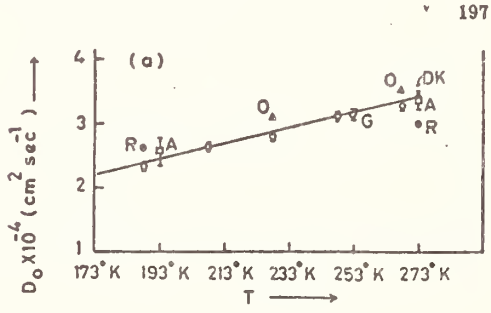

Fig. 14. Comparison of the experimental and theoretical results of the diffusion coefficient D_0 for ice as a function of temperature. ○ Silver[62]; □ Antonov et al[63], X Dloughy and Kvitek[40], Salaita[64], ● Reichardt[65], ▲ Ohanian[82], — present calculations.

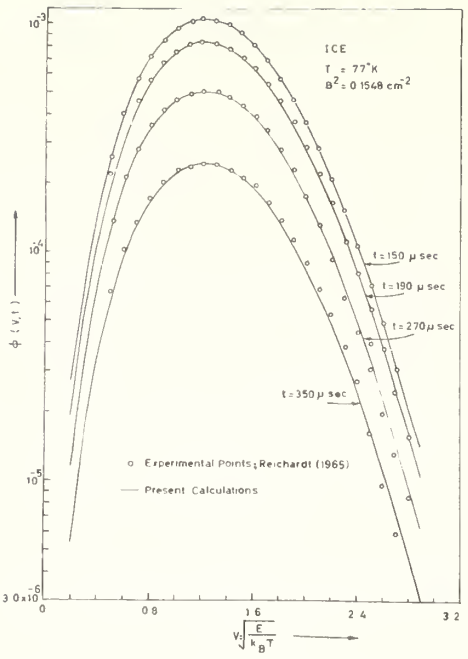

Fig. 15. Comparison of experimental and theoretical spectra at different times in ice at temperature 77°K and $B^2 = 0.1548$ cm^{-2}. Experimental points are from Reichardt[65].

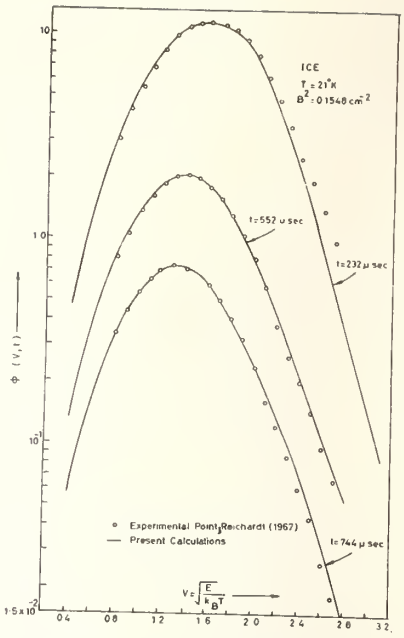

Fig. 16. Comparison of experimental and theoretical neutron spectra at different times in ice at T=21°K and $B^2=0.1548$ cm^{-2}. Experimental points are from Reichardt[65].

(a cube of nearly 17 cm side) are shown in fig. 17. The experimental results are those of Whittemore and McReynolds[69]. It will be observed that both experimentally as well as theoretically one gets the same steady-state spectrum at 21° K and 4° K. It was also observed as early as 1961 by these authors[70] that the effective temperature of the neutron distribution does not go below 40° K, however much one may reduce the temperature of ice. We[71] have shown that this arises because of diffusion hardening. To some extent the situation can be changed by adding some D_2O to H_2O. If we consider a pure D_2O assembly even then thermalization is incomplete in fairly large assemblies.

The values of effective temperature. $T_{eff} = \frac{2}{3}\frac{\bar{E}}{k_B}$ ($\bar{E}$ is mean energy of the distribution and k_B is the Boltzmann constant) in D_2O ice at various temperatures and in assemblies of various bucklings are given in Table I. We note that, unlike in H_2O ice, here there is a strong dependence of T_{eff} on buckling.

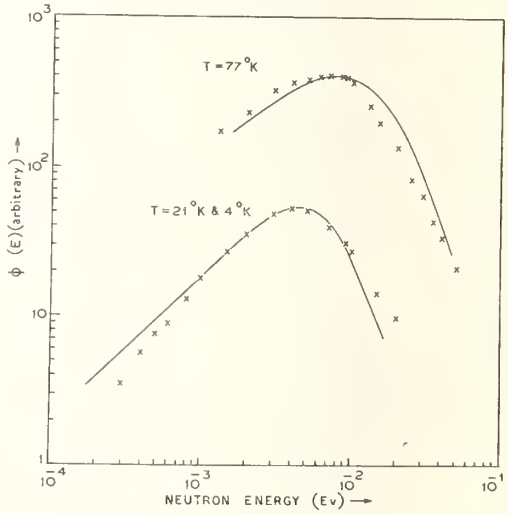

Fig. 17. Comparison of the calculated steady state neutron spectra in ice block with $B^2=0.1113$ cm^{-2} kept at 77, 21 and 4°K with the spectra measured by Whittemore et al[70]. Experimental points are reported by crosses.

Table 1

T_{eff}(°K) of Steady-State Neutron Spectra in D_2O Ice at Various Temperatures

B^2(cm^{-2})	Temperature of D_2O Ice (°K)		
	77	21	4
0.0	77.2	24.1	16.9
0.005	96.5	54.5	53.9
0.01	112.5	69.5	69.3
0.0158	128.6	82.1	82.1
0.02	138.8	89.4	89.5
0.03	159.9	103.3	103.4

Figs 18 and 19 show steady-state spectra in a 17 cm cube at 21° K for different H_2O, D_2O proportions. The vertical lines at 0.0017 eV and 0.005 eV correspond to Bragg cut-off energies in graphite and beryllium. For this buckling (0.1113 cm^{-2}) we find that the proportion of cold neutron flux is maximum in case of a mixture with 70% H_2O + 30% D_2O (by weight). (These curves are all normalized at 0.0168 eV.) Both for lower as well as higher D_2O contents, the fraction of cold neutrons decreases. The optimum mixture depends upon the size of the assembly. This is borne out by figures 20 and 21, where steady-state spectra in an assembly of B^2 = 0.0158 cm^{-2} (cube of ~ 45 cm side) at 21 K are shown. For this assembly the optimum mixture is 30% H_2O + 70% D_2O.

The variation of T_{eff} with change in D_2O concentration, in assemblies of various bucklings, is shown in Fig. 22. It will be observed that in an infinite assembly T_{eff} decreases steadily with increase in D_2O concentration, but it fails to attain the temperature of the medium even in 100% D_2O. In H_2O assemblies, the effective temperature hardly changes, as one goes from an infinite assembly down to a cube of almost 20 cm side. On the other hand, for D_2O, T_{eff} increases rapidly as B^2 increases.

For a given buckling, there is a range of optimum D_2O concentration. For large B^2 values, about 20% D_2O is expected to give the best results, whereas for small B^2 values 90% D_2O and 10% H_2O would

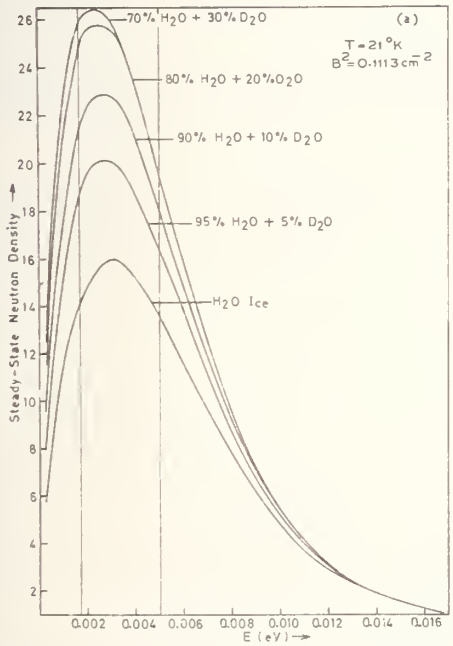

Fig. 18. Steady State neutron spectra in mixtures with 0, 5, 10, 20 and 30% D_2O at 21°K in an assembly with B^2=0.1113 cm^{-2}. All the curves are normalized at the cut off energy E_c. Also drawn in the figure are lines corresponding to energies of 20 and 60 k_B.

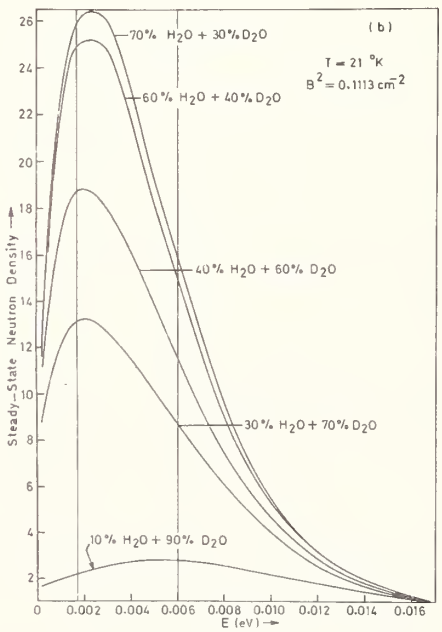

Fig.19. Steady state neutron spectra in mixtures with 30,40,60,70 and 90% D_2O at 21 K° in an assembly with B^2= 0.1113 cm^{-2}. All the curves are normalized at the cut off energy, E_c. Also drawn in the figure are lines corresponding to energies of 20 and 60 k_B.

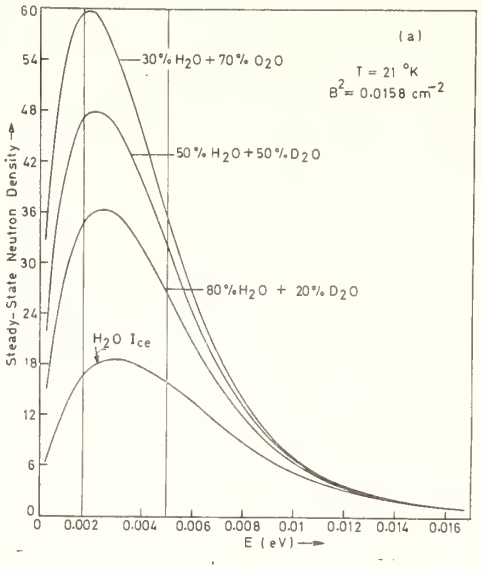

Fig. 20. Steady state neutron spectra in mixtures with 0, 20, 50 and 70% D_2O at 21° K in an assembly with B^2= 0.0158 cm^{-2}. All the curves are normalized at the cut off energy, E_c. Also drawn in the figure are lines corresponding to energies of 20 and 60 k_B.

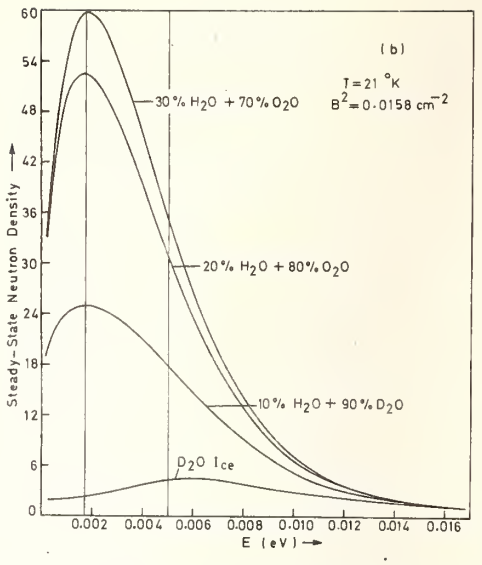

Fig. 21. Steady state neutron spectra in mixtures with 70, 80, 90 and 100% D_2O at 21 K in an assembly with B^2=0.0158 cm^{-2}. All the curves are normalized at the cut off energy, E_c. Also drawn in the figure are lines corresponding to energies of 20 and 60 k_B

give the lowest T_{eff} values. We also note that for certain buckling values, here ~ 0.05 cm^{-2}, T_{eff} remains almost constant for changes in D_2O concentration from almost 20% to 70% .

Liquid H_2, D_2 and mixtures have been widely used as cold neutron sources in European reactors[71]. Considerable theoretical work has also been done on the thermalization of neutrons in H_2 and D_2. One has to take account of the existence of the ortho-and para-spin states of the homopolar molecules, each of which has markedly different scattering properties. A further complication H_2, D_2 mixture would be the formation of HD molecules.

At room temperature the para:ortho ratio is nearly 1:3, whereas at 20 K ortho reverts to para and the equilibrium mixture contains nearly 99.7% para-hydrogen.

Neutron scattering cross section[71] for H_2 is shown in Fig. 22, alongwith available experimental results[73-75]. The scattering cross section for para hydrogen increases by almost a factor of 10 around neutron energy 0.015 eV. This is because of the excitation of the J=1 rotational level. At neutron energies below the threshold of any rotational excitations, the ortho-hydrogen cross section is almost 30 times that of para-hydrogen. At high energies both cross sections tend to the free atom value of 20 b.

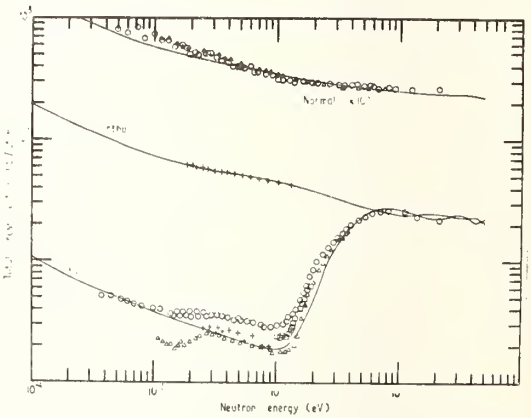

Fig.22. Comparison of predictions by the Young-Koppel scattering model with measurements of neutron total cross sections in normal ortho and para hydrogen at various temperatures: △ Seiffert[73] (para at 14 K, normal at 16 K); □ McReynolds and Whittemore[74](21 K); o McReynolds and Whittemore[74] (higher resolution measurements); + Squires and Stewart[75](20..4 K) (ref. Moon and Beynon[71]).

Since the spin-flip interaction from ortho to para (J=1 to J=0) will result in energy gain for the neutron, it might appear that para-hydrogen is a better moderator at low temperatures. In actual practice this is not so, since the scattering cross section of para-hydrogen at low energies is very much smaller than that of ortho-hydrogen.

Jacrot[75] studied neutron moderation in H_2, D_2 mixtures and found, the optimum mixture to be $\frac{1}{3}$ H_2 + $\frac{2}{3}$ D_2 by weight (50% ortho-hydrogen). On the other hand Davies et al[76] reported the optimum mixture to be $\frac{1}{4}$ H_2 + $\frac{2}{4}$ D_2 by weight. This difference in optimum mixtures is attributed to different sizes of cold neutron sources used by the two groups. More recently Carter and Jones[77] at Harwell have studied neutron moderation in H_2, D_2 and mixtures at 20.4 K inside a cylinderical assembly of internal diameter 20 cm and thickness varying from 1 to 15 cm. The effective temperatures measured by them are reported in Table II. One will observe close similarity between these results and our calculated results for ice, presented in Fig. 23. Here too we find that in H_2 assembly the effective temperature hardly changes as the thickness of the assembly is changed from 1 to 15 cm, and its value is almost the same as that in the case of H_2O ice at 21 K. In the case of D_2, in larger assemblies the effective temperature is lower than in H_2 and also shows some dependence on assembly size. In the case of mixtures inside small assemblies (2 cm thickness), T_{eff} increases with increase in H_2 concentration but in the intermediate assembly (5 cm) the temperature remains nearly constant over a very wide range of H_2 concentration (25% to 74%). This is very similar to our results for ice with B^2 = 0.05 cm^{-2} (Fig. 23). In large size, results are available only for low H_2 concentrations and here again T_{eff} shows some dependence on H_2 concentration.

Table II

Effective Temperature in Various Assemblies of H_2, D_2 and Mixtures at 20.4 K

Chamber Thickness (cm)	Moderator	Effective Temperature (K)
1	H_2	38
2	H_2	38
5	H_2	37
10	H_2	37
15	H_2	37
1	D_2	-
2	D_2	-
5	D_2	-
10	D_2	29
15	D_2	24
2	H_2/D_2(33% H_2)*	39
2	H_2/D_2(58% H_2)*	46
5	H_2/D_2(25% H_2)*	39
5	H_2/D_2(46% H_2)*	39
5	H_2/D_2(74% H_2)*	39
15	H_2/D_2(8.5% H_2)*	30
15	H_2/D_2(18.6% H_2)*	32.5

*Atomic percent

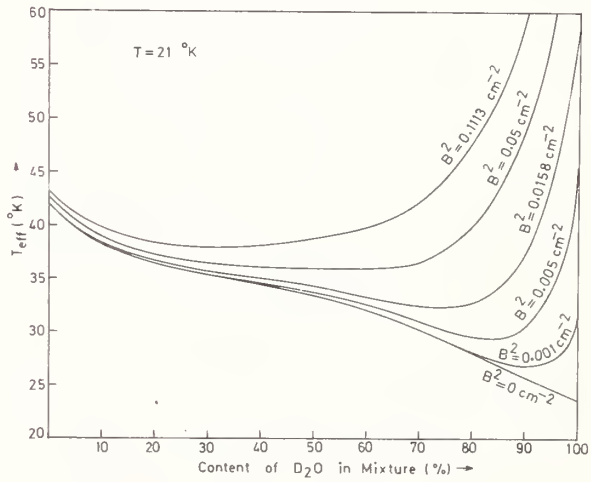

Fig. 23. Variation of T_{eff} with content of D_2O in the mixture for assemblies at 21° K with different values of B^2.

Inoue et al[78] have studied neutron thermalization in methane at low temperatures. They find that because of the near free rotational modes of this molecule, it is able to thermalize neutrons to lower temperatures than H_2 + D_2 mixtures. This is a very promising material and more studies may be made on this in coming years[79].

Neutron thermalization has also been studied in a number of other hydrogenous materials, including zirconium hydride, benzene polyethylene and some organic materials. Zirconium hydride has been used as a moderator in a number of experimental reactors. In this material hydrogen acts essentially as an Einstein oscillator, with a fairly well defined frequency. Once the neutron energy gets below the energy of the oscillator, thermalization will essentially stop.

Lattice dynamics of polyethylene corresponds to that of a chain structure. Wunderlich[80] proposed a model for the frequency distribution of this material to explain the temperature variation of the specific heat. More recently an alternative model has been proposed, which in many ways, is physically more satisfactory[81]. Neutron scattering on the basis of this model is being investigated.

There is still considerable work to be done on the thermalization of neutrons in small cold moderator assemblies. This has assumed some urgency because of the great interest currently being shown by solid state physicists in the study of the condensed state by the scattering of very long wavelength neutrons.

Part of the work presented here was supported by NSF grant No. 01P72-02844 A01. I am thankful to Mr. R.M. Bansal for his help in the preparation of this manuscript.

References

1. Goyal, I.C. and Kothari, L.S., Phys. Rev. 168, 752 (1968); Agarwala, S., Goyal, I.C. and Kothari, L.S., J. Nucl. Energy 26, 409 (1972).
2. Wigner, E.P. and Wilkins (Jr.), J.E., Report AECD - 2275 (1944).
3. Radkowsky, A., Report ANL-4470 (p.89) (1950) Argonne National Laboratory.
4. Nelkin, M.S., Phys. Rev. 119, 741 (1960).
5. Fujino, M., Hoshino, T. and Sumita, K., J. Nucl. Sci. Technol. 8, 423 (1971).
6. Askew, J.R., Fayers, F.J. and Fox, W.N., Report AEEW - R886, UK Atomic Energy Authority AEE-Winfritu, UK (1973).
7. Kosaly, G. and Valko, J., Nukleonik, 12, 237 (1969).
8. Ardemte, V. and Gallus, S., Nukleonik 11, 251 (1968).
9. Each, L.J., Yeater, M.L., Moore, W.E. and Seeman, K.W., Nucl.Sci.Eng. 46, 223 (1971).
10. Gotoh, Y. and Takahashi, H., Nucl. Sci. Eng. 45, 126 (1971).
11. Honeck, H.C., Trans. Am. Nucl. Soc. 5, 47 (1962).
12. Egelstaff, P.A. and Schofield, P., Nucl. Sci. Eng. 12, 260 (1962).
13. Koppel, J.U., Report GA - 7055, Gulf General Atomic (1966).
14. Haywood, B.C., J. Nucl. Energy 21, 249 (1967).
15. Bernal, J.D. and Fowler, R.M., J. Chem Phys. 1, 515 (1933).
16. Larsson, K.E. and Dahlborg, U., Reactor Sci. Technol. 16, 81 (1962).
17. Burgmann, J.U., Sciesinski, J. and Skold, K., Phys. Rev. 170, 808 (1968).
18. Szkatula, A. and Fulinski, A., Physica, 36, 35 (1967).
19. Golikov, V.V. et al., Inelastic Scattering of Neutrons in Solids and Liquids (IAEA, Vienna) Vol. II, p. 201 (1965).
20. Bansal, R.M., Tewari, S.P. and Kothari, L.S., J. Phys. D (Appl. Phys.) 7, 1132 (1974).
21. Bansal, R.M., Ph.D. Thesis (University of Delhi) 1974.
22. Gangwani, G.S., Tewari, S.P. and Kothari, L.S., Nucl. Sci. Eng. 50, 337 (1973).
23. Hughes, D.J. and Schwartz, R.B., Report BNL-325 (2nd Ed.) Brookhaven National Laboratory, 1958.
24. Neill, J.M., Russell (Jr.), J.L. and Browns, J.R., Nucl. Sci. Eng. 33, 265 (1968).
25. Whittemore, W.L. and McReynolds, A. W., Inelastic Scattering of Neutrons in Solids and Liquids (Vienna:IAEA), 1961. (p. 511).
26. Dardel, G.F., Trans. Roy, Inst. Technol., Stockholm No. 75 (1954).
27. Corngold, N., Michael, P. and Wollman, W., Nucl. Sci. Eng. 15, 13 (1963).
28. Kothari, L.S., Nucl. Sci. Eng. 23, 402 (1965).
29. Kothari, L.S. and Duggal, V.P., Advances in Nucl. Sci. and Tech. 2, 185 (Academic Press, New York, 1964).
30. Cokinos, D., Advances in Nucl. Sci. and Tech. 3, 1 (Academic Press, New York, 1966).
31. Kussmaul, G. and Meister, H., Reactor Sci. and Technology (J.Nucl. Energy Parts A/B) 17, 411 (1963).
32. Jones, H.G., Ph. D. Thesis Virginia Polytechnic Institute and State University (1965).
33. Parks, P.B., Pellarin, D.J., Prochnow, N.H. and Baumann, N.P., Nucl. Sci. Eng. 33, 209 (1968).
34. Clendenin, W.W., Nucl. Sci. Eng. 18, 351 (1964).

35. Von Dardel, G.F. and Sjöstrand, N.G., Phys. Rev. 96, 1245 (1964).
36. Kuchle, M., Nucl. Sci. Eng. 8, 88 (1960).
37. Antonov, A.V., Grantkin, B.V., Merkule'v, Y.A. and Smalik, Ch. K. Inelastic Scattering of Neutrons in Solids and Liquids (Vienna:IAEA) pp. 377, 1961.
38. Meadows, J.W. and Whalen, J.F., Nucl. Sci. Eng. 9, 132 (1961).
39. Lopez, W.M. and Beyster, J.R., Nucl. Sci. Eng. 12, 190 (1962).
40. Dloughy, Z. and Kvitek, I., Reactor Sci. Technol. 16, 376 (1962)
41. Dio, W.H. and Schopper, E., Nucl. Phys. 6, 75 (1958).
42. Kobayashi, K., Seki, Y., Mizoo, N., Watanabe, T. and Nishihara, N., J. Nucl. Sci. Technol. 3, 275 (1966).
43. Paiano, M.C. and Paiano, S., Neutron Thermalization and Reactor Spectra, Vol. II (Vienna: IAEA) pp. 395 (1968).
44. Salaita, G.N. and Robeson, A., Nucl. Sci. Eng. 46, 214 (1971).
45. Williams, P.M. and Munno, F.J., Nucl. Sci. Eng. 43, 120 (1971).
46. Bretscher, M.M., Proc. Indiana Acad. Sci. 72, 249 (1962).
47. Honeck, H.C. and Michael, P., Nucl. Sci. Eng. 16, 140 (1963).
48. Ganguly, N.K., Cobb, F.C. and Waltner, A.W., Nucl. Sci. Eng. 17, 223 (1963).
49. Westfall, F.R. and Waltner, A.W., Trans. Nucl. Soc. 5, 386 (1962).
50. Malaviya, B.K. and Profio, A.E., Trans. Am. Nucl. Soc. 8, 58 (1963).
51. Raievsky, V. and Horowitz, J., Comptes Rendus Acad. Sci. Paris, 238, 1993 (1954).
52. Silk, M.G. and Wade, B.O., Report AERE-M2034 (1968).
53. Daughtry, J.W. and Walter, A.W., Pulsed Neutron Research, Vol. I, (Vienna; IAEA) pp. 65 (1965).
54. Ishmaev, S.N., Mostovoi, V.I., Sadikov, I.P. and Chernyshov, A.A., Pulsed Neutron Research, Vol. I (Vienna:IAEA) pp. 643 (1965).
55. Menzel, J.H., Slovacek, R.E. and Gaerttner, E.R., Nucl. Sci. Eng. 42, 119 (1970).
56. Poole, M.J. and Wydler, P., Pulsed Neutron Research, Vol. I (Vienna, IAEA) pp. 425, (1965).
57. Wydler, P., Nucl. Energy 20, 981 (1966).
58. Kryter, R.C., Calame, G.P., Fullwood, R.R. and Gaerttner, E.R., Pulsed Neutron Research, Vol. I (Vienna:IAEA) pp. 465 (1965).
59. Meadows, J.W. and Whalen, J.F., Nucl. Sci. Eng. 9, 132 (1961).
60. Larsson, K.E. and Moller, E., Nucl. Sci. Eng. 33, 218 (1968).
61. Tewari, S.P. and Kothari, L.S., Nucl. Sci. Eng. 39, 193 (1970).
62. Silver, E.G., Ph.D. Thesis, ORNL-TM-1204, Oak Ridge National Laboratory (1965).
63. Antonov, A.V., Grantkin, B.V., Yu Merkulev, A., Pusanov, V.V. and Smolik, K.Ch. At. Energy (USSR), 12, 1, 22; 13, 4, 373 (1962).
64. Salaita, G.N., Ph.D. Thesis, Virgina Polytechnic Institute, Virginia (1965).
65. Reichardt, W., Proc. Symp. Neutron Thermalization and Reactor Spectra, Ann Arbor paper No. S.M. 96/- 15, (1967).
66. Gangwani, G.S., Tewari, S.P. and Kothari, L.S., Nucl. Sci. Eng. 47, 153 (1972).
67. Gangwani, G.S., Tewari, S.P. and Kothari, L.S., Nucl. Sci. Eng. 50, 337 (1973).
68. Gangwani, G.S., Tewari, S.P. and Kothari, L.S., Nucl. Sci. Eng. (to be published).
69. Whittemore, W.L. and McReynolds, A.W., "Differential Neutron Thermalization", Report GA-2503, General Atomic.
70. Gangwani, G.S. and Kothari, L.S., Nucl. Sci. Eng.
71. Moon, J.R. and Beynon, T.D., J.Phys. D (Appl. Phys.) 6, 427 (1973).
72. Sieffert, W.D., Euratom Report No.EUR-4455d (1970).
73. McReynolds, A.W. and Whittemore, W.L., Proc. Conf. on Inelastic Scattering of Neutrons in Solids and Liquids, Chalk River Vol. I (IAEA, Vienna) p. 263 (1963).
74. Squires, G.L. and Stewart, A.T., Proc. Roy. Soc. A230, 19 (1955).
75. Jacrot, B., Pile Neutron Research, (IAEA, Vienna), 393 (1960).
76. Davies, F. et al., Neutron Inelastic Scattering (Copenhagen) Vol. II, (IAEA, Vienna) p. 341 (1968).
77. Carter, P. and Jones, D.M., J. Nucl. Energy 26, 237 (1972).
78. Inoue, K., Otomo, N. and Utsuro, M., J. Nucl. Sci. Technol. (Japan) 9, 364 (1972).
79. Utsuro, M., J. Nucl. Sci. Technol. (Japan) 11, 434 (1974).
80. Wunderlich, B., J. Chem. Phys. 37, 1203, 1207 (1962).
81. Swaminathan, K. Tewari, S.P. and Kothari, L.S., Phys. Letters (submitted for publication).

Discussion

M.P. Navalkar

I have done a lot of experiments and analysis in pulse neutron technique using moderators such as H_2O, BeO, Pb etc. In BeO we have come to the conclusion that it is not possible to measure diffusion coefficient because asymptotic decay constant dose not exist below a certain size. What is your conclusion regarding this aspect for BeO?

L.S. Kothari

In pulsed neutron experiments one may not observe an asymptotic decay if the buckling exceeds the critical buckling. But I did not go into that aspect of the problem since it would have taken one away from the line I wanted to develop. I agree that in doing pulsed neutron experiments, particularly in D_2O assemblies, one must be careful to choose assemblies so that $B^2 < B_c^2$.

NEUTRON TRANSPORT STUDIES IN FAST REACTOR SHIELDS

R. Vaidyanathan, K.P.N. Murty and
R. Shankar Singh
Reactor Research Centre, Kalpakkam
India

The present study aims at evaluating the relative accuracies with which the different approximations to the transport theory represent the spatial and spectral distribution of neutrons in a typical fast reactor shield. Diffusion, removal diffusion and discrete ordinate transport calculations, with and without the inclusion of anisotropic scattering effects, have been performed for the lateral and axial shield configurations of the French fast reactor Rapsodie. The results have been compared, with the measurements made in Rapsodie and the NIOBE calculations made earlier.

(Approximations; diffusion; neutron; NIOBE; Rapsodie; reactor; shielding; transport calculation)

Introduction

The prediction of the spatial and spectral distribution of neutrons through the reactor shield is a vital requirement for shield design. In fast reactors, due to the small size of the core and the absence of a moderator, there is a high leakage flux from the core with long migration lengths in the surrounding material. Clearly, the diffusion theory can not adequately represent the asymptotic neutron angular flux, which exhibits severe anisotropy, especially near boundaries. Further, the major fraction of neutrons leaking into the reflector of a fast reactor is in the intermediate energy range ($<$ .5 MeV). With such source spectrum and the poorly moderating materials like sodium and steel as penetrating media, the virgin beam should principally consist of intermediate neutrons. Thus, one expects that the removal treatment which gives the penetration of fast neutrons would reduce to normal diffusion theory. All the same, it has been found[1] that the diffusion theory would yield accurate results with an empirically optimised energy group structure. But a practical limitation of this procedure is that the predictions are very sensitive to the group structure in regions of short slowing down lengths.

Another aspect of the neutron attenuation problems in fast reactor shields is the marked variation in neutron spectrum with propagation through the shield. Earlier studies[2] indicate that this effect is so severe that few-group calculations would not yield desired accuracy.

Scope of Calculations

The investigations were carried out with the following specifications:

a) The calculations were performed for the axial and radial shield configurations of Rapsodie, which is a 40 MW fast reactor at Cadarache, France. Both axial and radial configurations were studied as spherical systems with the specifications given in Table-1 with 12 energy groups.

Table-1a

Axial Configuration of Rapsodie

Zone	Radius (Cms)
Core (Driver Zone)	16.00
Expansion chamber	32.60
Transition Zone-5	36.95
Axial Blanket	64.60
Transition Zone.6	67.10
Sodium	258.80
Borated Graphite	278.40
Steel Virgo 14 SB	288.40
Borated Graphite	376.40
Steel A-42	386.40
Borated Graphite	436.40
Steel X C-18S	481.40

b) The transport equation was solved with S_4 approximation using DTF IV. To see the effect of anisotropic scattering considerations, the axial calculations were again performed with the sodium cross sections represented in 3 Legendre moments. The diffusion calculations were performed with ONEDX and a program

was developed here to solve the removal diffusion scheme. A 70-group S_4 calculation was performed to estimate the variation of spectrum due to spatial traverse in the radial shield. The 70-group cross sections were taken from JAERI fast reactor group constants[3].

Table-1b

Radial configuration of Rapsodie

Zone	Radius (Cms)
Test Zone	7.07
Driver Zone	23.0
UO_2 Blanket-I	28.0
UO_2 Blanket-II	63.5
S.S. reflector	73.5
Thermal shield	117.5
Stainless steel	121.5
2% borated concrete	181.5
0.5% borated structural concrete	396.5

c) We choose to compare here, the different methods with measurements made in the axial configuration of Rapsodie[4] with respect to the following integral parameters.

i) Thermal equivalent dose in Mn:

$$D_{th.eq.}(\underset{\sim}{r}) = \frac{1}{\sigma_{th}} \int_0^{Emax} \sigma(E)\varphi(\underset{\sim}{r},E)dE$$

ii) Fission equivalent dose in Ni:

$$D_{fis.eq.}(\underset{\sim}{r}) = \frac{1}{\hat{\sigma}} \int_0^{Emax} \sigma(E)\varphi(\underset{\sim}{r},E)dE.$$

where $\sigma = \int_0^{Emax} \sigma(E)\,\chi(E)dE$

$\chi(E)$ - U-235 fission spectrum
$\sigma(E)$ - Activation cross section
σ_{th} - Activation cross section at 2200 ms/sec.

The following approximations were made in the investigations:

a) Only coarse group fluxes (12 groups) were available at the core-reflector boundary. A white boundary condition was used to specify the source for the 70-group calculations.

b) The argon cover gas between liquid sodium surface and the rotating plug was ignored in the axial calculations.

Results and Conclusions

Fig.1 gives the spatial profile of the integral parameters mentioned in Section 2, in the axial shield configuration. DTF IV is seen to agree with the measurements within a factor of two to three. The diffusion theory underestimates the high energy fluxes by several orders of magnitude at deep penetration. It is better in predicting the thermal equivalent dose and hence the slow flux. The removal diffusion procedure is seen to make a feeble attempt to improve upon the diffusion theory results. Anisotropic scattering considerations give rise to substantial deviations in the neutron spectrum, though the differences are less pronounced in the integral parameters used for comparison here. The neutron

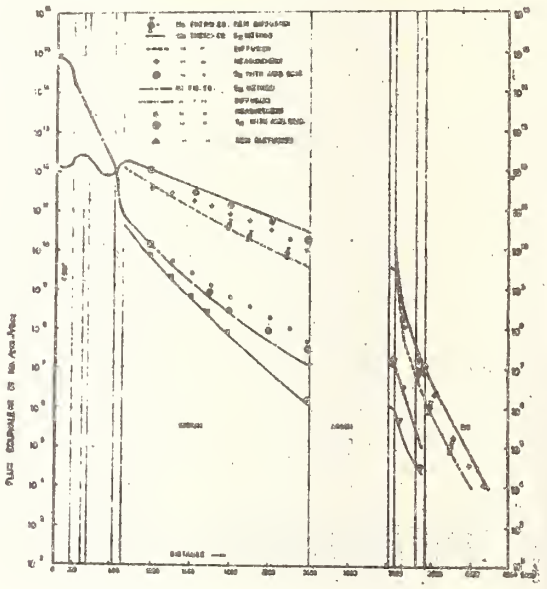

Fig. 1. Comparison of the calculated integral parameters in the axial configuration.

spectra at selective points, obtained by the 70-group calculation are given in Fig. 2. It is seen that the spectrum within a shield zone in the present configuration does not vary so markedly, as to give rise to difficulties in performing few group calculations. The present investigations indicate that -

a) The diffusion scheme can not adequately represent the neutron distributions in the fast reactor shield.

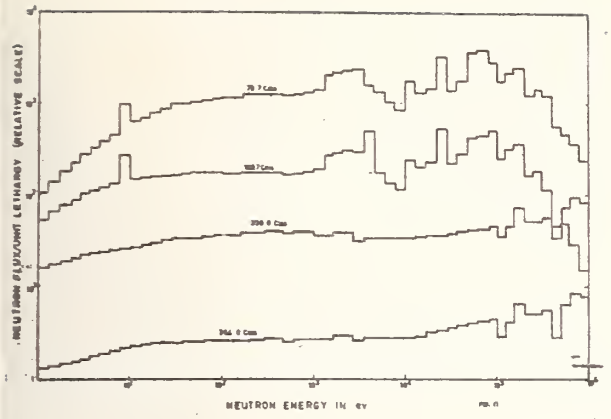

Fig. 2. Spatial variation of neutron spectrum in the radial shield.

b) The removal treatment is not very effective and almost reduces to straightforward diffusion scheme.

c) Many group calculations should be carried out if the shield regions are so thick that the spectral variation with space traverse is sharp.

Acknowledgement

The authors are thankful to M.S. Krishnan for lively discussions during the analysis of numerical results.

References

1. Avery, A.F. et.al., Neutron Attenuation studies in fast reactor shields, AERE(R) 5773, (1967).
2. Sumar Sahin, Comparison of Transport Theory and Diffusion Theory for Fast Reactor Shielding Calculations, Atomkernenergie - Sep. 1973.
3. Katsuragi et al. JAERI Fast Reactor Group Constants Systems Part I - JAERI - 1195, Aug. (1970).
4. Chaplet, M. et al., Etude experimentale des protections de Rapsodie, CEA-R-3626.

SHIELDING FOR THE VARIABLE ENERGY CYCLOTRON AT CALCUTTA

*G. Muthukrishnan, Hari Singh and
*R. Mukherjee
Health Physics Division, Bhabha
Atomic Research Centre, Trombay
Bombay-400085
India

Shielding calculations are done for the AVF Cyclotron under construction at Calcutta. Concrete shields are designed to reduce the fast neutron flux to less than the maximum permissible levels outside the shields. Earth shields are designed to reduce the fast neutron flux outside the building to less than the maximum permissible levels for public exposure. Experimentally measured values of half-value layer thickness are used in the calculations. Neutron source strengths are obtained by extrapolation to higher energies from published values at lower energies. Total neutron spectra consisting of both cascade and evaporation neutrons are computed for the bombardment of 60 MeV protons on a Li target, using semiempirical relations. In order to calculate the roof shield thicknesses calculated total neutron emission spectrum due to the bombardment of 60 MeV deuterons on a Be target is considered. Shield thicknesses thus obtained, are comparable with values calculated for a similar cyclotron at Texas A & M University. The calculated neutron dose outside the shield agrees well with the values predicted by Monte Carlo calculations.

(Calculation; concrete; cyclotron; design; earth shield; neutron spectra; shield thickness; shielding)

Introduction

The AVF cyclotron, under construction at Calcutta, is based on the design of the 88 inch AVF cyclotron at the Lawrence Radiation Laboratory Berkeley[1]. The design specifications are as follows:

Protons 6 - 60 MeV
Deuterons 12 - 65 MeV
Alphas 25 - 130 MeV
Internal beam current 1.0 mA
External beam current 100 μA.

Facilities include two high intensity caves with three beam ports and two high resolution caves with six beam ports. Figure 1 shows the proposed layout of the experimental facilities.

The shields consist of concrete shields outside the experimental caves and earth shields outside the building. The philosophy behind adequate shielding is to limit the radiation intensity in occupational areas to a dose rate of 5 Rem/Year and in public areas to 0.5 Rem/Year. Shielding calculations are done for the maximum operating conditions of the Cyclotron.

Neutron Production

Neutron production, due to the bombardment of Protons on a Li target, is calculated using the semiempirical relationship, developed by Yucker[2]. The program "CASCAD" calculates the total neutron spectrum and the differential spectra at various angles. The total cascade neutron spectrum is shown in Figure 2. Figures 3 and 4 show the differential spectra at various angles. The evaporation spectrum is shown in Figure 5. Neutron yields at higher energies due to the bombardment of deuterons and alpha particles are extrapolated from published values at lower energies. Table 1 gives the fast neutron yields due to the bombardment of alphas on Ta and deuterons on Be[3,4,5,6].

The angular distribution of neutrons due to the bombardment of 135 MeV alphas on Ta is assumed to be the same as that due to 80 MeV alphas. This is justified because there is no observed change in the angular distribution of neutrons due to the bombardment of 40 and 80 MeV alphas on Ta[4]. The same was

*Permanent address: VEC Project, Bidhan Nagar, Calcutta-700064.

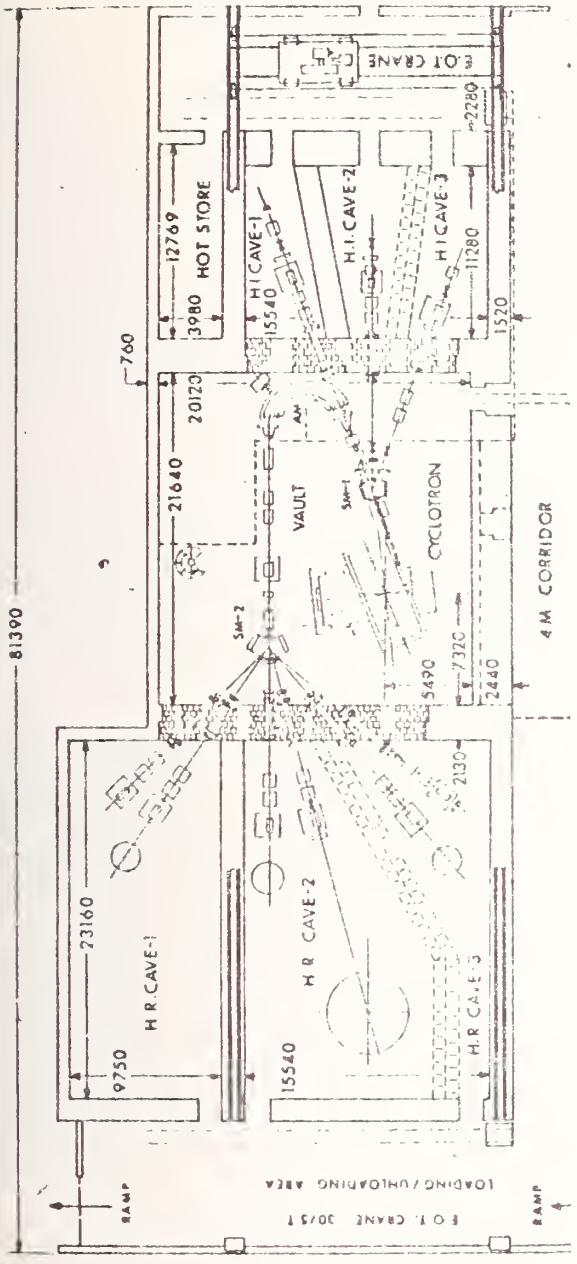

Fig. 1. V.E.C. Laboratory - Experimental Area.

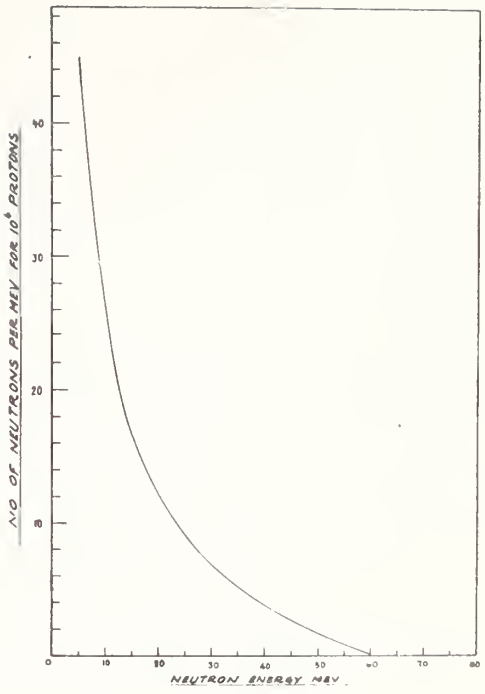

Fig. 2. Total cascade neutron spectrum.

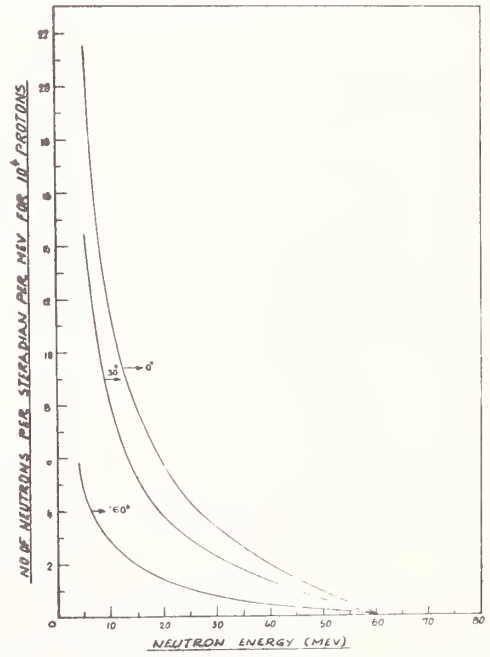

Fig. 3. Differential cascade neutron spectrum at 0°, 30° and 60°.

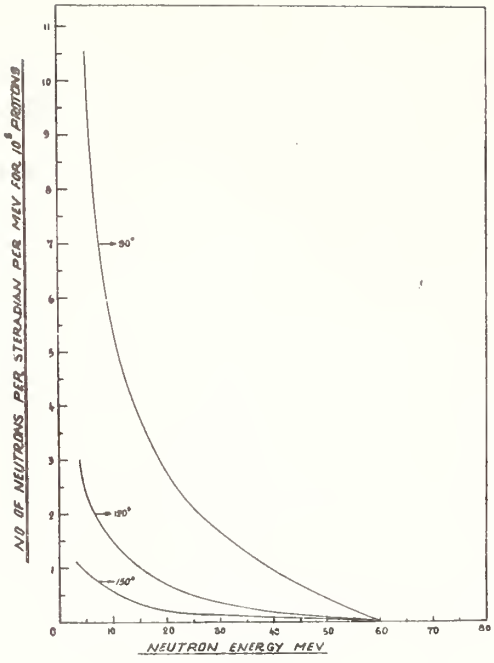

Fig. 4. Differential cascade neutron spectrum at 90°, 120° and 150°.

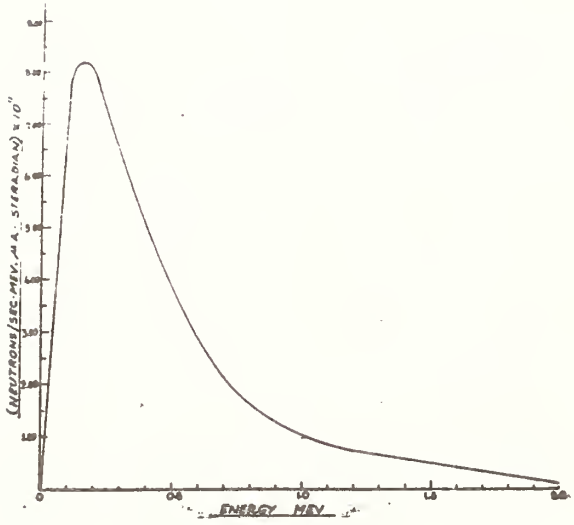

Fig. 5. Differential evaporation neutron spectrum.

Table-1

Neutron yields from (α,n) and (d,n) reactions.

ALPHAS ON Ta			
Energy MeV	Yield ns/sec-μA	Energy MeV	Yield ns/sec-μA
30	1.00×10^{8}	10	3.23×10^{10}
40	1.96×10^{10}	20	6.60×10^{10}
50	6.00×10^{10}	30	1.23×10^{11}
80	3.00×10^{11}	60	1.30×10^{12}
120	8.00×10^{11}	65	2.06×10^{12}
135	1.08×10^{12}		

Extrapolated values.

extrapolated to 120 MeV alphas on Ta by Wadman[6].

While considering the skyshine effect, the total emission spectrum, due to the bombardment of deuterons on a thick Be target, Calculated by Moyer[11] using Serber theory is taken as the source of neutrons.

Shields

Concrete and earth shields are used inside and outside the laboratory respectively. The concrete used is ordinary density concrete (density 2.4 gm/c.c.). Experimentally measured values of half-value layer thickness of concrete[6] are used in the calculations. The same was extended to other shield materials, taking into account the density effect[8]. Table 2 gives the fast neutron fluxes at 15 cms from the target and the corresponding values of the half value layer thickness. From experimental studies[13], it is observed that it is only the higher energy component of the incident neutron spectrum that determines the half value layer thickness of the shield material. Using these values, the shield thickness are calculated.

Calculations are carried out to determine the neutron fluxes outside the existing shields. These results are published elsewhere[9]. Table 3 shows shield thickness recommended to reduce the fast neutron fluxes to the maximum permissible level of 17 ns/cm^2 sec.

Table-2

Fast neutron fluxes at 15 cms from the target and the corresponding values of the half value layer thickness for the concrete shield.

Particles	Energy	Target	Angle from Target	Fast neutron flux at 100 μA ns/cm^2 sec.	Half value layer thickness cms.
Deuteron	65	Be	0°	6.0×10^{10}	12.70
Deuteron	65	Be	90°	6.246×10^{9}	10.16
Alphas	135	Ta	0°	1.45×10^{11}	18.54
Alphas	135	Ta	90°	4.028×10^{10}	10.16

Table-3

Recommended concrete shield thicknesses to reduce the fast neutron flux to the maximum permissible level at 7.2 meters from the target for 100 μA beam current.

Particle	Energy	Target	Angle from the target	Shield thickness (in meters)
Alpha	135	Ta	0°	3.90
Alpha	135	Ta	90°	2.18
Deuteron	65	Be	0°	2.58
Deuteron	65	Be	90°	1.92

Distance from target is 3.90 m.

Earth shields are provided outside the building adjacent to experimental and vault areas. Measured values of half value layer thickness of concrete are extended[8] for this shield, by taking into account the density effect of the shield material. (density 1.76 gms/cc) A value of 25.3 cms is taken for the half-value layer thickness of the earth shield. The shield thickness is calculated to be 12.5 meters of earth.

Skyshine Calculations

Skyshine calculations have been carried out by Lindenbaum[10]. Based on this, skyshine calculations are, done, considering the bombardment of 100 μA deuterons (energy 60 MeV) on a thick Be target. The total emission neutron spectrum, calculated by Moyer[11], is taken as the source.

The attenuation properties of the roof shield are taken into account in the calculation. A roof shield of 1.65 meters thick concrete is found adequate to reduce the fast neutron flux to a level of 2n/cm^2 - sec at a distance of 100 meters from the source.

Using the transmitted dose obtained by the Monte Carlo Calculations[14,15] for different neutron energies and shield thicknesses the transmitted dose rate due to neutrons produced by the bombardment of 60 MeV deuterons on a thick Be target was computed for a concrete shield of thickness 2.58 meters. The dose rate thus calculated is 1.55 mrem/hr against our computed value of 2.5 mrem/hr.

References

1. Phadke, D.Y. "Project Report on Variable Energy Cyclotron for Inter University Centre" April, 1967.
2. Yucker, W.R. "Empirical Formulae for secondary Nucleon Production cross sections". Proceedings of the special sessions on Accelerator shielding presented at the 1965 winter meeting of the American Nuclear Society. ANS-SD-3 (1965).
3. Allen, N.J., Nechaj, J.F., Sun, K.H. and Jennings, B. "Thick Target Fast Neutron yield from 15 Mev deuteron and MeV Alpha Bombardment". Phys. Rev. 81 (1951) 536.
4. **Wadman, William W.,** "Angular Distribution of Neutrons Produced by 40 and 80-MeV alpha particles on a Thick Tantalum Target". Health Physics 11 (1965) 659.
5. Smith, L.W. and Gerald Kruger, P. "Thick Target Yields from the (D,n) reaction at 10 MeV". Phys. Rev. 83 (1951) 1137.
6. **Wadman, William W.,** "Summary of shielding calculations based on Texas A and M University 88. inch cyclotron specifications" UCID 2437 (1964).
7. Tochilin, E., Ross, S.W., Shumway, B. W., Kohler, G.D. and Golden, R. "Cyclotron Neutron and Gammaray dosimetry for animal irradiation studies". Radiation Research 4 (1956) 158.
8. Wilson, Richard. "A Revision of shielding calculations". CEA-73(1959).
9. Muthukrishnan, G. and Hari Singh. "Summary of shielding calculations for the Proposed Variable Energy Cyclotron at Calcutta. BARC./I-81-(1970).
10. Lindenbaum, S.J., "Conference on shielding of High Energy Accelerators, Oak Ridge". TID-7545, 101 (1957).
11. Moyer, B.J., Some observations on Cyclotron Shielding, Unpublished.
12. Case, K.M., De Hoffman, F. and Placzek, G. "Introduction to the Theory of Neutron Diffusion". Volume I. Los Alamos Science Laboratory (1953).
13. **Stephens, L.D. and Miller, A.J., Radiation Studies at a**

Medium Energy Accelerator". UCRL - 19386 (1969).
14. Roussin, R.W. and Schmidt, F.A.R., Nucl. Eng. & Design 15, 319 (1971).
15. Roussin, R.W., Alsmiller, Jr., R.G. and Barish, J., ORNL-TM-3659 (Rev.) 1972.

COMPUTER CODES AND DATA AVAILABLE FROM THE RADIATION SHIELDING INFORMATION CENTER *

D.K. Trubey, Betty F. Maskewitz,
R.W. Roussin
Radiation Shielding Information Center
Oak Ridge National Laboratory
Oak Ridge, Tennessee - 37830, USA

The Radiation Shielding Information Center (RSIC)[1,2] is a technical institute serving the international shielding community. It acquires, selects, stores, retrieves, evaluates, analyzes, synthesizes, and disseminates information on shielding and ionizing radiation transport. The major activities include: (1) operating a computer-based information system and answering inquiries on radiation analysis, (2) collecting, checking out, packaging, and distributing large computer codes and evaluated and processed data libraries. The data packages include multigroup coupled neutron-gamma-ray cross sections and kerma coefficients, other nuclear data, and radiation transport benchmark problem results.

(Computer code; data library; information; RSIC; radiation; radiation analysis; shielding)

As an integral part of its information collection and processing activities, RSIC collects, makes operable, packages, and distributes computer code packages to nuclear scientists and engineers engaged in shielding research or design[3-5]. The various codes are designed for calculations related to radiation from fission and fusion reactors, radioisotopes, weapons and accelerators and to radiation occurring in space. The Center uses the word "package" to mean all the items needed to utilize a code effectively. The package normally includes documentation describing the theory and code operation (contributor's report plus RSIC abstract and notes) and one or more reels of tape on which is written the source program, operating (binary or hex) program, input and output for a sample problem, data libraries, and auxiliary routines.

Most of the codes are written in FORTRAN IV, which makes them nearly machine independent. Several of the packages actually represent coding systems. These are represented in the collection by prototypes, which are not necessarily useful in themselves, but which achieve generality in that they are designed to be easily changed. Such code systems are most useful to the research worker who will invest a great deal of effort in learning to use the system. Other packages are groups of interdependent codes which constitute a complete analysis system making use of a number of techniques.

The radiation treated by the majority of the codes is either neutron or gamma radiation or both, but some codes treat charged particles. The types of geometry treated vary widely, with many codes allowing a general three-dimensional geometry.

For convenience, the available codes are grouped into two classes: (1) those which treat radiation transport and identified by Computer Code Collection (CCC) numbers and (2) those performing auxiliary data processing useful for other radiation analysis purposes and identified by Peripheral Shielding Routine (PSR) numbers. The numerical methods applied in the CCC codes are primarily discrete ordinates (1- and 2-dimension), Monte Carlo (up to 3-dimension), and kernel integration (generally 3-dimension). The remaining include removal-diffusion (Spinney), moments, spherical harmonics, and invariant embedding transport theory codes and miscellaneous codes to calculate fission product buildup, release and resulting dose, stopping power, optimization, sensitivity analysis, and others.

*Research sponsored jointly by the U.S. Atomic Energy Commission and the Defense Nuclear Agency under contract with Union Carbide Corporation.

The PSR codes include multigroup cross section generation and handling, nuclear models, experimental energy spectra unfolding, optimization, plotting, coupling discrete ordinate results to Monte Carlo, random number generation, and others.

As an adjunct to the computer code exchange, RSIC is involved in many data activities, with most emphasis being placed on nuclear cross section data. Through cooperation with various agencies, RSIC assists in improving the adequacy of basic evaluated cross section data and packages and distributes various types of data libraries useful in radiation transport analysis. The emphasis of the effort is on the improvement of calculational tools available to the shielding analyst.

This work involves collaboration with the National Neutron Cross Section Center (NNCSC) at Brookhaven National Laboratory, the Shielding Subcommittee of the Cross Section Evaluation Working Group (CSEWG), Atomic Energy Commission Controlled Thermonuclear Research Division, the U.S. Nuclear Data Committee, especially the CTR subcommittee, and the Defense Nuclear Agency (DNA).

The Center's role in the Evaluated Nuclear Data File (ENDF) development is to assist in the acquisition, checkout, and review of "shielding" cross sections in ENDF format which may ultimately be placed in the ENDF/B file. In this context, "shielding" cross sections are evaluations performed in the shielding, radiation effects, or weapons radiation transport communities which are likely to have an emphasis on gamma-ray production cross sections, gamma-ray interaction cross sections, and neutron cross sections in the energy range of interest for shielding with detailed energy and angular distribution resolution. RSIC maintains and distributes the Defense Nuclear Agency (DNA) evaluated cross-section library. This is working library in ENDF format whose content can be modified and revised as often as the evaluator deems such changes to be necessary. The key to this approach is a selected evaluator, the person responsible for making the original evaluation for a particular nuclide or element. He is then responsible for authorizing changes in evaluations for that nuclide. The evaluated data are for those materials of interest to DNA, whose cross-section values were originally in a state of rapid change, and with emphasis placed on neutron energies up to 20 MeV and on secondary gamma-ray production. Evaluations which are not being modified frequently are found in the ENDF/B library, which is available in the USA from NNCSC at Brookhaven National Laboratory.

For workaday problem solving, it has been found useful to generate and collect multigroup cross section sets, and package, document, and distribute them in a format suitable as input to the most-used computer codes. Each data set, packaged as a unit, carries a Data Library Collection (DLC) number. As with the code packages, a particular data package does not remain static but is subject to revision, updating, and expansion as required. Such changes are announced in the RSIC Newsletter. Other data in the collection include gamma-ray interaction cross sections, neutron induced gamma-ray production spectra, fluence-to-kerma coefficients, radioactive decay spectra and decay schemes, and detailed output from transport calculations.

A continuing project, in cooperation with the American Nuclear Society, is to collect, edit, and publish reference data in the form of "benchmark problems"[7]. The objective is to compile in convenient form a limited number of well-documented problems in radiation transport which will be useful in testing computational methods used in shielding analysis. The problem solutions, having been determined by several methods, should be representative of the state of the art. The problem descriptions are published in looseleaf form so that revisions and additions can be easily made. In conjunction with benchmark work, data sets are packaged which allow the recalculation, with a particular calculational method, of already published results.

Lists of selected codes and data packages are given in the following table. These are typical of the most used but not necessarily the best for any particular application. Further information on these or any other codes or data are available from RSIC upon request.

Table

1. Neutron/Gamma-Ray Transport Discrete Ordinates Multigroup	1-Dimension	CCC-42/DTF IV
		CCC-82/ANISN
		CCC-126/ASOP (optimization)
		CCC-130/DTF-69 (X-ray)
		CCC-204/SWANLAKE (sensitivity analysis)
		CCC-204/INAP (activation)
	2-Dimensions	CCC-222/TWOTRAN II
		CCC-209/DOT III
		CCC-230/TRIPLET (triangular mesh)
Monte Carlo	3-Dimensions	CCC-230/MORSE-CG (multigroup)
		CCC-187/SAM-CE
2. Multigroup Cross Section	Neutron	PSR-13/SUPERTOG
		PSR-52/MACK (kerma factors)
	Gamma Ray	PSR-51/SMUG
	Coupled	PSR-63/AMPX
3. Kernel Integration	3-Dimensions	CCC-48/QAD
		CCC-94/KAP VI
		CCC-213/ACRA (radioactive cloud)
4. Spectra Unfolding		PSR-17/FERDOR-COOLC
		PSR-41/MAZE
		CCC-112/SAND II
		CCC-233/CRYSTAL BALL
5. Fission Product Inventory		CCC-217/ORIGEN
		CCC-225/REST
		CCC-237/BURP 2
6. Multigroup Data Libraries	Neutron	DLC-2/100G (100-group from ENDF/B)
		DLC-33/MONTAGE (100-group activation)
	Coupled	DLC-23/CASK (22-n, 21-γ)
		DLC-27/AMPX01 (104-n, 22-γ)
		DLC-31/FEWG1(37-n, 21-γ)

References

1. Trubey, D.K., The Radiation Shielding Information Center - A Technical Information Service for Nuclear Engineers, Nucl.Eng.Des. 9 (1969) 392-5.
2. Maskewitz, B.F., Trubey, D.K., Roussin, R.W. and Clark, F.H., The Radiation Shielding Information Center: A Unifying Force in the International Shielding Community, Fourth International Conference on Reactor Shielding, Paris, France (Oct. 1972), CONF-721018, Vol. I, pp. 215-225.
3. Trubey, D.K. and Maskewitz, Betty F., Computer Codes for Shielding Calculations - 1969, Nucl. Eng. Des. 10 (1969) 505-17.
4. Maskewitz, Betty F. and Trubey, D.K., Computer Codes for Shielding Calculations - 1970, Nucl. Eng. Des. 13 (1970) 448-9.
5. Maskewitz, Betty F., Clark, Francis H., Trubey, D.K., Computer Codes for Shielding and Related Calculations - 1972, Nucl.Eng.Des.22 (1972) 334-341.
6. Roussin, R.W., Trubey, D.K. and Maskewitz, Betty F., Data Activities of the Radiation Shielding Information Center, Fourth International Conference on Reactor Shielding, Paris, France (October 1972), CONF-721018, Vol. 4, pp. 1191-1201.
7. Profio, A.E., Editor, Shielding Benchmark Problems, ORNL-RSIC-25(ANS-SD-9) (Sup.1, 1970, Sup.2, 1974) Oak Ridge National Laboratory.

GAMMA RAY BUILD-UP FACTORS FOR FINITE MEDIA

K.John and D.V.Gopinath
Health Physics Division
Bhabha Atomic Research Centre
Bombay-400085

Using the transport code ASFIT, energy build-up factors are calculated for various energies and different systems. The results presented here are the energies 0.05, 0.1, 0.2, 0.4, 0.66, 0.8, 1.0, 1.25, 1.5, and 2.0 MeV. Media considered are air, aluminium, beryllium, calcium, carbon, hydrogen, iodine, iron, lead, magnesium, molybdenum, oxygen, silicon, sulphur, tin, uranium and water and their thicknesses are 1.0, 2.0, 4.0, 6.0, 8.0, 10.0, 15.0 and 20.0 mean free paths. Empirical formulae of the exponential polynomial type have been obtained for these finite region build-up factors. Dependence of the constants in the empirical formulae on the material property Z has been discussed.

(ASFIT ; build-up factor ; empirical ; energy ; gamma ray ; mean free path)

Introduction

The build-up factor defined as the ratio of the total detector response to the virgin radiation's response is a convenient concept in radiation attenuation calculations. In notation it can be written as

$$B = \frac{I}{I_o e^{-\mu x}}$$

where I = the total flux and

$I_o e^{-\mu x}$ = the uncollided flux

Any given build-up factor depends upon the material constituting the medium, the source energy or energies, the location in the medium and the source geometry. An extensive study of build-up factors has been done by Goldstein and Wilkins[1] using the moments method. This method assumes the medium as infinite and homogeneous. But in most of the shielding calculations one of the important parameter is the transmitted flux. Due to the assumption of the infinite medium moments method does not provide this. Another drawback of this method is that it is unsuitable for the calculations of heterogeneous shields.

Present Work

In this paper we present the energy build-up factors in finite media for one dimensional slabs obtained using the ASFIT (Anisotropic Source Flux Iteration Technique)[2] transport code which overcomes the above mentioned drawbacks of the moments method. The cross section data used for the computation is given in NSRD-NBS 29[3]. The media considered for the calculations are Air, Aluminium, Beryllium, Calcium, Carbon, Hydrogen, Iodine, Iron, Lead, Magnesium, Molybdenum, Oxygen, Silicon, Sulphur, Tin, Uranium and Water. The source energies considered are 0.05, 0.1, 0.2, 0.4, 0.66, 0.8, 1.0, 1.25, 1.5 and 2.0 MeV and the thickness are 1.0, 2.0, 4.0, 6.0, 8.0, 10.0, 15.0 and 20.0 mean free paths. We analysed for empirical relations by fitting the data for each media and energy as a function of thickness using the exponential polynomial[4].

Results

A very useful form for the build-up factors has been given by Taylor[5]. He expressed the build-up factor as a sum of the two exponentials, given by

$$B(\mu x) = A\, e^{-\alpha_1 \mu x} + (1-A) e^{-\alpha_2 \mu x}$$

where A, α_1, and α_2 are constants.

In our study we tried different types of exponential polynomials and saw that the function

$$B(x) = A_o + A_1 e^{-B_1 x} \quad (x \text{ in mean free paths})$$

is the simplest and the best fit to almost all the data from energies 1.0 MeV onwards. The constants are listed in Table-1. Table-2 gives the media in which the maximum error is above 6% . In all other cases the error is less than 6% . The constants obtained are given in Figs. 1a to 1d as a function of atomic number (z) for energies 1.0, 1.25, 1.50, 2.0. Below 1.0 MeV we could not obtain a smooth curve for constants versus Z.

Table-1

Constants of the curve $B(X)=A0+A1 \cdot EXP(-B1 \cdot X)$

Z	MEDIA		Energy (MeV) 1.00	1.25	1.50	2.00
1.0	HYDROGEN	A0	3.537+02	6.614+01	3.353+01	1.831+01
		A1	-3.532+02	-6.538+01	-3.259+01	-1.725+01
		B1	3.014-03	1.363-02	2.361-02	3.635-02
4.0	BERYLLIUM	A0	3.270+02	5.867+01	3.159+01	1.873+01
		A1	-3.265+02	-5.788+01	-3.063+01	-1.768+01
		B1	3.232-03	1.517-02	2.484-02	3.543-02
6.0	CARBON	A0	2.653+02	5.680+01	3.117+01	1.869+01
		A1	-2.648+02	-5.599+01	-3.021+01	-1.763+01
		B1	3.920-03	1.551-02	2.498-02	3.530-02
7.2	AIR	A0	3.044+02	5.807+01	3.150+01	1.900+01
		A1	-3.039+02	-5.727+01	-3.054+01	-1.795+01
		B1	3.437-03	1.525-02	2.482-02	3.486-02
8.0	OXYGEN	A0	2.753+02	5.526+01	3.056+01	1.900+01
		A1	-2.748+02	-5.445+01	-2.959+01	-1.795+01
		B1	3.764-03	1.589-02	2.542-02	3.473-02
10.0	WATER	A0	3.034+02	5.689+01	3.099+01	1.891+01
		A1	-3.030+02	-5.609+01	-3.002+01	-1.786+01
		B1	3.448-03	1.554-02	2.520-02	3.503-02
12.0	MAGNESIUM	A0	1.787+02	5.031+01	2.937+01	1.866+01
		A1	-1.781+02	-4.947+01	-2.839+01	-1.790+01
		B1	5.533-03	1.693-02	2.589-02	3.431-02
13.0	ALUMINUM	A0	1.625+02	4.908+01	2.918+01	1.900+01
		A1	-1.619+02	-4.823+01	-2.820+01	-1.795+01
		B1	6.021-03	1.723-02	2.594-02	3.415-02
14.0	SILICON	A0	1.470+02	4.885+01	2.932+01	1.910+01
		A1	-1.464+02	-4.800+01	-2.834+01	-1.805+01
		B1	6.571-03	1.720-02	2.570-02	3.383-02
16.0	SULPHUR	A0	1.207+02	4.591+01	2.856+01	1.894+01
		A1	-1.201+02	-4.504+01	-2.757+01	-1.788+01
		B1	7.786-03	1.796-02	2.604-02	3.383-02
20.0	CALCIUM	A0	9.243+01	4.167+01	2.729+01	1.904+01
		A1	-9.172+01	-4.078+01	-2.630+01	-1.799+01
		B1	9.708-03	1.917-02	2.662-02	3.312-02
26.0	IRON	A0	5.920+01	3.510+01	2.520+01	1.878+01
		A1	-5.837+01	-3.417+01	-2.420+01	-1.773+01
		B1	1.402-02	2.160-02	2.775-02	3.272-02
42.0	MOLYBDENUM	A0	2.186+01	1.991+01	1.796+01	1.698+01
		A1	-2.085+01	-1.887+01	-1.691+01	-1.592+01
		B1	3.012-02	3.208-02	3.405-02	3.281-02
50.0	TIN	A0	1.407+01	1.469+01	1.465+01	1.543+01
		A1	-1.301+01	-1.363+01	-1.359+01	-1.437+01
		B1	4.123-02	3.919-02	3.834-02	3.376-02
53.0	IODINE	A0	1.264+01	1.350+01	1.363+01	1.469+01
		A1	-1.157+01	-1.244+01	-1.256+01	-1.363+01
		B1	4.389-02	4.105-02	3.983-02	3.443-02
82.0	LEAD	A0	5.281+00	6.453+00	7.453+00	9.283+00
		A1	-4.234+00	-5.401+00	-6.398+00	-8.229+00
		B1	6.285-02	5.456-02	4.836-02	3.836-02
92.0	URANIUM	A0	4.539+00	5.600+00	6.607+00	8.301+00
		A1	-3.495+00	-4.551+00	-5.556+00	-7.250+00
		B1	6.023-02	5.271-02	4.646-02	3.736-02

Table-2

Media	Error(%)
Hydrogen	13
Beryllium	13
Carbon	12
Air	13
Oxygen	12
Water	13
Magnesium	10
Aluminum	9
Silicon	9
Sulphur	8

[Only for energy 1.0 MeV at thickness 1 mfp. In all other cases the error is less than 6%]

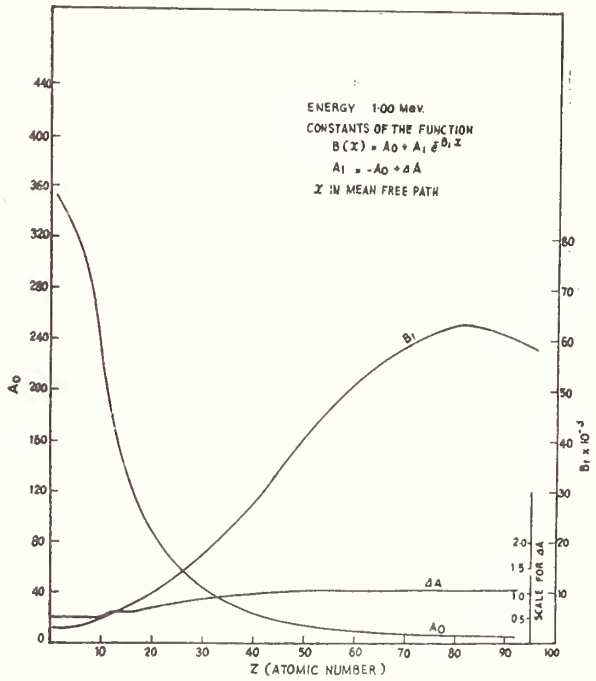

Fig. 1a

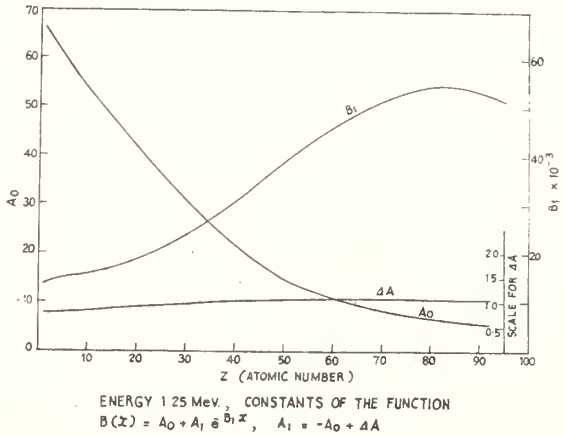

Fig.1b

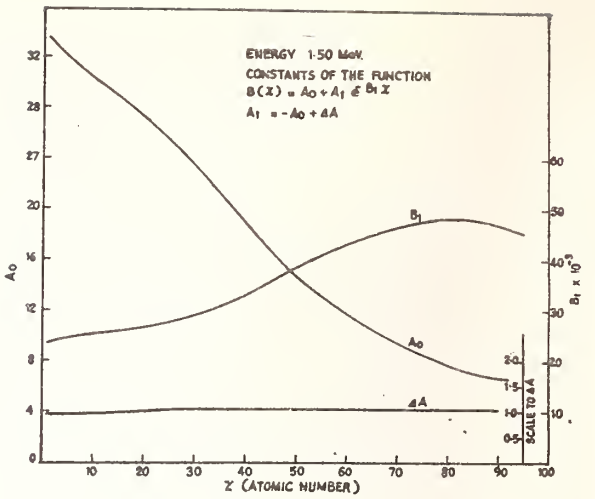

Fig. 1c

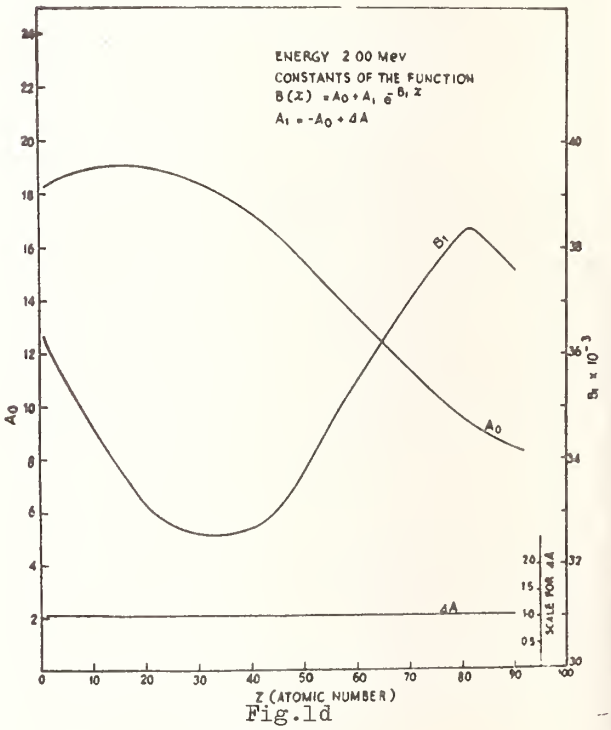

Fig.1d

References

1. Goldstein,H. and Wilkins,J.E., Calculation of the Penetration of Gamma rays, NYO 3075 (1954).
2. Gopinath,D.V. and Santhanam,K., Radiation Transport in one dimensional systems-Part I, Nuc.Sci.ε Engg. 43 186-196 (1971).
3. Hubbell,J.H., Photon Cross sections, Attenuation Coefficients, and Energy Absorption Coefficients from 10 keV to 100 GeV 1969, NSRDS-NBS 29.
4. Buckingham,R.A., Numerical Methods, Sir Isaac Pitman ε Sons Ltd., London, p.329.
5. Taylor,J.J., "Application of Gamma Ray Build-up Data to Shield Design", WAPD memo BM-217.

PHYSICAL PRINCIPLES OF PHOTON DOSIMETRY*

Walter S. Snyder**
Health Physics Division
Oak Ridge National Laboratory
Oak Ridge, Tennessee 37830

Estimation of dose absorbed in the human body is important from the point of view of health physics as well as because of the increased utilization of nuclear radiation in clinical and diagnostic medicine or therapy. An idealized mathematical model of the human body was developed and Monte Carlo calculation was applied to evaluate the photon dose. In this paper the attention is restricted to certain physical results or principles which are a by-product of such studies. These relate to evidence on the validity of the reciprocity theorem, use of the build-up factor for an infinite medium of tissue in calculating absorbed fractions, scaling absorbed fractions for the weight of the target organ, and the effects of non-homogeneity of the body on absorbed dose to the organs.

(Dose, dosimetry, Monte Carlo, organ, phantom, photon, reciprocity theorem, source, target, tissue.)

Introduction

Estimation of dose is important for medical uses of x-rays and in nuclear medicine, whether for diagnostic uses or for therapy. Also it is of great importance for health physics since use of nuclear energy requires careful control of sources so that no undue exposure of the occupational worker of the general public results. This paper is limited to consideration of dose from sources of photons within the body because the short range of electrons and alpha particles considerably reduces the complexity of estimation of the average dose to an organ, and it is this concept of average dose in an organ or tissue that is considered throughout this paper. Although many of the principles given here can be applied to micro-dose or to the other concepts of dose these are not considered in this paper.

Some ten years ago the author and his associates began to develop an idealized mathematical model of the human body to use for Monte Carlo type calculations of photon dose. The story is lengthy and not without interest, but in this paper the attempt is to focus on what has been learned about dosimetry in a complex phantom resembling in some respects the human body. In Figure 1 the exterior form of the phantom is shown and in Figure 2 some of the internal organs

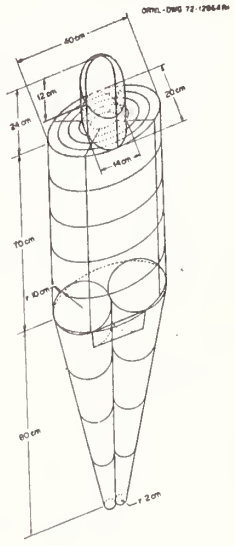

Fig. 1. The adult human phantom.

are shown, while Figure 3 displays a sketch of a skeleton together with the idealization of it for the phantom. All of these organs are described by rather

*Research sponsored by the U.S. Atomic Energy Commission under contract with Union Carbide Corporation.

**Consultant

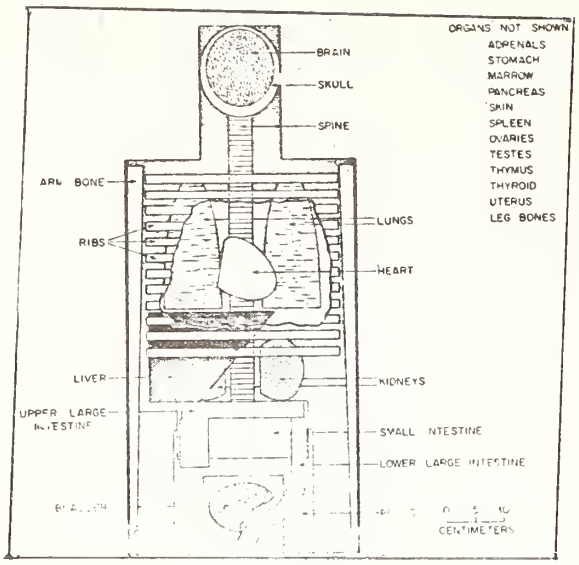

Fig. 2

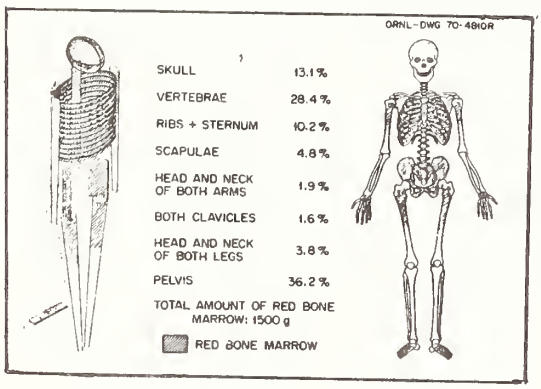

Fig. 3. Idealized Model of the Skeleton for Computer Calculations (left) and a More Realistic Representation (right) with Percentages of Red Bone Marrow Found in the Shaded Portions of the Bones.

simple mathematical formulae which are easily adapted to computation on a large scale digital computer.

The mass absorption coefficients are chosen for three distinct types of tissue; namely, bone plus bone marrow which is homogeneous with a density of about 1.5 g/cm^3, lung tissue which has a density of about 0.3 g/cm^3 and the remainder of the phantom which has density near 1 g/cm^3. Each of these tissues has its own characteristic composition and while each is homogeneous, the phantom as a whole has some of the diversity of the body. Thus the organs of the phantom approximate actual body organs in size, shape, composition and density. However, there has been no attempt to reproduce minor details of either the organs or of appendages, such as fingers, ears, etc. which are presumed to have a small effect on photon scattering.

Some of the results of our studies have been published in MIRD Phamphlet No. 5 and more special results have been published in Health Physics[2,3] and in ORNL reports[4-13]. There have been sixteen organs used as a "source" organ and in each case twelve monoenergetic sources of photons were distributed uniformly in these organs. When a calculation is completed one has dose to all twenty-three "target" organs of the phantom from a uniformly distributed source provided the statistics are good. Frequently they are not, but this is discussed below. An extensive tabulation of results is in course of publication as ORNL-5000 (in press),[14] but here attention is restricted to certain physical results or principles which are a by-product of the studies.

Variation of Dose with Organ Mass

To a first approximation, the average dose to an organ from a source outside the organ and some distance away is independent of the organ mass or size. Strictly, the principle cannot be correct in all cases as is evident if the target organ increases so greatly that the solid angle subtended from the source is changed significantly or if the distance from source to target is markedly changed. Except for these extremes the dose is relatively insensitive to the mass of the target organs. As one example, in Figure 4 are plotted the dose per photon to three different models of the solid bladder which is given three different weights. Although the weights vary by a factor of two, the doses are so close they can barely be distinguished on the figure. The sources are in the ovaries and in the kidneys which are reasonably close to the bladder. This and similar examples provide an answer to many questions medical people frequently ask; "Your calculations are for a standard man, but my patient is not standard in many respects. What difference in dose will result if his liver is larger than usual?" From sources outside the liver the evidence indicates little difference provided the average distance from source to target remains about the same.

If the liver is both the source and target organ the answer is rather different. If the source is uniformly

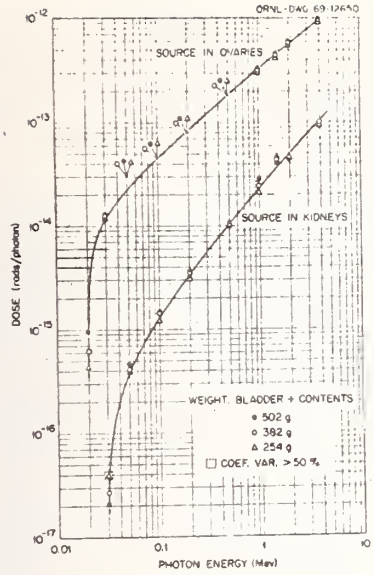

Fig. 4. Dose for Three Bladder Sizes and Two Source Organs.

distributed in a sphere and if multiple scattering is neglected (mean free path much greater than the radius r) the absorbed fraction of energy is $3r\mu_{ab}/4$ and this implies that the dose varies inversely as $M^{-2/3}$. It is surprising how well this formula holds for target organs whose shape is not approximately spherical. In Figure 5, the absorbed fraction, AF, divided by $\mu_{ab}\sqrt[3]{M}$ is

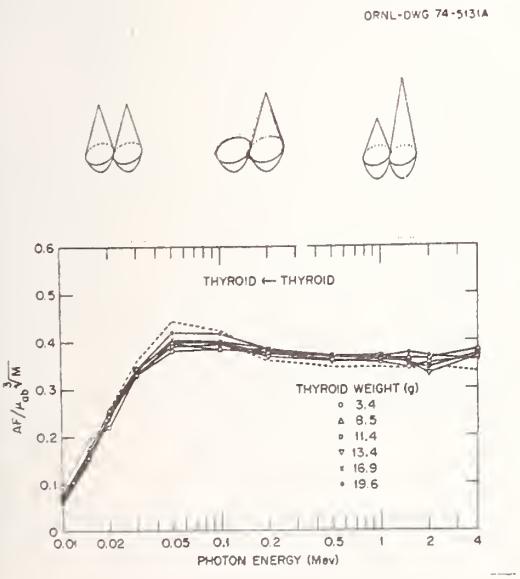

Fig. 5. Absorbed Fraction of Photons in the Thyroid in Relation to Size and Shape of Organ. (Source in Thyroid).

plotted for three shapes of thyroid which are sketched at the top of the figure and for masses ranging from 3.4 g to 19.6 g. One can scarcely distinguish the different points they lie so closely together and the curves do seem approximately constant for photon energies above 0.1 MeV. Below that, the curves are still close together but now the mean free path does not greatly exceed the diameter of the thyroid and so the curve is not flat. This is only one of many illustrations which indicate the relative insensitivity of this quotient which is, however, only for sources distributed uniformly in the organ. Other illustrations are given in Reference 15.

The Reciprocity Theorem

The interplay of theory and practice is illustrated by the reciprocity theorem first stated by Mayneord, (1945)[16]. This theorem states that if the same activity is distributed uniformly in two subregions A and B of an infinite homogeneous scattering medium, the dose rates produced in the other regions are equal. In symbols, $D(A \leftarrow B) = D(B \leftarrow A)$ where $A \leftarrow B$ indicates the source region B and the target region A. Now the body is neither infinite nor homogeneous and one may wonder whether the theorem is useful in practice. One of the by-products of the Monte Carlo type of calculation is that when A and B have each been used as a source organ one can test to see whether the equation above holds--at least within the limits of statistical accuracy. In Figure 6 the results of several hundred tests are recorded. The ratio $D(A \leftarrow B)/D(B \leftarrow A)$ is calculated, where $D(A \leftarrow B)$ is the larger of the two dose rates for all choices of A and B such that the coefficient of variation (= 100 σ/m) did not exceed 50%. The bar graph indicates the percentage of cases where the ratio did not exceed 1.2, 1.4, 1.6 etc. At the low photon energies none of the ratios exceeded two, but at higher energies there were a few exceptions and these are indicated. In all these cases about 60% or more of the ratios were below 1.2, while 95% or greater were below 1.8. Moreover, a part of this inaccuracy may be due to the statistical scatter of the Monte Carlo data. In fact, as the coefficient of variation is limited to 30% and then to 20% the exceptional cases where the ratio exceeds 2 tend to disappear. This is the basis for the claim that the ratio is, in most cases, below 1.3. The data shown are only for organs composed of soft tissue and when bone is one of the organs the above result no longer holds but an adjustment can be made which is given in reference 15. Thus, although

there is no doubt that the reciprocity theorem is not exact for organs of the body, it can still be used if one is willing to accept a limited accuracy of 20-30% .

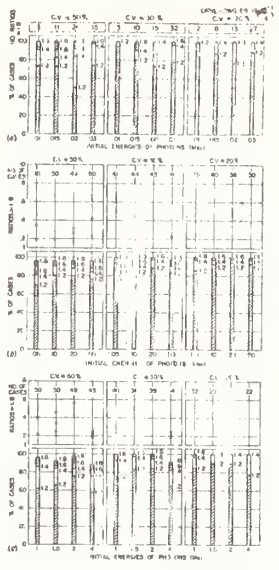

Fig. 6. Distribution of Reciprocity: Tissue Organ and Tissue Target.

The Build-up Factor

For many source and target organs the Monte Carlo estimates are statistically uncertain and the authors have therefore sought other methods which, while less exact, would not involve large errors. The specific absorbed fraction, that is the fraction of photon energy absorbed per gram of the target organ, can be written as

$$\Phi(A \leftarrow B) = \frac{1}{|A|\,|B|} \int_A dx \int_B dy \, \frac{\mu_{ab}\, e^{-\mu |X-Y|}}{\pi |X-Y|^2} B(\mu |X-Y|) \quad \ldots (1)$$

where the integral is of the product space AxB and μ and μ_{ab} denote the mass attenuation and mass absorption coefficients for photons of the required energy and $|A|$ denotes the mass of organ A and $|X-Y|$ the distance from point X to point Y.

This expression can be integrated using statistical methods and when it is compared with the results obtained from the Monte Carlo technique a surprising fact emerges. In effect, the build-up factor has been tabulated by Berger (1969)[17] for an infinite space of water so that in effect the body is enlarged to an infinite extent and is also homogeneous. But this change has remarkably small effect on the value of Φ obtained for the body.

In Figures 7-9 the results are displayed, the value of Φ obtained by the Monte Carlo calculation being the abscissa and the result of the evaluation of (1) the ordinate. When the two are equal the point should fall on the line bisecting the angle. It is found that for cases where the Monte Carlo results are reasonably exact, say with a coefficient of variation not exceeding 50%, the two results agree within a

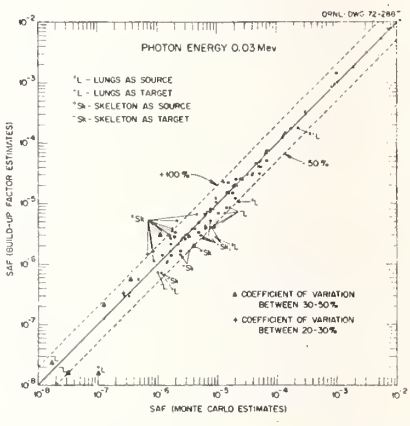

Fig. 7. Monte Carlo Estimates of Specific Absorbed Fractions Compared with Build-up Factor Estimates.

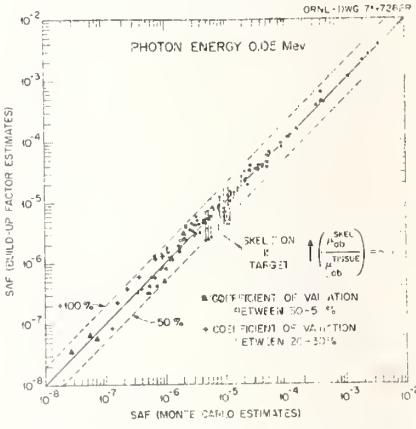

Fig. 8. Monte Carlo Estimates of Specific Absorbed Fractions Compared with Build-up Factor Estimates.

factor of about 2 and usually are much closer than this. This agreement is not due to the lack of influence of the

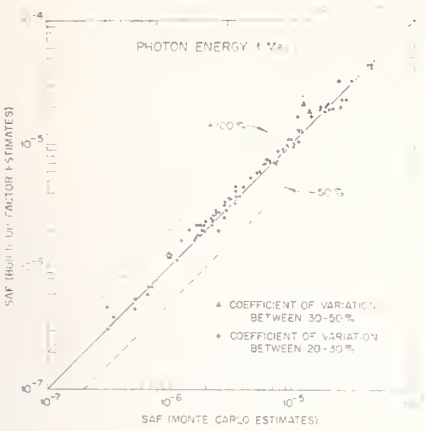

Fig.9. Monte Carlo Estimates of Specific Absorbed Fractions Compared with Build-up Factor Estimates.

build-up factor, for it has values of the order of 10^3 at 20 mean free paths in many cases. Only the results for photons of energy 0.03, 0.05 and 1 MeV are shown here but they are typical of the others. In particular, note the values with arrow attached on the two plots for the lower energies. These represent the ratio where bone is one of the organs and the arrow represents the displacement that would occur if one replaced μ_{ab} for soft tissue with μ_{ab} for bone. Thus this method seems to afford a means of getting values of Φ which are sufficiently accurate to bring one within a factor of 2 of the correct result and do not involve inordinately large sample sizes.

Special Studies

The Monte Carlo technique can be applied to a wide variety of exposure situations, for example, dose to the fetus from a radionuclide in the body, dose to an individual surrounded by a large cloud of radioactive material, and also to children. It is particularly instructive to note that preliminary phantoms have been designed for children and the results obtained indicate that dose per photon increases by an order of magnitude or more as the phantom becomes smaller. These phantoms are now in the process of being refined at ORNL to better represent the child. The study of dose to the bladder, an organ for which the dose per photon changes greatly during the process of filling, has been published[13]. No doubt these are only a few examples of the many uses to which the Monte Carlo method of calculation can provide answers.

References

1. Snyder, W.S., Ford, M.R., Warner, G.G. and Fisher, H.L., "Estimates of Absorbed Fractions for Monoenergetic Photon Sources Uniformly Distributed in Various Organs of a Heterogeneous Phantom," MIRD Pamphlet No.2, J. Nucl. Med., Suppl. No.1, 15 (1969).
2. Cloutier, R.J., Smith, S.A., Watson, E.E., Snyder, W.S. and Warner, G.G., "Dose to the Fetus from Radionuclides in the Bladder", Health Physics, 26, No.4 (1974).
3. Poston, J.W. and Snyder, W.S., "A Model for Exposure to a Semi-Infinite Cloud of a Photon Emitter," Health Physics, 26, No.4 (1974).
4. Snyder, W.S., Ford, Mary R. and Warner, G.G., "Estimation of Dose and Dose Commitment to Bladder Wall from Radionuclides Present in Urine", Health Phys. Div.Ann.Prog.Rept. for Period Ending July 31, 1970, ORNL-4584, 206.
5. Snyder, W.S., Cloutier, R.J. and Smith, S., "Dose to a Developing Fetus from a Gamma Emitter in the Bladder," Health Phys.Div.Ann.Prog.Rept. for Period Ending July 31, 1971, ORNL-4720, p. 119.
6. Snyder, W.S. Ford, Mary R., Warner, G.G. and Brindza, P.,"Absorbed Fractions for Internal Emitters," Health Phys.Div.Ann.Prog.Rept. for Period Ending July 31, 1971, ORNL-4720, p. 121.
7. Snyder, W.S., Ford, M.R. and Warner, G.G., "Estimates of Absorbed Fractions for Photon Emitters within the Body," Health Phys.Div.Ann.Prog.Rept. for Period Ending July 31, 1972, ORNL-4811, p. 86.
8. Hilyer, M.J.C., Snyder, W.S. and Warner, G.G., "Estimates of Dose to Infants and Children from a Photon Emitter in the Lungs," Health Phys. Div.Ann.Prog.Rept. for period ending July 31, 1972, ORNL-4811, p. 91.
9. Snyder, W.S., Poston, J.W. and Dillman, L.T., "A Model for Exposure to a Semi-Infinite Cloud of a Photon Emitter," Health Phys.Div.Ann.Prog. Rept. for Period Ending July 31, 1973, ORNL-4903, p. 110.
10. Snyder, W.S. and Ford, M.R., "Estimation of Dose and Dose Commitment to the Bladder Wall from a photon Emitter Present in Urine," Health Phys.Div.Ann.Prog.Rept. for Period Ending July 31, 1973, ORNL-4903, p. 115.
11. Hilyer, M.J.C., Hill, G.S. and Warner, G.G., "Dose from Photon Emitters Distributed Uniformly in the Total Body as a Function of Age," Health

Phys.Div.Ann.Prog.Rept. for Period Ending July 31, 1973, ORNL-4903, p. 119.
12. Snyder, W.S. and Ford, M.R., "Estimates of Dose Rate to Gonads of Infants and Children from a Photon Emitter in Various Organs of the Body," Health Phys.Div.Ann.Prog.Rept. for Period Ending July 31, 1973, ORNL-4903, p. 125.
13. Snyder, W.S., Poston, J.W., Warner, G.G. and Owen, L.W., "Dose to a Dynamic Bladder for Administered Radionuclides," Health Phys.Div.Ann. Prog.Rept. for Period Ending July 31, 1974, p. 13.
14. Snyder, W.S., Ford, Mary R., Warner, G.G. and Watson, Sarah B., "A Tabulation of Dose Equivalent per Microcurie-Day for Source and Target Organs of an Adult for Various Radionuclides," ORNL-5000, (in press).
15. Snyder, W.S. "Estimation of Absorbed Fractions of Energy from Photon Sources in Body Organs," Medical Radionuclides: Radiation Dose and Effects, USAEC report CONF-691212 (1970),p.33-49.
16. Mayneord, W.V., "Energy Absorption: IV. The Mathematical Theory of Integral Dose in Radium Therapy", Brit. J. Radiol. 18, 12 (1945).
17. Berger, M.J., "Energy Deposition in Water by Photons from Point Isotropic Sources," MIRD Pamphlet No.2, J.Nucl. Med., Suppl. No.1, p. 15 (1968).

TRACK THEORY APPLIED TO PHYSICAL, CHEMICAL AND BIOLOGICAL SYSTEMS*

S.C. Sharma and Robert Katz
Behlen Laboratory of Physics
University of Nebraska
Lincoln, Nebraska 68508, U.S.A.

The conceptual structure of the δ-ray model of track effects will be presented. Its universal applicability to a wide spectrum of radiation detectors and radiation environments will be shown. For 1-hit detectors, the response with LET variation is described by two parameters, the D-37 dose for gamma-rays and the size of the sensitive element. The role of 1-hit detectors in the measurement of radiation quality will be briefly outlined. A simple cellular model which applies to cells whose radiosensitivity parameters have been determined experimentally yields the cellular survival, RBE, OER etc. for heavy ions, neutrons and pions.

(Cell; delta ray; dose; ions; LET; model; neutron; OER; one-hit detector; pion; radiation; track)

Introduction

Studies of track effects in emulsion and other physical, chemical and biological media indicate that secondary electrons are the principal agents coupling the track-forming particle to the medium through which it passes. The spatial distribution of ionization energy by the secondary electrons about the path of the particle determines the track structure and is a relevant parameter to describe radiation effects. Since gamma-rays are also coupled to an irradiated medium through secondary electrons, differences in the effects observed in these kinds of irradiations arise either from the time schedule with which the electrons are generated or from their spatial distribution, or both. Track effects may be correlated with effects observed from gamma-ray irradiation by assuming that the response of small subvolumes of the medium near the path of an energetic particle is as if these subvolumes are part of a larger system irradiated with gamma-rays to the same dose. Thus the knowledge of the dose-response function of a medium to gamma-rays may be coupled with the spatial distribution of dose from secondary electrons to yield the spatial distribution of response about the path of a charged particle. The theory has been applied to a variety of detectors of interest in dosimetry, including nuclear emulsion, scintillation counters, plastics, glass, thermoluminescence, and chemical dosimeters, enzymes, viruses, and biological cells. It is applicable to track-segment bombardments as well as to mixed radiation environments including stopping particles[2].

Dose - Response Functions

The transition from gamma-ray to heavy ions is achieved by using gamma-ray dose-response transfer functions. Most of the detectors display a 1 - or - more hit response to dose. That is, the probability P that a detector is activated at dose D may be expressed as:

$$P = 1 - e^{-D/E_o} \qquad (1)$$

where E_o (also called the D-37 dose) is the dose of gamma-rays at which 37% of the detector's sensitive elements survive (or at which 63% are activated). At this dose there is an average of 1 hit per sensitive element. These are on-off detectors. If they are not activated by a passing particle their response to the next particle is as if there were no prior irradiation. Among the detectors, which are classified as 1-hit detectors, are photographic nuclear emulsions.

Biological cells display a different sort of response, described by the mathematical form of a multi-target, single-hit model, expressed as:

$$P = (1 - e^{-D/E_o})^m \qquad (2)$$

where m is the multiplicity of the target structure, and it is taken that each of the m elements of the target must be inactivated, by a single hit, for the cell to be killed. If some lesser number

* Supported by the USAEC and the NSF (RANN)

of elements than m have been affected by the radiation, it can be said that the cell has accumulated sub-lethal damage.

Theory

The size of a sensitive element plays an indirect role in determining the response of a detector to gamma-rays, as it affects the D-37 dose, but it plays a direct role in heavy ion irradiation. We take each sensitive element to act collectively, and find the radial distribution in energy density $\bar{E}$ deposited in sensitive elements of radius a_o as a function of the elements' radial distance t from the ion's path. The result, shown in Fig. 1 as a graph of $\bar{E}(z, \beta, t, a_o)\cdot\beta^2 a_o^2/z^2$ vs. t/a_o, is the basis of the calculations of the theory. The gamma-ray dose-effect relationship (Eqs. 1 or 2) is used as a transfer function by applying it to Fig. 1 to find the radial distribution of effect about the path of an ion of charge number z, moving at relative speed β through the medium. To calculate $\bar{E}$, a simple delta-ray distribution formula is used, which gives the number of rays per unit path length per unit energy interval. The delta rays are taken to be ejected radially, to loose energy at a constant rate, to move in straight line paths, to be limited in energy where $T_{max} = 2mc^2\beta^2(1-\beta^2)^{-1}$, which is determined by kinematics[1]. The maximum radial penetration τ has a nominal value (in water) of about $10^{-2}\beta^2$ cm.

At distances where both t and a_o are substantially less than τ, the normalized curves of Fig. 1-lie atop one another, with the essential result that sites for which $t/a_o < 1$ experience a "local dose" which varies as $z^2\beta^{-2}a_o^{-2}$, while sites for which $t/a_o > 3$ experience a local dose which varies as $z^2\beta^{-2}t^{-2}$. In both cases the local dose varies as z^2/β^2.

1 - hit Detectors

When Eq. (1) is applied to Fig. 1, with a suitable value of E_o and a_o, we obtain the probability P for inactivation. Since the radial integral of the probability is the cross-section σ for the (in)activation of a sensitive element by a single passing ion, we may find the radiosensitivity of a detector to this mode of inactivation.

$$\sigma = \int_0^\infty 2\pi t P \, dt \qquad (3)$$

Radiosensitivity k_i may be calculated from:

$$k_i = \sigma/L \qquad (4)$$

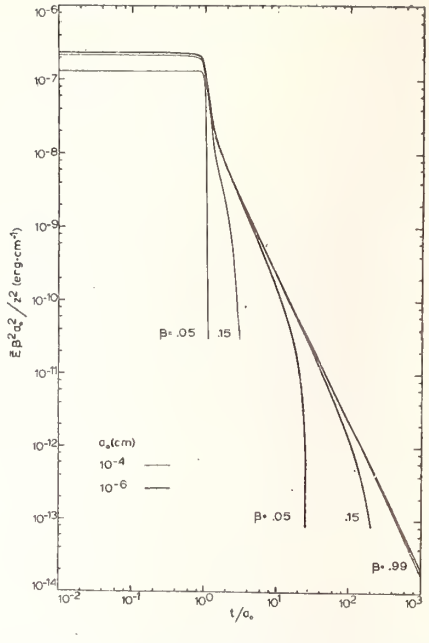

Fig. 1. Radial distribution of the local dose $\bar{E}$, in water, deposited by delta rays in sensitive elements of radius a_o whose center is at radial distance t from the path of an ion of effective charge number z and relative speed β.

where L is the stopping power of the ion.

$$RBE = (\sigma/L)\, D_\gamma^{37} \qquad (5)$$

From Eqs. (1) and (3) we note that the response of a 1-hit (m = 1) detector may be found from the two detector parameters D_γ^{37} and a_o. We also note that detector parameters and ion parameters are not separable variables. Dosimeters we now identify as 1-hit detectors are shown in Table-I. In most cases the characteristic target size is only poorly evaluated. The identification is based on gamma-ray, or heavy ion response or both. Having the parameters E_o and a_o we can calculate the response of a detector to any radiation environment[3] In Fig. 2 we show the systematic variation of RBE with an increase in LET. In Fig. 3, we show the predictions that were made and sent to Appleby[7] before his measurements of the yield of the Fricke dosimeter in the PPA nitrogen beam. Results are in quite good agreement.

To summarize the features and characteristics of 1-hit detectors, we note that when energy is deposited diffusely, it is most efficiently used by a 1-hit detector because there is no

Table-I

PROPERTIES OF 1-HIT DETECTORS

	D_γ^{37} erg/cm^3	a_o Å	G_o #/100eV	κ
Radical Production				
Valine	5.0×10^9	15	2.0	610
DL αAlanine	1.8	15	6.0	210
Thymine	1.3	85	0.05	110
Glycine	7.7×10^8	20	5.3	170
Cytosine	3.0×10^7	150	0.4	320
Inactivation (enzymes)				
Lysozyme	3.3×10^9	14	4.5	310
Trypsin	2.5	18	2.7	400
DNA-ase	1.7	25	1.4	540
β-galactosidase	3.1×10^8			
Inactivation (viruses)				
T-1	5.7×10^7			
φx-174 (243-252Å)	5.0			
T-7 (wet)-(590-650Å)	8.5×10^6	300	0.17	360
Optical Rotation				
Arabinose-3% solution	3.1×10^9			
5% solution	5.7			
Pararosanaline-CN	5.0×10^8			
Cobalt glass	8.0			
Fricke-aerated	5.0×10^7	60	15.6	90
-deaerated	1.0×10^8	60		
Luminescence				
Glass-Ag activated	1.0×10^8			
CaF_2:Mn	2.0			
$CaSO_4$:Mn	1.0			
LiF	1.0×10^7			
Scintillators				
NaI:Tl	4.0×10^7	35	22.3	12
Organic solids	1.0×10^6			
liquid	1.0×10^4			
Emulsions				
K-2	3.0×10^7	1200	7×10^{-4}	2×10^4
K.0	2.0×10^6	1200		
K.2	5.0×10^5	1200		
K.5	1.0	1200		
G.5	3.0×10^4	2000	0.16	60

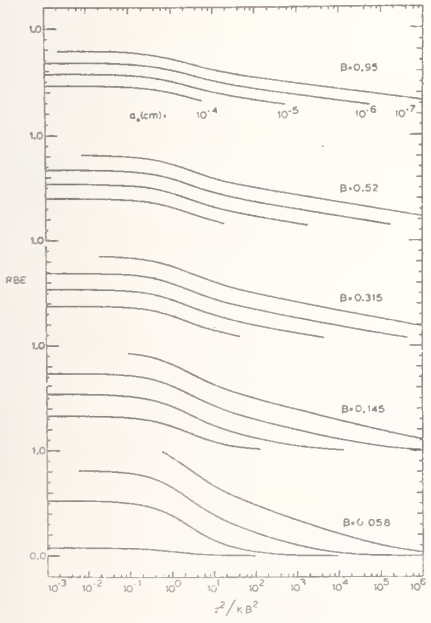

Fig. 2. Radiation detectors. The numerical values of the detector parameters have been found in different ways for the different detectors, and must be regarded as somewhat tentative.

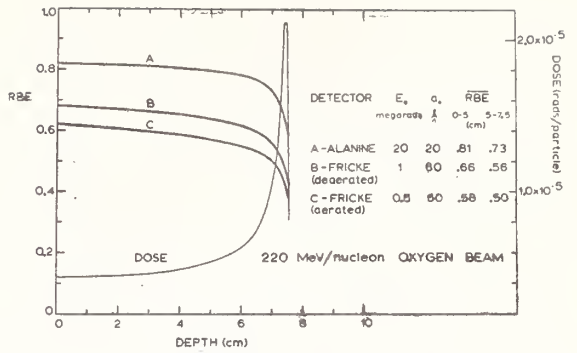

Fig. 3. Calculated values of the RBE of 1-hit detectors at different values of the relative speed of a bombarding ion, are plotted at five ion speeds from 0.95c to 0.058c and $a_o=10^{-7}$ to 10^{-4} cm. All plots are given as a function of $z^2/k\beta^2$ where $k=E_o a_o^2/2\times10^{-7}$. By matching experimental plots of the radiosensitivity (or RBE) vs. z^2/β^2, to the theoretical curves, we can determine k.

over-kill. The radiosensitivity and RBE decline with increasing values of the LET and they are both multiple-valued and non-linear. Since RBE may be found from the product of D_γ^{37} and the radiosensitivity, k, we note that the RBE of 1-hit detectors is always less than 1. The role of the 1-hit detector in the measurement of radiation quality will be shown in the last section of this paper.

A Model for Cellular Survival

When m = 1, the detector cannot accumulate sub-lethal damage. The probability that it will survive irradiation by a beam of particles of fluence F is $e^{-\sigma F}$. When m > 1, the sensitive element can accumulate sub-lethal damage. We take the gamma-ray dose-response curve for biological cells to be of the form as given in Eq. (2). We follow the mathematical operations as outlined in 'Theory' and arrive at the delta ray theory of the inactivation of cells. Just as in the 1-hit detector, a cell can be inactivated by the passage of a single ion, which is called ion-kill mode, and they may be inactivated in a second mode, called gamma-kill, through the participation of many delta-rays from different ions. The surviving fraction of a biological species when a dose D of the radiation is deposited is given by

$$N/N_o = e^{-\sigma_o PF}[1-(1-e^{-(1-P)D/E_o})^m] \quad (6)$$

$$P=\sigma/\sigma_o = (1-e^{-z^2/k\beta^2})^m \quad (7)$$

where σ_o, k, m and E_o constitute a set of four fitted parameters.

$$D = FL \tag{8}$$

$$z = Z(1 - e^{-125\beta Z^{-2/3}}) \tag{9}$$

$$\Gamma = D_\gamma / D \tag{10}$$

where D_γ = dose in gamma-kill mode.

For biological materials there are two size parameters which we have called σ_o and k. The first of these is nominally the cross-sectional area of a cell nucleus. The second parameter k is formally the value of $z^2/4\beta^2$ at which plateau (or saturation cross-section) is achieved when cells are bombarded with various heavy ion beams. Parameters E_o and m are extracted from the x-ray survival curve of a biological cell. One compact set of four parameters describes the cell survival curves for all track-segment and stopping particles. The extension to the mixed radiation environments arising from heavy ion beams, neutrons and pions is straight forward provided that we know the spectrum of secondary charged particle distribution[4].

In Fig. 4 the parameters for T - 1 human kidney cells and the survival curves they generate are shown in comparison with the data to which the parameters were fitted[4].

A beam of heavy charged particles can be approximated by a simple model incorporating attenuation and straggling, but neglecting secondary particle production, beam contamination, energy inhomogeneity and focusing[5]. Use of the heavy ion beam model yields cell survival as a function of depth in a 230 MeV/amu oxygen beam to be compared with experimental data of Roisman et al. (LBL-2016, 1973). These results[4,5] as shown in Fig. 5 were predicted before the experiment was actually performed.

With this model, we have designed ridge filters (to obtain iso-survival regions of any desired width), have calculated survival, OER, RBE, dose as a function of the depth in a phantom for different cell lines and have compared some of these calculations to the calculations of the response of different 1-hit detectors. In Fig. 6, we show the calculated response of an alanine dosimeter, here labelled as its RBE, in a cross-field irradiation with a neon beam, and compare it with the calculated

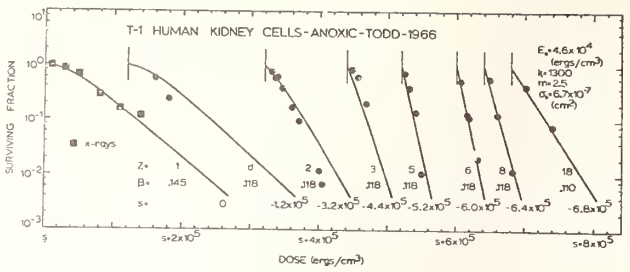

Fig.4. Calculated values of the response of alanine, the deaerated and the aerated Fricke dosimeters as a function of depth in a Bevalac beam irradiated phantom having the stopping power of water, after irradiation with 220 MeV/nucleon oxygen beam. The predicted values of the average RBE in plateau and peak regions agree with recent measurements of Appleby[7].

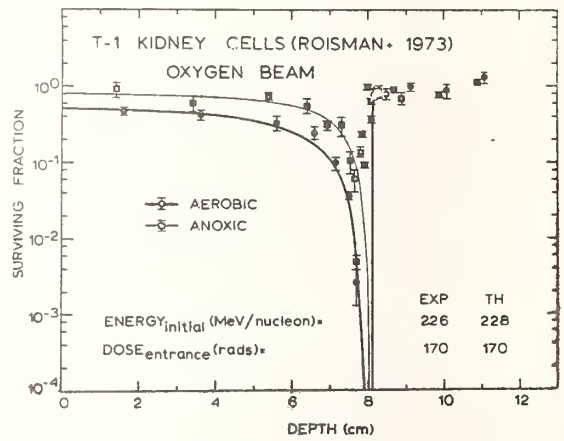

Fig.5. Survival data (Todd) for anoxically exposed T-1 human kidney cells are superimposed on a family of theoretical curves from fitted parameters[4].

value of the fraction of the dose delivered to kidney cells in the gamma-kill mode (Eq. 10), for both aerobically and anoxically irradiated cells[6]. This demonstrates that the RBE of a 1-hit detector must decline with an increase with the 'LET' of the radiation. Both F and OER show a similar decline. Thus it is suggested that an alanine dosimeter, or other suitable 1-hit detector, can be used alongside a conventional dosimeter in the measurement of radiation quality, particularly in the case where quality is changing[6].

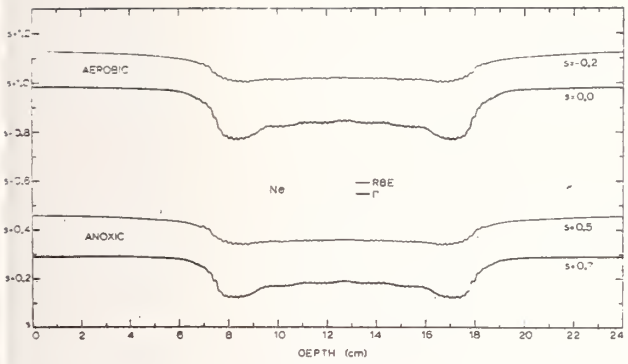

Fig.6. Experimental values of the surviving fraction of kidney cells irradiated aerobically and anoxically, at different depths in a "submarine" with a beam of oxygen ions at an initial energy of 226 MeV/nucleon at the BEVALAC (From Roisman et al., LBL-2016, 49, Sept. 1973) are compared with predictions of the delta-ray theory[4,5].

Acknowledgement

We thank Rose Ann Nelson for her assistance in the course of these investigations, and in the preparation of materials for publication.

References

1. Butts, J.J. and Katz, R., Radiat. Res. 30, 855 (1967).
2. Katz, R., Sharma, S.C. and Homayoonfar, M., The Structure of Particle Tracks, in Topics in Radiation Dosimetry, F.H. Attix, ed., Academic Press, New York (1972).
3. Katz, R., Sharma, S.C. and Homayoonfar, M., Nucl. Instr. and Meth. 100, 13 (1972).
4. Katz, R. and Sharma, S.C.,Nucl. Instr. and Meth. 111, 93 (1973).
5. Katz, R. and Sharma, S.C., Phys. Med. Biol. 19, No. 4, 413 (1974).
6. Sharma, S.C. and Katz, R., The 1-hit Detector in the Measurement of Radiation Quality, in Proceedings of the Fourth Symposium on Microdosimetry, Verbania-Pallanza (Italy), Euratom (1973).
7. Appleby, A., private communication.

Discussion

A.K. Ganguly

I am intrigued by the track model you present. Can you extend the model to deal with tracks in individual high molecular weight systems, arising out of single or a few radioactive atoms incorporated in them.

S.C. Sharma

The theory specifically avoids the assignment of the microscopic interactions between radiation and matter which are ultimately responsible for the observed effects. We understand the structure of the track common to all the detectors rather than the individual phenomena different in each detector. We have simulated tracks in different emulsions and work is in progress to understand the parameters of significance in track structure. So the answer is 'no' at the present time.

S. Mukherji

1. Is the theory on delta ray production tested in the single case of ion-pair formation in elemental gases ?

2. The energy-loss rate for heavy ions is not always given by Bethe's equation.

S.C. Sharma

1. I believe there is good deal of information on delta-ray production in elemental gases. We use simple delta-ray distribution formula and are always interested in knowing more about the finer details of the variation of ω-values in gases for various energies.

2. I agree. For our computations, we use standard tables for energy-loss and range-energy values for heavy ions. Although the stopping power information is not very accurate for very low energy and relativistic heavy ions, yet the final results are not affected a great deal.

P.S. Nagarajan

Could your theory predict the RBE, OER etc. when the high LET and low LET are deliberately used, i.e. the synergestic effects ?

S.C. Sharma

The theory can predict the response of any detector to any mixed radiation environment. For cells the high LET and low LET parts are apportioned in ion-kill and gamma-kill modes respectively. For details, please refer to our paper in Physics in Medicine and Biology (1974).

SPECTRUM SHAPES OF LOW-ENERGY PHOTON SOURCES

R.C. Sharma, S. Somasundaram, K. Unnikrishnan
and Shiv Datta
Body Burden Measurement Section
Health Physics Division
Bhabha Atomic Research Centre
Bombay-400 085

The spectrum shapes of low-energy photon (LEP) sources undergo interesting changes in the presence of scattering media of low atomic numbers. Two readily observed changes in the spectrum shape are (a) downward shift of the peak energy and (b) apparent deterioration of the energy resolution of the detector. A study of these changes is useful for in vivo assessment of LEP-emitters such as ^{241}Am, ^{239}Pu, U, ^{210}Pb etc. A computer program, based on Monte Carlo principles, has been evolved to compute the magnitudes of these changes in pulse-height distribution. Calculations were performed for point sources of low-energy photons located on the axis of the detector and for different thicknesses of the scattering medium interposed between the source and the detector. The variable parameters considered in these calculations are initial photon energy, thickness of the interposed material and type of detector. The magnitudes of both the above-mentioned changes in the pulse-height spectra of LEP sources embedded under media of low effective atomic number, such as water ($\bar{Z}$ = 7.42), tissue ($\bar{Z}$ = 7.33) and perspex ($\bar{Z}$ = 6.47), are found to be dependent to a great extent on the energy resolution of the detector employed, apart from the electron density and effective atomic number of the scattering medium. The theoretical results are presented and compared, wherever possible, with experimental values obtained with NaI (Tl) detector.

(Detector; Monte Carlo; perspex; photon energy; pulse height; resolution; scattering media; tissue; water).

Introduction

It has been observed recently in connection with in vivo detection of low-energy photon (LEP) emitters ($E_\gamma < 100$ keV) with thin NaI(Tl) scintillation or NaI(Tl)-CsI(Tl) phoswich detectors[1-4] that the presence of tissue produces appreciable changes in the original pulse-height spectrum which may be exploited advantageously to estimate the depth at which activity is located. Two most readily observed changes in the spectrum of a monoenergetic LEP source located in a medium of low effective atomic number ($\bar{Z}$), such as tissue ($\bar{Z}$ = 7.33) or water ($\bar{Z}$ = 7.42), are (a) downward shift of the peak energy and (b) apparent deterioration of the energy resolution of the system. Experimental work in our laboratory has indicated that the magnitudes of these effects are in general different for different absorber-scatterers, which could be explained qualitatively on the basis of differences in the effective atomic numbers and the electron densities (number of electrons/cm^3) of the material[4]. Experimental studies with point sources of LEP emitters embedded at various depths in a tissue-equivalent material have also indicated the feasibility of correlating with depth the observed peak-shift or the change in resolution[1-3]. On the basis of such correlations, it would be possible to derive effective soft tissue thicknesses for individuals of differing body builds to facilitate correction of the calibration factors. Besides, in the literature the occurrence of these phenomena has usually been explained qualitatively as being exclusively due to Compton scattering in the intervening medium.[1-4] The present work describes a computer program evolved to compute the changes in pulse-height spectra for a wide range of low energies and depths of source in tissue-like media. The calculations provide a better insight into the actual mechanisms leading to the observed changes in pulse-height spectra of LEP sources. The results of calculation are presented and compared with the experimental values.

Computer Program

Mathematically, the problem is specified by referring to fig. 1 in which C represents the NaI(Tl) detector of radius R and thickness T, on the axis of which is placed a point source S at a distance t from the detector face. The intervening space between S and C is filled with water W, also of radius R. It is desired to construct the pulse-height response of C due to monoenergetic photons emitted by S. This is achieved in two steps:

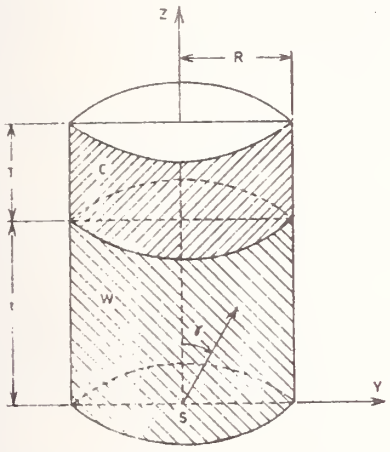

Fig. 1. Source detector geometry used in computational scheme.

First, the line spectrum incident on the detector face, hereafter referred to as the "exit photon spectrum", is determined by the Monte Carlo technique. Scattering from the surroundings is not taken into account. This idealization is quite justified since only low-energy photons are involved. The Monte Carlo simulation of (a) is achieved by following the sampling techniques described by Cashwell and Everett[5]. Fig. 2 shows the flow chart of the computer program schematic used in the present studies to compute the exit photon spectrum. The relevant cross sections for water are taken from reference[6].

The second step required is the derivation of the pulse-height spectrum resulting from the interaction between the exit photon spectrum and the NaI(Tl) detector. A rigorous derivation would require that each photon of the exit spectrum be followed individually into the detector in order to compute the actual energy deposited in C. However, extension of our calculations for thin NaI(Tl) detectors[7] to a detector of thickness 5 mm confirmed that below 100 keV, most of the photons incident on the face of the crystal are completely absorbed. The presence of iodine escape peaks would not affect the present calculations. It is therefore assumed that the interaction of the exit photon spectrum with the detector could be adequately represented by the smearing of the former by the Gaussian resolution function associated with the latter. Experimental measurements at four photon energies below 100 keV show that the standard deviation of the Gaussian peak can be expressed as a function of energy by the relation

$$\sigma(E) = A\sqrt{E} + B$$

The constants A and B are determined from the experimental plot of $\sigma(E)$ vs. $\sqrt{E}$. Smearing of the exit photon spectrum is then accomplished by computing the contributions from each channel to the others, using the Gaussian distribution function and is carried out as follows:

The contribution from the kth channel of the exit photon spectrum to the jth channel of the smeared pulse-height spectrum is given by

$$B(K,J) = \frac{A(K)}{\sigma_K\sqrt{2\pi}} \int_{C(J-1)}^{C(J)} \exp\left[-\frac{(E-E(K))^2}{2\sigma_K^2}\right] dE$$

where A(K) is the number of counts in the kth channel of the exit photon spectrum, E(k) is the mean energy corresponding to the kth channel of the exit photon spectrum, C(j) and C(j-1) are the upper and lower limits of the jth channel of the smeared pulse-height spectrum and σ_k is the standard deviation of the Gaussian peak in the pulse-height spectrum at energy E(k). Expressed in terms of normal probability function P(x),

$$B(K,J) = A(K)[P(X_2) - P(X_1)]$$

where $X_1 = \frac{C(J-1) - E(K)}{\sigma_K}$ and $X_2 = \frac{C(J) - E(K)}{\sigma_K}$

Thus, using the normal probability function values and experimentally obtained σ_k's, the contribution from all the k channels (k = 1 .... n') of the exit photon spectrum to every jth channel (j = 1 ... n) is calculated to get the smeared pulse-height distribution. The location of the peak is found by using the technique of "linearization of the peak". In practice five channels on either side of the peak were used for this purpose.

Experimental Setup And Calculations

A Harshaw integral assembly (10.16 cm dia x 5 mm thick NaI(Tl) having 1 mm Be as radiation entrance window) is currently in use in our laboratory for detection of Pu/Am in vivo. The NaI(Tl)

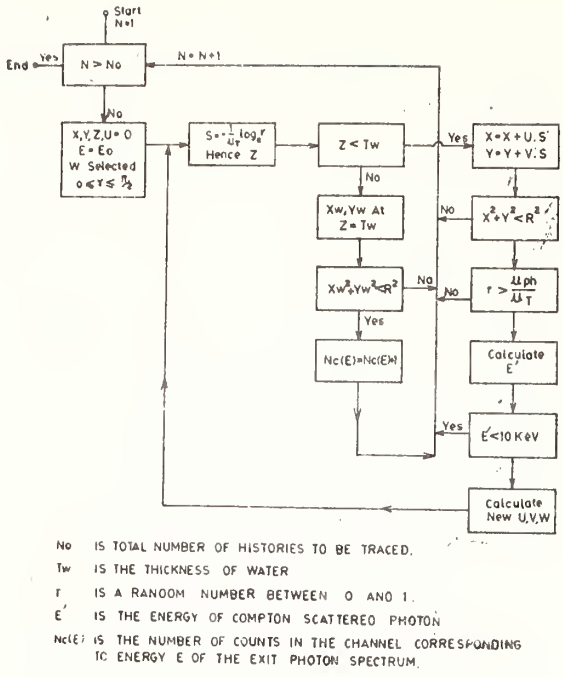

Fig. 2. Flow chart for computing exit-photon spectrum.

scintillation crystal is coupled to a 2.54 cm thick quartz light pipe and mounted on a RCA 8055 phototube. The output from the phototube is routed through a FET pre-amplifier to a 400 channel pulse-height analyser. In order to have a meaningful comparison between theory and experiment, the computations were performed for point sources of low-energy photons located on the axis of a NaI(Tl) detector of the available size and for different thicknesses of the scattering material interposed between the source and the detector. The variable parameters considered are (a) initial photon energy (from 20 keV to 100 KeV at intervals of 10 KeV), (b) thickness of interposed scattering material varying from 1 cm to 12 cm and (c) type of detector - the energy resolution distinguishing each type. The experimental results were obtained with a point source of ^{241}Am (60 keV) with different thicknesses of distilled water in a thin perspex container interposed between the source and the detector. Another scatterer employed was perspex.

Results and Discussion

In fig. 3 are shown a typical exit-photon spectrum as a histogram, the resulting peak in the smeared pulse-height spectrum as a smooth curve and the experimental values (normalized to the smeared spectrum at the new peak channel) as circles. The detector is a

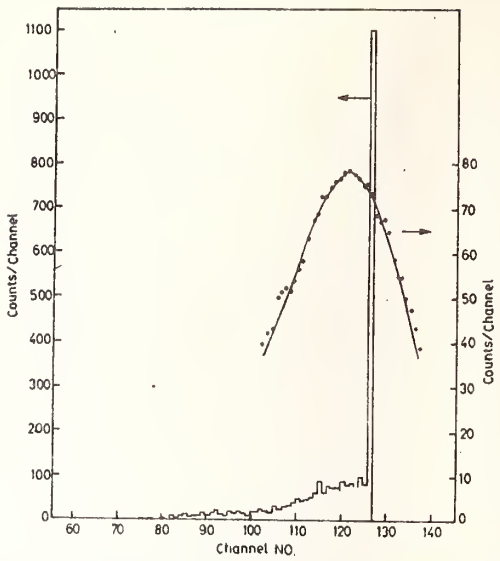

Fig. 3. The exit spectrum (histogram) of photons for initial energy 60 KeV and water thickness 6.3 cm and the resultant peak in the pulse-height spectrum (continuous line) from a NaI(Tl) detector of dimensions 10.15cm x 5 mm. The points indicate the corresponding experimental data.

NaI(Tl) scintillator as described above and a point source of initial photon energy 60 KeV is used, the thickness of the interposed water scatterer being 6.3 cm. The exit photon spectrum and the theoretical peak are for 20,000 source photon histories. The figure illustrates how the peak-shift is introduced. The exit photon spectrum does not show any shift in the maximum photon energy and the number of counts in the original peak channel is still overwhelmingly large. This would be representative of the case of an ideal detector having an infinitely fine resolution, introducing no line broadening. In actual practice, however, the exit photon spectrum would be distorted due to the finite energy resolution of the detector and its variation with energy (fwhm vs. photon energy relation). Since the peak-shift appears only after the smearing of the exit photon spectrum with the experimentally determined values of fwhm, it may be concluded that it is the energy resolution of the NaI(Tl) detector which introduces the peak-shift in the pulse-height spectrum. Different exit photon spectra, incident on the same detector, would also indicate different values of peak-shift (ΔE). The smeared spectrum in fig. 3 has a peak at 58.07 KeV, i.e. $\Delta E = 1.93$ KeV. After smoothing, the peak-shift in the experimental pulse-height spectrum for the same case is

to be 1.97 keV.

We may next consider some hypothetical detectors having the same fwhm vs. peak energy relation as the NaI(Tl) detector but having different energy resolutions; i.e. we consider detectors with

$$\sigma'(E) = K\sigma(E)$$

where $\sigma'(E)$ is the standard deviation of normal distribution centred at energy E for a hypothetical detector, $\sigma(E)$ is the standard deviation of normal distribution centred at energy E for the NaI(Tl) detector and K is a constant. Therefore

$$\sigma'(E) = A' \sqrt{E} + B'$$

and $$\text{fwhm} = 2.355\sigma'$$

The exit photon spectrum in fig. 3 is smeared using several values of σ' and the peak-shifts (ΔE) are observed. Fig. 4 depicts this dependence; ΔE is plotted as a function of K. It is seen that when the same exit photon spectrum is incident on detectors having different energy resolutions, the peak-shifts observed are different. In the typical case given, the peak-shift could vary from 0 keV to 3.09 keV, depending upon the energy resolution of the detector. ΔE appears to saturate for a detector having an energy resolution twice as bad as that of our detector.

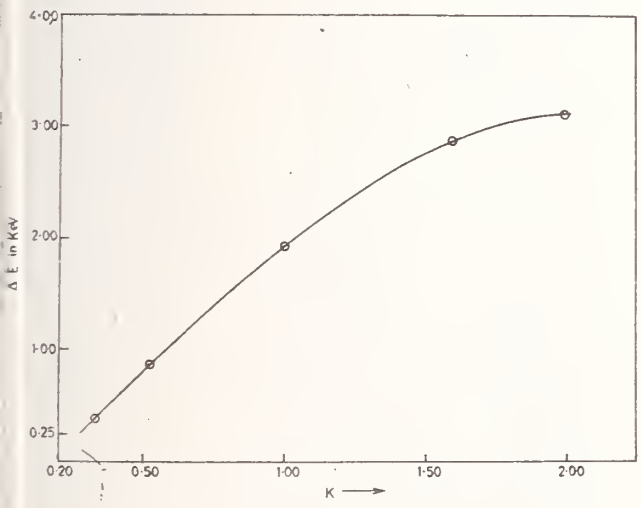

Fig. 4. Theoretical predictions of peak-shift (ΔE in KeV) for hypothetical detectors having standard deviation of Gaussion peak $\sigma' = K\sigma$; σ being the parameter for NaI(Tl) detector and K a constant. The results are for a point source of initial photon energy 60 keV under water depth of 6.3 cms.

Fig. 5 shows the variations of ΔE and fwhm with depth of a point isotropic source of 60 keV photons under water when NaI(Tl) detector described earlier is used. The continuous curve shows the computed values and the experimentally measured values are shown by the points. The experimental values of ΔE fall close to those predicted by calculations. The experimental fwhm values are slightly higher than the predicted values probably due to very little back scatter from 1 mm thick perspex source container. The small difference between the fwhm values does not seem to introduce significant difference in ΔE values.

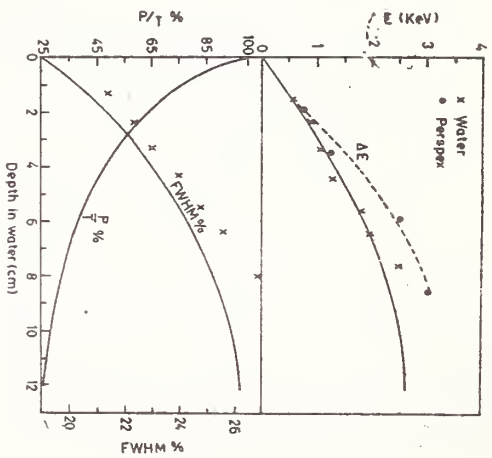

Fig. 5. Theoretical variations (continuous curves) of peak shift, FWHM and P/T ratio of the number of photons in the 60 keV channel to the total number of photons in the exit spectrum) with depth of a point source of photons of energy 60 keV under water. Experimentally measured values are indicated by marked points.

Fig. 6 illustrates the variation of ΔE with the initial energy of source photons when the source is located at a constant depth of 3, 5 and 7 cm of water. These results are obtained from our program by treating the initial photon energy as a variable parameter. Since fwhm is a function of the incident photon energy and increases with energy, ΔE would increase. In the initial stages this increase will be augmented by the rapid decrease of P/T (the ratio of the number of photons in the 60 KeV channel to the total number in the exit-photon spectrum) which in turn is caused by the predominance of the photoelectric effect in this region. Beyond this, P/T increases slowly in accordance with the decrease in mass absorption coefficient which works

against the increase in ΔE. The combined effect of all is that ΔE first increases steeply with E and then falls to a lower value.

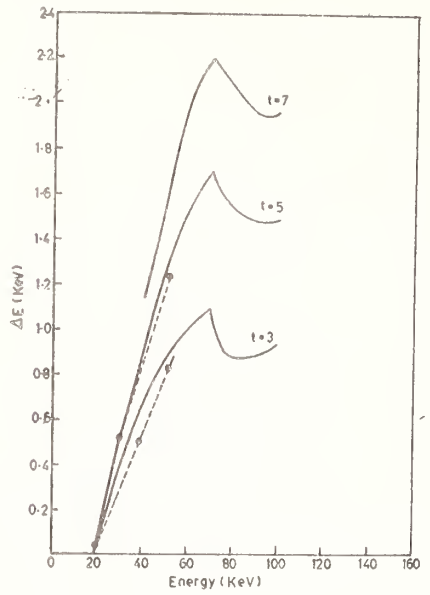

Fig. 6. Theoretical peak-shift (ΔE) as a function of initial photon energy for point isotropic sources under constant water depths of 3, 5 and 7 cm as continuous curves. Broken curves are for perspex.

The dotted curves in fig. 6 are for the same detector and perspex scatterer. The calculations yield ΔE values less than those for water, whereas the experimental values are higher than those for water (fig.5). We have used the cross section data in ref. 8 for perspex (density taken as 1.0 g/cc) and in ref. 6 for water. We have not used the cross section data from any other reference to resolve this difference.

Fig. 7 shows fwhm plotted as a function of $\sqrt{E}$, E being the observed 'peak' energy. Deviations from the approximately linear relation observed when no scatterer-absorber is present are evident. This deviation increases with the thickness of the scatterer (water) and there seems to be no significant departure from linearity below an energy of 25 keV.

Conclusion

A computer program using Monte Carlo techniques has been described to calculate changes in the pulse-height spectra obtained from detectors exposed to low-energy photon sources embedded in media of low effective atomic numbers. The role of the detector in introducing such changes has been delineated.

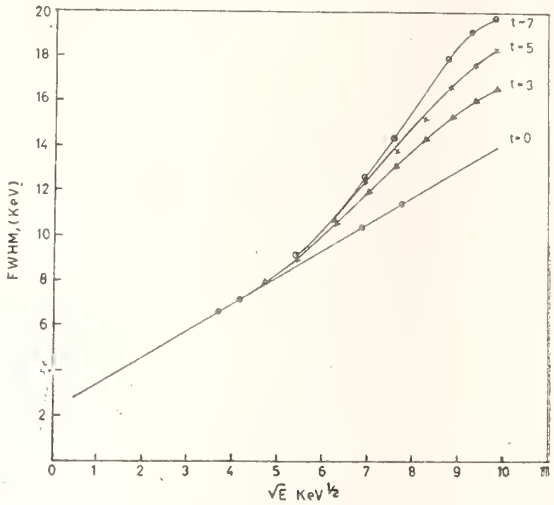

Fig. 7. Computed FWHM as a function of $\sqrt{E}$ for the cases of point source under water thickness of 0,3,5 and 7 cms.

Acknowledgement

The authors wish to express their sincere thanks to Shri T.K. Haridasan for his assistance in the present work.

References

1. Morsy, S.M., El-Assaly, E.M. and Aloush, A.A., Assessment of radioactive contamination in man, IAEA (1972) p. 115.
2. Rundo, J., Keane, A.T. and May, H.A. ibid, p. 579.
3. Wrenn, M.E., Rosen, J.C. and Cohen, N. ibid, p. 595.
4. Sharma, R.C., Somasundaram, S., Surendran, T., Kapur, D.K. and Garg, S.P., BARC report No.BARC-748 (1974).
5. Cashwell, E.D. and Everett, C.V. A practical manual on the Monte Carlo method for random walk problem, Pergamon Press, London (1959).
6. Sieg̃bahn, K., Alpha, Beta and Gamma-ray spectrometry, Elsevier, Amsterdam (1955).
7. Sharma, R.C., Garg, S.P. and Somasundaram, S. Nucl. Instr. Methods, 101 (1972) 413.
8. Hubbell, J.H., US National Bureau of Standards report No. NSRDS-NBS 29.

DOSE FUNCTION FOR BETA DOSIMETRY

S.J. Supe and Shiv Datta
Division of Radiological Protection
Modular Laboratories, Bhabha Atomic
Research Centre, Trombay
Bombay-400085, INDIA

The feasibility of using various shapes and sizes of field limiting devices and collimators with beta ray eye applicators has necessitated the study of dosimetry for these fields. A method of obtaining dosimetry for any shaped field from the data for circular fields is presented. The method is based on a similar procedure for X and gamma rays. The surface dose computation is done based on Clarkson's method but without splitting the surface dose into air dose and back-scatter dose. The depth dose evaluation is based on depth dose function which is defined as the dose rate at a particular depth for particular circular field. The usual method of splitting depth dose into primary and scatter doses was not found necessary. The evaluated values for the surface and depth dose were compared with experimentally obtained values for three non circular fields. The good agreement in these data indicates the practicability of the method suggested.

(Air dose; arbitrary shaped field; back-scatter factor; Clarks' method; dosimetry; depth dose; surface dose)

Introduction

The early cases of lesions of eye were treated by X-radiation and have resulted in radiation cataract. With the use of β-ray emitters like radium D + E and radon, the eye lense dose was appreciably reduced. When ^{90}Sr - ^{90}Y, a pure beta emitter, was available for use as eye applicators, the gamma component of eye lense dose was eliminated. This reduced the frequency of incidence of radiation cataract and no further attempts were reported to reduce the eye lense dose. These applicators were usually used without any field limiting or collimating devices regardless of size of the lesion resulting in much larger doses to the lens of the eye. Recently, use of field limiting devices[1] as well as collimators[2,3] has been investigated and shown to be possible for almost all cases. The feasibility of matching the field shape to that of lesion size has raised new problems of dosimetry. As various lesion shapes are encountered the present dosimetric data of circular fields[4-7] is insufficient for the treatment of widely varying shapes of the lesions. Further, it is virtually impossible to carry out dosimetric studies for the numerous field shaping devices of variety of sizes and shapes. In this work a method of estimation of surface and depth dose for any shaped field from the available data for circular fields on the same lines as X and Gamma fields was tried.

Clarkson[8], Meredith and Neary[9] and Johns and Cunningham[10] described the method for roentgen and gamma radiations for such estimation. This method consists of measurement of air dose, use of back scatter factor and scatter functions for estimation of this data. The air dose is to be actually measured for the field size under consideration. However, for the estimation of surface dose the small variation of air dose with field size is neglected and air dose assumed to be a constant. The non-circular field size is divided in a large number of segments of circles with different radii drawn at equal angles. The back scatter factors for these are averaged to give the effective back scatter factor for the field under consideration.

To obtain the dose at any depth the dose is divided into its two components, the primary dose and the scatter dose. The primary dose is obtained by extrapolating the central axis depth dose for various field sizes to zero field size. The scatter dose is evaluated by obtaining the average scatter function for the field under consideration by the same method as used for back scatter factor. The data so obtained are used for getting the central axis as well as off axis depth doses for the field under consideration. Further interpolation of this data yields complete isodose curves.

Air Dose for Beta Rays

Adoption of this procedure in case of beta rays is handicapped by difficulties. The measurement of air dose for betas is rather difficult[11]. Air dose

with beta rays is possible only if the collecting electrode of an extrapolation chamber or a flat ionization chamber is equally thin as the upper or polarizing electrode. If a thicker plate is used the contribution due to back scatter from the plate will not permit the measurement of the air dose.

Further, the increase in air dose is going to be very rapid with increasing field size as a large active area would be contributing to the dose. A constant dose output is not possible with the beta ray sources when used with the field limiting diaphragms and hence it was decided to try and find out whether dosimetry at surface and in tissue could be developed on similar lines as that of X and gamma rays but without the help of a constant air dose.

Surface Dose

The variation of surface dose was studied with the field size splitting it into air dose and the back scatter dose. For this purpose using an extrapolation chamber, doses were measured for a RA- (tracerlab) type eye applicator with increasing field limiting diaphragm diameters. Measurements were also repeated for 450 mCi ^{90}Sr- ^{90}Y source with a collimator of 1.05 cm length. The surface dose rates for rectangular shaped field sizes have been evaluated from the dose rate for circular fields by using Clarkson[12] method. These are presented in Table I. In addition, surface dose measurements for the applicator with the corresponding shapes of field limiting devices have been carried out with an extrapolation chamber and the results thus obtained are presented in column 4 of Table I. The evaluated values agree well within $\pm$ 5% with the experimentally obtained ones.

Depth Doses

A further difficulty was observed in calculating the dose at any point in tissue on similar lines as those for X and gamma rays. In the case of beta rays, obtaining the value of the primary component of dose was found to be rather difficult. The central axis depth dose data for beta rays are available from the maximum field size of about 8 mm down to about 2.00 mm and would not yield by extrapolation the primary dose with the required accuracy. Any attempt to measure doses for field sizes smaller than about 2 mm diameter is handicapped with inaccuracies introduced in making electrodes of extrapolation chamber smaller than this diameter[12] and the primary component of beta dose at various depths cannot be obtained with sufficient accuracy.

Close scrutiny of the procedures for calculating the dose at any point within the field and at any depth revealed that such separation of scatter dose from primary component is not necessary. It was noted whether primary dose is determined separately and added to the average value of scatter function or whether the average of the total dose is estimated, the same results are obtained. Thus it was decided to use dose function for beta rays rather than scatter functions. The dose function is defined as the dose rate at the particular depth on the central axis of a circular field. The dose functions were evaluated in the following manner. The surface dose rate for a particular field size was multiplied by the percentage depth doses at different depths for the same field. These dose functions for various field sizes and

TABLE-I

SURFACE DOSE RATES FOR VARIOUS FIELD LIMITING DEVICES & COLLIMATORS

Sr. No.	Collimator/ field limiting device size(mm)	Source to surface distance(cms)	Dose rate(rad/s) Extrapolation chamber measurements	Dose rate(rad/s) evaluated values
1.	6 x 6	0	117.0	118.2
2.	6 x 4	0	77.5	81.2
3.	6 x 3	0	65	62.1
4.	6.6 x 8.2	1.05	19.2	18.7
5.	6 x 8	1.05	20.1	19.5
6.	6 x 6	1.05	14.5	13.8

depths are shown in fig. 1.

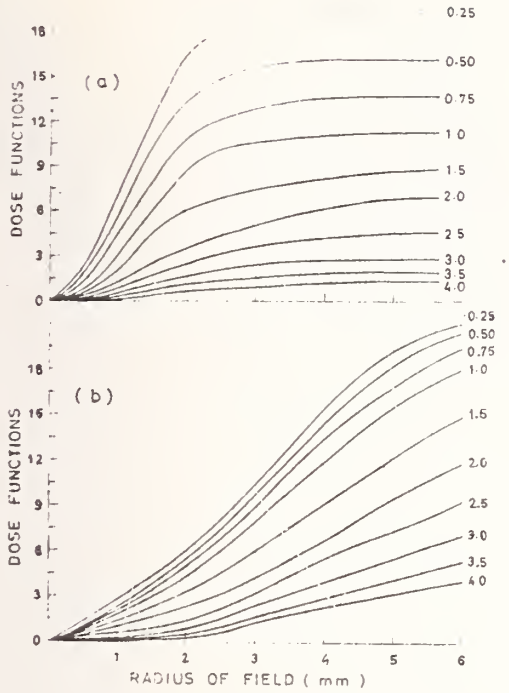

Fig. 1. Dose functions at different depths for various radii of field sizes.

a) RA-1 applicator with field limiting devices.
b) 450 mCi source with collimators.

Using the surface dose rates and the dose functions for circular fields as basic data for Clarkson's method, computation of depth dose in the space around the source could be easily carried out. This has been done for three fields and the depth dose data thus obtained are presented in Table I and II.

Non-circular field limiting diaphragms were constructed and using the experimental method already described dose data were obtained for these fields which are also presented in the same tables. It can be seen that the depth dose data obtained by the computation and those obtained experimentally are in fairly agreement for the three shapes. This agreement indicates that the procedure suggested here is practicable enough for therapeutic purpose. The computation can be carried out within a period of a few hours with some practice. A computer programme can also be easily written for this purpose.

Acknowledgements

We are indebted to Shri G. Subrahmanian for his keen interest in these investigations. Grateful thanks are also due to Shri S.M. Rao for his help in experimental measurements.

TABLE-II

EXPERIMENTAL AND EVALUATED DEPTH DOSE DATA
RA-1 Applicator with field shaping devices.

Depth (mg/cm^2)	Percentage depth dose data for collimators sizes of					
	6 x 8		6 x 6		6 x 3	
	Experimental	Evaluated	Experimental	Evaluated	Experimental	Evaluated
0.	100	100	100	100	100	100
100.	49.0	45.3	46.5	44.9	46.0	43.7
200	26.5	22.7	24.5	21.7	23.5	20.6
300	13.3	11.3	12.2	10.2	11.0	9.0
	450 mCi Source with collimators					
	6.6 x 8.2 mm		8 x 8 mm		6 x 6 mm	
0	100	100	100	100	100	100
100	64.9	71.7	66.6	73.0	64.9	69.0
200	40.9	41.8	46.7	43.0	38.7	38.7
300	26.1	25.1	29.0	26.0	24.4	22.3

References

1. Supe, S.J. and Cunningham, J.R., Am. J. Roentgenol. and Rad. Therapy , 79, 570 (1963).
2. Supe, S.J., Am. J. Roentgenol. and Rad. Therapy , 114, 24 (1972).
3. Supe, S.J. and Rao, S.M., Brit. J. Radiol., 31, 786 (1974).
4. Krohmer, J.S., Am. J. Roentgenol and Rad. Therapy, 66, 791 (1951).
5. Jones, C.H., and Dermentzoglou, F., Brit. J. Radiol. 44, 203 (1971).
6. Mc Taggart, W.G., West, W.D., Claypool, H.A., and Collins, V.P., Radiology, 76, 278 (1961).
7. Sinclair, W.K. and Trott, N.C., Brit. J. Radiol., 29, 15 (1956).
8. Clarkson, J.R., Brit. J. Radiol, 14, 265 (1941).
9. Meredith, W.J. and Neary, G.J., Brit. J. Radiol., 17, 75 (1944).
10. Johns, H.E., and Cunningham, J.R., Spring field, Illinois, Chas. C. Thomas (1969). The Physics of Radiology.
11. Sheppard, C.W., and Abele, R.K., AECU-655, (ORNL-265) (1949).
12. Supe, S.J., Int. J. Appl. Radiat. Isotopes, 24, 545 (1972).

ACTUAL PROBLEMS IN PHOTON DOSIMETRY*

D. F. Regulla and G. Drexler
Gesellschaft für Strahlen-und Umweltforschung mbH München
D-8042 Neuherberg, Ingolstädter Landstrasse I
Germany, F.R.

A brief review of the evolution of quantities and units in dosimetry is given, and the relevance of the dosimetry concept to applications in medicine, technique and health physics is pointed out. While radiation dosimetry seems to have, from a physical point of view, achieved an adequate status, handling of the physical fundamentals as well as practical application of quantities, units and measurement methods to operational dosimetry appears to be limited mainly to the level of highly competent authorities in dosimetry, such as ICRU or, on a national basis, to primary standard laboratories. This consequence is based on the authors' experience, that there is hardly a country, in which the numerical value of a dosimetrical quantity can be determined reproducibly through the different institutions engaged with practical dosimetry. WHO and IAEA, for this reason, started to establish a net-work of secondary standard laboratories, recently, with the aim of an improvement of dosimetry in medicine, radiation protection and radiation research. Details of this joint international effort on standardization are given, results already evident in some countries are presented. Recent advances, **particularly in** solid state dosimetry, are discussed together with the scientific aspects of physics in diagnostic radiology. To the authors' opinion almost every effort in the field of diagnostic radiology is worthy and promising for reasons of reduction of population dose and amelioration of information but also due to the broad interdisciplinary possibilities, the immediate output of applied research and, last not least, the benefit to mankind. Some examples on new results of medical physics as well as an outlook to future developments are given.

Introduction

From literature study we found keynote addresses to be often characterized by two formalities: On the one side, the speaker wishes to express his gratitude to the responsibles of the conference for the honour of invitation - which practice we should like to join - and, on the other side, he searches for a concept of the lecture by interpretation of the term keynote. Following this example we found the term keynote defined in the dictionary as "fundamental tone of a scale". Seeking for a relationship between this definition and the subject of the present session "Radiation Dosimetry and Instrumentation" one is inclined to correlate the term fundamental tone merely with the physical basis of dosimetry which could function as a connecting link between the diverging topics, such as microdosimetry, calculation of stopping power, solid state dosimetry etc. Doubtlessly, at this place a keynote address could exceptionally be presented on the basic physical aspects of dosimetry.

However, to the authors' opinion it should be pointed out, that dosimetry even after its physical definition and interpretation in terms of the respective quantities and units is gaining importance and justification only by imbedding it into the matrix of the manifold applications. Thus, dosimetry is loosing the character of ending in itself and becomes a tool for a relevant qualitative and quantitative description of the radiation field and its interaction with the absorber medium. On the basis of

*Dedicated to Professor Dr. F. Wachsmann on the occasion of his 70th birthday.

this approach one has - by returning to the dictionary definition of the keynote - to see the fundamental tone of dosimetric physics in connection with the scale of applications, at least, in biology, medicine industry, agriculture, health physics and research.

The dosimetric procedure self-evidently practiced today by starting from the physical fundamentals and adapting them to the respective field of application has not been common as far as to the beginning of the sixties. For a long time, any quantification of the radiation effect was performed by description of type and intensity of the effect under consideration. The early biological dosimetry methods to be designated as "analog techniques" such as the erythema dosimetry, the epilation dosimetry or even mouse-dead dosimetry become understandable by the lack of a relevant dosimetric philosophy and physical concept of measurement. Time was not yet ripe for a detailed application to photon fields of the fundamental concepts of particle fluence, flux density and energy spectra - familiar from the kinetic theories of gases—because theories of the dual corpuscular and wave nature of photons were still evolving. It was the application of ionization as a physical pre-condition for a dosimetric digitalization of the measuring procedure that first made a definition of physical quantities possible in dosimetry and established a connection to the exact natural sciences by introducing well-defined and reproducible units. Nevertheless, the concepts of exposure and fluence are philosophically rather close: They both attempt to define the radiation field independently of its interaction with matter.

The importance of, and the state of art achieved in modern dosimetry may be measured against the fact, that dosimetry and its aspects are discussed within the frame of physical symposia and conferences, today. Nevertheless, there has up to recently been much discussion of the fundamental concepts and quantities employed in radiation dosimetry. This has arisen partly from the rapid increase in the number of individuals using these concepts in the expanding field of science and technology, partly because of certain obscurities in the existing formulation of the quantities and units themselves. For instance, a serious source of confusion has been the failure to define adequate, and that in time, the radiation quantity of which "roentgen" was said to be the unit[1]. As a consequence of this ommission the roentgen had gradually acquired a double role: The use of this name for the unit had become recognized as a way of specifying not only the magnitude but also the nature of the quantity measured. This practice conflicts with the general usage in physics, which permits, within the same field, the use of a particular unit for all quantities having the same dimensions.

A number of dosimetric quantities and units have been introduced in course of time, but only those that are of importance in the framework of the dosimetry concepts discussed here, will be reviewed.

Objectives of Dosimetry

The term "dose" is biologically oriented and originating from the early medical use of X-rays. In order to reproduce medical and biological radiation effects, compare different radiation effects among each other and estimate the amount of ionizing radiation for any application one needs an effect caused by and related to the dose, which can well be defined, measured and quantified along a scale. This, however, is no more a medical or biological problem but a physical one. Therefore, dose has at least been defined in terms of physically measurable quantities.

The ideal unit of dose from the standpoint of radiation protection and biophysics would be the one which would produce the same biological effect independent of the kind and energy of radiation. Such an ideal is, particularly on biological basis, probably unattainable because of the extreme complexity of radiation-induced damage in living systems. For realization, a physical dose unit is applied which gives nearly the same biological effect independent of the energy of a given kind of radiation.

Thus, it is the aim of dosimetry to determine a physical quantity to which the chemical, biological and medical effects can be related. In this connection particularly those quantities will be of importance, which describe the physical interaction of radiation with matter.

Radiation Quantities and Units

From results of radiobiology it is obvious that local radiation effects can well be correlated with local energy density. Therefore, it appears logical to choose the energy absorbed (or alternatively imparted to) a mass of matter for dose description. The energy imparted by ionizing radiation to the matter (ΔW_D) in a volume is the difference between the sum of the energies of all the directly and indirectly ionizing particles which have entered the volume (ΔW_E) and the sum of the energies of all those which have left it (ΔW_L), minus the energy equivalent (ΔW_R) of any increase in the mass that took place in nuclear or elementary particle reactions within the volume

$$\Delta W_D = \Delta W_E - \Delta W_L - \Delta W_R)$$

On the basis of "energy imparted to matter", the concept of absorbed dose D has been defined and recommended by ICRU 11[2] as "the quotient of dW_D by dm', where dW_D is the energy imparted to the matter by the ionizing radiation in a volume element dV, and $dm = \rho dV$ is the mass of the matter with the density ρ in that volume,

$$D = \frac{dW_D}{dm} = \frac{1}{\rho} \cdot \frac{dW_D}{dV}$$

By this definition the absorbed dose has the dimension energy per mass which in terms of the SI units refers to J kg^{-1}. The special unit of the absorbed dose is the rad.

$$1 \text{ rad} = 0.01 \text{ J kg}^{-1}, \text{ formerly}$$
$$1 \text{ rad} = 100 \text{ erg g}^{-1}$$

The definition of absorbed dose is valuable for all types of radiation and radiation energies in all kinds of matter. However, the indication of absorbed dose is only useful if the conditions of irradiation and the material, in which the absorbed dose has been determined, are reported. Moreover, the definition appears incomplete without specification of the size of the volume element[3].

Apart from the absorbed dose, additional quantities and units common in dosimetry should be mentioned here:

i) For protection purposes it is useful to define a quantity which will be termed the "dose equivalent", (DE). (DE) is defined as the product of absorbed dose, D, quality factor, (QF), dose distribution factor, (DF), and other necessary modifying factors.

$$(DE) = D(QF).(DF) \ldots$$

The dose equivalent is a rather hybrid quantity compounded of three elements, the first consisting of physical data, the second concerning factors derived from radio-biology and the third consisting of administrative factors. Thus, dose equivalent is by definition immeasurable.

The unit of dose equivalent is the "rem". The dose equivalent is numerically equal to the dose in rads multiplied by the appropriate modifying factors.

ii) Recently defined is the quantity "kerma" which represents the kinetic energy transferred to charged particles by the uncharged particles per unit mass of the irradiated medium. This is the same as one of the common interpretations of a concept 'first collision dose', that has proved to be of great value in fast neutron dosimetry. The concept is also closely related to the energy equivalent of exposure in an X-ray beam.

Per definition, the "kerma" (K) is the quotient of dW by dm, where dW_K is the sum of the initial kinetic energies of all the charged particles liberated by indirectly ionizing particles in a volume element of the specified material, dm is the mass of the matter in that volume element dV.

$$K = \frac{dW_K}{dm} = \frac{1}{\rho} \cdot \frac{dW_K}{dV}$$

Kerma can be a useful quantity in dosimetry when charged particle equilibrium exists at the point and in the material of interest and bremsstrahlung losses are negligible. It is then equal to the absorbed dose at that point. From the more specific definition $K = \Psi . \mu_{tr}/\rho$ (where Ψ = energy fluence of the photons; μ_{tr} = mass energy transport coefficient) it becomes evident that it allies the primary and secondary components of the radiation field for mathematical treatment of dosimetrical problems. The unit of kerma is equal to that one of absorbed dose.

iii) While for photons, the reduction of fluence or energy fluence is primarily caused by a reduction of particles, the energy fluence in case of charged particles decreases mostly by energy losses of the particles with practically constant particle flux density. For characterizing these energy losses, the mass stopping power S has been introduced.

The mass stopping power of a material with the density ρ for charged particles with the energy E is the quotient of dE and the product of ρ and dl

$$S = \frac{dE}{\rho . dl}$$

where dE is the mean energy loss within the path length dl in material with the density ρ.

iv) A quantity closely allied to stopping power is the linear energy transfer, abbreviated LET. This is defined as the linear-rate of loss of energy (locally absorbed) by an ionizing particle traversing a medium and may conveniently be expressed in keV/μ. The use of the concept of LET concentrates attention in the transfer of energy to the material, rather than on the loss by the particle as does mass stopping power.

Physical Concept of Radiation Dosimetry

So far, the concepts of some dosimetric quantities and units and their definitions have been reviewed; it is pertinent to examine physical concepts and practical techniques currently used in operational dosimetry.

Implied in the term radiation dosimetry is the central problem of the radiation field characterized by specific field parameters. Within the radiation field there are interactions between the ionizing particles and the atoms or molecules of matter. The absorbed dose refers to such interactions. Though absorbed dose does not give a final answer on the kind of expected biological effect, it is that dose quantity which corresponds with the observed biological reaction in the most promising way. It seems important to point out this fact, in particular, as the opinion can be heard that it is sufficient to refer chemical or biological radiation effects solely to,for instance, particle fluence. Nevertheless, field quantities such as particle flux density, particle fluence, energy flux density and energy fluence are related to dose quantities by physical laws via the interaction coefficients dependent on radiation energy and matter for the different types of radiation, for instance, the attenuation coefficient, the energy absorption coefficient, stopping power as well as capture and scattering cross sections.

We shall distinguish between the two basic approaches to radiation dose determination at a specific point of interest in matter:

a) The first approach gives primary attention to the radiation field itself; in concept, measurements of energy-angle distributions of particles in the field are carried out to specify the radiation at each point in terms of physical quantities, giving rise to direct absorbed dose calculations.

b) The second approach characterizes the field primarily in terms of its interaction with matter in local vicinity of the point of dosimetric interest, by appropriate measurements. This approach is of great practical value and has formed the basis of almost all radiation dosimetry.

The distinction between the two approaches is somewhat arbitrary in that we know the radiation field only through its interaction with matter.

Calculation of Absorbed Dose from Field Parameters

The calculation of absorbed dose provides the term energy imparted to matter, W_D. The concept of energy imparted will be considered from the point of view of a macroscopic field theory.

A complete specification of the field can be made in terms of (i) the nature of particles, (ii) the spatial density of particles, (iii) the energy of the particles and (iv) the direction of the particles. This can conveniently be expressed by $n(\vec{r}, E.\vec{\Omega}, t)\, d^3r\, dEd\Omega$, which is the number of particles at time t in the volume element d^3r around $\vec{r}$ with the energies between E and E + dE and with the velocity vectors in the solid angle element of $d\Omega$ around the unit vector $\vec{\Omega}$. Other parameters, such as polarization[5] will not be regarded.

In the present case of a field of photons and electrons, W_D on the basis of ICRU definition is given by the general expression, in which the temporal variations are neglected.

$$W_D = \int K(\vec{r})\, \rho dV - \int dV \int d\Omega . diV[\vec{\Omega} . \int E^e I^e (r, \vec{\Omega} E^e)\, dE^e]$$

where:

$$K(\vec{r}) = \iint dE^p \frac{\mu_{tr}(E^p)}{\rho} I^p(\vec{r},\vec{\Omega},E^p)\, d\Omega$$

The indices p, e refer to the photon or electron component the radiation field.

$I(\vec{r},\vec{\Omega}, E)dEd\vec{\Omega}$	the fluence of the respective radiation component in the energy and angle range under consideration
E	the energy of electrons or photons
dV	the volume element
$d\Omega$	the solid angle element
μ_{tr}/ρ	mass energy transfer coefficient
$\int K_\rho dV$	the total kinetic initial energy of electrons of the volume dV, which have been released by the photons through photo and Compton effect

For the calculation of the electron fluence I^e of the first generation of photo or Compton electrons one can proceed as follows:

$$I_1^e(\vec{r},\vec{\Omega}, E_1^e)dD_1^e d\Omega = N.J_o^p(\vec{r}_1,\vec{\Omega}_o,E_o^p).$$

$$\frac{d\sigma(E_o^p - E_1^e)}{dD_1^e d\Omega_1}\, d\Omega_o d\Omega dE_o^p dE_1^e .$$

In this equation is :

N	the number of electrons per unit volume of the absorber
$\vec{\Omega}_o$	direction of primary photons
$d\sigma/dE_1^e d\Omega_1$	differential cross section for the generation of photo or Compton electrons
$\vec{\Omega}_1$	direction of photo or Compton electrons of the first generation relative to the direction $\vec{\Omega}_o$
E_1	energy of photo or Compton electrons

The absorbed dose D in the point $\vec{r}$ is then calculated by

$$D(\vec{r}) = \lim_{V\to 0} \frac{W_D}{\int \rho dV}$$

Calculation alone is rarely sufficient for dose determination but will provide a limited number of measurements. In principle, the determination of field parameters such as particle fluence and energy spectra are well-established physical concepts and permit quantification of unperturbed radiation fields by utilizing highly sophisticated techniques.

From this, any absorbed dose may be calculated using the fluence $(\vec{r},\vec{\Omega},E)$ distribution for each kind of radiation incident on the medium. However, to make thorough determination of field parameters in, as is normal, an unknown radiation field is complicated and time-consuming; in most cases it may even be impossible and, moreover, not all input data concerning interaction with matter will be known with sufficient accuracy. Particularly, the respective interaction coefficients for a certain material change with the particle energy thus providing knowledge in its spectral distribution. This distribution may change with penetration depth for reasons of interaction with matter, and that both for photons and secondaries. Moreover, the consistency of most absorbers is normally not homogeneous causing serious discontinuities in the field parameters and requiring differentiation of the interaction coefficients.

After this short analysis of the more theoretical approach of absorbed dose some actual problems in photon dosimetry shall be pointed out. At first, basic field parameters, such as low energy photon spectral distributions, still look for an intensive investigation. The evident output of those investigations influences the largest field of X-ray application, the X-ray diagnosis. As a high proportion of the ionizing radiation received by the population is due to medical X-ray diagnosis it is essential that the necessary diagnostic information should be obtained with the least possible amount of radiation.

In the range where the energy dependence on the mutual effect of patient and detector systems is great, as is the case with the usual polychromatic X-ray spectrum. X-ray spectrometry is indispensible in answering the

questions which arise. From the spectra of a diagnostic X-ray tube (operating at 120 kV) monitored in front of and behind a phantom it can distinctly be seen, that the low-energy component of the primary radiation merely contributes to the exposure of the patient but is hardly noticeable any more in the image forming radiation (Fig. 1). Different filtration at the tube strongly affects the spectral distribution of the primary radiation whereas the spectrum of the image forming radiation is mainly influenced by the object and the tube voltage. Hence, the necessity for higher filtration to reduce radiation dose to the patient is evident.

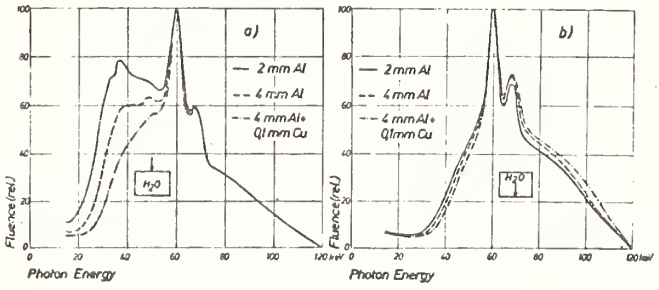

Fig. 1. Primary radiation (a) in front of and (b) attenuated by a 20 cm water phantom for different tube filtration. Tube voltage 120 kV.

However, comparison of the spectra of the image forming, attenuated primary radiation, and the scattered radiation both incident at an image point clearly shows the limits of scatter elimination (Fig. 2). The spectrum of scattered radiation includes a large portion of the same energy range as the primary radiation spectrum thus hardly rendering feasible an energy-selective filtration of the scatter component behind the patient. Furthermore, a strong increase in scatter proportional to the increase in volume irradiated can be recognized. Problems of adaptation of the spectral sensitivity of the image recording system to the available radiation qualities as well as those relating to the improvement of grids can also be solved by spectrometric methods.

For measurements of the spectroscopic field quantities, semiconductor detectors represent state of art since the interpretation of their pulse height spectra into polychromatic spectral fluence is feasible with the well-known characteristics of the detectors. In particular, the constant resolution over the areas of interest simplifies the calculation of true spectra. By contrast,

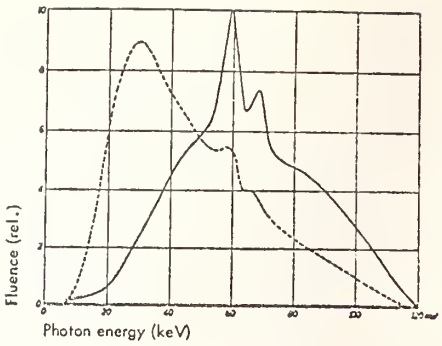

Fig. 2. Comparison of an attenuated primary radiation (___, measured) to the integral scattered radiation(---, calculated) at an image point. Phantom thickness 20 cm H_2O, tube voltage 120 kV, field size 10 x 10 cm^2.

the widely used scintillation spectrometer with limited resolution depending on energy would yield serious problems in unfolding the pulse height spectra. Fig. 3 shows the deterioration of an assumed but typical test spectrum by the inherent qualities of two spectrometric systems (System I : fwhm=const, System II: fwhm=f(E)). Thus considering the exposure of patient quantitatively the determination of fluence together with geometric data must only be regarded as the first step for solving the above introduced fundamental integral equation.

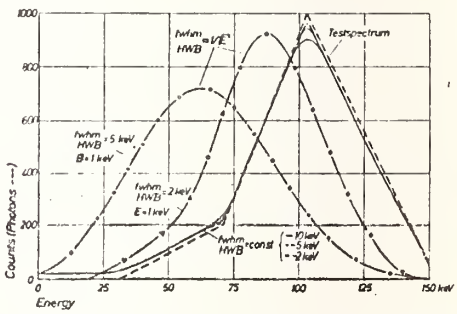

Fig. 3. Influence of energy resolution of a detector on the pulse height spectrum.

Many attempts have been carried out to determine attenuated photon and electron spectra within organs of interest together with the interaction and energy absorption coefficients. Since a considerable lack of information of those data exists, approximations by Monte-Carlo transport codes together with an appropriate mathematical description of the human body's shape and of

its dimensions have been carried out[6]. Problems arise from considering all interactions possible as well as their mathematical treatment. From results already available agreement within a factor of 2 is supposed to justify those extensive calculations, in principle.

Determination of Absorbed Dose by Measurements

Absorbed dose evaluation and calculations are generally verified by an experimentally determined description of the field parameters in terms of its interactions with matter. The objective of this approach of absorbed dose is to avoid the complete field characterization by taking into account that the dose quantities are integral quantities providing integration over the different spectral field components. Thus, instead of using integration procedures on a calculative basis and the application of more or less known coefficients, one can alternatively apply selected measuring techniques which are able to approximatively perform the intended integration experimentally.

In order to perform such a measurement, one must use an effect caused by irradiation which is easy to measure and, moreover, in magnitude proportional to absorbed dose. Since the medium to which the radiation dose is applied does, in general, not yield a proper measurable effect, a radiation sensitive detector is brought to the point of dosimetrical interest. It is the detector material in which the dose-proportional effect is measured. For certain pre-conditions, i.e. charged particle equilibrium, CPE, or the fulfillment of the Bragg-Gray conditions, one can - by means of the measured dose effect - perform the determination of absorbed dose generated in the irradiated medium as if it were there instead of the substituting detector. A suitable measuring effect is the ionization of gases. As pertinent dose quantity the "exposure" (X) has been introduced, for air as a detector material.

The "exposure" is defined as the quotient of dQ by dm, where dQ is the sum of the electrical charges on all the ions of one sign produced in air when all the electrons liberated in a volume element of air with the mass dV, are completely stopped in air.

$$X = \frac{dQ}{dm} = \frac{1}{\rho} \cdot \frac{dQ}{dV}$$

The special unit of exposure is the roentgen (R); $1\ R = 2.58 \times 10^{-4}\ C\ kg^{-1}$. With present techniques it is difficult to measure exposure when the photon energies involved lie above a few MeV or below a few keV. The principal quantity in the relationship between exposure and absorbed dose is the average energy required to produce an ion pair (w-value). The "exposure" is measured with ionization chambers which in dimensions and wall material must fulfill the conditions of CPE or Bragg-Gray.

CPE is achieved with chambers walls consisting of air equivalent materials so that

$$\left(\frac{\mu_{en}}{\bar{S}}\right)_{wall} = \left(\frac{\mu_{en}}{\bar{S}}\right)_{air},$$

and a linear extension $d \gg R_{max}$ of the secondaries.

The BRAGG-GRAY principle describes the possibility to express the absorbed dose D_M in a material by the specific ionization J in a small air filled cavity imbedded in the material by use of the equation

$$D_M = \frac{(\bar{S}/\rho)_M}{(\bar{S}/\rho)_{air}} D_{air} = \frac{(\bar{S}/\rho)_M}{(\bar{S}/\rho)_{air}} = w \cdot J$$

provided the following pre-conditions are fulfilled: (i) the cavity dimension must be such that particle flux density is not changed, i.e. $\Psi_{air} = \Psi_M$, (ii) for non-ionizing radiation the ionization in the cavity must be small against the secondaries of the material, i.e. $(\mu_{en})_M > (\mu_{en})_{air}$, (iii) the cavity wall $d_W \ll R$, which is the range of secondaries, or is made of tissue equivalent material in case of biological measurements.

Determination of absorbed dose (D_M) in an arbitrary material from exposure (X) measured in air by means of the BRAGG-GRAY principle is characterized, as mentioned above, by

$$D_M = \frac{(\bar{S}/\rho)_M}{(\bar{S}/\rho)_{air}} \cdot D_{air}$$

For conditions of CPE, defined by the conditional equation $(\mu_{en}/S)_M = (\mu_{en}/S)_{air}$, one obtains with

$$\frac{(\bar{S}/\rho)_M}{(\bar{S}/\rho)_{air}} = \frac{(\mu_{en}/\rho)_M}{(\mu_{en}/\rho)_{air}}$$

the special form of the BRAGG-GRAY-principle for X and γ-rays:

$$D_M = \frac{(\mu_{en}/\rho)_M}{(\mu_{en}/\rho)_{air}} \cdot D_{air}$$

By using $D_{air}[rd] = 0.869 \cdot X\,[R]$ which is the absorbed dose in air one receives the general formula:

$$D_M[rd] = 0.869 \frac{(\mu_{en}/\rho)_M}{(\mu_{en}/\rho)_{air}} \cdot X[R] = f \cdot X[R]$$

The f-factor implying measurements of exposure under conditions of CPE converts exposure values to absorbed dose; another conversion factor, g, implies measurements of ionization under Bragg-Gray conditions. Usually, the factors f and g are calculated from the ratios of the mean values of the mass energy absorption coefficients and the mass stopping power of the two media, respectively:

$$f = 0.869 \frac{\int (\mu_{en}(E^p)\rho^{-1})_M \frac{d\sigma}{dE^p} dE^p}{\int (\mu_{en}(E^p)\rho^{-1})_{air} \frac{d\sigma}{dE^p} dE^p}$$

$$g = 0.869 \frac{\int (S(E^e)\rho^{-1})_M \frac{d\sigma}{dE^e} dE^e}{\int (S(E^e)\rho^{-1})_{air} \frac{d\sigma}{dE^e} dE^e}$$

It can be shown that the dose conversion factors f and g are not dependent on geometrical factors, such as depth in water or the field size. Further detailed parameters of interest can be taken from the respective ICRU-Reports[7-11].

For soft tissue $\frac{(\mu_{en}/\rho)_{tissue}}{(\mu_{en}/\rho)_{air}} = 1.1$ approximately energy independent between 0.1 and 10 MeV; the resulting absorbed dose $D_{tissue}[rd] = 0.97 \cdot X\,[R]$.

Obviously, also the above shown way of dose determination is dependent on interaction coefficients which provide prior knowledge of the quality of radiation or making assumptions as to its composition. However, it is the ratio of interaction coefficients for the medium of interest and air as detector material which influences the calculation. Particularly, in case of approximately equivalent materials this ratio will change much less with the spectrum than the single coefficient. Therefore, the radiation spectrum does not affect the dose determination so significantly as in case of dose calculations from the field parameters.

The concept, as well as the methods and techniques in dose measurements are well established, thus meeting the requirements of a high accuracy standard. But problems may arise from field application and control of procedures and equipment. This is shown at the determination of a basic property of a radiation detector as is the energy dependence of its signal response in Fig. 4. Even for the same detector different energy calibration factors may be achieved at different labs for reasons of differing calibration spectra applied. It is obvious that these discrepancies refer to different approaches of effective energy with non-compatible spectra since monochromatic X-rays are, up to now, not common in the range of low energy photons. In other terms, it appears possible to produce any response curve which you are asked for, even a flat response, by use of an adequately filtered bremsstrahlung. The resulting serious problem may only be solved sufficiently by standardization of calibration procedures. This was urgently called for at the IAEA-Symposium on Advances in Physical and Biological Radiation Detectors in fall 1970, however, without leaving a sound effect.

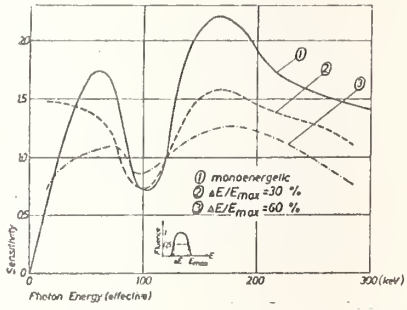

Fig. 4. Response of a dosimeter for different qualities of calibration radiations (The curves are fitted to unit sensitivity a 120 keV)
1. Assumed response to monoenergetic sources
2. Calculated response to calibration set with ΔE/Emax = 30
3. Calculated response to a calibration set with ΔE/Emax = 60%

Operational Dosimetry and Problems

From a recent directory published by the International Atomic Energy Agency one can find that the high energy radiotherapy equipments are concentrated in advanced centres of preferably developed nations. This inequity certainly has created a separation of the level of dosimetry as practiced by the countries involved. The need for constant development and improvement of new, reliable dosimetric techniques has no doubt thrust the advanced institutions into the front line in the field of radiation dosimetry. Radiotherapy centres in some of the developing nations certainly cannot afford to catch up with this trend due to the lack of both equipment and trained personnel. Moreover, facilities in such parts of the world have frequently experienced neither the urge nor the need for new techniques while other pressing problems claim higher priority.

In general, the most observable deficiency in these centres is the lack of some of the equipment considered essential for basic dosimetry work. This includes various types of ionization dosemeters but, equally, education and dosimetric joining to reference labs.

The necessity for transferring radiation quantities between different labs has become evident by multinational surveys for cobalt-60 radiation therapy dosimetry, by means of a postal dose intercomparison service. These surveys, based on a joint WHO/IAEA[8] project, pointed out that more than 40% of the participating institutes exceeded by partly significantly more than ± 5% the reference dosimetry value.

These findings for cobalt-60 gamma dosimetry which dosimetry somehow is simple to proceed, give a certain imagination upon the dosimetric problems in that practice where X-rays are applied and where, in addition, the accuracy of dose distributions is of interest. In this case all uncertainties of an X-ray generator application must be taken into account. In this connection one again must point out the need of establishing characteristic field parameters, i.e., at least, the penetrability or the HVL of the X-ray quality under consideration. However, as can be seen from Fig. 5 which shows the spectra of two calibration qualities with the same HVL, even this first approximation to the radiation energy by its penetrability characteristics, is a doubtful value.

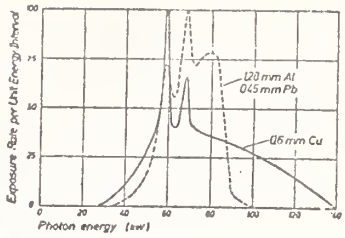

Fig. 5. Spectral distribution of two X-ray qualities of the same HVL (0.75 mmCu) achieved with different tube voltages and filtrations.

As a result, one has really to be in doubt, if the problem of the establishment of absorbed dose or exposure measurements with an ideal uncertainty of around ± 4% is furtheron of exclusive priority. Eventually it should be of preference to direct main effort to the proper definition and application of radiation fields in terms of the respective parameters. A IAEA panel on the activities of Secondary Standard Dosimetry Laboratories (SSDL), taking place at Rio de Janeiro still at the end of this year will try to balance both the aspects of calibration and education in order to overcome those problems, world-wide. The installation of SSDL's by WHO/IAEA has already encouraged improvement at many institutions and thus, in turn, has increased the standard of medical dosimetry practices. Standardization of procedures and techniques in these regions, however, seems to be a difficult task at the present time.

A useful tool in the field of applied dosimetry, supplying standard ionization techniques can be the solid state dosimetry, which is based on measurable changes of, at least, one property of the solid body as a function of interaction with radiation. Some newer solid state dosemeters, for instance thermoluminescent or photoluminescent dosimetry, have proved particularly suitable for special problems such as storage of dose information, use in very confined spaces or measurements of extremely low or extremely high doses. Further, for certain detector materials there is a relatively small to negligible energy dependence of the relative mass stopping power compared with water or soft tissue. The geometrical and mechanical features of the detectors are outstanding together with a reasonably good reproducibility of the radiation induced signal, which has just again been

proven for thermoluminescent dosimetry (TLD) on the occasion of an International Euratom Intercomparison on Nov. 11 to Nov. 15, 1974 at Bologna, Italy. The results of that meeting, clearly point out the necessity for a new generation of read-out devices to achieve higher precision and that more reliably. The new readers should be automated in cycling with a multi-step temperature program and diminish the influence of planchet reflectance on the signal, f.i. by using hot gaz heating. Nevertheless, TLD is worthwhile to be shortly reviewed on its possibilities and the problems still to be solved. Multiprobe TLD measurements in medical physics can be recommended as routine procedure for the determination of dose distributions, surveys of radiation burden in critical organs during radiation treatment as well as for equipment checks. Problems of sterilisation or handling of the detectors can be overcome.

In the large field of radioecology, a number of surveys and an equal number of different results due to inadequate dose assessments can be found in literature. These surveys involve investigations of radiation burden from natural sources (terrestrial and cosmic radiation, radiation resulting from building materials) and sources caused by civilization and technical progress (medical diagnosis, nuclear power plants). Of particular interest will be exact data on the medical radiation burden causing around 95% of the artificial radiation burden as well as routine dosimetry in the populated environment of nuclear power stations for permanent control of the radiation level. The importance of quantititative information on the effect of radiation on human beings justifies any effort.

In all these application fields of radioecology TLD could be of major importance. However, sensitivity and energy dependence are still lacking improvement. Basic features of the detectors would be a lower limit of detection of µrad and particularly, an energy independent response down to around 10 keV. At the moment, there is, to the authors' knowledge, no detector material fulfilling both requirements.

In occupational monitoring the possibilities of dose assessment with TLD meet, in general, the requirements of modern health physics trends for higher possible accuracy and that to better respect the MPD values and determine also low doses for an amelioration of the working conditions.

However, there are still fundamental monitoring problems due to discrepancies between the objectives of radiological protection measurements and its physical practicability. As a common basis of understanding, the principal objectives of personnel monitoring are the demonstration that the level of radiological safety meets appropriate standards, and the provision of information that allows improvements of working conditions if necessary. In more specific terms, the objectives are to achieve compliance with the recommendations of ICRP as reflected to national legislation. These specific objectives can only be met if measurements of the personnel dose allow estimation of the mean dose in various organs, since this is the basis of ICRP recommendations. In practice, however, the radiation field will neither be locally nor temporally constant for simple straight-forward measurements, i.e. each point of the body surface will be exposed to a radiation field different in intensity, spectral distribution and incident direction. For these reasons, the relationship between measured personnel dose at the surface and required organ dose is rather complex and ambiguous.

Because of the lack of physical realization of the measurement of organ doses an appropriate philosophy has been installed declaring the surface dose measured at a representative place of the trunk to be equal to the respective body dose. This philosophy is valid for external radiation coming from directions predominantly within one hemisphere, i.e. the direction towards which the individual is facing.

In order to meet the requirements of this philosophy, the dosimeter should be approximately tissue-equivalent between photon energies from 10 keV to 3 MeV. For discrimination between the radiation burden of the skin, due to β's and low-energy photons and of organs in the depth due to higher energy photons a simple dosimeter system should be sufficient consisting out of two detectors differently shielded - in compliance with recommendations of ICRP publication[12,13]. In this dosimeter-system one detector behind 10 - 20 mg/cm^2 filtration would differentiate the non-penetrating radiation, the second detector behind 0.5 - 1 g/cm^2 tissue equivalent filtration would give a measure of radiation of higher penetrability which could be set equal to the organ dose.

TLD is able to meet the requirements of this philosophy, within the error

limits acceptable of a factor 1.5 in Fig. 6. However, there still remains the problem of more specific data interpretation in case of doses in the vicinity or in excess of MPD's.

While personnel dosimetry is well installed in developed nations, using partly highly sophisticated dosimeters and discussing problems of philosophy as mentioned above[14], more than 30% of occupationally exposed personnel in developing countries is not monitored. Even in countries with monitoring services which I got to know as an IAEA-expert, this service was partly done quite unsufficiently. For instance, one service applying a four-filter badge, evaluated only the open-window field for all kinds of radiation workers. Further, the calibration has been done only with a 70 kV radiation X-ray quality using no additional filtration to the inherent filter. It is obvious, that energy independent TLD introduced to personnel monitoring in these countries will be of major help and effectiveness in radiation protection.

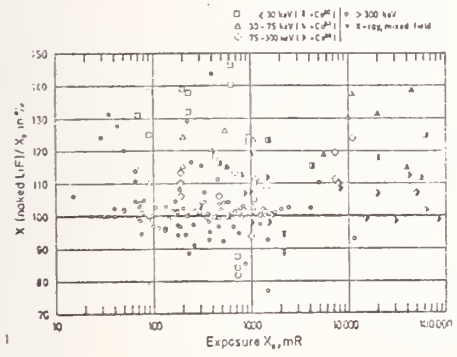

Fig. 6. Reading of TL dosimeter shielded with 300 mg/cm in dependence of the dose applied (Parameter: photon energy).

For the understanding of radiation mechanisms in radiobiology and radiochemistry it is important to intruduce further parameters for field description in addition to the absorbed dose. Particular interest is given to the density of energy imparted along the path of a particle (LET concept), to the energy deposed in a certain object size or to the statistical distributions of these energy amounts deposed in certain object sizes. The quantities and methods important for the studies of reaction mechanisms and describing microdosimetry shall not be further discussed, here.

Modern solid state dosimetry techniques eventually matching the requirements of microdosimetry, such as thermally stimulated exoelectron emission (TSEE), are still under elaboration. TSEE promises a detector depth around some 100 Ångstroem. However, at the moment, the investigations deal still with the interpretation of the TSEE mechanism prior to dosimetry application. Results of unexpected high exoelectron energies in Fig. 7 are first steps of better understanding of the phenomenon[15]. Particularly for measurements in vacuo, high reproducibility and linearity has been found for TSEE output versus alpha or gamma fluence for different grades of ceramic beryllium oxide in Fig. 8.

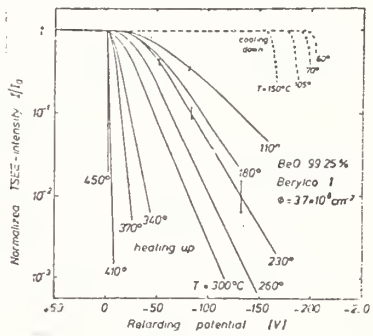

Fig. 7. Integral exoelectron energy distributions for ceramic BeO (Beryllium Consolidated) during the heating and cooling cycle. Parameter glow temperature.

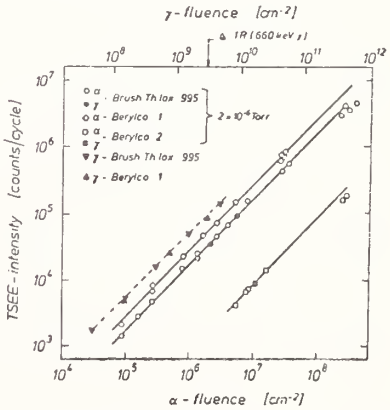

Fig. 8. Integral TSEE output of different ceramic BeO versus α- and γ-fluence.

Conclusion

Although the concept of energy absorption in matter represented a philosophical departure from the idea of quantifying the radiation field per se, the absorbed dose probably is, at present, the central physical dose quantity, while other dose quantities are auxiliary quantities supporting, for instance, the determination procedure of absorbed dose (exposure) or requirements of health physics (dose equivalent). But, reviewing all the dose quantities existing and having in mind, that even the main quantity, the absorbed dose, cannot be measured simply in practice, one is inclined to think of DENNIS[16] exclaiming: "Once upon a time we had the Roentgen, which we could measure but didn't want; then we had the rad which we wanted but couldn't measure; and now we have got the kerma which we don't want and can't measure".

Both the approaches of absorbed dose pointed out above, i.e. starting indirectly, from the determination of field parameters or from direct measurements of the radiation interaction with matter, are still lacking further and more exact data concerning basic parameters of interaction. For instance, there are serious doubts as to the adequacy of w-values, there is a need for stopping power data and spectroscopy of secondaries in matter; further there are problems in measuring compatible characteristics of field instruments for bremsstrahlung due to the absence of standardization of calibration conditions. Thus, care has to be given to the correlation between the measurement output and the absorbed dose. In applied dosimetry there is the further problem of data interpretation which often are measured at a point different from the one of dosimetric interest. Further, absorbed dose cannot be seen isolated from considerations of LET and microdosimetry in the fields of radiobiology and radiotherapy.

However, emphasis should be given to the importance of ensuring that the **inevitable** imprecision of data measurement, estimation and transfer is not reflected in a corresponding imprecision of concept.

References

1. Fränz, H. and Hobner, W. Proc. 2nd Int. Conf. on the Peaceful Uses of Atomic Energy, Geneva 1958, P/971 21, p. 101.
2. ICRU-Report 11, 1968, Radiation Quantities and Units.
3. Rossi, H.H., Microscopic Energy Distribution in Irradiated Matter, Radiation Dosimetry, Vol. I, Acad. Press, New York (1968).
4. Rindi, A. and Thomas, R.H. Health Phys. 23, 715 (1972).
5. Fano, U., Spencer, L.V. and Berger, M.J. Penetration and Diffusion of X-Rays, Handbuch der Physik 38/2, 660 (1959).
6. Jones, T.D., Auxier, J.A. and Snyder, W.S. Health Physics 24, 241 (1973).
7. ICRU-Report 10 a, 1962, Radiation Quantities and Units.
8. ICRU-Report 14, 1969, Radiation Dosimetry: X-Rays and Gamma Rays with Maximum Photon Energies between 0.6 and 50 MeV.
9. ICRU-Report 17, 1970, Radiation Dosimetry: X-Rays generated at Potentials of 5 to 50 kV.
10. ICRU-Report 19, 1971, Radiation Quantities and Units.
11. ICRU-Report 23, 1973, Measurement of Absorbed Dose in a Phantom Irradiated by Single Beam of X- or Gamma-Rays.
12. Moos, W.S., Balamutov, V.G. and Abedin-Zahed, R., National and International Radiation Dose Intercomparisons, IAEA-PL-479/18.
13. ICRP-Report 12, General Principles of Monitoring for Radiation Protection of Workers.
14. Dunster, H.S., Symposium Radiation Protection - Philosophy and Implementation, Aviemore / Scotland, June, 1974.
15. Ecker, K.H., Wittmaack, K., Regulla, D.F. and Schulz, F., Proc. 4th Int. Conf. on Luminescence Dosimetry, Krakow (1974).
16. Dennis, J.A., Personnel Dosimetry Techniques for External Radiation, p. 207, European Nuclear Agency, Madrid (1963).

NEUTRON DOSIMETRY BY THERMOLUMINESCENCE DOSIMETER

Yutaka Furuta and Shun-ichi Tanaka
Japan Atomic Energy Research Institute
Tokai Research Establishment
Tokai-mura, Naka-gun, Ibaraki-Ken, Japan

In this report, a historical survey of neutron dosimetry by thermoluminescence dosimeter (TLD) is made to begin with and then, as the basic problems for neutron dosimetry, the energy response to neutrons, gamma-ray discrimination performance in gamma neutron mixed fields, and sensitivity improvement are described. Furthermore, two types of conversion efficiencies are introduced to obtain the integral glow value of TLD from its kerma value. These efficiencies are given for any charged particle and may serve not only to estimate neutron energy response of any TLD but also to study the energy transfer to material from charged particles. As applications of these studies, the possibility of development of a rem response TLD or absorbed dose measurements for neutrons by TLD are also described.

(Charged particle, dosimeter, dosimetry, efficiency, gamma ray, kerma, neutron).

Introduction

Because of its many superior characteristics, studies of the thermoluminescence dosimeter (TLD) have rapidly increased during the past ten years. Especially, some of TLD's have an effective atomic number similar to that of air and most of the studies have been devoted to gamma-ray exposure measurements. Therefore, the studies of TLD as a gamma-ray dosimeter are considered to have proceeded fairly well at present.

On the contrary, investigations on neutron dosimetry can not be considered as sufficient and there are many problems yet to solve.

In the present report, the authors will survey the historical development of neutron dosimetry by TLD and will show the approaches to develop a new dosimeter or dosimetry to neutrons.

Historical Survey

The discovery of radiation-induced thermoluminescence goes back to the beginning of the present century. It was reported recently that Mme. Curie wrote in her thesis her discovery of the phenomena in the course of studying the various physical and chemical effects produced by exposing various substances to radium[1]. Rapid development of the studies, however, may be considered to have started in 1950.

Daniel et al[2] had introduced wide feasibility of the thermoluninescence (TL) phenomena including radiation dosimetry as a research tool. In early days, studies were mainly made for X or gamma rays, but in later 1950s considerable effort was concentrated on the practical means of measuring neutrons with TL materials.

Häring and Schoen[3] tried to detect neutrons by a CaF_2 film with ^{10}B or ^{6}Li film held in front of the CaF_2 film. The CaF_2 TLD responds to alpha particles produced by (n,α) reaction of ^{10}B or ^{6}Li with neutrons of a high reaction cross section. These materials serve as the radiator of alpha particles. They described that the lower limit of neutron detection in the case of using ^{10}B film was 3×10^5 neutrons, and besides, ^{6}LiF film was more energetic and found to be more suitable and 5×10^3 neutrons could still be detected. Furthermore, they used simultaneously a second CaF_2 film without the radiator film in order to eliminate the contribution of gamma rays to the TLD. In their report, it was also suggested that the utilization of protons recoiled by neutrons in radiator was a disadvantage because of their rather small energies, but the utilization of neutrons to be moderate, which could possibly be done by the human body, was promising. We see in their report many fundamental concepts for neutron dosimetry by TLD used in these days.

A neutron dosimeter using TLD in conjunction with a fast neutron moderator and a radiator was reported by Surjadi[4]. His dosimeter consisted of a layer of CaF_2 TLD enveloped by a LiF film and a

paraffin ball surrounding the detector device. He studied the relation between the sensitivity and the ball radius from 4 to 12 cm and the energy response to monoenergetic neutrons of 1,2 and 14 MeV.

The sensitivity to fast neutrons can be considerably increased by suspension of LiF TLD in alcohol, and the method was practiced by Karzmark et al[5]. In this case, alcohol serves both as the moderator for fast neutrons and as the radiator of recoil protons. Furthermore, it is convenient to use a volatile liquid like alcohol because it is readily evaporated at room temperature prior to read-out.

At that time, Harshaw Chemical Company (Cleveland, Ohio, U.S.A.) had developed activated LiF crystals specifically for TLD in cooperation with the University of Wisconsin. These materials were identified as TLD-100 (natural Li containing LiF TLD) and TLD-700 (^{7}Li enriched LiF TLD). Cameron et al[6] of the university studied the characteristics of these TLD's and showed that thermal neutron dose in gamma neutron mixed fields may be estimated by subtracting the light output of TLD-700 from that of TLD-100, because of the response of TLD-700 to thermal neutrons was less than 0.5% of TLD-100.

The 1st International Conference on Luminescence Dosimetry was held in 1965 at Stanford and many papers were submitted. In this conference, the major reports concerning neutron dosimetry were as follows:

1. Wingate et al.[7] reported the TL response of TLD-700 to thermal and fast neutrons at energies from 0.26 to 14 MeV. From the results, they concluded that TLD--700 made a convenient gamma-ray dosimeter in mixed gamma neutron fields because of its low neutron sensitivity. Furthermore, they indicated that the thermal neutron fluence may be conveniently measured with normal LiF(TLD-100) with linear relationship between light output and neutron fluence up to about 10^{12} neutrons/cm^2, and also pointed out from their results of glow curve that a higher read-out temperature was required than gamma-dose measurements.

2. A pair use of TLD-100 and TLD-700 was proposed by Simpson[8] to obtain gamma-ray dose in gamma neutron mixed fields of a reactor environment utilizing the characteristic of the same response to gamma rays and different response to neutrons. He also obtained the linear relationship between light output and thermal neutron fluence similarly to the case of Wingate et al.[7].

3. Endres[9] reported a pair of capsules of LiF TLD's used at Hanford as a neutron dosimeter, of which one was filled with a phosphor alone for measurement of gamma-ray exposure and the other filled with the same phosphor and alcohol (or other hydrogenous material) for measurement of the gamma-ray plus neutron exposure.

4. At Brookhaven National Laboratory, a neutron dosimeter system has been developed by using LiF TLD within a Bonner sphere. In the report by Distenfeld et al.[10] a 12" diameter polyethylene sphere modifies the neutron response characteristics of the LiF TLD to reasonably resemble the dose equivalent response characteristics of neutrons in tissue from thermal energies to approximately 20 MeV. Evaluation of the gamma-ray response is made by using ^{6}LiF TLD (^{6}Li enriched LiF TLD) and ^{7}LiF TLD (^{7}Li enriched LiF TLD) pair simultaneously in the system.

To evaluate experimentally the neutron shielding performance, Gayton et al.[11] reported several methods using LiF TLD. One of them was a new type of spectrometer, the DELTA spectrometer, which used LiF TLD's along the axis of a cylindrical moderator irradiated on one face. The spectral information was obtained from the thermal neutron fluence distribution by an iterative solution to a matrix equation. The report described that the device covered nine decades of energy and was sufficiently sensitive to measure fluence levels of 10^6 neutrons/cm^2.

Kuz'min et al.[12] studied the relation between sensitivity and phosphor layer thickness of TLD with recoiled proton radiator, and obtained a flat response dosimeter to neutrons having energies of 0.2 to 4.5 MeV.

Stolterfoht and Jacobi[13] also obtained energy response of ^{7}LiF TLD with and without alcohol using two kinds of capsule made of teflon and polyethylene to fast neutrons of 3 to 15 MeV.

In 1968, the 2nd International Conference on Luminescence Dosimetry was held at Gatlinburg. In this conference, energy responses were reported by Endres and Kocher[14] to neutrons of several types of TLD's (TLD-100, TLD-600 (^{6}Li enriched LiF TLD made by Harshaw Chemical Co.), $Li_2B_4O_7$, CaF_2, and BeO) placed on a polyethylene phantom with and

without Cd or ^{10}B shield.

Use of a TLD with neutron activation material was proposed by Kocher and Endres[15] as a personnel neutron dosimeter, of which TL is induced by radiations emitted from the material activated by neutrons. In their dosimeter, Rh was used as a neutron activation material.

A pair of ceramic BeO discs, of which one was covered with a non-hydrogenous material (graphite) and the other with a hydrogenous material (polyethylene) was reported by Becker and Crase[16]. For read-out, thermally stimulated exoelectron emission (TSEE) technique was used.

Busuoli et al.[17] showed that the ratio of the main peak (210°C) and the high temperature peaks (250 - 300°C) of the glow curve of TLD-100 is 24.5 for gamma rays and 2.4 for slow neutrons, and suggested that this characteristic makes it possible to use LiF TLD for measuring neutron dose in gamma neutron mixed fields.

Falk[18] reported a personnel neutron dosimetry system consisting of three pairs of LiF TLD's (TLD-600, -700) shielded with Cd. In his system, one of the pairs is shielded from the front, one pair from the back, and the third pair is shielded from both front and back.

An application of the LiF-teflon discs using ^{6}LiF and ^{7}LiF TLD's pair laminated between the plastic layers of an identification card was reported by Nash and Attix[19] as accident dosimeters.

In July 1971, the 2nd AEC Workshop on Personnel Neutron Dosimetry was held in New York[20]. In this meeting, many researchers participated from main establishments in the United States. It was then reported that most of the establishments employed the albedo type TLD neutron dosimeter, and the following was concluded at the meeting.

1. Neutron dosimeters utilizing the albedo neutrons require a fixed or well known spacing between the dosimeter and the body of the individual.

2. Energy dependence is still an important problem, but the dosimeters can give good results when properly worn and when calibrated with neutron spectra approximating those to which they will be exposed.

The 3rd International Conference on Luminescence Dosimetry was held in October 1971 in Risö. In the conference, a new idea was reported by Mayhugh et al.[21]. They tried to apply the activation of TLD composite material for thermal neutron dosimetry. That is, after exposure of a TLD in gamma neutron (thermal) mixed fields the TLD is annealed. When a constituent nucleus has an activity by thermal neutrons, the TLD undergoes self-irradiation (self dose) from the internal radioactive nucleus. A period of time after, the TL is read. The read corresponds to the neutron exposure, independent of the gamma-ray contribution during exposure in the mixed fields. They suggested ^{44}Ca or ^{146}Dy as suitable isotopes contained in the TLD.

In November of the same year (1971), a Symposium on New Development in Physical and Biological Radiation Detectors was held by IAEA in Vienna. In the symposium, Attix[22] discussed the neutron luminescent dosimetry problem and proposed a TLD system to obtain the neutron tissue dose by BeO TLD for thermal neutrons, for intermediate neutrons by a mixture of some TLD-100 powder with TLD-700, and for fast neutrons by TLD-600 and TLD-700 combination.

Neutron dosimetry technique utilizing TLD self dose proposed by Mayhugh[21] for thermal neutrons was extended for fast neutrons by Pearson et al[23]. They used phosphors such as MgF_2 TLD which contain two activating nuclei with different threshold energies and different decay times, and suggested some neutron spectrum analysis.

Efforts to utilize TLD's for personnel neutron monitoring are continuing at several major laboratories. At the Savannah River Laboratory a prototype badge had already been developed[24], and further development have been made by Hoy[25]. The newly developed dosimeter consists of a 2" diameter polyethylene hemisphere which is divided into two parts at 1/4" from the rounded end, and only a large part is covered with Cd plate. Both parts have recesses for a pair of ^{6}LiF and ^{7}LiF TLD's and the whole placed in a stainless steel housing and attached to a belt. The report concluded that it has limitations in certain energy regions of the spectrum, but the dosimeter provides a reasonably accurate method of integrating personnel exposures from unknown spectra at installations where neutron sources are contained or sufficient scatter is present.

The response of LiF and $Li_2B_4O_7$ TLD to thermal neutrons has been investigated by Majborn et al.[26] primarily with a view to using them for personnel moni-

toring in areas with mixed gamma neutron fields. The investigations include: 1) measurements of TL response vs. thermal neutron fluence, 2) measurements of TL response vs. dosimeter thickness, 3) measurements of TL response vs. isotopic abundance of ^{6}Li and ^{10}B, and 4) measurements of backscattering and gamma-ray contribution from a phantom in a collimated-beam geometry.

Blum et al.[27] reported a usage of a mixture of highly sensitive $CaSO_4$ TLD ($CaSO_4$(T/M/28)) and glucose (3 parts of glucose and 1 part of $CaSO_4$(Tm) powder) for fast neutron dosimetry. The same authors[29] also reported the results of fast neutron dosimetry by CaF_2 TLD in pair use with hydrogenous (polythene) and with non-hydrogenous (lead) screens. They concluded that lead was a convenient material for the latter and recommend microrod type TLD rather than disk type because of the directional dependence of the former dosimeter.

Attix et al.[30] reported that an attempt was made to determine the gamma-ray dose component in the neutron beam from a cyclotron by CaF_2 and ^{7}LiF TLD (TLD-700) at U.S. Naval Research Laboratory.

Kocher et al.[31] reported a five-element TLD using LiF blocks for beta particles, photons, and neutrons used at Hanford, of which ^{7}LiF block is shielded to provide interpretation of the 1 cm tissue depth dose, and a second ^{7}LiF block is unshielded to provide the kerma dose interpretation, and two ^{6}LiF and one ^{7}LiF blocks are used for fast and thermal neutron dose interpretation.

Calculated response of several albedo neutron dosimeters using ^{6}LiF TLD was reported by Alsmiller and Barish[32] for neutron energies lower than 400 MeV. They obtained the results for each of the dosimeter geometry considered, which were presented for both mono-energetic and continuous incident neutron spectra and for both normally and isotropically incident neutron fluences.

The 4th International Conference on Luminescence Dosimetry was held in Kraków this summer (1974). The present authors have not acquired yet the proceedings except manuscripts of a few papers. In these, there is a paper on composite dosimeters using $CaSO_4$ and BeO phosphors for x-ray, gamma-ray, beta-ray, and neutron dosimetry reported by Iga et al.[33] In their dosimeter, $CaSO_4$(Tm) powder and Non-TL ^{6}Li or ^{7}Li compound mixtures in a weight ratio of 1 : 1 are used.

Basic Problems

If we wish to use TLD for neutron dosimetry, some basic properties must be taken into consideration. These are the energy response, gamma-ray discrimination, and sensitivity. We will describe about these problems.

Energy Response

In any case, one of the most basic requirements for radiation detection is to know the energy response of the detector to objective radiations.

Figures 1 and 2 show the energy response of typical TLD's to neutrons. Experimental results were obtained to mono-energetic neutrons produced by Van de Graaff accelerator. In the same figures the energy responses obtained by calculations are also shown. These were obtained as follows:

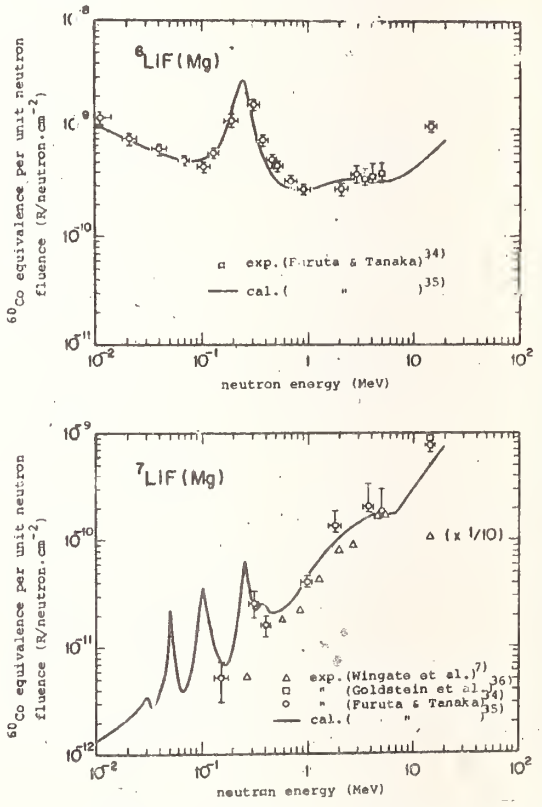

Fig. 1. Energy responses of ^{6}LiF and ^{7}LiF thermoluminescence dosimeters.

When the TLD is calibrated by ^{60}Co gamma rays, the integral glow value to neutrons is obtained by the kerma calculation

$$G(E_n) = \sum_i \bar{\eta}_{(i)} \cdot K_{(i)} \qquad (1)$$

$$K_{(i)} = C.\varepsilon_{(i)}.(E_n + Q_{(i)}).\sigma_{(i)}(E_n) \cdot \Phi(E_n).N_{(i)} \qquad (2)$$

where

$G(E_n)$: integral glow value (R ^{60}Co equivalence/neutron.cm^{-2}),

E_n : incident neutron energy (MeV),

$\bar{\eta}_{(i)}$: mean conversion efficiency for i-th particle produced or recoiled by incident neutron to obtain integral glow value from kerma value of the particle (R_1 ^{60}Co equivalence/$erg.g^{-1}$),

$K_{(i)}$: kerma value of i-th particle ($erg.g^{-1}$),

C : conversion factor to obtain erg unit from MeV unit,

$\varepsilon_{(i)}$: fraction of energy transfer to i-th particle from incident neutron,

$Q_{(i)}$: Q-value of nuclear reaction concerning i-th particle production (MeV),

$\sigma_{(i)}(E_n)$: reaction cross section with neutrons of energy E_n concerning i-th particle (cm^2),

$\Phi(E_n)$: fluence of neutrons having energy E_n (neutron.cm^{-2}),

$N_{(i)}$: number of atom concerning i-th particle in unit weight of TLD (g^{-1}).

If we know the value of the mean conversion efficiency for each particle produced or recoiled by incident neutrons, we may estimate the energy response of any TLD to neutrons by the above calculations. Therefore, it is clear that the conversion efficiency is also very important in developing a new TLD, and we will describe the efficiency further in a later section.

We may also estimate the energy response of the moderator type or the albedo type dosimeter by this method in conjunction with the calculations, such as the Monte Carlo calculation, of neutron spectrum at the TLD set position.

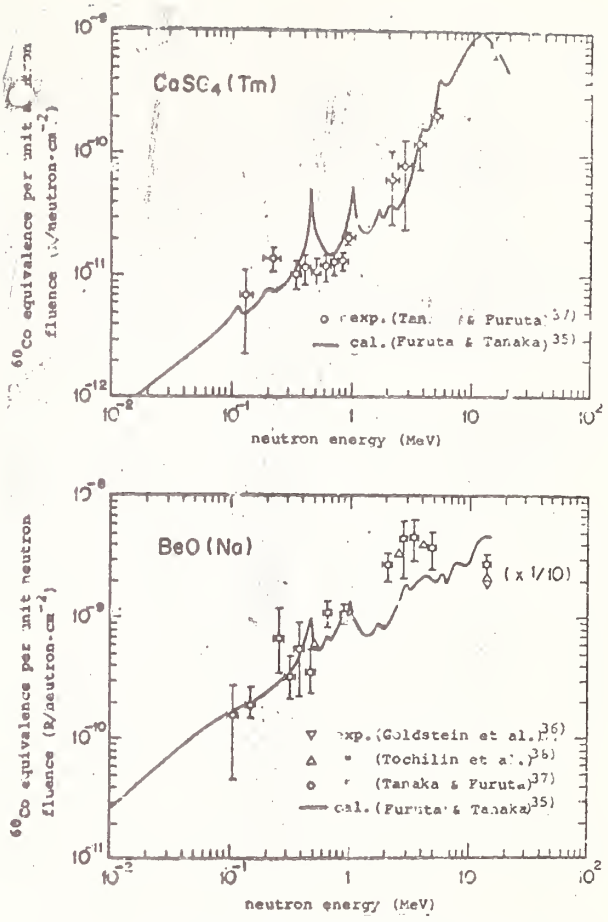

Fig. 2. Energy responses of $CaSO_4$ and BeO thermoluminescence dosimeters.

Gamma-ray Discrimination

In most cases, neutron fields are accompanied by gamma rays, and to obtain the neutron dose in these gamma-neutron mixed fields gamma-ray discrimination must be taken into consideration. As seen in the historical survey, the following methods have generally been used.

i) Utilizing a pair-use of two types of TLD which show the same responses to gamma rays but different responses to neutrons; for example, ^6LiF and ^7LiF TLD's.

ii) Utilizing the difference of glow curve shape; for example, ^6LiF TLD.

iii) Utilizing the reaction caused only by neutrons; for example, the self dose induced by neutron-activated nucleus.

These methods are also useful for future development of a new TLD's.

Care must be taken in the facts that any TLD has non-negligible response to the fast neutrons as seen from the energy responses to neutrons, and that ^{7}LiF TLD is sensitive to thermal neutrons because of large cross section of ^{6}Li(n,α)T reaction to thermal neutrons inspite of small contents of ^{6}Li in ^{7}LiF TLD. Therefore, as described in the literature, it is not suitable to use TLD in fast neutron fields.

Sensitivity

As seen from the energy responses of TLD's, the sensitivity of TLD to neutrons generally is not so large except for some TLD's containing elements of high reaction cross section with neutrons. On the whole, it is about 10^{-10} R ^{60}Co equivalence for 1 MeV and about 10^{-9} R ^{60}Co equivalence for 10 MeV to unit neutron fluence in rough estimation. For the moderator type or the albedo type dosimeter, increment of the sensitivity by several digits may be expected. The sensitivity of them, however, should be changed by geometrical conditions of the moderator, and the energy response must be obtained for each geometry.

The development of new phosphors of high sensitivity or new method to readout the luminescence should be expected. The photon counting or the TSEE method is considered to be promising.

Recently, new phenomena were found by Podgorsak and Moran.[39] The phenomena concern the electrical polarization phenomena in dielectic solids which can be induced by ionizing radiation. According to their report, radiation-induced thermally activated depolarization (RITAD) effects are quite different from radioelectret effects, and for normally pure CaF_2 sample, the RITAD signals showed a signal-to-noise power advantage of 40 decibels. They suggested that the phenomena will be a great potential for use as a dosimetry technique.

Conversion Efficiency

To develop a new TLD having desired response to neutrons, its energy response must be estimated. As seen in the preceding section, it may be done by calculation if we know the mean conversion efficiencies for all charged particles produced or recoiled by neutrons. We may consider two types of conversion efficiencies for the TL phenomena. They are the mean conversion efficiency and the differential conversion efficiency. The mean (conversion) efficiency is defined as "the ratio of the integral glow value, say the whole luminescence, G_0 to the initial energy E_0 of a charged particle which induce the TL (G_0/E_0)." The differential (conversion) efficiency is defined as "the ratio of the partial glow value dG to the differential energy loss dE by which the partial glow is induced (dG/dE)." In general, both the efficiencies are not necessarily equivalent.

The response of TL material to neutrons provides much information with many applications for radiation physics including health physics and reactor physics, which could not be obtained from the investigation for gamma rays. The reason is the response resulting from the migration of many kinds of charged particle composing TL material, which is considered as a fundamental phenomena in radiation physics. The differential efficiency may serve to theoretical treatment of these phenomena and the mean efficiency may serve to practical use for estimating the energy response of TLD to charged particles or neutrons.

The mean efficiency (relative to that for electrons) as a function of the mass stopping power for the initial energy of charged particles is shown in Fig. 3 (upper), and the differential efficiency (relative to that for electrons) as a function of the mass stopping power of a charged particle for the energy at each instant during energy loss in material is shown in the figure (bottom). These were obtained for a chain of particles one after another from experimental data of electron (for LiF and other TLD), proton (for LiF TLD), triton (for ^{6}LiF TLD), alpha (for LiF and CaF_2 TLD), beryllium (for BeO TLD), oxygen (for $CaSO_4$ TLD) and so on. The story of obtaining the efficiencies should be interesting. It is described, however, more fully in another report.[35]

In Fig. 3, the ranges of the mass stopping power which must be considered to reactor neutrons are shown for several types of particles.

New Approach for Neutron Dosimetry by TLD

Dose Equivalent Measurements

As seen in the historical survey, the TLD dosimeters already developed may be mainly classified as follows or a combination of the following:

1) moderator type,

2) albedo type,
3) self dose type.

At present, all of them do not necessarily satisfy the desired conditions for neutron dosimetry. Especially, it is difficult to obtain a significant value by moderator type dosimeter to neutrons because neutron spectrum is not well known usually. The same thing may be said for albedo type dosimeter. The self dose method is rather hopeful in estimating neutron spectrum reasonably using many types of TLD as threshold detectors. It is unsuitable for personnel monitoring, but, though only rough estimation of fast neutron dose can be obtained, it may serve an accident neutron personnel monitor even if single TLD is used. For example, $CaSO_4$ TLD, which is usually used as a gamma-ray personnel dosimeter, can be used as a fast neutron monitor utilizing $^{32}S(n,p)^{32}P$ reaction.

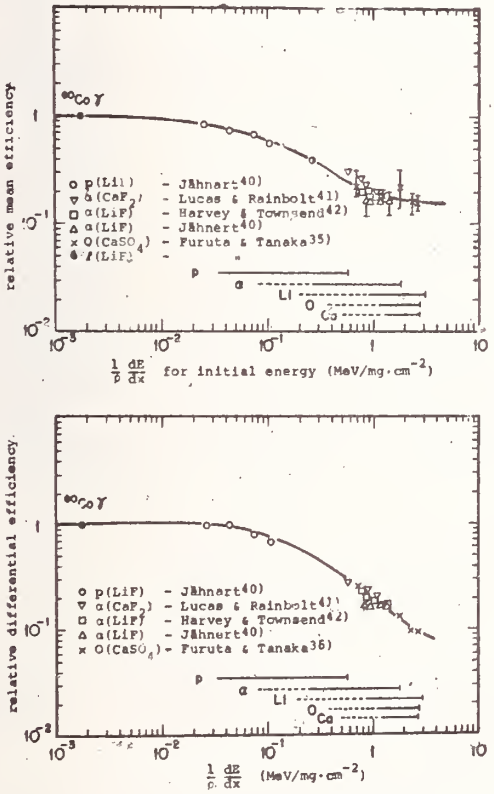

Fig. 3. Mean conversion efficiency and differential conversion efficiency.

One of the reasons for the difficulty in obtaining the significant value by moderator type or albedo type dosimeter is that the information obtained from the TLD is too simple. If we can make, however, a new TLD which shows a neutron response similar to that of dose equivalent, the defect becomes no longer a problem and it may be applied to neutrons having any spectrum. Hence, we will call hereafter the TLD having such property as the rem response TLD, and will introduce our approach to develop the TLD.

As described in the preceding section, we already obtained the conversion efficiency for any charged particles and the energy response to neutrons of any TLD may be estimated by calculation.

The rem response TLD now considered is consisted by a pair of two types of TLD having almost the same response to gamma rays and one type sensitive to neutrons while the other is not. Fig. 4 shows an estimated neutron response of the TLD. It was obtained by subtraction of the integral glow value of the neutron insensitive TLD from that of the neutron sensitive TLD. In the same figure, the maximum dose equivalent for monoenergetic neutron of unit fluence incident normally on a 30 cm thick tissue equivalent phantom[43] is also shown. From the figure, a fairly good agreement is seen between both responses.

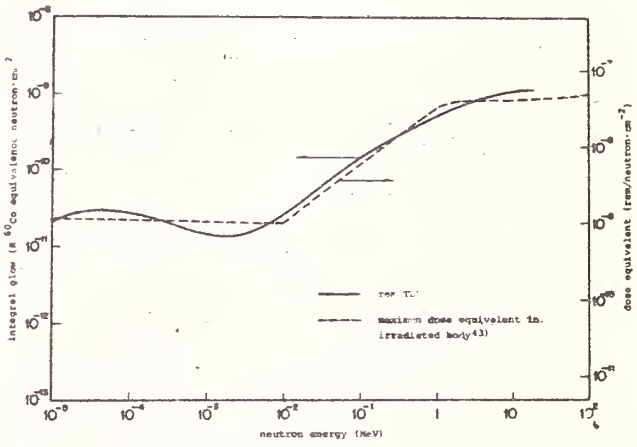

Fig. 4. Energy response of a newly developed rem response thermoluminescence dosimeter.

Absorbed Dose Measurements

In reactor physics or engineering, including fusion reactor, we often encounter the necessity to obtain the absorbed dose or energy deposition by neutrons for any material. Estimation of radiation heating in shield materials or damage of structural materials are considered as the example. These problems

are very important in reactor physics or engineering even at present, and the importance will rapidly increase in the near future especially in fusion reactor.

Recently, applications of TLD in gamma-ray heating estimation have been reported.[44,45] For neutrons, however, applications in absorbed dose or energy deposition measurements are not reported yet. In this report, we will offer a suggestion of the feasibility of TLD in neutron absorbed dose or energy deposition measurements.

As described previously, we had obtained experimentally the energy responses of several TLD's. From the results it was seen that the responses of some TLD's very much resembled the calculated kerma of some material. We will show two examples from the results in the present report. Fig. 5 is a comparison between the energy response of ^{7}LiF TLD to neutrons obtained by experiment and the calculated kerma of aluminum, and Fig. 6 is also the energy response of UD137N TLD (made by Matsushita Electric Industrial Co., Ltd.) ($CaSO_4$(Tm) and non-TL ^{7}LiF TLD)[33] and the kerma of iron. Good agreement may be seen from the figures.

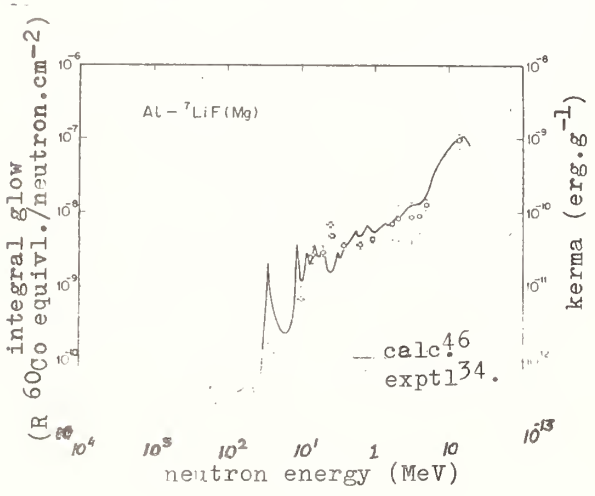

Fig. 5. Energy response of ^{7}LiF thermoluminescence dosimeter and kerma of aluminum.

It may be concluded that if the neutron field is not disturbed by positioning a TLD, and if the contribution of gamma rays to the integral glow value of the TLD may be estimated, the absorbed dose of some material may be estimated by TLD.

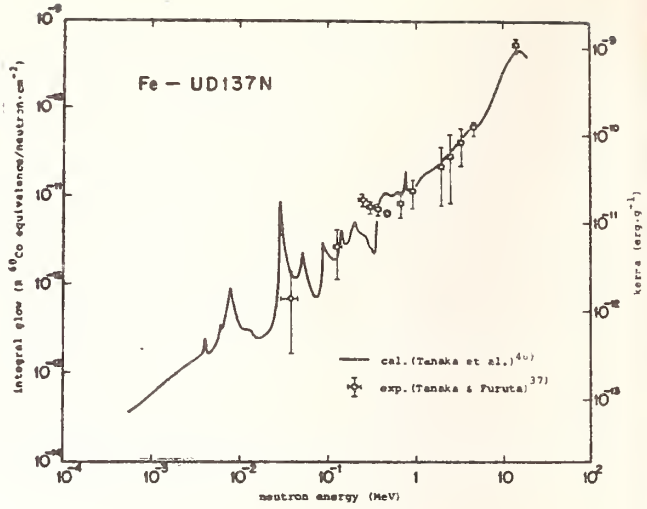

Fig. 6. Energy response of UD137N thermoluminescence dosimeter and kerma of iron.

At present, the following combinations are considered as giving good results.

material	TLD	f
Aluminum	^{7}LiF	1.0×10^{2}
Sodium	UD137N	2.7×10^{2}
Iron	UD137N	5.0×10

The value of f shows a fitting factor to obtain the kerma of a material K_m in erg.g^{-1}/unit neutron fluence from the integral glow value G_{TLD} of the corresponding TLD in R ^{60}Co equivalence/unit neutron fluence for each neutron energy E_n, that is

$$K_m(E_n) = f.G_{TLD}(E_n).$$

Conclusion

Recently, the necessity of a neutron dosimeter having high sensitivity and accuracy is increasing at rapid rate in health physics and in reactor physics and engineering.

As may readily be seen from the historical survey, personnel neutron dosimeters practically used at present are not necessarily sufficient to the purposes. For neutron absorbed dose or energy deposition measurements the same may also be the case. The thermoluminescence dosimeter, however, has many superior characteristics compared with other dosimeters, and it should be

utilized in various fields. The authors believe it has the ability, and they feel honoured if some suggestions described in this report might be of service to the development of new neutron dosimeters or dosimetry.

Acknowledgement

The authors express their thanks to the Organising Committee of this symposium and to Professor Ghose for their kind offer of a chance to deliver this Key-note address in this symposium.

One of the authors, Y.Furuta, is also indebted to IAEA for making his attendance to this symposium possible.

References

1. Eisenbud, M., Health Phys., 26, 110 (1974).
2. Daniels, F. and Saunders, D.F., The thermoluminescence of crystals; Final report, AECU-1583, 261p (1951).
3. Häring, N. and Schoen, M., Proc. Symp. Selected Topics in Radiation Dosimetry, 541-548 (Vienna, 1960).
4. Surjadi, A.J., Atomkernenergie, 8, 435-437 (1963).
5. Karzmark, C.J., White, J. and Fowler, J.F., Phys. Med. Biol., 9, 273-286 (1964).
6. Cameron, J.R., Zimmerman, D., Kinney, G., Buch, R., Bland, R. and Grant, R., Health Phys., 10, 25-29 (1964).
7. Wingate, C.L., Tochilin, E. and Goldstein, N., Proc. Intern. Conf. Luminescence Dosimetry, 421-434 (Stanford, 1965).
8. Simpson, R.E., Proc. Intern. Conf. Luminescence Dosimetry, 444-456 (Stanford, 1965).
9. Endres, G.W.R., Proc. Intern. Conf. Luminescence Dosimetry, 435-443 (Stanford, 1965).
10. Distenfeld, C., Bishop, W. and Colvett, D., Proc. Intern. Conf. Luminescence Dosimetry, 457-466 (Stanford, 1965).
11. Gayton, F.M., Hall, J.A. and Webb, G.A. M., Proc. Intern. Conf. Radiation Measurements in Nuclear Power, 152-161 (Berkeley, 1966).
12. Kuz'min, V.V., Lushchik, Ch.B., Savikhin, F.A., Sokolov, A.D. and Yaek, I.V., Atomnaya Energiya, 22, 482-488 (1967).
13. Stolterfoht, N. and Jacobi, W., Strahlentherapie, 134, 536-544 (1967).
14. Endres, G.W.R. and Kocher, L.F., Proc. 2nd Intern. Conf. Luminescence Dosimetry, 486-500 (Gatlinburg, 1968).
15. Kocher, L.F. and Endres, G.W.R., BNWL SA 1831 Rev., 17p (1968).
16. Becker, K. and Crase, K.W., Nucl. Instr. and Meth., 82, 297-298 (1970).
17. Busuoli, G., Cavallini, A., Fasso, A. and Rimondi, O., Phys. Med. Biol., 15, 673-681 (1970).
18. Falk, B., RFP-1581, 18p (1971).
19. Nash, A.E. and Attix, F.H., Health Phys., 21, 435-439 (1971).
20. Second AEC Workshop on Personnel Neutron Dosimetry, BNWL-1616, 109p (New York, 1971).
21. Mayhugh, M.R., Watanabe, S. and Muccillo, R., Proc. 3rd Intern. Conf. Luminescence Dosimetry, Risö Report No. 249, 1040-1050 (Risö, 1971).
22. Attix, F.H., Proc. of a Symp. on New Developments in Physical and Biological Radiation Detectors, IAEA-SM-143/25, 3-15 (Vienna, 1971).
23. Pearson, D., Wagner, J., Moran, P.R. and Cameron, J.R., COO-1105-175, 8p (1972).
24. Korba, A. and Hoy, J.E., Health Phys., 13, 581-584 (1970).
25. Hoy, J.E., Health Phys., 23, 385-389 (1972).
26. Majborn, B., Bøtter-Jensen, L. and Christensen, P., Proc. Symposium Dosimetry Techniques Applied to Agriculture, Industry, Biology, and Medicine, 169-177 (Vienna, 1972).
27. Blum, E., Bewley, D.K. and Heather, J.D., Phys. Med. Biol., 17, 661-662 (1972).
28. Yamashita, T., Nada, N., Onishi, H., and Kitamura, S., Proc. 2nd Intern. Conf. Luminescence Dosimetry, pp 4-17 (Gatlinburg, 1968).
29. Blum, E., Bewley, D.K. and Heather, J.D., Phys. Med. Biol., 18, 226-234 (1973).
30. Attix, F.H., Theus, R.B., Shapiro, P., Surratt, R.E., Nash, A.E. and Gorbics, S.G., Phys. Med. Biol., 18, 497-507 (1973).
31. Kocher, L.F., Nichols, L.L., Endres, G. W.R., Shipler, D.B. and Haverfield, A. J., Health Phys., 25, 567-573 (1973).
32. Alsmiller, R.G., Jr. and Barish, J., Health Phys., 26, 13-28 (1974).
33. Iga, K., Yamashita, T., Takenaga, M., Ohta, T. and Oonishi, H., Composite dosimeters based on $CaSO_4$:Tm and BeO phosphors for X-ray, γ-ray, β-ray and neutron dosimetry, presented in the 4th Intern. Conf. Luminescence Dosimetry (Krakow, 1974).
34. Furuta, Y. and Tanaka, S., Nucl. Instr. and Meth., 104, 365-374 (1972).
35. Furuta, Y. and Tanaka, S., The relation between light conversion efficiency and stopping power of charged particles in thermoluminescence dosimeter, presented the 4th Intern. Conf. Luminescence Dosimetry (Krakow, 1974).
36. Goldstein, N., Miller, W.G. and Rago, P.F., Health Phys. 18, 157-158 (1970).
37. Tanaka, S. and Furuta, Y., Neutron responses of thermoluminescence dosimeters, BeO(Na), $CaSO_4$(Tm), and mixture with ^{6}LiF or ^{7}LiF, presented the 4th Intern. Conf. Luminescence Dosimetry (Krakow, 1974).
38. Tochilin, E., Goldstein, N. and Miller, W.G., Health Phys. 16, 1-7 (1969).

39. Podgorsak, E.B. and Moran, P.R., Science, 179, 380-382 (1973).
40. Jähnert, B., Proc. 3rd Intern. Conf. Luminescence Dosimetry, 1031-1039 (Risö, 1971).
41. Lucas, A.C. and Rainbolt, C., Proc. 2nd Intern. Conf. Luminescence Dosimetry, 456-463 (Gatlinburg, 1968).
42. Harvey, J.R. and Townsend, S., Proc. 3rd Intern. Conf. Luminescence Dosimetry, 1015-1030 (Risö, 1971).
43. Radiation protection instrumentation and its application, ICRU Report No. 20 (1971).
44. Simons, G.G. and Yule, T.J., Nucl. Sci. Eng., 53, 162-175 (1974).
45. Simons, G.G. and Olson, A.P., Nucl. Sci. Eng., 53, 176-197 (1974).
46. Tanaka, S., Takeuchi, K. and Furuta, Y., in preparation.

Discussion

A.K. Ganguly

What is the highest energy of neutron upto which you feel you can use the TL dosimetry?

Y. Furuta

It may be considered that the problem depends on the size of TLD used. When most of the lost energy of the produced or recoiled particles is absorbed in the TLD, good results may be expected.

W.S. Snyder

Are the comparisons with dose based on the "air-dose", that is the dose to a small dosimeter, or are they based on the maximum dose within the body?

Y. Furuta

Our rem response TLD introduced in this symposium has a neutron response similar to that of the maximum dose equivalent when it was used in a free space. We are also considering now another TLD which shows similar response to the maximum dose equivalent when put in front of a human body.

S. Makra

Adding a small-size polyethylene moderator to a paired TLD detector which is located on the body improves the response very slightly. I think there is very little point in doing so.

I feel that the delta-spectrometer has a poor resolution thus the practical importance of this instrument is limited.

Hydrogeneous radiator - TLD combination is a very promising device, I hope it will be used more widely.

Y. Furuta

In our rem response TLD, hydrogeneous material only use for the purpose to slight compensate the slope for 10^{-2} 1 MeV region neutron energies to the MADE response.

I also think so, but for some purpose it may be useful.

I also think so.

EFFECT OF HEAT TREATMENTS ON THERMOLUMINESCENCE OF PURE Al_2O_3

A.S. Basu and A.K. Ganguly
Health Physics Division
Bhabha Atomic Research Centre
Bombay-400085

Six TL glow-peaks at the temperatures 100°C, 150°C, 200°C, 275°C, 310°C and 415°C are observed in pure Al_2O_3 after gamma irradiation. For higher exposures (>1000 R) the 275°C TL glow-peak is masked by the lower temperature peaks and is not seen. Thermoluminescence of this pure Al_2O_3 is investigated after different thermal treatments. The overall sensitivity increases with annealing temperatures and reaches a maximum at about 1200°C. The results are explained in terms of the structural change in alumina during these heat treatments.

(Aluminium oxide; glow; heat treatment; impurity; temperature; thermoluminescence)

Introduction

Rieke and Daniels[1] have shown that gamma ray induced thermoluminescence of aluminium oxides depends on the extent of hydration and the crystal form produced by different calcining treatments. A peak at 236°C depends on sodium impurity. They have used different samples of Al_2O_3 with varying impurity contents and prepared with different calcining treatments. In the present paper thermoluminescence of Al_2O_3 is studied with one sample of spec pure quality alumina (with impurity contents in ppm level) after different thermal treatments.

Experimental

Phosphor Characteristics and Preparations

The starting material of spec pure Al_2O_3 used in the present investigation contains the following impurities (data supplied by the manufacturer)

Chloride	-	0.05%
Sulphide	-	0.01%
Fe	-	0.01%
Loss on ignition	-	1%

The general method of preparing Al_2O_3 consists of precipitating $Al(OH)_3$ which after repeated washing is fired at 1100°C to remove the last trace of H_2O. Hence it can be presumed that the above sample had been fired at about 1100°C.

For studying the effect of thermal treatment on alumina, the sample is heated at temperatures ranging from 700°C to 1400°C. The heating is done for two hours in air at any given temperature and cooled in the switched off furnace. The sample so prepared are referred to as treated Al_2O_3 at that temperature and are stored in light tight containers.

TL Glow Curve Recording

For studying the TL output, the samples were given gamma exposure of 3.3×10^5 R from a ^{60}Co gamma irradiation facility. The glow curves were then recorded at a linear heating rate of 25°C/min using 2 mg of irradiated powder, in the temperature range of 25°C to 500°C. The details of the TL Reader set up used is fully described elsewhere[2].

Results

Fig. 1 shows the TL glow curves of Al_2O_3 treated at temperatures as indicated and also of untreated Al_2O_3 (virgin sample without giving any heat treatment) after gamma irradiation.

From the figure it can be seen that Al_2O_3 exhibits six peaks in its TL glow curve at temperatures of 100°C, 150°C, 275°C, 310°C and 415°C. The 275°C and 310°C peaks are not easily discernible from a visual inspection of the TL glow curves but can be distinctly seen by partial bleaching techniques. If an irradiated powder is heated at 220°C for half an hour, the TL recorded, it exhibits clearly the 275°C peak. Similarly TL glow curve of irradiated powder after heating at 280°C for half an hour exhibits clearly the 310°C peak.

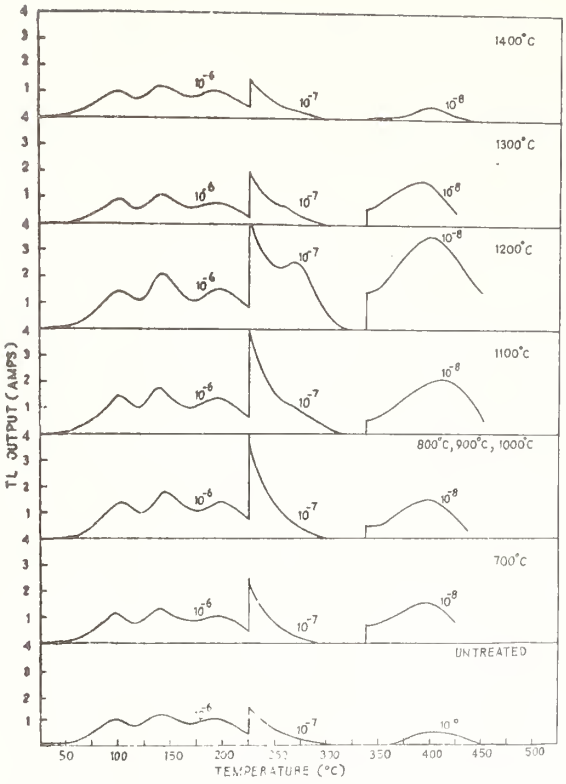

Fig. 1. TL glow curve of Al_2O_3 heated at different temperatures for two hours and cooled in the furnace.

The total thermoluminescence output (area under the TL glow curves) increases as we go from untreated Al_2O_3 to 1200°C treated samples as in fig. 2. As the treatment temperature is increased from 700°C to 1200°C, the area goes to a maximum and then falls for any further increase in the treatment temperature.

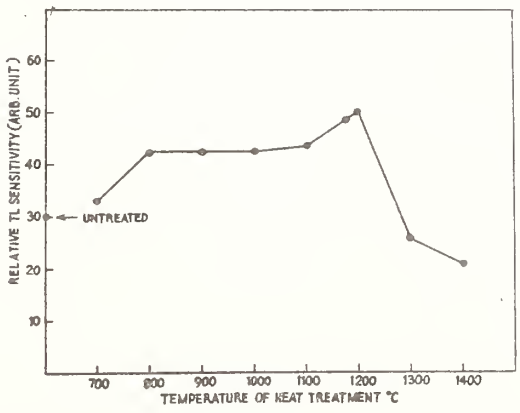

Fig. 2. Relative TL sensitivity of Al_2O_3 at different temperatures and cooled in the furnace.

Figure 3 shows the glow curves of Al_2O_3 when the sample is quenched i.e. when it is removed directly from the indicated temperature to the room temperature from 1000°C onwards. The TL glow curve of quenched as well as furnace cooled Al_2O_3 is the same for treatment temperatures upto 900°C. Figure 4 shows the glow curves of Al_2O_3 when it is heated under vacuum (atmospheric pressure of $(1\text{-}1.5)\times10^{-4}$ Torr) at a few indicated temperatures. Table 1 gives a comparative study of the relative TL outputs of Al_2O_3 when it is heated under these three conditions. From the above table is is clearly seen that the TL output of quenched Al_2O_3 is less than that of furnace cooled Al_2O_3 from treatment temperatures of 1000°C onwards. The TL output reduces still more when it is heated under vaccum.

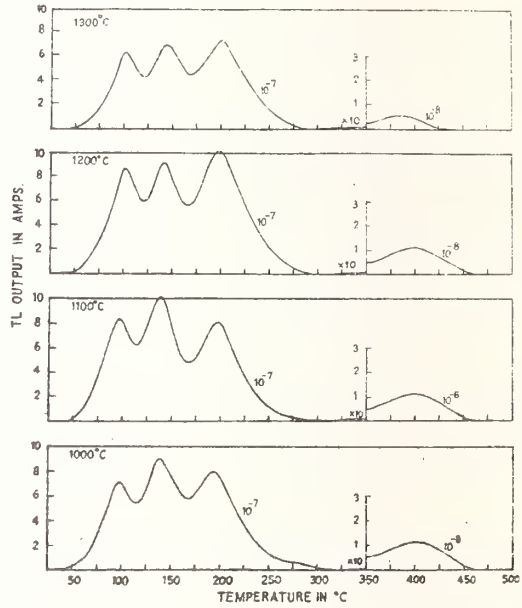

Fig. 3. TL glow curves of Al_2O_3 when at different temperatures for two hours and quenched.

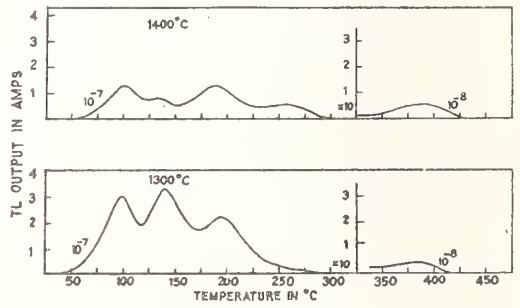

Fig. 4. TL of Al_2O_3 samples heated at different temperatures in vacuum for two hours.

Table-1

Comparative study of relative TL sensitivity of Al_2O_3 when heated under different conditions.

Temp. of treatment for two hours (^oC)	Relave TL output when cooled in the furnace	Relative TL output when the sample is quenched	Relative TL output when heated in vacuum
700	33.2	33.2	
800	42.5	42.5	
900	42.5	42.5	
1000	42.5	21.5	
1100	43.2	21.9	
1200	50.5	25.2	
1300	26.17	17.6	7.32
1400	21.4		3.3

Relative TL output for untreated sample - 30.65

Discussions

The different modification of Al_2O_3 obtained on annealing[3] at different temperatures are

$$Al_2O_3\ 3H_2O \xrightarrow{150^oC} Al_2O_3\ 1H_2O \xrightarrow{300^oC}$$

$$\gamma\ Al_2O_3 \xrightarrow{1000^oC} \alpha\ Al_2O_3$$

γ-Al_2O_3 is a face centred close packed oxygen lattice which transforms into a hexagonal close packing - the α form on heating at 1000°C. This transformation γ to α is complete when heated at 1200°C in air. Annealing temperatures below 1200°C is likely to produce a mixture of γ/α.

It is known from Low Energy Electron Diffraction[4] that α alumina undergoes a change of surface structure upon heat treatment under vacuum above 1250°C accompanied by a change in the chemical composition of the surface by the loss of oxygen. This structural change is reversible and can be changed back to the initial stage by heating at 1200°C in presence of oxygen (10^{-4} Torr of oxygen pressure).

In the light of the above discussions, our TL results can be interpreted to indicate that α alumina is the most sensitive TL emitter among various forms of alumina and presence of oxygen during any heat treatments to alumina helps to preserve the TL sensitivity. For temperature of treatments higher than about 1000°C, fast cooling of the sample reduces the TL sensitivity perhaps because the surface structural changes occuring in α alumina get frozen.

References

1. Ricke, James K. and Daniels, Farrengton, J.Phys.Chem., 61, 629 (1957).
2. Sunta, C.M., Ph.D.Thesis, Agra University, 1970.
3. Holzapfel, G. and Chrysson, E., Third Internat.Conf. Luminescence Dosimetry, Riso, Oct. 11 - Oct. 14, 1971.
4. French, T.M. and Somorjai, G.A., J.Phys.Chem., 74, 2489 (1970).

THERMOLUMINESCENCE MECHANISMS IN LITHIUM FLUORIDE

S.P.Kathuria, V.N.Bapat, C.M.Sunta and V.K.Jain
Health Physics Division
Bhabha Atomic Research Centre
Trombay, Bombay-400085, India

Five glow peaks upto 200°C are well known in lithium fluoride after gamma irradiation. Seven new glow peaks above 200°C are reported in the present work. They are designated as I to XII in the ascending order of temperature of appearance. Activation energies are determined by initial rise method for five glow peaks, which could be well isolated by partial annealing from the lower temperature glow peaks. TL emission from the prominent glow peaks is similar and contains four bands with maxima at 370nm, 390 nm, 415 nm and 470 nm approximately. The spectral distribution of the total TL emission and emission from glow peaks V (195°C) and XII (400°C) are obtained also by plotting the integrated intensities of individual glow curves recorded at every 5 nm interval from 250 nm to 800 nm. The TL emission spectra obtained in this way are corrected for the instrument response. Optical absorption spectrum of lithium fluoride crystal is recorded after gamma irradiation. Distinct absorption bands are observed at 225 nm, 250 nm, 310 nm and 380 nm. Absorption spectra are recorded also after various thermal annealing treatments. The spectral similarity of individual glow peaks and the continuous bleaching of F band (250 nm) with the annealing of individual peaks, shows that F centre takes part in recombination process at each stage of glow peak emission. The thermally released carrier at individual glow peaks is therefore of hole type.

(Irradiation; gamma rays; LiF; optical absorption; spectral distribution; thermoluminescence)

Introduction

Thermoluminescence of lithium fluoride has been studied extensively by a number of workers[1-5]. Five glow peaks upto 200°C have been observed by all workers but observation of TL emission at temperatures higher than 200°C has varied from worker to worker. Sunta et al[6,7] observed ten glow peaks upto 400°C.

There are conflicting opinions regarding the nature of charge carriers released on heating and also about the thermoluminescence mechanism[3,7-10]. Christy et al[8] proposed the recombination centre as the impurity centre absorbing at 196 nm. TL emission occurs when a hole freed by thermal heating is captured by this centre. The crystal is restored to its initial state by an electron tunneling from a nearby F centre, to the impurity ion with the emission of a second photon. However, Claffy[11] observed thermoluminescence in the absence of 196 nm absorption band also.

Mayhugh et al[10] found that trapped charge carriers responsible for TL are electrons. On heating the irradiated LiF phosphor, electrons from their respective trap centres are liberated and captured at V_3 centres containing two trapped holes[12]. This would result in a single hole centre (V_k centre) which is unstable at room temperature. The indirectly produced mobile hole then undergoes recombination at an impurity site with electron from F centre resulting in light emission. In the present work, a study of optical absorption spectra and TL emission spectra in LiF after gamma irradiation is undertaken to identify the luminescence centres and nature of charge carriers released on heating.

Experimental

Lithium fluoride samples used are (i) LiF (T) powder (140 to 200 mesh) from crystal grown in the Technical Physics Division of this centre and (ii) TLD-100 of Harshaw Chemical Co., USA. Before use the powders were annealed at 400°C for 1 hour and cooled to room temperature by leaving in air on a block of aluminium. Irradiation was carried out in ^{60}Co gamma cells having dose rates of 2.3 KR/min and 7.0 KR/min. TL measurements were carried out using 5 mg of powder at a linear heating rate of 25°C/min with a reader system described by Sunta[13].

Experimental arrangements for recording optical absorption spectra and TL emission spectra have been described elsewhere[14].

Results and Discussion

Glow Curves

TL glow curves of five LiF samples are shown in Fig. 1. Qualitatively all the five glow curves are similar. It is also evident from the figure that while the general structure of the glow curves remains the same, the relative peak heights may vary from sample to sample. The TL of LiF obtained from whatever source, does not seem to depend, critically on the impurities so far as the glow curve structure is concerned[15]. However, it does depend upon the impurity and preparation parameters if one looks at the sensitivity, relative peak heights and response characteristics of various peaks. In the sample TLD-700 (Batch 48 DZ) there are ten distinct glow peaks seen at the temperature 62°C, 102°C, 142°C, 175°C, 195°C, 215°C, 232°C, 257°C, 287°C and 403°C. In other four samples, glow peaks at the temperature 215°C, 232°C, and 287°C are not clearly seen but there exists a faint suggestion of their presence.

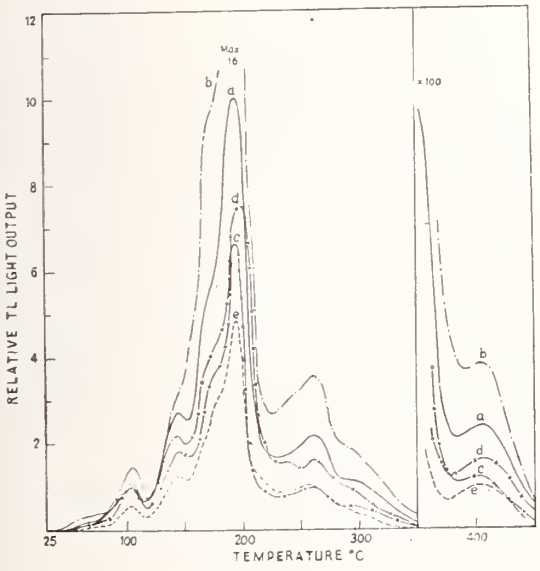

Fig. 1. TL Glow curves of LiF samples for the gamma exposure 7.05 x 10^5R (a) TLD-100 (48 DW) (b) TLD-100 (LJL) (c) TLD-600 (26 EAD) (d) TLD-700 (48 DZ) (e) LiF (T).

To ascertain the exact number of glow peaks beyond 200°C one of the LiF samples (TLD-100) was annealed at 160°C for 30 minutes after gamma irradiation so as to erase the first 5 glow peaks and then quenched to room temperature. The glow curve recorded after this annealing treatment shows a clear glow peak at 220°C which was not seen before the annealing treatment. (Fig. 2 curve b). This peak was obviously submerged below the 195°C glow peak. Aliquots of the irradiated sample were then successively annealed at higher temperatures. These annealing temperatures and time are chosen in such a way that the glow peaks preceding the one under examinations are completely eliminated during each anneal. The glow curves recorded after each such thermal annealing are given in fig. 2 (curve b to h). Following this procedure, seven more TL glow peaks above 200°C which were not obvious (curve a) are observed at 220°C, 237°C, 260°C, 295°C, 312°C, 337°C and 405°C. Following the similar procedure, these new peaks clearly showed up in other samples also. Thus, a total of twelve glow peaks are observed in all the LiF samples studied. They are designed as I to XII in the ascending order of the temperature of appearance.

Thermal activation energy of glow peaks II, V, VIII, XI and XII are determined by initial rise methods for LiF (T) and TLD-100 samples and are given in Table-1.

Table-1

Thermal activation energies of glow peaks II, V, VIII, IX and XII determined using initial rise method

Glow peak No.	Glow peak Temperature (°C)		Thermal activation Energy (eV)	
	LiF(T)	TLD-100	LiF(T)	TLD-100
II	102	103	1.36	1.25
V	195	195	1.63	1.5
VIII	257	260	2.10	2.08
XI	332	337	1.97	1.97
XII	402	405	1.54	1.37

TL Emission Spectra

The annealed TLD-100 samples are irradiated to 10^5R and 10^6R and the glow curves with 10 mgm of each of these samples are recorded at intervals of 5 nm from 250 nm to 800 nm. The area under each glow curve is determined and plotted against the respective wavelength after correcting for the system response (curves a of figs. 3 and 4). Curves b of figs 3 and 4 show the TL emission spectra of glow peaks V and XII respectively recorded in a similar way with 10^5R and 10^6R irradiated TLD-100 samples. It is seen from these figures that there

are four emission bands appearing at 370 nm, 390 nm, 415 nm and 470 nm and qualitatively all the TL emission spectra are similar. However, there is variation in relative intensity of emission bands.

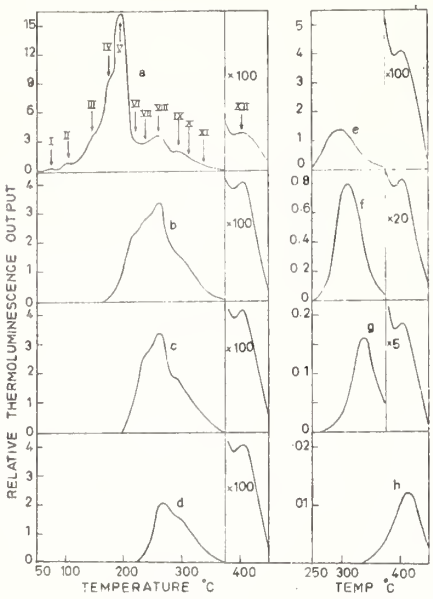

Fig.2. TL glow curves of TLD-100 (IJL)

(a) After 7.05×10^4R of gamma irradiation
(b) 'a' followed by 30 min annealing at 160°C
(c) 'a' followed by 20 min annealing at 180°C
(d) 'a' followed by 10 min annealing at 220°C
(e) 'a' followed by 20 min annealing at 240°C
(f) 'a' followed by 30 min annealing at 260°C
(g) 'a' followed by 10 min annealing at 300°C
(h) 'a' followed by 2 hrs annealing at 330°C

Similar results were obtained when emission spectra were recorded at the temperatures 85°C, 135°C, 180°C and 380°C[16]. At these temperatures prominent glow peaks II, III, V and XII are emitted respectively. This shows that the same luminescence centres are involved in the thermoluminescence process at all temperatures. The change in the relative intensity of TL emission bands is possibly because of the change in the configuration of the luminescence centres with temperature.

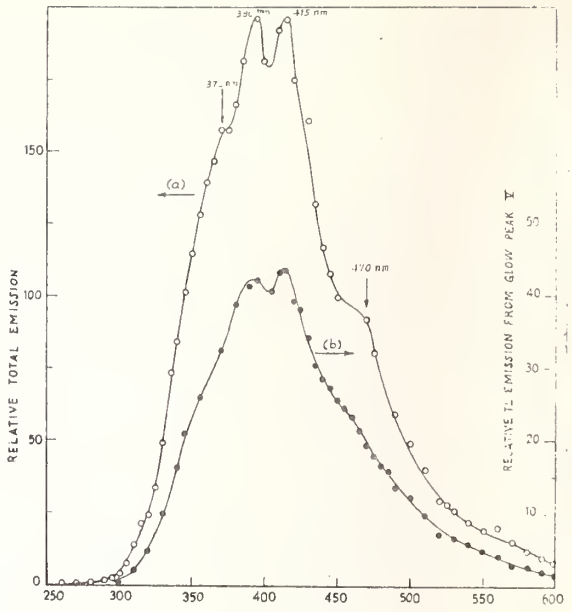

Fig. 3. TL emission spectra of TLD-100 (IJL) after 10^5R gamma irradiation (a) Total TL emission (b) TL emission from glow peak V.

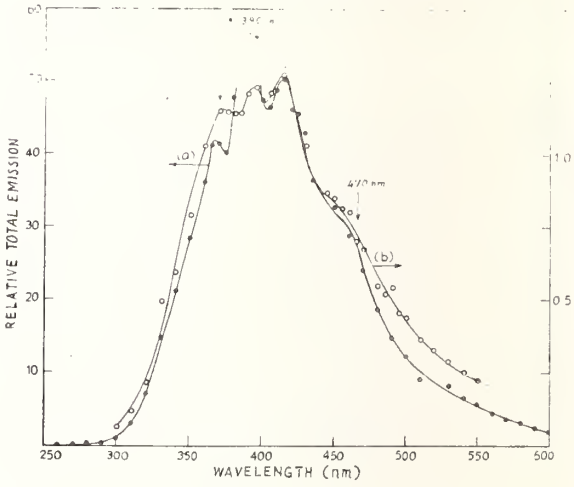

Fig. 4. TL emission spectra of TLD-100 (IJL) after 10^6R gamma irradiation (a) Total TL emission (b) TL emission from glow peak XII.

Optical Absorption Spectra

Fig. 5 shows the absorption spectra of LiF(T) crystal after gamma irradiation and annealing at 100°C, 150°C, 200°C, 250°C and 350°C for 30 minutes each. After gamma irradiation three absorption bands at 250 nm, 310 nm and

380 nm are seen clearly and there is a suggestion of another absorption band at 225 nm. 250 nm absorption band is a well known F-band and is due to the electrons trapped at the negative ion vacancies.

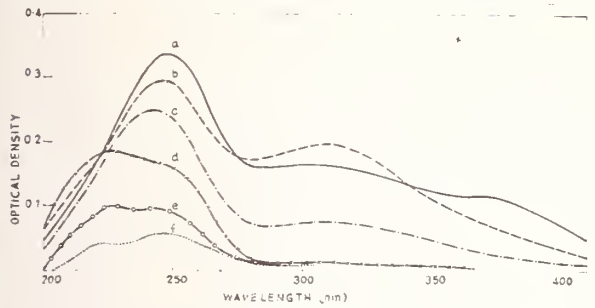

Fig. 5. Optical absorption spectra of LiF(T) crystal after

(a) 7.05×10^4R gamma irradiation
(b) 'a' followed by 30 min annealing at 100°C
(c) 'b' followed by 30 min annealing at 150°C
(d) 'c' followed by 30 min annealing at 200°C
(e) 'd' followed by 30 min annealing at 250°C
(f) 'e' followed by 30 min annealing at 350°C.

The F-band decreases progressively after each thermal annealing (curves a to f). After annealing the crystal at 350°C, the absorption at 225 nm and a part of the F-band only are left (curve f) and in the corresponding glow curve there is only one glow peak present at 402°C. Both the absorption bands, 225 nm and F-band disappear together with the 402°C glow peak after annealing the crystal at 400°C for 1 hour. If it is assumed that an electron and hole centre are required for TL emission, it would appear that the 225 nm absorption is due to hole centres and is correlated with 402°C TL glow peak (XII). Klick et al[9] have suggested that the absorption at 225 nm arises from a centre which traps two holes. Such a centre has been identified in KCl:Ca[17].

All the glow peaks are regenerated by irradiating the LiF sample, having glow peak XII as residual to Hg lamp UV light[18]. UV light photons release the charge carriers from the peak XII traps which are captured by the trapping sites corresponding to lower temperature glow peaks, emptied during thermal annealing.

The glow peak XII has been correlated with the optical absorption found at 225 nm which is due to hole centres. Therefore charge carrier involved in the transfer process from peak XII traps are the holes which are being captured by the trapping sites corresponding to lower temperature glow peaks.

The progressive decrease in F-band optical density after different thermal annealings (fig. 5 curves a to f) shows that F-centres take part in the recombination process. The exact configuration of the luminescence centre is not identified in the present work. Thus on heating the gamma irradiated LiF sample, holes are released from traps of different thermal stability which recombine with electrons of the F-centres - part of the luminescence centres. Energy is supplied to the luminescence centre by the recombination of the hole with an electron which appears as light. The emitted TL emission bands correspond to the energy states of the luminescence centre modified by the crystal field.

Acknowledgements

Authors are grateful to Dr. A.K. Ganguly, Director, Chemical Group for his keen interest in the work and many helpful discussions.

References

1. Daniels, F., Boyd, C.A. and Saunders, D.F., Science 117, 343 (1953).
2. Daniels, F., Lum. Dosimetry, AEC Symp. Ser. Vol. 8, CONF-650637, Stanford (1965).
3. Claffy, E.W., Lum. Dosimetry, AEC Symp. Ser. Vol. 8, CONF-650637, Stanford (1965).
4. Cameron, J.R. and Daniels, F. Science, 134, 333 (1961).
5. Cameron, J.R., Zimmerman, D.W., Kenney, G., Buch, R., Bland, R. and Grant, R., Health Physics, 10, 25 (1964).
6. Sunta, C.M. and Kathuria, S.P. Advances in Physical and Biological Radiation Detectors, SM-143/24, IAEA, Vienna (1971).
7. Sunta, C.M., Bapat, V.N. and Kathuria, S.P. Proc. 3rd Int. Conf. Lum. Dosimetry, Oct. 11-14, Riso (DAEC and IAEA), (1971).
8. Christy, R.W., Johnson, N.M. and Wilbarg, R.R.,J.Appl. Phys. 38, 2099 (1967).
9. Klick, C.C., Claffy, E.W., Gorbies, S.G., Attix, F.H., Schulman, J.H. and Allard, J.G., J. Appl. Phys. 38,3867 (1967).
10. Mayhugh, M.R., Christy, R.W. and Johnson, N.M., J. Appl. Phys. 41, 2968 (1970).
11. Claffy, E.W., Phys.Stat.Sol. 22, 71 (1967).
12. Winter, E.M., Wolfe, D.R. and Christy, R.W., Phys. Rev. 186, 949 (1969).
13. Sunta, C.M. Ph.D.Thesis, Agra Univ. (1971).

14. Kathuria, S.P., M.Sc. Thesis, Bombay University (1974).
15. Jones, D.E. and Burt, A.K., Lum. Dosimetry, AEC Symp. Ser. Vol. 8, CONF-650637, Stanford (1965).
16. Kathuria, S.P., Indo-Soviet Conference on Solid State Material, Dec. 11-16, Bangalore (1972).
17. Crawford, J.H.Jr. and Nelson, C.M., Phys. Rev. Letters 5, 314 (1960).
18. Kathuria, S.P., Bapat, V.N. and Jain, V.K., Presented at the Fourth Int. Conf. Lum. Dosimetry, Aug. 27-31, 1974, Krakow, Poland.

THERMOLUMINESCENCE RESPONSE OF LiF TO GAMMA RAYS

V.K. Jain and S.P. Kathuria
Health Physics Division
Bhabha Atomic Research Centre
Trombay, Bombay 400085
India

The thermoluminescence of lithium fluoride shows twelve peaks, of which II (100°C), III (135°C) and V (190°C) grow linearly first and then become nonlinear, eventually saturate and finally show decreased response or damage. Peaks beyond the Vth peak on the other hand seen to grow supralinearly right from the beginning. None of the available explanations for the supralinearity of the dosimetry peak (V) is entirely satisfactory. Similarly damage too is not understood. In this paper it has been shown that the radiation induced sensitisation is linked with the XIIth peak (400°C). It is postulated that this peak is created as a result of irradiation and hence is supralinear right from the beginning. The other high temperature peaks, though supralinear, are not found to be responsible for radiation induced increase in sensitivity of lower temperature peaks. It is shown that the trap centres (TC's) responsible for the XIIth peak are generated as a result of the break up of complex centres TCLC's on irradiation. This break also causes the addition of luminescence centres (LC's) which leads to increase in sensitivity. The complex centres (TCLC's) themselves are formed due to the 400°C annealing. Decreased response or damage after saturation is the result of loss of luminescence centres while the traps remain unaffected.

(Dose; gamma rays; LiF; response; sensitivity. supralinear; thermoluminescence)

Introduction

Many aspects of TL response to X- and gamma rays of LiF dosimetry phosphor are vaguely understood. For example, the complicated annealing behaviour[1,2] and radiation sensitization[3,4,5] are not satisfactorily explained. Similarly, radiation damage in LiF is quite critical and needs investigation.

The glow curve of LiF has many more peaks than are generally reported in literature[6]. In this paper the TL response of some of these peaks is reported. The model proposed earlier[7], to explain radiation sensitization and supralinearity in LiF is elaborated. Some aspects of the lowering of response, due to radiation damage are reported and the involvement of luminescence centres in this is discussed.

Experimental

Lithium fluoride samples used were (i) LiF (T) powder (140 to 200 mesh) from crystal grown in the Technical Physics Division of this Centre and (ii) TLD-100 of Harshaw Chemical Co., USA. Before use the powders were annealed at 400°C for one hour and cooled to room temperature by leaving in air on a block of aluminium. Irradiation was carried out in Co-60 gamma cells having dose rates of 2.3 kR/min and 7.0 kR/min. TL measurements were carried out using 5 mg of powder at a linear heating rate of 25°C/min with a reader system described by Sunta[8].

Results and Discussion

Thermoluminescent Response of Some Peaks

Fig. 1 shows the glow curves of lithium fluoride after gamma irradiation. There are total of twelve glow peaks present in the glow curves of LiF samples[9]. But for the first peak which decays rapidly and XIth peak which is hidden under Xth peak, ten peaks can be clearly seen. In Fig. 2 the response of some of the peaks viz. II, III, V, VIII, and XII is shown. From the growth pattern it appears that the TL peaks in LiF fall into two groups: one group comprises peaks upto the Vth (dosimetry peak) and the other of peaks beyond the Vth. The first-group peaks initially rise linearly and become supralinear at higher exposures. The second-group peaks seem to respond supralinearly right

from the beginning (VIII and XII in fig. 2). Also shown in this figure is sensitization by gamma irradiation and annealing at 350°C for 15 min for peaks V and VIII. The well known sensitization procedure enhances the response of not only the Vth (dosimetry) peak but also of the VIII peak as shown and other peaks, not shown. Sensitization is shown for two gamma pre-exposures and it can be seen that when the sensitization is incomplete the phosphor still responds supralinearly though at a higher exposure.

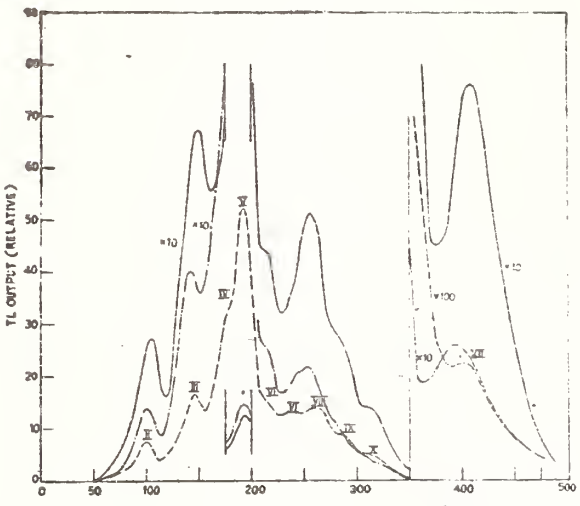

Fig. 1. TL glow curves of LiF TLD-100 exposed to 2.3×10^5R and LiF(T) exposed to 6.9×10^4R and 2.3×10^5R.

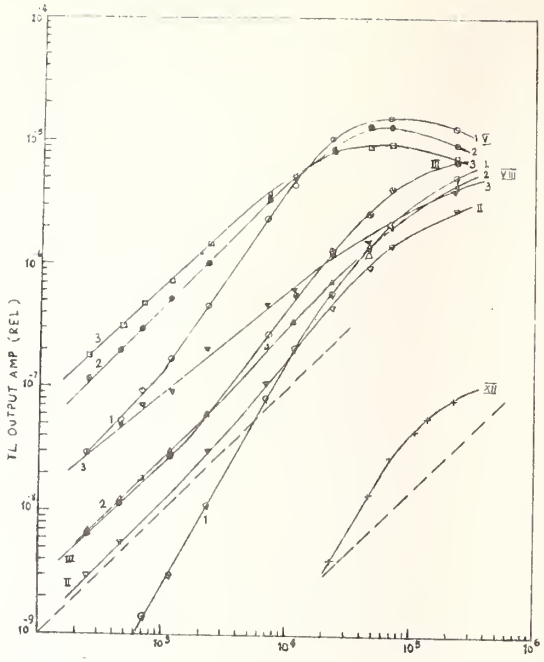

Fig. 2. Response of peaks II, III, V, VIII and XII in LiF(T). Peak V and VIII (1) LiF(T) annealed at 400°C for 1 hour (2) 1 followed by 1.15×10^4R of sensitization exposure and annealing at 350°C for 15 min (3) 1 followed by 6.9×10^4R of sensitization exposure and annealing as in 2. Peak XII as in above.

One of the reasons for the thermoluminescence peaks to be supralinear throughout could be that they are created by irradiation as has been suggested by Mason and Linsely[10]. The VIIIth peak and the XIIth peak both are supralinear but with a difference. The VIIIth peak is radiation sensitized but not the XIIth. In fact radiation sensitization is dependent on the XIIth peak which is 'created' (see next section). If the VIIIth peak were due to traps which captured more than one charge carrier, its growth would be supralinear*.

Supralinearity and Sensitization

The ratio of the response to 100 R of gamma rays of TLD-100 sensitized by 4.0×10^4R of gamma rays and subsequent annealing (S) and that of the unsensitized TLD-100 (S_o) gives the sensitization factor (S/So). Also the area of the glow curve remaining after the gamma exposure and subsequent annealing gives the residual thermoluminescence (RTL). How S/So varies with RTL remaining as a result of annealing at different temperatures for various periods is shown in Fig. 3. From these curves it is apparent that S/So does not depend critically on RTL except when the latter has decreased to a negligible proportion which corresponds to peak XII. Sunta et al[11] concluded that glow peak XII alone is responsible for sensitization. A model was proposed earlier[6] to explain supralinearity and sensitization. The model postulated the formation of a complex centre (TCLC) consisting of a trap centre (TC) and a luminescence centre[10]. Initially the number of such complexes is small. By annealing at high temperatures (400°C), trap centres and luminescence centres are brought together to form more complexes[7]. On irradiation this complex breaks up into its constituents (TC and LC). As irra-

*The fact that for densely ionizing radiations like alpha rays the relative response of the high temperature peaks is more, suggests this.

diation progresses, more and more luminescence centres are added which cause increase in TL response leading to supralinearity. Annealing the irradiated powder at a lower temperature say 350°C does not reform the complex and the added luminescence centres continue to be available resulting in sensitization.

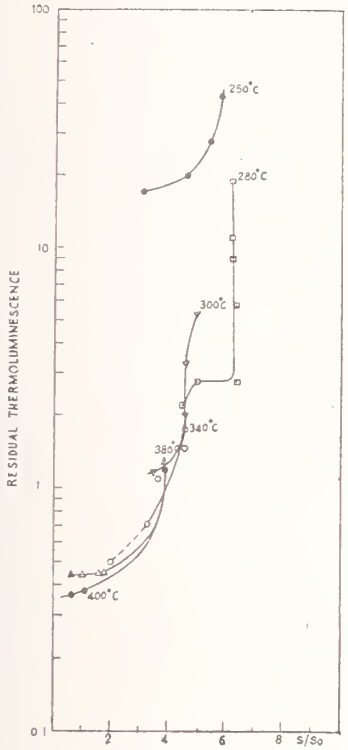

Fig. 3. Change in sensitization factor with annealing at different temperatures for different times.

As has been indicated by Zimmerman[12], we postulate further an association between the TL trap and the luminescence centre. Thus when the luminescence centres increase on irradiation as a result of break up of TCLC, they get spatially associated with the nearest trap available. Now on release of the charge carrier from the trap there is greater probability of recombination with the luminescence centre. When this number has increased sufficiently, as happens after an exposure of about 5×10^4R for glow peak V, there is no further increase in the probability of recombination and maximum response is reached. Similarly after a pre-exposure of the same order followed by 280°C annealing for 1 hour, though the trap responsible for lower temperature peaks have been emptied, the recombination centres continue to be associated with the respective traps. The 280°C annealing does not destroy this association. The TL response of the powder is therefore that enhanced by radiation (radiation sensitization). At 400°C however, the "created trap", TC and the added luminescence centre, LC, combine to form the complex (TCLC). The increased sensitivity is thus removed.

Radiation Damage

The response curves of fig. 2 show decrease beyond the saturation point. The decrease depends upon the total exposure given to the phosphor (order of graphs 1,2 and 3 reverse to 3,2 and 1 beyond saturation). This decrease in response is due to damage effects (13) and is a general feature of LiF thermoluminescence. This is presented in fig. 4. From these graphs as well as those of fig. 2 it appears at least for the first group of peaks, that even after damage the saturation exposure does not alter indicating no change in trap population. This has been verified for various initial exposures. The thermoluminescence output, however, decreases throughout indicating less recombinations. Thus damage to TL in LiF can be attributed to loss of recombination or luminescence centres. This is also indicated by the change in the TL emission spectrum of LiF after damage[14].

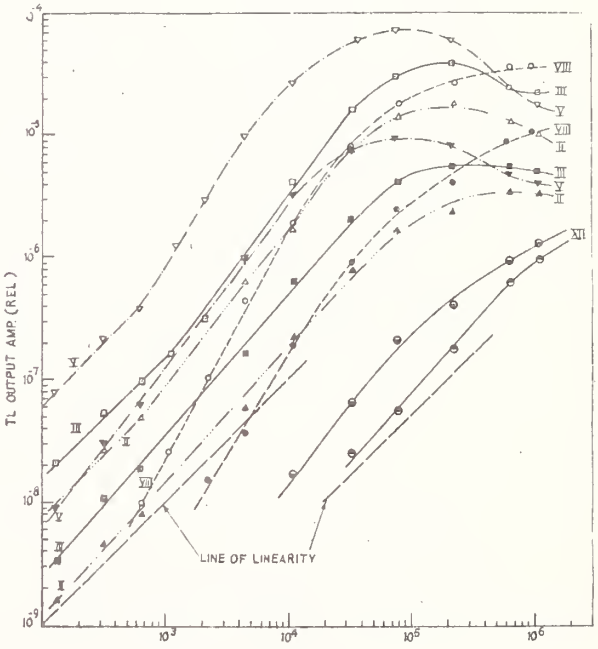

Fig. 4. Damage effect in LiF (T) for 8.3×10^6R. For each peak (Not marked), upper curve is without damage and lower with damage.

Conclusion

The main characteristic required to be seen for LiF in dosimetry is sensitivity. The radiation sensitization in LiF is due to the break up on irradiation of a complex centre (TCLC) into TC and LC which itself is formed while annealing at 400°C.

References

1. Cameron, J.R., Suntharalingam, N. and Keney, G.N., Thermoluminescent Dosimetry, University of Wisconsin Press, Madison, Wisconsin, U.S.A., (1968).
2. Zimmerman, D.W., Rhyner, C.R. and Cameron, J.R., Health Physics 12, 525, (1966).
3. Suntharalingam, N. and Cammeron, J.R. Phys. Med. Biol. 14, 397 (1969).
4. Cameron, J.R. and Zimmerman, D.W., Modifications of the Mathematical model reported in COO-1105-102 and Report COO-1105-113, (1966).
5. Claffy, E.W., Klick, C.C. and Attix, F.H., Proc. 2nd Int. Conf. on Luminescence Dosimetry, Gatlinburg, eds. J.A. Auxier et al. (CONF-680920, NBS, Springfield, Virginia, USA (1968)
6. Kathuria, S.P., M.Sc. Thesis, University of Bombay, Bombay (1974).
7. Jain, V.K., Kathuria, S.P., and Ganguly, A.K., J. Phys. C (Solid St. Physics) 8, (1974).
8. Sunta, C.M., Ph.D. Thesis, Agra University, Agra, (1971).
9. Kathuria, S.P., Bapat, V.N., Sunta, C.M. and Jain, V.K., Paper in this conference.
10. Mason, E.W. and Linsley, G.S., Proc. 3rd Int. Conf. on Luminescence Dosimetry, Riso, ed. V. Mejdahl, (Riso Report No. 249) (Riso: Danish AEC and IAEA) (1971).
11. Sunta, C.M., Bapat, V.N. and Kathuria, S.P., Proc. 3rd Int. Conf. on Luminescence Dosimetry, Riso, ed. V. Mejdahl, (Riso Report No. 249) (Riso:DAEC and IAEA) (1971).
12. Zimmerman, J., J. Phys. C (Solid St. Physics) 4, 3277 (1971).
13. Marrone, M.J. and Attix, F.H., Health Physics 10, 431, (1964).
14. Jain, V.K., Bapat, V.N. and Kathuria, S.P., J.Phys.C(Solid St. Phys.) 6,L343, (1973).

CHANGE IN TL SENSITIVITY OF QUARTZ DUE TO STRESS

M. David and A.K. Ganguly
Health Physics Division
Bhabha Atomic Research Centre
Bombay-400085

Stress and strain caused by progressive and impact pressure loading can change the TL sensitivity of natural quartz. Stress due to progressive loading enhances the TL sensitivity considerably. It is found that sensitisation increases as the amount of stress increases and reaches a maximum at about 1400 kg cm^{-2}. The TL sensitisation obtained is correlated to 'strain hardening' by the dislocation nets produced by stress. In the case of stress caused by impact loading, TL sensitivity is reduced. This may be due to the conversion of quartz to a glassy state at a high stress.

(Quartz; sensitivity; stress; thermoluminisum)

Introduction

TL of quartz has been observed to be affected by the stress to which the crystal is subjected prior to irradiation. The effects of stress on the TL output of quartz have significance in both understanding and applications of TL phenomenon in (i) archaeological and geological datings[1-3] and (ii) radiation dosimetry[4].

This paper reports the results obtained in the studies carried out on the effect of stress on TL of natural quartz.

Experimental Methods

Thin plates (0.5 cm thickness) were cut from naturally available transparent single crystal of quartz along the directions perpendicular to c-axis. These plates were then polished very carefully to obtain flat surfaces to ensure uniformity of stress all over the crystal.

An Instron Universal Tensile Testing Machine was used to give various stresses to the samples.

Two kinds of stresses were applied to the crystal plates: (i) stress by progressive loading along the c-axis and (ii) stress by impact loading along the c-axis. These quartz plates were then powdered using agate mortar to sizes less than 0.151 μ and were used for TL studies.

All the irradiations to gamma-rays were done in ice bath at a rate of 6.9×10^3 R/min.

Results

Effect of Stress by Progressive Loading

The crystals were subjected to stresses of different peak loadings. The desired stresses were developed on the sample by loading at rate of 500 kg/min. The sample was kept in the state of peak stress for three minutes and then the stress was released at the same rate as loading. The stresses given to different plates were 308 $kg.cm^{-2}$. No visible deformation was found in the samples for stresses upto 1400 $kg.cm^{-2}$. For stresses above 1400 $kg.cm^{-2}$ extensive cracks developed in the crystal.

Natural thermoluminescence (NTL, the TL signal naturally present inside the sample prior to any artificial irradiation) glow curves were recorded using 5 mg of the samples. A linear heating rate of 25°C/min was employed over a temperature range of 25°C-500°C. Figure 1 shows the NTL glow curves obtained from all the five samples. Two TL peaks were observed, one at 260°C and

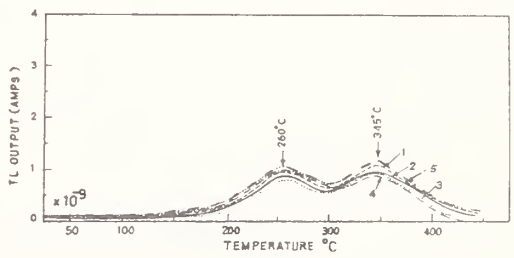

Fig. 1. TL glow curves of unirradiated quartz samples after giving different amounts of stress by progressive loading.

another at about 350°C. No significant difference in TL output was observed between the stressed and unstressed samples.

The stressed samples were subjected to a heat treatment of 400°C for 90 mins. along with an unstressed sample so as to remove the NTL completely. These samples were then given an artificial irradiation (test dose) of 2.4 x 10^5R from a Co-60 gamma source and the glow curves were recorded. There were mainly five glow peaks present in all the samples viz: at 75°C, 110°C, 180°C, 235°C and 320°C. Areas under glow curves are plotted against stresses in Figure 2.

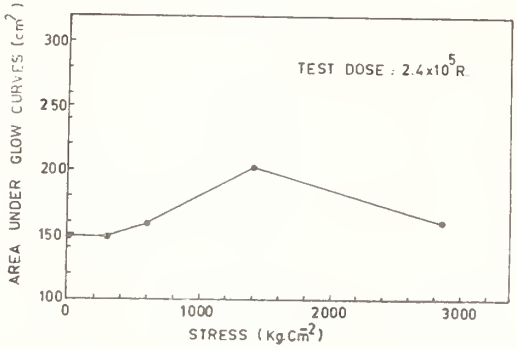

Fig. 2. Effect of stress (by progressive loading) on Thermoluminescence of Transparent quartz.

TL output is enhanced very slowly with the increase in stress till 600 kg cm^{-2} beyond which it goes through a stress developing maximum sensitivity in the crystal and falling back to almost the value obtained with the unstressed crystal at 2875 $kg.cm^{-2}$. The fall in the TL output beyond 1400 $kg.cm^{-2}$ appears to be associated with plastic deformations occurring to the samples at heavy loads.

The sensitisation produced is by overall enhancement of the entire glow curve. Even though the change in sensitisation is observed no change in behaviour in respect of linearity of response to gamma dose was observed. The glow peaks of the samples subjected to stress, saturate at the same dose as that of unstressed sample.

Activation energies of the glow peaks of the stressed samples were calculated using the initial rise method[5] (see Table-1). Average activation energies of the glow peaks of the samples are plotted against the stresses in figure 3. It is seen that the activation energies increases in the cases of all the peaks and reaches a maximum at 1435 $kg.cm^{-2}$. It is to be remembered that TL emission also was maximum around this stress.

Table-1

Effect of stress on thermal activation energy of different TL glow peaks of transparent quartz

Peak temp.	Activation energy (eV) Natural sample	Sample after stress (kg/cm²) 308	1436	2873
70°C	.658	.658	.732	.621
110°C	.298	.653	.675	.582
180°C	.718	.784	.843	.814
235°C		.873	.906	.829
320°C	.831	.865	.911	.878

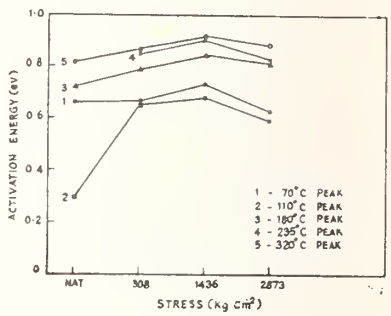

Fig. 3. Effect of stress on Thermal Activation Energy of different glow peaks of transparent quartz.

Effect of Stress by Impact Loading

Stress by impact loading was done by dropping a load of 200 kg from a height of 30 cm on a (10 x 8 x 5 mm) plate. The sample got crushed and was further crushed to a standard mesh size (0.151 mcs). This sample was heated at 400°C for 90 minutes and then given a test gamma dose of 2.4 x 10^5R and the TL was measured. It was found that the sensitivity was reduced considerably. The glow curves of the stressed and unstressed samples are given in Figure 4.

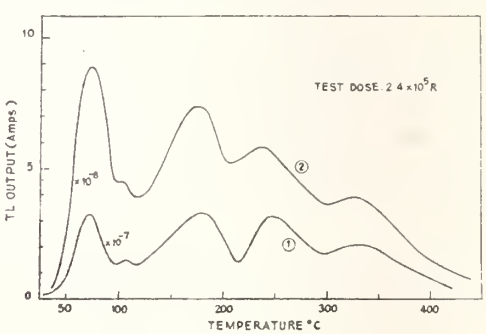

Fig. 4. Effect of stress by impact loading on TL of transparent quartz.

The activation energies of the TL glow peaks of the sample subjected to impact loading were also found to have reduced considerably.

Discussion and Conclusion

Mc Dougall[4] explained the effect of stress on the TL output of quartz as due to variation in free energy associated with trapped electrons of the crystal, which in turn is related to the formation and annihilation of lattice dislocations.

The initial increase in the observed TL (cf. fig. 2) after giving different stresses can be correlated to the strain hardening due to the development of dislocation nets in the crystal. If the argument is valid, the stress induced sensitisation should be initiated at the elastic limit of the crystal and should reach a maximum during the early stage of permanent deformations. The sensitisation of the sample starts around a stress of 600 kg cm^{-2}. This means that the 'hardening' due to the development of dislocations starts at about this stress. It is possible that the TL sensitisation by stress is associated with 'strain hardening' in quartz crystals and that the elastic limit for this sample is at about 1400 $kg.cm^{-2}$, beyond which the crystal damage occurs. The fall in sensitisation may be due to the plastic deformations in the lattice and annihilation of dislocations during the recovery from strain hardening.

The reduction observed in TL output after impact loading of the crystal may be due to the conversion of quartz to a glassy state at a high stress. Short[6] gives data showing the conversion of quartz to a glassy state at a load of 300 K.bars. It is to be noted that in our studies the stress given to the crystal by impact loading was also well above the suggested pressure for the conversion.

In archaeological and geological dating of the samples, natural TL and its calibration against artificial TL is very important. The present investigations bring out that in these types of applications of TL, the geological stress that the sample might have received, should be taken into consideration.

References

1. Ichikava, Y. and Higashimura, T. Application of TL of quartz, paper presented in conference on TL at Tennessee (1969).
2. Aitken, M.J. TL Dating in Archaeology, in TL of Geological Materials (Mc Dougall, D.J.; Ed) Academic Press, London and New York, p. 369 (1968).
3. Zeller, E.J. Geological Age Determination by TL, in TL of Geological Materials (Mc Dougall D.J.; Ed). Academic Press, London and New York (1968).
4. Mc Dougall, D.J.; Some TL Properties of quartz and its potential as accident radiation dosimeter, Paper presented in 3rd International Conf. on TL (1971).
5. Randall, J.T. and Wilkins, M.H.F. Proc. Roy. Soc., A-184, 366 (1945).
6. Short, M.N.; J. Geology, 78 705 (1970).

Discussion

D.V. Gopinath

Does this enhanced sensitivity change with time or is it permanent ?

If permanent, does it mean that by pounding it in different ways, one can obtain different sensitivities?

M. David

Yes, it is a permanent sensitisation in the sense, it will not be desensitised by itself with time. The sensitisation produced is not dependent on the method of powdering; it depends on the amount of stress to which the sample was subjected.

ESR-TL CORRELATION STUDIES IN $CaSO_4$(RE) PHOSPHORS

K.S.V. Nambi
Health Physics Division
Bhabha Atomic Research Centre
Bombay-400085, INDIA

ESR and TL glow curve measurements were done after gamma irradiation at room temperature of $CaSO_4$ samples doped individually with all the lanthanide series rare earth (RE) elements, an yttrium doped sample and a few undoped samples of different origins. Samples were prepared in the laboratory using standardized techniques and concentration of the dopant in individual doped samples was maintained at a typical value of 0.1% by weight in $CaSO_4$. ESR as well as the TL glow curve patterns of all the sixteen samples were almost identical excepting for relative intensity differences. By observing the build up of these signals with increasing gamma dose and also by following the decay of these for storage at room temperature, it could be inferred that the nature of the trapping species indicated in the ESR and TL glow curve patterns are the same. The behaviour of these patterns for various thermal annealings at different temperatures have revealed that the trapping species might have configurations like SO_4^-, SO_3^-, O_3^- etc. having different thermal stabilities and these are responsible for the observation of the multi-peak TL glow curve structure involving a variety of thermal activation energies. The increased intensities observed in the ESR and TL signals of the differently doped samples indicate that presence of various RE impurities in $CaSO_4$ enhances to different extents the stabilities of these trapped species after gamma irradiation.

($CaSO_4$; correlation; dose; ESR; gamma ray; glow curve; irradiation; TL)

Introduction

In thermoluminescence, trapped electrons and holes either at an impurity ion or at a host lattice ion or at a complex involving both, play the key role and if any of these are paramagnetic in nature, it is evident that ESR technique can be effectively applied to determine the structure of these trapping centres. This paper presents the results obtained in an attempt to correlate ESR-TL characteristics of rare-earth doped calcium sulphate [$CaSO_4$(RE)] phosphors after gamma irradiation at room temperature (RT).

Experiments

$CaSO_4$ (polycrystalline) samples doped individually with all the rare earths of the lanthanide series and an yttrium doped sample were prepared in the laboratory by the simple technique of coprecipitation and evaporation. The dopant concentration chosen was about 0.1% by weight. A blank $CaSO_4$ sample without addition of any dopant was also prepared.

A varian dual cavity X-Band ESR spectrometer employing 100 KC/sec field modulation was used to record the ESR spectra of gamma irradiated samples at room temperature. The TL recorder used has been described in detail elsewhere[1].

Results and Discussions

TL Glow Curves of Gamma Irradiated $CaSO_4$ (RE) Phosphors

All the $CaSO_4$ samples (doped and undoped) exhibited varying TL outputs but their TL glow curves were characterised by the appearance of glow peaks at more or less the same temperatures; the relative intensities of the various glow peaks were also varying from sample to sample[1]. Actually about twelve glow peaks could be resolved in each glow curve by 'partial bleaching technique' and fig. 1 gives TL glow curve obtained from gamma irradiated $CaSO_4$(Dy) phosphor, with all the glow peaks labelled from I to XII.

It is known that TL glow curves are characteristic of the various traps exis-

ting in a phosphor which are thermally deactivated as the temperature is progressively increased. From the similarity of the glow peak temperatures obtained for the sixteen samples it is amply demonstrated that the dopants have not altered the basic nature of the traps already existing in the base matrix; they result only in different luminescence efficiencies. In fact the activation energies of these traps have been found to be directly proportional to the peak temperatures independent of the dopant added. That the impurities already present in the starting material of $CaSO_4$ had no influence on the characteristic TL glow peak temperatures obtained in all the doped specimens was confirmed by studying the TL glow curve pattern of pure $CaSO_4$ samples of different origins all of which gave the same glow peak temperatures[1].

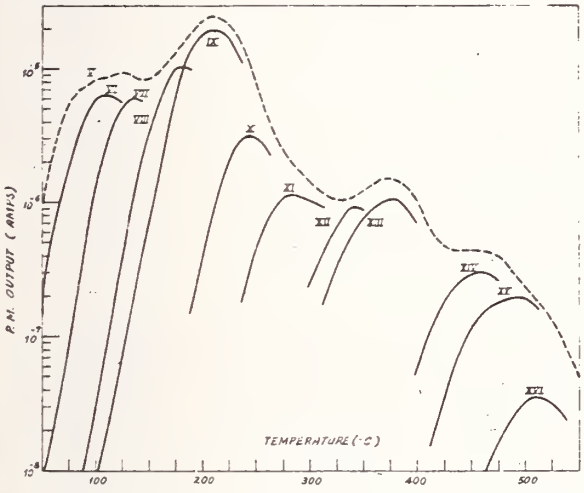

Fig. 1. TL glow curve of gamma irradiated $CaSO_4$(Dy).

ESR Spectra of Gamma Irradiated $CaSO_4$(RE) Phosphors

None of the samples gave any ESR signal prior to gamma irradiation. The ESR patterns show some remarkable similarities except for the cases of La, Lu, Gd and Eu dopants in $CaSO_4$. The cause for this exception has not been analysed in the present work. In general, a six peak spectral pattern is seen having the same set of g-values (2.001, 2.0022, 2.003, 2.004, 2.0057 and 2.0113) and even the four exceptional cases exhibit peaks which could have enveloped the above generally observed six peak spectral patterns.

As the ESR of irradiated solids is due to the unpaired trapped charge carriers in the material, the similarity of the ESR patterns obtained above can be construed to demonstrate that the different traps are the basic nature of the host material and the dopants influenee only the relative populations in the various traps. Whether the trapping species shown in the ESR spectra are the same which are involved in the TL glow curves was verified by ESR-TL correlation studies the result of which are shown in the next section.

ESR-TL Correlations

Gamma Dose vs. ESR-TL Signals Build-up

The ESR signal intensity obtained for various gamma irradiations has been monitored and plotted in fig. 2 for the case $CaSO_4$ (Tm). The ESR signal intensity increases with dose till about 10^6R beyond which saturation sets in. This pattern is very much analogous to the TL intensity vs dose relationship shown in the same figure. A condition has thus been satisfied for a possible conclusion that the trapping species involved both in ESR and TL are the same.

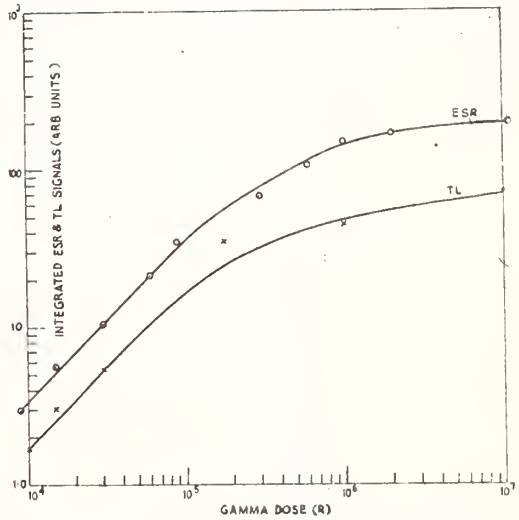

Fig. 2. Gamma dose build-up curves for ESR and TL in $CaSO_4$ (Tm).

Room Temperature Decay Characteristics of ESR-TL Signals

Further evidence for the nature of the trapping species being the same both in the TL and ESR, has been provided by the parallel nature of the decay patterns of these signals for storage of the gamma irradiated sample at room temperature. Fig. 3 presents the results obtained for the case of $CaSO_4$ (Tm).

Thermal Annealing Characteristics of ESR-TL Signals

The bleaching of the ESR signals of

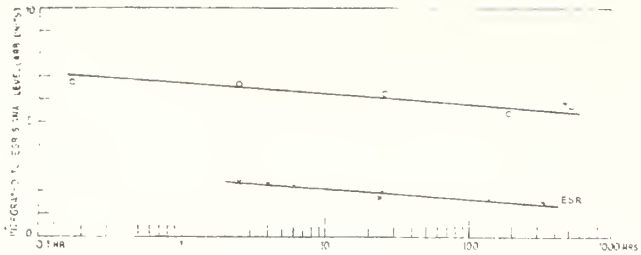

Fig. 3. Decay of TL and ESR of gamma irradiated $CaSO_4$(Tm) for storage at RT.

gamma irradiated $CaSO_4$ phosphors corresponding to various stages of bleaching of the TL signal was studied after annealing the samples at different temperatures successively. The temperatures chosen were 400°K, 500°K, 675°K and 800°K and samples were heated for half an hour each at these temperatures. These treatments successively erased the TL signals in four stages of three peaks each: I-III, IV-VI, VII-IX and IX-XII respectively. The ESR patterns were almost identical for all the samples and fig. 4 presents the thermal annealing behaviour of the ESR signal for the case of gamma irradiated $CaSO_4$(Tm).

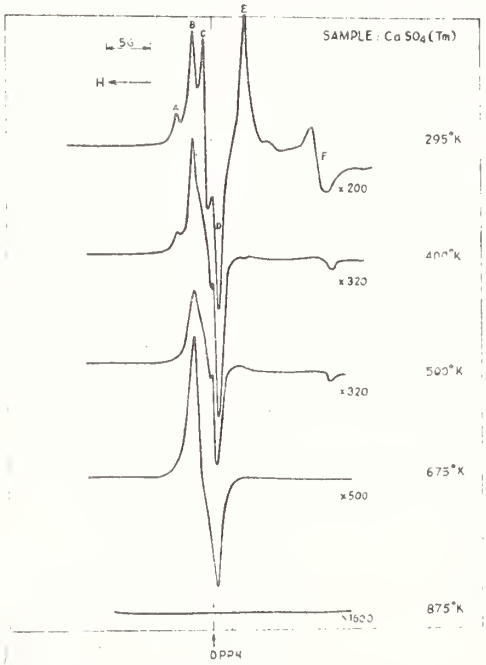

Fig. 4. Typical thermal annealing characteristics of ESR signals of gamma irradiated $CaSO_4$ powders.

The presence of isolated paramagnetic radicals like SO_4^-, SO_3^- etc. in gamma irradiated sulphate salts like K_2SO_4, Na_2SO_4, $BaSO_4$ etc almost independent of their environment in the crystal lattice, has been verified by many workers. Hariharan et al obtained isotropic lines with g-values of 2.0045 and 2.01 respectively for SO_3^- and anisotropic lines for SO_4^- and SO_2^- in irradiated Na_2SO_4 crystals at room temperature; Gromov et al[4] obtained axially symmetric lines for SO_3^-, O_2^- and O^- in K_2SO_4; Morton et al[5] observed that SO_4^- could be observed even upto 300°K in irradiated K_2SO_4 and SO_3^- is the more stable radical at higher temperatures; Spitsyn et al[6] detected SO_4^- in irradiated $SrSO_4$ even upto 350°C; Gupta et al[7] identified the complicated powder spectrum obtained at LNT for irradiated $BaSO_4$ with radicals like SO_4^-, SO_3^-, SO_2^-, SO_2^+ and O_3^-.

The range of g-values deducible for the various signals in the six-peak envelope obtained for the $CaSO_4$ powder in the present study compare well with the range of g-values reported for many of the radicals mentioned above. It is, therefore, reasonable to expect that ESR signals obtained in the present study of gamma irradiated $CaSO_4$ are mostly due to host lattice radicals like SO_4^-, SO_3^-, O_3^- etc and that the stability of these radicals has been affected by the individual RE dopants to different extents as indicated by the differences in the intensities of these signals.

The individual indentification of the various radicals in the complicated six-peak ESR spectra obtained, is rather difficult as these have been obtained for powder samples and at a single frequency. However a careful examination of the spectrum and its annealing behaviour (fig. 4) does reveal that the various radicals are bleached effectively at different temperatures (the ESR spectrum does not bleach uniformly over its entire field range). The less complicated, nearly isotropic line (g 2.0040) seen in the penultimate stage of the annealing process, perhaps belongs to SO_3^- radical which has been observed at comparably high temperatures with more or less the same g-value in sodium and potassium sulfates. The line F is evidently composed of superimposed signals and the signal represented by the part which is completely bleached by annealing at 400°K is probably due to O_3^- having a near isotropic g-value of about 2.012. In the context of TL, these various radicals, expecially SO_4^-, SO_3^- and O_3^- represent radicals with trapped holes characterised by different activation energies.

Conclusion

From the foregoing results and dis-

cussions, it can be concluded that hole traps provided by the host lattice ions having configurations of SO_4^-, SO_3^-, O_3^- etc. give rise to the observed TL glow curve pattern in $CaSO_4$ and addition of rare-earth ions seem to affect the stability of these various traps to different extents. Combined with our findings on the TL emission spectra it could be said that the TL process in $CaSO_4$ (RE) is perhaps similar to that in CaF_2(RE) involving $RE^{3+} \underset{\text{heat}}{\overset{\text{irradiate}}{\rightleftharpoons}} RE^{2+}$ reactions with simultaneous trapping and release of holes at the sulphate sites during irradiation and heating respectively.

Acknowledgements

I am grateful to M.V. Krishnamurthy and M.D. Sastry or Radiochemistry Division for their help in recording the ESR spectra. Thanks are also due to V.N. Bapat for the help he rendered during the course of this work.

References

1. Nambi, K.S.V, Ph.D. Thesis, Gujarat Univ., Ahmedabad (1974).
2. Atkins, P.W. and Symons, M.C., 'The Structure of Inorganic Radicals' Elsvier Pub. (1967).
3. Hariharan, N. and Sobhanadri, Mol. Phys. 17, 507 (1969).
4. Gromov, V.V. and Morton, J.R., Can. J. Chem. 44, 527 (1966).
5. Morton, J.R., Bishop, D.M. and Randic, M., J. Chem. Phys. 45, 1885 (1966).
6. Spitsyn, V.I., Gromov, V.V. and Karaeva, C.G., Dokl. Akad. Nauk, S. S.S.R., 159, 178 (1964).
7. Gupta, N.M., Luthra, J.M. and Shankar, J., Rad. Eff. 21, 151 (1974).

Discussion

S. Makra

I feel that heating the sample and detecting the emitted light is not the only possibility for TL evaluation. Efforts like yours besides theoretical importance are of practical importance too.

K.V.S. Nambi

Thank you for your kind comments.

NEUTRON DOSE EVALUATION USING CALCULATED NEUTRON SPECTRA

S. Makra
Central Research Institute for Physics
1525 Budapest 114. P.O.B. 49 Hungary

Measurements carried out at shielded neutron sources such as nuclear reactors and neutron generators showed the importance of intermediate energy neutrons not recorded by most of the commonly used monitors. Based on these measurements correction factors were established for scintillation survey instruments, track plates, activation detectors and other routinely used devices. Although this simple technique has proved to be very useful, the need for a more sophisticated evaluation method was evident. With this in mind we started with the calculation of neutron spectra transmitted through and reflected from shielding slabs. Calculations were performed by using the MUSPALB albedo code developed in our Institute as well as with the 05R code written in Oak Ridge, USA. Over the last four years spectra for different reactor and neutron generator sources with H_2O, polythene, concrete, beryllium, aluminium, graphite, iron, boron loaded polythene and iron-concrete mixture shields were calculated for thicknesses ranging from 5 cm to 200 cm. Calculated spectra were used for personnel-, survey-, and nuclear accident dosimetry evaluation. International comparison measurements have shown the value of this evaluation method. For illustration several examples are given.

(Computer code, dose, dosimetry, monitor, neutron, shielding, spectrum)

Introduction

Early measurements of the stray neutron field carried out at shielded neutron sources showed, that the energy spectrum of the neutrons in such circumstances is quite wide. The leakage spectrum of shielded nuclear reactors, radioactive neutron sources, or even 15 MeV neutron generators span from the source energy down to the eV range or even to thermal energies. Dosimeters used for personnel monitoring, on the other hand, in spite of the considerable progress achieved in the past decades, do not cover this wide energy range in Fig. 1. In my lecture I intend to show how evaluation techniques can be established to take into account the fraction of the neutron dose not recorded by a given dosimeter. This requires the knowledge of the spectrum in question. In the first part I shall deal with investigations performed with moderator devices, these bulky instruments are not used as personnel dosimeters (it's somewhat difficult to wear a 20 lb sphere on top of your working clothes!) but the information yielded by them is readily applicable to dosimetry evaluation. In the second part I shall discuss problems concerning leakage spectrum calculations and their applications in dosimetry evaluation.

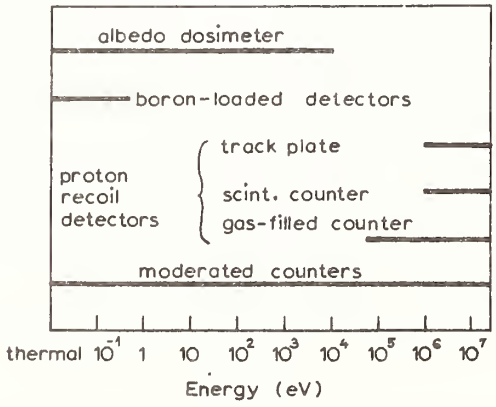

Fig. 1. Diagram showing the energy range of some commonly used neutron monitors.

Dose Fraction Measurements

Theoretical considerations as well as monitoring results showed the importance of the intermediate energy neutrons not monitored by the commonly used neutron dosimeters.

Nachtigall's measurements[1] showed that the contribution of the neutrons in the energy range 0.5 eV - 0.1 MeV to the total dose is quite high: sometimes exceeding 90 % in the vicinity of experimental and power reactors in Fig. 2. Another important conclusion was that the intermediate dose fraction varies by more than an order of magnitude depending on several parameters, which were not established

during the course of these investigations.

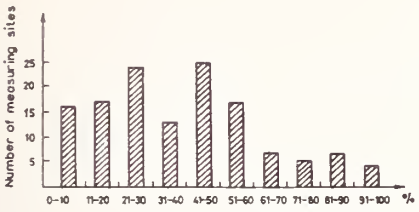

Fig. 2. Dose percentage due to 0.5 eV - 0.1 MeV neutrons averaged from data for 135 measuring sites (Nachtigall, 1965).

In Budapest in 1967, we commenced with the investigation of the stray radiation field of our experimental reactors using a measurement technique similar to that developed by Nachtigall[2]. The neutron dose rate for the whole energy spectrum in question was monitored by rem-counters, the dose resulting from the slow and fast neutrons being monitored by scintillation counters. Owing to the similarity in the responses of the slow neutron survey and personnel monitors (boron-loaded scintillators and cadmium covered films) on the one hand, and those responses of the fast neutron survey and personnel monitors (proton recoil scintillation counters and track plates) the results were applicable for personnel dose evaluation. Figures 3 and 4 illustrate typical monitoring results[3]. Based on several measurements similar to the one shown here calibration factors were established.

For instance the multiplication factor of 9 - 32 was established as that applied to track plates in order to obtain the total neutron dose for the hall of our WWR-S type reactor. The introduction of this correction considerably improved the accuracy of our dose evaluation and at the same time emphasized the importance of the search for dosimeters with a wider energy range.

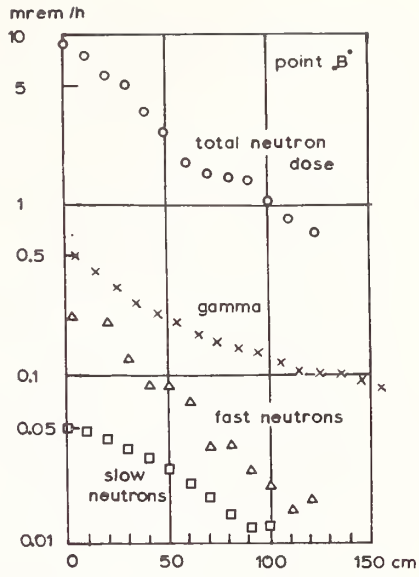

Fig. 3. Dose equivalent vs. height over the top shield of the WWR-S reactor for neutrons in the 10^{-2} - 10^{7} eV, E<0.5 eV and E>1 MeV energy range (denoted as "total neutron dose", "slow neutrons", and "fast neutrons", respectively) as well as for gamma radiation.

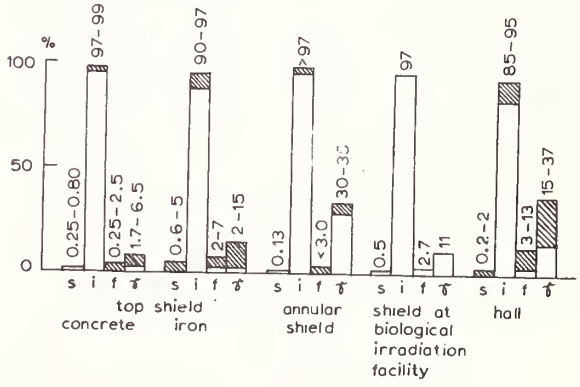

Fig. 4. Percentage dose of slow, intermediate and fast neutrons, as well as gamma rays at different sites of the shield of the WWR-S reactor.

Average Energy Determinations

Average energy determinations of the radiation field yield information which is also applicable for dosimetry evaluation. For this purpose several techniques were developed. One, developed in the Lawrence Radiation Laboratory[4] is based on the determination of the spatial distribution of the thermalized neutrons inside a moderator. For source energies from a few tens of keV up to 15 MeV the shape of the distribution is a measure of the source energy. The multisphere technique[5] makes use of the variation in the counting rate ratio of different diameter Bonner-sphere counters when irradiated with different energy neutrons. In our laboratory both techniques were investigated with the aim of developing a theory for average energy determina-

tions and for checking calculations and measurements. It was shown that both techniques, owing to unavoidable instrument distortions, measure a quantity differing from the mean energy[6,7].

Mean energy and another widely used quantity the effective energy, are defined as follows:

$$\text{mean energy } \bar{E} = \frac{\int E.\varphi(E)\,dE}{\int \varphi(E)\,dE}$$

$$\text{effective energy } E_{eff} = \frac{\int_E d(E).\varphi(E)\,dE}{\int d(E).\varphi(E)\,dE}$$

where $\varphi(E)$ represents flux density and the $d(E)$ weight function is the flux-to-dose conversion function. Both $\bar{E}$ and E_{eff} have a practical significance. However measurement techniques determine a quantity $\tilde{E}$ which is defined as

$$\text{average energy } \tilde{E} = \frac{\int E.k(E).\varphi(E)dE}{\int k(E).\varphi(E)dE}$$

where $k(E)$ is a weight factor, characteristic for the instrument, $\tilde{E}$ the quantity measured but $\bar{E}$ or E_{eff} is the one actually used.

A monitoring result is given in Fig. 5 as an example showing the relationship between these quantities. These results not only show a good agreement between theory and measurement but emphasize the importance of using well-defined terms, as a discrepancy of a factor of two may occur if instrument response is not correctly taken into account.

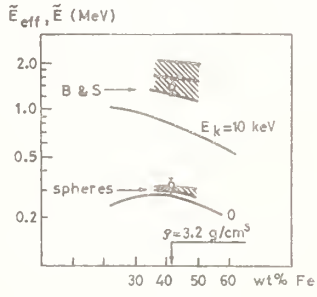

Fig. 5. Calculated and measured effective energies, and average energies behind a 100 cm thick iron-loaded concrete wall. Measured and calculated effective energies (open circles and hatched stripes, respectively) are presented for both the Block and Shon, and the paired spheres technique. The horizontal range of the hatched stripes corresponds to the estimated uncertainty in the fraction of the iron aggregate (35-50 wt %).

Although average energies and dose fractions obtained by measurements proved to be very useful in dosimeter evaluation, the need for a more sophisticated evaluation method was evident. With this in mind we started with the calculation of neutron spectra transmitted through and reflected from different shielding slabs.

Spectrum Calculations

For the calculation of the spectrum modifying effect of different shields we used two computer codes: one, the MUSPALAB code developed by Vertes[8] makes use of the so called albedo formalism, the other, the 05R5S, is a Monte Carlo code. The original version of this code, the 05R, was written in Oak Ridge[9], and was adapted to our institute's ICL 1905 computer, and several modifications were performed in order to reduce the running time[10,11]. Both codes can handle neutron sources with different energy and angular distributions. The shielding layers are taken as planar, calculations can be made for one-component slabs, for mixtures and for laminated shields. Both transmitted and reflected neutron spectra are calculated. The energy range of the output spectra spans from the maximum source energy down to thermal energies.

Using the computer codes MUSPALB and 05R5S spectrum calculations were performed for several different reactor and monoenergetic sources and for several shielding layers. Fission, light-water moderated reactor, fast reactor escape and monoenergetic neutrons were taken as source, the shielding layer composition was water, polyethylene, lucite, concrete, aluminium, beryllium, iron, and several mixtures of iron, concrete and boron. The shield thickness ranged from 10 to 60 cm in the 05R5S calculations, and from 5 upto 120 to 200 cm when using the MUSPALB code.

Some typical results are shown in the following figures: Fig. 6 shows fission neutrons after passing through 20 cm and 100 cm thick boron-loaded concrete; in Fig. 7 spectra of fission neutrons are plotted after passing through 100 cm thick iron-concrete shields of different mixing ratio[12]; for neutron generator survey evaluation, the spectra displayed in Fig. 8 were applied[13].

Spectrum Comparison and Evaluation

In 1972 after calculating several hundreds of leakage spectra we commenced the compilation and evaluation of spectra calculated by us or taken from the literature . The final purpose of this work is to prepare a compendium of neutron leakage spectra to facilitate dosimetry, primarily nuclear accident dosimetry

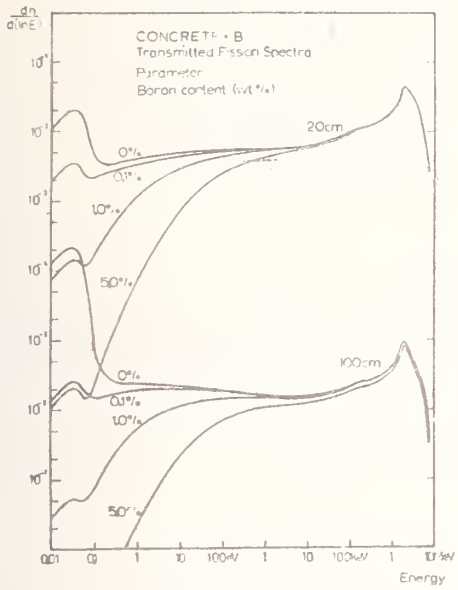

Fig. 6. Flux density vs. energy plots of fission neutrons after passing through 20 cm and 100 cm thick concrete with different boron contents (in wt %).

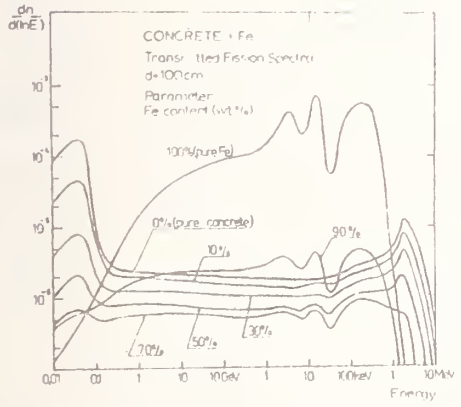

Fig. 7. Effect of the concrete-iron mixing ratio on the shape of the spectrum and on the flux reduction of fission neutrons after passing through a slab 100 cm thick. Parameter: Fe content in wt %.

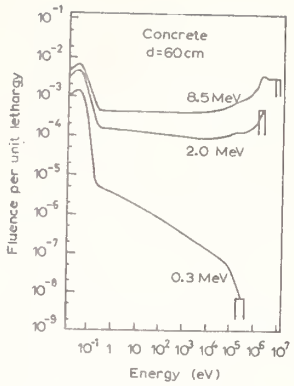

Fig. 8. Spectra of monoenergetic neutrons transmitted through 60 cm concrete. The flux density of thermal neutrons depends only slightly on source energy.

evaluation, by making available spectra to laboratories involved in dosimetry, but lacking manpower and/or computers to develop their own computation techniques.

In order to facilitate spectrum comparison and evaluation several handling codes were written. SPECTRANS-2[14], for instance, calculates the spectra for 48 predetermined energy intervals, computes kerma and dose-equivalent spectra as well as dose fractions and average energies. The calculated spectra are written on a magnetic tape and plotted in a variety of different formats. Another computer code used for spectrum handling is the TRESPASS[15].

Some representative results are presented in Figs. 9 and 10: Fig. 9 shows spectra of fast neutron sources transmitted through 30 cm thick iron as measured in the Soviet Union and calculated by us; Fig. 10 shows fission neutrons passed through 40 cm water slabs calculated by the O5R5S and the MUSPALB code[16]; Fig. 11 gives results for 5 MeV monoenergetic neutrons and a 10 cm borated Polythene slab[17,18].

For the calculation, handling and application for evaluation of neutron spectra a computer code family has been developed, which is shown schematically in Fig. 12.

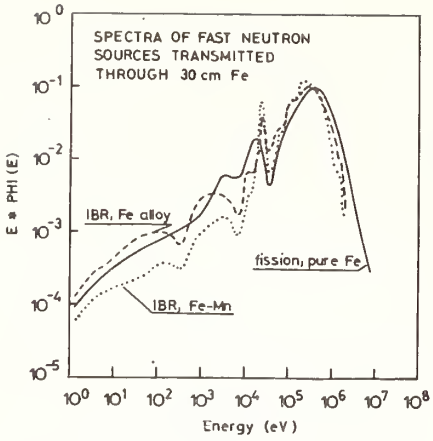

Fig. 9. Spectra transmitted through 30 cm iron or steel slabs. The calculation for a fission spectrum and pure iron (solid line) is compared with two spectra measured at the IBR fast reactor; the "Fe-Mn" curve (dotted line) is for a ferro-manganese steel, while the "Fe alloy" curve (dashed line) is for a steel containing Mn, Cr, Ni and Co.

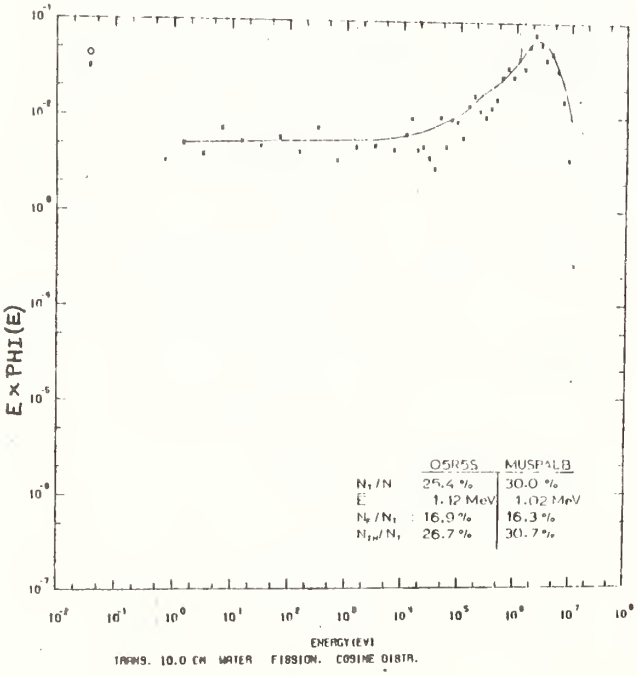

Fig. 10. Fission neutrons after passing through 10 cm water calculated by the O5R5S and the MUSPALB codes. For comparison the following quantities are given: fraction of transmitted neutrons, mean energy, percentages of slow and E>2.5 MeV neutrons in the transmitted spectrum.

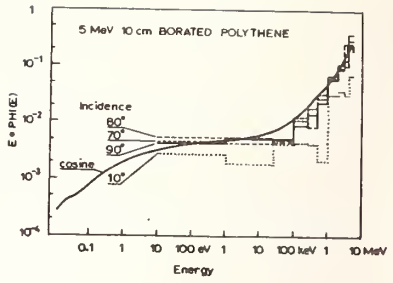

Fig. 11. Spectra of 5 MeV neutrons transmitted through a 10 cm thick polyethylene slab for various angles of incidence.

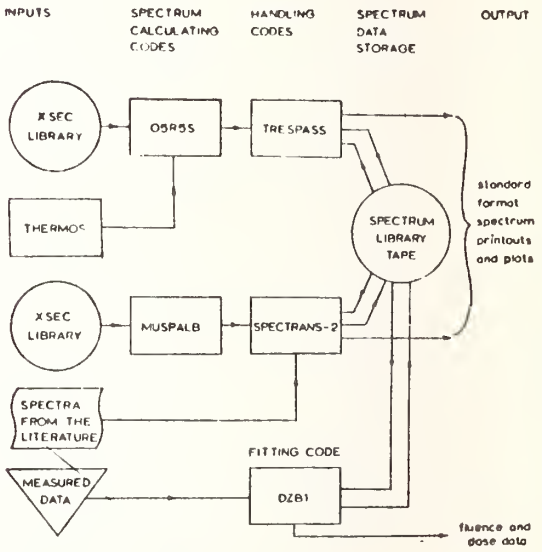

Fig. 12. Scheme showing the computer code family used for spectrum calculation and dosimetry evaluation.

Spectrum Applications for Dosimeter Evaluation

Survey Results of Shielded Reactors

In the early sixties only fast and slow neutron detectors (cadmium covered film, slow and fast neutron scintillation counters, track plates) had been used in our institute for reactor surveys and personnel monitoring. In 1966, Bonner sphere techniques were introduced. In order to improve the precision of the neutron dose evaluations, calculations were performed for determining the readings of the devices mentioned above. Calculated results[19] for two rem counters are given in the following three figures (Figs. 13-15)[19], and their response functions are shown in Fig. 16. Results show that, as a rule, Bonner sphere survey results can be considered as quite

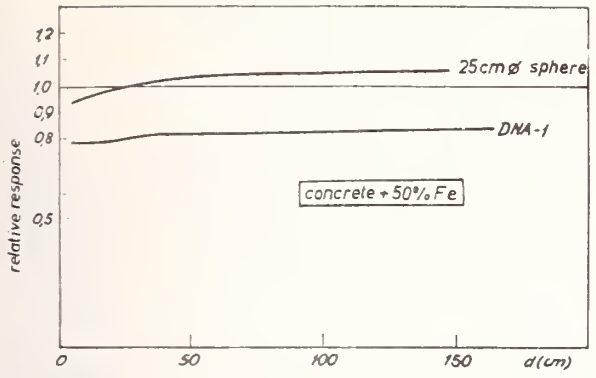

Fig. 13. Relative response of two rem counters for fission neutrons which have passed through concrete + iron layers of different thicknesses.

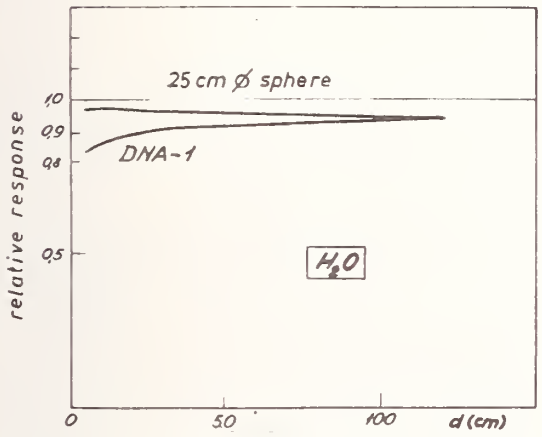

Fig. 14. Relative response of two rem counters for fission neutrons which have passed through water layers of different thicknesses.

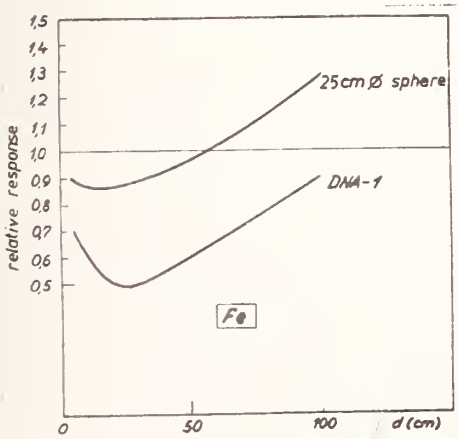

Fig. 15. Relative response of two rem counters for fission neutrons which have passed through iron layers of different thicknesses.

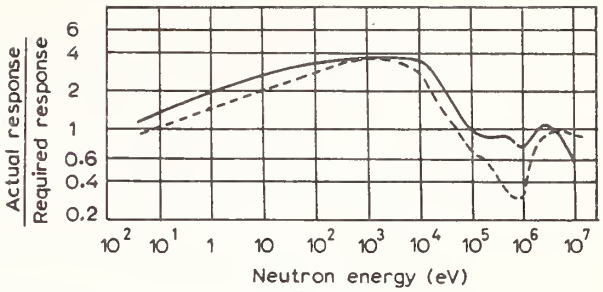

Fig. 16. Relative deviations of the DN-A-1 rem counter (dashed curve) and a 10-in. Bonner sphere (solid curve) from the ICRP response curve.

accurate (there is little point in applying a correction smaller than 10%), however for a 100 cm thick iron-shielded reactor a 30% over-reading occurs which we consider to be significant.

The evaluation of a proton recoil scintillation survey instrument measurement requires much sophistication, as the set of graphs shown in Fig. 17 proves it. Here, the instrument reading is plotted against shield thickness for a light-water reactor. Parameters are shielded composition and detector discrimination level. The two upper graphs show that for iron-loaded concrete, independent of the mixing ratio as well as the discrimination level, the relative reading is 0.4 - 0.5, i.e. an average correction factor ~ 2 can be applied. This is not true for iron shields where the detector reading happens to be one or even two orders of magnitude lower than the actual dose strongly depending both on shield thickness and discriminator setting.

Dose percentages of intermediate energy neutrons (1 eV $<$ E $<$ 1 MeV i.e. the energy range not monitored by the old-

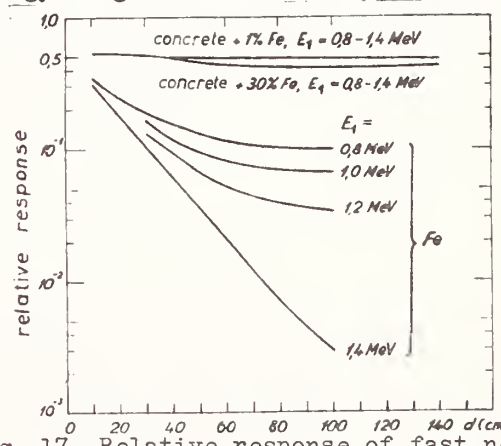

Fig. 17. Relative response of fast neutron detector for various shield materials and discrimination levels.

fashioned slow and fast neutron survey instruments) are illustrated in Fig. 18 determined by measurement and calculation. It should be noted that the fairly good agreement between theory and experiment may be misleading, for in many cases complicated shield geometry, scatter, or other factors impossible to include into the calculation model may cause large discrepancies.

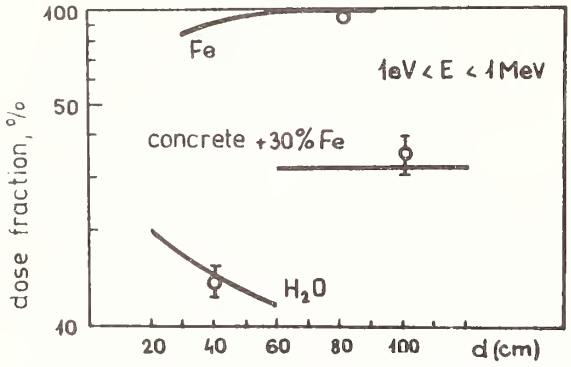

Fig. 18. Dose fractions of intermediate energy neutrons behind the shields of light-water reactor sources. Circles: measured values; lines: calculated data.

Evaluation for a Scattered Neutron Field

The following results show an example of the application of backscattered spectra in dosimetry evaluation for complex geometries. The ZR-6 critical assembly is a light-water moderated, enriched uranium fuel system, located in a well some distance below floor level. Neutron radiation in the reactor hall is due mainly to scattering from walls and other structures. The walls are of concrete, while aluminium and iron are the other structural materials. The contribution to the dose of the radiation scattered from different materials varies from point to point in the hall. Thus the dose at a given point can be expressed as the linear combination of the doses due to the scatter by concrete, Al, and Fe:

$$D = k_c D_c + k_{Fe} D_{Fe} + k_{Al} D_{Al}$$

where D_c, D_{Fe} and D_{Al} denote the respective doses resulting from the scattering by concrete, iron and aluminium, and k_i-s are the relevant weight factors. Owing to the complexity of geometry the k factors cannot be determined. Instead, we determined the maximum possible variation in spectral shape, in Fig. 19 (Makra, 1973).

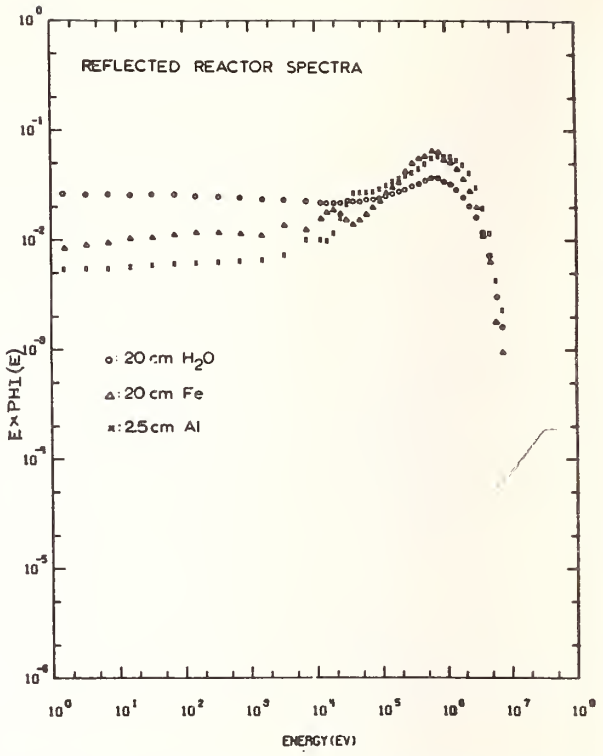

Fig. 19. Spectrum from a light-water reactor after being reflected from slabs of different materials.

By using these spectra correction factors for the nuclear emulsions and fast neutron scintillation monitors, as well as for sulphur activation detectors routinely used for neutron monitoring were obtained (Table 1). These results - which were proved by measurements for some selected cases - show that average correction factors can be used with reasonable accuracy:

$$K(E > 1 \text{ MeV}) = 2.1 \pm 0.5$$

for nuclear emulsion and scintillation proton recoil detectors and

$$K(E > 2.5 \text{ MeV}) = 8.5 \pm 3$$

for sulphur activation detectors.

Nuclear Accident Dosimeter Calibrations

The two preceding examples were for complex situations where simplifications were unavoidable. Far more accurate evaluation was applied in the problems discussed here.

Highly sophisticated evaluation techniques can be used when the source spectrum and the irradiation geometry are

Table 1

Correction factors for detectors having 1 MeV and 2.5 MeV energy thresholds, irradiated with the radiation of the ZR-6 critical assembly, scattered from the walls and from other structures. The spread of the values is caused by the spectrum changes of the assembly due to differences in water reflector thickness.

Reflecting material	Correction factor (fission - reactor)	
	E > 1 MeV	E > 2.5 MeV
concrete	1.7 - 2.2	5.6 - 7
iron	1.9 - 2.6	8.3 - 11.5
aluminium	1.6 - 2.1	5.9 - 8.0

well known. This was the case when we performed calibration runs at the Oak Ridge National Laboratory with the Dosar facility[20] or in Vinca near Belgrade, Yugoslavia, with a heavy water assembly[21]. As an example the dose evaluation procedure for NAD dosimeters positioned on human phantoms will be discussed here. For the Dosar irradiations the following calculation steps were used: 1) the leakage spectrum of the facility was determined by the ORNL staff using the DOT code[22]; 2) we determined the modifying effect of the shields, by using the MUSPALB code. 3) The backscattering effect of the phantom was taken into account modelling the phantom with a water slab and determining the backscattered spectrum with the MUSPALB code using the spectrum obtained in the previous step as input. 4) The summed direct + reflected spectra were used as a model spectrum for fitting to flux values of the NAD activation detectors. As an illustration, spectra for a 13 cm thick iron shield are shown in Fig. 20.

The same procedure was applied for the evaluation of our measurements performed at the Vinca heavy-water reactor. In this case the reactor escape spectrum was calculated at Chalk River using the 05R code[23], otherwise the procedure was identical with that discussed previously.

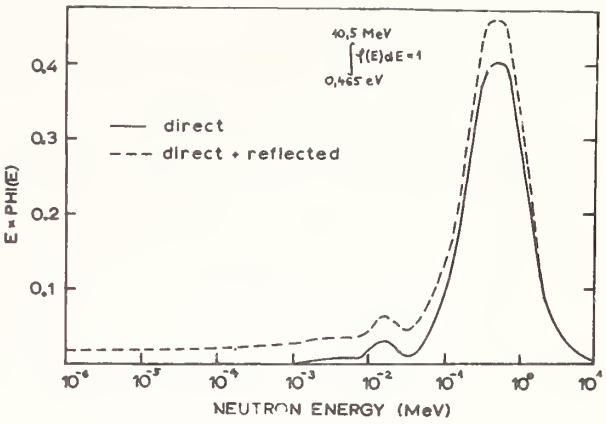

Fig. 20. Steel filtered spectrum of the Oak Ridge Health Physics Research Reactor (solid line) and the same as modified by the reflection of a water-filled human phantom (dashed line).

Conclusion

Spectra of neutrons passed through or reflected from different slabs may be calculated and applied for dosimeter evaluation. As the use of such spectra considerably improves evaluation techniques the application of spectrum calculations is being continued. One of the purposes of our work is to prepare a compendium of neutron spectra which makes available these spectra in a readily applicable form to scientists involved in neutron dosimetry evaluation.

Acknowledgements

Thank are due to my co-workers, J. Palfalvi, L. Koblinger and P. Zarand for their contribution, as well as to Dr. P. Vertes for the development of the MUSPALB computer code and to Dr. H. Ing (Chalk River Nuclear Laboratories, Canada) for the valuable discussions.

References

1. Nachtigall, D., Atompraxis 11 (1965) 203.
2. Nachtigall, D., Proc. Conf. Neutron Monitoring for Radiological Protection 329 IAEA Vienna 1967.
3. Makra, S., Toth, M., KFKI Közl. 16 (1968) 381.
4. Block, S., Shon, F.J., Health Physics 8 (1962) p. 533.
5. Nachtigall, D., Rohloff, F., Jül-213 -ST report (1964).
6. Makra, S., KFKI-70-6-HP report (1970) and lecture No. 107, Second IRPA congress, May 3-7 1970, Brighton, England.
7. Attix, F.H. (editor), Topics in Radiation Dosimetry. Academic Press, New York, London, 1972 p. 433.
8. Vertes, P., Nukleonik 12 (1969) 67.
9. Irving, D.C., Freestone, R.M., Kam, F.B.K., ORNL-3622 (1965).
10. Lux, I., Koblinger, L., KFKI-73-2 report (1973).
11. Koblinger, L., KFKI-74-47 report (1974).
12. Makra, S., Vertes, P., Kernenergie 16 (1973) p. 378.
13. Makra, S., Palfalvi, J., Vertes, P., Health Phys. 26 (1974) 29.
14. Palfalvi, J., KFKI-73-57 report (1973).
15. Palfalvi, J., KFKI-74-48 report (1974).
16. Palfalvi, J., Koblinger, L., KFKI-74-63 report (1974).
17. Makra, S., Palfalvi, J., Zarand, P., Proc. Conf. Neutron Monitoring for Radiation Protection Purposes, 47, IAEA Vienna, 1973.
18. Allen, F.J., Futterer, A., Wright, W., Budka, A., BRL 1130 report (1961).
19. Makra, S., Bekes, E., Proc. Conf. Advances in Physical and Biological Radiation Detectors p. 425, IAEA, Vienna, 1971.
20. Makra, S., Zarand, P., KFKI-71-82 report (1971).
21. Palfalvi, J., Makra, S., KFKI-74-68 report (1974).
22. Poston, J.W., Knight, J.P., Whitesides, G.E., Health Phys. 26 (1974) 217.
23. Ing, H., Private communication 1973.

Y.T. Song

1) Mixed use of average and mean energy need clarification.

2) Calculating fast neutron spectra through iron, what cross-section did you use?

3) Direct + scattered and Direct neutron spectra were compared. However, direct and direct + scattered had exactly same spectrum, though scattered were about 20% need clarification.

4) You made comment on optimum mixing ratio in connection of your spectrum calculation. How could it be used?

S. Makra

1) The terms I used are defined in some of my earlier papers (e.g. 1st IRPA Congress Lecture, Brighton, 1970) and in condensed form in Attix's recent Radiation Dosimetry book. Mean energy is a mean value without any weight factor; effective energy is weighted by kerma or dose-equivalent, effective energy is weighted by detector response.

2) The earlier calculations Abagian data were used, for recent calculations the 05R library was obtained from RSIC.

3) The direct and direct + reflected spectra displayed were flux per unit lethargy (linear scale) vs. energy (log scale) plots. The very similar shape in this case actually means that the low energy neutron contribution for the upper curve is considerably higher than for the lower one.

4) We did not develop any code for optimum mixing ratio determination. However, comparison of results for several mixing ratios can be used for a general orientation.

UTILIZATION OF PLASTIC SCINTILLATOR IN THE MEASUREMENT OF UNCHARGED RADIATIONS

P.K. Sarkar and K.N. Kirthi
Health Physics Division
Bhabha Atomic Research Centre
Bombay-400085

Uncharged radiations like neutrons and gamma rays produce scintillations in plastic scintillator through secondary charged particles. The energy distributions of these recoil particles are related to the energy distribution of the incident radiation. An attempt has been made in the present work to get back the original incident spectrum from the recoil distribution. The computer code UNFOLD designed for the purpose makes a minimum-variance, maximum likelihood estimate of the incident spectrum by iterative least square technique. Neutron spectra from different Be(α,n) source and ^{252}Cf spontaneous fission have been measured. The results agree well with those published. Plastic scintillator proves to be more useful when the incident gamma spectrum is continuous in nature because the Compton continuum produced in the scintillator has a well defined integral relationship with the incident gamma spectrum. Continuous gamma spectrum in Apsara reactor beam hole has been estimated using the technique developed.

(Apsara; energy distribution; gamma ray; iterative; neutron; plastic; recoil; scintillator; UNFOLD)

Introduction

Mixed radiation fields exist in many nuclear environments of applied and basic interest. An example of particular importance is the incore radiation field of a reactor, consisting, mainly of neutrons and gamma rays. In the measurement of a radiative component of such mixed fields the usual procedure is to employ a certain detection system which responds only to that particular component and discriminates against others. Though it is well known that total discrimination against background is impossible, the actual choice of detection system is often based primarily upon this very requirement. Existence of a non-zero sensitivity to background implies an experimental interdependence among the components of a mixed radiation field. Due to this complementary relationship, an improved definition of any given component automatically provides more precise knowledge of the remaining ones.

The present effort is directed towards the development of a general method for measuring both the continuous gamma and neutron component of a mixed radiation field. The technique applied is charged particle recoil, the recoil medium being a plastic scintillator. Protons and electrons are the recoil particles produced when plastic scintillator is exposed to neutrons and gamma rays respectively.

Plastic scintillator is one of the proton recoil detectors that can efficiently be used as a neutron spectrometer. It has a basic advantage over the liquid scintillators for its high detection efficiency and convenience of handling. Unlike anthracene or stilbene the pulse height produced in plastic scintillator does not depend on the direction of neutron incidence nor it is sensitive to thermal or mechanical shock. Kim[1] has pointed out that if the disadvantage of gamma response can be removed then plastic scintillator promises to be a very simple neutron spectrometer with high efficiency and moderate energy resolution. Young[2] has shown that the resolution of a scintillator detector increases with the decrease in the thickness till proton escape from the scintillator tries to affect resolution. Now, if proton escape is also accounted for in estimating the neutron spectrum a thin plastic detector can give a high degree of resolution. Apparently, it seems meaningless to use plastic scintillator in gamma spectrum analysis because of its comparatively bad resolution and mainly because it produces a smeared rectangular distribution rather than clear photopeaks for monoenergetic gammas. But when it becomes evident that it is the Compton recoil spectrometers that only can be used in the precise determination of the continuous gammas ray spectra[3], the plastic scintillator has the advantage due to the fact that scintillations are mainly by the Compton electrons produced

in it due to the incident gamma radiation.

In the recoil detection technique the problem basically lies with the unfolding of the incident distribution. The energy spectrum of the recoil particles gets a complicated smear in the observed pulse height distribution due to multiple scattering, non-linear light output and photomultiplier statistics. Still, if the response of the detector to mono-energetic incident radiation is known, the incident spectrum can be estimated by inverting the equation that relates the incident spectrum to the observed distribution. But if straight forward matrix inversion or iterative techniques are employed amplification of the fluctuations in the experimental pulse height distribution or large oscillations are likely to occur.

Calculation of the Response Function

In view of the practical difficulty associated with obtaining series of monoenergetic neutron or gamma sources, the response of the scintillator to those radiations were calculated theoretically. It is not practicable to use an analytic expression for the response function, since in general, the extremely complicated analytic expressions which exist are approximations not easily related to practical counter configurations. Several attempts were made to calculate the response function in different ways. They have been discussed elsewhere[4]. In the present case Monte Carlo technique has been employed to calculate the response functions.

Computer codes MECROS-N and MECROS-G[4] were developed to get the response of the scintillator to neutrons and gamma rays respectively. The present calculations follow the course of each neutron or gamma photon inside the scintillator, collision by collision, and calculates the energy deposited by the charged particles produced due to elastic scatterings and reactions. The light pulse produced by the incident radiation is obtained by summing up the contributions of all the charged particles after multiplying them with proper statistical weights and using proper formulations for light output vs. particle energy. Biased Monte Carlo technique i.e. Russian roulette and splitting is adopted. The statistical weight of the incident radiation after each collision is multiplied with the non-escape probability and is allowed to make further collisions inside the scintillator. The finite resolving power of the spectrometer system has been considered by making a random fluctuation being gaussian in nature.

Monte Carlo technique, though it gives the desired accuracy, does not yield an analytical expression from which the incident spectrum can be deduced directly. It requires an unfolding based on matrix configuration of response function.

Unfolding the Measured Distribution

When a measuring instrument is fed with a distribution g(s), the output obtained becomes y(t). Thus the function of the instrument can be looked upon as an operator O and the situation can be expressed in mathematical terms as

$$\boxed{O}\ g(S) = y(t)$$

This equation can be written in matrix notations as K.G. = Y where K is the response matrix of n x m elements, Y is the proton recoil distribution, and G is the spectrum to be evaluated. An easy solution to this equation is

$$G = K^{-1}\ Y$$

But this solution is not unique and also it can be shown[5] that G will not be known accurately due to the statistics associated with the observed data, what at the most can be obtained is the maximum likelihood estimate of 'G', based on 'a priori' informations with error and variance minimised as far as possible. Error minimisation is carried out by the usual least square techniques. Variance is minimised by using the weighting matrix and iterative techniques, resulting in a minimum variance maximum likelihood estimate of the spectrum. In order to remove spurious fluctuations smoothing has been applied to the observed data, using time series and Fourier analyses.

Experiment and Results

For measuring the neutron spectrum different thicknesses of scintillator were coupled to photomultipliers and pulses were fed to a multichannel analyser after a stage of conventional amplifiers. Channel calibration was done by a ^{60}Co gamma source. Neutron spectrum from different Be(α,n) sources and from spontaneous fission of ^{252}Cf was estimated. Details of the experimental set up and results have already been published[4,6]. Figs. 1,2,3 give the estimated spectra of Pu-Be, Ra-Be and ^{252}Cf respectively. For measuring gamma spectrum a single thickness of the scintillator has been used. The

selection of the thickness has been made by optimising resolution of the detector and electron escape from the scintillator. Continuous gamma background at Apsara beam hole number 3 was measured. The experiment was repeated with a lead shielding of 2.5 cms thickness. The observed and unfolded spectra are plotted in Figs. 4 and 5.

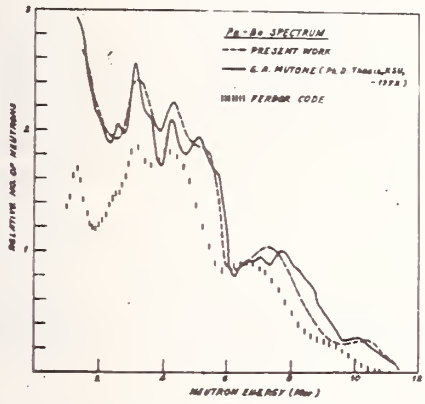

Fig. 1. Pu-Be Neutron Spectrum.

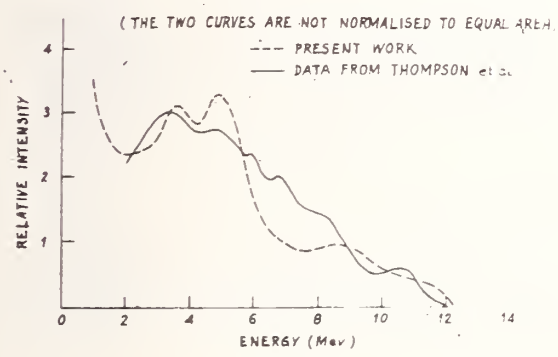

Fig. 2. Ra-Be Neutron Spectrum.

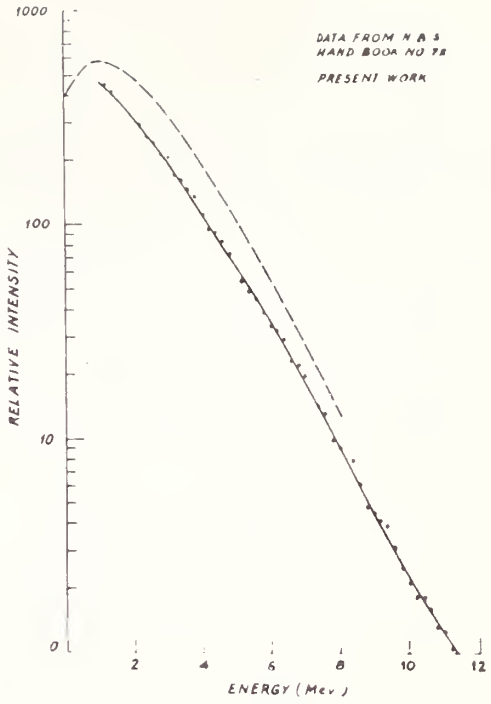

Fig. 3. Californium-252 Spontaneous fission neutron spectrum.

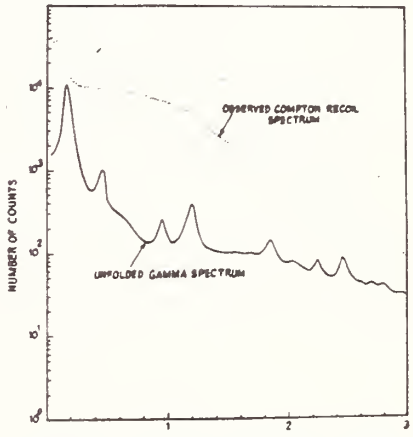

Fig. 4. Observed and Unfolded Gamma Spectrum taken with Plastic Scintillator at Apsara Beam Hole No.3. (The Number of counts for the unfolded spectrum is plotted in an arbitrary scale. The areas under the curves are not normalised).

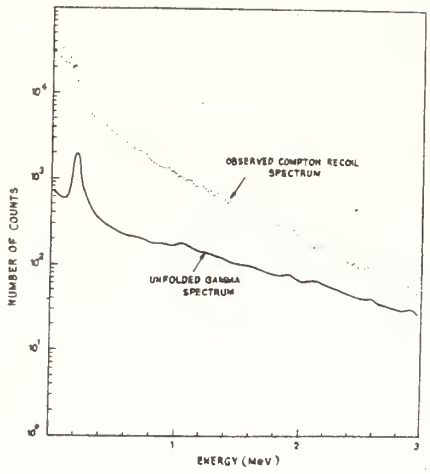

Fig. 5. Observed and Unfolded Gamma spectrum taken with Plastic scintillator at Apsara Beam Hole No.3 after 2.5 cms Lead shielding. (The number of counts for the unfolded spectrum is plotted in an arbitrary scale. The areas under the curves are not normalised).

Discussion

It is evident from the results shown that both the continuous gamma spectrum and the neutron spectrum in presence of gamma field can be estimated by plastic scintillator with fairly good accuracy. In order to separate out the two components of a mixed radiation field, first the neutron spectrum has to be estimated, then it has to be converted to the proton recoil distribution in the scintillator used to measure the gamma spectrum. The pulse height spectrum due to proton recoil distribution has to be subtracted from the observed pulse height spectrum. The pulse height distribution thus obtained can be used to unfold the gamma component.

Though plastic scintillator has poor resolution in case of discrete gamma peaks, the high degree of Compton dominance makes it very useful where the spectrum is continuous. In the case of neutron spectrum estimation, the most important limitation lies in the judicious selection of number and energy range of thin scintillator employed to resolve the spectrum. However, this limitation becomes insignificant when we take into cognizance the fact that plastic scintillator can efficiently be used to determine both the neutron and gamma component of a mixed field. Work is in progress in determining the two components seperately, using the method suggested in the present paper.

Acknowledgements

The authors are thankful to Dr. A.K. Ganguly for his constant encouragement and valuable guidance and also to Shri S. D. Soman for his keen interest in the work. We thank Dr. M.R. Iyer and Shri Hari Singh for their help.

References

1. KIM, C.M., A theoretical comparision of 4π fast neutron spectrometers, UCRL-9604 (1960).
2. Young, W.R., Neutron spectra from organic scintillators, UCRL-16149 (1965).
3. Gold, R. and Olson, I.K., Analysis of Compton continuum measurements, ANL-7611
4. Sarkar, P.K.; Kirthi, K.N. and Ganguly, A.K., Response of plastic scintillator to neutrons, gamma-rays and charged particles, BARC 756 (1974).
5. Burrus, W.R., Utilization of 'a priori' information in the statistical interpretation of measured distributions, ORNL-3743 (1964).
6. Sarkar, P.K., Kirthi, K.N. and Ganguly, A.K., A Technique of measuring neutron spectrum. Proc. 2nd Symposium on neutron dosimetry in biology and medicine, Munich, Sept. 30 - Oct. 4 (1974).

Discussion

K.V.S. Nambi

Have you attempted to measure the 'skyshine' spectrum from the gamma garden at BARC using a plastic scintillator and your unfolding technique?

P.K. Sarkar

Because of the experimental difficulties associated with such measurements so far no attempt has been made. We have a plan to do it in future.

H. Sanjeeviah

1. Can one use a plastic scintillator to measure bremsstrahlung spectra?

2. Bremsstrahlung radiation (EB or IB) is generally of low intensity. So will not the low efficiency of the plastic scintillator hinder the measurement ?

P.K. Sarkar

1. The continuous nature of

Bremsstrahlung spectra indicates that plastic scintillator can be used to measure such spectra. But care should be taken to have the response function very precisely estimated. In fact experimental estimation will be more valuable than the theoretically calculated ones.

2. The efficiency factor can be increased by increasing the thickness (or volume) of the scintillator. In fact provisions can be made to arrest all the bremsstrahlung radiations. But care should be taken to optimise the thickness because of light attenuation in the scintillator.

Y. Furuta

1. What is the lowest detectable energy of neutrons ?

2. What data did you take from for the relation between charged particle energy and obtained pulse height of charged particles ?

P.K. Sarkar

1. The lowest energy which can be discriminated against gamma background is 1 MeV.

2. We have considered the formulation given by Lindstrom et al (Nucl. Instr. and Methods 98 (1972) 413) primarily. But we also have performed experiments at a Van-de-Graaff accelerator using our scintillator to check the validity of the relationship for the present scintillator (supplied by Technical Physics Division, BARC).

NEUTRON SPECTROMETRY BY SANDWICH SURFACE BARRIER TECHNIQUE *

O.P. Joneja
Bhabha Atomic Research Centre
Trombay, Bombay-400085
India

A neutron spectrometer using silicon surface barrier detectors employing ^{6}LiF as a radiating material is developed. An incident neutron interacts with the radiating atom resulting in two charged particles, which are detected by sandwich detector geometry and the corresponding sum pulses from both the detectors shall uniquely define the incident neutron energy. This paper also presents results obtained by Monte Carlo simulation of all the correction factors for the detector head employed. A new concept for resolution correction is developed which brings down the lower energy limit of the detector system. The spectrometer is employed for incore spectrum studies in case of a thermal reactor 'Kahter' and the results obtained exhibit a good agreement with that of calculations by GAM THERMOS EXTERMINATOR Code.

(Detector; energy leakage; ^{6}LiF; Monte Carlo; neutron; sandwich; spectrometry; surface barrier)

Introduction

The study of neutron spectrum in reactors offers an effective tool to check the validity of calculational methods, in addition, the damage suffered by construction material in high flux experimental and power reactors requires the knowledge of fast neutron spectrum. The neutron energy of interest in case of fast and epithermal reactors is considered to extend from $\sim$ 10 keV to 10 MeV and uptil now the results from several experimental techniques are normalized to scan such a wide energy region. The present method, however provides the spectrum information for most of the energy region of interest in a single shot. The spectrometer head consists of two silicon surface barrier detectors sandwiching a ^{6}LiF layer. Although charged particles produced due to ^{6}Li (n, α)T reaction receive energy depending upon their angle of ejection, the sum of their kinetic energy in principle remains constant and is equal to energy of the incident neutron plus Q value of the reaction. Thus, for a continuous incident neutron spectrum there will be one to one correspondence between neutron energy and sum pulses but since the cross section of ^{6}Li(n, α)T reaction depends on neutron energy, therefore spectrum unfolding from pulse height information shall require an efficiency correction.

Experimental Set-up

Two identical silicon surface barrier detectors each having an area $\simeq$ 260 mm^2 and a depletion depth of 500 microns, enclosing 150$\mu gm/cm^2$ of ^{6}LiF layer in a sandwich geometry and housed in a steel container forms a detecting head. For the purpose of calibration, each leg, comprising a detector and a set of amplifying units, is adjusted to exhibit identical pulses for a given energy loss in the respective detectors. A fast coincidence along with a gate unit ensures detection of coincidence events and elimination of single particle events. The calibration is accomplished by thermalizing neutrons from an Am - α - Be neutron source.

Monte Carlo Method

It can be easily visualized that a sandwich system operating in coincidence mode shall suffer from the following losses:

1) When either one or both the particles escape from the finite separation between the detectors, i.e., gap leakage.

2) There is no coincidence response when both the particles hit the same detector, i.e., double response leakage.

* The work done at KFA-IRE, Juelich in West Germany

3) An event is also considered lost when the pulse height resulting from either detector falls below the threshold setting, i.e., bias leakage.

Now, in case the failure of coincidence response due to above losses depends upon neutron energy then spectrum unfolding without considering above effects shall results in a distorted spectrum. In order to evaluate all the leakages, a Monte-Carlo Code 'COINCIDE' is develcped in Fortran IV[1]. The leakage simulation is accomplished for an isotropic incident neutron flux assuming that the lighter charge particle is ejected isotropically in the laboratory system. The output lists all the leakages per observed coincidence count for several neutron energies and the results obtained for the detector head employed are presented in Fig. 1.

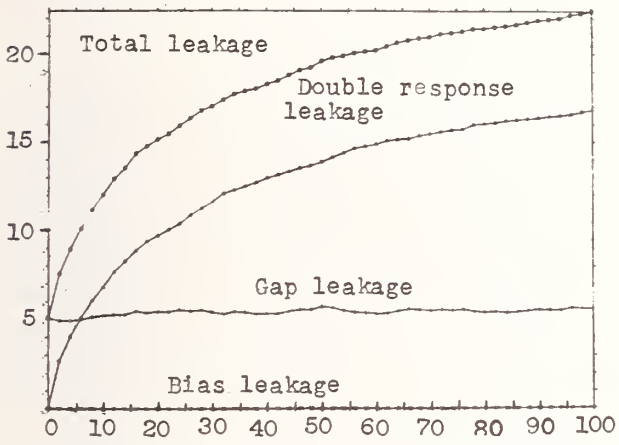

Fig. 1. Leakage factors obtained by Monte Carlo for a ^{6}Li system (a-2.60, c=C.C12 cm) x-axis -n.energy (MeV), y-axis leakage factors/ registered count: for bias=1.5 MeV.

Description of Thermal Assembly 'Kahter'

The spectrometer is used for incore spectrum studies in the case of a graphite moderated assembly 'Kahter', at the institute of reactor development at Juelich in West Germany. The fuel $(U\text{-}Th)O_2$ is fabricated in the form of balls, each containing one gm of ^{235}U and 5 gms of ^{232}Th. A uniform mixture of coated particles and graphite compressed to a diameter of 5 cms forms the core of a fuel ball, which is further enclosed by a 5 mm thick graphite jacket. A cylindrical graphite structure 40 cms thick having an inner diameter of 2.16 metres and height of 2.40 metres with a slanting base and an additional cylindrical passage leading to a carrier belt forms core of the reactor. The assembly is controlled with the help of nine boron carbide rods. The detector head in the present experiment is located in an aluminium channel situated at a distance of about 30 cms from the central absorber rod and about 140 cms from bottom of the core.

Resolution Correction and Comparison with Calculations

The subject of resolution correction in general has been dealt by R. Gold[2] and the standard expression for numerical solution can be written as

$$\underline{Y} = R\underline{X} \qquad \underline{Y} = \text{output reactor}$$

$$R = \text{Response matrix} \qquad \underline{X} = \text{input reactor}$$

The input vector $\underline{X}$ can be determined by matrix inversion, however this method quite often is found to yield oscillatory solutions and that is why one finds number of iterative schemes available in literature but unfortunately none of them can be recommended for a particular measurement. It is interesting to state that available iterative methods aim at correcting the experimental data for resolution whereas in the present work correction is attempted through cross section. In this method one has to construct an advancing matrix from a detector response to thermal neutrons and then transform the cross section vector by matrix operation. The advancing response matrix and the cross section transformation for thermal response obtained at different power levels is presented in Figs. 2 and 3. The measured lethargy spectrum after all the corrections is shown in fig. 4 along with fission spectrum and calculated reactor spectrum. It can be seen that measured and calculated spectra agree within $\pm 12\%$ over most of the energy region of interest. The larger discrepancies below about 250 keV might result from non reproducibility of the response function and also lower moderation in experimental results might be due to the fact that during experiment detector head was not completely surrounded by fuel balls. Also a relatively larger error in one of the higher energy bands is expected to result from the fact that the code employed for calculations was good for thermal reactor calculations and moreover the calculated spectra is averaged over a large volume containing the site of experiment.

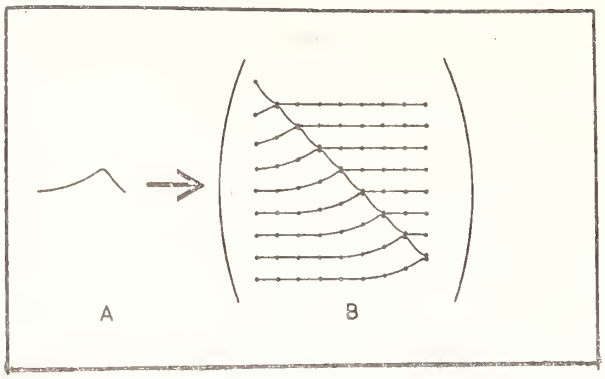

Fig. 2. Response matrix constructed from thermal neutron response.

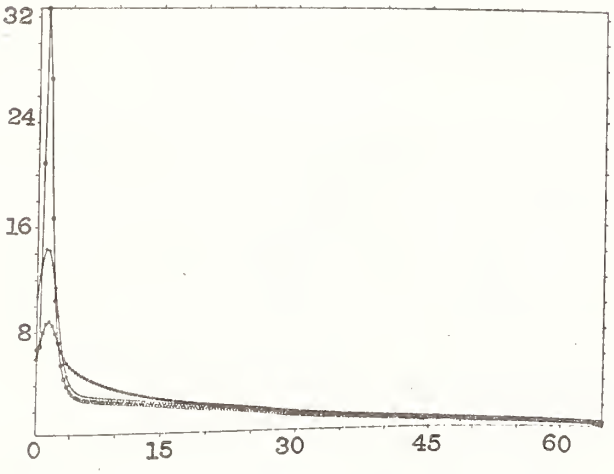

Fig. 3. Plot detects the actual cross section data and the resolution corrected cross section data

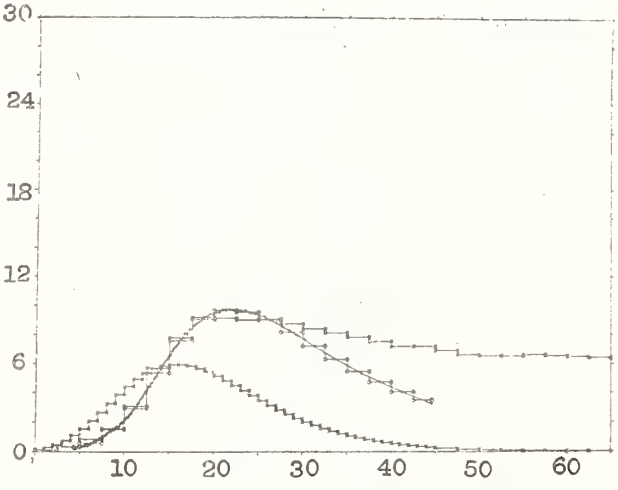

Fig. 4. Comparison of measured:calculated and fission $\varphi^{*}(U)/U$ in Kahter core.

Acknowledgements

My sincere thanks are due to Dr. R. Hecker for providing all the facilities and valuable suggestions. I shall also like to thank Dr. P. Cloth for the discussions. I would like to thank Dr. P.K. Iyengar for suggesting the problem and useful discussions. Also, I would like to thank Dr. M.P. Navalkar for his interest and suggestions.

References

1. Joneja, O.P., Fast Spectrum Studies with ^{3}He Surface Barrier Sandwich Detector KFA, Internal report IRE - 25-73.
2. Gold, R., An iterative unfolding method for response matrices, ANL - 6984 (Dec. 1964).

ROLE OF HIGH RESOLUTION Ge(Li) DETECTOR IN TRACE ELEMENT STUDY IN WATER ACTIVATED WITH THERMAL NEUTRONS

J.M. Chatterjee (Das)*, E. Peeters and M.A. Castiaux
Institut Royal des Sciences Naturelles de Belgique
Rue Vautier 31, 1040 Bruxelles, Belgium

While chemical analysis is limited in its application of element detection, gamma-ray spectrometry plays a big role in the nondestructive element detection in the neutron activated samples with large volume high resolution Ge(Li) detector. The water samples from the volcanic region of the island SANTORINI (Greece) have been activated with thermal neutrons, and the gamma-rays emitted by the long-lived radioisotopes have been detected with high resolution Ge(Li) detector. The analyzed results show the high concentrations of alkaline and magnetic elements if compared with that of these elements in the normal sea water samples. The presence of some rare earth elements has been observed as well.

(Activation; analysis; element; gamma rays; Ge(Li) detector; neutron; nondestructive; resolution; spectrometry; water)

Introduction

The activation analysis has its important role in the various fields of radio analytical chemistry. The procedure is applied successfully to the trace element study in the samples of biology, metallurgy, mineralogy, medicine, water, air (pollution study) and also for industrial process control in different laboratories. The direct counting with the high resolution large volume Ge(Li) detector has made possible the rapid and precise determination of elements of multielemental samples.

The procedure has been used to study the trace elements of the water collected from the region of living volcano Santorini (Nisos-Thira, Greece).

Site Choice and Sample Collection

The region was chosen for several reasons, particularly

a) Mere sight has been enough to realize the existence of some elements; the pronounced rusty red colour of iron oxide visible on the rocks of the volcano and the green sea water extending few km from the source show the presence of high concentrations of iron.

b) The information on this region is very scanty; only some geological study has been reported[1].

c) The place is very near to the residential area and considered one of the tourists' places in Greece.

d) The local people are living on fishing in the Aegean Sea and the sea of Crete which surround the island.

Seven places including the bays were chosen to cover the whole rim as well as the body of the volcano (fig. 1). The hot water sources under the huge rocks (steno source 1 and 2), the bays flowing to the sea (Erinia, St. Georgia, St. Nicolas), the natural lake of the volcano, the hot vapour coming out had been considered the main reservoirs of different elements. The water from these places and the vapour condensed were collected for sampling by sucking with plastic syringe; 2 ml of sample was poured into the sterilized quartz vials; precautions were taken not to contaminate them during collection. The vials are then sealed in the flame.

Fig.1. Shows the sites for sample collection.

*Present address - E.S.C. Division, Saha Institute of Nuclear Physics, Calcutta-9

Experimental Procedure

With thermal neutrons of estimated flux 3 x 10^{12} n/s/cm^2, the samples were irradiated in the reactor of C.E.N. (Saclay-France) for five days along with standards prepared from Zn, Co, Br and Hg compounds. The standards are used as comparator and also for checking the neutron flux in the reactor canal. An empty quartz vial was irradiated to check the impurity added to the sample from the wall of the container.

The activated samples were then cooled down for four weeks, the reason is, during the irradiation extremely large amounts of ^{24}Na, ^{38}Cl, ^{42}K and ^{82}Br are produced and these short-lived nuclides present an initial radiation problem and their gamma-ray spectra mask the spectra of other trace activation products.

1 ml of the activated sample was inserted into the disc of plexiglass (internal diameter 19.9 mm and thickness 3.7 mm). Two ccxial rightangled Ge(Li) detectors - ORTEC and PHILIPS - of active volumes 31.4. and 64 cc respectively were used in combination with 16 K multichannel pulse height analyser (Intertechnique BA 163). The analyser has the provision for simultaneous accumulation of four separate spectra with proper analogue-to-digital converter (Intertechnique CT 102). The detectors were incorporated with preamplifier and the signals were amplified by ORTEC spectroscopy amplifiers; their resolution had been 2.2 keV for ORTEC and 1.8 keV for Philips on 1,332 keV gamma-ray from ^{60}Co.

30-35 photopeaks of energy ranges 100-2,000 keV from each sample were detected with the time interval of 14-15 weeks. The counting time was adjusted according to the counting statistics desired. The major isotopes searched had been of half-lives from few days to several years.

Results and Discussions

The elements found are Ce, Hg, Cr, Sr, Cs, Rb, Zn, Co, Fe, Sc, Eu, Se and Br. Br is not observed in the measurements taken 18 weeks after irradiation. Very interesting observations are made in this region. Variable concentrations of most of the elements are observed. Ce and Cr are not found in all the samples. Hg content is very high (500%) in comparison with that in the normal sea water[2]. (14-20 mg/l of Sr is found in the water samples but is totally absent in both the samples of condensed vapour). Extremely large concentrations of Cs and Fe are found, the large quantity of iron is visible from the rusty red colour of the rocks. All other observed elements have their concentrations more than those present in the normal sea water. The absence of Sr, Cs and Rb in the sample taken by condensing the hot vapour from the outlet of orater may be due to (1) some geochemical change in the molten part of the volcano and (2) the filtration by the various earth layers inside the volcano. Two more elements Eu and Se have been detected in the sample of vapour condensed. The large concentration of Se in this sample is noticeable.

The presence of sulphur is apparent from the yellow layer in the orater and from the smell of H_2S in the water sample from hot source. But this element could not be detected because of its very short half-life (5.07 m). However, a gradual and careful activation analysis of sea water and marine organisms will provide much information about the geochemical change and pollution of this region.

Acknowledgements

The authors wish to express their heartiest thanks to Prof. A. Capart, Director of the I.R.S.N.B., Bruxelles for his active help during the measurement and participation in sample collection. One of the author J.M.C. is grateful to IAEA, Vienna for sponsoring the fellowship for the post-doctorate research during this period.

References

1. Nikovich, D. and Heezen, B.C., Submarine Geology and Geophysics; edited W.F. Whittard and R. Bradshaw, Proceedings of the 17th Symposium of the Colston Research Society held in the University of Bristol, 1965.
2. Bowen, H.J.M. and Gibbons, D., Radioactivation Analysis; Clarendon Press, Oxford (1963).

SUMMING UP OF THE DELIBERATIONS OF THE INTERNATIONAL SYMPOSIUM ON RADIATION PHYSICS

By A.K. Ganguly
Director, Chemical Group
Bhabha Atomic Research Centre
Trombay, Bombay-400085
INDIA

At the near conclusion of this Symposium, a very successful one at that, thanks are due to the untiring efforts of Professor A.M. Ghose and to his wonderful band of enthusiastic workers.

Historically, a national symposium on metrology of radio-nuclides was held in 1966 in Trombay which finally emerged from its deliberations as essentially a symposium on Instrumentation in Radiation Physics. This was then appropriately renamed as National Symposium on Radiation Physics organised in 1970. Now, at the end of 1974, we are witness to this International Symposium on Radiation Physics. Papers, presented, and deliberations in the Symposium have also been marked by progressive enlargement of scope and enhancement of standards. My intention in this summing up effort is not to restate what has been stated; in fact I find the summary of this Symposium has already appeared as a publication of this symposium as abstracts of papers. Barring only a few all of them were presented during these 4½ days. What this publication does not contain, is free for discussion during these scientific sessions.

In view of the above, I should like only to re-state some of the high-lights of the papers and discussions that appear to me as significant. So, I hope, you will excuse me since this talk will have some of my personal bias built into it. I could not avoid this inspite of myself.

The papers were excellently classified under broad headings of the scientific sessions as 'Basic Interaction Cross-Sections', 'Radiation Transport Theory and Applications', 'Radiation Scattering in Bulk Media', 'Radiation Shielding' and 'Radiation Dosimetry and Instrumentation'.

There had been at the back of the minds of most of the Indian participants, the fact of the near completion of the big radiation production machine, the Variable Energy Cyclotron in this city. Right in the beginning of the symposium, the proceedings sounded to me as an exercise in thinking aloud as to what of the many good things we can do in Radiation Physics and in Nuclear technology besides carrying out the basic nuclear physics experiments with this machine. Dr. Hubbell from the United States presented to us the status of photon cross-section data from 100 eV to 100 GeV range. Our interest at the present moment is still towards lower energies of this range, say from 100 MeV to 100 eV. Workers are comfortable in keV to a few MeV range. Radiation Physics in this country has to take better cognizance of the energies below few keV and above a few MeV. The **tradition of radiation physics, which in this country started with Sir J. C. Bose and Prof. M. N. Saha, as emphasized at this Conference, in this country and elsewhere has to expand the domain of energies indicated above.**

Dr. P. K. Iyengar in his talk on radiation physics and nuclear technology eloquently emphasized the needs of R and D efforts that can readily be undertaken in this country using the nuclear reactors and the cyclotrons for the development of material sciences. Using radiation production machine as a tool for Radiation Physics experiments, research work has to come of age now in this country in the light of the programme in technology and nuclear researches. Work in this line has been going on for some time with the coming of the fast reactor technology and the high energy accelerators. This line of activity is bound to take a new enlarged dimension.

Professor A.M. Ghose emphasized new techniques for measurement of angular scattering and his ideas about the development of double scattered neutron polarimeter are indications of some important developments. The Bose Institute shows great promise in the future developments in these directions.

Dr. F. Perey's talk on Gamma photon production programme at ORNL appeared particularly relevant in our context as well. It was stimulating to find reappearance of a great interest in the basic gamma spectrometry using sodium iodide and development of the powerful technique of spectrum unfolding. We, in this country, have still a sustained interest in sodium iodide crystal spectrometry for very pragmatic reasons

and simultaneously we have also been sustaining an interest in high energy neutron (60 MeV neutron) spectrometry using plastic scintillators. This work is going to receive a fresh impetus since mono-energetic neutrons of energy higher than those available at Trombay, would be available in Variable Energy Cyclotron.

Dr. D.V. Gopinath's presentation of a generalised formulation of radiation transport problems that has the sphere to deal, in the onset, with photons, neutral and charged particles, would be a commendable attitude to maintain. In covering the energy range, we are talking about, it would be necessary that we need further development in techniques for precision measurement of cross sections in the low and high energy ranges that have been indicated earlier. Because in the final analysis, this is an essential input experimental data for computational physics. A number of other papers related to computational physics as presented, laid very great emphasis on the Monte Carlo techniques. Still we do not have precision data at the low energy end of the degraded high energy particles of photons. Dr. D.K. Trubey, from a very good practical angle laid emphasis on development of shielding standards. This is an activity which we are yet to handle systematically.

Professor T. Hyodo discussed the problems of gamma back-scattering and techniques of measurements. It appeared that the problems of low energy end of the back-scattered spectrometry are still to be handled coherently, specially when the incident energy is comparable with the K electron binding energy of heavy nuclides.

Professor P.P. Kane produced an evidence, during the discussion, indicative of the influence of the K electron binding energy on the scattering of low energy photons. The difficulty of dealing with the multiply charged heavy ions as pointed out by Dr. S. Mukherjee is a problem in its own right. Researches on the stopping of multiply charged accelerated heavy particles produced in the accelerators can be undertaken for experimentation. Here I would like to mention that the possible future programme of VEC includes acceleration of multiply charged heavy ions.

Dr. D.K. Trubey's talk giving comprehensive description of the ORNL Shielding Information Centre, naturally attracted attention for obtaining information on the very topics on shielding enumerated in the talk.

Dr. W.S. Snyder's talk on radiation dosimetry of human organs used for computational purposes - the concept of a Phantom of a Phantom and again the computational techniques were based on the Monte Carlo methods.

S.C. Sharma presented a model based on the experimental track structure for computation of internal dose delivered to an organ from an external source. On first hearing the approach developed by Sharma and Katz, it appeared that the model could be handled for micro dosimetric computation of internally deposited radio nuclides.

Dr. D.F. Regulla, while discussing the versatility of luminescent dosimeters, attracted attention to a phenomenon in his experiment of TSEE. An irradiated phosphor gave indications of the emissions of exoelectrons of about 300 eV. We are yet to understand what these mean.

Dr. Y. Furuta emphasized the present state of all-out development in the field of neutron dosimetry by T.L. Phosphors like ^{6}LiF and ^{7}LiF. The problems of dosimetry of high energy neutrons in the tens of MeV range are still to be resolved for health and safety operations.

We have listened to an extremely interesting lecture by Shri C. Ambasankaran, where the VEC machine was described in many of its constructional details. It is heartening to note that the various parts of the cyclotron, such as the main magnet, coil, resonator tank etc. are being fabricated indigenously. When the machine is in operation, towards the end of 1975, it will fulfil the long felt need in India to carry out studies of high energy neutrons, gamma rays and multiply charged heavy ions. In his talk on solar energy, a topic apparently not directly associated with the radiation physics, Dr. V.G. Bhide laid emphasis on the possibilities of solar energy becoming a great hope for the future energy requirements.

Dr. S. Makra in his talk on "Neutron Dose Evaluation using calculated Neutron Spectra", brought up very significantly the question of shield optimisation. Even at this stage of development of Codes and Techniques for radiation transport, practical shielding problems are still being handled on empirical or adhoc basis in great majority of situations. Dr. Gopinath and Dr. Trubey brought to our attention, the existence of a code for optimisation

for a given sequential shield. It is felt that it is still worth looking for prescription of shields both in regard to thicknesses of the individual layer of materials and their sequence for a given set of shield materials.

We have been listening to a whole series of excellent papers from Indian authors and the abstracts to which I made a mention earlier gives an account of the present state of activities in radiation physics research. We missed listening to new efforts in radiation physics based on the recent developments of theoretical principles.

Professor L.S. Kothari dealt with the theory of neutron thermalization and Dr. Sharma dealt with the model of a track structure and Professor Ghose indicated some indigenous methods for using the principles of geometrical optics in the development of techniques for radiation measurements. While explaining the mechanism of Radiation Damage, Dr. P.K. Iyengar mentioned development of theoretical models for development in radiation physics. Dr. R. Ramanna, in his inaugural speech felt that this symposium will be able to give some indication as to where we go from here in radiation physics. I feel that in some later symposia we should also invite some of those theoreticians who are also interested in seeing some applications of their theory.

NBS-114A (REV. 7-73)

U.S. DEPT. OF COMM. BIBLIOGRAPHIC DATA SHEET	1. PUBLICATION OR REPORT NO. NBS SP-461	2. Gov't Accession No.	3. Recipient's Accession No.

4. TITLE AND SUBTITLE

RADIATION PHYSICS - Proceedings of the International Symposium on Radiation Physics, held at Bose Institute, Calcutta, India, Nov. 30-Dec. 4, 1974

5. Publication Date: January 1977

6. Performing Organization Code

7. AUTHOR(S) Proceedings Editors: A. M. Ghose, D. V. Gopinath, J. H. Hubbell, S. C. Roy.

8. Performing Organ. Report No.

9. PERFORMING ORGANIZATION NAME AND ADDRESS

NATIONAL BUREAU OF STANDARDS
DEPARTMENT OF COMMERCE
WASHINGTON, D.C. 20234

10. Project/Task/Work Unit No. 2400105

11. Contract/Grant No.

12. Sponsoring Organization Name and Complete Address (*Street, City, State, ZIP*)

Organized by: Bose Institute, Calcutta, India
Co-sponsored by: Dept. of Atomic Energy (DAE), India
Assistance from: International Atomic Energy Agency (IAEA); National Bureau of Standards

13. Type of Report & Period Covered: final

14. Sponsoring Agency Code

15. SUPPLEMENTARY NOTES

Library of Congress Catalog Card Number: 76-608379

16. ABSTRACT (*A 200-word or less factual summary of most significant information. If document includes a significant bibliography or literature survey, mention it here.*)

These proceedings contain invited and contributed papers presented at the International Symposium on Radiation Physics organized by and held at the Bose Institute, Calcutta, India Nov. 30-Dec. 4, 1974. The purpose of this symposium, recognizing radiation physics as the thread held in common by a variety of medical, engineering and scientific disciplines, was to bring together specialists from these disciplines to report on, exchange, and make available through these proceedings, information and experiences of common interest to workers in these diverse disciplines. Topics thus brought together in this symposium include new measurements, theoretical developments, compilations and applications of basic cross section and transport data for photon, electron, neutron and heavy ion beams interacting with matter.

17. KEY WORDS (*six to twelve entries; alphabetical order; capitalize only the first letter of the first key word unless a proper name; separated by semicolons*)

Cross sections; dosimetry; electrons; neutrons; photons, radiation physics; symposium.

18. AVAILABILITY

[X] Unlimited

[ ] For Official Distribution. Do Not Release to NTIS

[X] Order From Sup. of Doc., U.S. Government Printing Office Washington, D.C. 20402, SD Cat. No. C13.10:461

[ ] Order From National Technical Information Service (NTIS) Springfield, Virginia 22151

19. SECURITY CLASS (THIS REPORT): UNCLASSIFIED

21. NO. OF PAGES: 268

20. SECURITY CLASS (THIS PAGE): UNCLASSIFIED

22. Price: $3.25

USCOMM-DC 29042-P74

☆U.S. GOVERNMENT PRINTING OFFICE: 1977 240-848/101 1-3

NBS TECHNICAL PUBLICATIONS

PERIODICALS

JOURNAL OF RESEARCH reports National Bureau of Standards research and development in physics, mathematics, and chemistry. It is published in two sections, available separately:

• Physics and Chemistry (Section A)
Papers of interest primarily to scientists working in these fields. This section covers a broad range of physical and chemical research, with major emphasis on standards of physical measurement, fundamental constants, and properties of matter. Issued six times a year. Annual subscription: Domestic, $17.00; Foreign, $21.25.

• Mathematical Sciences (Section B)
Studies and compilations designed mainly for the mathematician and theoretical physicist. Topics in mathematical statistics, theory of experiment design, numerical analysis, theoretical physics and chemistry, logical design and programming of computers and computer systems. Short numerical tables. Issued quarterly. Annual subscription: Domestic, $9.00; Foreign, $11.25.

DIMENSIONS/NBS (formerly Technical News Bulletin)—This monthly magazine is published to inform scientists, engineers, businessmen, industry, teachers, students, and consumers of the latest advances in science and technology, with primary emphasis on the work at NBS. The magazine highlights and reviews such issues as energy research, fire protection, building technology, metric conversion, pollution abatement, health and safety, and consumer product performance. In addition, it reports the results of Bureau programs in measurement standards and techniques, properties of matter and materials, engineering standards and services, instrumentation, and automatic data processing.

Annual subscription: Domestic, $9.45; Foreign, $11.85.

NONPERIODICALS

Monographs—Major contributions to the technical literature on various subjects related to the Bureau's scientific and technical activities.

Handbooks—Recommended codes of engineering and industrial practice (including safety codes) developed in cooperation with interested industries, professional organizations, and regulatory bodies.

Special Publications—Include proceedings of conferences sponsored by NBS, NBS annual reports, and other special publications appropriate to this grouping such as wall charts, pocket cards, and bibliographies.

Applied Mathematics Series—Mathematical tables, manuals, and studies of special interest to physicists, engineers, chemists, biologists, mathematicians, computer programmers, and others engaged in scientific and technical work.

National Standard Reference Data Series—Provides quantitative data on the physical and chemical properties of materials, compiled from the world's literature and critically evaluated. Developed under a world-wide program coordinated by NBS. Program under authority of National Standard Data Act (Public Law 90-396).

NOTE: At present the principal publication outlet for these data is the Journal of Physical and Chemical Reference Data (JPCRD) published quarterly for NBS by the American Chemical Society (ACS) and the American Institute of Physics (AIP). Subscriptions, reprints, and supplements available from ACS, 1155 Sixteenth St. N.W., Wash. D. C. 20056.

Building Science Series—Disseminates technical information developed at the Bureau on building materials, components, systems, and whole structures. The series presents research results, test methods, and performance criteria related to the structural and environmental functions and the durability and safety characteristics of building elements and systems.

Technical Notes—Studies or reports which are complete in themselves but restrictive in their treatment of a subject. Analogous to monographs but not so comprehensive in scope or definitive in treatment of the subject area. Often serve as a vehicle for final reports of work performed at NBS under the sponsorship of other government agencies.

Voluntary Product Standards—Developed under procedures published by the Department of Commerce in Part 10, Title 15, of the Code of Federal Regulations. The purpose of the standards is to establish nationally recognized requirements for products, and to provide all concerned interests with a basis for common understanding of the characteristics of the products. NBS administers this program as a supplement to the activities of the private sector standardizing organizations.

Consumer Information Series—Practical information, based on NBS research and experience, covering areas of interest to the consumer. Easily understandable language and illustrations provide useful background knowledge for shopping in today's technological marketplace.

Order above *NBS publications from: Superintendent of Documents, Government Printing Office, Washington, D.C. 20402.*

Order following *NBS publications—NBSIR's and FIPS from the National Technical Information Services, Springfield, Va. 22161.*

Federal Information Processing Standards Publications (FIPS PUBS)—Publications in this series collectively constitute the Federal Information Processing Standards Register. Register serves as the official source of information in the Federal Government regarding standards issued by NBS pursuant to the Federal Property and Administrative Services Act of 1949 as amended, Public Law 89-306 (79 Stat. 1127), and as implemented by Executive Order 11717 (38 FR 12315, dated May 11, 1973) and Part 6 of Title 15 CFR (Code of Federal Regulations).

NBS Interagency Reports (NBSIR)—A special series of interim or final reports on work performed by NBS for outside sponsors (both government and non-government). In general, initial distribution is handled by the sponsor; public distribution is by the National Technical Information Services (Springfield, Va. 22161) in paper copy or microfiche form.

BIBLIOGRAPHIC SUBSCRIPTION SERVICES

The following current-awareness and literature-survey bibliographies are issued periodically by the Bureau:

Cryogenic Data Center Current Awareness Service. A literature survey issued biweekly. Annual subscription: Domestic, $20.00; Foreign, $25.00.

Liquified Natural Gas. A literature survey issued quarterly. Annual subscription: $20.00.

Superconducting Devices and Materials. A literature survey issued quarterly. Annual subscription: $20.00. Send subscription orders and remittances for the preceding bibliographic services to National Bureau of Standards, Cryogenic Data Center (275.02) Boulder, Colorado 80302.

U.S. DEPARTMENT OF COMMERCE
National Bureau of Standards
Washington, D.C. 20234

OFFICIAL BUSINESS

Penalty for Private Use, $300

POSTAGE AND FEES PAID
U.S. DEPARTMENT OF COMMERCE
COM-215

SPECIAL FOURTH-CLASS RATE
BOOK